UNIVERSIDAD AUTÓNOMA DE MADRID

Departamento de Biología Molecular

Facultad de Ciencias

Regulation and diagnosis of cardiovascular diseases by microRNAs derived from immune cells

Tesis doctoral presentada por el Graduado en Biotecnología:

Rafael Blanco Domínguez

Para optar al título de:

Doctor en Biociencias Moleculares

por la Universidad Autónoma de Madrid

Directora de tesis:

Dra. María Pilar Martín Fernández

Este trabajo ha sido realizado en el Centro Nacional de Investigaciones Cardiovasculares (CNIC)

Madrid, 2022

Madrid, October 25, 2021

Dr. María Pilar Martín Fernández, Associate Professor and Group Leader of the "Regulatory Molecules of Inflammatory Processes" group of the Vascular Pathophysiology Area at the Spanish National Center for Cardiovascular Research (CNIC), CERTIFIES THAT:

The doctoral thesis entitled: **"*Regulation and diagnosis of cardiovascular diseases by microRNAs derived from immune cells*",** has been carried out by Rafael Blanco Domínguez, Bachelor in Biotechnology by the Universidad Pablo de Olavide, under my supervision and direction. I consider this PhD thesis satisfactory and I authorize its presentation for the evaluation by the corresponding committee.

To whom it may concern, I sign this certificate in Madrid, on October 25, 2021.

The director María Pilar Martín Fernández

Associate Professor
Group Leader Regulatory Molecules Lab.
Vascular Pathophysiology Area
Centro Nacional de Investigaciones cardiovasculares (CNIC)
28029 Madrid, Spain
Phone: +34 91 453 1200-ext 2009
pmartinf@cnic.es

"Penicillin cures, but wine makes people happy"

Alexander Fleming

AGRADECIMIENTOS

En primer lugar, me gustaría agradecer a Pilar el haber apostado por mí desde aquella llamada telefónica en 2015 hasta hoy. En aquella llamada, recuerdo que me detalló una serie de proyectos científicos que quería explorar. Confieso que no me enteré de mucho, pero ella parecía convencida y eso me gustó. Hoy, gran parte de aquello que me quiso contar está desarrollado en esta tesis. Le agradezco el haberme otorgado todos los medios que estaban en su mano para poder desarrollar el trabajo de investigación aquí recogido. También le agradezco el haberme pasado su lema, que ya casi he asimilado como mío: la gente pesada gobierna el mundo. Verdad absoluta.

En su laboratorio he aprendido a ser científico. Tanto las personas que están como las que estuvieron han aportado de una forma u otra a desarrollarme personal y profesionalmente. Tengo que resaltar la labor de Raquel, de la cuál he aprendido la mayor parte de técnicas y destrezas que conozco actualmente. Con ella he trabajado codo con codo todos estos años para sacar gran parte de lo que está aquí incluido. Ella es la verdadera artífice de la validación del biomarcador humano aquí desarrollado y merece ser reconocida por ello. También tengo que hacer mención especial a Rosa, por haber estado ahí casi todo el camino compartiendo poyata. También compartiendo dramas e impotencias. Y éxitos, menos. Junto a Rosa, debo agradecer a Laura e Iker por su contribución activa en muchos de los experimentos aquí expuestos y por su compañerismo. A todos los que han sido lab PM. Y a los Pacos, por apoyarnos en ocasiones como una extensión de su grupo.

Este trabajo de investigación ha sido posible gracias a las distintas unidades técnicas e instalaciones del CNIC, así como al apoyo científico y moral de muchos compañeros y colaboradores. En la parte de investigación clínica de esta tesis han participado profesionales de distintos hospitales aquí detallados, los cuales han contribuido aportando muestras humanas y conocimiento médico para la aplicabilidad clínica de nuestros resultados. Por ello, merecen un agradecimiento. También agradecer al Dr. Klaus Ley por permitirme realizar una estancia de investigación con su maravilloso equipo en mitad de aquel paraíso californiano.

Tengo que agradecer también a mis padres, que me han apoyado incondicionalmente desde siempre, aun sin saber muy bien dónde me metía. A mi familia, por su confianza. A la familia que se escoge, mis amigos y amigas, ya que juntos hemos desarrollado patas de gallo, celebrando penas y ahogando logros durante todo este recorrido y lo que queda por recorrer. Y a Charlotte, por transmitirme su calma y su paciencia, y por estar siempre que la he necesitado.

A los que olvido y no me olvidan.

Gracias.

SUMMARY

SUMMARY

Cardiovascular diseases are the main cause of mortality and morbidity worldwide. Adequate management of acute cardiac conditions, such as myocarditis and myocardial infarction (MI), relies on an early diagnosis. However, diagnosis is often presented as a clinical challenge due to the uncharacteristic nature of their symptoms and the lack of non-invasive and cost-effective tools for discrimination. Emerging evidence acknowledges the participation of T cells in the origin and resolution of different cardiovascular disorders, constituting a broad field for the exploration of new clinical candidates. We aimed to deepen our knowledge in the T cell responses underlying myocarditis and MI, to elucidate novel molecular targets that ultimately will improve diagnosis and management of patients.

In this study, we characterized that Th17 cells increase in the peripheral blood of myocarditis patients and experimental autoimmune myocarditis (EAM) mice, but not in MI patients or MI mice. Profiling of miRNAs in T cells and plasma identified mmu-miR-721 as secreted by Th17 cells into plasma extracellular vesicles (EVs) during EAM. We defined that this miRNA promotes Th17 cell responses by targeting *Pparg*, which is an inhibitor of RORγt expression. Thus, blockade of mmu-miR-721 *in vivo* dampens Th17 cell responses and ameliorates EAM progression. Subsequently, hsa-miRNA-Chr8:96 was cloned and validated as a human consensus sequence to the murine mmu-miR-721, which exhibits miRNA properties and is upregulated in the plasma EVs of myocarditis patients. The analysis of four independent patient cohorts validated hsa-miR-Chr8:96 as a biomarker that discriminates myocarditis from MI, other Th17-related diseases and healthy individuals. The identification of this biomarker in plasma provides an avenue for the advancement of non-invasive and accurate diagnosis of myocarditis.

In a parallel study, an extensive analysis of immunological markers in MI patients showed an expansion of peripheral $CD69^+$ Treg cells after MI. We showed that *Cd69*$^{-/-}$ mice develop strong IL-17^+ γδT cell responses after MI that increase myocardial inflammation and, consequently, worsen cardiac function and decrease survival. Mechanistically, $CD69^+$ Treg cells inhibit IL-17^+ γδT cells in a CD39-dependent manner. Adoptive transfer of $CD69^+$ Treg cells to *Cd69*$^{-/-}$ mice after MI reduces IL-17^+ γδT cell recruitment and improves survival. Consistently, clinical data from two cohorts of patients indicate that increased CD69 expression on Treg cells after acute MI is associated with a lower risk of re-hospitalization for chronic heart failure (CHF) after 2.5 years of follow-up. In addition, hsa-miR-155-5p and CD69 expression coincide in Treg cells of MI patients. This miRNA is upregulated in the plasma of MI patients with high CD69 expression, designating those at low risk of developing CHF. Our data highlight that the CD69/miR-155-5p axis on Treg cells is a therapeutic and prognostic candidate for preventing MI-derived CHF.

RESUMEN

RESUMEN

Las enfermedades cardiovasculares constituyen la primera causa de muerte y morbilidad en el mundo. Las diferentes afectaciones cardiacas, como el infarto de miocardio (MI) y la miocarditis, requieren de un diagnóstico precoz para llevar a cabo un tratamiento eficaz. Sin embargo, el diagnóstico suele ser difícil debido a que comparten síntomas y a la falta de herramientas rápidas y no invasivas. Evidencias científicas apoyan cada vez más la participación de las células T en el origen y la resolución de enfermedades cardiovasculares, suponiendo un terreno amplio para la investigación de nuevos candidatos diagnósticos, pronósticos y terapéuticos. Por ello, nos propusimos profundizar en las respuestas T tras la miocarditis y el MI para descubrir nuevas dianas moleculares que mejoren en última instancia el diagnóstico y manejo de pacientes.

En este estudio, hemos confirmado que las células Th17 se incrementan en la sangre de pacientes y ratones con miocarditis, y no en ratones ni pacientes con MI. El análisis del perfil de miRNAs en células T y plasma encontró que el mmu-miR-721 es secretado por células Th17 en vesículas extracelulares (EVs) durante la miocarditis. Además, definimos que este miRNA promueve las respuestas Th17 al inhibir su diana *Pparg*, que a su vez reprime la expresión de RORγt. Así. el bloqueo del mmu-miR-721 *in vivo* restringe la respuesta Th17 y mejora la miocarditis. Posteriormente, clonamos y validamos la secuencia humana hsa-miR-Chr8:96 como consenso del mmu-miR-721, presentando propiedades de miRNA y encontrada incrementada en EVs de plasma de pacientes con miocarditis aguda. El análisis de cuatro cohortes independientes de pacientes validó el hsa-miR-Chr8:96 como biomarcador capaz de diferenciar una miocarditis de un MI, de otras enfermedades dependientes de Th17 y de individuos sanos. La identificación de este biomarcador en plasma supone un avance para el diagnóstico no invasivo de la miocarditis.

En un estudio paralelo en el que se analizaron marcadores inmunológicos sanguíneos se mostró que las células CD69^{+} Treg aumentan tras MI. Animales *Cd69*$^{-/-}$ desarrollan una fuerte respuesta de células IL-17^{+} γδT tras infarto que promueve la inflamación y la disfunción cardiaca, empeorando la supervivencia. Demostramos que las células CD69^{+} Treg inhiben las IL-17^{+} γδT mediante la actividad de CD39. La terapia con células CD69^{+} Treg en ratones tras MI disminuye el reclutamiento de células IL-17^{+} γδT, mejorando la supervivencia. A su vez, pacientes con MI con altos niveles de células CD69^{+} Treg, presentan menor riesgo de ser rehospitalizados por fallo cardiaco crónico (CHF) en 2.5 años. Además, la expresión del hsa-miR-155-5p y CD69 correlacionan en células Treg de pacientes con MI. Este miRNA está aumentado en plasma de pacientes con MI que expresan altos niveles de CD69, señalando aquellos que tienen menos riesgo de CHF. Estos datos subrayan la importancia del eje CD69/miR-155-5p en células Treg como candidato terapéutico y pronóstico para prevenir el CHF derivado de MI.

INDEX

INDEX

LIST OF ABBREVIATIONS

List of Abbreviations

AAR: area at risk

ACTB: beta-actin

AGO: argonaute

ANOVA: analysis of the variance

APCs: antigen presenting cells

AUC: area under the curve

BSA: bovine serum albumin

CAD: coronary artery disease

CCL20: C-C-motif ligand 20

CCR6: CC chemokine receptor 6

CFA: complete Freund adjuvant

CHF: chronic heart failure

CI: confident interval

CK-MB: creatine kinase MB

CMR: cardiac magnetic resonance (imaging)

CMV: cytomegalovirus

Co-IP: co-immunoprecipitation

CRP: C-reactive protein

CTA: computerized tomography angiogram

CTLA-4: cytotoxic T lymphocyte antigen 4

CVD: cardiovascular disease

DAMP: danger-associated molecular pattern

DC: dendritic cell

DCM: dilated cardiomyopathy

EAM: experimental autoimmune myocarditis

ECG: electrocardiogram

EF: ejection fraction

EV. extracellular vesicles

FMO: fluorescence minus one

Foxp3: forkhead box protein 3

Gal-1: galectin 1

GAPDH: Glyceraldehyde 3-phosphate dehydrogenase

GITR: glucocorticoid-induced TNF receptor

H&E: hematoxylin and eosin

HF: heart failure

HODE: 13s-hydroxyoctadecadienoic acid

HSV-TK: herpes simplex virus-1 thymidine kinase promoter

ICI-irAEs: immune checkpoint inhibitor therapy-immune related adverse effects

IFNγ: interferon gamma

IL: interleukin

IL-17R: IL-17 receptor

IL-2R: IL-2 receptor

I/R: ischemia/reperfusion

iTh17: *in vitro* differentiated Th17 cells

iTreg: *in vitro* differentiated regulatory T cells

IP: immunoprecipitation

LAD: left anterior descending (coronary artery)

LCX: left circumflex (coronary artery)

LDH: lactate dehydrogenase

LN: lymph node

LV: lentivirus

mAb: monoclonal antibody

MHC: major histocompatibility complex

MI: myocardial infarction

MINOCA: MI with non-obstructive coronary arteries

miRNA: microRNA

MIR155HG: miR-155 host gene

MS: multiple sclerosis

mTEC: medullary thymic epithelial cells

MyHCα: myosin heavy chain, isoform alpha

MyHCα-p: Immunogenic peptide of the MyHCα

MVA: multivariate analysis

NSTEMI: non-ST-segment elevation myocardial infarction

OM: obtuse marginal (coronary artery)

Ox-LDL: oxidized low-density lipoprotein

PBLs: peripheral blood leukocytes

PCI: percutaneous coronary intervention

PEG: Polyethylene glycol

PKC: protein kinase C

PMA: phorbol myristate acetate

Pre-miR: precursor microRNA

Pri-miR: primary microRNA

PPARg: peroxisome proliferator-activated receptor gamma

qPCR: quantitative polymerase chain reaction

RA: rheumatoid arthritis

RCA: right coronary artery

RFP: red fluorescent protein

RISK: RNA-induced silencing complex

RPMI: Roswell Park Memorial Institute

ROC: receiver-operating characteristic

RORγt: retinoic acid-related orphan receptor gamma t

SD: standard deviation

SEM: standard error of the mean

SN: supernatant

SPA: spondyloarthritis

STAT: signal transducer and activator of transcription

STEMI: ST-segment elevation myocardial infarction

S1P: sphingosine 1-phosphate

S1P1: sphingosine 1-phosphate receptor 1

Tbet: T-box expressed in T cells

Tc: T cytotoxic cell

TCR: T cell receptor

TFOS: time from onset of symptoms

TGF-β: transforming growth factor beta

Th: T helper cell

Th17ag-sp: (ovalbumin) antigen-specific Th17 cells

TLR: toll-like receptor

TNFα: tumor necrosis factor alpha

TnI: troponin I

TnT: troponin T

Treg: regulatory T cells

TTC: triphenyltetrazolium chloride

TTE: transthoracic echocardiography

t-SNE: t-distributed stochastic neighbor embedding

UTR: untranslated region

WHO: World Health Organization

INTRODUCTION

INTRODUCTION

1. Cardiovascular diseases

Acute and chronic pathologies that affect the heart or the blood vessels at different levels, impeding a proper blood circulation, are classified as cardiovascular diseases (CVDs). According to the World Health Organization (WHO), CVDs are the leading cause of death worldwide. The most common CVD-related events, which are myocardial infarction (MI) and cerebral stroke, occur as a consequence of atherosclerosis. Atherosclerosis is a process that consists in the accumulation of lipids in the arterial wall, originating a plaque in the intimal layer of the vessels that restricts blood flow. Spontaneous rupture of the plaque results in a rapid thrombus formation that occludes the artery and causes tissue hypoxia and subsequent damage of the affected organ (Wolf and Ley 2019). Infections or autoimmune reactions are also the origin of severe inflammatory pathologies affecting the heart muscle, such as myocarditis, or the vasculature, such as vasculitis. Congenital causes or metabolic disorders also underlie different manifestations of CVD.

1.1. Myocardial infarction

Among CVDs, MI accounts for the highest morbidity and mortality. The number of people dying from MI worldwide has increased in recent decades, accounting for 9.14 million deaths in 2019 (Roth et al. 2020), and remaining the leading cause of death during the COVID-19 pandemics (Ahmad and Anderson 2021). The universal definition of MI denotes the presence of myocardial injury in the clinical setting consistent with acute myocardial ischemia (Thygesen et al. 2018). Destabilization of an atherosclerotic plaque and subsequent thrombosis at the level of the coronary arteries is typically the origin of the myocardial ischemia. Different genetic and environmental contexts, including hypertension, smoking, high cholesterol levels, concomitant diabetes or obesity, constitute cardiovascular risk factors that contribute to the development and rupture of the atherosclerotic plaque (Rahman and Woollard 2017). Oxygen deprivation leads to cardiomyocytes death and loss of cardiac tissue that may result in severe outcomes such as cardiogenic shock or heart failure (Bahit, Kochar, and Granger 2018).

Patients with MI often present with acute chest pain. Hypoxia results in a rapid damage of the myocardial tissue and thus, release of myocardial injury markers into the circulation, such as cardiac troponins T (TnT) and I (TnI) and creatine kinase MB (CK-MB) (Ooi, Isotalo, and Veinot 2000; Thygesen et al. 2018). Tissue injury causes cardiac contractility malfunction evidenced as electrocardiogram (ECG) and/or echocardiography alterations. However, appearance of these cardiac injury biomarkers in blood and cardiac dysfunction may be due to other pathologies, requiring

angiography to confirm coronary artery occlusion. A sustained occlusion of the artery may appear on the ECG as an ST-segment elevation in MI patients, which are then termed STEMI patients. In contrast, patients without ST-segment elevation, likely due to a transient occlusion, are referred to as non-ST-segment elevation MI (NSTEMI) patients (Ibanez et al. 2018; Thygesen et al. 2018).

Reperfusion of the myocardium after MI is urgently needed to minimize irreversible damage. For this purpose, the preferred strategy is primary percutaneous coronary intervention. In this procedure, a stent is introduced with a catheter to unblock the coronary blood vessel. Treatment of patients after MI, designed to prevent chronic heart failure (CHF) development and reduce the risk of re-infarction, usually includes anti-thrombotic drugs like aspirin, beta-blockers to prevent malignant arrhythmias and lipid-lowering compounds such as statins (Ibanez et al. 2018).

Multiple experimental models have been developed to induce MI-like myocardial damage in different species of small and large animals. In mice, permanent ligation of the left-anterior-descending (LAD) coronary artery is the most widely used MI model, since it mimics the myocardial ischemia and infarction with high reproducibility. Ischemia/reperfusion (I/R) models, in which coronary arteries are transiently ligated, are also widely used, although they are more difficult to reproduce surgically (Abarbanell et al. 2010). Myocardial cryoinjury, induced with a liquid nitrogen-cooled probe, is another model used to study ischemia-independent processes such as wound healing, as it is easy to perform and also highly reproducible and replicable (Strungs et al. 2013).

1.2. Myocarditis

Myocarditis is an inflammatory process affecting the cardiac muscle or myocardium with heterogeneous etiology. The inflammation may be originated by an infectious agent, namely, viruses (enteroviruses such as Coxsackie virus, as well as some strains of coronaviruses, adenoviruses or parvoviruses), bacteria (*Borrelia burgdorferi*), fungi (Aspergillus, Candida), protozoa (*Tripanosoma cruzi*) or parasites (visceral larva migrans). Non-infectious causes including toxins, drugs, sarcoidosis or autoimmune reactions are also often behind myocarditis (Cooper 2009; Caforio et al. 2015; Heymans et al. 2016; Kawakami et al. 2021). Persistent inflammation may progress to tissue remodeling, fibrosis and myocardial death and dysfunction (Caforio et al. 2013). Progression to chronic damage results in the development of irreversible dilated cardiomyopathy (DCM) and other severe cardiac complications (Caforio et al. 2013; Ekström et al. 2016). Indeed, myocarditis is the cause of 10 to 50 % of DCM cases, involving dilation of heart chambers and CHF, whose only definitive treatment is usually transplantation (Kindermann et al. 2008).

Acute myocarditis presents a wide variety of clinical features, ranging from asymptomatic to life-threatening. In fact, it is the cause of sudden death in 8 to 12 % of cases (Fabre and Sheppard 2006; Doolan, Langlois, and Semsarian 2004). Chest pain is often accompanied by ST-segment elevation and other ECG alterations, elevation of cardiac damage markers such TnI, TnT or CK-MB, as well as

echocardiographic evidence of heart dysfunction (Caforio et al. 2013). These symptoms, which overlap with other heart diseases with high incidence, such as MI, together with a lack of noninvasive specific diagnostic tools, make myocarditis an underdiagnosed disease with uncertain prevalence (Golpour et al. 2021). Although underdiagnosis complicates the estimation, some studies report the prevalence of myocarditis to be around 10 to 100 per 100,000 patients annually (Heymans et al. 2016; Golpour et al. 2021). Myocarditis is the most frequent final diagnosis in patients with MI with non-obstructive coronary arteries (MINOCA), a challenging clinical entity occurring in 5 to 25 % of patients presenting *prima facie* symptoms of MI (Tamis-Holland et al. 2019; Sucato et al. 2021; Ibanez et al. 2018). Therefore, angiography is often performed to rule out coronary artery disease. In recent years, cardiac magnetic resonance (CMR) has evolved as a tool to efficiently detect myocardial edema, hyperemia and necrosis defined in the Lake Louise Criteria (Friedrich et al. 2009; Gannon et al. 2019). However, CMR is not immediately available in all centers and its sensibility decreases overtime (Ferreira et al. 2018; Caforio et al. 2019). The gold standard for the diagnosis of myocarditis remains the detection of infiltrating inflammatory cells by endomyocardial biopsy, an invasive procedure that is rarely performed due to the risk of complications (Cooper et al. 2007). Reliable, specific and non-invasive early diagnostic tools are an urgent clinical necessity.

Treatment of myocarditis patients consists of etiology-specific protocols and symptomatic management of cardiac and hemodynamic disease (Caforio et al. 2013). Immunosuppression is used in treatment of aggressive forms of myocarditis of autoimmune origin such as giant cell myocarditis (Ekström et al. 2016). Immunomodulatory approaches, for example high doses of intravenous immunoglobulins, are used to alleviate the progression of myocarditis (Jensen and Marchant 2016). Patients with infectious myocarditis may be treated with antibiotics, antifungal or antiviral drugs, depending on the infectious agent (Pollack et al. 2015; Jensen and Marchant 2016). Treatment with interferon α and β has also been described to improve the outcome of viral myocarditis (Kühl et al. 2003).

Several rodent models have been developed to study autoimmune and infectious myocarditis. Experimental Autoimmune Myocarditis (EAM) is induced by immunizing susceptible mice with an alpha cardiac myosin heavy chain peptide (MyHCα-p) or other immunogenic cardiac antigens, which elicits an autoimmune reaction toward the heart. As observed in myocarditis patients, EAM mice develop an acute phase of heart inflammation within two-to-three weeks that progresses toward chronic dilated cardiomyopathy with heart dysfunction. Infection of mice with the cardiotropic strain of coxsackievirus B3, capable of inducing heart inflammation within ten days, is the most widely used mouse model to study viral myocarditis (Cihakova and Rose 2008).

2. The immune response

The immune system is a complex network of cells and molecules that defends the organism against infection and disease. It detects and responds against a wide range of foreign bodies or pathogens such as microorganisms, macromolecules or toxins. In addition, the immune system reacts against host cells that need to be eliminated such as tumor or damaged cells. The coordinated process by which the immune system fights against these intruders or altered cells is called inflammation or immune response. There are two types of immune response or immunity: innate immunity and adaptive immunity. Innate immunity, which is activated rapidly after the onset of an infection, constitutes the first line of defense of an organism and does not require previous exposure to the foreign agent. In contrast, adaptive immunity, which requires more time to be activated, evolved to increase intensity and efficacy after repeated exposure to the strange agent, since it exhibits pathogen-specific memory (Flajnik and Du Pasquier 2004).

Adaptive immunity is further subdivided into humoral and cellular immunity. Briefly, during humoral immunity, B lymphocytes are activated to produce antibodies. Antibodies recognize specific antigens, which are molecules present on the aggressor agent capable of generating adaptive immune responses, and neutralize them to induce their destruction by different mechanisms. Cellular immunity is mediated by antigen-specific T lymphocytes, which clonally expand upon encountering host cells that present specific antigens, called antigen presenting cells (APCs), and coordinate and enhance the immune response (Silverstein 2003). Although the innate and adaptive responses are often described as separate arms of the host response, they usually act in concert, with innate immunity representing the first line of host defense and adaptive immunity gaining prominence after several days, when antigen-specific B and T cells have undergone expansion. The components of the innate system contribute to the activation of adaptive antigen-specific cells and eliminate antibody-neutralized foreign bodies. Antigen-specific cells amplify their responses by recruiting innate effector components that successfully control invading agents. Thus, synergy between both branches is essential for a fully effective immune response.

3. T cell-mediated immunity

T lymphocytes comprise a heterogeneous group of immune cell subsets characterized by the expression of the T cell receptor (TCR), which mediates antigen recognition, and the co-receptor CD3. The T cell branch of the adaptive immunity is predominantly mediated by T cells expressing the α and β chains of the TCR (αβT cells). Shortly after the discovery of the TCRαβ in the 80s (Saito et al. 1984), another less abundant population of T cells expressing the γ and δ chains of the TCR (γδT cells) emerged as an independent T cell subset (Brenner et al. 1986; Born et al. 1987) with functions between innate and adaptive immunity discussed below.

In the thymus, αβT cells differentiate with specificity for random antigens. The adaptive immune response consists of three steps: antigen recognition, lymphocyte activation and effector function. During the first step, naïve T cells leave the thymus to reach peripheral lymphoid organs, such as the spleen and lymph nodes, where they encounter APCs. APCs migrate from the site of infection or damage to peripheral lymphoid organs to expose peptides from the strange antigens on their membranes through the Major Histocompatibility Complex (MHC). When a naïve T cell recognizes an antigen presented by APCs through the TCR, together with costimulatory molecules, this cell becomes activated and releases cytokines. These cytokines act in an autocrine manner for the induction of proliferation of this T cell, in a process called clonal expansion, and in a paracrine manner for the stimulation of other effector immune cells (Hommel 2004).

There are two main types of αβT cells: $CD8^+$ T lymphocytes capable of eliminating infected or tumor cells are termed cytotoxic T cells (Tc); $CD4^+$ T lymphocytes or T helper cells (Th) induce proliferation and recruitment of innate cells to combat the pathogens (Fleisher 1997; Dutton, Bradley, and Swain 1998). $CD4^+$ T cells differentiate into effector or regulatory subsets with different cytokine-releasing profile and functions (**figure I.1**). Th1, Th2 and Th17 cells are the main subtypes of effector $CD4^+$ T cells (Spinner and Lazarevic 2020; Bluestone et al. 2009; Tada et al. 1978).

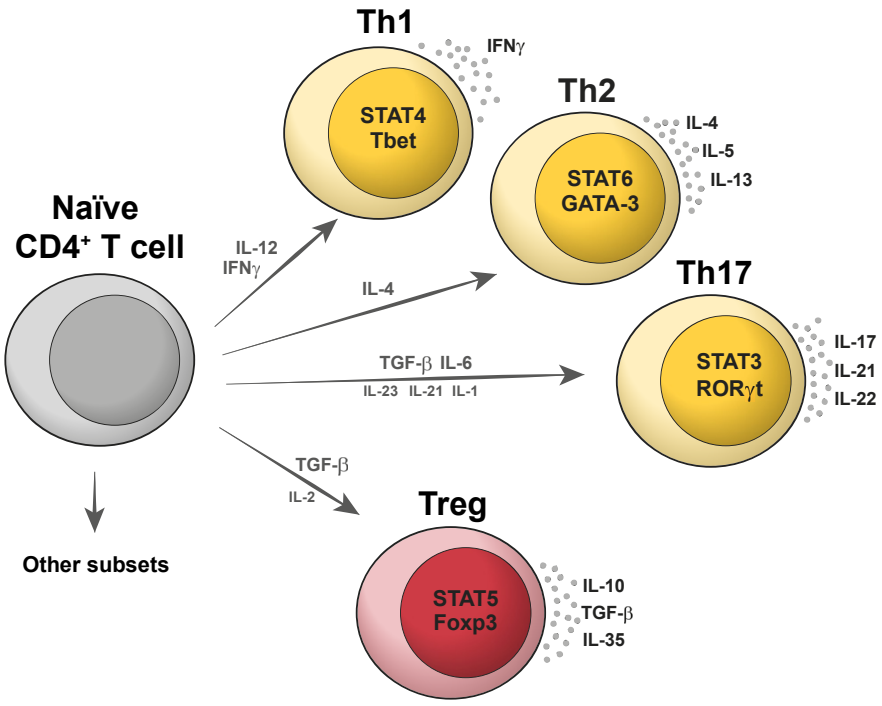

Figure I.1. Main $CD4^+$ T cell subsets. Each effector or regulatory $CD4^+$ T cell subset differentiates from naïve $CD4^+$ T cells. Upon APC encountering, the signaling through the TCR, costimulatory molecules and a particular combination of cytokines activates specific transcription factors that will drive the differentiation toward either one or another mature T cell subset. Each mature T cell subset releases a particular cytokine cocktail that will contribute to their immune function.

Th1 cells release mainly interferon-gamma (IFNγ) mediated by the phosphorylation of Signal transducer and activator of transcription (STAT)4 and further activation of the T-box expressed in T cells (Tbet) transcription factor. Th1 cells activate macrophages and are critical in controlling intracellular infections (Szabo et al. 2000; Grogan et al. 2001). Th2 cells contribute to the humoral immunity against extracellular pathogens and allergic responses by the secretion of interleukin- (IL-) 4, IL-5 and IL-13, in a mechanism mediated by STAT6 and the transcription factor GATA3 (Zheng and Flavell 1997; Paliard et al. 1988; Grogan et al. 2001). Th17 cells, defined by the secretion of IL-17, are mainly involved in autoimmune and chronic inflammation, as well as in the maintenance of mucosal homeostasis (Singh et al. 2014). In contrast, regulatory T cells (Treg) secrete anti-inflammatory molecules to counteract effector cells and prevent exacerbated inflammatory reactions (Josefowicz, Lu, and Rudensky 2012). Regulation and function of Th17 and Treg cells are detailed below.

3.1. Th17 cells

Th17 cells were discovered as an independent subset of $CD4^+$ T cells that produce mainly IL-17A, IL-17F, IL-21 and IL-22, but neither IFNγ nor IL-4 (Aggarwal et al. 2003; Langrish et al. 2005; Zhou et al. 2007; Korn et al. 2007). These cells are involved in multiple inflammatory processes, chronic inflammation and also in autoimmune diseases, in which a failure in immune tolerance mechanisms results in an expansion of T cells that recognize self-antigens and attack tissues and organs. Examples of reported Th17-mediated diseases include asthma (Barczyk, Pierzchala, and Sozañska 2003), encephalomyelitis or multiple sclerosis (Kebir et al. 2007; Cua et al. 2003), contact hypersensitivity (Nakae et al. 2002; He et al. 2006), rheumatoid arthritis (Bush et al. 2002; Kirkham et al. 2006), psoriasis (Kanda, Koike, and Watanabe 2005; Zheng, Danilenko, et al. 2007; Wilson et al. 2007), colitis (Fujino et al. 2003; Nielsen et al. 2003; Kullberg et al. 2006) and myocarditis (Rangachari et al. 2006).

The differentiation of Th17 cells requires the combination of IL-6 and transforming growth factor beta (TGF-β) signaling (Bettelli et al. 2006; Mangan et al. 2006; Veldhoen and Stockinger 2006) and is enhanced in the presence of IL-1β (Higgins et al. 2006; Sutton et al. 2006). Activation of the IL-6 receptor induces the phosphorylation of STAT3, which is translocated to the nucleus to activate the retinoic acid-related orphan receptor gamma t (RORγt) expression, encoded by the *Rorc* gene. RORγt is the main transcription factor that drives the differentiation toward the Th17 phenotype by the direct induction of the *Il17* gene and other genes important for cell maintenance and function (Ivanov et al. 2006; Yang et al. 2007). Depletion of RORγt does not completely suppress Th17 differentiation, since RORα is also activated by STAT3 and acts synergistically with RORγt to favor Th17 polarization (Yang, Pappu, et al. 2008). IL-23, secreted mainly by dendritic cells (DC) and some stromal cells, amplifies Th17 cell expansion and maintains IL-17 production. The IL-23 receptor is not present in naïve CD4 T cells, but its transcription is induced by RORγt. Therefore, IL-23 acts on already commited cells to stabilize the Th17 cell lineage (Aggarwal et al. 2003; Harrington et al. 2005; McGeachy and

Cua 2007; Zhou et al. 2007). In addition, IL-21 produced by Th17 cells in autocrine manner, but also by natural killer cells, cooperates with TGF-β to promote the differentiation of Th17 cells (Korn et al. 2007).

The effector function of Th17 cells is exerted mainly by the release of cytokines that amplify and mantain inflammation by different mechanisms. Different immune and stromal cell types express the IL-17 receptor (IL-17R) and so they are able to react to IL-17 in different ways. IL-17 stimulate granulopoiesis (Schwarzenberger et al. 1998; Schwarzenberger et al. 2000) and promote the activation and recruitment of neutrophils to inflamed tissues (Hsu et al. 2013; Laan et al. 1999; Nakae et al. 2007). IL-17 signaling also results in the macrophage skewing toward more pro-inflammatory phenotypes (Jovanovic et al. 1998; Chen et al. 2013). IL-17 also activates fibroblasts, which also express the IL-17R, accelerating fibrosis and pushing fibroblasts to consequently synthetize more pro-inflammatory cytokines, which continue potentiating inflammation and damage (Molet et al. 2001; Yamamura et al. 2001; Nakae et al. 2007). Furthermore, IL-17 triggers the secretion of pro-inflammatory cytokines and chemokines such as IL-6, IL-8, GM-CSF, Prostaglandin-E2 and nitric oxide by stromal cells, contributing to the overall amplification of inflammation (Fossiez et al. 1996; Attur et al. 1997; Teunissen et al. 1998; Jovanovic et al. 1998).

Despite their contribution to chronic inflammation, Th17 cells play a beneficial role in maintaining mucosal homeostasis (Maloy and Kullberg 2008), as they control infections of multiple microorganisms such as fungi and bacteria, being more important for extracellular than for intracellular pathogens (Aujla et al. 2008). In the gut, Th17 cells orchestrate the response to foreign pathogens and control bacterial dissemination (Blaschitz and Raffatellu 2010).

3.2. Treg cells

Regulatory T cells have evolved to balance the immune responses in order to avoid the detrimental consequences of uncontrolled immune system activity. These cells are indispensable for maintaining immune self-tolerance and homeostasis by releasing inhibitory signals in peripheral lymphoid organs and tissues (Josefowicz, Lu, and Rudensky 2012). Treg cells were first called as a subset of $CD4^+$ T cells expressing the IL-2 receptor alpha-chain (IL-2Rα or CD25) (Sakaguchi et al. 1995). Subsequently, expression of the transcription factor Forkhead box protein 3 (Foxp3) was described as a distinct feature of this population, intervening in the differentiation and suppressive function of *bona fide* Treg cells (Hori, Nomura, and Sakaguchi 2003; Fontenot, Gavin, and Rudensky 2003). A different subset of T cells that lacks Foxp3 but also exhibits regulatory properties are Tr1 cells, which are able to produce anti-inflammatory IL-10 and TGF-β (Pot, Apetoh, and Kuchroo 2011). The membrane of Treg cells present a repertoire of activating and inhibitory receptors that control their expansion, survival or function (Martín, Blanco-Domínguez, and Sánchez-Díaz 2021), including glucocorticoid-induced TNF receptor (GITR) (Shimizu et al. 2002), cytotoxic T lymphocyte antigen-4 (CTLA-4) (Read, Malmström,

and Powrie 2000), CD27 (Mack et al. 2009), CD69 (Cortes et al. 2014), CD39 and CD73 (Deaglio et al. 2007).

Treg cell generation may occur in the thymus and then migrate to peripheral organs, or they can differentiate from naïve $CD4^+$ T cell in peripheral tissues and lymphoid organs (Bluestone and Abbas 2003). The general idea is that thymic Treg cells tend to recognize self-antigens, in contrast to peripheral Treg cells that likely respond to foreign antigens (Coutinho et al. 2005; Hsieh et al. 2006). In the thymus, T cell precursors recognizing self-antigens with high affinity are depleted, but those recognizing self-antigens with medium affinity are programmed to differentiate into Treg cells, as a way to prevent autoimmune responses (Hsieh et al. 2004). In addition, IL-2 signaling is important for Treg cell differentiation and crucial for their maintenance in the periphery (Fontenot et al. 2005). IL-2R activation induces the Jak3-mediated STAT5 phosphorylation, which activates the *Foxp3* locus by binding to its promoter and regulatory elements (Burchill et al. 2008). Independently, cooperation between the CD69 receptor and miR-155-5p in a positive feedback loop is important to amplify STAT5 phosphorylation and sustain Treg cell differentiation (Sanchez-Diaz et al. 2017) (**figure I.2**).

To a lesser extent, TGF-β signaling also induces a Smad-NFAT-dependent activation of *Foxp3* expression (Tone et al. 2008) **(figure I.2).** Ablation of the TGF-β signaling transiently impairs thymic Treg development, a defect that is afterwards compensated with an age-dependent increase in IL-2 levels (Liu et al. 2008). Thus, in the thymus, the importance of TGF-β signaling is limited to conferring survival advantage to Treg precursors (Ouyang et al. 2010; Zheng et al. 2010)**.** Differentiation of inducible Treg cells is slightly different in peripheral organs, where TGF-β, as is the case for IL-2, is indispensable for Treg cell development. CTLA-4 is also required for peripheral TGF-β-mediated induction of Foxp3, although it is dispensable for the origination of Treg cells in the thymus (Zheng et al. 2006).

The immunosuppressive function of Treg cells consists mainly in the antigen-dependent inhibition of effector $CD4^+$ and $CD8^+$ T cells by cell-to-cell contact or by secretion of anti-inflammatory cytokines such as IL-10, TGF-β or IL-35 (Chen et al. 2003; Collison et al. 2007; Papiernik et al. 1998). These processes are able to dampen effector T cell differentiation, activation and proliferation. They can also attenuate the maturation and antigen presentation capacity of APCs (Misra et al. 2004; Taams et al. 2005). In addition, Treg cells have antigen-independent mechanisms of suppression of different target cell types. For instance, Treg cells are able to reduce proliferation and cytokine production of intestinal γδT cells (Park et al. 2010) in an antigen-independent manner. Treg cells can release cytotoxic molecules such as perforins and Granzyme B to eliminate effector cells (Gondek et al. 2005; Grossman et al. 2004). CD39 and CD73 are expressed in most Treg cells and also contribute to their antigen-independent suppressor function. The consecutive action of CD39 and CD73 ectoenzymes catalyzes the conversion of extracellular ATP to adenosine. Uptake of adenosine by innate and T effector cells

promotes apoptosis and inhibition (Deaglio et al. 2007; Fabbiano et al. 2015), but uptake by Treg cells triggers anti-inflammatory properties (Ohta and Sitkovsky 2014). Other indirect mechanisms of suppression by Treg cells relay on IL-2 deprivation from the media, since they uptake higher amounts than effector T cells, which also require this cytokine for proliferation (Pandiyan et al. 2007), or on the inhibition of co-stimulation through CTLA-4-mediated depletion of CD28 ligands (Qureshi et al. 2011).

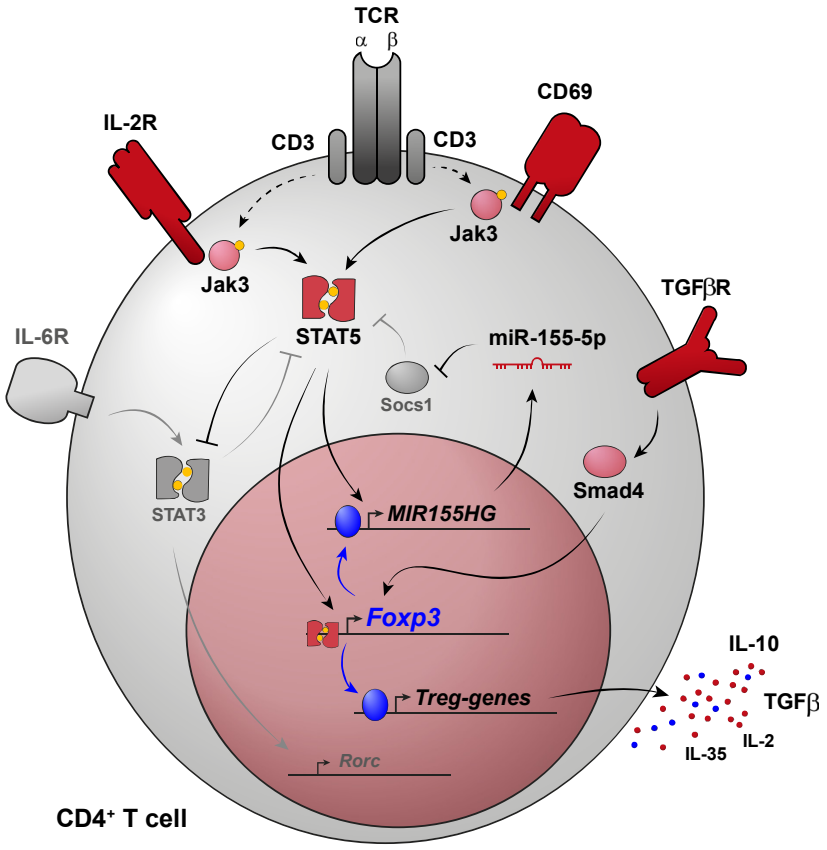

Figure I.2. Signaling pathways driving Treg cell differentiation. Antigen recognition by the TCR, together with the activation of IL-2R and CD69 synergistically, induces the phosphorylation of the Jak3 kinase. Jak3 phosphorylates and activates STAT5, that dimerizes and is translocated to the nucleus to promote the expression of *Foxp3*. Foxp3 induces the expression of cytokines and molecules involved in the Treg cell differentiation and function such as IL-10, TGF-β and miR-155. In the cytoplasm, miR-155-5p targets and inhibits Socs1, which is an inhibitor of STAT5, thus maintaining STAT5 activation. Additionally, TGF-β recognition by its receptor activates Smad4, which also promotes Foxp3 expression. Oppositely, the signaling downstream the IL-6 receptor activates STAT3 and subsequent *Rorc* expression. STAT5 inhibits STAT3 to prevent Th17 cell differentiation and favor Treg cell differentiation.

3.3. γδT cells

Bridging the gap between innate and adaptive immunity are the γδT cells. They represent less than the 5 % of T lymphocytes, although their proportion is increased in epithelial and mucosal barriers, as well as in certain diseases. Due to their ability to express regulatory and effector molecules, they can contribute to both the maintenance of tissue homeostasis and the development of inflammatory diseases

(Paul and Lal 2016). They recognize a wide repertoire of self and non-self antigens not restricted to MHC-presentation such as soluble proteins, peptides, phosphoantigens, pyrophosphates, MHC class I chain-related protein A and B (MICA/MICB) and non-classic MHC class I molecules (Deseke and Prinz 2020). Both αβ and γδT lymphocytes develop in the thymus from common progenitor cells. The most widely accepted model describes that strong TCR stimulation commits progenitors to the γδ lineage (Haks et al. 2005; Hayes, Li, and Love 2005). Unlike αβ $CD4^+$ T cells, most mouse γδT cells exit the thymus with an already acquired effector potential (Muñoz-Ruiz et al. 2017). Some may exit the thymus in a naïve-like state and fully differentiate into secondary lymphoid organs. Unlike the pre-programmed murine γδ thymocytes, most human γδT cells require peripheral activation to become mature and acquire effector phenotypes (Ribot et al. 2014). They do not require classic MHC class II restriction for proper development and function (Bigby et al. 1993). The development of γδT cells relies on the dynamics of TCR somatic recombination and the rearrangements of the variable regions of the TCR chains (Vγ and Vδ), which is often linked to different effector functions (O'Brien and Born 2010).

In mice, there are mainly two thymic effector γδT cells that can be distinguished by IL-17 or IFNγ production (Jensen et al. 2008). Expression of the CC chemokine receptor 6 (CCR6) is characteristic of IL-17^+ γδT cells (Haas et al. 2009), whereas the costimulatory receptor CD27 is a specific marker of IFNγ^+ γδT cells (Ribot et al. 2009). Signals from the mouse thymic epithelium to γδ T cell precursors drive the differentiation of the different subsets. Although γδ and $CD4^+$ T cells share RORγt and T-bet as the determinant transcription factors for IL-17- or IFNγ-producing subsets, respectively, they are regulated by T cell type-specific auxiliary molecular signaling pathways (Barros-Martins et al. 2016). In particular, Sox13 induces the expression of the signal transducer BLK (Laird, Laky, and Hayes 2010), which cooperates with Sox4 to promote RORγt expression and IL-17^+ γδT cell differentiation (Malhotra et al. 2013). In contrast, activation of Egr2 and Egr3 induces Id3, which, on the one hand inhibits RORγt expression (Xi et al. 2006; Narayan et al. 2012) and, on the other hand, activates T-bet and IFNγ^+ γδT cell polarization (Lauritsen et al. 2009). Moreover, downstream transcription factors of the Wnt-signaling, such as TCF1 and Lef1, contribute to the IFNγ^+ γδT cell development (Malhotra et al. 2013), whereas Hes-1, downstream of Notch signaling, is involved in the differentiation of IL-17-producing γδ T cells (Shibata et al. 2011). Nevertheless, γδT cell subsets exhibit some plasticity in periphery and can express both IL-17 and IFNγ upon sustained inflammation *in vivo* (Sheridan et al. 2013).

Functional activation of γδT cells in the periphery occurs more rapidly than that of other T cells. In fact, these cells are usually the first source of IL-17 in the early stages after infections or sterile inflammatory triggers (Papotto, Ribot, and Silva-Santos 2017). For example, *in vitro* stimulation with IL-23 and IL-1β is sufficient to induce secretion of high amounts of IL-17 by pre-programmed IL-17^+ γδT cells, even without TCR co-stimulation (Sutton et al. 2009). They are able to recognize danger-associated molecular patterns (DAMP) due to the expression of different toll-like receptors (TLR) in an innate-

like manner (Mokuno et al. 2000; Sutton et al. 2009; Martin et al. 2009; Ribot et al. 2010). On top of that, these cells can also undergo rapid polarization in secondary lymphoid organs following TCR stimulation for a sustained IL-17 production. This occurs in an adaptive-like manner but without requiring extensive clonal expansion, making the response more rapid than that of other T lymphocytes (Zeng et al. 2012).

Early cytokine production positions γδT cells at the first line of defense for pathogens. While IFNγ activates early innate responses, IL-17 attracts neutrophils and activates pro-inflammatory monocytes for pathogen clearance (Nakasone et al. 2007; Hamada et al. 2008). A fraction of γδ lymphocytes expanded during primary infection may remain as a memory reservoir for long periods, contributing to adaptive immune responses upon secondary challenges (Sheridan et al. 2013).

Despite their protective function in tissue surveillance, γδT cells can accumulate and exert damage to target tissues, boosting pathological inflammation in multiple inflammatory disease contexts. Due to the fact that IL-17$^+$ γδT cells are a prominent and early source of IL-17 and other cytokines such as IL-22, they amplify Th17 cell responses and IL-17-mediated inflammatory activation and damage. Thus, they accelerate the early inflammatory stages of autoimmune diseases such as psoriasis (Laggner et al. 2011; Cai, Shen, et al. 2011), encephalomyelitis (Malik, Want, and Awasthi 2016), arthritis (Roark et al. 2007) or type 1 diabetes (Markle et al. 2013). Tissue damage, such as that caused by myocardial ischemia, can also trigger γδT cell infiltration. In the first days after MI, C-C-motif ligand 20 (CCL20) released from damaged cardiomyocytes rapidly recruits IL-17$^+$ γδT cells that express CCR6 (the receptor for CCL20), enhancing myocardial inflammation and damage (Yan et al. 2012).

4. Immunomodulatory molecules

4.1. CD69

The early leukocyte activation molecule CD69 belongs to the C-type lectin membrane receptor family and is expressed in all types of bone-marrow-derived cell except erythrocytes (Testi et al. 1994). The *Cd69* gene is located on the chromosome 6 and chromosome 12 of mice and humans, respectively (López-Cabrera et al. 1993), within a region called natural killer gene complex (Ziegler et al. 1994). CD69 is a dimeric transmembrane receptor formed by two identical polypeptide chains that differ only in their glycosylation state (Sánchez-Mateos and Sánchez-Madrid 1991).

Leukocytes express CD69 on the membrane between 2 and 4 hours after activation, so it is considered a marker of early activation (López-Cabrera et al. 1993). CD69 expression requires the synthesis *de novo* in T lymphocytes upon activation, triggered by induction of protein kinase C (PKC). This can be achieved by treatment with anti-CD3 monoclonal antibodies, phorbol esters or mitogenic stimulators

such as phytohemagglutinin (Cebrián et al. 1988). In a TCR-independent mechanism, IL-2, IL-6, IL-15 or tumor necrosis factor alpha (TNFα) signaling also increment CD69 expression (Unutmaz, Pileri, and Abrignani 1994; Kanegane and Tosato 1996). Constitutive expression of CD69 is restricted to differentiating thymocytes (Swat et al. 1993; Barthlott, Kohler, and Eichmann 1997), some populations of Treg cells (Han et al. 2009; Cortes et al. 2014), resident memory T cells and tissue-infiltrating leukocytes in chronic inflammatory diseases (Laffón et al. 1991; Samat et al. 2021), in tumors (Coventry et al. 1996), as well as in persistent infections (García-Monzón et al. 1990; Zajac et al. 1998).

Some natural ligands of CD69 have been described. Unlike other C-type lectin receptors, CD69 does not bind monosaccharides and has low affinity for some sulfated polysaccharides (Childs et al. 1999). Galectin-1 (Gal-1) expressed by DCs can bind CD69 on T cells, prompting anti-inflammatory cell skewing (de la Fuente et al. 2014). The S100A8/S100A9 complex is another ligand of CD69, whose interaction promotes Treg cell differentiation (Lin et al. 2015). Binding of soluble oxidized low-density lipoprotein (ox-LDL) to CD69 on T cells has also been described to promote a regulatory T cell phenotype in the context of atherosclerosis (Tsilingiri et al. 2019). In addition, CD69 can interact laterally at the membrane with other molecules such as sphingosine 1-phosphate receptor 1 (S1P1) to inhibit cell egress from lymph nodes (Shiow et al. 2006) and LAT1-CD98 to control L-tryptophan uptake (Cibrian et al. 2016).

It is well established that CD69 behaves as a negative regulator of inflammation, since the depletion of this receptor exacerbates mouse models of T-cell-mediated autoimmune and inflammatory diseases such as arthritis (Sancho et al. 2003), asthma, skin contact hypersensitivity (Martín, Gómez, Lamana, Matesanz Marín, et al. 2010), colitis (Radulovic et al. 2012) and autoimmune myocarditis (Cruz-Adalia et al. 2010). The mechanisms underlying this regulatory effect of CD69 rely on its ability to act as a brake for Th17 cell differentiation and as a promoter of Treg cell differentiation and function. The cytoplasmic tail of CD69 interacts with and activates Jak3, which phosphorylates and activates STAT5. Dimerization and nuclear translocation of phosphorylated-STAT5 induces Foxp3 transcription and inhibits STAT3 and subsequent RORγt expression (Martín, Gómez, Lamana, Cruz-Adalia, et al. 2010). In the thymus, CD69 is involved in Treg cell differentiation by inducing Foxp3 expression in an IL-2-independent manner as aforementioned (Sanchez-Diaz et al. 2017). In addition, CD69 confers suppressive capacity to Treg cells, since CD69-deficient Treg cells express lower levels of suppressive markers such as CTLA-4, ICOS, CD38 and GITR, resulting in impaired effector T cell suppression and tolerance (Cortes et al. 2014). Thus, CD69 signaling balances T cell responses by favoring Treg cell function and preventing pro-inflammatory IL-17 responses in homeostasis and inflammatory diseases (Gonzalez-Amaro et al. 2013).

4.2. PPARγ

Peroxisome proliferator-activated receptor gamma (PPARγ) is a nuclear receptor that functions as a ligand-activated transcription factor. Ligand binding promotes heterodimerization with retinoic X receptor and subsequent promote activation of target genes (Amber-Vitos et al. 2016). Natural ligands such as the linoleic acid derivative, 13s-hydroxyoctadecadienoic acid (HODE), as well as synthetic agonists can successfully activate PPARγ (Straus and Glass 2007). PPARγ expression and activity are regulated by a complex network of epigenetic players including histone and DNA modifications and microRNAs (Porcuna, Mínguez-Martínez, and Ricote 2021).

PPARγ plays an essential role in the regulation of metabolism. It is highly expressed by adipocytes and promotes adipogenesis. It also promotes insulin secretion by pancreatic β cells, induces liver gluconeogenesis, contributes to insulin sensitization by the striated muscle and controls cholesterol homeostasis (Hong et al. 2019).

PPARγ is also an important regulator of inflammation at different levels (Glass and Ogawa 2006). This nuclear receptor is a key modulator of macrophage homeostasis and polarization, functioning as a negative regulator of pro-inflammatory response programs in this cell type (Ricote, Valledor, and Glass 2004). Furthermore, PPARγ is an inhibitory regulator of dendritic cell maturation and function, thereby promoting $CD4^+$ T cell anergy and tolerance (Klotz et al. 2007; Szatmari et al. 2007). In 2000, it was shown that T cells express PPARγ with remarkable relevance as PPARγ activation inhibits cytokine production and activation of $CD4^+$ T cell clones (Clark et al. 2000). Subsequently, it was described to behave as a brake for Th17 responses. PPARγ prevents the removal of co-repressors from the *Rorc* promoter, thus preventing RORγt expression and subsequent IL-17 production and Th17 cell differentiation (Klotz et al. 2009). In this direction, depletion of PPARγ in T cells results in exacerbated Th17-responses and autoimmunity in a mouse model of encephalomyelitis (Klotz et al. 2009). A mutation of the *Pparg* gene (encoding the PPARγ protein) in mice, which decreases about 75 % of gene expression (Tsai et al. 2009), leads to a lupus-like phenotype with splenomegaly and generalized autoimmunity (Liu et al. 2016). Mechanistically, reduced PPARγ levels exacerbates Th17 polarization that contributes to B cell hyperactivation and uncontrolled autoantibody production, accompanied by reduced S1P1 expression and lymphocytes retention in the spleen (Liu et al. 2016). Conversely, activation of PPARγ with ligands ameliorates the progression of autoimmune diseases such as myocarditis (Yuan et al. 2003) or thyroiditis (Niino et al. 2001).

5. Adaptive immunity in heart diseases

It is well documented that some myocardial diseases are primary triggered by T cell responses. In this case, T cells react against cardiac self-antigens as in autoimmune myocarditis, or against foreign antigens as in heart transplant rejection (Lichtman 2013). In these scenarios, T-cell reactivity triggers direct cytotoxicity or boosts other inflammatory effector cells, resulting in permanent myocardial tissue damage that is replaced by fibrosis and progresses to dilated cardiomyopathy and CHF. In recent years, increasing evidence has highlighted the importance of T cell responses in other disorders leading to heart failure such as myocardial infarction or hypertension. In these conditions, T cells are recruited secondarily to the stressed myocardium, where regulation of T cell activation and cytokine production contributes to control inflammation after the initial stimulus, cardiac remodeling and progression to CHF (Blanton, Carrillo-Salinas, and Alcaide 2019).

5.1. T cells and myocarditis

Autoreactive $CD4^+$ T cells recognizing cardiac antigens are the main driving force in the development and progression of myocarditis and are a common feature of different etiologies (Smith and Allen 1991; Cooper 2009). Autoreactive T cells are depleted during differentiation in the thymus by exhibiting high affinity for self-antigens exposed by medullary thymic epithelial cells (mTEC). Interestingly, the gene encoding for the intracellular MyHCα, one of the most important self-antigens in myocarditis, is not represented in the self-antigen repertoire of mTEC (neither in mice nor in humans), so cardiac-specific $CD4^+$ T cells scape the thymic negative selection (Lv et al. 2011). Impairment or inhibition of tolerance mechanisms involving Treg cells and immune checkpoints, which normally suppress these autoreactive cells, may trigger cardiac autoimmunity (Grabie, Lichtman, and Padera 2019). Indeed, myocarditis is an important side effect of the therapy with immune checkpoint inhibitors in cancer patients (Mocan-Hognogi et al. 2021). In addition, different insults such as infection, ischemia or toxins cause cardiomyocytes damage, which expose intracellular antigens such as MyHCα, lead to T cell activation and myocarditis in susceptible individuals (Pollack et al. 2015). In general, overactivation of the immune system, such as in that occurring during vaccination, may increase the chances of developing myocarditis. This might explain the cases reported of myocarditis associated with vaccines against COVID-19 and other diseases (Mei et al. 2018; Dionne et al. 2021; Hajjo et al. 2021; Mevorach et al. 2021). T cells are orchestrated with innate immunity, which potentiate and sustain the adaptive immune response, as evidenced by the need for adjuvants and/or activation of TLRs to induce autoimmune myocarditis in mouse models. In this regard, infectious agents also play the role of adjuvants that activate innate inflammatory mechanisms that amplify autoreactive T cell clones (Fairweather et al. 2001; Fairweather, Frisancho-Kiss, and Rose 2005). Interestingly, due to the resemblance of certain microbial antigens with the MyHCα, they may also activate cardiac-specific autoimmune $CD4^+$ T cells in the gut in a process named molecular mimicry (Massilamany et al. 2011; Gil-Cruz et al. 2019).

Th17 cells are the main pro-inflammatory T cell subtype involved in the progression of myocarditis (Sonderegger et al. 2006; Rangachari et al. 2006; Myers et al. 2016). IL-23-induced Th17 cells are required for the development of EAM (Sonderegger et al. 2006; Wu et al. 2016). In patients, increased Th17 response is a characteristic feature of peripheral blood during acute myocarditis (Myers et al. 2016), and IL-17 and RORγt are detected in myocarditis heart biopsies (Yuan et al. 2010). T cell-derived IL-17 helps B cells to produce cardiac-specific antibodies (Yuan et al. 2010), promotes fibrosis and contributes to recruitment and activation of effector pro-inflammatory monocytes/macrophages (Wu et al. 2014; Barin et al. 2012). Moreover, IL-17 signaling is essential for the progression to DCM and heart failure (Baldeviano et al. 2010). Th1 cells are important for the IFNγ-mediated clearance of infection in viral myocarditis. IFNγ participates in controlling the autoimmune response and fibrosis after experimental myocarditis induction (Eriksson, Kurrer, Bingisser, et al. 2001; Fairweather et al. 2004; Rangachari et al. 2006). In contrast, other Th1-derived cytokines such as IL-12 and TNFα play pro-inflammatory roles during myocarditis development (Eriksson, Kurrer, Sebald, et al. 2001; Eriksson, Kurrer, Bingisser, et al. 2001). Th2-derived cytokines also exhibit opposing effects, with IL-13 being beneficial and IL-4 detrimental for the progression of myocarditis in some animal models and some mouse strains (Cihakova et al. 2008; Afanasyeva et al. 2001). Although a strong Th2 response leads to severe eosinophilic myocarditis in mice lacking both IFNγ and IL-17 (Barin et al. 2013), the role of Th2 cells in this disease remains controversial,.

5.2. T cells and myocardial infarction

Inflammation plays an important role not only during atherosclerosis progression (Roy, Orecchioni, and Ley 2021) but also in the resolution of post-ischemic myocardial damage (Swirski and Nahrendorf 2013). An optimal balance of inflammatory responses is important to promote cardiac repair and prevent further cardiac deterioration. It is well-established that myeloid populations, mostly neutrophils and monocytes, are rapidly mobilized to the infarcted tissue during the first days after MI, being main mediators of the human and mouse heart inflammation (Nahrendorf et al. 2007; Tsujioka et al. 2009; Yan et al. 2013; Swirski and Nahrendorf 2018). A growing body of evidences following the finding of infiltrating T cells in the human infarcted heart (Abbate et al. 2008) illustrates a crucial role of also T cells in controlling both acute inflammation and progression to CHF scenarios (Hofmann and Frantz 2016).

A few days after MI, $CD4^+$ T cells become activated by autoantigens presented by MHC class II molecules and proliferate in the mediastinal lymph nodes draining the heart and in the spleen, inducing myocardial repair (Hofmann et al. 2012). Evidence for this activation of cardiac-specific T cell is the fact that transfer of splenocytes isolated from MI mice is able to trigger autoimmune myocarditis in recipient mice (Maisel et al. 1998). Recognition of cardiac autoantigens such as MyHC peptides promotes the acquisition of pro-healing Treg phenotypes (Rieckmann et al. 2019). Rapid recruitment

of Treg cells to the infarcted tissue, in part mediated by Gal-1 (Seropian et al. 2013), is required to prevent an uncontrolled early inflammation. In mouse models, Treg cell depletion results in an increased mortality rate and an overall worsening of post MI immune-mediated outcomes (Weirather et al. 2014; Saxena et al. 2014). In the same direction, adoptive transfer of activated Treg cells improves healing and survival post MI. In addition to dampening autoreactive effector T cell responses, Treg cells induce macrophage polarization toward anti-inflammatory phenotypes (Weirather et al. 2014) and inhibit fibrosis (Saxena et al. 2014). Different human studies reported that Treg cells are also mobilized in MI patients, changing their proportion in peripheral blood (Sardella et al. 2007; George et al. 2012; Mao et al. 2019) and accumulating in coronary thrombi (Klingenberg et al. 2015) and myocardium (Rieckmann et al. 2019) after MI.

During the first week post MI, γδT cells accumulate in the myocardium and are the main source of IL-17. Th17 cells are virtually absent during the early days post ischemia. In the infarcted heart, IL-17 contributes to amplify inflammation, induce cardiomyocyte apoptosis and accelerate fibrosis (Mora-Ruiz et al. 2019). Due to the abundant IL-17 secretion, γδT cells are associated with increased morbidity in mouse models (Yan et al. 2012; Yan et al. 2013) and MI patients (Chen et al. 2018). The contribution of other T cell subsets in the pathophysiology post MI remains elusive.

6. miRNAs

6.1. Biogenesis and function of miRNAs

MicroRNAs (miRNAs) are short non-coding ribonucleic acid of about twenty nucleotides-long involved in the regulation of post-transcriptional gene expression (Pillai 2005). Since their discovery in *Caenorhabditis elegans* in 1993 (Lee, Feinbaum, and Ambros 1993; Wightman, Ha, and Ruvkun 1993), they have emerged as important agents controlling multiple biological processes in homeostasis and disease across most eukaryotic species. Three letters denotating the species before and a specific number after the abbreviation 'miR' is the main rule for denotating miRNAs (i.e. hsa-miR-155 is the human homolog of the murine mmu-miR-155).

miRNAs are typically encoded in introns of protein-coding genes or in separate non-coding transcript units. They are generally transcribed by RNA polymerase II as longer sequences called primary microRNA (pri-miR) (Rodriguez et al. 2004). Pri-miRNAs are processed into mature miRNAs by the successive action of RNAse-III family of endonucleases (Kim 2005). In the nucleus, Drosha excises out a typically 70 to 100 nucleotides-long precursor called pre-miRNA, which folds into a secondary stem-loop structure (Lee et al. 2003). Exportin-5 exports out the pre-miR to the cytoplasm (Yi et al. 2003), where Dicer crops the stem-loop structure to generate a two-stranded molecule of about twenty base pairs (Hutvágner et al. 2001; Ketting et al. 2001). This duplex is loaded into the RNA-induced

silencing complex (RISC) by binding Argonaute (AGO) proteins (Sontheimer 2005; Kobayashi and Tomari 2016). AGO unwinds the duplex during RISC assembly (Kwak and Tomari 2012) (**figure I.3**). Either of the two strands, called 5p (5') and 3p (3'), respectively, according to their location in the pri-miR sequence, may become a mature miRNA, although one of the strands is usually more abundant or unique depending on thermodynamic stability (Meijer, Smith, and Bushell 2014). Non-canonical Drosha- or Dicer-independent pathways have also been described as minor mechanisms of miRNA biogenesis, reflecting evolutionary flexibility of these processes (Yang and Lai 2011; Xie and Steitz 2014).

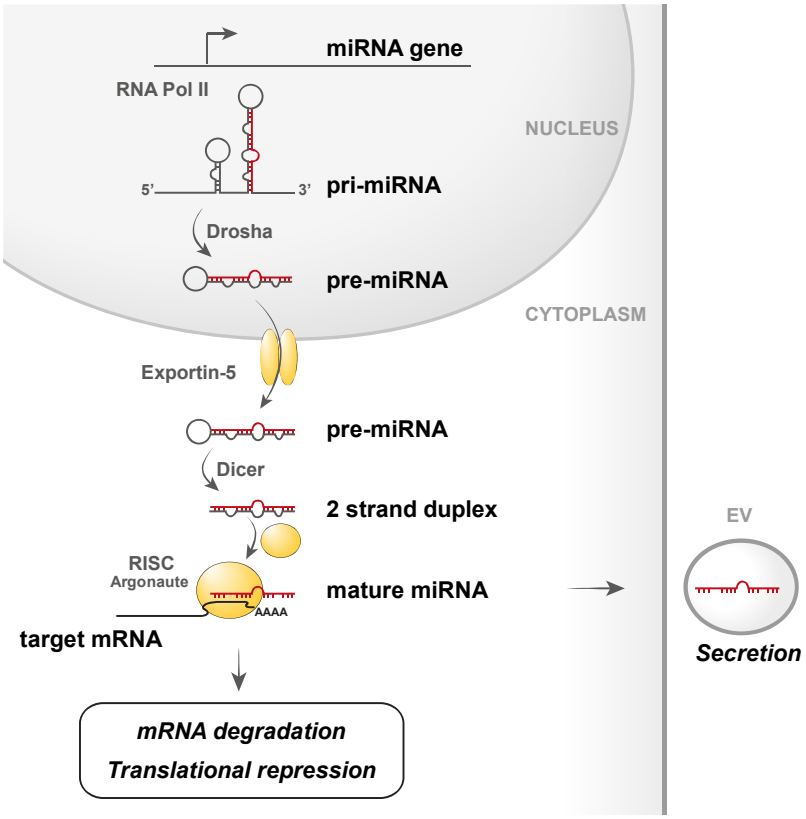

Figure I.3. Biogenesis and function of miRNAs. After transcription by the RNA polymerase II, pri-miRNAs are cleaved by the consecutive action of the endonucleases Drosha and Dicer. Mature miRNAs, loaded onto the RISC, recognize 3'UTR sequences of target mRNAs to inhibit their translation. Some miRNAs can be secreted into extracellular vesicles to play a role elsewhere in the organism.

Mature RISC-associated miRNAs recognize regions of the 3' untranslated regions (UTR) of target messenger RNAs (mRNA). The binding to partially complementary 3'UTR sequences recruits factors that typically induce mRNA degradation or translation blockade, thus ultimately preventing protein synthesis from target mRNAs (Iwakawa and Tomari 2015). Most mammalian protein-coding genes contain miRNA binding sites and a single miRNA targets multiple mRNAs, so most cellular processes are under the control of miRNAs (Friedman et al. 2009). For this reason, the biogenesis and function of miRNAs are regulated at different levels by mechanisms involving the balance of RNA-binding proteins, posttranscriptional nucleotide modifications or inhibitory complementary sponge RNA molecules (Michlewski and Cáceres 2019).

Beyond intracellular activity, miRNAs also exist extracellularly and are able to inhibit targets in distant cells, participating in intercellular communication (Ramachandran and Palanisamy 2012). Upon certain stimuli, cells are able to secrete miRNAs protected in extracellular vesicles (EVs) like exosomes (Valadi et al. 2007), which can be detected in different biofluids such as circulating plasma and serum (Hunter et al. 2008) (**figure I.3**). Cell-free miRNA profiles can act as biomarkers of intracellular state and tissue pathology. Therefore, determination of circulating miRNA levels in biofluids has emerged as powerful non-invasive diagnostic tools in multiple disease contexts such as CVDs (Navickas et al. 2016; Poller et al. 2018).

6.2. miR-721

In 2006, mmu-miR-721 was first cloned in the central nervous system of mouse embryos (Wheeler et al. 2006) and subsequently described in preimplantation embryos (Yang, Bai, et al. 2008; Maserati et al. 2011). The mmu-miR-721 sequence is located on the murine chromosome 5, within a non-coding region of the gene *Cux1*. Although the 3' 18 nucleotides of the murine mature miRNA are conserved in humans as well as in other mammalian species, the homolog of miR-721 has not yet been annotated in the human genome. Additionally, some regions around the mmu-miR-721 sequence are also evolutionary conserved around the human consensus sequence and support a possible folding like a pre-miRNA stem-loop structure (Wheeler et al. 2006). Remarkably, the identification of three mature miRNAs mapping different regions of the pre-miRNA hairpin of mmu-miR-721, presenting common and different putative target genes, suggested that this miRNA might undergo alternative processing, probably in a tissue- or stimulus-dependent manner (Humphreys et al. 2012).

Meox2 was the first target gene described for mmu-miR-721. As a part of the miRNA family miR-130/301/721, miR-721 downregulates *Meox2* mRNA, thus enhancing inducible pluripotent stem cell generation (Pfaff et al. 2011). Other experimentally validated targets described for mmu-miR-721 are *Nos2* and *Pparg*. The *in vitro* inhibition of PPARγ by mmu-miR-721 in adipocytes decreases glucose uptake and promote insulin sensitivity (Ke et al. 2017). In the context of Leishmania infection, the downregulation of *Nos2* by mmu-miR-721 in macrophages, reduces nitric oxide production and facilitates infectivity (Muxel et al. 2017).

6.3. miR-155-5p

The miR-155 is processed from a host gene primary transcript, known as B-cell integration cluster (*BIC*) or MIR155 host gene (*MIR155HG*), located on mouse chromosome 16 and human chromosome 21 (Lagos-Quintana et al. 2002; Eis et al. 2005). The 5' strand of the miR-155 hairpin, miR-155-5p, is widely expressed one or two orders of magnitude more than miR-155-3p, so it has been studied more deeply (Landgraf et al. 2007). Nevertheless, miR-155-3p has also been described to regulate pathways redundantly, synergistically or independently of those regulated by miR-155-5p (Zhou et al. 2010; Tarassishin et al. 2011).

The miR-155-5p is a miRNA well studied in the field of inflammation, being a key regulator of both innate and adaptive immune responses. It is rapidly upregulated upon cell activation (Haasch et al. 2002; Thai et al. 2007; O'Connell et al. 2007; O'Connell et al. 2010) and is indispensable for the proper differentiation and function of T and B lymphocytes, as well as for that of myeloid cells, such as macrophages, monocytes and dendritic cells (Calame 2007; Rodriguez et al. 2007; Squadrito et al. 2013; Chen et al. 2020). Particularly in Treg cells, the absence of miR-155-5p hinders thymic and peripheral cell differentiation. Mechanistically, miR-155-5p promotes Foxp3 expression by inhibiting its target SOCS1, which enables STAT5 activation and binding to the Foxp3 promoter (Lu et al. 2009; Kohlhaas et al. 2009). In turn, Foxp3 binds and activates *MIR155HG,* inducing the expression of the miRNA (Cobb et al. 2006; Zheng, Josefowicz, et al. 2007; Marson et al. 2007). This feedback loop is in part regulated by CD69, which maintains STAT5 phosphorylation and subsequent induction of *MIR155HG* (Sanchez-Diaz et al. 2017) **(figure I.2**).

In addition, this miRNA participates in paracrine communication as it can be transported to adjacent and distant cells into extracellular vesicles or exosomes. Consequently, circulating hsa-miR-155-5p has been validated as a biomarker of different pathological conditions, especially in the field of oncology (Bertoli, Cava, and Castiglioni 2015; Due et al. 2016; Shao et al. 2019; Zheng et al. 2020). This miRNA is upregulated in the circulation of critically ill COVID-19 patients and can discriminate COVID-19 from influenza patients (Garg et al. 2021). It has also been proposed as a marker of response to asthma treatment (Li et al. 2020). In the cardiovascular field, miR-155 has been reported to be upregulated in the periphery of patients with heart failure (Ding et al. 2020) and inflammatory cardiomyopathy (Obradovic et al. 2021) and after heart transplant rejection (Duong Van Huyen et al. 2014) or atherosclerotic plaque rupture (Li et al. 2017). Levels of miR-155 are inversely correlated with the severity of atherogenic coronary lesions (Zhu et al. 2014) and this miRNA is a predictor of cardiac death after MI (Matsumoto et al. 2012). There are conflicting data findings on the relative levels of this miRNA in circulation after MI, mostly due to the low number of patients analyzed or the use of different comparators or control groups. In this regard, miR-155 appeared upregulated in MI patients compared with healthy donors consistent with inflammatory responses (Kazimierczyk et al. 2019) but not significantly elevated when compared with unstable angina patients (Li et al. 2019). In another study, authors reported a correlation of plasma miR-155 with Th17 responses in MI and unstable angina patients, although in this case miR-155 was found to be downregulated in MI patients when compared with other acute coronary syndromes (Yao et al. 2011). In any case, observations in patients highlights a possible role of this miRNA in MI patients although the mechanism of action and cellular source remains challenging.

Although the main effects of miR-155-5p in CVDs are through its regulation of inflammation, this miRNA is expressed by multiple cell types and tissues, making it a multifunctional molecule that can lead to different clinical outcomes depending on cell-specific regulations (Ma, Ma, and Zheng 2013).

In the context of MI, different roles have been attributed to miR-155-5p that have been studied in animal models. As a matter of fact, *miR-155*$^{-/-}$ mice showed smaller area of necrosis after ischemia-reperfusion injury because the target SOCS1 controls the generation of reactive oxygen species (Eisenhardt et al. 2015). Moreover, the miR-155 knockout has been reported to improve survival of mice after permanent LAD-ligation, whereas overexpression produces the opposite effects (Wang et al. 2017; He et al. 2016). In contrast, atherosclerotic (*ApoE*$^{-/-}$) *miR-155*$^{-/-}$ mice showed neither an improvement nor an aggravation of heart dysfunction and damage after LAD-ligation, but just an excessive accumulation of myofibrils (Schumacher et al. 2021). Probably due to differential kinetics of miR-155 expression and its varied functions in different tissues, modulation of this miRNA in different contexts results in different effects. As an example of this, secretion of miR-155 into exosomes by macrophages regulates cardiac fibroblast proliferation and inflammation in a paracrine manner (Wang et al. 2017). The uptake of these miR-155-containing exosomes by endothelial cells inhibits angiogenesis and subsequent cardiac dysfunction (Liu et al. 2020). Importantly, miR-155 is also abundant in T and B lymphocytes, however, due to the fact that these cells are a minority after MI, the role of this miRNA in lymphocytes in the pathology after coronary artery occlusion remains unexplored. Further cell-specific approaches will facilitate the understanding of the miR-155 function to develop it as a strong candidate for both therapy and/or diagnosis.

OBJECTIVES

OBJECTIVES

T cell responses have been acknowledged as important mediators of cardiovascular diseases, although the particular mechanisms involved remain elusive. In addition, the discrimination of different acute heart diseases remains clinically challenging due to the lack of non-invasive cell- and disease-specific biomarkers. In this regard, miRNAs are emerging as important regulatory and stable diagnostic molecules in the field of inflammatory and cardiovascular diseases.

Consequently, our main objectives are divided into the following points:

a. To confirm that Th17 cells are specific to the acute phase of myocardial injury in patients with myocarditis and not in patients with myocardial infarction.

b. To identify a Th17 cell-derived miRNA biomarker for the diagnosis of patients with myocarditis.

c. To profile the peripheral immune repertoire of patients with myocardial infarction.

d. To study the role of $CD69^{+}$ Treg cells in inflammation and subsequent heart damage and failure after myocardial infarction.

e. To explore the clinical value of the CD69/miR-155-5p axis in Treg cells for prognosis after myocardial infarction.

MATERIAL AND METHODS

MATERIAL AND METHODS

1. Mouse models and animal procedures

1.1. Mice

Throughout this study, the different experimental groups were sex- and age-matched with littermates mice on C57BL/6 or BALB/c background, depending on the experimental model and the susceptibility of the strain.

C57BL/6 Foxp3-mRFP/IL17-eGFP reporter mice were kindly provided by Dr. R. A. Flavell (Yale University) and crossed with *Cd69*$^{+/+}$ or *Cd69*$^{+/+}$ mice. C57BL/6-Tg (TcraTcrb) 425Cbn/J (called OTII) mice expressing a TCR specific for ovalbumin peptide (residues 323-339) in the context of I-Ab (Barnden et al. 1998) were purchased from the Jackson Laboratory (stock number 004194). OTII mice were backcrossed with CD69-deficient mice in the C57BL/6 background.

Mice were housed under specific pathogen-free conditions at the CNIC animal facility. All procedures involving mice were approved by the Comunidad Autónoma de Madrid and conducted in accordance with Directive 2010/63/EU of the European Parliament and of the Council of September 22, 2010, on the protection of animals used for scientific purposes.

1.2. Mouse models of myocarditis

For Experimental Autoimmune Myocarditis (EAM) induction, 8-12 weeks-old BALB/c mice were immunized subcutaneously on days 0 and 7 with 100 µg/0.2 mL of cardiac MyHC-α peptide (MyHCα-p, residues 614–629; Ac-RSLKLMATLFSTYASADR-OH), emulsified 1:1 in complete Freund adjuvant (CFA, 1 mg/mL) and PBS. Mice reached the EAM acute phase of heart inflammation three weeks post-immunization; the chronic phase with heart dysfunction is achieved from day 56.

Viral myocarditis was induced in BALB/c and C57BL/6 mice upon infection with Coxsackievirus B3. Coxsackievirus B3 (Nancy strain) was obtained from the American Type Culture Collection (ATCC, Manassas, Virginia), grown in Vero cells (ATCC) and passaged through the heart, as described previously (Myers et al. 2013). Eight-week-old female mice were inoculated intraperitoneally with sterile PBS (controls) or with 10^3 plaque forming units of heart-passaged coxsackievirus B3, containing infectious virus and heart tissue, diluted in sterile PBS. Sera and hearts were collected at day 10 post infection during acute myocarditis, as described previously (Myers et al. 2013).

1.3. Mouse model of myocardial infarction

For MI induction, a permanent ligation of the left-anterior-descending coronary artery was performed. Briefly, 8 to 12 weeks-old mice were anesthetized with sevoflurane (4%), and intubated using a 24-gauge catheter with a blunt end. Mice were artificially ventilated with a mixture of O_2 and air (1:1, vol:vol) using a rodent ventilator (minivent 845, Harvard) with 160 strokes/min in a total volume of 250 µl. Mice were placed on a heating pad to maintain body temperature at 37 °C. A thoracotomy was performed through the fourth left intercostal space, the pericardium was opened and the heart was exposed. The proximal LAD coronary artery was localized and permanently ligated by passing a 7-0 silk suture around the artery. Sham operated mice were analyzed in parallel as controls of surgery.

MI was induced in C57BL/6 mice except for the experiments in which LAD-ligation was compared with EAM mice, in which BALB/c mice were used for both models.

1.4. Adoptive transfer of iTreg cells

Treg cells were *in vitro* differentiated (iTreg) from isolated naïve $CD4^+$ T cells from either Foxp3-mRFP/IL17-eGFP/*Cd69*$^{+/+}$ or Foxp3-mRFP/IL17-eGFP/*Cd69*$^{-/-}$ mice as described below. After determining the purity of $CD4^+CD25^+Foxp3^+$ cells, a single injection of 1.5 x 10^6 iTreg cells were intravenously injected to *Cd69*$^{-/-}$ mice 4-6 h after LAD ligation. Mice were monitored daily and sacrificed 7 days after infarction.

1.5. Echocardiography acquisition and analysis

Transthoracic echocardiography was performed by a blinded expert operator using a high-frequency ultrasound system (Vevo 2100, Visualsonics Inc., Canada) with a 30-MHz linear probe. Two-dimensional (2D) and M-mode (MM) echography were performed at a frame rate over 230 frames/sec. Mice were lightly anesthetized with 0.5-2% isoflurane in oxygen, adjusting the isoflurane delivery to maintain the heart rate in 450±50 bpm. Mice were placed in supine position and maintained normothermia using a heating platform and warmed ultrasound gel. A base apex electrocardiogram (ECG) was continuously monitored. Longitudinal and short axis views of the left ventricle were acquired at the level of the papillary muscles for M-mode and also medium and apical levels for 2D.

For the analysis of the wall motion score using echocardiography, regional left ventricular function was evaluated in the parasternal long-axis view. The left-ventricular wall was subdivided into six segments (basal,mid, and apical in the anterior and posterior walls). Each segment was scored by an independent blinded evaluator based on its motion and systolic thickening, according to the guidelines of the American Society of Echocardiography (Lang et al. 2015): (1) normal or hyperkinetic, (2) hypokinetic (reduced thickening), (3) akinetic (absent or negligible thickening, e.g., scar), and (4) dyskinetic (systolic thinning or stretching, e.g., aneurysm). The number of dysfunctional segments was quantified,

and the total wall motion score index (WMSI) representing the sum of the score of the six individual segments in each heart was calculated.

1.6. Measures of biomarkers of cardiac injury

Serum samples collected during one month after induction of myocardial infarction or autoimmune myocarditis were analyzed for cardiac troponin I, creatine kinase MB and lactate dehydrogenase using the Dimension RxL Max Integrated Chemistry System.

1.7. Isolation of heart infiltrating cells

Hearts were perfused with 10 ml of cold PBS and removed from the chest cavity. The hearts were then minced and digested with collagenase IV (100 U/mL; Gibco) for 45 minutes at 37 °C under constant agitation. The resulting cell suspensions were filtered through 40-µm cell strainers (BD Falcon) and washed twice with PBS, 0.5% bovine serum albumin (BSA), 1 µM EDTA. Erythrocytes were removed using hypotonic buffer. The number of leukocytes was assessed. Single cell suspensions were stained as described elsewhere and the different cell populations where analyzed by FACs.

2. Histopathological analysis in mice

2.1. Mouse infarct size quantification

Animals were anesthetized and 0.5 ml of 1% (weight/volume) Evan's Blue dye was infused intravenously through the cava vein 36 hours post surgery. Rapidly we opened the thoracic cavity to perfuse hearts with PBS to wash out the excess of Evan's Blue. Heart was then harvested, rinsed and atria were removed. The hearts were photographed before being cut into transverse slices (4-5 per ventricle), and then slices were weighted. The palish negative area for Evan's Blue delineates the area at risk (AAR): myocardium lacking blood flow. In order to differentiate infarcted from viable tissue, the same slices were then incubated in triphenyltetrazolium chloride (TTC, 1% (wight/volume) in PBS) at 37 °C for 15 minutes. The sections were then re-photographed and weighed. After the incubation with TTC, Evan's Blue staining clears out and sections present two areas: one necrotic (palish negative for TTC staining: infarcted myocardium) and one alive (red positive for TTC staining). Regions negative for Evan's Blue staining (AAR) and for TTC (infarcted myocardium) were blindly quantified using ImageJ with FIJI image processing package (NIH). Percentages of AAR and Infarcted myocardium were weighted and corrected independently of each slice, and the total mg of AAR and TTC-negative region was calculated for each heart. The AAR were determined as the mg:mg ratio of AAR:Ventricle weight, and the Infarct Size were determined as infarcted myocardium:AAR.

2.2. Histological assessment of heart inflammation

Mouse hearts were fixed in 10% buffered formalin and stained with hematoxylin and eosin (H&E) to assess inflammation. Myocarditis was assessed as the percentage of the heart section with inflammation compared to the overall size of the heart section using a microscope eyepiece grid, as previously described (Myers et al. 2013).

3. Collections of human samples

3.1. Patient cohorts for the discovery of a myocarditis miRNA biomarker.

Blood samples from the main cohort of the study were collected within the first 24h after admission and prior to the administration of heparin (if it was prescribed therapeutically). Blood collection was performed in BD-Vacutainer EDTA-tubes (4-10 ml per patient). When possible, 1 ml of blood was used for the analysis of leukocyte populations by FACS. The remaining blood was centrifuged to separate platelet-poor plasma and store at -80ºC.

The *miRNA Main Study Cohort* was obtained from a Spanish multicenter registry that included 132 patients with initial clinical suspicion of acute myocarditis based on clinical criteria at emergency room presentation (chest pain syndrome, electrocardiographic changes and/or positive biomarkers) and imaging suggestive of myocardial injury or ventricular dysfunction (**table 1** and **table 2**). The final diagnosis was myocarditis in 42 patients, STEMI in 45 patients, and NSTEMI in 45 patients. Final diagnoses were established based on findings on coronary arteriography and CMR, using standardized clinical criteria. In the case of myocarditis, diagnosis required the absence of coronary disease plus CMR with typical Lake Louise diagnostic criteria. Biopsy-proven diagnosis was not required. Patients included here presented myocarditis with infectious and non-infectious origins. The different etiologies and comorbidities of the myocarditis patients are summarized in **table 2**.

A total of 80 healthy participants with no abnormal findings on electrocardiography or echocardiography were included as additional controls.

The study was approved by the research ethics committees from the participating hospitals (Hospital Universitario de la Princesa, Fundación Jiménez-Díaz, Hospital Universitario HM Montepríncipe, Hospital Universitario Central de Asturias, Hospital Universitario Doce de Octubre) and the ethics committee of the Spanish Institute of Health Carlos III. Written informed consent was obtained from all participants.

Parameter	Healthy Control	Acute Myocarditis	STEMI	NSTEMI
N	80	42	45	45
Age, years	42.31±1.21	40.36±19.40	60.31±12.61	65.69±14.41
Sex (women/men), N (%)	41 (51.25) / 39 (48.75)	10 (23.80) / 32 (76.19)	11 (24.44) / 34 (75.56)	16 (35.56) / 29 (64.44)
TFOS, days	NA	4.167±5.951	0.814±1.419	1.462±2.063
CRF, N (%)	NA	23 (54.76)	40 (88.63)	41 (91.11)
Dyslipidemia, N (%)	NA	9 (21.43)	19 (43.18)	29 (64.44)
History of smoking, N (%)	NA	14 (33.33)	26 (60.00)	20 (44.44)
Hypertension, N (%)	NA	6 (14.29)	17 (37.78)	30 (66.67)
Diabetes, N (%)	NA	3 (7.14)	7 (15.56)	13 (28.89)
Renal Insufficiency, N (%)	NA	1 (2.38)	2 (4.44)	3 (6.67)
Peripheral Artery Disease, N (%)	NA	1 (2.38)	2 (4.44)	2 (4.44)
Laboratory findings				
Peak Troponin I, ng/ml	NA	9.042±9.646	42.02±35.16	13.16±20.59
Peak Troponin T, ng/l	NA	1217±1274	3378±3302	1189±2303
Peak CK-MB, U/l	NA	50.59±35.29	96.44±57.72	60.74±26.67
ECG alterations, N (%)	0 (0.00)	28 (66.67)	45 (100.00)	35 (77.78)
ST segment elevation, N (%)	0 (0.00)	28 (66.67)	45 (100.00)	0 (0.00)
Q-wave, N (%)	0 (0.00)	8 (19.05)	5 (11.11)	10 (22.22)
CT or coronary angiography performed, N (%)	0 (0.00)	19 (45.24)	45 (100.00)	45 (100.00)
Coronary Artery Disease, %	-	1 (5.26)	44 (97.78)	40 (88.89)
Echocardiography at admission, N (%)	80 (100.00)	41 (93.18)	43 (95.56)	35 (77.78)
Left Ventricular Ejection Fraction, %	63.81±0.55	54.07±13.04	51.42±11.69	57.66±10.39
Segmental contraction abnormalities, N (%)	0 (0.00)	19 (46.34)	34 (79.07)	24 (68.57)
CMR, N (%)	9 (11.25)	42 (100.00)	7 (15.91)	1 (2.22)
Myocarditis diagnosed by CMR (Lake Louise criteria), N (%)	0 (0.00)	42 (100.00)	0 (0.00)	0 (0.00)

Table 1. Baseline characteristics of the *miRNA Main Study Population*. Data are expressed as means ± SD or as number of patients (N) with percentages in brackets. NA, not assessed; TFOS, time from the onset of symptoms until hospital admission; ECG, electrocardiogram at admission; CK, creatine kinase; CMR, cardiac magnetic resonance during hospitalization; CRF, cardiovascular risk factors.

Comorbidities	Myocarditis (N=42)	Myocardial Infarction (N= 90)
Pneumonia	1	0
Diabetes	2	20
Gastroenteritis	1	0
Tonsillitis	1	0
Flu	1	0
Q-fever	1	0
Lupus	0	2
R. Arthritis	0	1
Renal insufficiency	0	5
Cancer	1	0

Etiology	Myocarditis (N=42)
Unknown	22
Bacteria	1 Chlamydophila 1 Coxiella
Virus	1 Adenovirus 1 Influenza
IC inhibitor-irAEs	1
Idiopathic	14[a] 1[b]

Table 2. Comorbidities and etiology of myocarditis in the *miRNA Main Study Population.* ICI-irAEs: immune checkpoint inhibitor therapy-immune related adverse effects. [a]Negative serology for suspected virus. [b]Negative serology for suspected Chagas' disease.

The *miRNA Validation Cohort 1* was provided by the Partners Biobank (now the Mass General Brigham Biobank) in Boston, Massachusetts (USA). These samples were collected from patients who consented to having their plasma stored for future research after their initial hospitalization and diagnosis of myocarditis (and do not correspond to the acute stage of myocarditis when patients initially presented to the hospital). As these patients were not part of a clinical trial, their diagnosis and management resembled real-world clinical practice. Diagnosis was made in most cases based on clinical criteria (presentation with chest pain syndrome and ECG changes or positive biomarkers) with imaging suggestive of myocardial injury or ventricular dysfunction, and without evidence of obstructive coronary artery disease. Biopsy-proven diagnosis was rare in this cohort as right ventricular biopsy is rarely obtained in cases of suspected myocarditis in this hospital (only 4 patients with myocarditis confirmation by biopsy). As reflected in the evolution of care of these patients (with diagnosis between 2006 and 2017, and one case in 1998), CMR was obtained more frequently in the later cases and showed 2/3 of the typical Louise-Lake diagnostic criteria for myocarditis (T2 myocardium to skeletal muscle ratio >1.9; delayed enhancement in subepicardial and or mid-myocardium in nonischemic distribution; increased global myocardial gadolinium enhancement ratio between myocardium and skeletal muscle) in 11 of 17 cases in which CMR was obtained. There may be some heterogeneity as to the actual diagnosis in this population (e.g. cases of MINOCA, viral myocarditis, giant cell or lymphocytic myocarditis) (**table 3**).

Parameter	Myocardial Infarction	Myocarditis
N	11	34
Age, years	61±15	54±16
Sex (Male), %	64	56
Sex (Female), %	34	44
CRF		
Hypertension, %	73	42
Hyperlipidemia, %	64	42
History of Smoking, %	37	42
Diabetes Mellitus, %	27	15
Presence of chest pain, %	100	67
EGC changes, %	64	80
ST elevation on ECG, %	56	26
Laboratory findings		
Peak Troponin-T, ng/mL	1.72±1.23 ng/mL TnT (n=6) 2.20±1.97 ng/L hsTnT (n=5)	0.58±0.93 ng/ml TnT (n=30) 3.1±4.2 ng/mL Trop-I (n=2)
Cardiac catheterization or CTA performed, %	100	73
Presence of obstructive CAD, %	100	9
Echocardiography (closest to presentation)		
Left Ventricular Ejection Fraction, %	58±11	47±18
CMR performed, %	NA	50
Myocarditis diagnosed by CMR (Lake Louise criteria), %	-	32
Treatment		
Beta blockers, N	9	24
Ace inhibitors or ARBs, N	3	19
Statins, N	10	21
Aspirin, N	10	17
Heparin products, N	10	1

Table 3. Patient characteristics of the *miRNA Validation Cohort 1* from MGH. Patients with myocarditis were selected from the Massachusetts General Hospital (MGH) Partners Biobank based on a diagnosis of myocarditis and verified by chart review. CRF, cardiovascular risk factors; ECG, Electrocardiogram; CTA: Computerized tomography angiogram; CAD: Coronary Artery Disease; CMR: Cardiac Magnetic Resonance Imaging; ARB: Angiotensin Receptor Blocker; NA: not assessed.

The *miRNA Validation Cohort 2* was provided by the Center for Molecular Cardiology of the University Hospital Zürich (Switzerland). Myocarditis was diagnosed based on clinical presentation, elevation of troponin T and CMR, after exclusion of obstructive coronary artery disease through coronary angiography. All patients received CMR. Endomyocardial biopsy at this center is reserved only for patients that are hemodynamically unstable, for example patients with severely reduced left ventricular ejection fraction, ventricular arrhythmia, high degree atrioventricular block, patients unresponsive to therapy or those patients who need inotropic support or ECMO. Endomyocardial biopsy was performed in 7 patients from this collection. Of these, 3 had giant cell myocarditis, 1 had lymphocytic myocarditis, 1 had Parvovirus B 19 and 2 endomyocardial biopsies showed nonspecific results. In addition, 2 patients had fulminant myocarditis, but there was no endomyocardial biopsy available (**table 4**).

Parameter	MINOCA excluded by CMR	MINOCA without CMR	Myocarditis confirmed by MRI
N	12	8	35
Age, years	42±16	35±16	40±15
Sex (Male), %	50	50	77
Sex (Female), %	50	50	23
CRF			
Hypertension, %	33	0	18
Hyperlipidemia, %	17	0	18
History of Smoking, %	17	50	36
Diabetes Mellitus, %	0	0	14
Presence of chest pain, %	67	100	68
ECG changes, %	33	50	73
ST elevation on ECG, %	0	50	50
Laboratory findings			
Peak Troponin-T, ng/mL	26±17	65±43	253±336
Cardiac catheterization or CTA performed, %	83	100	100
Presence of obstructive CAD, %	17	0	0
Echocardiography at admission			
Left Ventricular Ejection Fraction, %	55±12	61±2	53±10
CMR performed, %	100	0	100
LGE/Inflammation/Edema on patients with CMR, %	0	0	100
Myocarditis on Endomyocardial Biopsy, N	0	0	4

Table 4. Patient characteristics of the *miRNA Validation Cohort 2* from UHZ. Patients with myocarditis were selected by the Center for Molecular Cardiology of the University Hospital Zürich (UHZ, Zürich, Switzerland) based on a diagnosis of myocarditis and verified by cardiac magnetic resonance imaging (MRI) and/or myocardial biopsy. Data are expressed as means ± SD, as number of patients (N) or as percentages. CRF, cardiovascular risk factors; ECG, Electrocardiogram; CTA, Computerized tomography angiogram; CAD, Coronary Artery Disease; LGE, Late Gadolinium Enhancement.

The *miRNA Validation Cohort 3* was composed of 40 consecutive patients selected from a prospective cohort of 800 patients recruited by the cardiology service at Padova University (Padua, Italy) with a diagnosis of biopsy-proven myocarditis. Of these patients, 39 had lymphocytic myocarditis and 1 had giant-cell myocarditis. With respect to etiology, 33 had autoimmune myocarditis and 7 had viral myocarditis (defined as virus-negative and virus-positive, respectively, by polymerase chain reaction on endomyocardial biopsy). All had unobstructed epicardial coronary arteries on selective coronary angiography, and 34 underwent CMR at the time of hospital admission. As comparators for this cohort, we included 49 samples from patients with myocardial infarction (STEMI) from the Biobank Regional Platform, Instituto Murciano de Investigación Biomédica (Murcia, Spain) (**table 5**).

Parameter	Myocarditis	Myocardial Infarction
N	40	49
Age, years	44.63±14.09	65.43±11.01
Sex (women/men), N (%)	13 (32.50) / 27 (67.50)	20 (20.41) / 39 (79.59)
CRF, N (%)	10 (25.00)	41 (83.67)
Dyslipidemia, N (%)	0 (0.00)	21 (42.86)
History of smoking, N (%)	6 (15.00)	28 (57.14)
Hypertension, N (%)	6 (15.00)	26 (56.06)
Diabetes, N (%)	1 (2.50)	17 (34.69)
Renal Insufficiency, N (%)	0 (0.00)	4 (8.16)
Peripheral Artery Disease, N (%)	0 (0.00)	3 (6.12)
Laboratory findings		
Peak Troponin I, ng/ml	9.43±24.71	196523±168058
Peak Troponin T, ng/ml	NA	22218±64093
ECG alterations, N (%)	39 (97.50)	49 (100.00)
ST segment elevation, N (%)	5 (12.50)	49 (100.00)
CT or coronary angiography performed, N (%)	40 (100.00)	49 (100.00)
Coronary Artery Disease, %	0 (0.00)	49 (100.00)
Echocardiography at admission, N (%)	40 (100.00)	48 (97.96)
Left Ventricular Ejection Fraction, %	38.61±15.53	50.79±10.25
Segmental contraction abnormalities, N (%)	32 (80.00)	49 (100.00)
CMR, N (%)	34 (85.00)	0 (0.00)
Myocarditis on Endomyocardial Biopsy, N (%)	40 (100.00)	0 (0.00)

Table 5. Patient characteristics of the *miRNA Validation Cohort 3* from Padua (Italy) and Murcia (Spain). A total of 40 patients with biopsy-proven myocarditis were selected from a prospective cohort of 800 patients recruited by the cardiology service at Padova University. As comparators, 49 patients with myocardial infarction were included from the Biobank Regional Platform from Murcia, Spain. Data are expressed as means ± SD or as number of patients (N) with percentages in brackets. NA, not assessed; CRF, cardiovascular risk factors; ECG, electrocardiogram at admission; CMR, cardiac magnetic resonance during hospitalization.

As additional control cohorts, we included retrospective samples of patients with Th17-related immunological diseases, including rheumatoid arthritis (RA, n= 40), spondyloarthritis (SPA, n= 27), psoriasis (n= 24) or multiple sclerosis (MS, n= 12), in a moderate-to-severe grade and without cardiac involvement. We also included control donors who were suspected of having SPA (C-SPA, n= 22) or RA (C-RA, n=15) with negative evaluations after 2 years of follow-up, and controls for MS (C-MS, n= 12). Samples were obtained from the Hospital Universitario de La Princesa (RA, C-RA, SPA, C-SPA and psoriasis) and from the Hospital Universitario Ramón y Cajal (MS and C-MS). All these patients and controls complete the *miRNA Th17-linked diseases Cohorts* (**table 6**).

	C-SPA	SPA	C-RA	RA	Psoriasis	C-MS	MS
N	22	27	15	40	24	12	12
Age, years	39.9±13.3	42.6±26.2	53.7±17.8	50.5±15.6	49.9±10.4	34.1±5.6	34.8±12.4
Sex (women/men)	9/13	13/15	13/2	36/4	14/10	5/7	8/4
CRP, mg/l	0.17±0.14	1.98±4.11	0.29±0.26	3.50±3.72			
Disease score							
ASDAS	1.92±0.69	2.74±1.13					
BASDAI	3.57±1.46	4.75±1.97					
DAS28			2.82±0.89	5.85±1.02			
PASI (<10)					15.61±5.37		
EDDS (0-10)						1±0.75	2.66±1.63

Table 6. Baseline characteristics of the *miRNA Th17-linked diseases cohorts*. Data are expressed as means ± SD. SPA: spondyloartritis; RA: rheumatoid artritis; MS: multiple sclerosis; control donors were studied after suspicion of SPA (C-SPA) or RA (C-RA) with negative result after 2 years follow-up, and controls for MS (C-MS). CRP: C - reactive protein; ASDAS: Ankylosing Spondylitis Disease Activity Score; BASDAI: Bath Ankylosing Spondylitis Disease Activity Index; DAS28: 28-joint Disease Activity Score; PASI: Psoriasis Area Severity Index. EDDS: Expanded Disability Status Scale.

3.2. Patient cohorts and controls analyzed for the assessment of the clinical value of CD69 and hsa-miR-155-5p in MI.

For the main study cohort of this part (*CD69 Main Study Cohort*), blood samples of MI patients were prospectively collected from the arterial sheath used for coronary angiography prior to the administration of heparin, between March 2017 and May 2019. All demographic, clinical, angiographic and procedural characteristics of patients with MI were also prospectively collected and are summarized in **table 7**. Revascularization and subsequent clinical management at the coronary care unit and at the cardiology ward was performed following the guideline recommendations for MI (Ibanez et al. 2018).

All patients with MI were systematically followed in a dedicated outpatient clinic. Re-admission for chronic heart failure and all-cause death are summarized (**table 8**).

In parallel, we analyzed blood samples from 80 healthy donors with absence of cardiac disease, as determined by no abnormal findings in electrocardiography or echocardiography.

A. Baseline clinical characteristics	
N	283
Age (years)	64 ± 13
Sex (male)	212 (74.9)
Ethnicity	
Caucasian	273 (96.5)
Latino American	4 (1.4)
Asian	2 (0.7)
Black	4 (1.4)
Measures	
Weight (kilograms)	78 ± 16
Height (meters)	168 ± 11
Body Mass Index (kg/m^2)	27 ± 4
CRF	
Systemic hypertension	153 (54.1)
Hyperlipidemia	163 (57.6)
Diabetes mellitus	63 (22.3)
Smoker	123 (43.5)
Ex-smoker	75 (26.5)
Family history of ischemic heart disease	21 (7.4)
Peripheral artery disease	15 (5.3)
Chronic kidney disease	22 (7.8)
Ischemic heart disease	34 (12)
Previous MI	29 (10.2)
Previous PCI	26 (9.2)
Previous CABG	2 (0.7)
Atrial fibrillation	12 (4.2)

B. Clinical presentation and in-hospital evolution	
Final diagnosis	
STEMI	209 (73.9)
NSTEMI	74 (26.1)
Culprit coronary artery	
Left main	8 (2.8)
LAD	114 (40.3)
LCX	43 (15.2)
RCA	115 (40.6)
Bypass	1 (0.4)
Unknown	2 (0.7)
Coronary artery affected	
Left main, N (%)	12 (4.2)
LAD, N (%)	165 (58.3)
LCX, N (%)	98 (34.6)
RCA, N (%)	166 (58.6)
N of coronary arteries affected	
1-vessel, N (%)	174 (61.5)
2-vessels, N (%)	61 (21.6)
3-vessels, N (%)	48 (16.9)
Killip-Kimball classification	
I, N (%)	246 (86.9)
II, N (%)	21 (7.4)
III, N (%)	4 (1.4)
IV, N (%)	12 (4.2)
Revascularization therapy	
PCI, N (%)	261 (92.2)
CABG, N (%)	8 (2.8)
Conservative, N (%)	14 (4.9)
Laboratory findings	
Peak creatine kinase, U/l	913 (308-1900)
Peak troponin T, ng/ml	2508 (660-5533)
Peak number of leukocytes, /mm^3	11820 (9450-14805)
Peak CRP level, mg/l	2.5 (0.7-11.4)
Left-ventricular ejection fraction, %	54±10
Reduced EF (<50%), N (%)	88 (31.1)
Acute decompensated HF, N (%)	38 (13.4)
Fever during admission, N (%)	33 (11.7)
Antibiotic therapy at admission, N (%)	33 (11.7)

Table 7. **Characteristics of the *CD69 Main Study Cohort* from the Hospital Universitario de La Princesa.** (**A**) Baseline clinical characteristics. (**B**) Clinical presentations and in-hospital evolution. Data are expressed as means with interquartile ranges between brackets or as number with percentages of patients between brackets. CRF: cardiovascular risk factors; PCI: percutaneous coronary intervention; CABG: coronary artery bypass grafting; STEMI: ST-elevation myocardial infarction; NSTEMI: non-ST-elevation myocardial infarction; RCA: right coronary artery; LAD: left anterior descending coronary artery; LCX: left circumflex coronary artery; CRP: C-reactive protein; EF: ejection fraction; HF: heart failure.

Parameters	N=187 patients
Time of follow-up (years)	2.5 (IQR 2.1-3.0)
All-cause death	2 (6.4 %)
New admission for heart failure	7 (3.7 %)

Table 8. **Follow-up data of patients from the *CD69 Main Study Cohort* from the Hospital Universitario de La Princesa**. At medium time of follow-up (2.5 y): 91.9 % free from composite all-cause death or admission for heart failure.

The independent validation cohort of this finding (*CD69 Validation Cohort*) consisted of a consecutive series of patients admitted to the Hospital de la Santa Creu i Sant Pau for MI. Blood samples were collected within the first 24h from the admission and prior to heparin administration. Baseline clinical characteristics, clinical presentation and in-hospital evolution are summarized in **table 9.** All patients were followed and the adverse clinical outcomes (chronic heart failure and all-cause death) are summarized in **table 10.**

A. Baseline clinical characteristics	
N	84
Age (years)	59.6 ±13.6
Sex (male)	64 (76.2)
Ethnicity	
Caucasian	81 (96.42)
Asian	3 (3.57)
CRF	
Systemic hypertension	44 (52.38)
Hyperlipidemia	38 (45.23)
Diabetes mellitus	13 (15.47)
Smoker	43 (51.19)
Ex-smoker	16 (19.04)
Family history of ischemic heart disease	19 (22.61)*
Peripheral artery disease	6 (7.14)
Chronic kidney disease	4 (4.76)
Ischemic heart disease	8 (9.5)
Previous MI	2 (2.4)

B. Clinical presentation and in-hospital evolution	
Final diagnosis	
STEMI	82 (97.61)
NSTEMI	2 (2.38)
Culprit coronary artery	
LAD, N (%)	40 (47.6)
RCA, N (%)	28 (33.3)
LCX, N (%)	7 (8.3)
OM, N (%)	6 (7.1)
Unknown, N (%)	3 (3.6)
N of coronary arteries affected	
1-vessel, N (%)	174 (61.5)
2-vessels, N (%)	61 (21.6)
3-vessels, N (%)	48 (16.9)
Revascularization therapy	
PCI, N (%)	84 (100)
Laboratory findings	
Peak troponin T, ng/ml	&3605 (204-10000)
Left-ventricular ejection fraction, %	†48±9.54
Antibiotic therapy during admission, N (%)	0 (0.00)

Table 9. Characteristics of the *CD69 Validation Cohort* from the Hospital de la Santa Creu i Sant Pau. Data are expressed as means with interquartile ranges between brackets or as number with percentages of patients between brackets. (**A**) Baseline clinical characteristics. (**B**) Clinical presentations and in-hospital evolution. Data are expressed as means ± SD or as number with percentages of patients between brackets. RCA: Right Coronary Artery; LAD: Left Anterior Descending Coronary Artery; LCX: Left Circumflex Coronary Artery; OM: Obtuse Marginal Coronary artery; PCI: Percutaneous Coronary Intervention. *73; &64 patients; †70 patients.

Parameters	N=84 patients
Time of follow-up (years)	2,15 IQR (1,76-2,68)
All-cause death	4 (4.8)
New admission for heart failure	9 (10.71)

Table 10. Follow-up data of patients from the *CD69 Validation Cohort* from the Hospital de la Santa Creu i Sant Pau.

Oral informed consent was obtained for patients requiring emergency coronary angiography and primary angioplasty and subsequently written informed consent was obtained immediately after the procedure. The study was approved by the Research Ethics Committees from the Hospital Universitario de la Princesa and Hospital Santa Creu i Sant Pau.

4. Flow cytometry analysis

Peripheral blood leukocytes (PBLs) were isolated from mouse or human blood samples using Ficoll-Isopaque (density=1.121 g/ml) gradient centrifugation. Human/Mouse PBLs or single cell suspensions of mouse lymph nodes or heart infiltrating leukocytes were incubated in PBS +0.05% BSA +0.01% EDTA buffer with fluorochrome-conjugated antibodies. PBLs were cultured overnight for bystander activation in plates coated with 3 µg/ml of purified anti-CD3 (for human cells: OKT3 clone, Biolegend; for mouse cells: 145-2C11 clone, BD PharMingen) in complete RPMI medium (Gibco) before cell staining. For cytokine production assessment, cells were stimulated with 50 ng/ml of phorbol myristate acetate (PMA, Sigma Aldrich), 1 µg/ml of ionomycin (Sigma Aldrich) and 1 µg/ml of GolgiPlug (BD PharMingen) in complete culture medium for 4 additional hours.

Staining of membrane markers was performed by incubating single cell suspensions with fluorochrome-conjugated antibodies in PBS +0.05% BSA +0.01% EDTA for 15 minutes at 4 ºC. When required, membrane-stained cells were further fixed and stained with the following intracellular or intranuclear protocols:

For Foxp3 evaluation, nuclear staining was performed using the Foxp3 staining buffer set (Miltenyi Biotec) for human cells and the Foxp3 kit (eBioscience) for mouse cells, following the providers' instructions.

For effector T helper cell evaluation, cells were fixed with PBS 2% paraformaldehyde for 10 minutes at room temperature and intracellularly stained with conjugated-antibodies against IL-17, IL-22 and IFNγ in PBS +0.05% BSA +0.01% EDTA +0.5% saponin for 45 minutes at room temperature. When

indicated, Foxp3-RFP/IL17-eGFP mice were used to track Foxp3$^+$ and/or IL-17$^+$ cells. The fluorochrome-conjugated clones of antibodies used are listed in **table 11**.

Cells were analyzed in an LSRFortessa or FACSymphony Flow Cytometer and the data were processed with FlowJo v10.0.4 (Tree Star).

Marker	Clone	Manufacturer
Human CD14	M5E2	Biolegend
Human CD16	DJ130	Dako
Human CD25	2A3	BD Biosciences
Human CD4	SK3	BD Biosciences
Human CD45RA	H100	BD Biosciences
Human CD45RO	UCHL1	BD Biosciences
Human CD66b	G10F5	Biolegend
Human CD69	FN50	BD Biosciences
Human Foxp3	3G3	Miltenyi Biotec
Human HLA-DR	G46-6	BD Biosciences
Human IFNγ	B27	BD Biosciences
Human IL-17A	SCPL1362	BD Biosciences
Human IL-22	142928	R&D Systems
Mouse CD11b	M1/70	BD Biosciences
Mouse CD3	145-2C11	Biolegend
Mouse CD39	24DMS1	eBioscience
Mouse CD4	RM4-5	BD Biosciences
Mouse CD45.2	104	Biolegend
Mouse CD69	H1.2F3	BD Biosciences
Mouse F4/80	BM8	Biolegend
Mouse Gr1	RB6-8C5	BD Biosciences
Mouse Ly6C	AL-21	BD Biosciences
Mouse TCRγδ	GL3	Biolegend

Table 11. List of human and mouse antibodies for flow cytometry used in this study.

5. T cell cultures

All primary cells (except for the EV secretion assays that required an exosome-free medium) were cultured in Roswell Park Memorial Institute (RPMI) 1640 medium (Sigma-Aldrich) supplemented with 20% heat-inactivated calf serum (Gibco), 20 mM HEPES, 2 mM L-Glutamine, 0.1 mM non-essential amino acids, 100 U/ml penicillin, 100 µg/ml streptomycin, 0.05 mM β-mercaptoethanol and 100 mM sodium pyruvate. Cultures were maintained at 37 ºC and 5% CO_2.

5.1. *In vitro* differentiation of Th17 cells

Naive CD4$^+$ T cells were obtained from single-cell suspensions of the spleen and mesenteric lymph nodes of OTII mice. The cell suspensions were incubated with biotinylated antibodies against CD24,

CD8, CD117, major histocompatibility complex (MHC) class II (I-Ab), CD19, CD16, CD11b, CD11c, and DX5 and subsequently with Streptavidin MicroBeads (MACS; Miltenyi Biotec). $CD4^+$ T cells were negatively selected in an auto-MACS Pro Separator (Miltenyi Biotec) according to the manufacturer's instructions. The naïve status was confirmed by expression of CD4, CD25, and CD62L by flow cytometry (data not shown). Naïve $CD4^+$ T cells (10^6 cells/ml) were cultured in the presence of irradiated antigen-presenting cells (APCs) (T-cell-depleted splenocytes) and ovalbumin peptide, residues 323-339 (10 µg/ml), plus the following combination for Th17 polarization: anti-IFN-γ (4 µg/ml), anti-IL-4 (4 µg/ml), recombinant IL-6 (10 ng/ml), recombinant IL-23 (10 ng/ml), and recombinant TGF-β1 (5 ng/ml). Where indicated, 3-day-differentiated Th17 cells from wild type BALB/c mice were analyzed as polyclonal Th17 cells.

5.2. *In vitro* differentiation of Treg cells

Naive $CD4^+$ T cells were purified from single-cell suspensions of the spleen, peripheral and mesenteric lymph nodes of the indicated mice. Cell suspensions were incubated with biotinylated antibodies against CD44, CD8, major histocompatibility complex (MHC) class II (I-Ab), CD19, B220, IgM, CD11b, CD11c, and DX5 and subsequently with Streptavidin Microbeads (MACS; Miltenyi Biotec). Naïve $CD4^+$ T cells were negatively selected in LD columns (MACS; Miltenyi Biotec) according to the manufacturer's instructions. The naïve status was confirmed by expression of CD4 and CD62L by flow cytometry (data not shown). Then, naïve $CD4^+$ T cells (10^6 cells/ml) were co-cultured for 72h with irradiated (30 Gy) APC in the presence of plate-bound anti-CD3 (2 µg/ml) and soluble anti-CD28 (2 µg/ml) plus recombinant TGF-β1 (10 ng/ml) and IL-2 (2 ng/ml). For antigen specific iTreg cells, naïve $CD4^+$ T cells were obtained from OTII mice and were differentiated in the presence of ovalbumin peptide, residues 323-339 (10 µg/ml).

5.3. *Ex vivo* cultures of Treg and Th17 cells

EAM was induced in Foxp3-RFP/IL17-eGFP reporter mice by immunization with MyHCα-p and CFA. EAM-draining (axillary and inguinal) lymph nodes were collected six days post-immunization. Cell suspensions from lymph nodes were cultured ($2x10^7$ cells/ml) during 48h in exosome-free TexMACS media (Miltenyl Biotec) in the presence of the peptide MyHCα-p (10 µg/ml) and IL-23 (10 ng/ml, R&D). $CD4^+$Foxp3-$mRFP^+$ (Treg) and $CD4^+$IL17-$eGFP^+$ (Th17) cells were sorted using a BD FACS Aria II cell sorter or iCyt Synergy 4L cell sorter. Sorted cells were cultured in TexMACS media for 48h with MyHCα-p and either recombinant IL-2 (R&D) for Foxp3$mRFP^+$ cells, or recombinant IL-23 (R&D) for IL-17$eGFP^+$ cells.

5.4. Co-cultures of γδT cells and natural Treg cells

Single cell suspensions of peripheral (axillary, inguinal and submaxillary) lymph nodes of Foxp3-mRFP/IL17-eGFP/*cd69*$^{+/+}$ or Foxp3-mRFP/IL17-eGFP/*cd69*$^{-/-}$ reporter mice were stained with fluorochrome-conjugated antibodies. Natural Treg cells ($CD3^+$Foxp3-$mRFP^+$) and γδT cells ($CD3^+$

TCRγδ$^+$ cells) were sorted using a BD FACSAria II cell sorter. Both cell populations were co-cultured at different ratios for 24h in the presence of plate-bound anti-CD3 (2 µg/ml) and soluble anti-CD28 (2 µg/ml) plus recombinant IL-2 (10 ng/ml) with or without ARL 67158 (250 µM, Tocris). Apoptosis of γδT cells was evaluated by flow cytometry using annexin V (BD Biosciences). For IL-17A-eGFP production assessment, cells were incubated 4 additional hours in the presence of PMA (Sigma Aldrich), ionomycin (Sigma Aldrich) and GolgiPlug (BD PharMingen).

6. RNA extraction and quantification

6.1. Quantification of miRNA levels by qPCR

MicroRNAs were extracted from human and mouse cells and plasma with the miRVana miRNA Isolation kit (Invitrogen) or miRNeasy mini kit (Qiagen) as recommended by the manufacturers. For plasma samples, reverse transcription was adjusted by volume. The volume of RNA retrotranscribed corresponds to 8 µl of initial volume of plasma per 10 µl of final volume, as recommended by the manufacturer. For miRNA analysis in cells, reverse transcription was performed from 100 ng of total RNA. For both plasma and cells, miRCURY LNA Universal RT microRNA PCR kit (Exiqon, later named as miRCURY RT kit by Qiagen) was used for reverse transcription. MicroRNA expression was analyzed by real-time quantitative PCR using specific microRNA LNA PCR primer sets (Exiqon/Qiagen) for each microRNA and miRCURY LNA SyBrGreen PCR Kit (Exiqon/Qiagen). RNA Spike-in kit (Exiqon/Qiagen) was used as an exogenous control of RNA extraction according to the manufacturer´s instructions. Two synthethic RNA spike-ins (UniSp5 and UniSp2) in different concentrations were used to control the quality of RNA quantification. Synthetic UniSp6 was used to monitor RT-PCR yield. The use of these spike-ins as exogenous controls allowed us to exclude samples not meeting amplification standards. We tested 7-10 different miRNAs to select the more stable ones in immune cells and in plasma as normalizers. MiR-423-3p and miR-103a-3p were proposed by NormFinder (https://moma.dk/normfinder-software, visited on 2017) as the most stable miRNAs among T cell and plasma sample groups and were used as endogenous normalizers.

Real-time quantitative PCR (qPCR) analyses were performed with an ABI Prism 7900HT SDS 384-well thermal cycler (Applied Biosystems). Relative miRNA expression was determined using the $2^{-\Delta\Delta CT}$ method.

6.2. Quantification of mRNA levels by qPCR

RNA was extracted from frozen human PBLs or mouse single cell suspensions with miRNeasy mini kit (Qiagen) as recommended by the manufacturer. Reverse transcription was performed from 200 ng of DNAse-treated RNA using the High Capacity cDNA RT kit (Applied Biosystems). Then, gene

expression was measured by real-time quantitative PCR using SYBR green PCR mix (*Applied Biosystems*) and mRNA specific primer pairs (Thermo Fischer Scientific) listed in **table 12**.

Real-time qPCR analyses were performed with an ABI Prism 7900HT SDS 384-well thermal cycler (*Applied Biosystems*). Relative gene expression was determined using the $2^{-\Delta\Delta CT}$ method, normalizing by beta-actin, (*ACTB/Actb*) and glyceraldehyde 3-phosphate dehydrogenase (*GAPDH/Gapdh)* housekeeping genes.

Gene	Forward primer (5' -> 3')	Reverse primer (5' -> 3')
Human *ACTB*	CATCGAGCACGGCATCGTCA	TAGCACAGCCTGGATAGCAAC
Human *CD69*	ATTGTCCAGGCCAATACACATT	CCTCTCTACCTGCGTATCGTTTT
Human *FOXP3*	GAGAAGCTGAGTGCCATGCA	GGAGCCCTTGTCGGATGAT
Human *GAPDH*	GAAGGTGAAGGTCGGAGTC	GAAGATGGTGATGGGATTTC
Mouse *Actb*	GGCTGTATTCCCCTCCATCG	CCAGTTGGTAACAATGCCATGT
Mouse *Gapdh*	TCAAGCAGGCATCTGAGGG	CGAAGGTGGAAGAGTGGGAG
Mouse *Il17a*	CTTTCCCTCCGCATTGACAC	TTTAACTCCCTTGGCGCAAAA
Mouse *Pparg*	AAGAGCTGACCAATGGTTG	GCATCCTTCAGACAAGCATGAA
Mouse *Rorc*	CCGCTGAGAGGGCTTCAC	TGCAGGAGTAGGCCACATTACA

Table 12. List of primers used for mRNA quantification by qPCR.

6.3. Microarrays of miRNAs

First, mouse microRNA microarray analysis (Agilent mouse miRNA array, 8x15K) was performed to assess expression of miRNAs in activated $CD4^+$ T cells, polyclonal Th17 cells (Th17poly), ovalbumin-specific Th17 cell (Th17ag-sp) skewed cultures and Th17ag-sp sorted cells. The chips were scanned using the Agilent G2567AA Microarray Scanner System (Agilent Technologies). Raw probe-level data were recovered with Agilent Feature Extraction 10.7.3.1 software. Data files were then imported into GeneSpring GX software version 10.0 (Agilent Technologies) and quantile normalization was performed. Probes were flagged (Present, Marginal, Absent) using GeneSpring default settings and filtered for further analysis according to expression (all miRNAs with raw expression levels within the range 20-100% of expression in 75% of replicates for at least one condition were retained) and flags (all miRNAs flagged as Present or Marginal in 75% of replicates for at least one condition were retained). To determine statistically significant differences between both conditions, a moderated t-test using the limma package from Bioconductor was applied to the filtered data. Benjamini-Hochberg p-value correction was used for control of the false discovery rate (FDR or corrected p-value) (**annex, tables A.1 and A.2**).

Second, mouse microRNA microarrays (Agilent release 21.0, 8x60K) were used to analyze expression of miRNAs in $CD4^+$ T cells from mice with myocarditis ($CD4^{EAM}$) *versus* mice with myocardial infarction ($CD4^{MI}$). After induction in mice of experimental autoimmune myocarditis or myocardial

infarction, axillary and mediastinal lymph nodes were collected at day 6 or 3, respectively. Single-cell suspensions were labelled with biotinylated antibodies against CD4 (Pharmingen, BD). $CD4^+$ T cells were incubated with Streptavidin Microbeads (MACS; Miltenyi Biotec) and positively selected with MS columns (MACS; Miltenyi Biotec). Microarray data were acquired with Agilent Feature Extraction 10.7.3.1 software. Raw probe-level signal intensities were processed with the AgiMicroRna Bioconductor package version 2.28.0 to obtain normalized expression levels for each miRNA, using the RMA algorithm with quantile normalization across samples. To avoid losing information for miRNAs expressed at lower levels, background correction and undetected probe filtering were omitted. Of 1881 miRNAs described by the array, 704 were detected as differentially expressed (with Benjamini-Hochberg adjusted p-values < 0.1). Of these, 367 were upregulated in $CD4^{EAM}$ relative to $CD4^{MI}$, and 337 were downregulated (**annex, table A.3**).

MicroRNA microarray data generated here are available at the Gene Expression Omnibus under the following accession codes: GSE109992, GSE109993 and GSE109994.

7. Extracellular vesicles assays

7.1. Isolation and characterization of extracellular vesicles

Extracellular vesicles (EVs) were isolated with polyethylene glycol (PEG) as previously described (Andreu et al. 2016) from 200µl of plasma or supernatants (SN) for qPCR analysis. Briefly, cell debris were pelleted by centrifugation at 1000g for 30 minutes. EVs were precipitated by adding 0.4 volumes of 50% PEG 6000 (Sigma Aldrich) in 375 mM NaCl followed by 30 minutes of incubation at 4 ºC. Samples were then spin down at 1500g for 30 minutes at 4ºC. For the characterization of extracellular vesicles derived from immune cells, EVs present in culture SN were analyzed by Nanosight LM10 and NTA 2.3 Software (NanoSight, Wiltshire, UK) after removal of cell debris by centrifugation at 10000g for 30 minutes.

7.2. Evaluation of miRNA secretion into extracellular vesicles

The ratio SN-EVs/Total-SN and Plasma-EVs/Total-plasma was calculated as follows. For SN, 5 x 10^5 cells from draining lymph nodes at day 6 of EAM were cultured in 200 µl of exosome-free TexMACS medium (Miltenyl Biotec) during 24h in the presence of the MyHCα-p, anti-CD3 and anti-CD28. SNs were collected after centrifugation at 1000g during 10 minutes, to remove cell debris. The volume of liquid (200 µl SN or plasma) was split in half; after PEG-isolation EVs from SN were solubilized in TexMACs and EVs from plasma were solubilized in PBS, (1:1 volume). The RNA-extraction lysis buffer was supplemented with the amount of spike-ins controls recommended by the manufacturer (RNA Spike-in kit, Exiqon/Qiagen). RNA extraction was then performed as described above. Without adjusting concentration, the same volume of RNA solution of each sample was used for RT-qPCR

(**figure M.1**). Normalization was performed *versus* the spike-ins controls using the $2^{-\Delta Ct}$ method to obtain linear values of relative quantity and avoid differences in the yield of the protocol. The ratios were then calculated using linear quantities as described (Andreu et al. 2016). The maximum value 1 indicates that the specific microRNA detected in plasma/SN samples is fully encapsulated into EVs; lower values indicate that part of this microRNA is released free in the medium and is lost after EV precipitation.

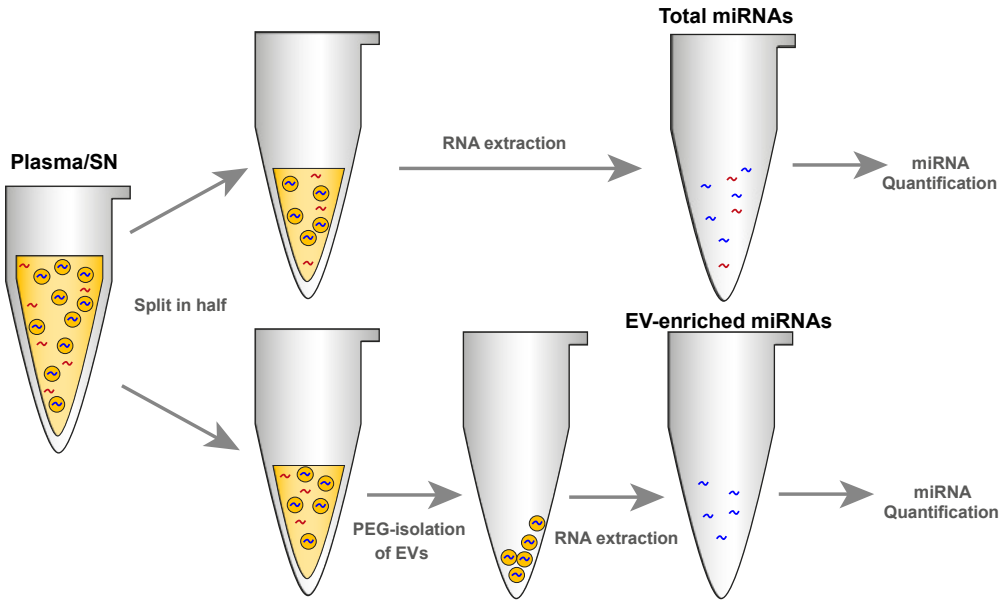

Figure M.1. Protocol for the evaluation of miRNA secretion into EVs. The plasma or supernatant (SN) is split in half and from one half we isolated EVs by precipitation with PEG. Then, RNA is extracted in both fractions and miRNA levels are compared in total SN/Plasma *versus* EV-enriched fractions.

8. miRNA validation and modulation assays

8.1. Cloning of the consensus sequence of mmu-miR-721 in humans

To identify the human homolog of mmu-miR-721, we analyzed qPCR products obtained with the specific probe for mmu-miR-721 against RNA from plasma and PBLs obtained from patients with myocarditis or myocardial infarction or from healthy controls. The products were analyzed using polyacrylamide gel electrophoresis (48% urea 15% acrylamide) with denaturing conditions to assess molecular weight. In order to quantify the intensity of the qPCR product obtained from the amplification with either mmu-miR-721or hsa-miR-Chr8:96 primers, methylene-blue stained bands were measured with Image Studio Lite v.4.0.We pooled qPCR reaction products of plasma from six patients or controls, and the product was purified with the QIAquick PCR Purification Kit (Qiagen). To obtain the sequence of the human homologous mmu-miR-721, the purified product was cloned into the pGEM-T vector (pGEM-T Vector System I A3600 Promega). The vector was transformed in competent bacteria (MAX

Efficiency DH5α Competent Cells, Invitrogen) and 96 clones of those obtained after transformation were sequenced with T7p primer.

8.2. RNA-Co-immunoprecipitation with Argonaute-2

To validate the hsa-miR-Chr8:96 sequence as a human mature miRNA, we cloned a 350 base-pair fragment of chromosome 8, between positions 96405654 and 96406003, containing the putative mature hsa-miR-Chr8:96 sequence in its core:

96406003 CCTTGGAGGG CGCACAATCA CTCAGCTGAT TTGATTTCGT ATACATGTAC GTAGGGCAGG
96405943 GATTCGTTAG AAAACATGTA TTGAGTCTAA TCATTGTGCA TATCACAGAG CTGTTTTTCT
96405883 GCCATATATT GGGGGTTAGG GAAAATGCAG GGGAACTGCT T**TCTTGCAAT TAAAAGGGGG**
96405823 **AA**AAAGTGCT AGGGGCACAT TGCACTACAT CCTAGAGCCT GACCAGAAGA CATCCTCATC
96405763 TTGCTTGTAT CCCTACCCCT CTTGTTCCTC TACTAGCACA AACAAGGCCT CCAAAGCCCA
96405703 CCCAGGACCC TTCCCCTGCA CCAGCACTGC CCTCTAGGAA GGAACTAGGA

To assess the processing of hsa-miRChr8:96 sequence by Argonaute-2 (AGO-2), the 350 base-pair cloned sequence was transiently overexpressed in HEK293T cells and RNA was extracted after co-immunoprecipitation with anti-AGO-2 antibody as follows. A total of 350 nucleotides encompassing the hsa-miRChr8:96 sequence and flanking regions were amplified by PCR with specific primers (Fw: 5′-CCTTGGAGGGCGCACAAT-3′, Rv: 5′-TCCTAGTTCCTTCCTAGAGGGC-3′) from genomic DNA of human PBLs and were inserted into the pCDH-CopGFP vector (System Biosciences). HEK293T cells were transfected with the pCDHCopGFP-hsa-Chr8:96 plasmid (24 µg) using Lipofectamine 2000 (Invitrogen). After 48 h., cells were lysed in 50 mM Tris-HCl, 150 mM NaCl, 5 mM EDTA, 1% NP-40, 1 mM DTT lysis buffer, supplemented with protease inhibitors (Complete Mini, Roche), phosphatase inhibitors (PhosStop, Sigma-Aldrich) and 100 U/ml RNase inhibitors (RNAsin plus Promega). The lysate was split in two, and 5 µg of anti-human AGO-2 antibody (Abcam) were added to one half and 5 µg of IgG1 isotype control to the rest. The mixes were incubated with shaking overnight at 4°C. Thereafter, 30 µl of equilibrated Dynabeads Protein G (Invitrogen) were added to assay/wash buffer (50 mM Tris-HCl, 150 mM NaCl, 5 mM EDTA, 0.1% NP-40, 1 mM DTT) and incubated for additional 4h at 4°C in constant shaking. After five washes, RNA was extracted using the miRNeasy Mini Kit (Qiagen). RT-qPCR analysis for hsa-miR-Chr8:96, hsa-miR-126-3p, and hsa-miR-423-3p was performed as indicated elsewhere. *RNU1A1* was used as an AGO-2-independent endogenous housekeeping control for qPCR analysis. A fraction of Dynabeads Protein G (Invitrogen) incubated with the lysates was analyzed by Western blot against human AGO-2 to examine the co-immunoprecipitation (co-IP) efficiency. Quantitative assessment of protein expression was performed with the Odyssey scanner and analyzed with Image Studio Lite v4.0 Western blot analysis software (Li-Cor).

8.3. Functional validation by luciferase activity assays

To further validate the putative mature hsa-miR-Chr8:96 sequence as a functional miRNA, we cloned a tandem (2-mer) of the reverse complementary sequence into a renilla/firefly luciferase dual reporter vector (Rao et al. 2010) as follows. Two complementary antisense sequences (2-mer) (5′-GGCCGCTTCCCCC TTTTAATTGCAAGACGATTTCCCCCTTTTAATTGCAAGAC-3′, Rv: 5′-TCGAGTCTTGCAATTA AAAGGGGG AAATCGTCTTGCAATTAAAAGGGGGAAGC-3′) of the hsa-miR-Chr8:96 separated by a 4-nucleotide spacer were inserted into the psiCHECK-2 reporter vector (Promega). HEK293T cells were transfected with the reporter plasmid psiCHECK-2-hsa-miR-Chr8:96 or the empty plasmid with Lipofectamine 2000 (Invitrogen) and were incubated for 18 h at 37°C in complete medium. Then 8 x 10^4 transfected cells were plated in a 24-well plate and incubated in 200 µl complete medium supplemented with 50 µl of supernatants from overnight-stimulated human PBLs. For the luminescence activity assay, Dual-Glo Luciferase Assay kit (Promega) was used following the manufacturer's instructions with slight modifications. Briefly, cells were lysed in 100 µl Luciferase lysis buffer. We added 5 µl of extract to 100 µl of Dual-Glo Luciferase reagent at room temperature and firefly luminescence was measured in a Sirius tube luminometer (Berthold). Renilla luminescence was analyzed by adding 100 µL of Dual-Glo Stop-Glo Substrate, incubating for 10 seconds and measuring luminescence in the same tube.

8.4. Overexpression of mmu-miR-721 in $CD4^+$ T cells from EAM mice

Lentiviral vectors expressing the pre-miR-721 (mature miRNA sequence flanked by aprox. 100 bp) were generated by co-transfection of the lentiviral vector pHRSIN/SINBX-pre-mmu-miR-721, with the plasmid 8.9 and plasmid PMD2, by the CaCl2 method. The generated lentiviruses were titrated in Jurkat ATCC cells growing in exponential phase. Since the generated lentiviral vector expresses the GFP, viral titers were determined by FACS. $CD4^+$ T cells were obtained from lymph nodes 6 days after EAM induction with the MyHCα-p. The multiplicity of injection (MOI) 1, MOI 2 and MOI 5 doses were tested to infect 600,000 cells to check a dose dependent overexpression of mmu-miR-721 by qPCR. After extensive washing, cells were cultured over 48h. Cytokine production was assessed by FACS and qPCR, and mRNA target modulation was assessed by qPCR.

8.5. *In vivo* blocking of mmu-miR-721

For the blocking of mmu-miR-721 expression *in vivo,* we use a sponge single-stranded molecule consisting of 4 tandem-repeated reverse complementary mature miR-721 sequence separated by three 4-6 base-pair-long spacer sequences as follows: 5′GGCC GC**TT CCCC CTTT TAAT TGCA CTG**C GAT**T TCCC CCTT TTAA TTGC ACTG** ACCG GT**TT CCCC CTTT TAAT TGCA CTG**T CAC**T TCCC CCTT TTAA TTGC ACTG** C 3′. A scramble sequence encoding a fragment of a recombinant GFP of similar size was used as control.

Reverse complementary mmu-miR-721 sequence: 5' TTCCCCCTTTTAATTGCACTG 3'

Scramble sequence: 5' AGAAGAACGGCATCAAGGTGA 3'

At the time of EAM induction, 50 pM of the sponge-miR-721 or scramble emulsified with the CFA plus MyHCα-p were subcutaneously administered at day 0 and day 7. To determine the inhibition efficiency of mmu-miR-721 and modulation of target mRNAs, some animals per group were sacrificed and axillary and inguinal draining lymph nodes were collected at day 9 for qPCR analysis. Acute EAM was evaluated at day 21.

9. Statistical analyses

For statistical analysis, the normality of the distributions was first evaluated using Shapiro-Wilk's test for mouse experiments and D'Agostino-Pearson's test for patient samples with higher number of samples. If distributions were normal, unpaired Student's *t*-test was used for two-group comparisons and one-way analysis of the variance (ANOVA) with Tukey's *post hoc* test when more than two groups were compared. If distributions were non-normal, Mann-Whitney's U-test was used for the analysis of two groups and Kruskal-Wallis test with Dunn's *post hoc* test for multiple comparisons. When the distributions were non-normal and the two groups of data analyzed were paired, we used Wilcoxon matched-pairs signed rank test. In the kinetic experiments, two-way ANOVA with the Sidak's multiple comparison *post hoc* test or one-way ANOVA with Dunnett's multiple comparisons *post hoc* test were performed. For consecutive variable measures of the same animals, repeated measures correction of the ANOVA was used. Survival curves were compared by long-rank (Mantel-Cox) test. Spearman´s correlation coefficient was used to analyze independence of continuous variables. Association between nominal variables was calculated by Chi-square (χ^2) test. These data analyses were performed with *GraphPad Prism* software (versions 7.0 and 8.0).

To assess the association of $CD69^+$ Treg cells with the development of CHF, multivariate logistic regression analysis was performed adjusting for sex, age, troponins (normalized values), CK and ejection fraction. To assess the association of hsa-miR-Chr8:96 with myocarditis, we performed logistic-regression analyses after adjustment for sex, age, troponin level (normalized value), and ejection fraction with or without the addition of hsa-miR-Chr8:96 as an independent variable. We performed analysis of the receiver-operating characteristic (ROC) curves to evaluate diagnostic performance and DeLong's test for comparisons. We estimated the best cut-off value for each parameter, as the one achieving both a sensitivity and specificity of more than 90% or the value presenting the highest likelihood ratio. Multivariate analyses and DeLong's tests were performed with R statistical software (version 3.6.2).

RESULTS

RESULTS

PART I. Th17 cell-derived mmu-miR-721/hsa-miR-Chr8:96 is a biomarker of myocarditis

1. Differential kinetics of Th17 responses during myocardial damage in acute myocarditis and acute MI

In order to assess T cell responses during myocardial damage we induced either MI by the permanent LAD-ligation or myocarditis with the EAM model in susceptible BALB/c mice (**figure R.1**). We evaluated the kinetics of cardiac injury after induction of each model by measuring serum biomarkers and transthoracic echocardiography. Significant elevation in the levels of cardiac troponin I, creatine kinase MB and lactate dehydrogenase suggests that, myocardial injury peaks around days 21 and 3 after the induction of EAM and MI, respectively (**figures R.1 and R.2A)**. Left-ventricular ejection fraction, as a measure of heart function, drops promptly after LAD-ligation, with a significant reduction of more than 50 % three days after MI. In myocarditis, ejection fraction also declines progressively, reaching a significant decrease at day 21 after EAM induction (**figure R.2B**). These data confirm that the pathophysiological kinetics of these two mouse models differ. In this sense, the acute phase of myocardial injury and dysfunction occurs three days after LAD-ligation and twenty-one days after EAM induction (**figure R.1**).

We next analyzed Th17 cells in peripheral blood of mice during four weeks after EAM induction or LAD-ligation. Th17 cells are virtually absent in blood from healthy mice and peak two weeks after EAM or MI induction (**figure R.2C**), in agreement with the time required for the development of adaptive immune responses. However, whereas Th17 cells is still significantly elevated twenty-one days after EAM induction, this T cell subset remains low or absent at three days after LAD-ligation (**figure R.2C**). Therefore, circulating Th17 cells appear to be characteristic of the acute phase of myocardial injury of EAM (day 21) but not of the acute phase of myocardial injury of MI (day 3) (**figure R.2**).

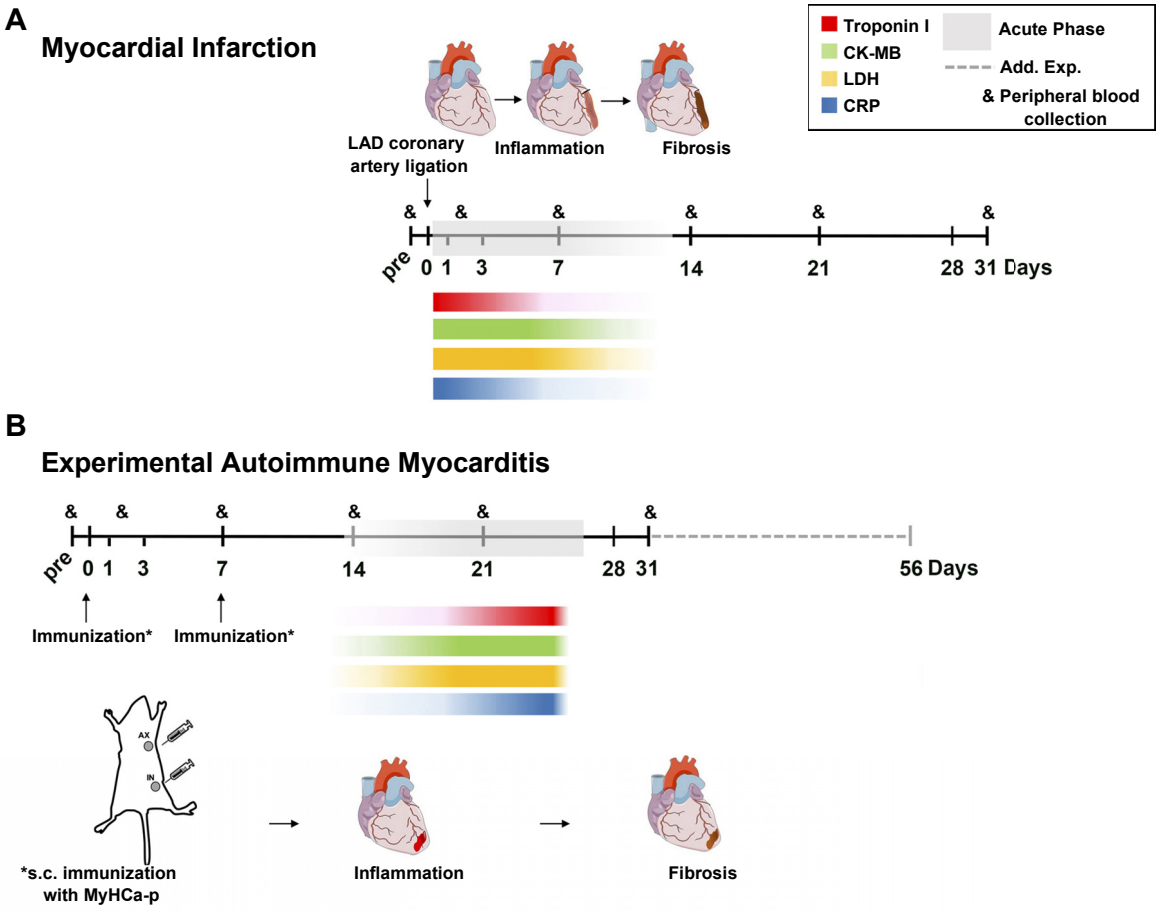

Figure R.1. Schematic view of the myocardial injury kinetics after permanent ligation of the left anterior descending coronary artery (myocardial infarction) and after experimental autoimmune myocarditis. (**A**) Mice were subjected to permanent ligation of the left anterior descending (LAD) coronary artery to induce myocardial infarction. (**B**) Experimental autoimmune myocarditis was induced by two subcutaneous immunizations, one week apart, at the axillary and inguinal regions of mice with a peptide derived from the cardiac alpha-myosin heavy chain (MyHCα-p, residues 614-629) emulsified in complete Freund's adjuvant. (**A-B**) Kinetics of biomarkers of myocardial injury in the serum of mice after myocarditis or myocardial infarction are represented. LDH, lactate dehydrogenase; CK-MB, creatine kinase MB; C-RP, C-reactive protein. Grey shadows depict the time frame of the acute phase of myocardial injury and inflammation in both models (around days 21 for EAM and 3 for MI, respectively). &, Blood samples were collected at the indicated time points. Ad. Exp., additional time of experimental analysis.

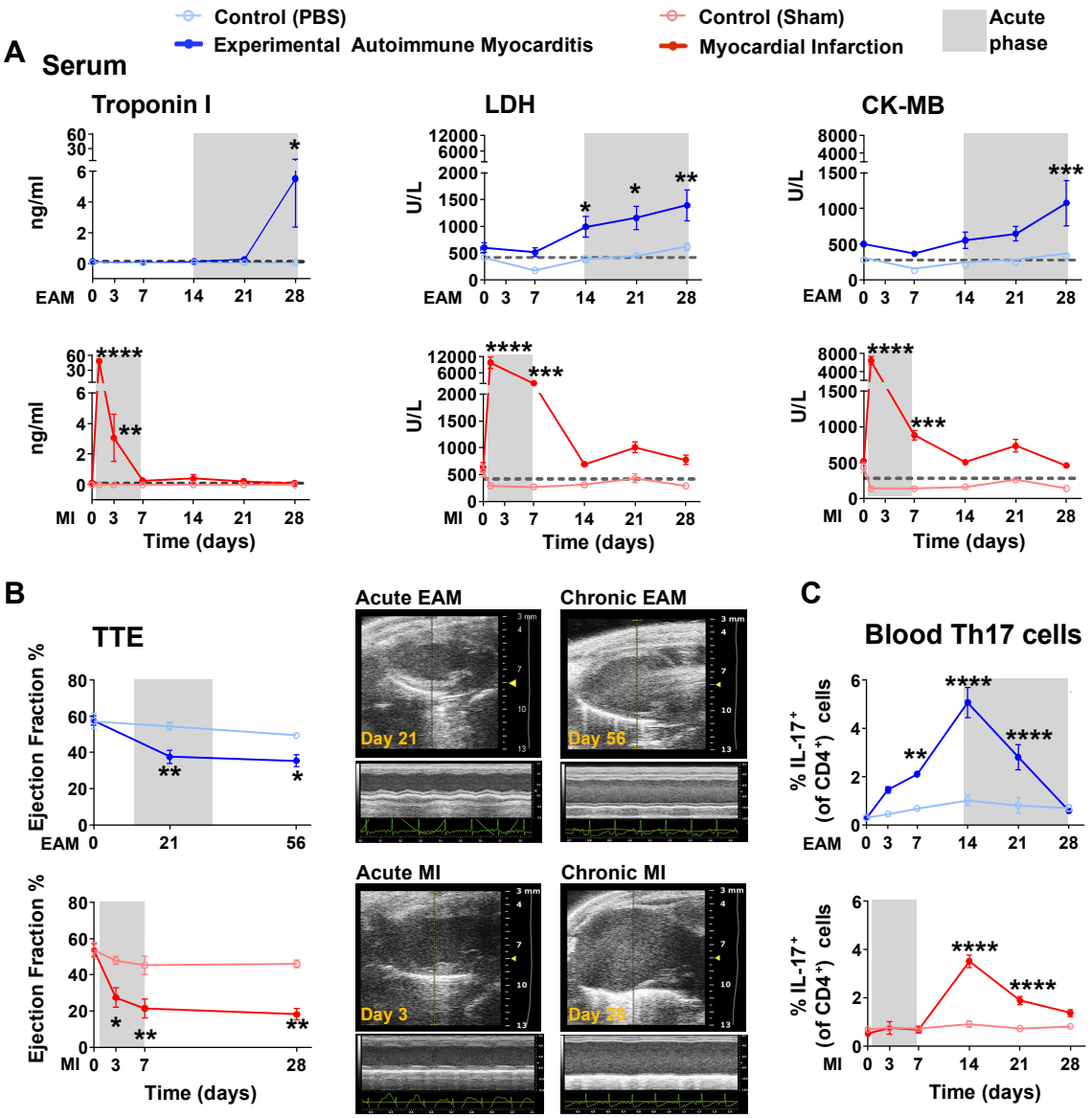

Figure R.2. Circulating Th17 cells coincide with the acute phase of cardiac injury in myocarditis mice. (**A**) Kinetics of biomarkers of myocardial injury (LDH, Lactate dehydrogenase; CK-MB, creatine kinase MB) in the serum of BALB/c mice after induction of EAM (immunization with MyHCα, dark blue) or control mice (immunization with PBS, light blue), and after the induction of MI (LAD-ligation, dark red) or control mice (sham operated, light red). Dashed lines represent basal levels of each biomarker. Two-way ANOVA with Sidak´s multiple comparisons test for EAM and MI *versus* their respective controls. * P< 0.05, ** P< 0.01, *** P< 0.001, **** P< 0.0001. Data are representative of more than 3 independent experiments and errors bars represent the mean ± SEM (n = 3-10 pools of 2 mice each). **(B)** Time course of changes in left ventricular ejection fraction after the induction of EAM or MI, quantified by B-mode transthoracic echocardiography (TTE), n= 4-7 mice per group. Representative TTC images of cardiac function are shown (upper panels, B-mode; lower panels, M-mode and ECG). (**C**) Time course of changes in the percentage of $CD4^{+}IL\text{-}17^{+}$ (Th17) cells in the blood of BALB/c mice after EAM or MI induction (and respective controls), analyzed by FACS; n= 6 mice per group. Data in **B** and **C** are representative of more than 3 independent experiments and errors bars represent the mean ± SEM. Two-way repeated-measures ANOVA (Sidak *post hoc* test). * P< 0.05, ** P< 0.01, **** P< 0.0001.

2. Th17 cell-response is enhanced in acute myocarditis patients

In parallel, we evaluated peripheral T cell responses in 42 patients with acute myocarditis, 90 patients with acute MI (45 STEMI and 45 NSTEMI) and 80 healthy donors (**figure R.3**). Demographic and clinical data are summarized on **table 1.** Comorbidities and etiology of the included myocarditis patients are summarized on **table 2**.

Among patients admitted to hospital with clinically suspected acute myocarditis, symptoms vary in type and severity. However, the most common presentations are typical symptoms indicative of MI (i.e. chest pain, ischemic-like electrocardiographic changes, and elevated troponins/CK values). Three illustrative patients included in the study exemplify this clinical challenge (**figure R.3A-C**). A first myocarditis patient presenting signs and symptoms suggestive of acute MI, but exhibiting non-obstructive epicardial coronary arteries on emergent coronary arteriogram (then classified as MINOCA) (**figure R.3A**). A second MI patient showing acute occlusion of the right coronary artery on an angiogram and inferoapical subendocardial enhancement on CMR images (**figure R.3B**). A third 22 year-old MINOCA patient with an infarct-like presentation whose CMR showed a typical pattern of acute myocarditis, including higher signal intensity on T2-weighted images, matching with increased areas of intramyocardial and subepicardial gadolinium enhancement in the apical septum and inferolateral walls (**figure R.3C).** Echocardiography might be useful for differential diagnosis, but its accuracy for the identification of acute myocarditis is limited, as we can see by the initial depression of the ejection fraction in both acute myocarditis and acute MI patients (**figure R.3D)**.

We collected blood samples during the acute phase of patients with myocarditis or MI at the time of hospital admission. In agreement with the data in mice, circulating Th17 cells are significantly elevated in peripheral blood of patients with acute myocarditis, compared with STEMI/NSTEMI patients and healthy controls (**figure R.3E**). Peripheral Treg cells are also significantly increased in acute myocarditis patients, as well as in STEMI patients, when compared with healthy controls but not when comparing among disease types (**figure R.3F**). Both groups of MI patients show incremented peripheral Th1 cell responses when compared with healthy donors, but this population does not significantly differentiate MI patients form acute myocarditis patients (**figure R.3F**). Increased Th17/Th1 and Th17/Treg ratios in acute myocarditis (**figure R.3G**) further highlight the predominant role of Th17 cells among effector T cell subsets in this heart disease. Therefore, we postulated that Th17 cells present in the blood during acute myocarditis might serve as a potential source of specific circulating markers for myocarditis patients.

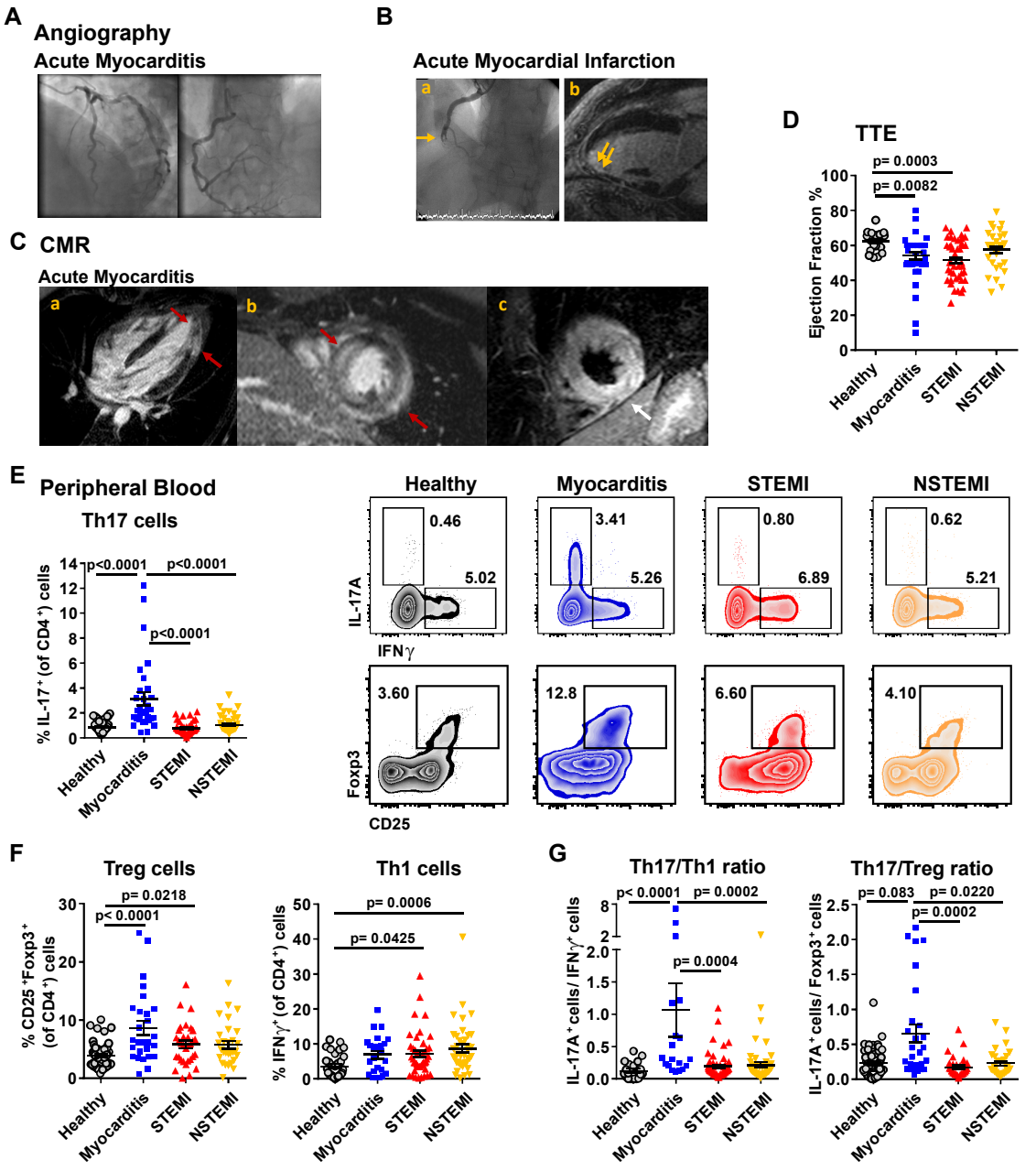

Figure R.3. Enhanced peripheral Th17 response in acute myocarditis patients. (**A**) Arteriogram of an acute myocarditis patient showing no obstruction of coronary arteries. (**B**) Panel *a* shows occlusion of the right coronary artery on angiography and Panel *b* shows subendocardial gadolinium enhancement at the infero-apical wall, consistent with an inferior MI (**C**) CMR imaging shows a MINOCA patient finally diagnosed as acute myocarditis. Panels *a* and *b* show increased areas of intramyocardial and subepicardial late gadolinium enhancement in the apical septum and lateral walls (red arrows), matching with the increased signal intensity areas, indicating regional injury typical of myocarditis. Panel *c*, short-axis T2-weighted spin-echo image with increased signal intensity (white arrow) of the apical septum and infero-lateral walls compared with the contralateral unaffected myocardium. (**D**) Left ventricular ejection fraction of 23 healthy donors and 43 myocarditis patients, 43 STEMI and 35 NSTEMI patients measured by transthoracic echocardiogram (TTE). (**E**) Quantification of $CD4^+IL\text{-}17^+$ (Th17) cells in PBLs from 33 acute myocarditis, 45 STEMI or 41 NSTEMI patients and from 66 healthy controls, analyzed by FACS. Right, representative density plots of Th17, $CD4^+IFN\gamma^+$ (Th1), and $CD4^+CD25^+$ $Foxp3^+$ (Treg) cells in human PBLs. (**F**) Quantification of Th1 and Treg cells in the blood of the above patients. (**G**) Th17/Th1 and Th17/Treg ratios of cell percentages. Data are represented as means ± SEM of each group and were analyzed by Kruskal-Wallis with Dunn´s *post hoc* test.

3. Mmu-miR-721 is selectively synthetized by Th17 cells during myocarditis

The discovery of miRNA candidates in different forms of CVDs have suggested that the release of some circulating miRNAs is a nonspecific indicator of cardiac damage and that the determination of the cellular source is crucial to exploit their clinical use (Li et al. 2017; Nie et al. 2020; Ding et al. 2020; Marketou et al. 2021; Obradovic et al. 2021). Unlike these previous studies, we investigated the expression of miRNAs synthetized by Th17 cells, as this cell subset appears specifically in the blood during acute myocarditis. With the aim of finding miRNAs derived from antigen-specific Th17 cells (Th17ag-sp), we used cells from transgenic OTII mice that exhibit TCR specificity for ovalbumin antigen (Barnden et al. 1998). We performed a comparative miRNA screening of activated $CD4^+$ T cells, polyclonal Th17 cells, and cultures enriched with Th17ag-sp cells or Th17ag-sp sorted cells (**figure R.4A)**. Microarray analysis identified 27 miRNAs overrepresented in both Th17ag-sp cultures and Th17ag-sp sorted cells (**figure R.4B and annex table A.1**).

Next, we compared the expression of those 27 miRNAs, specific of Th17ag-sp cells, in Th17ag-sp sorted from *Cd69*$^{-/-}$ mice, in which a severe form of EAM develops (Cruz-Adalia et al. 2010), with Th17ag-sp obtained from wild type mice. This analysis showed mmu-miR-721 and mmu-miR-483-5p as the strongest upregulated miRNAs in *Cd69*$^{-/-}$ Th17ag-sp cells (**figure R.4C and annex table A.2**) Analysis by qPCR of mmu-miR-721 and mmu-miR-483-5p expression in sorted $CD4^+$ T cells and *in vitro* differentiated antigen-specific Th17 cells and Treg cells from OTII mice, validated mmu-miR-721 as specifically overexpressed in antigen-specific Th17 cells (**figure R.4D)**. *Ingenuity* pathway analysis identified roles of the selected miRNAs in T cell homeostasis and differentiation (**figure R.4E**) and revealed validated target genes of interest related to Th17 cells such as *Pparg*, *Nos2*, *Stat1*, *Stat3*, *Socs3, Foxo1, Tgfb1* and *Cd69* (**figure R.4C**).

To assess the differential expression of these miRNAs by T cells in the pathophysiological context of myocarditis and MI, we analyzed miRNA profiles in sorted $CD4^+$ T cells isolated from draining lymph nodes 6 days after the induction of EAM ($CD4^{EAM}$) and 3 days after MI ($CD4^{MI}$) (**figure R.5A**). We analyzed these time points as they are the time when T cell responses are generated in these models. $CD4^{EAM}$ cells were isolated from axillary and inguinal lymph nodes, as they are the closest ones to the sites of MyHCα-p immunization. $CD4^{MI}$ were isolated from heart-draining mediastinal lymph nodes, were the T cell response is developed after LAD-ligation. The analysis by miRNA-microarray revealed that the two miRNAs with the highest expression in Th17ag-sp cells from *Cd69*$^{-/-}$ mice, namely, mmu-miR-721 and mmu-miR-483-5p, were overexpressed in $CD4^{EAM}$ when compared with $CD4^{MI}$ cells (**figure R.5B and R.5C and annex table A.3**), indicating their specificity for myocarditis-related $CD4^+$ T cells. Expression analysis by qPCR in different sorted $CD4^+$ T cell subsets from EAM/PBS-induced mice (**figure R.5D**) and MI mice (**figure R.5A**) confirmed that mmu-miR-721 is preferentially synthetized by myocarditis-specific Th17 cells (**figure R.5E**).

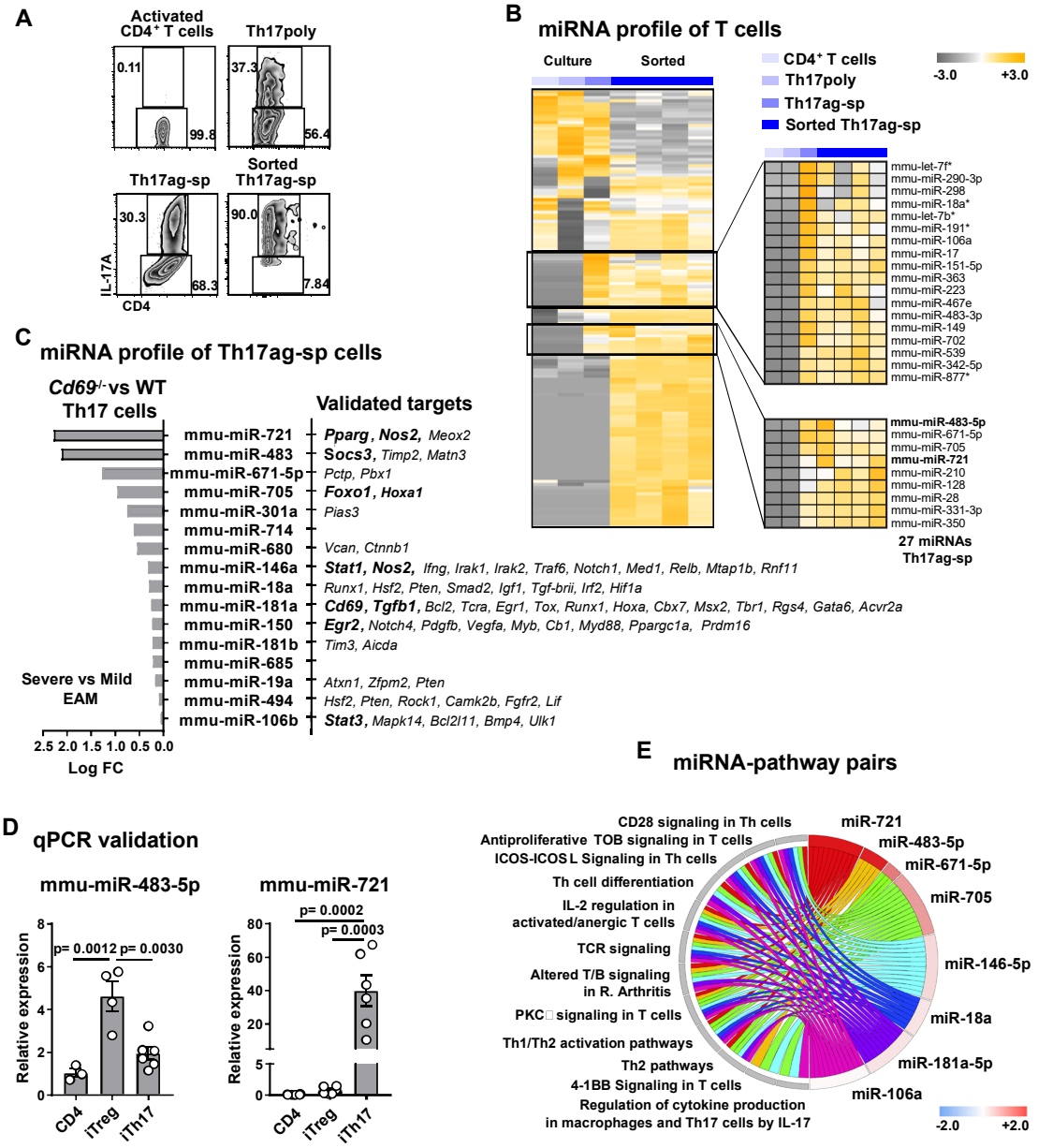

Figure R.4. Antigen-specific Th17 cells synthesize mmu-miR-721 *in vitro*. (**A**) Representative density plots of CD4$^+$ T cells activated for 48h with anti-CD3/anti-CD28 mAbs, polyclonally differentiated Th17 (Th17poly) cells or ovalbumin antigen-specific cultured or sorted Th17 cells (Th17ag-sp), used for the microRNA expression analysis by microarray. (**B**) Heat map represents unsupervised hierarchical clustering for the commonly expressed miRNAs analyzed by miRNA-microarray in the populations shown in **A** (n= 4). All data were median normalized by miRNAs and the color scale indicates the relative expression of each miRNA. Gate includes 27 miRNAs overexpressed by Th17ag-sp cells (magnified on the right). (**C**) Th17ag-sp miRNAs in **B** were analyzed by microarray between sorted Th17ag-sp from *Cd69*$^{-/-}$ (severe EAM) *versus* sorted Th17ag-sp from wild type (EAM) mice. Differentially expressed miRNAs are shown together with a list of their experimentally validated targets. In bold, targets involved in Th17 cell biology. (**D**) Mmu-miR-483-5p and mmu-miR-721 relative expression in naïve CD4$^+$ T cells and cultures of *in vitro* differentiated Th17 cells (iTh17) and Treg cells (iTreg) analyzed by qPCR (n= 3-6). One-way ANOVA with Tukey's *post hoc* test. (**E**) Chord diagram of miRNAs – pathways pairs. Color scale indicates miRNAs logFC in *Cd69*$^{-/-}$ *versus* wild type Th17ag-sp.

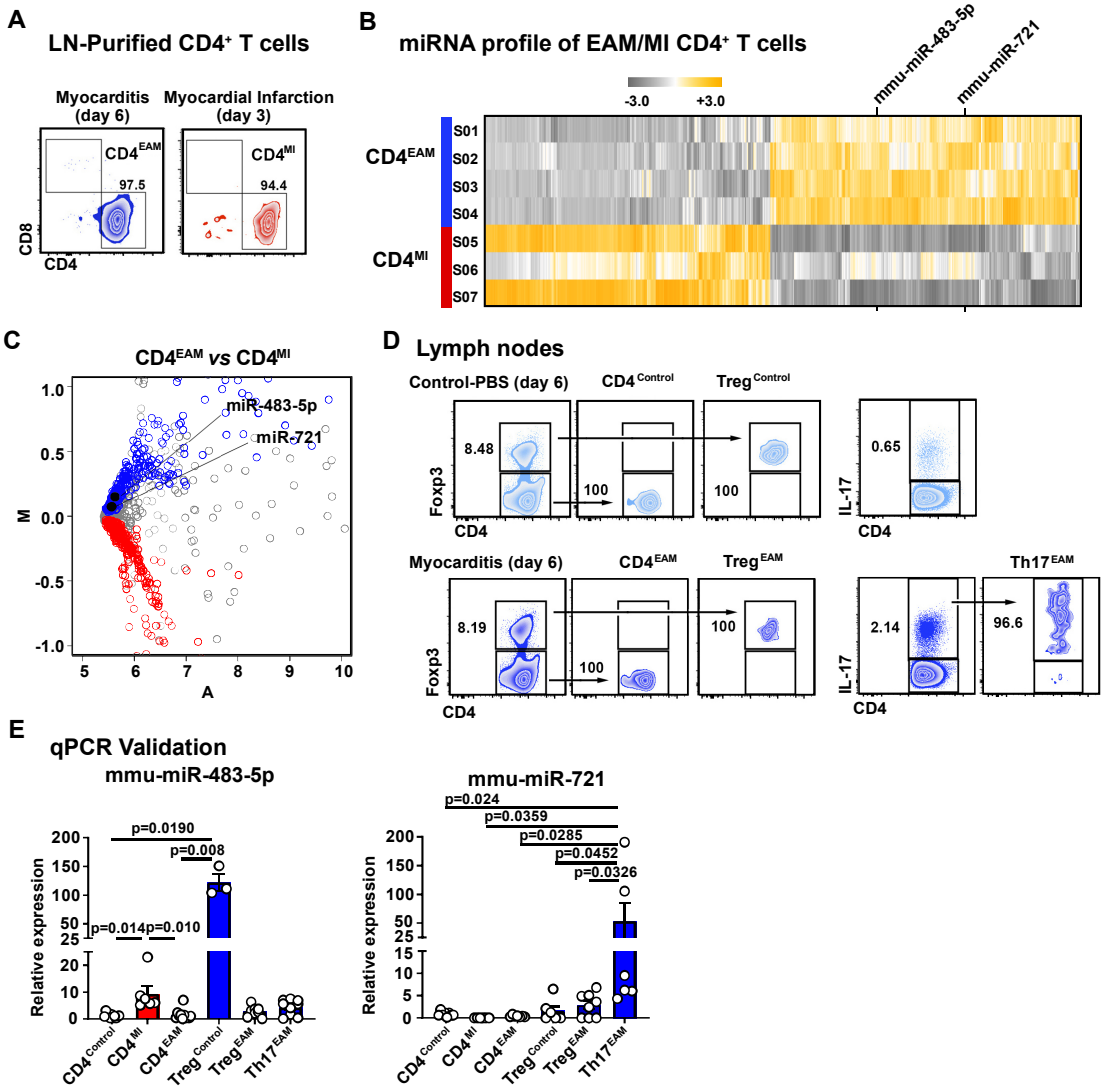

Figure R.5. Th17 cells synthesize mmu-miR-721 during myocarditis. (**A**) Purity of CD4^{+} T cells used for miRNA microarray analysis, obtained from BALB/c axillary lymph nodes, 6 days after experimental autoimmune myocarditis induction (CD4^{EAM}), or from mediastinal lymph nodes, 3 days after myocardial infarction (CD4^{MI}). (**B**) Heat map for the differentially expressed miRNAs with significant expression variance between CD4^{EAM} (n= 4) and CD4^{MI} (n= 3, each sample is a pool of 2 mice). Color scale indicates relative expression after normalization by the median of each miRNA. miRNAs of interest are highlighted. (**C**) The MA plot indicates the average expression (A) *versus* the $\log_2$ of the mean difference (M) of miRNAs detected in the microarray. In blue, miRNAs significantly overrepresented in CD4^{EAM} cells with adjusted p-value <0.1; in red, miRNAs significantly overrepresented in CD4^{MI} cells; in grey, miRNAs with adjusted p-value >0.1. (**D**) Sorting strategy of T cells from axillary lymph nodes from BALB/c mice 6 days after EAM induction or immunization with PBS (as controls) for miRNA validation by qPCR. (**E**) Relative expression of mmu-miR-483-5p and mmu-miR-721 by qPCR in sorted T cell subsets as in **A**-**D**. Histograms and error bars indicate the mean ± SEM. Data from three independent sorting experiments. P-values were calculated by one-way ANOVA with Tukey's *post hoc* test for mmu-miR-721 (n= 5-7 pools of 2 mice each) and non-parametric Kruskal-Wallis with Dunn's *post hoc* test for mmu-miR-483-5p (n= 3-7 pools of 2 mice each).

4. Mmu-miR-721 inhibits *Pparg*, enhancing RORγt, Th17 responses and EAM

In order to determine the role of mmu-miR-721 in Th17 cell differentiation during myocarditis, we overexpressed this miRNA in $CD4^+$ T cells from draining lymph nodes 6 days after EAM with the use of lentiviral transduction. We designed lentiviral vectors encoding primary (pri)-miR-721 (**figure R.6A**), and confirmed overexpression of the miRNA by real-time PCR in $CD4^+$ T cells isolated from EAM mice (**figure R.6B and R.6C**). Overexpression of mmu-miR-721 results in enhancement of IL-17 production at the protein and mRNA levels (**figure R.6D and R.6E**). It has been previously reported that *Pparg* is a direct target of mmu-miR-721 (Ke et al. 2017). PPARγ is a nuclear receptor that negatively regulates Th17 cell differentiation by repressing *Rorc* induction (Klotz et al. 2009), a master transcription factor of Th17 cells (Ivanov et al. 2006). For clarification of the terminology, *Rorc* refers to the gene/mRNA and RORγt refers to the protein counterpart of the retinoic-acid-related orphan receptor that drives Th17 differentiation and function. Hence, to understand how mmu-miR-721 regulates Th17 cell function, we analyzed the expression of *Pparg* and *Rorc* at the mRNA level after miRNA overexpression. We confirmed the effective reduction of *Pparg* in EAM-derived $CD4^+$ T cells after mmu-miR-721 overexpression with lentiviral vectors (**figure R.6D**). In parallel, we observe increased levels of *Rorc* mRNA (**figures R.6E**) and RORγt protein (**figure R.6F**). These data suggest a direct role of mmu-miR-721 in Th17 cell responses during myocarditis development through the control of *Pparg*/*Rorc* axis.

Since mmu-miR-721 controls myocarditis-induced Th17 responses, we next aimed to ascertain whether the functional blockade of this miRNA has an implication in the progression of the disease. For this purpose, we designed a sponge molecule with 4 tandem-repeated reverse complementary sequences of the mature mmu-miR-721 separated by spacers, namely, random sequences, that is able to block and inhibit the miRNA (miR-721-sponge, **figure R.7A)**. EAM was induced in BALB/c by subcutaneous immunization with the MyHCα–p along with either the miR-721-sponge or a scramble sequence of similar size as a control. Analysis by qPCR confirmed mmu-miR-721 downregulation (**figure R.7B**) and overexpression of its target *Pparg* (**figure R.7C**) in draining lymph nodes from the sites of injection in the presence of the miR-721-sponge. Heart inflammation and function was assessed twenty-one days after EAM induction, during the acute phase of myocarditis. Mice treated with the miR-721-sponge exhibit reduced of heart inflammation, measured by a reduction in the number of heart-infiltrating leukocytes (**figure R.7D**). Decreased inflammation is accompanied by improved heart-to-body weight ratio (**figure R.7E**) and left ventricular function analyzed by echocardiography (**figure R.7F**), suggesting an overall reduction in myocardial disease. Furthermore, the recruitment of heart-infiltrating $CD4^+$ T cells expressing RORγt and IL-17A is significantly inhibited in mice treated the miR-721-sponge (**figure R.7G**). Thus, the functional blockade of mmu-miR-721 protects against the development of myocarditis by inhibiting Th17 responses.

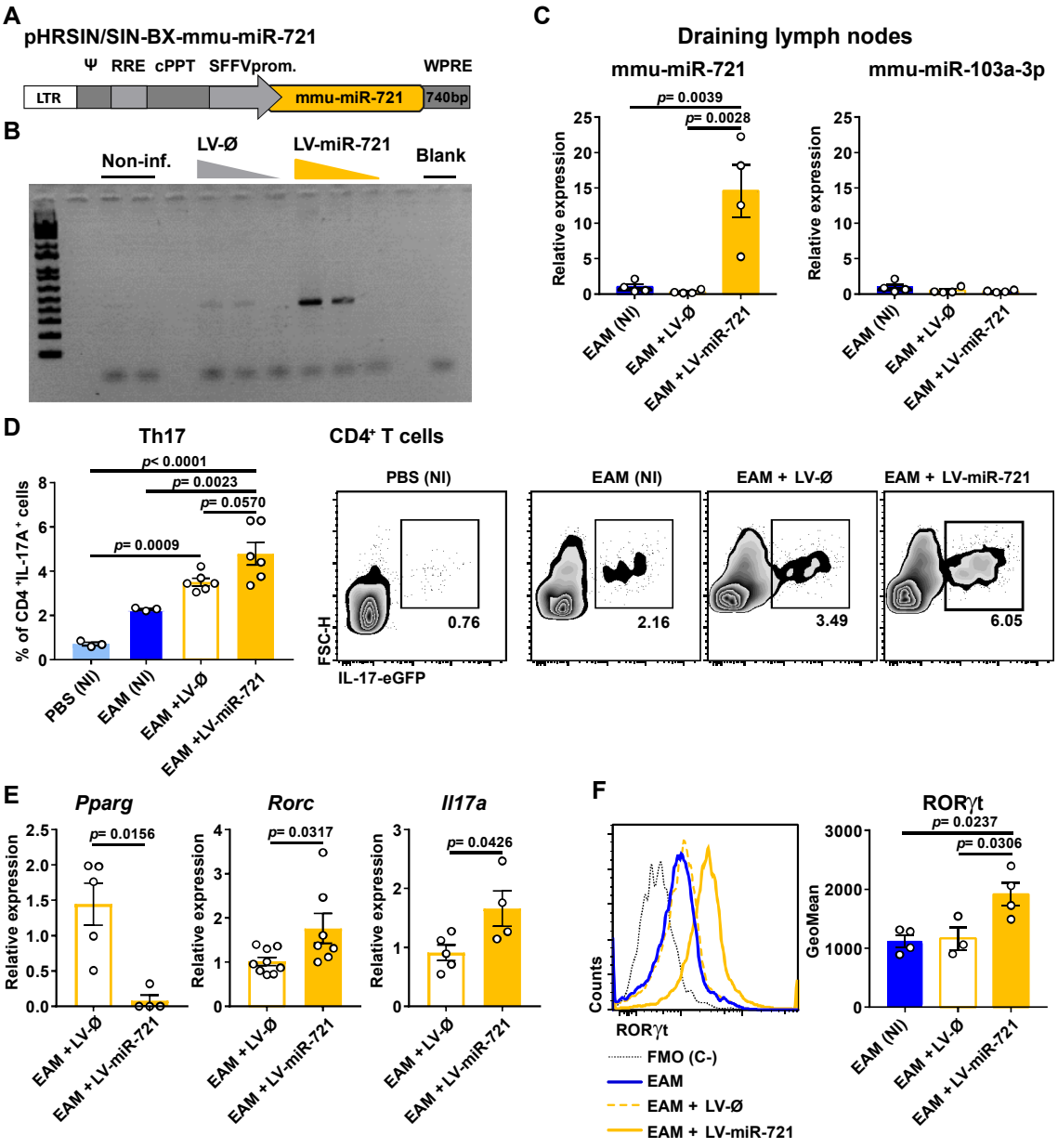

Figure R.6. Overexpression of mmu-miR-721 enhances Th17 responses in EAM. (**A**) Schematic representation of the lentiviral vector generated for the overexpression of mmu-miR-721. LTR, 5´long terminal repeat; Sequence Ψ, packaging sequence; cPPT, central sequence Polypurine Tract; SFFV, lentiviral promoter; WPRE (Woodchuck hepatitis virus (WHP) Posttranscriptional regulatory element; mmu-miR-721, sequence of 399 bp containing the sequence of the mmu-pre-miR-721. (**B**) PCR analysis of mmu-miR-721 expression in non-infected EAM-isolated CD4$^+$ T cells or after infection with lentiviral vectors expressing miR-721 (LV-miR-721) or empty vectors (LV-Ø) at MOI 5, MOI 2 and MOI 1. (**C**) Analysis of mmu-miR-721 and control mmu-miR-103a-3p expression after infection with MOI 5. *Rnu1a1* small nuclear RNA was used as normalizer for qPCR. (**D**) Lymph nodes were collected after EAM/PBS-control induction and infected with LV-Ø or LV-miR-721 (MOI 5). Quantification ± SEM and representative density plots of Th17 cells after infection. (**E**) Analysis of *Pparg*, *Rorc* and *Il17a* mRNA levels by qPCR in sorted CD4$^+$ T cells from LV-infected EAM-lymph nodes. (**F**) RORγt expression in CD4$^+$ T cells as above analyzed by FACS. FMO (fluorescence minus one) indicates negative staining control. Data from one representative out of three independent experiments (n=4-6). In **C, D** and **F**, one-way ANOVA with Tukey's *post hoc* test. In **E**, unpaired *t*-test (*Rorc* and *Il17*) or Mann-Whitney U test for non-normal distributions (*Pparg*).

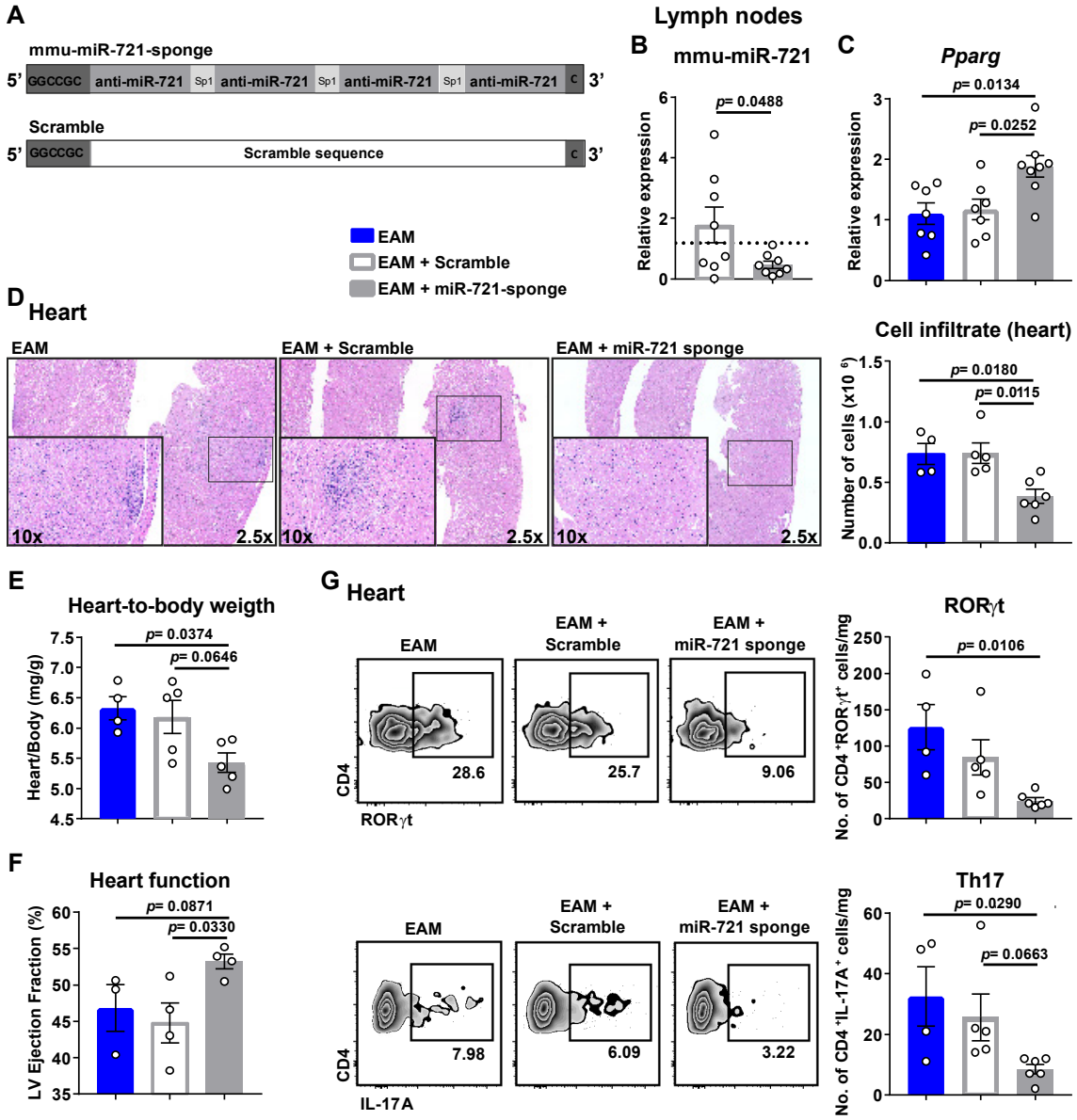

Figure R.7. Blockade of mmu-miR-721 ameliorates EAM development *in vivo*. (**A**) Schematic view of mmu-miR-721 sponge molecule (miR-721-sponge) for silencing mmu-miR-721. Anti-miR-721, reverse complementary sequence of the mature mmu-miR-721; SP1-3, random spacer sequences of 4-6 nt. A scramble non-complementary nucleotide sequence of the same size was used as control. (**B**) Blocking efficiency of miR-721 and (**C**) relative expression of *Pparg* mRNA in axillary and inguinal draining lymph nodes at day 9 after EAM induction (n= 8). In **B**, dotted line represent the levels of the miRNA in non-infected cells. (**D**) Representative H&E staining of heart sections 21 days after EAM. Cell infiltrate indicates the number of heart-infiltrating leukocytes per heart (n= 4-6). (**E**) Ratio of heart weight (mg) to body weight (g) (n= 4-6). (**F**) Left ventricular (LV) ejection fraction as a measure of heart function, assessed by transthoracic echocardiography (n= 4). (**G**) Representative density plots and percentages of RORγt$^+$ and IL-17$^+$ heart-infiltrating CD4$^+$ T cells 21 days after EAM. Cell numbers per mg of heart tissue are quantified (n= 4-6). Data are represented as means ± SEM. One representative out of two independent experiments. Data in **B** were analyzed by unpaired *t*-test. In **C-G**, one-way ANOVA with Tukey's *post hoc* test or Kruskal-Wallis with Dunn's *post hoc* test when non-normal distributions.

5. Mmu-miR-721 is detected in plasma from mice with autoimmune and viral myocarditis

As Th17 cells circulate in peripheral blood during acute myocarditis, we next examined the expression of circulating mmu-miR-721 in plasma from myocarditis and MI mice, to test its potential as a non-invasive biomarker. Analysis of miRNAs levels by qPCR in plasma revealed an upregulation of miR-721 in the acute phase of EAM mice when compared with PBS-induced control mice. This upregulation is not detected in mice during acute MI when compared with sham-operated control mice. The highest mmu-miR-483-5p expression coincides with the acute phase of MI, although without reaching statistical significance (**figure R.8A**).

In addition, we analyzed the levels of these two miRNAs in circulation of EAM-induced *Cd69*$^{-/-}$ mice that develop a severe form of the disease (Cruz-Adalia et al. 2010). The relative expression of circulating mmu-miR-721, but not mmu-miR-483-5p, increases more prominently in *Cd69*$^{-/-}$ mice than in wild type mice during EAM (**figure R.8B**), suggesting a correlation with disease severity.

During EAM progression, the time course of rise and fall of circulating mmu-miR-721 in plasma coincides with that of circulating Th17 cells, confirming their concomitant existence in blood during the development of myocarditis (**figure R.8C**).

Viral infections are within the main causes of myocarditis (Pollack et al. 2015) so we analyzed the miRNA levels in a murine model of viral myocarditis induced by infection with coxsackievirus B3 (CVB3). Circulating mmu-miR-721 levels in the plasma of mice 10 days post infection with CVB3 (the time point of acute heart inflammation in this model) (Myers et al. 2013) are significantly higher than in control mice (**figure R.8D**). This data highlight a specificity of mmu-miR-721 for myocarditis of different origins, advocating for a diagnostic potential of this miRNA.

Remarkably, mmu-miR-721 upregulation was higher in CVB3-infected C57BL/6 mice, in which severe heart inflammation develops, than in BALB/c mice, in which mild inflammation develops (**figure R.8D and R.8E**). Mmu-miR-721 detection in plasma is higher in the most susceptible mouse models of autoimmune myocarditis (*Cd69*$^{-/-}$) and viral myocarditis (C57BL/6), suggesting a possible prognostic value of this miRNA.

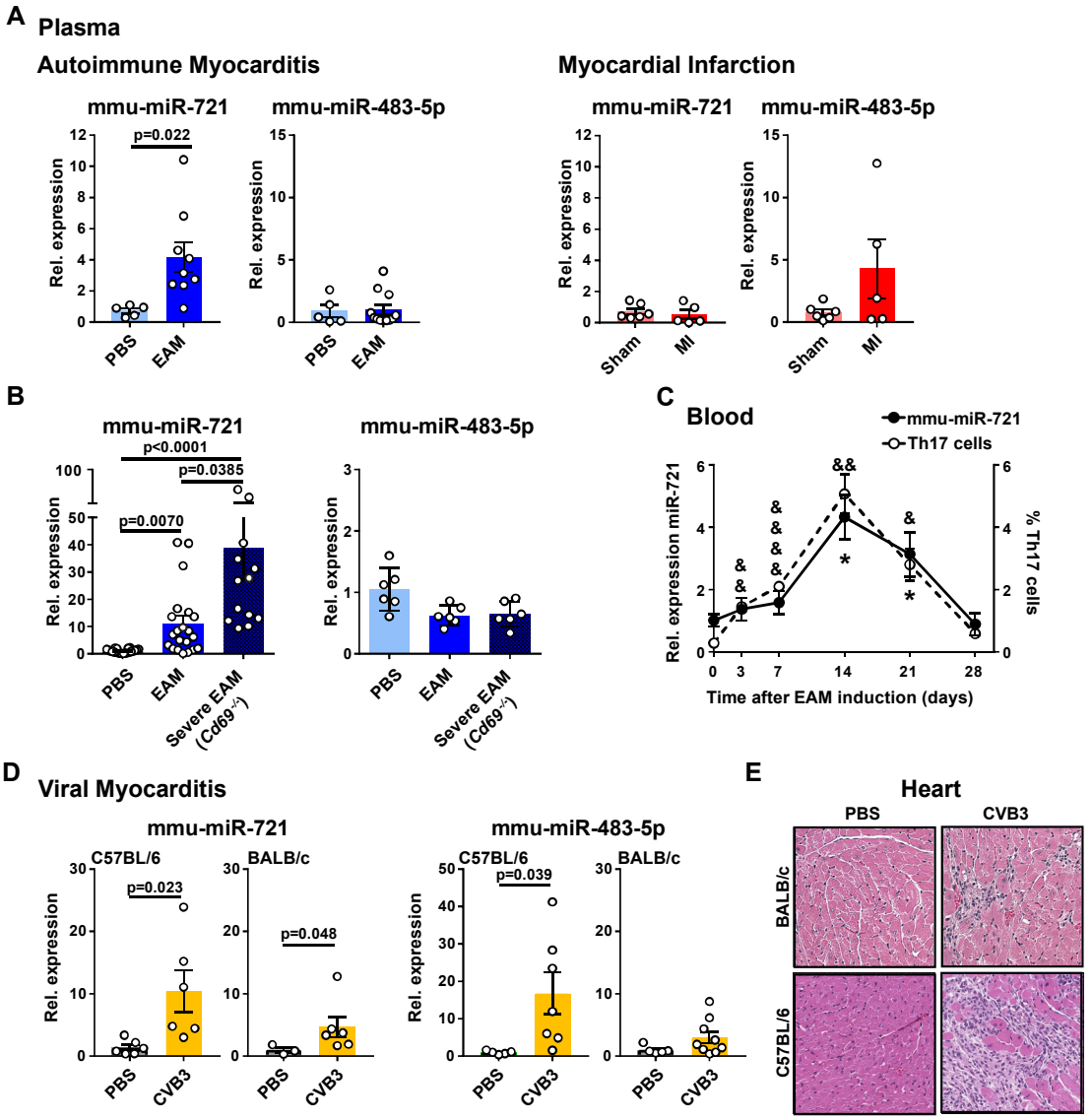

Figure R.8. Mmu-miR-721 is upregulated in the plasma of autoimmune and viral myocarditis mice. (**A**) Expression of mmu-miR-721 and mmu-miR-483-5p analyzed by qPCR in plasma from BALB/c mice twenty-one days after immunization with MyHCα-p (EAM) or with PBS (control), or three days after the LAD-ligation (MI) or sham-operated mice (control). Data are represented as means ± SEM from one representative out of three independent experiments (n= 5-9 mice per group). Unpaired *t*-test. (**B**) Relative expression of mmu-miR-721 and mmu-miR-483-5p in serum from mice developing severe myocarditis (*Cd69*$^{-/-}$ BALB/c) moderate myocarditis (wild type BALB/c) and PBS-control mice (n= 6-21 mice per group), analyzed by qPCR. Histograms and error bars indicate the mean ± SEM. One-way ANOVA with Tukey's *post hoc* test. (**C**) Relative expression of mmu-miR-721 and percentage of Th17 cells in peripheral blood analyzed by qPCR and flow cytometry, respectively from mice at different time points after EAM induction (n= 6 mice). Error bars show SEM. One-way repeated-measures ANOVA with Dunnett´s multiple-comparison test between values at day 3 to 28 *versus* day 0 after EAM induction. *mmu-miR-721, $^{\&}$ Th17 cells, analyzed independently. */$^{\&}$ P <0.05, $^{\&\&}$ P <0.01, $^{\&\&\&\&}$ P <0.0001. (**D**) Circulating miRNA levels were assessed by qPCR during viral myocarditis, 10 days after infection with coxsackievirus B3 (CVB3). Expression in BALB/c and C57BL/6 mouse strains was analyzed in parallel with uninfected control groups (n= 5-7 mice per group). Data represented as means ± SEM were analyzed by unpaired t-test (C57BL/6) and Mann-Whitney U test (BALB/c). (**E**) Representative H&E staining of heart sections of mice 10 days post CVB3 infection and control mice (10x magnification).

6. Mmu-miR-721 is secreted by Th17 cells protected into extracellular vesicles during EAM

Circulating miRNA species in plasma are typically protected from ribonuclease degradation by encapsulation into EVs. The sequence of mature miRNAs have been postulated to predict their predisposition to be sorted EVs. For instance, guanine-rich sequences (Momose et al. 2016) and particular 3' end motifs, also called EXOmotifs, such as the GGNG (in which the N can be equally A, C or G indistinctly) (Villarroya-Beltri et al. 2013), are predominant features of EV-miRNAs. The 3´ end positions of mmu-miR-721 and mmu-miR-483-5p sequences contain the previously described EXOmotif and polyG sequences (**figure R.9A**).

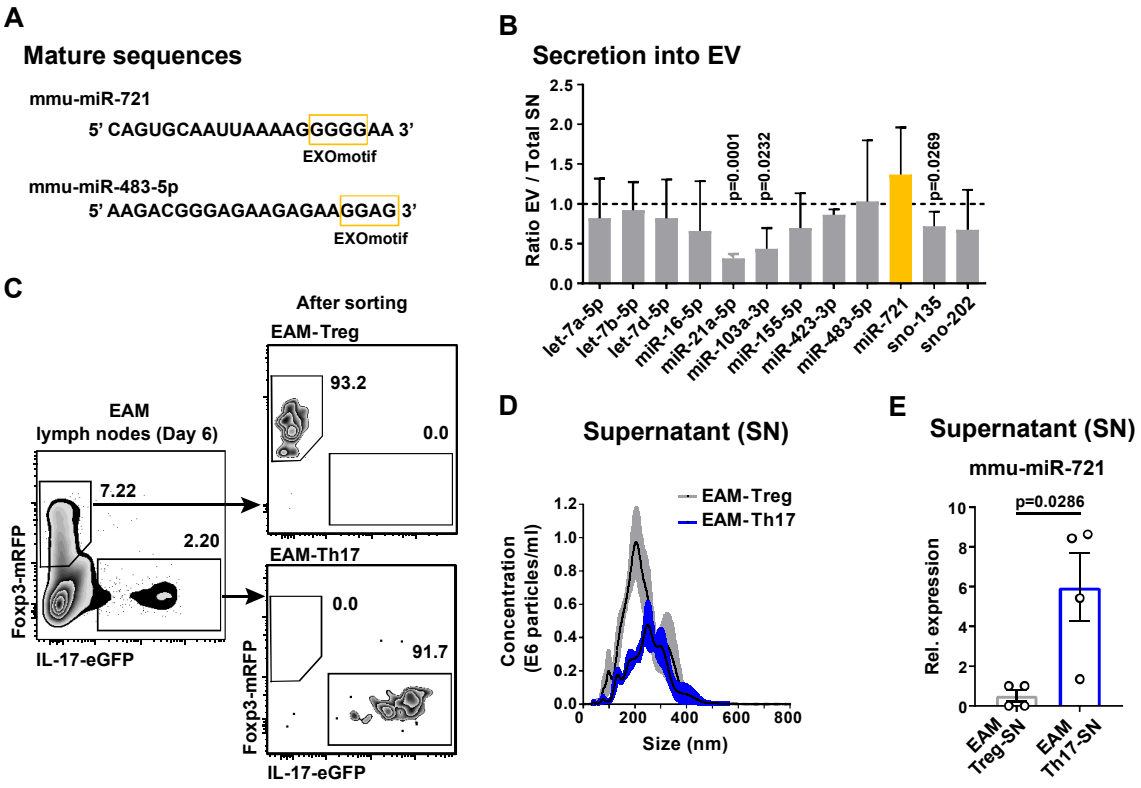

Figure R.9. Th17 cells secrete mmu-miR-721 into extracellular vesicles. (**A**) Mature sequences of mmu-miR-721 and mmu-miR-483-5p, EXOmotifs in yellow. (**B**) Lymph nodes from EAM mice six days after immunization were cultured 48 hours with MyHCα-p. Ratio between the relative expression of miRNAs in PEG-isolated EVs from supernatants (SN) *versus* total SN, calculated after correction for the yield of the extraction using UniSp5 spike-in control (n= 6-10). Dotted line indicate ratio =1. Data pooled from 3 independent experiments. Means ± SEM are represented and analyzed against a hypothetical value 1 by one-sample *t*-test. (**C**) Th17 and Treg cell sorting strategy from EAM lymph nodes. (**D**) Distribution of EV concentration *vs* EV size in the supernatant of these cells, analyzed by *Nanosight*. Black lines indicate the mean and shadows depict the SEM. (**E**) Mmu-miR-721 relative expression in SN-isolated EVs from sorted Th17 and Treg cells after 48 hours culture (n=4 of 6 pooled mice). Mann-Whitney U test.

To determine the potential of the selected miRNAs to be exported into EVs, we cultured draining lymph nodes for 48h, collected from the site of immunization with MyHCα-p six days after EAM induction, and isolated EVs from supernatants (SN) by precipitation with polyethylene glycol (PEG) (Andreu et al. 2016). Both mmu-miR-721 and mmu-miR-483-5p were indeed detected in total SN as well as in EV-enriched fractions. We compared the levels of the selected miRNAs in EVs isolated from the supernatant and in total supernatants (**figure M.1**). For both mmu-miR-721 and mmu-miR-483-5p their ratios of relative quantity between EVs and total SN can be considered equal to 1. Hereby, the quantity that we detect of these miRNAs in total SNs is equal to what we detect in EV-enriched fractions, unlike other miRNAs released free into the SN whose EV/total SN ratio is <1. These data indicate that mmu-miR-721 and mmu-miR-483-5p are preferentially secreted into EVs (**figure R.9B**).

Next, we cultured sorted Th17 and Treg cells from EAM mice for 48h (**figure R.9C**) and analyzed the features of the EVs secreted by both cell subsets (**figure R.9D**). The analysis of miRNAs in the SN of these cultured cell types revealed that mmu-miR-721 is released mainly by Th17 cells in the context of myocarditis (**figure R.9E**).

In addition, we evaluated the miRNA levels in plasma-derived EVs. Mmu-miR-721 is significantly overrepresented in plasma-EVs of mice during acute EAM but not during acute MI (**figure R.10**), supporting that this putative circulating biomarker for myocarditis is protected into plasma EVs.

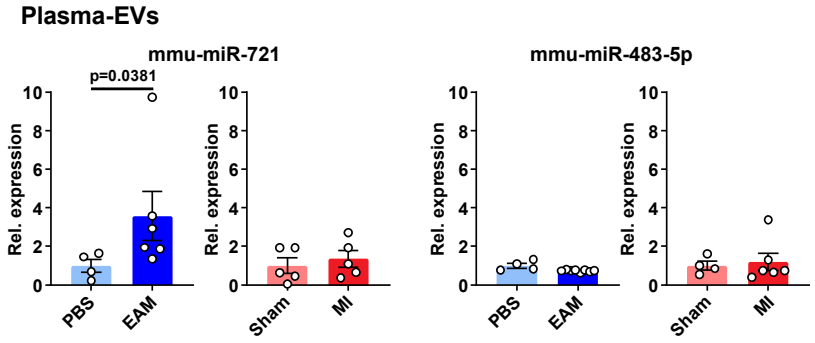

Figure R.10. Mmu-miR-721 is upregulated in plasma EVs of acute myocarditis mice. Quantification of mmu-miR-721 and mmu-miR-483-5p by qPCR in PEG-isolated extracellular vesicles from acute EAM (day 21) and acute MI (day 3) mice, compared with respective controls. Data represent means ± SEM and were analyzed by Mann-Whitney U test.

7. Identification and cloning of the miR-721 human homolog

The human miRNA homolog has neither been identified nor validated (Wheeler et al. 2006) so we screened the genome of human and other mammalian species for homologous sequences to mmu-miR-721 (**figure R.11A**). *In silico* analysis of conserved nucleotides showed that the mature murine miRNA,

as well as regions probably involved in the folding of the miRNA precursor, were highly conserved in *Homo sapiens* and in other mammalians such as *Macaca mulatta* and *Sus scrofa* (**figure R11.A**).

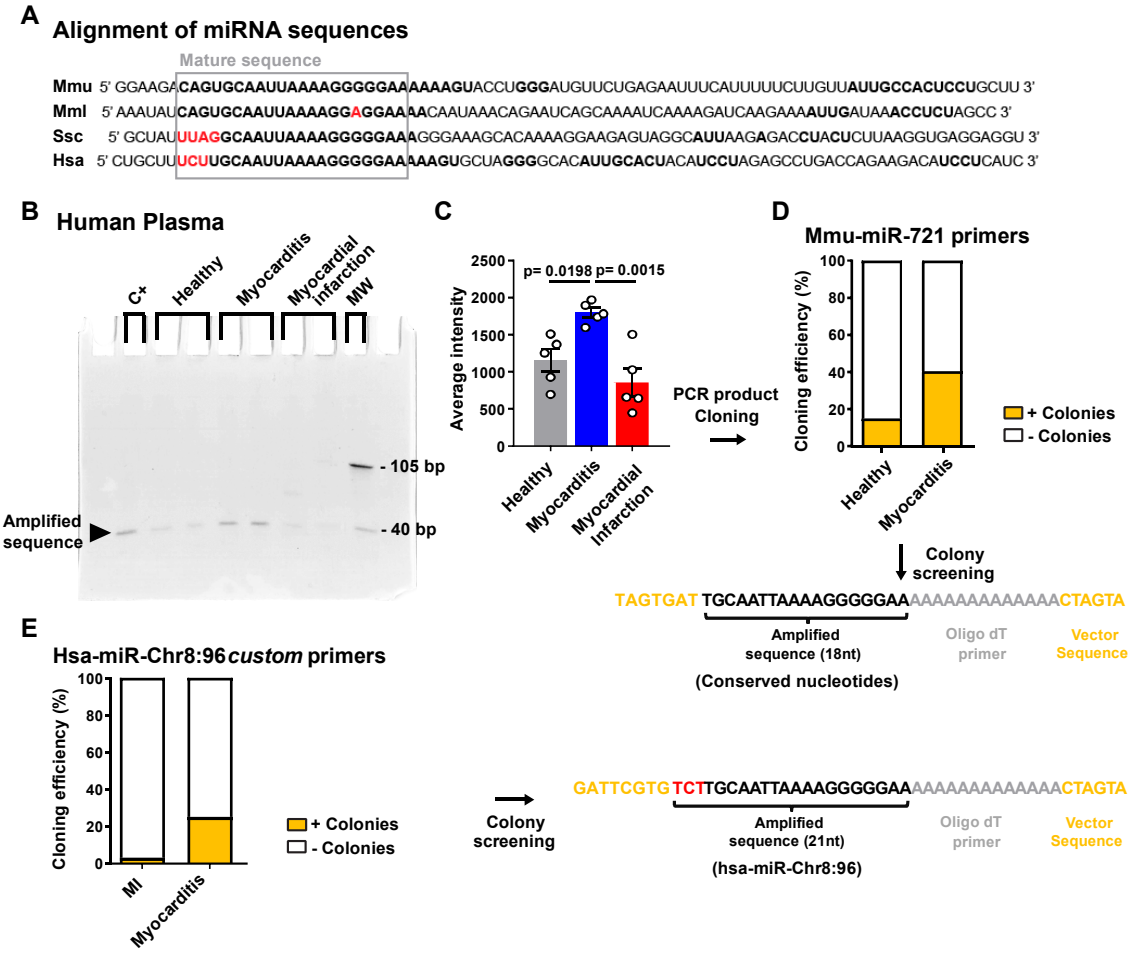

Figure R.11. Cloning of a consensus human RNA sequence to the mmu-miR-721 in plasma from myocarditis patients. (**A**) The grey square delineates the sequence of the mature *Mus musculus* mmu-miR-721, aligned with the consensus sequences from *Macaca mulatta* (Mml), *Sus scrofa* (Ssc) and *Homo sapiens* (Hsa). Conserved nucleotides are shown in black-bold and non-conserved nucleotides are shown in red-bold. Conserved sequences in the precursor miRNA, likely involved in the processing toward mature miRNA, are also highlighted in bold. (**B**) Polyacrylamide gel showing the qPCR product (black arrowhead) obtained using the primers for mmu-miR-721 to amplify human plasma samples from patients with acute myocarditis or acute MI or from healthy controls. Transfected mmu-miR-721 in human cells was used as a positive control (C+). MW: molecular-weight markers. Gel stained with methylene blue. (**C**) Quantification of the average intensity of the qPCR product (quantified with Image Studio Lite v.4.0). Data are pooled from two independent gels. Histograms represent the means ± SEM and were analyzed by one-way ANOVA with Tukey's *post hoc* test (n= 5). (**D**) The qPCR products were cloned in a pGEM-T vector for sequencing. Quantification of the cloning efficiency of the qPCR products obtained using mmu-miR-721-specific primers with myocarditis patients' plasma. Colonies were sequenced and the product obtained (below) included 18 nucleotides (black) of the conserved sequence with a polyA tail (grey), added as a poly dT reverse primer during RT-qPCR, inserted into vector sequence (yellow). (**E**) Quantification of the cloning efficiency of the qPCR products obtained using custom-made primers for the putative mature hsa-miR-Chr8:96 with myocarditis patients' plasma. The product obtained after colony sequencing is shown on the right. In red, the three nucleotides differing from the murine sequence, present in the sequenced product.

We designed a strategy to identify and amplify the miR-721 human homolog in the plasma from human samples (healthy donors, acute myocarditis and MI) with the murine primers for mmu-miR-721 (**figure R.11B**). Both the yield of amplification product as well as the cloning efficiency were higher in plasma from patients with myocarditis than in patients with MI or healthy controls (**figure R.11B-D**). Colonies screened by sequencing harbored an 18-nucleotide sequence (TGCAATTAAAAGGGGGAA) identical to mmu-miR-721 (**figure R.11D**), coinciding with the 3' 18-nucleotides conserved in mice ad humans (**figure R.11A**). A poly-A tail added to miRNAs in the process of RT-qPCR is also present in the sequenced product. We identified the sequence in the human genome located within chromosome 8, positions 96405822 and 96405839 (genomic sequence, NC_018919.2). Since miRNAs typically consist of 20-22 nucleotides (Iwakawa and Tomari 2015), we postulated that the 3 differential nucleotides (TCT) at the 5′end could complete the putative mature human homolog of mmu-miR-721 (*TCT*TGCAATTAAAAGGGGGAA), thereafter referred as hsa-miR-Chr8:96.

In a second approach, we amplified plasma samples from myocarditis patients using custom-made primers for the putative hsa-miR-Chr8:96 21-nucleotides sequence designed by *Exiqon/Qiagen* (Custom LNA™ primer set PER-206999-721). We have also cloned and sequenced the qPCR fragment amplified and the unique product obtained this time was: *TCT*TGCAATTAAAAGGGGGAA, the full mature sequence of the hsa-miR-Chr8:96 (**figure R.11E**).

8. Validation of hsa-miR-Chr8:96 as a potentially functional mature miRNA

MicroRNAs are defined by their length and their association with the family of AGO proteins, key components of the RISC (Kobayashi and Tomari 2016). To validate hsa-miR-Chr8:96 as a mature functional miRNA, we cloned in an expression vector a 350 base-pair fragment of human chromosome 8 containing the putative novel miRNA sequence and study the interaction with AGO2 (**figure R.12A**). Biochemical analysis of RNA-protein co-immunoprecipitation assays (**figure R.12B**) support a binding of the cloned RNA sequence to the AGO2 complex. The qPCR analysis with custom-made primers for mature hsa-miR-Chr8:96, revealed higher levels of the miRNA in the AGO2 co-immunoprecipitation fractions after overexpressing the region containing the putative human pre-miRNA. This result indicates that the cloned fragment is processed toward a mature miRNA (**figure 12C**).

For functional validation, we next cloned two reverse complementary sequences of hsa-miR-Chr8:96 in tandem in a luciferase dual reporter vector (**figure R.12D**), so the functional miRNA would bind the cloned sequence and downregulate the luciferase levels. HEK2963T cells expressing the aforementioned luciferase vector or a control empty luciferase vector were cultured in the presence of supernatants from PBLs cultured overnight, obtained from patients with acute myocarditis, with MI or healthy donors. Supernatants from PBLs of myocarditis patients, containing EVs with higher levels of hsa-miR-Chr8:96 (**figure R.12E**), downregulates the luciferase activity significantly more efficiently

than supernatants from MI or healthy donors (**figure R.12F**). These data support that the mature hsa-miR-Chr8:96 sequence is secreted by PBLs from myocarditis patients and is functionally active.

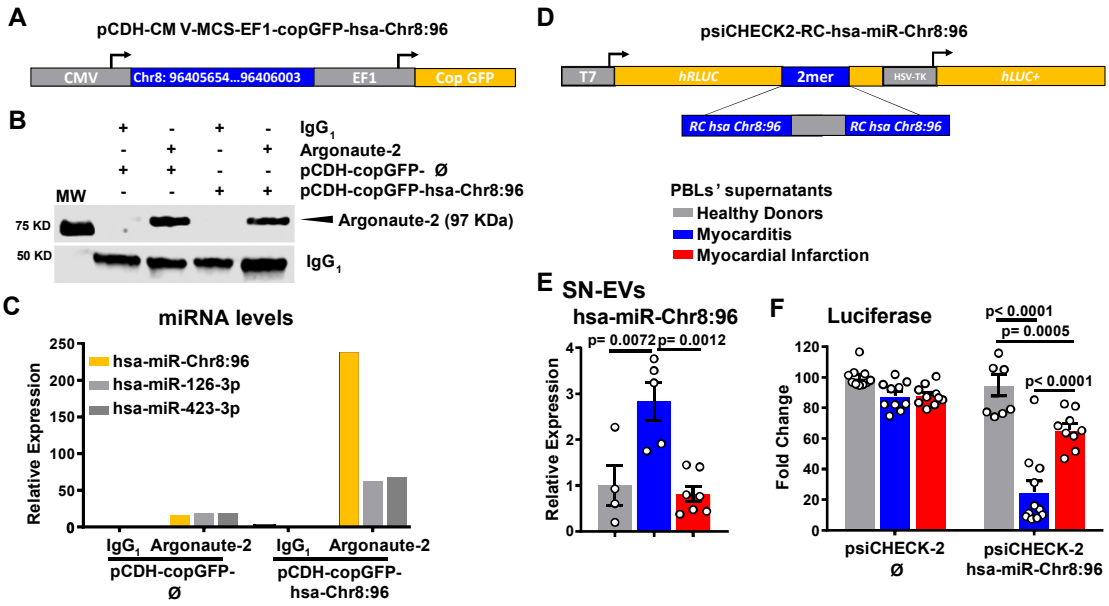

Figure R.12. Validation of hsa-miR-Chr8:96 as a mature functional miRNA. (A) Diagram of pCDH-CMV-MCS-EF1-copGFP-based lentiviral vector used to express the sequence of Chr8: 96405654…96406003, containing 350 nucleotides including the putative primary sequence of hsa-miR-Chr8:96. (**B**) Representative blotting with Argonaute-2 antibody of the RNA-Argonaute-2/IgG1 co-IP fraction. (**C**) Levels of the indicated miRNAs in the co-IP fractions were evaluated by qPCR. Hsa-miR-Chr8:96 was quantified with custom-made primers recognizing the putative mature hsa-miR-Chr8:96. *RNU1A1*, a small nuclear RNA that is processed independently of Argonaute-2, was used as endogenous control. One representative out of four independent experiments. (**D**) Diagram of psiCHECK2-RC-hsa-miR-Chr8:96 luciferase dual reporter vector. The 2-mer insert consists of a tandem repeat of the reverse complementary (RC) sequence of the mature hsa-miR-Chr8:96. (**E**) PBLs obtained from healthy controls, patients with acute myocarditis or MI, were cultured overnight and supernatants were collected. Quantification of hsa-miR-Chr8:96 in PEG-isolated EVs from the supernatants of human PBLs is shown (n= 4-7). Means ± SEM. One way ANOVA with Tukey's *post hoc* test. (**F**) Renilla and firefly luciferase dual reporter assays were performed after transiently transfecting HEK293T cells with an empty plasmid (psiCHECK2) or psiCHECK2-RC-hsa-miR-Chr8:96-expressing plasmid, and by adding the supernatant of the different human PBLs (n= 8-11). Data represented as means ± SEM and analyzed by two-way ANOVA with Sidak's *post hoc* test. CMV, cytomegalovirus promoter; EF1, elongation factor 1 promoter; CopGFP, GFP-expressing vector; T7, T7 promoter; hRLUC, synthetic renilla luciferase reporter gene; HSV-TK, herpes simplex virus-1 thymidine kinase promoter; hLUC+, synthetic firefly luciferase gene.

9. Plasma hsa-miR-Chr8:96 is a specific biomarker for acute myocarditis patients

We analyzed plasma samples from the main cohort of participants for miRNA profiling by qPCR. Relative expression hsa-miR-Chr8:96 expression was quantified in 39 myocarditis patients, MI patients (39 STEMI and 38 NSTEMI) and 31 healthy donors (**figure R.13**). For comparison, the levels of hsa-

miR-483-5p and hsa-miR-21, previously described as abundant in MI or after myocardial injury (Li et al. 2019; Wang et al. 2014), and hsa-miR-132-3p and hsa-miR-212-3p, which are involved in Th17 cell differentiation (Nakahama et al. 2013), were analyzed. The levels of hsa-miR-Chr8:96 were higher in plasma from acute myocarditis patients than in STEMI/NSTEMI patients or healthy donors, whereas hsa-miR-483-5p was detected in all groups with myocardial injury. Hsa-miR-21-5p, hsa-miR-132-3p and hsa-miR-212-3p values in plasma were not specific to any group (**figure R.13A**).

Then, we tested the expression of hsa-miR-Chr8:96 in sorted $CD4^+$ T cell subsets from patients with acute myocarditis, showing that the miRNA is predominantly synthetized by Th17 cells (**figure R.13B**).

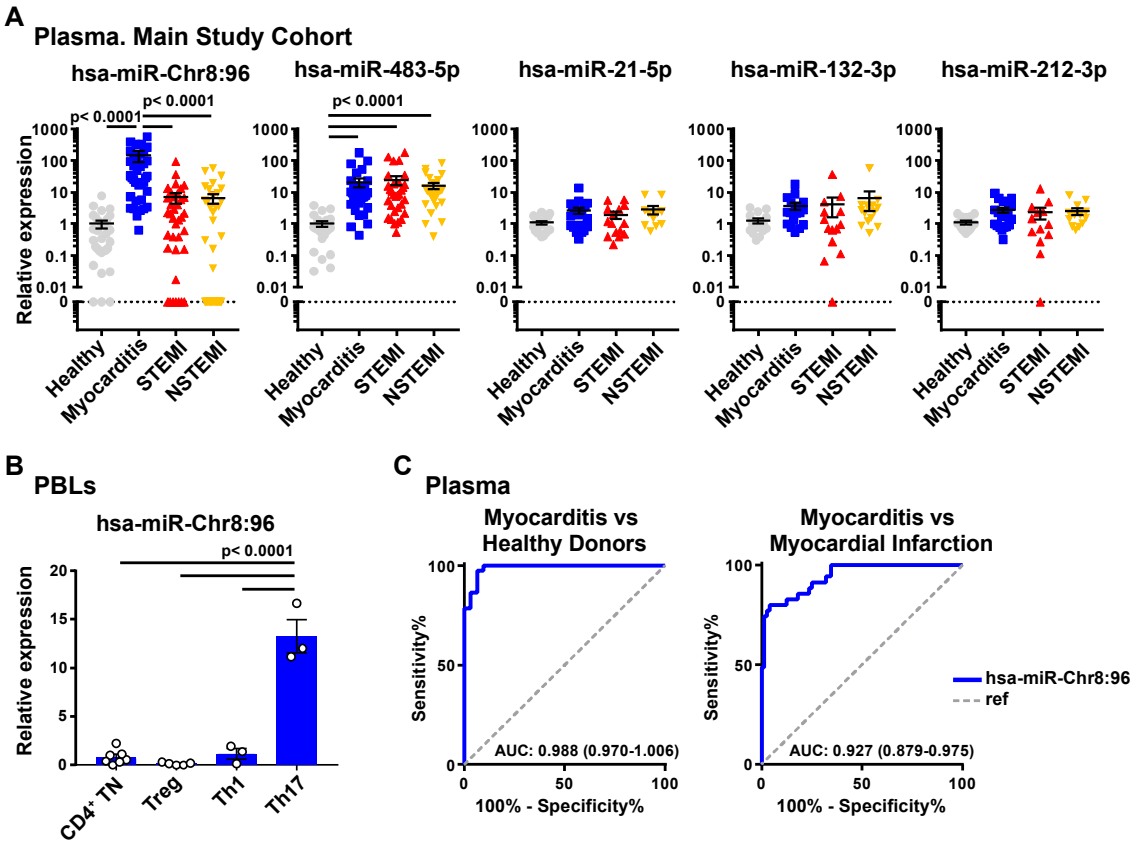

Figure R.13. Hsa-miR-Chr8:96 is upregulated in plasma from acute myocarditis patients. (**A**) Quantification of miRNAs by qPCR in circulating plasma from patients with acute myocarditis (n= 39), STEMI (n= 39) or NSTEMI (n= 38) and from healthy controls (n= 31) from the main study cohort (Spain). Data are represented as log10 of miRNA relative expression in plasma. Error bars depict the SEM. Kruskal-Wallis with Dunn's *post hoc* test. (**B**) Quantification of hsa-miR-Chr8:96 by qPCR in sorted naïve $CD4^+$ T cells, Treg cells ($Foxp3^+$), Th1 cells ($IFN\gamma^+$), and Th17 cells ($IL\text{-}17^+$) isolated from blood of patients with myocarditis (n= 3-6 pools of 2 patients each). Data represented as means ± SEM. One-way ANOVA with Tukey's *post hoc* test. (**C**) Receiver operating characteristic (ROC) curves of hsa-miR-Chr8:96 determinations, using $2^{-\Delta\Delta Ct}$ values in plasma, were generated to evaluate the potential to discriminate patients with acute myocarditis from healthy controls and patients with acute myocardial infarction. The area under the ROC curve (AUC) with 95% confidence interval between brackets for each comparison are indicated.

Receiver operating characteristic (ROC) curves analysis was performed to evaluate the potential diagnostic value of hsa-miR-Chr8:96, other analyzed circulating miRNAs and peripheral T cells (**annex table A4**). Th17 cells showed a significant area under the ROC curve (AUC) for the discrimination of acute myocarditis patients from MI patients (AUC= 0.883, 95% CI, 0.798 - 0.967) and from healthy controls (AUC= 0.866, 95% CI, 0.782 - 0.951), reinforcing their potential as a cellular source of myocarditis biomarkers. Plasma hsa-miR-Chr8:96 showed an even higher AUC, being 0.927 (95% confident interval, 0.879-0.975) for the differentiation of myocarditis from MI, and 0.988 (95% confident interval, 0.970-1.006) for the differentiation from healthy controls (**figure R.13C, annex table A4**). These data evidence a robust diagnostic value of hsa-miR-Chr8:96 for acute myocarditis patients.

Additionally, the expression of selected hsa-miRNAs was studied in the EV-fraction after PEG precipitation from plasma. While both hsa-miR-Chr8:96 and hsa-miR-483-5p were sorted into the EV-fraction (**figure R.14A**), hsa-miR-Chr8:96 detection was increased in plasma-EVs from acute myocarditis patients and hsa-miR-483-5p was increased in all patients with myocardial disease (**figure R.14B**).

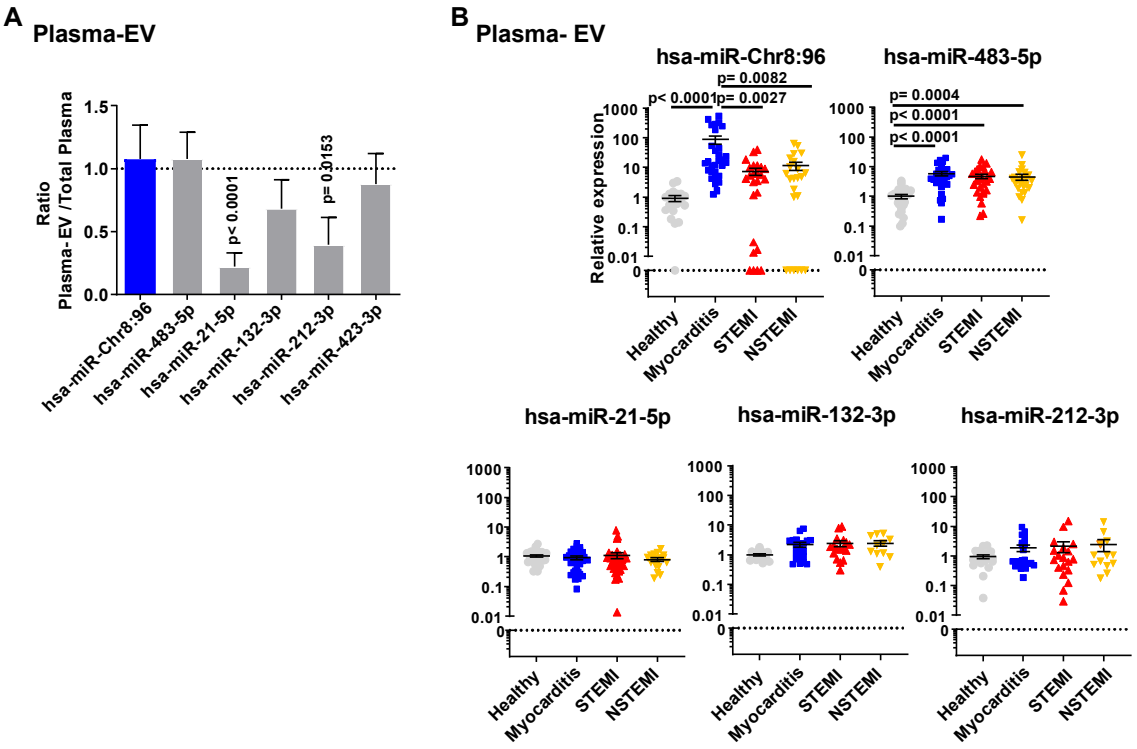

Figure R.14. Hsa-miR-Chr8:96 is protected into plasma-EV of myocarditis patients. (**A**) Ratio of relative miRNA levels in PEG-isolated EVs from plasma *versus* in total plasma. Data are represented as means ± SEM and interference with hypothetical value= 1 was analyzed by one sample t-test. (**B**) Quantification of miRNAs in PEG-isolated EV fractions from circulating plasma of healthy donors (n= 20), myocarditis patients (n= 30), STEMI patients (n= 25) and NSTEMI patients (n= 23). Data are represented as log10 of miRNA relative expression. Means ± SEM. Data were analyzed by one-way ANOVA with Tukey's *post hoc* test or, when non-normal distributions, by Kruskal-Wallis with Dunn's *post hoc* test.

With the aim to validate the diagnostic potential of hsa-miR-Chr8:96 we analyzed three additional independent cohorts of patients with myocarditis from different centers located in Boston (*miRNA Validation Cohort 1*, **table 3**), Zurich (*miRNA Validation Cohort 2*, **table 4**) and Padua (*miRNA Validation Cohort 3*, **table 5**). The data confirmed in all independent cohorts that hsa-miR-Chr8:96 is specifically elevated in plasma from myocarditis patients, as compared with either acute MI or MINOCA patients (**figure R.15A-C**). In addition, we evaluated the expression of hsa-miR-Chr8:96 in the plasma of patients with other Th17-related diseases such as rheumatoid arthritis, spondyloarthritis, psoriasis and multiple sclerosis (**table 6**). Although marginal elevation of the miRNA was obtained in some of the studied Th17-linked conditions, hsa-miR-Chr8:96 expression was significantly enhanced in plasma from myocarditis patients compared to the other pathologies (**figure R.15D**).

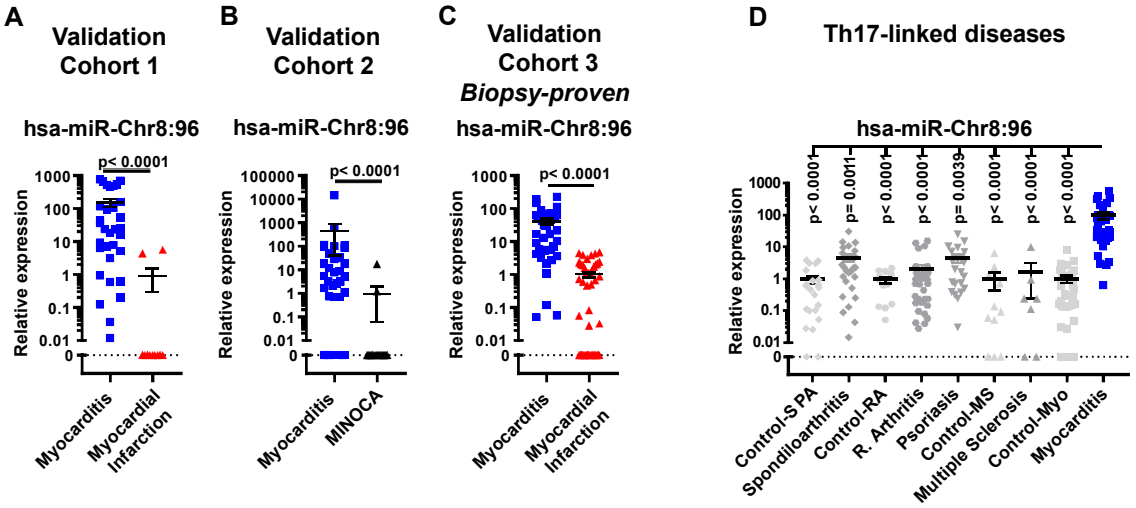

Figure R.15. Validation of hsa-miR-Chr8:96 as a myocarditis biomarker in independent cohorts. Analysis of circulating hsa-miR-Chr8:96 by qPCR in different cohorts expressed as means ± SEM. (**A**) Validation Cohort 1 of patients with myocarditis or acute MI from Boston (MA, USA). (**B**) Validation Cohort 2 of myocarditis patients compared to MINOCA patients from the Zürich (Switzerland). (**C**) Validation Cohort 3 of patients with biopsy-proven acute myocarditis from Padova (Italy) and patients with acute MI from Murcia (Spain). In **A-C**, Mann-Whitney U-test. (**D**) Analysis of hsa-miR-Chr8:96 in patients with other Th17-linked diseases and control patients that were finally excluded after suspicion of these diseases. Data were analyzed by Kruskal-Wallis with Dunn's *post hoc* test.

The discrimination ability of hsa-miR-Chr8:96 in distinguishing acute myocarditis from MI remained significant after considering other biomarkers as ejection fraction and troponins levels, and after adjusting by age and gender (**figure R.16A**). Additionally, it improved the diagnosis value when added to a model including conventional cardiac injury markers and potential demographic confounders (**figure R.16B**). Altogether, our data endorse the use of hsa-miR-Chr8:96 as a myocarditis biomarker.

A Main Study Cohort

	Odds Ratio (95% CI)	P-value
(Intercept)	130.967 (0.732, 46741.671)	0.080
Sex (women)	0.858 (0.189, 3.869)	0.840
Age (years)	0.902 (0.86, 0.937)	<0.001
Troponins (Normalized)	0.998 (0.994, 1.001)	0.282
Ejection Fraction %	1.004 (0.933, 1.083)	0.907

	Odds Ratio (95% CI)	P-value
(Intercept)	1.417 (0.003, 643.699)	0.909
Sex (women)	1.562 (0.268, 10.2)	0.624
Age (years)	0.901 (0.848, 0.943)	<0.001
Troponins (Normalized)	0.998 (0.993, 1.002)	0.404
Ejection Fraction %	1.031 (0.943, 1.13)	0.505
Log10 (hsa-miR-Chr8:96 + 1)	16.659 (4.716, 92.949)	<0.001

B

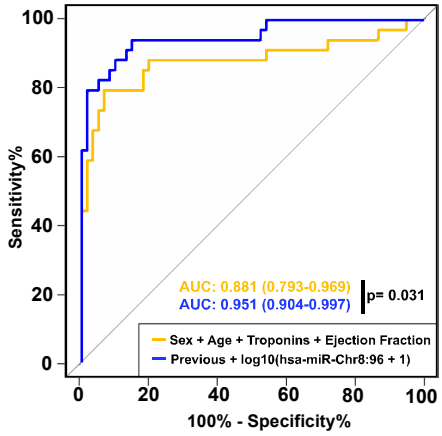

Figure R.16. Hsa-miR-Chr8:96 remains a predictor of myocarditis after adjusting by cardiac injury biomarkers and potential confounders. (**A**) Multivariate (MVA) logistic regression models with or without inclusion of hsa-miR-Chr8:96, controlling for the potential confounders listed, to discriminate patients with myocarditis from patients with MI. (**B**) ROC curves for the MVA logistic regression models with or without hsa-miR-Chr8:96 and the variables of sex, age, serum troponin levels and ejection fraction. DeLong´s test was used for comparison of ROC curves.

PART II. CD69$^+$ Treg cells control inflammatory damage after myocardial infarction and produce miR-155-5p

1. Enhanced peripheral CD69$^+$ Treg cell response in patients with acute MI

The blood immune phenotype was determined in a cohort of 283 participants with acute MI and 80 healthy donors. Demographic and clinical data are summarized in **table 7**. Regarding cardiovascular risk factors, the percentage of patients presenting at least one risk factor was greater than 90%; the three most frequent being dyslipidemia, arterial hypertension and history of smoking. **Table 7** also summarizes the data regarding biomarkers, presence of ECG abnormalities, number of diseased vessels and echocardiographic findings, including segmental wall motion abnormalities and left ventricular function. Most patients presented as ST-segment elevation MI. The culprit lesion was mainly located in the left-anterior descending coronary artery or right coronary artery, although 38.5% of patients had multivessel disease. Left ventricular ejection fraction was generally preserved and only one-third of patients exhibited a reduction in this echocardiographic measurement.

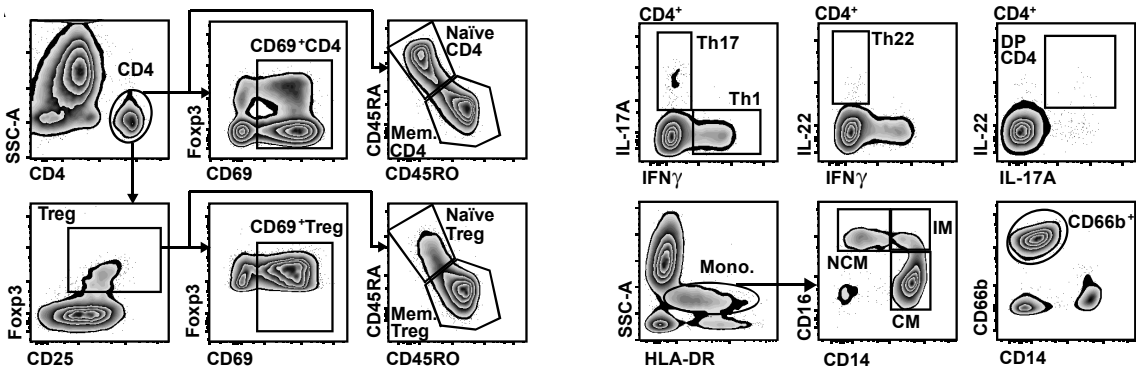

Figure R.17. Gating strategy for human immune cell population analysis by FACS. PBLs after excluding doublets and autofluorescent cells. DP, IL-17A$^+$IL-22$^+$ double positive CD4$^+$ cells; Mem., Memory; Mono., Monocytes; CM, Classical Monocytes; NCM, Non-classical Monocytes; IM, Intermediate Monocytes

We performed an extensive analysis of lymphoid and myeloid cell populations by FACS in peripheral blood in the first 24 hours after the ischemic event (**figure R.17**). Elevation of serum cardiac injury markers after MI, such as troponins and creatine kinase, are correlated with CD69 expression on circulating CD4$^+$ T cells and CD4$^+$CD25$^+$Foxp3$^+$ Treg cells, as well as with the ratios of effector T cells to CD69$^+$ Treg cells. These correlations suggest that CD69 expression is induced upon myocardial injury (**table 13**).

	Troponin T			CK			LV Ejection Fraction		
	r	p-value	N	r	p-value	N	r	p-value	N
CD4	**-0.3449**	**<0.0001**	**182**	**-0.3095**	**<0.0001**	**196**	**0.1967**	**0.0062**	**192**
CD45RA$^+$ CD4	0.0146	0.8449	182	0.0109	0.88	196	0.0228	0.7527	192
CD45RO$^+$ CD4	-0.0146	0.8441	182	-0.0122	0.8646	196	-0.0224	0.7576	192
CD69$^+$ CD4	**0.2188**	**0.003**	**182**	**0.1928**	**0.0068**	**196**	-0.1167	0.1068	192
Treg (CD4$^+$CD25$^+$Foxp3$^+$)	-9.8E-05	0.999	182	0.0067	0.9254	196	0.0224	0.7568	192
CD45RA$^+$ Treg	-0.0129	0.8623	182	0.0141	0.8446	196	-0.0626	0.388	192
CD45RO$^+$ Treg	0.0042	0.9547	182	-0.0301	0.6755	196	0.0614	0.397	192
CD69$^+$ Treg	**0.1931**	**0.009**	**182**	**0.2042**	**0.0041**	**196**	-0.0659	0.3633	192
Th1 (CD4$^+$IFNg$^+$)	-0.1049	0.1814	164	-0.0618	0.4118	178	0.0425	0.5774	174
Ratio Th1/Treg	-0.0915	0.2438	164	-0.0542	0.4721	178	0.0049	0.9484	174
Ratio Th1/CD69$^+$ Treg	**-0.2117**	**0.0067**	**163**	**-0.1869**	**0.0127**	**177**	0.1113	0.1451	173
Th17 (CD4$^+$IL-17$^+$)	-0.0439	0.5775	163	-0.0660	0.3825	177	-0.0094	0.902	173
Ratio Th17/Foxp3	-0.0161	0.838	163	-0.0300	0.6913	177	-0.0168	0.8256	173
Ratio Th17/CD69$^+$ Treg	**-0.1867**	**0.0167**	**164**	**-0.2398**	**0.0013**	**178**	0.0858	0.2598	174
CD4$^+$IL17$^+$IL22$^+$ (DP)	-0.0692	0.378	164	-0.0907	0.2281	178	0.0172	0.8213	174
Th22 (CD4$^+$IL-22$^+$)	-0.1104	0.1592	164	-0.1246	0.0975	178	0.1209	0.1121	174
Ratio Th22/Treg	-0.0834	0.2852	166	-0.1065	0.1548	180	0.0757	0.318	176
Ratio Th22/CD69$^+$ Treg	**-0.1971**	**0.0107**	**167**	**-0.2354**	**0.0014**	**181**	0.1373	0.0685	177
Monocytes	-0.1762	0.1156	81	-0.1942	0.075	85	0.0202	0.8549	84
Classical Monocytes	0.2102	0.0613	80	0.0532	0.631	84	-0.1856	0.093	83
Intermediate Monocytes	-0.1228	0.2747	81	-0.0681	0.5354	85	0.2214	0.043	84
Non-classical Monocytes	-0.2074	0.0632	81	-0.1433	0.1907	85	0.1031	0.3507	84
CD66b$^+$CD14^{lo}	0.2158	0.0546	80	0.0827	0.4545	84	-0.0792	0.4761	83

Table 13. Correlations between immune populations and cardiac damage biomarkers in MI patients. Spearman correlation coefficient (r) and p-values were calculated between the percentages or the ratio of percentages of the different immune cell populations, measured by flow cytometry, and the levels of serum troponin T, serum creatine kinase (CK) and left ventricular (LV) ejection fraction, measured by echocardiography. The numbers of samples (N) indicate the number of XY pairs for each comparison. Significant p-values are highlighted in bold.

Indeed, the analysis of CD4$^+$ T cells by flow cytometry revealed that a subset of CD69$^+$CD25$^+$Foxp3$^+$ Treg cells expand after MI in peripheral blood (**figure R.18A**). CD4$^+$ T and Treg cell populations are decreased and augmented, respectively, in MI patients compared with healthy controls (**figure R.18B**). CD69 is virtually absent in circulating blood lymphocytes due to the high concentration of sphingosine-1-phosphate (S1P) which maintains the receptor S1P1 levels high (Shiow et al. 2006), suppressing CD69 expression (Bankovich, Shiow, and Cyster 2010). Therefore, we analyzed CD69 expression on circulating CD4$^+$ T cells in the blood after overnight bystander activation on a plate loaded with anti-CD3 antibody. The percentage of CD69$^+$ Treg cells increases in the circulation in MI patients (**figure R.18C**), determined by an overall increase in CD69 expression on Treg cells after infarction in most patients (**figure 19**).

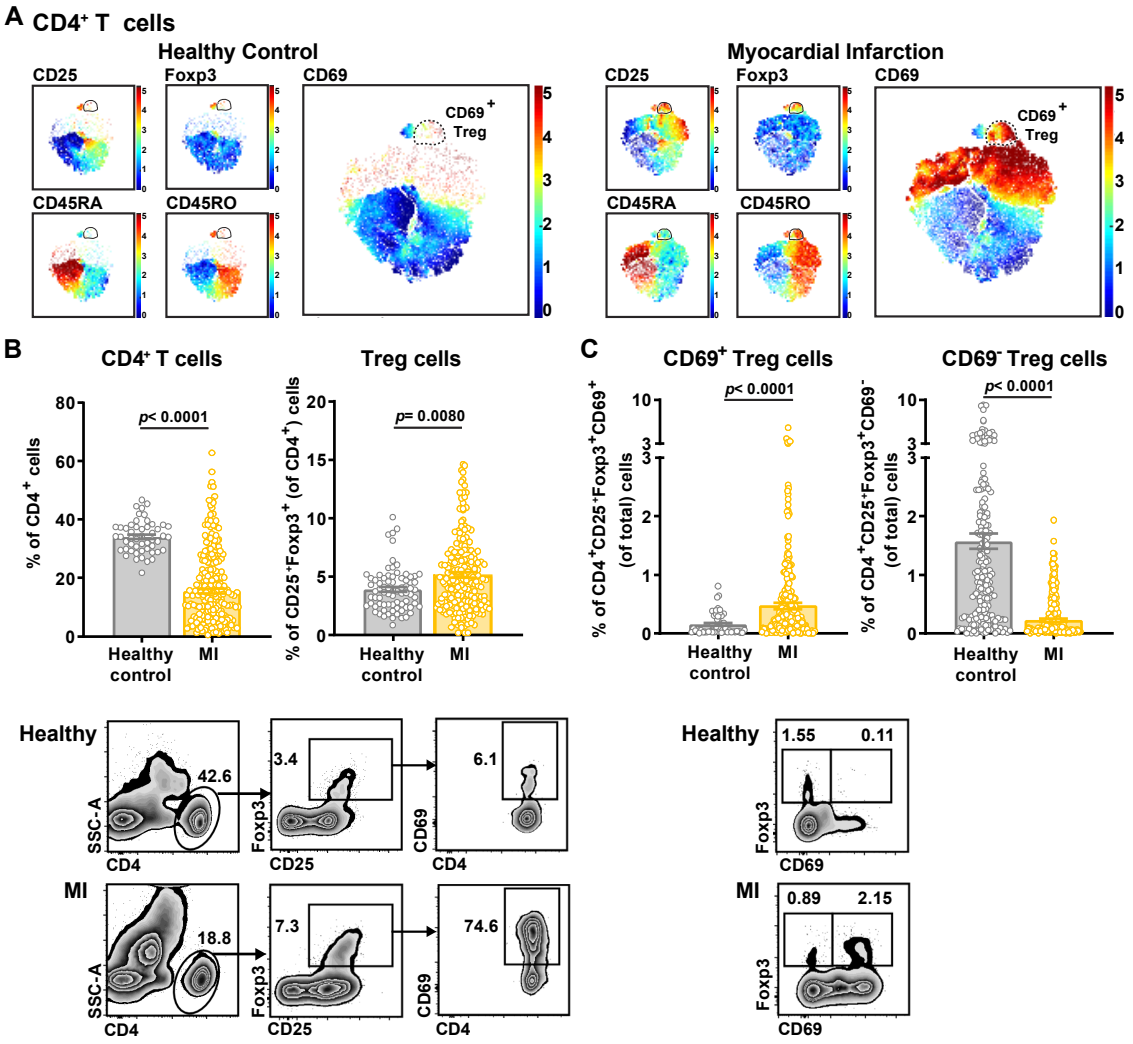

Figure R.18. MI patients exhibit an enhanced CD69$^+$ Treg cell response in peripheral blood. (**A**) t-distributed stochastic neighbor embedding (t-SNE) plots of CD4$^+$ T cells from PBLs from a representative healthy control and MI patient, considering the indicated markers, measured by flow cytometry. The color bars indicate the relative intensity of the markers. Dots represent individual cells. (**B**) Quantification of the percentages of CD4$^+$ and CD4$^+$CD25$^+$Foxp3$^+$ (Treg) cells in peripheral blood of healthy donors (n= 77) and MI patients (n= 156) at the time of hospital admission. (**C**) Percentages of CD69$^+$ Treg cells and CD69$^-$ Treg cells out of total PBLs. Representative density plots are shown below. Means ± SEM are indicated. Mann-Whitney U-test.

However, we found two groups of patients according to CD69 expression levels on Treg cells, so we subdivided the population as patients with high CD69 expression (65% of patients) or low CD69 expression (35% of patients) for further analyses in this study (**figure R.19A**). Unsupervised hierarchical clustering of patients based on myeloid and lymphoid cell types analyzed by FACS (**figure R.17**) evidences that high and low CD69 patients present different immune phenotypes as they cluster in distinct groups (**figure R.19B**). Patients with high CD69 expression exhibit higher percentages of CD4$^+$ T and IL-22$^+$CD4$^+$ T cells but lower percentages of Treg cells. In addition, high CD69 patients present more naïve and less memory Treg cells, according to the expression of CD45RA$^+$ and CD45RO$^+$, respectively (**figure R.19C and R.19D**).

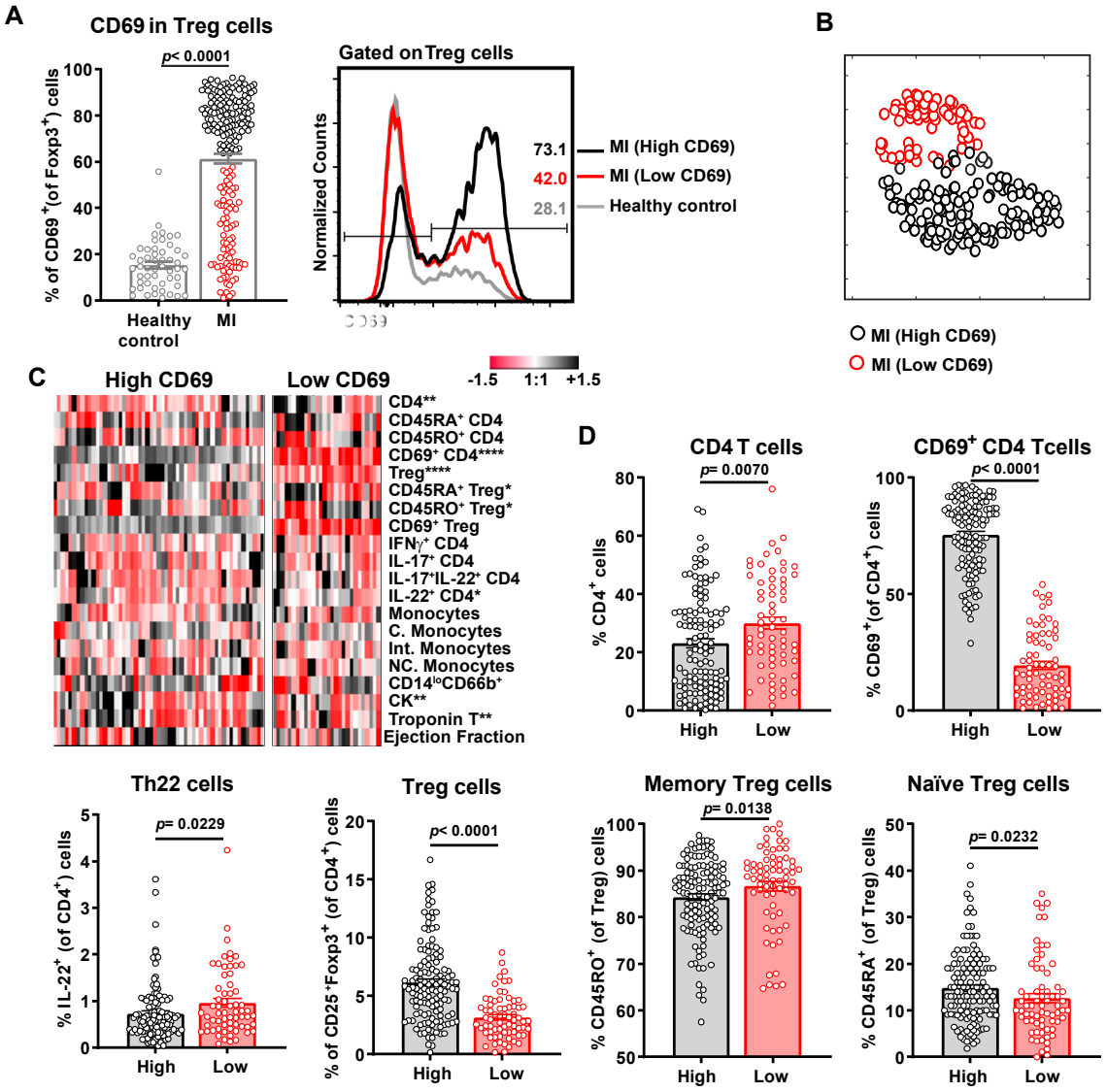

Figure R.19. CD69 expression on Treg cells classifies two group of MI patients with different immune phenotypes. (**A**) CD69 expression on Treg cells, quantified as percentage of CD69$^+$ cells after gating on Treg cells. Two groups of MI patients are differentiated according to the CD69 expression on Treg cells: patients with high levels of CD69 (High CD69, black circles) and patients with low levels (Low CD69, red circles). Data represent means ±SEM and were analyzed by Mann-Whitney U-test. Representative histograms and percentages of CD69$^+$ Treg cells are shown on the right. (**B**) t-SNE plot was made based on the proportions of the cell populations analyzed by FACS shown in **figure R.17**. Dots represent individual MI patients. High CD69 and Low CD69 MI patients are show as black and red dots, respectively. (**C**) The heat map shows the levels of the different cell populations analyzed by FACS and the cardiac damage markers in High CD69 and Low CD69 MI patients. Each column represents one patient. Data were normalized by subtracting the mean and dividing by the standard deviation. The color bar indicates the relative levels of each parameter with black indicating high expression and red, low expression. Differences between High and Low CD69 patients were analyzed by Mann-Whitney U-test and significance is indicated as *p< 0.05, **p< 0.01 or ****p< 0.0001. (**D**) Quantification of different immune populations, measured by FACS in High and Low CD69 MI patients. Data represent means ±SEM and were analyzed by Mann-Whitney U-test.

2. CD69 expression alleviates cardiac damage and improves survival and recovery of mice after LAD-ligation

To evaluate the role of CD69 expression in recovery after MI, we analyzed the survival and body weight loss after LAD-ligation in CD69 knockout mice in comparison with wild type mice. Survival is significantly reduced in *Cd69*$^{-/-}$ mice compared with their wild type littermates and sham-operated controls of surgery (**figure R.20A**). CD69-deficient mice recover worse after infarction, as they are unable to reach baseline body weight one week after LAD-ligation (**figure R.20B**).

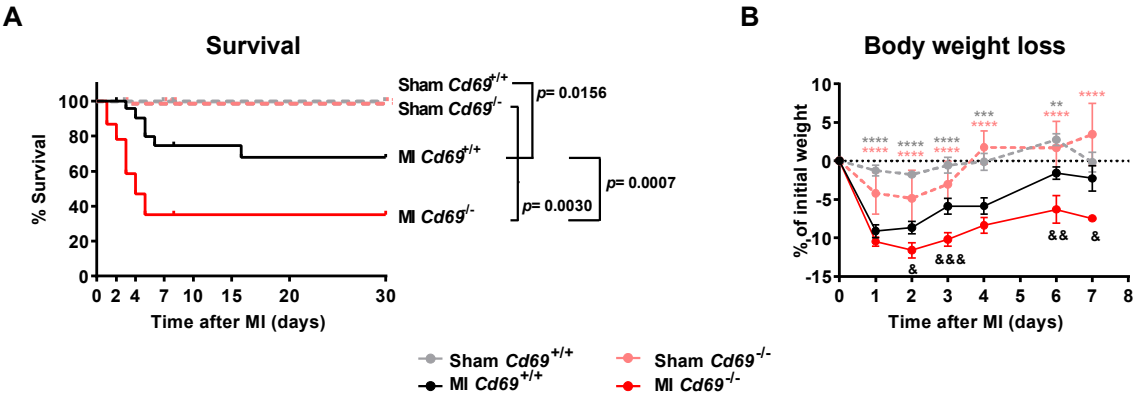

Figure R.20. CD69 contributes to survival and recovery in mice after LAD-ligation. (**A**) Survival curve of mice after LAD-ligation (n= 23-29 MI, n= 11-20 Sham). Data were pooled from five independent experiments and were analyzed by long-rank (Mantel-Cox) test. (**B**) Kinetics of the percentage of body weight loss after LAD-ligation (n= 9-17). Data represent means ± SEM and were analyzed by two-way ANOVA with Sidak's multiple comparisons test. * Differences between MI and Sham groups (gray for *Cd69*$^{+/+}$ mice, light red for *Cd69*$^{-/-}$ mice); $^{\&}$ differences between *Cd69*$^{+/+}$ and *Cd69*$^{-/-}$ MI mice.

In addition, *Cd69*$^{-/-}$ mice showed elevated myocardial damage **(figure R.21A)** and increased heart-weight to body-weight and heart-weight to tibia-length ratios two days after LAD-ligation, indicating that *Cd69*$^{-/-}$ hearts are swollen and might be more inflamed **(figure R.21B)**. Analysis of infarct size by triphenyltetrazolium chloride (TTC) staining and ischemic area at risk by Evan´s blue two days after infarction indicate that *Cd69*$^{-/-}$ hearts have increased infarct size and necrosis (**figure R.21C and R.21D**). Evaluation of cardiac function by echocardiography indicates that the ventricular wall motion score index increases in *Cd69*$^{-/-}$ mice as the disease progresses, reaching significance *versus* wild type mice one month after infarction, supporting a worse prognosis in *Cd69*$^{-/-}$ mice after LAD-ligation (**figure R.21E**).

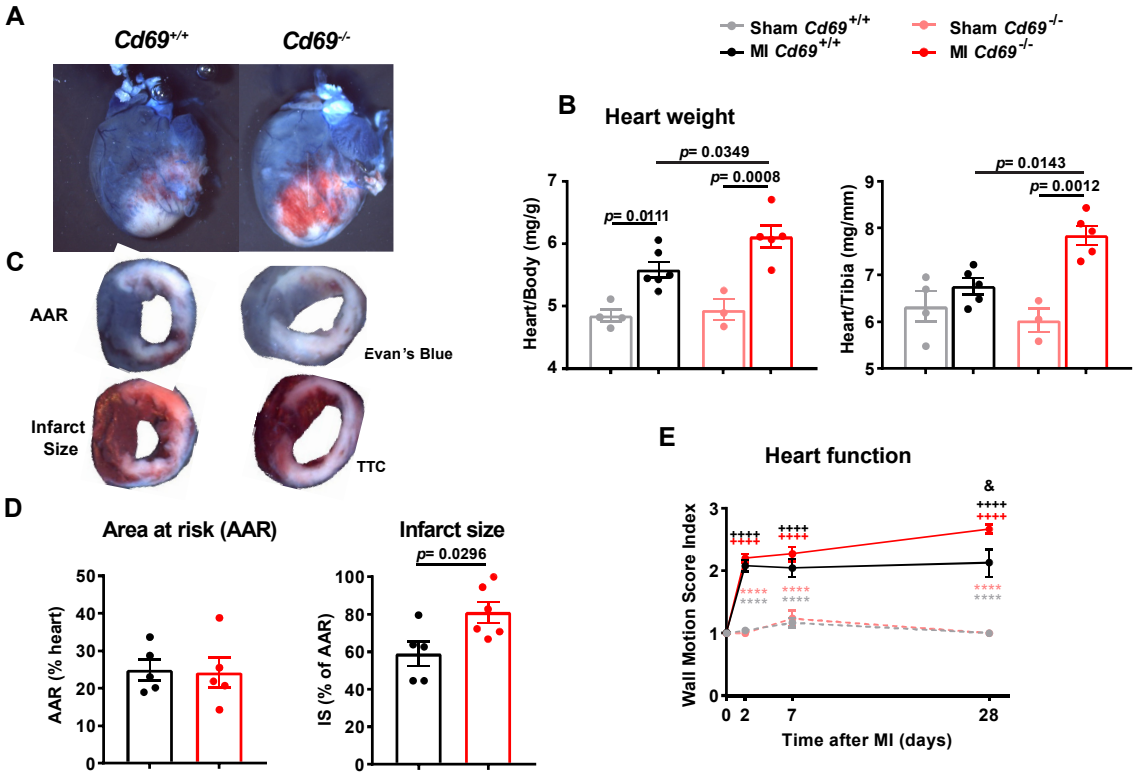

Figure R.21. CD69 depletion increases myocardial damage after LAD-ligation in mice. (**A**) Representative images of infarcted hearts collected after Evan's Blue intravenous injection at day 2 post-surgery. (**B**) Heart weight normalized *versus* body weight and tibia length at day 2 after LAD-ligation (n= 3-4 Sham mice and n= 5-6 MI mice). Data are representative of three independent experiments. Bars indicate means ± SEM, one-way ANOVA with Tukey's *post hoc* test. (**C**) Representative images of heart slices showing ischemic area at risk (AAR, negative for Evans Blue) in upper panels and extent of necrosis (negative for triphenyltetrazoliumchloride, TTC staining) in lower panels. (**D**) Histological quantification of the percentage of the left-ventricular AAR and percentage of infarct size (IS) (n= 5-6). Data expressed as means ± SEM and analyzed by unpaired t-test. (**E**) Time course of the heart dysfunction as a function of the Wall Motion Score Index measured by echocardiography (n= 6-16 MI, n= 4-8 Sham). Data were pooled from three independent experiments, represent means ± SEM and were analyzed by two-way ANOVA with Sidak's multiple comparisons test. *Differences between MI and Sham (grey for $Cd69^{+/+}$ mice, light red for $Cd69^{-/-}$ mice); $^{\&}$differences $Cd69^{+/+}$ and $Cd69^{-/-}$ MI mice; $^{+}$ differences between each day and day 0. $^{*/+/\&}p< 0.05$, $^{**/\&\&}p< 0.01$, $^{***/+++/\&\&\&}p< 0.001$, $^{****/++++/\&\&\&\&}p< 0.0001$.

3. IL-17^{+} γδT cells are the main source of peripheral IL-17 shortly after infarction and are increased in *Cd69*$^{-/-}$ mice

The mobilization and role of myeloid cells after infarction have been described (Swirski and Nahrendorf 2013; Swirski et al. 2009; Swirski and Nahrendorf 2018), whereas the kinetics of adaptive immunity and, in particular, of T cells remained poorly understood. It is well known that the number of CD4^{+}CD25^{+}Foxp3^{+} Treg cells increases in the heart during the first day after infarction (Bansal et al. 2019), indicating an antigen-independent migration of Treg cells into the injured myocardium. We observed a specific mobilization of CD69^{+} Treg cells in wild type mice after infarction, with a 2.5-fold increase in peripheral blood in the first 24 hours (**figure R.22**), mimicking the peripheral response in

MI patients (**figure R.18 and R.19**). This mobilization is not observed in either wild type CD69^{-} or *Cd69*$^{-/-}$ Treg cells (**figure R.22**).

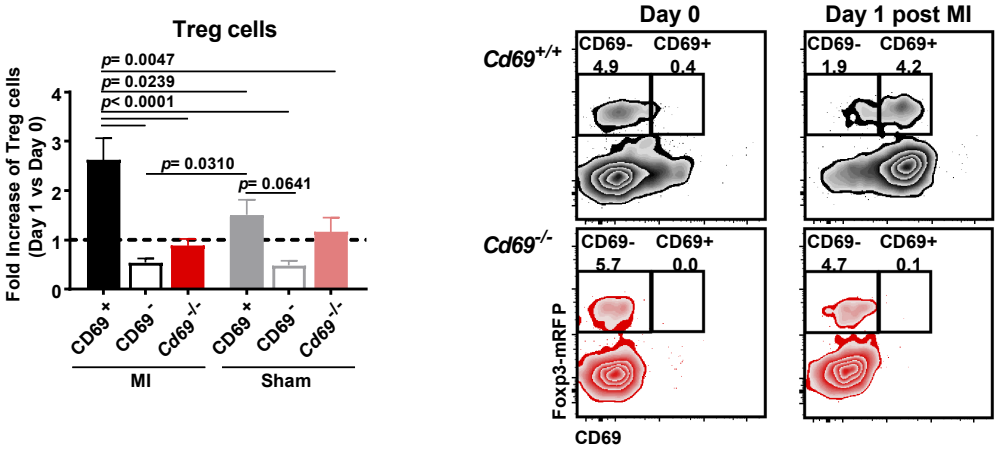

Figure R.22. CD69^{+} Treg cells are expanded in peripheral blood of MI mice. Fold Increase of the percentages of wild type CD69^{+} Treg cells, wild type CD69^{-} Treg cells and *Cd69*$^{-/-}$ Treg cells out of CD4^{+} cells in peripheral blood one day after LAD-ligation/sham surgery, compared with the percentages at day 0 (dotted lines). Representative density plots of Treg cells at day 0 and day 1 post MI are shown on the right. Histograms indicate means ± SEM (n= 10-20). Data were analyzed by one-way ANOVA with Tukey's *post hoc* test.

Since *Cd69*$^{-/-}$ mice exhibit exacerbated Th17 responses in different inflammatory diseases (Gonzalez-Amaro et al. 2013), we analyzed the kinetics of IL-17^{+} cells in blood one week after infarction. *Cd69*$^{-/-}$ mice have a significantly increased IL-17 response during the first week after LAD-ligation, which is not observed in *Cd69*$^{+/+}$ mice (**figure R.23A**). The majority of IL-17A producing cells in peripheral blood after infarction are CD3^{+} T cells in *Cd69*$^{+/+}$ and *Cd69*$^{-/-}$ mice (**figure R.23B**). Further characterization of the nature of these IL-17-producing T cells confirmed that γδT cells, but not Th17 cells, are the main source of IL-17 in the blood during the first week after infarction (**figure R.23B**). *Cd69*$^{-/-}$ γδT cells express higher levels of IL-17A even in steady state and *Cd69*$^{-/-}$ mice amplify the IL-17^{+} γδT cell response in peripheral blood shortly after MI (**figure R.23C and R.23D**). As IL-17^{+} γδT cells are well known as initiators of inflammation (Papotto, Ribot, and Silva-Santos 2017) and induce apoptosis of cardiomyocytes (Huber 2000), we postulate that this population may contribute to the increased damage observed in *Cd69*$^{-/-}$ mice after LAD-ligation.

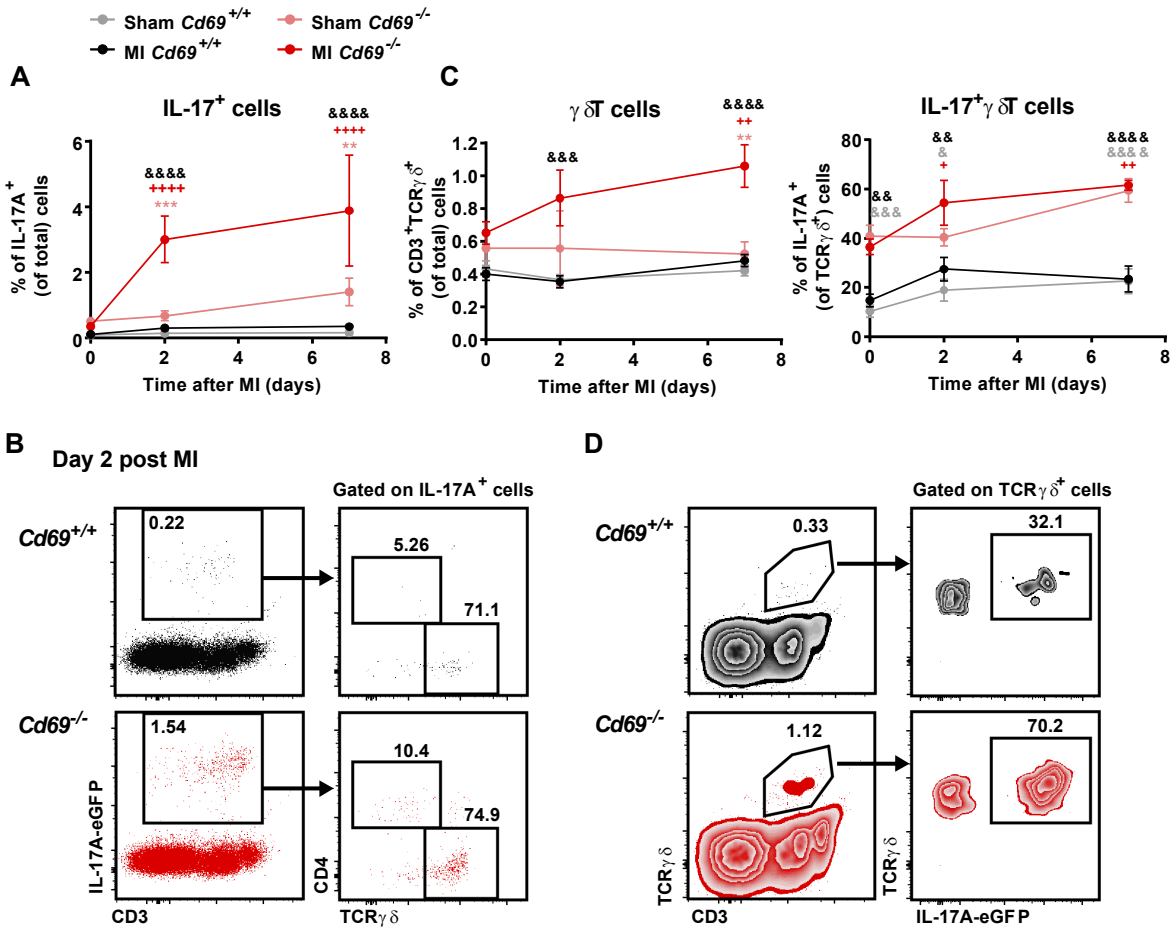

Figure R.23. IL-17$^+$ γδ T cells are upregulated in peripheral blood of CD69-deficient mice after MI. (**A**). Kinetics of IL-17A$^+$ cells in peripheral blood after surgery, expressed as percentage of total cells. (**B**) Left, representative dot plots of IL-17A$^+$ cells, percentages of total cells are indicated inbox. Right, representative dot plots showing the main populations positive for IL-17A. (**C**). Kinetics of the percentages of γδT cells and IL-17$^+$ γδT cells in peripheral blood after LAD-ligation/sham surgery. Data in **B** and **D** are representative of more than three independent experiments and show means ± SEM (n= 6-10). Data were analyzed by two-way ANOVA with Sidak's multiple comparisons test. * Differences between MI and Sham groups (in grey for *Cd69*$^{+/+}$ mice, in light red for *Cd69*$^{-/-}$ mice); $^{\&}$ differences between *Cd69*$^{+/+}$ and *Cd69*$^{-/-}$ MI mice; $^{+}$ differences between each day and day 0. $^{+/\&}$ p< 0.05, $^{**/++/\&\&}$ p< 0.01, $^{***/+++/\&\&\&}$ p< 0.001, $^{++++/\&\&\&\&}$ p< 0.0001.

4. CD69$^+$ Treg cells are recruited to the heart after MI in mice

Next, we analyzed the myocardial infiltrating leukocyte populations to characterize inflammation in infarcted tissue from *Cd69*$^{-/-}$ mice. Quantification of the total number of leukocytes per miligram of infarcted tissue shows that the hearts of *Cd69*$^{-/-}$ mice exhibit increased inflammation at day 2 after MI compared with their *Cd69*$^{+/+}$ littermates (**figure R.24A**). Consistent with previous studies, we found that Treg cells are recruited to the heart after ischemia. However, we found an increased number of CD69$^+$ Treg cells and higher CD69 expression on Treg cells in the myocardium of MI mice *versus* sham

mice, indicating a selective migration of these cells to the myocardium after LAD-ligation (**figure R.24B**).

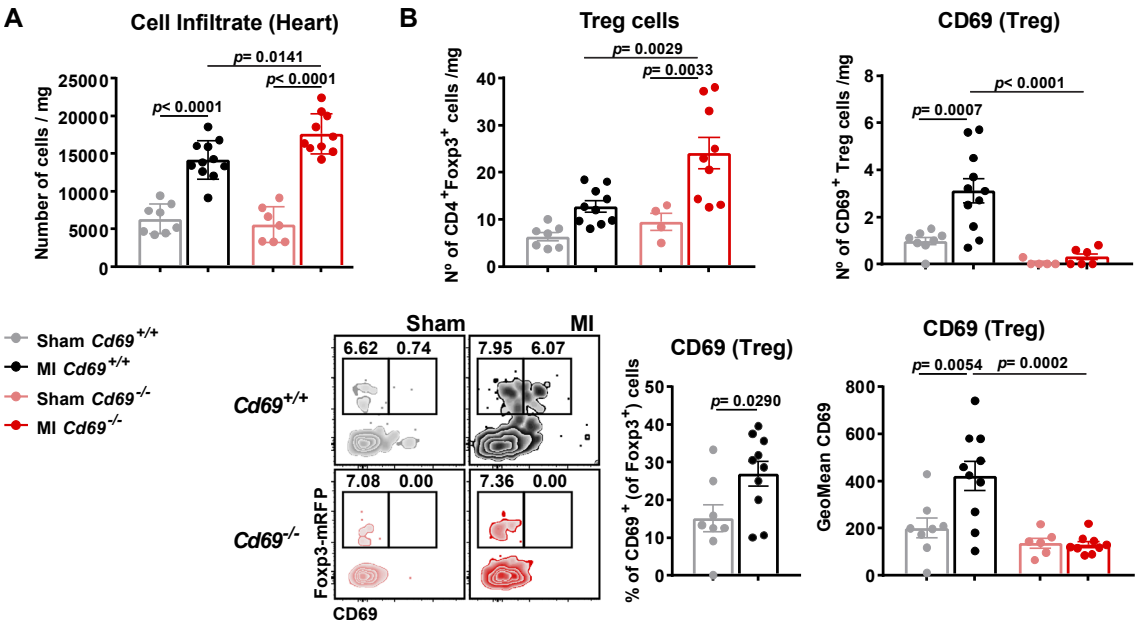

Figure R.24. CD69$^+$ Treg cells are accumulated in the infarcted myocardium after LAD-ligation. Infiltrating populations in the heart were evaluated 2 days post infarction (**A**) Leukocyte cell number per milligram of tissue in the myocardium. (**B**) Quantification of the number of Treg (CD4$^+$Foxp3$^+$) cells and CD69$^+$ Treg (CD4$^+$Foxp3$^+$CD69$^+$) cells per mg of heart tissue, percentage of CD69$^+$ Treg cells and CD69 geometric mean (GeoMean) fluorescence expression on Treg cells. Representative density plots and percentages are shown after gating on CD45$^+$CD11b$^-$CD4$^+$ cells. Data are representative of more than three independent experiments. Bars indicate means ± SEM (n= 6-11 animals per group) and data were analyzed by one-way ANOVA with Tukey's *post hoc* test.

Evaluation of CD69 expression after MI in different cardiac cell types revealed that CD45$^-$CD31$^+$ endothelial cells, CD11b$^+$ myeloid cells and CD11b$^-$CD4$^+$Foxp3$^-$ T effector cells do not upregulate CD69 after MI in the extent of Treg cells (**figure R.25**). Although the effect of CD69 expression by other cell types remains to be explored, these data support a dominant role of CD69 expression in the Treg cell compartment after MI. Therefore, we focused on the understanding of the role of CD69 expression by Treg cells in the regulation of the post-MI inflammation.

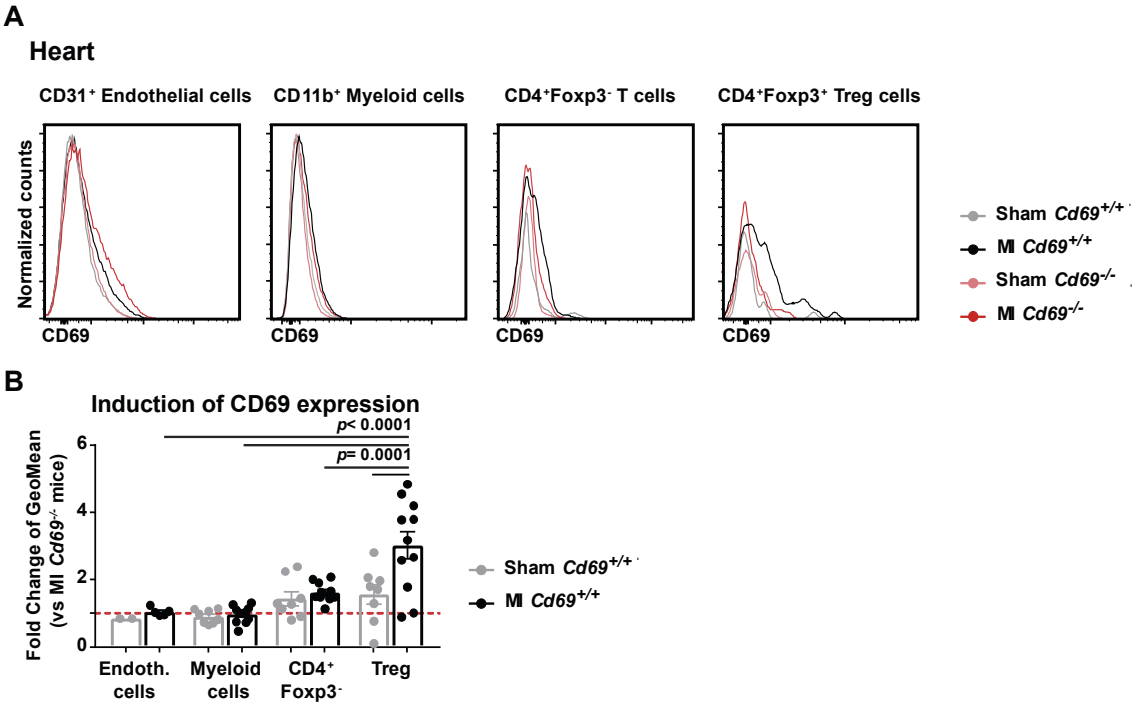

Figure R. 25. CD69 expression on cardiac cell populations after LAD-ligation. (**A**) Histograms show the representative expression of CD69 on $CD45^{-}CD31^{+}$ endothelial cells, $CD45^{+}CD11b^{+}$ myeloid cells, $CD45^{+}CD11b^{-}CD4^{+}Foxp3^{-}$ T effector cells and $CD45^{+}CD11b^{-}CD4^{+}Foxp3^{+}$ Treg cells in the heart two days after MI. (**B**) Quantification of CD69 geometric mean (GeoMean) of expression in the populations above. Each population was normalized (fold change) *versus* the GeoMean of MI *Cd69*$^{-/-}$ mice (red dotted line), as considered the baseline of fluorescence. Data are represented as means ± SEM and were analyzed by two-way ANOVA with Sidak's multiple comparisons test (n= 8-11).

5. IL-17^{+} γδT cells rapidly accumulate in the myocardium after LAD-ligation in the absence of CD69

In the infarcted myocardium, γδT cells peak one week after ischemia and are the main producers of IL-17 with deleterious functions (Yan et al. 2012). Indeed, we confirmed that the majority of IL-17A producing cells are TCRγδ^{+} cells (about 75%) in both *Cd69*$^{+/+}$ and *Cd69*$^{-/-}$ mice, although γδT cells and IL-17^{+} γδT cells infiltration in the myocardium is significantly increased in *Cd69*$^{-/-}$ mice as early as two days after LAD-ligation (**figure R.26A**). Neither *Cd69*$^{+/+}$ nor *Cd69*$^{-/-}$ mice show a significant recruitment of Th17 cells at this early time point (**figure R.26B).** In parallel, the pathogenic IL-17^{+} γδT cell population is significantly increased in the mediastinal lymph nodes of *Cd69*$^{-/-}$ mice two days after infarction (**figure R.26C**), suggesting a local expansion of this cell type in the lymph nodes draining the heart.

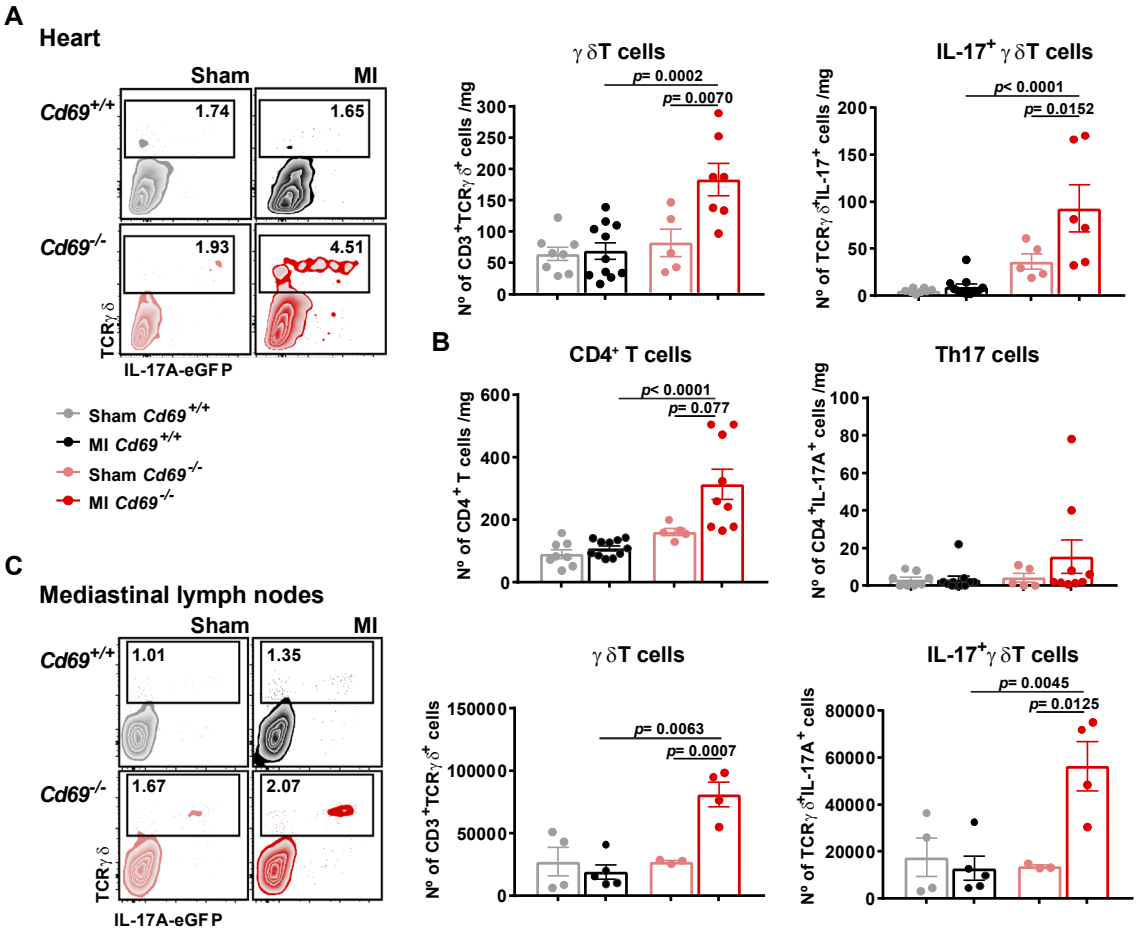

Figure R.26. IL-17$^+$ γδT cell response is increased in the heart and mediastinal lymph nodes of *Cd69*$^{-/-}$ mice two days after LAD-ligation. Heart-infiltrating populations were analyzed two days after surgery. (**A**) Representative density plots gated on CD45$^+$CD11b$^-$CD3$^+$ cells and numbers of γδT cells and IL-17$^+$ γδT cells per milligram of tissue. (**B**) Numbers of CD4$^+$ T cells and Th17 cells per milligram of tissue in the heart (n= 5-11). (**C**) Representative density plots and absolute numbers of γδT cells and IL-17$^+$ γδT cells in the mediastinal lymph nodes (n= 4-5). Representative data of three independent experiments. Data are represented as means ± SEM and were analyzed by one-way ANOVA with Tukey's *post hoc* test or, for non-normal distributions, by Kruskal-Wallis with Dunn's multiple comparisons test.

Furthermore, although no clear differences in the number of CD11b$^+$ myeloid cells or CD11b$^+$Gr1^{hi} granulocytes are observed between genotypes (**figure R.27A**), *Cd69*$^{-/-}$ mice show a higher number of inflammatory Ly6C^{hi} monocytes accumulated in the infarcted myocardium (**figure R.27B**), indicating a more pro-inflammatory scenario (Swirski et al. 2009).

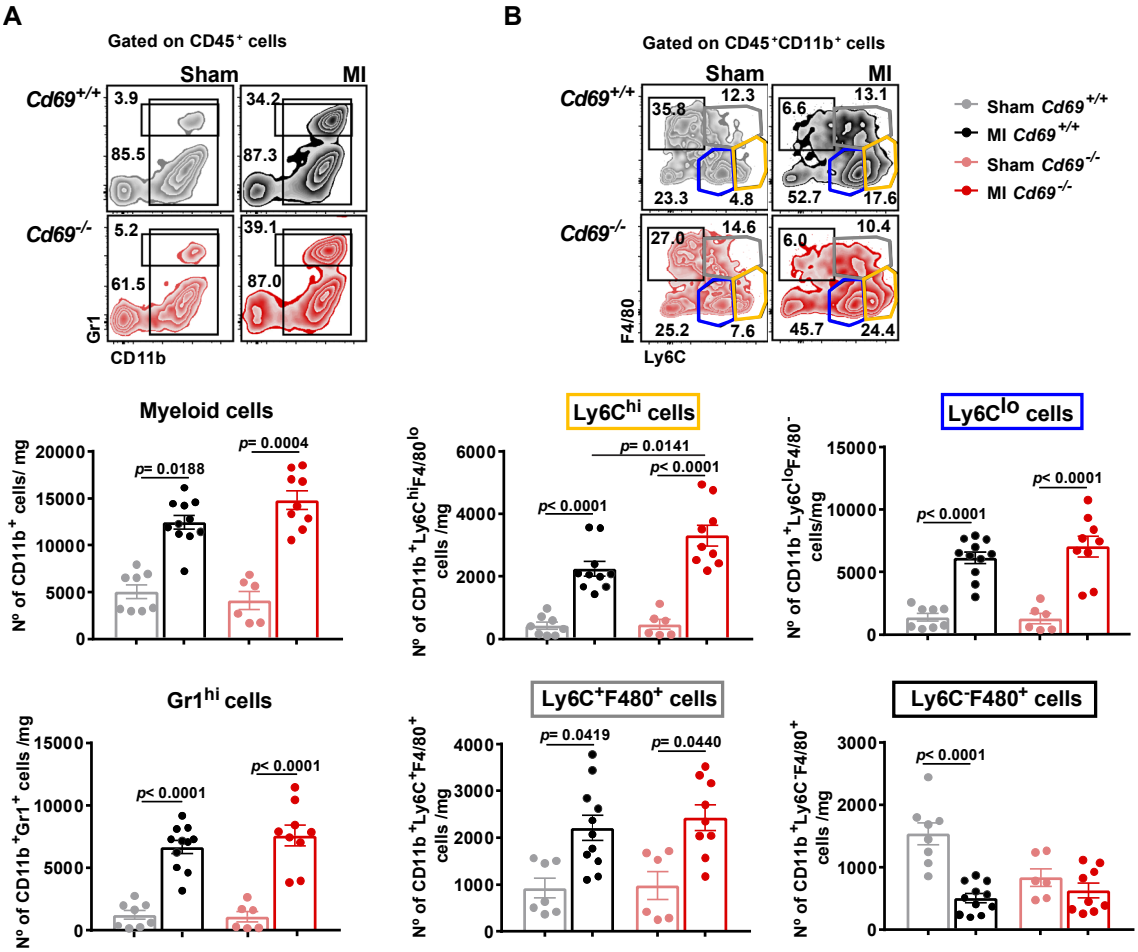

Figure R.27. Heart-infiltrating myeloid populations after LAD-ligation. (**A**) Gating strategy with representative percentages and quantification (cells/mg of heart tissue) of myeloid CD45$^+$CD11b$^+$ cells and CD45$^+$CD11b$^+$Gr1^{hi} granulocytes populations. (**B**) Gating strategy, after gating on CD45$^+$CD11b$^+$ cells, and quantification of the main CD45$^+$CD11b$^+$ myeloid populations in the heart (n= 6-11). Representative data from three independent experiments, expressed as means ± SEM (n=6-11). One-way ANOVA with Tukey's *post hoc* test.

6. CD69$^+$ Treg cells inhibit γδT cells in a CD39-dependent manner in mice

Previous studies provide evidence for antigen-independent inhibition of γδT cells by Treg cells (Park et al. 2010; Kunzmann et al. 2009), although the mechanisms remained poorly understood. Our data suggest that CD69 expression on Treg cells may be involved in limiting γδT cells activity. To test this hypothesis, we co-culture sorted *Cd69*$^{+/+}$ or *Cd69*$^{-/-}$ natural Treg cells (nTreg) with *Cd69*$^{+/+}$ γδT cells from peripheral lymph nodes (**figure R.28A**). Our data indicate that CD69$^+$ nTreg cells induce apoptosis in γδT cells more efficiently than *Cd69*$^{-/-}$ nTreg cells (**figure R.28B**). Both *Cd69*$^{+/+}$ and *Cd69*$^{-/-}$ nTreg cells successfully decrease IL-17A production in a dose-dependent manner. However, at lower doses

of nTreg cells, *Cd69*$^{+/+}$ nTreg cells show more significant reduction of IL-17A production (**figure R.28C**).

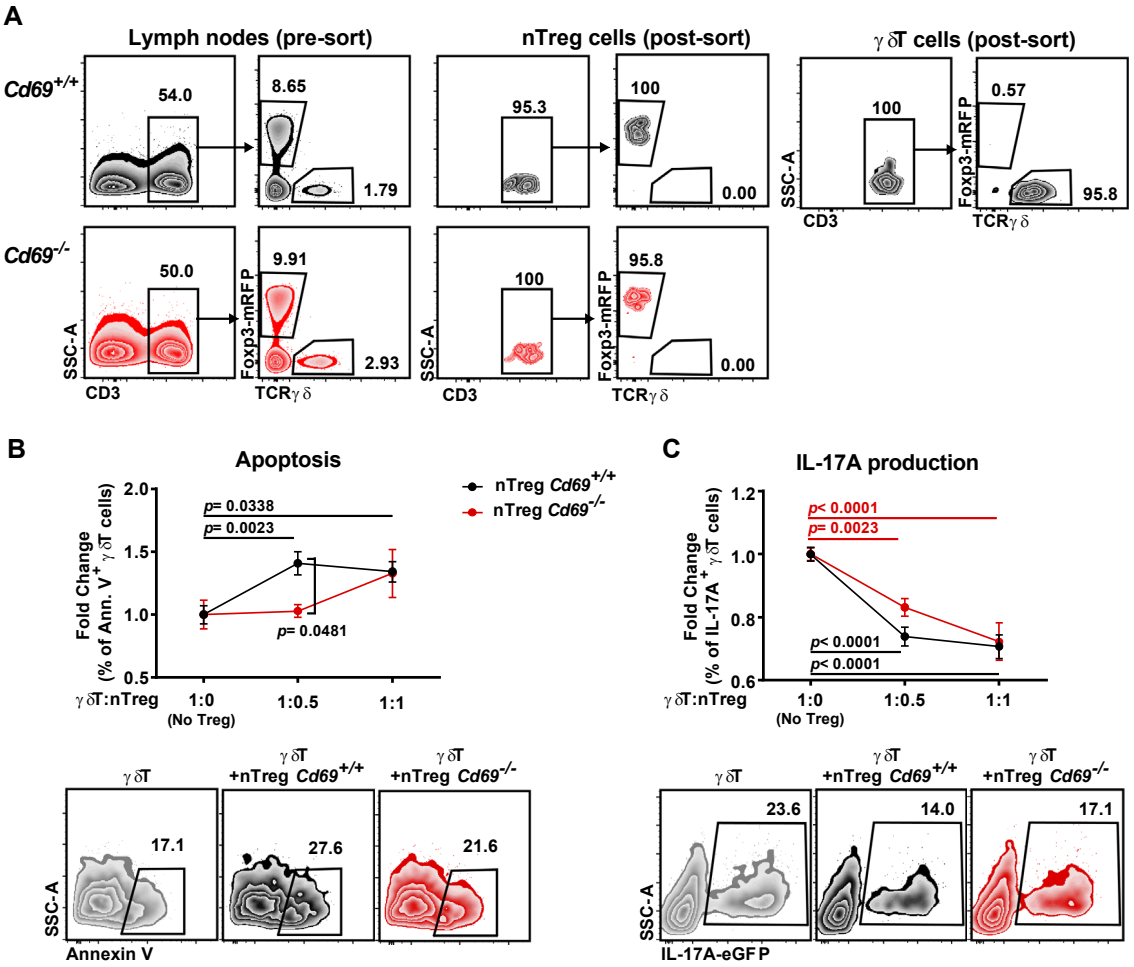

Figure R.28. CD69^{+} Treg cells induce apoptosis and inhibit IL-17 production in γδT cells. (**A**) Sorting strategy, representative frequencies in peripheral lymph nodes, and purity of sorted γδT cells and natural Treg cells used for co-culture experiments in **B** and **C**. (**B**) Sorted wild type γδT cells were co-cultured for 24h with sorted natural Treg cells from either *Cd69*$^{+/+}$ or *Cd69*$^{-/-}$ mice at the indicated γδT:nTreg ratios. Quantification of the apoptosis induction of γδT cells, represented as the fold increase of Annexin V^{+} γδT cells *versus* the condition without adding nTreg cells (ratio 1:0) (n= 4-10). Representative zebra plot of the 1:0.5 ratio, gated on γδT cells, are shown below. (**C**) Quantification of the inhibition of IL-17A production by γδT cells, represented as the fold change of IL-17A^{+} γδT cells for each ratio *versus* the 1:0 ratio (n= 6-12). Representative zebra plot of the 1:0.5 ratio, gated on γδT cells, are shown below. Data in **B** and **C** are a pool of four independent experiments. Each point depicts the mean ± SEM. Data were analyzed by two-way ANOVA with Sidak's multiple comparisons test. Significant p-values are shown (black for nTreg *Cd69*$^{+/+}$ and red for nTreg *Cd69*$^{-/-}$).

CD39 is a membrane ectonucleotidase expressed in most Treg cells that, together with CD73, converts extracellular ATP to adenosine (Borsellino et al. 2007; Deaglio et al. 2007). It has been shown that CD39 can mediate inhibition of innate cells (Fabbiano et al. 2015), independently of antigen-specific

Treg cell immunosuppression, by induction of apoptosis upon tissue injury. We have evaluated whether the observed inhibition of γδT cells by $CD69^+$ Treg cells after infarction is mediated by CD39. $CD69^+$ Treg cells express higher levels of membrane CD39 than $CD69^-$ and *Cd69*$^{-/-}$ Treg cells in peripheral blood, mediastinal lymph nodes and cardiac infiltrate two days after MI (**figure R.29A**). The reduction of IL-17A production in γδT cells by $CD69^+$ nTreg cells is impaired when a CD39 inhibitor (ARL 67156) is added to the co-culture medium. No effect of ARL 67156 is observed on *Cd69*$^{-/-}$ nTreg (**figure R.29B**). We ruled out a direct action of ARL 67156 on γδT cells since no γδT cell inhibition is observed when adding ARL 67156 in the absence of nTreg cells. These data suggest that $CD69^+$ Treg cells inhibit $IL\text{-}17^+$ γδT cells through CD39 to control inflammation after MI.

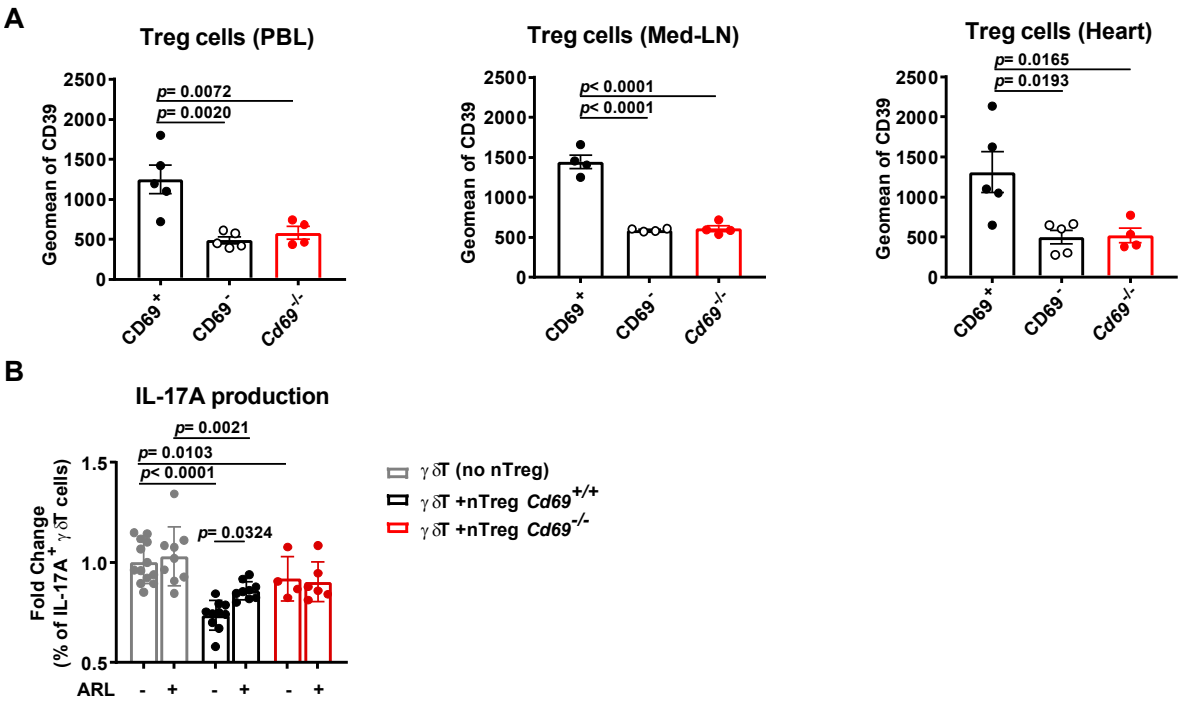

Figure R.29. $CD69^+$ Treg cells inhibit $IL\text{-}17^+$ γδT cells in a CD39-dependent manner. (**A**) CD39 expression in $CD4^+Foxp3^+$ Treg cells in peripheral blood (PBL), mediastinal lymph nodes (Med-LN) and heart, measured by flow cytometry in mice two days after LAD-ligation (n=4-5). One representative out of three independent experiments. Data, represented as means ± SEM, were analyzed by one-way ANOVA with Tukey's *post hoc* test. (**B**) IL-17A production by sorted γδT cells in the presence of nTreg cells and/or the CD39 inhibitor ARL 67156 (ARL), fold change *versus* the percentage of $IL\text{-}17^+$ γδT cells alone (n= 3-7). Data pooled from three independent experiments. Means ± SEM are shown and data were analyzed by two-way ANOVA with Sidak's multiple comparisons test.

7. Adoptive transfer of CD69-sufficient Treg cells to *Cd69*$^{-/-}$ mice restores survival, inflammation and cardiac damage after MI

In order to assess the specific role of CD69 on Treg cells in the control of inflammation and recovery after infarction we performed adoptive transfer experiments with Treg cells. *In vitro* differentiated Treg cells (iTreg) from naïve *Cd69*$^{+/+}$ and *Cd69*$^{-/-}$ CD4^{+} T cells were injected intravenously into *Cd69*$^{-/-}$ mice 4-5 h after LAD-ligation and mice were monitored for one week (**figure R.30A**). Therapy with *Cd69*$^{+/+}$ iTreg cells improved survival of *Cd69*$^{-/-}$ mice after infarction (**figure R.30B**), supporting that CD69 expression on Treg cells is sufficient to ameliorate progression after MI.

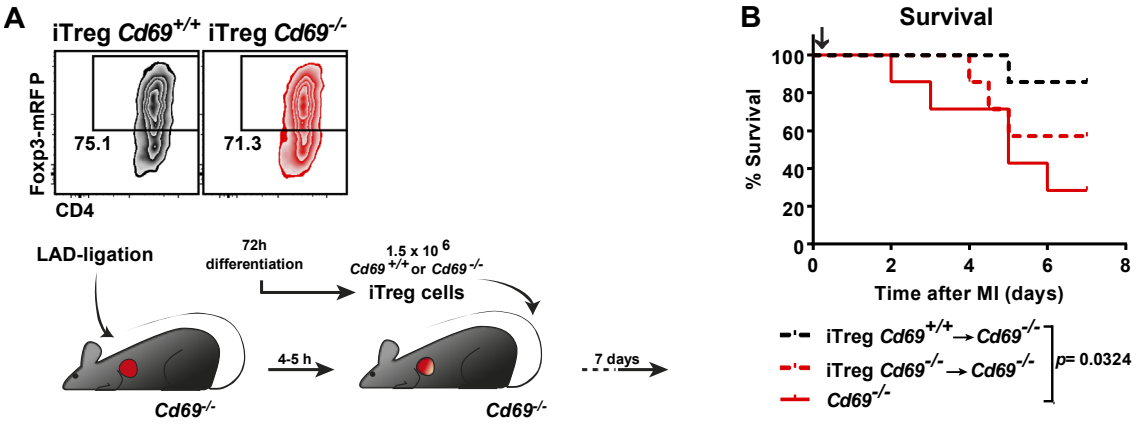

Figure R.30. Adoptive transfer of CD69-suficient Treg cells improves survival of *Cd69*$^{-/-}$ mice after MI. (**A**) Schematic workflow of iTreg adoptive transfer 4-5 h after LAD-ligation. The density plots represent the purity of 72 h-differentiated iTreg cells intravenously injected to receptor mice 5-6 h after infarction. (**B**) Survival after LAD-ligation (n= 7). Black arrow depicts the time of iTreg cell inoculation (4-5h post-infarction). *Cd69*$^{-/-}$ mice without cell transfer were used as controls. Data pooled from three independent experiments. P-value was calculated by long-rank (Mantel-Cox) test.

Analysis of hearts one week after adoptive transfer revealed that the heart-to-body weight ratio is preserved in the *Cd69*$^{-/-}$ mice transferred with *Cd69*$^{+/+}$ iTreg cells, as is the total number of leukocytes infiltrating the myocardium (**figure R.31A**). Interestingly, infiltrating IL-17^{+} γδT cells are reduced in the myocardium after transfer of *Cd69*$^{+/+}$ iTreg but not *Cd69*$^{-/-}$ iTreg cell, supporting a CD69-mediated inhibition of this population by Treg cells (**figure R.31B**). In parallel, myeloid cells, including pro-inflammatory Ly6C^{hi} monocytes and Gr1^{hi} granulocytes, are also reduced (**figure R.31C**). All these data suggest that CD69^{+} Treg cell transfer ameliorates the immune-mediated cardiac damage after LAD-ligation.

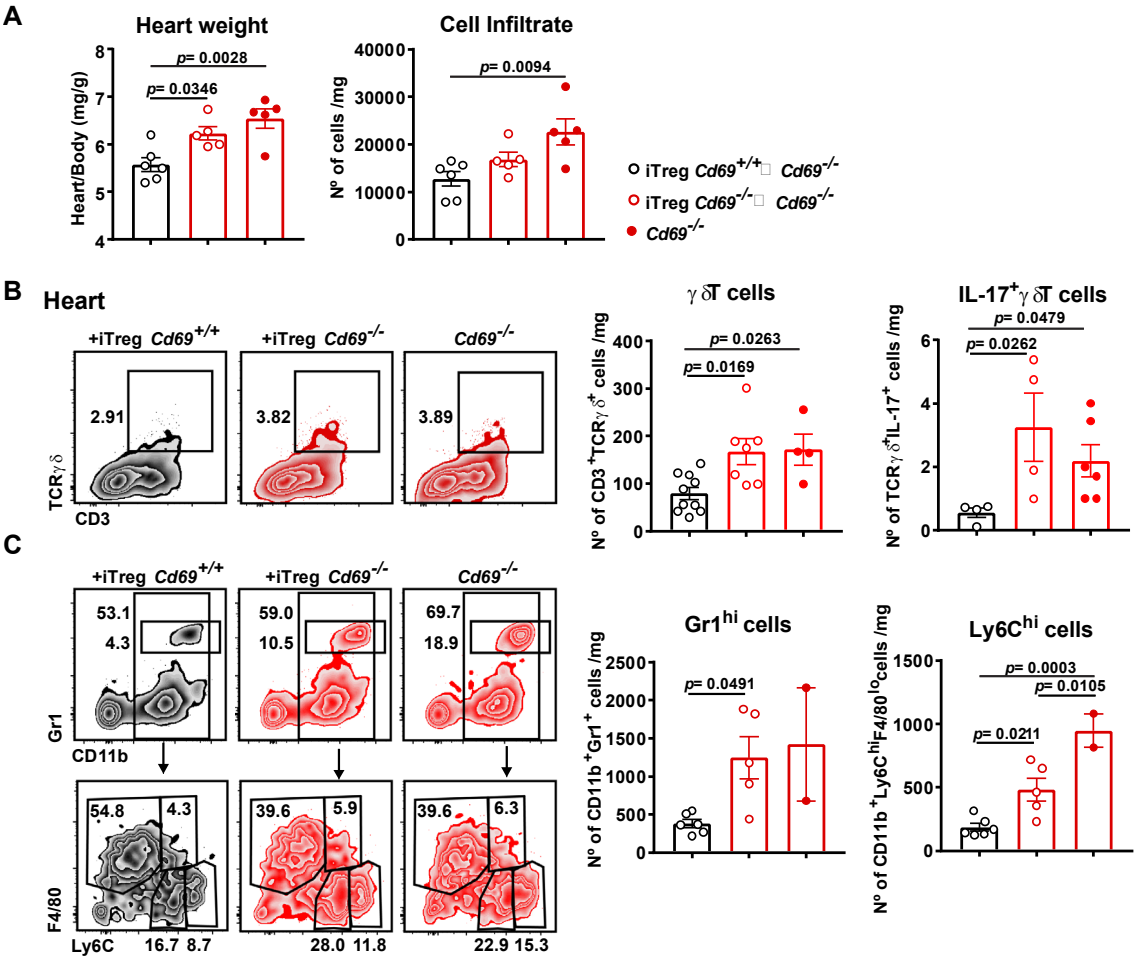

Figure R.31. Transfer of CD69-suficient Treg cells reduces IL-17$^+$ γδT cell infiltration and myocardial inflammation after MI. (**A**) Heart-to-body weight ratio and total leukocyte number per mg of heart tissue 7 days after LAD-ligation and adoptive transfer (n= 5-6). (**B**) Representative density plots (gated on CD45$^+$CD11b$^-$ cells) and quantification of the numbers of γδT cells and IL-17$^+$ γδT cells per mg of myocardial tissue 7 days post infarction. (**C**) Representative zebra plots and quantification of myeloid cell populations in the myocardium 7 days post infarction. Up, plots gated on CD45$^+$ cells. Down, plots gated on CD45$^+$CD11b$^+$ cells. Data correspond to one representative out of three independent experiments Bars indicate means ± SEM and data were analyzed by one-way ANOVA with Tukey's *post hoc* test.

8. Early expression of CD69 on Treg cells is associated with a lower risk of developing chronic heart failure in MI patients

We tested the prognostic value of CD69 expression after MI in those patients who completed 2.5 years of follow-up in our CD69 main study cohort (**table 8**). CD69 expression on Treg cells, measured at the time of hospital admission during acute MI, was lower in patients who were subsequently re-hospitalized for CHF (**figure R.32A**). Importantly, only left-ventricular ejection fraction, but neither CK or Troponin T levels, also changed (decreased) during acute MI in patients who developed CHF (**figure R.32B**). After stratifying patients according to high or low CD69 expression, as in **figure R.19**,

we observe that most patients who developed CHF belong to the group expressing low CD69 levels during acute MI (**figure R.32C**). The analysis of *CD69* mRNA levels in PBLs by qPCR revealed that CHF-developing patients also present reduced *CD69* transcription during acute MI (**figure R.32D**). *CD69* mRNA expression in PBLs correlates with *FOXP3* mRNA levels, establishing the association between CD69 expression and the Treg subset (**figure R.32E**). Importantly, the percentage of $CD69^+$ Treg cells remains a significant predictor of the CHF development after adjusting for traditional biomarkers of cardiac injury and confounders, such as sex and age (**figure R.32F**).

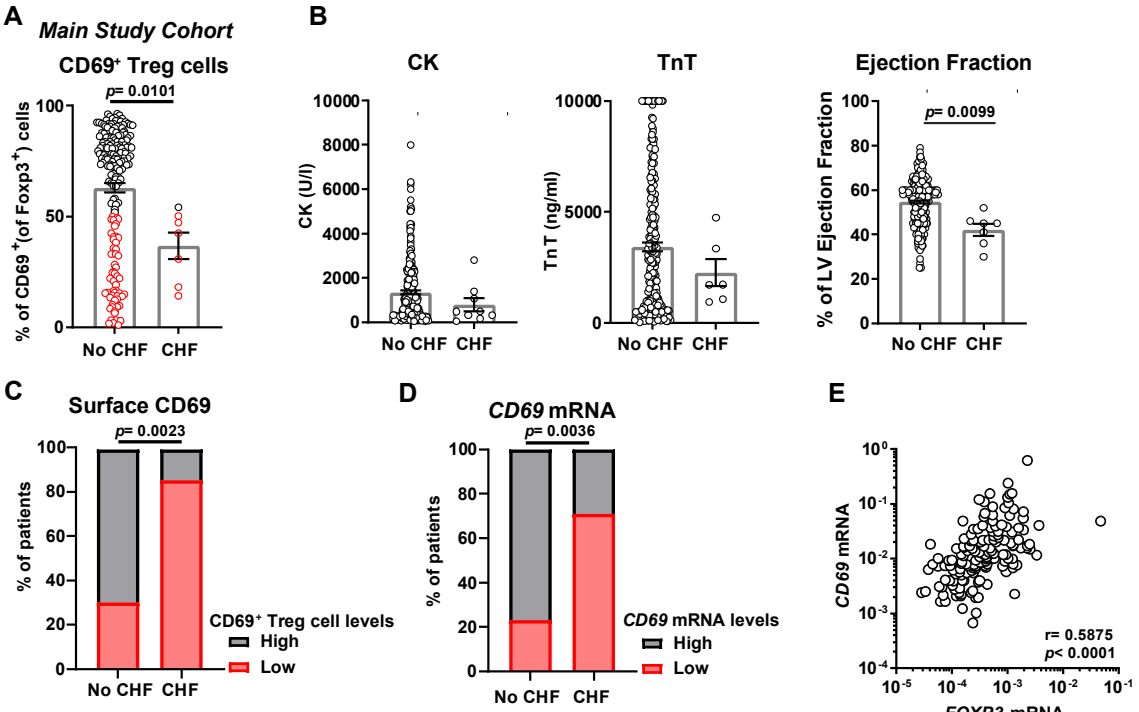

F

CHF vs No CHF

	Odds ratio (95% CI)	*p*-value
(Intercept)	0.000 (0.000-0.136)	0.0938
Troponin s (Norm.)	0.992 (0.974-0.974)	0.2049
LV Ejection Fraction(%)	0.907 (0.759-1.044)	0.1888
CK (U/l)	1.001 (0.999-1.005)	0.4089
$CD69^+$ Treg cells (%)	0.929 (0.838-0.980)	0.0409*
Sex	11.1 (0.404-4765.4)	0.2471
Age	1.430 (1.128-2.482)	0.0444*

Figure.32. High CD69 expression in MI patients at admission is associated with a decreased risk of developing chronic heart failure. After 2.5 years of clinical follow-up, patients were stratified depending on whether they have or have not developed CHF. **(A)** CD69 expression on Treg cells and (**B**) biomarkers of cardiac injury at the time of hospital admission for acute MI. Data expressed as means ± SEM (n= 7 CHF and n= 180 No CHF). Mann-Whitney U-test. (**C**) Percentage of patients with low/high levels of surface CD69 expression on Treg cells measured by FACS. (**D**) Percentage of patients with low/high levels of *CD69* mRNA expression measured by qPCR in PBLs. P-value was calculated by χ^2 test. (**E**) Correlation between *FOXP3* and *CD69* mRNA levels in PBLs of MI patients. Spearman correlation coefficient (r) and p-value are shown. (**F**) Multivariable logistic regression model to discriminate patients with and without CHF, controlling for potential confounders.

In parallel, we prospectively analyzed the contribution of early CD69 expression (i. e. within the first 24 h from hospital admission) to clinical outcome after MI in an additional independent validation cohort of 84 patients with similar time of follow-up (**tables 9 and 10**). Quantification of *CD69* mRNA levels in PBLs confirmed that patients who developed CHF expressed lower *CD69* levels during acute MI in an independent cohort (**figure R.33A and R.33B**). As in the main study cohort, *CD69* mRNA expression correlates significantly with the expression of the Treg-master transcription factor *FOXP3* (**figure R.33C**). Thus, these data corroborate that early CD69 expression in MI patients is associated with a lower risk of developing CHF.

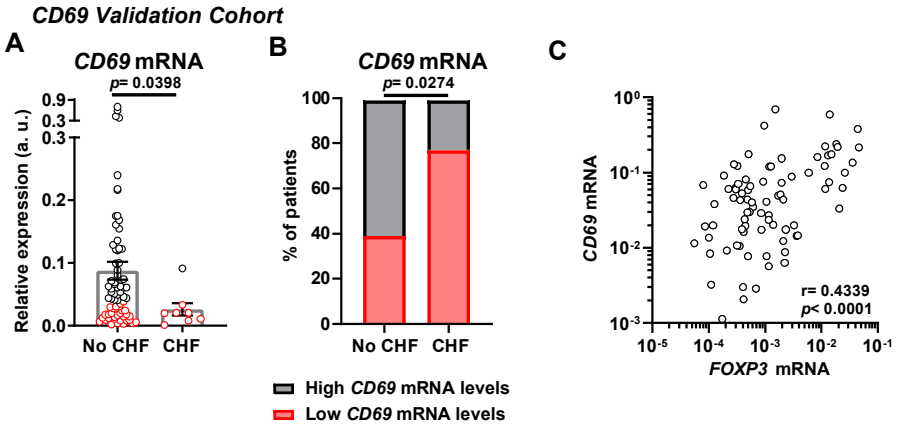

Figure R.33. Validation of CD69 expression as negatively associated with CHF in an independent cohort of MI patients. (A) *CD69* mRNA levels measured by qPCR in total PBLs from the independent validation cohort of patients. Means ± SEM (n=75 No CHF and n= 9 CHF). Mann-Whitney U-test. (**E**) Frequency of patients with low/high levels of *Cd69* mRNA, measured by qPCR ($2^{-\Delta Ct}$ values were used to discriminate between low and high expressing patients). P-value was calculated by χ^2 test. (**F**) Correlation between *FOXP3* and *CD69* mRNA expression in PBLs of the validation cohort. Spearman's correlation coefficient (r) and p-values are shown.

9. CD69$^+$ Treg cells synthetize hsa-miR-155-5p during MI

We have previously reported that the cooperation between CD69 and miR-155-5p is crucial for the differentiation of Treg cells. The miR-155-5p pathway is enhanced by CD69 expression in Treg cells upon activation and differentiation (Sanchez-Diaz et al. 2017). We aimed to investigate if miR-155-5p expression could be an indicator of functional CD69$^+$ Treg cell responses for the control of inflammation and prognosis after infarction. For this purpose, we first analyzed the expression of hsa-miR-155-5p and surface CD69 in sorted Treg cells from PBLs of MI patients (**figure R.34A**), confirming that CD69 and hsa-miR-155-5p levels are correlated in Treg cells after MI (**figure R.34B)**. Secondly, we separated Treg cells based on membrane CD69 expression after overnight bystander TCR stimulation (**figure R.34C)**. The data indicate that CD69$^+$ Treg cells express higher levels of hsa-miR-

155-5p than CD69$^-$ Treg cells (**figure R.34D**), highlighting an activation of the hsa-miR-155-5p pathway by CD69 expression in Treg cells after MI.

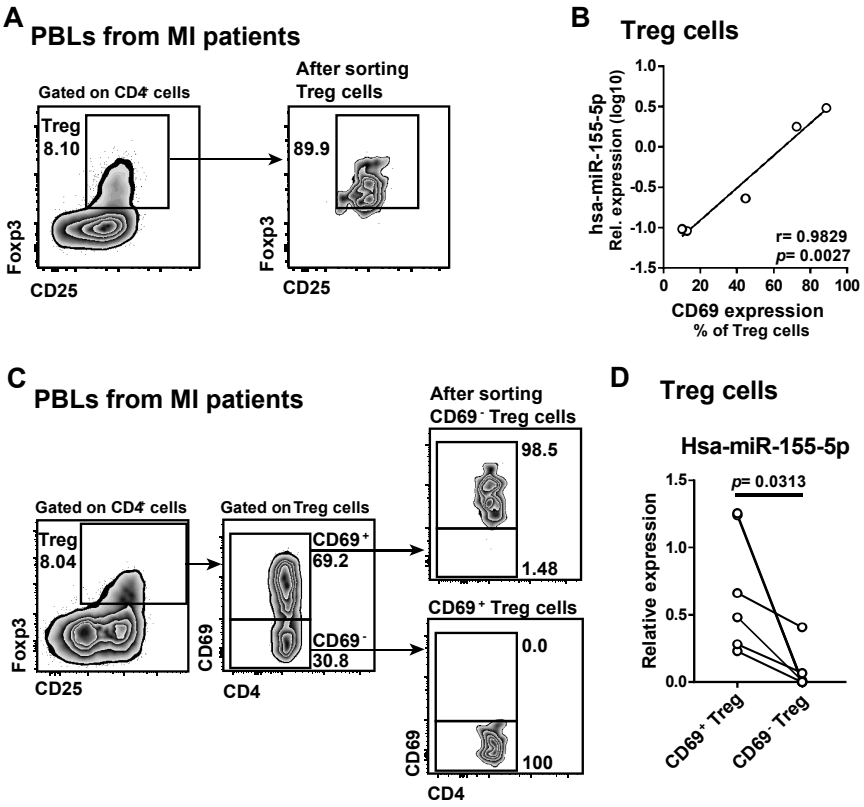

Figure R.34. CD69$^+$ Treg cells synthesize hsa-miR-155-5p during MI. (**A**) Sorting strategy and after-sorting purity of Treg cells from PBLs of MI patients. (**B**) Correlation between CD69 expression, measured as a percentage of Treg cells, and hsa-miR-155-5p levels, measured by qPCR in sorted Treg cells from MI patients (n= 5). Spearman's correlation coefficient (r) and p-value are shown. (**C**) Sorting strategy of CD69$^+$ Treg cells and CD69$^-$ Treg cells from PBLs of MI patients. (**D**) Relative expression of hsa-miR-155-5p in sorted CD69$^+$ and CD69$^-$ Treg cells. Lines link populations from the same patient (n= 6). Data analyzed by Wilcoxon matched-pairs signed rank test.

10. Circulating hsa-miR-155-5p mirrors the peripheral CD69$^+$ Treg cell response in MI patients

In order to study the peripheral hsa-miR-155-5p response after infarction, we analyzed the miRNA levels in plasma of patients with MI from our main study cohort (**table 7**). We found that hsa-miR-155-5p is upregulated in plasma during acute MI when compared with healthy controls (**figure R.35A**).

Different immune cell types can express this miRNA, so we analyzed the correlation of hsa-miR-155-5p plasma levels and different lymphoid and myeloid populations present in peripheral blood (**figure**

R.17 and table 14). Remarkably, only $CD69^+$ Treg cells correlated positively and significantly with the plasma levels of hsa-miR-155-5p (**table 14 and figure R.35B**), suggesting that this population could be the major source of this miRNA and that the overall miRNA expression in plasma may depend on CD69 expression on Treg cells. Additionally, the miRNA levels were inversely correlated with Th17 cells, Th17/Treg and Th17/$CD69^+$ Treg cell ratios, in agreement with an association with anti-inflammatory responses (**table 14**).

	Plasma hsa-miR-155-5p		
	r	p-value	N
CD4	0.02371	0.7597	169
$CD45RA^+$ CD4	-0.0165	0.8314	169
$CD45RO^+$ CD4	0.02129	0.7835	169
$CD69^+$ CD4	0.08441	0.2752	169
Treg ($CD4^+Foxp3^+CD25^+$)	0.09579	0.2154	169
$CD45RA^+$ Treg	-0.02338	0.7628	169
$CD45RO^+$ Treg	0.02148	0.7817	169
$CD69^+$ Treg	**0.1559**	**0.0430**	**169**
Th1 ($CD4^+IFNg^+$)	-0.04237	0.5983	157
Ratio Th1/Treg	-0.09317	0.2354	164
Ratio Th1/$CD69^+$ Treg	-0.1322	0.0915	164
Th17 ($CD4^+IL\text{-}17^+$)	**-0.1896**	**0.0174**	**157**
Ratio Th17/Foxp3	**-0.1899**	**0.0146**	**165**
Ratio Th17/$CD69^+$ Treg	**-0.1513**	**0.0496**	**169**
$CD4^+IL17^+IL22^+$ (DP)	0.01799	0.823	157
Th22 ($CD4^+IL\text{-}22^+$)	0.009988	0.9012	157
Ratio Th22/Treg	-0.01349	0.8618	469
Ratio Th22/ $CD69^+$ Treg	-0.03949	0.6102	169
Monocytes	0.1331	0.2548	75
Classical Monocytes	-0.07365	0.5300	75
Intermediate Monocytes	-0.009929	0.9326	75
Non-classical Monocytes	0.03508	0.7651	75
$CD66b^+CD14^{lo}$	-0.1385	0.2360	75

Table 14. Correlations between hsa-miR-155-5p plasma levels and peripheral blood immune populations in MI patients. Spearman correlation coefficient (r) and p-values were calculated between the percentages or the ratio of percentages of the different immune cell populations in peripheral blood, measured by flow cytometry, and the $2^{-\Delta\Delta Ct}$ qPCR values of hsa-miR-155-5p (normalized *versus* healthy individuals). The numbers of samples (N) indicate the number of XY pairs for each comparison. Significant p-values are highlighted in bold.

Last, we compared the expression levels of the miRNA between MI patients with high CD69 levels and low CD69 levels, since we have validated them to differ in terms of clinical evolution. MI patients with low CD69 levels, associated with a higher risk of developing CHF (**figures R.32 and R.33**), exhibited decreased expression of hsa-miR-155-5p in plasma (**figure R.35C**), advocating for the study of this miRNA as a progression marker of MI.

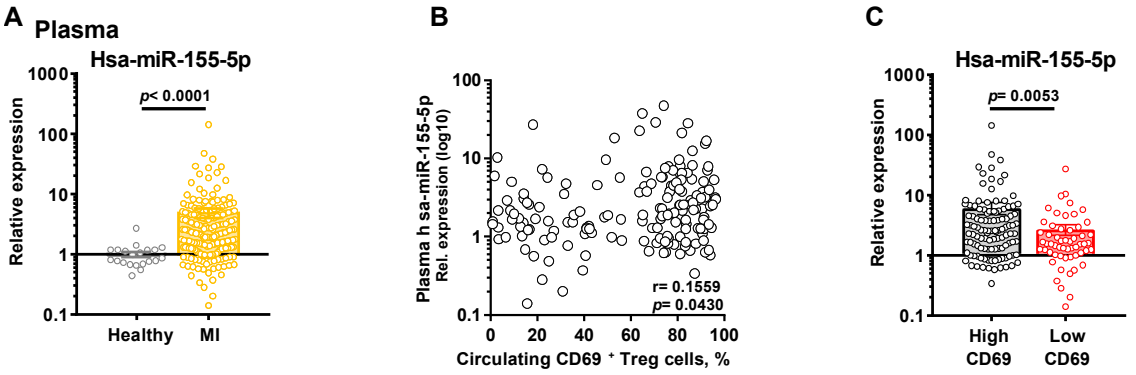

Figure R.35. Hsa-miR-155-5p is upregulated in plasma from MI patients correlating with the CD69$^+$ Treg cell response. (**A**) Analysis of hsa-miR-155-5p levels in peripheral plasma form healthy donors (n= 21) and MI patients (n= 188). Data are represented as log10 of miRNA relative expression. (**B**) Correlation between hsa-miR-155-5p plasma levels and percentage of circulating CD69$^+$ Treg cells per patient, analyzed by Spearman correlation coefficient (r) (n=169 XY pairs). (**C**) Comparison of miRNA levels in plasma from patients expressing high levels of CD69 (n= 113) and low levels of CD69 (n= 56) on Treg cells. Data are represented as log10 of miRNA relative expression. Data in **A** and **C** are represented as means ± SEM and were analyzed by Mann-Whitney U test.

DISCUSSION

DISCUSSION

Increasing number of evidences illustrate the important contribution of miRNAs in the regulation and diagnosis of cardiovascular and inflammatory diseases. In addition, different cardiomyopathies differ on the nature and kinetics of their immune responses. By combining preclinical and clinical research approaches, we have defined novel mechanisms in which T-cell-derived miRNAs and other molecules appear as relevant candidates for precision medicine in myocarditis and myocardial infarction.

1. Mmu-miR-721/Hsa-miR-Chr8:96 as a biomarker of myocarditis

Myocarditis remains a diagnostic challenge in clinical practice due to the atypical nature of its clinical presentation and the lack of easily accessible and accurate diagnostic methods (Caforio et al. 2013). An early diagnosis is essential for establishing an appropriate treatment and, consequently, improving outcomes (Heymans et al. 2016). Although endomyocardial biopsy remains the reference standard, it is not routinely performed in clinical practice as it is a highly invasive method with associated risks and limited sensitivity (Sato 2019). The advent of CMR has notably improved the diagnosis of acute myocarditis (Kotanidis et al. 2018). Identification of myocardial oedema, vascular permeability and fibrosis by CMR evidences the presence of myocarditis with acceptable efficacy (Lurz et al. 2016; Ferreira et al. 2018). Even though CMR is a non-invasive tool, it has limitations such as the lack of accessibility in many hospitals and in the ambulatory setting and the decrease in sensitivity for oedema detection and vascular permeability overtime (Lurz et al. 2016). These limitations hinder the rapid use of CMR at the time of initial clinical suspicion. Therefore, there is a need for new diagnostic methods that ideally combine precision, together with precocity and usefulness in differential clinical scenarios.

Multiple studies have increasingly endorsed the importance of T cells and adaptive immunity in acute coronary syndrome (Zhao et al. 2011; Simon et al. 2013; Weirather et al. 2014) and myocarditis (Daniels et al. 2008; Sonderegger et al. 2008) over the last years. However, due to the heterogeneity or low sample size of these studies, the role and the proportion of each T cell subset in heart and blood remained poorly characterized. The immune response has surged as a source of disease-specific biomarkers of different cardiac affectations (Frangogiannis 2014; Zhang, Bauersachs, and Langer 2017; Chaikijurajai and Tang 2020). We have studied the adaptive immune responses, using FACS in freshly isolated PBLs, in animal models and in patients at the time of hospital admission confirming that circulating Th17 cells are characteristic of the acute phase of cardiac injury in myocarditis of different etiologies, but not in MI.

Circulating miRNAs are secreted to human biofluids into extracellular vesicles during pathological conditions, offering a unique opportunity to develop non-invasive molecular diagnostic tools. In recent years, these biomarkers have been used more frequently for the diagnosis of certain types of cancer, enhancing the progression in the field of detection to facilitate its implementation in clinical settings (Moody et al. 2017). Nowadays, the widely clinically used PCR technology, in parallel with the development of portable point-of-care devices for the detection of circulating miRNAs is a growing field of research (Vaca 2014). This is improving the detection of miRNA-biomarkers without the need of expertise in molecular biology techniques. Thus, the determination of circulating miRNAs is becoming a fast, reliable, easy-to-handle, and cost-efficient method for diagnosis.

In order to search for myocarditis-specific biomarkers, we profiled miRNAs in Th17 cells and plasma obtained from autoimmune and viral myocarditis mice, identifying mmu-miR-721 as an exclusive marker of myocarditis. Cloning of a consensus sequence of the mmu-miR-721 in the plasma of patients with acute myocarditis allowed us to identify hsa-miR-Chr8:96. Structural and functional validation, including the co-immunoprecipitation with AGO2 and luciferase reporter assays, suggests that the conserved sequence hsa-miR-Chr8:96 is compatible with a miRNA. As for mmu-miR-721, hsa-miR-Chr8:96 is also upregulated by human Th17 cells and plasma during acute myocarditis. Hsa-miR-Chr8:96 was validated in four independent patient cohorts worldwide as a diagnostic biomarker of myocarditis, able to discriminate between this pathology from healthy individuals and patients with MI.

Even though it is a Th17-derived biomarker, the levels of circulating hsa-miR-Chr8:96 remained elevated in myocarditis when compared with those in patients with different autoimmune diseases that occur with activation of Th17 responses. Although without reaching the levels of myocarditis, a partial elevation of the biomarker was found in patients with psoriasis and spondyloarthritis, in which cardiovascular affectation is an important comorbidity presentation (Boehncke 2018; Caiazzo et al. 2018; Moltó and Nikiphorou 2018; Kim and Choi 2021). This observation might be explained by the fact that hsa-miR-Chr8:96 could be preferentially produced by heart-specific Th17 cells. It might also be explained by a diversity in the prominence of the peripheral acute Th17 response in the different autoimmune manifestations.

Although ROC curves analyses revealed a marginal overlap with MI patients, we noted a high variability in the levels of hsa-miR-Chr8:96 among patients with myocarditis that remains unexplained. According to preclinical data, mice developing more aggressive forms of myocarditis present higher levels of mmu-miR-721. Nevertheless, a follow up of the myocarditis patients included in this study was not available so to ascertain whether variations in the levels of hsa-miR-Chr8:96 might reflect the differences in the disease outcome. Even though preclinical data suggest a possible prognostic value of the biomarker, this aspect should be studied in detail in humans. In addition, the biomarker has not been assessed in other chronic scenarios such as in dilated cardiomyopathy patients or other entities that

might present resemblance with myocarditis in the clinical setting. Since hsa-miR-Chr8:96 has been measured with *ad-hoc* synthesized miRNA primers not commercially available, technical yield fluctuations in the primers production might also explain the variability in the measurements.

We showed that mmu-miR-721/hsa-miR-Chr8: 96 contains the EXOmotif GG(A/G)G and so they are encapsulated into plasma EVs. A previous work has already detected mmu-miR-721 enriched into exosomes (Jovičić and Gitler 2017). Here we found that Th17 cells secrete this miRNA during EAM. The sorting of miRNAs into EVs preserves their stability in plasma and protects them from degradation by RNAses (Villarroya-Beltri et al. 2013; Santangelo et al. 2016). The fact that hsa-miR-Chr8:96 is contained in plasma EVs, being upregulated in plasma EVs from myocarditis patients, reinforces its use as a stable biomarker candidate in clinical practice.

The development of a disease biomarker requires the validation in different cohorts. In this regard, hsa-miR-Chr8:96 demonstrated a significant diagnostic value to discriminate patients with myocarditis from those with MI or MINOCA in four independent cohorts from Madrid (Spain), Boston (MA, USA), Zurich (Switzerland) and Padua (Italy). In addition, the biomarker retained its diagnostic value when adjusted by age, sex, ejection fraction and troponins. The availability of hsa-miRNA-Chr8:96 as a biomarker for the early detection of acute myocarditis could assist the clinicians in difficult scenarios, as those with low grade of clinical suspicion, avoiding the risks and costs associated with invasive procedures and improper therapies. Thus, hsa-miR-Chr8:96 stands as a molecular biomarker for improving the diagnosis of acute myocarditis, although further studies are necessary to confirm its impact on clinical decision making and patient management in the context of a clinical trial.

2. miR-721 as an immunomodulator of myocarditis

Beyond its potential as a biomarker, we found that this miRNA plays a role in regulating Th17 responses during myocarditis development. Interestingly, two of the validated targets for mmu-miR-721 in mice, being, *Nos2* and *Pparg*, have been related with Th17 cell biology. PPARγ restrains Th17 differentiation (Klotz et al. 2009). The role of Nos2 is more controversial. Although it was described to maintain stability of human Th17 cells (Obermajer et al. 2013), in different mouse models of autoimmunity, Nos2 functions as a brake for Th17 cell differentiation and cytokine production (Niedbala et al. 2011; Jianjun et al. 2013).

Our data demonstrate that mmu-miR-721 overexpression downregulates *Pparg* in *ex vivo* $CD4^+$ T cells isolated from EAM mice, revalidating this target in T cells. PPARγ is a repressor of *Rorc* transcription (Klotz et al. 2009). Consequently, mmu-miR-721 overexpression results in increased *Rorc* mRNA and RORγt protein levels, enhancing IL-17 production (**figure D.1**). Overexpression of mmu-miR-721 in $CD4^+$ T cells lacking PPARγ would be of interest to confirm that the effect observed on Th17 cell

polarization is due to the modulation of PPARγ by mmu-miR-721. Inversely, we found that the *in vivo* inhibition of mmu-miR-721 with blocking antisense sponge molecules augments *Pparg* levels in the draining lymph nodes of EAM mice. This blockade of mmu-miR-721 decreases the amount of Th17 cells in the myocardium, thus ameliorating EAM progression. Therefore, mmu-miR-721 works as an immunomodulator of myocarditis development by boosting Th17 responses. In this regard, this miRNA appears as a candidate for the development of therapeutic approaches for myocarditis. Data from our laboratory not shown here showed that overexpression of hsa-miR-Chr8:96 in human PBLs downregulates endogenous PPARγ levels. More research has to be brought forward to evaluate whether hsa-miR-Chr8:96 regulates human T cell responses in the same way than mmu-miR-721.

The active secretion of this miRNA into circulating EVs leads us to conjecture that it may play a role not only within Th17 cells but also in distant cells and tissues. For instance, mmu-miR-721 plays a role in macrophages, contributing to pathogen infectivity of this cell type by modulating Nos2 (Muxel et al. 2017). In the context of myocarditis, specific experiments designed to identify the target cells that uptake the Th17-cell-derived mmu-miR-721 would clarify a possible function of this miRNA in intercell communication.

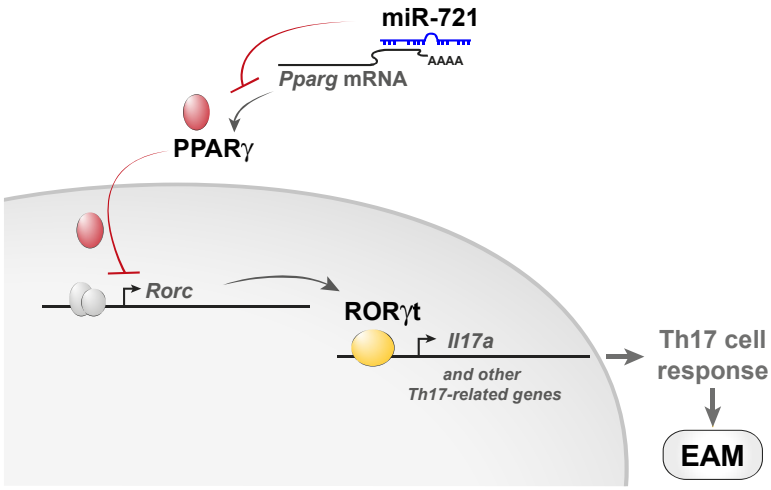

Figure D.1. miR-721 controls Th17 cell responses and EAM progression by inhibiting *Pparg*. In the cytoplasm, mmu-miR-721 binds the 3' UTR of *Pparg* mRNA, downregulating its expression. PPARγ keeps repressor molecules on the *Rorc* promoter, contributing to the transcriptional inhibition of this gene. Thus, in the presence of mmu-miR-721, *Pparg* is inhibited and *Rorc* derepressed, increasing the expression of RORγt target genes, such as IL-17, and consequently favoring Th17 cell responses and EAM progression.

3. CD69^{+} Treg cells control MI-induced myocardial inflammation and damage

Multiple studies have documented that Treg cells are recruited to the myocardium during the first days after MI to control excessive inflammation and prevent cardiac deterioration (Sharir et al. 2014; Weirather et al. 2014; Xia et al. 2015; Bansal et al. 2019; Wang et al. 2019). Our results illustrate that

CD69 expression contributes to the anti-inflammatory properties of Treg cells in the context of MI. CD69 is an inflammatory brake that promotes Treg cell differentiation and suppressor function and prevents pro-inflammatory T cell responses in multiple disease scenarios (Gonzalez-Amaro et al. 2013). It was shown that CD69 expression on lymphocytes prevents atherosclerosis progression in mice, and that low CD69 levels in PBLs predicts subclinical atherosclerosis in asymptomatic individuals after adjustment for traditional cardiovascular risk factors (Tsilingiri et al. 2019). Here we demonstrate that CD69 also plays a role after ischemic events in the myocardium. Mice lacking CD69 exhibit increased myocardial inflammation and heart dysfunction, leading to a prompt decrease in survival during the first week after infarction. Therapy with $CD69^+$ Treg cells in the first hours after LAD-ligation alleviates cardiac inflammation and improves survival of *Cd69*$^{-/-}$ mice, revealing that CD69 expression specifically on the Treg subset is sufficient to ameliorate the recovery after MI.

In order to shed light on the regulatory mechanism of CD69 after MI, we explored in detail the peripheral and myocardial inflammatory responses after LAD-ligation. We found that Treg cells expressing CD69 are mobilized and recruited to the infarcted tissue shortly after LAD-ligation. In contrast, the absence of CD69 results in a rapid and excessive recruitment of heart-infiltrating leukocytes in mice as early as two days after MI. The recruitment of these antigen-independent $CD69^+$ Treg cells is critical for the control of the inflammatory burden in the ischemic tissue and recovery of the mice. Different natural ligands of CD69, such as Gal-1 (de la Fuente et al. 2014) or S100A8/A9 (Lin et al. 2015), are upregulated after MI and contribute to immune cell recruitment (Seropian et al. 2013; Sreejit et al. 2020). Particularly, Gal-1 is expressed by damaged cardiomyocytes in mice and humans (Seropian et al. 2013). Gal-1-deficient mice present exacerbated inflammation and damage and decrease survival during the first week post LAD-ligation, similarly to *Cd69*$^{-/-}$ mice. The release of Gal-1 by cardiomyocytes under hypoxic conditions (Al-Salam and Hashmi 2014) works as a chemoattractant to call Treg cells to the ischemic myocardium and maintain homeostasis (Seropian et al. 2013). The aforementioned mechanism might explain why $CD69^+$ Treg cells, sensitizing Gal-1, are selectively recruited to the heart after MI, although this hypothesis should be demonstrated experimentally.

Increased numbers of IL-17^+ γδT cells characterize the cellular infiltrate of the heart of *Cd69*$^{-/-}$ mice, being the main source of IL-17A already two days after MI. IL-17^+ γδT cells express the surface CCR6 (Haas et al. 2009), which sensitizes CCL20 released by the infarcted myocardium, contributing to their recruitment (Yan et al. 2012). The increased recruitment of IL-17^+ γδT cells is in agreement with the worse prognosis of *Cd69*$^{-/-}$ mice after MI, as γδT cells induce apoptosis of cardiomyocytes (Huber 2000) and the production of IL-17 promotes fibrosis, sustains neutrophil/monocyte infiltration and polarizes macrophages toward a pro-inflammatory phenotype (Yan et al. 2012). This fact could explain the increased levels of infiltrating pro-inflammatory $Ly6C^{hi}$ cells in *Cd69*$^{-/-}$ mice. Reciprocally, macrophage

and neutrophils cells locally sustain IL-17$^+$ γδT cell polarization in an inflammatory feedback loop. Upon TLR recognition of DAMPs, these innate cells secrete IL-23 and IL-1β, which stimulate IL-17 production by γδT cells (Sutton et al. 2009). Since γδT cells also express some TLRs (Martin et al. 2009; Mokuno et al. 2000; Ribot et al. 2010), they are able to directly respond to DAMP signals released by the injured tissue (Yan et al. 2012) (**figure D.2**). Notably, we observed that peripheral *Cd69*$^{-/-}$ γδT cells express significantly higher levels of IL-17A in basal conditions, suggesting that CD69 might be also playing a role in the intrinsic regulation of this T cell subset. This observation open venues for the study of CD69 in the ontogeny and differentiation of γδT cells.

It is well established that Treg cells suppress effector CD4$^+$ T cells and CD8$^+$ T cells (Shevach 2009; Josefowicz, Lu, and Rudensky 2012). However, these populations play a minor a role during the first days after MI. It has been described that Treg cells can reduce the proliferation of human phosphoantigen-expanded γδT cells (Kunzmann et al. 2009) and the proliferation and cytokine production of murine intestinal γδT cells (Park et al. 2010) in an antigen-independent manner, evidencing that Treg cells are also capable of inhibiting this T cell subset. Our data show that mouse γδT cells undergo apoptosis and decrease IL-17A production *in vitro* when Treg cells are added to the culture, supporting the inhibitory effect of Treg cells on γδT cells. This effect is dose-dependent and is mediated by CD69, as *Cd69*$^{-/-}$ Treg cells show a lower inhibitory capacity. These results may explain the decrease in the number of IL-17$^+$ γδT cells in the infarcted heart after the adoptive transfer of *Cd69*$^{+/+}$ Treg cells. Interestingly, the accumulation of IL-17$^+$ γδT cells in the heart is impaired when *Cd69*$^{+/+}$ but not *Cd69*$^{-/-}$ Treg cells are transferred, reinforcing that CD69 mediates the inhibition of IL-17$^+$ γδT cells by Treg cells *in vivo*. Therefore, CD69$^+$ Treg cells counteract the inflammatory loop in the microenvironment of the infarcted myocardium by targeting γδT cells (**figure D.2**). Whether CD69$^+$ Treg cells directly inhibit other inflammatory subsets remains unexplored.

In order to deepen in the molecular basis of this rapid inhibition of γδT cells, we examined the CD39-mediated antigen-independent mechanisms of Treg suppression. CD39 is an ectonucleotidase that hydrolyzes extracellular ATP, released from damaged tissue like the injured myocardium (Dolmatova et al. 2012), to AMP, which is further degraded to adenosine by CD73. Adenosine promotes apoptosis and cell inhibition of innate and T effector cells (Deaglio et al. 2007; Fabbiano et al. 2015) and adenosine uptake by Treg cells sustains suppressive functions (Ohta and Sitkovsky 2014). Also, extracellular ATP depravation by CD39 contributes to the Treg-mediated protection of tissue injury (Wang et al. 2012). Our work shows that CD69$^+$ Treg cells in peripheral blood, draining lymph nodes and infiltrating the heart express higher levels of membrane CD39 compared with CD69$^-$ or *Cd69*$^{-/-}$ Treg cells two days after LAD-ligation. Consistently, we report that chemical inhibition of CD39 results in impaired suppression of γδT cells by CD69-sufficient Treg cells, whereas no effect is observed on CD69-deficient Treg cells, suggesting that CD69$^+$ Treg cells exert their inhibition of γδT in a CD39-

dependent manner. Nevertheless, expression of CD39 and CD73 was also detected in other cardiac infiltrating leukocyte subsets (Bonner et al. 2012). Although we observe no inhibitory effect when treating γδT cells with a CD39 inhibitor in the absence of Treg cells, demonstrating that CD39 specifically on Treg cells inhibits γδT cell inhibition, the contribution of CD39 in other cardiac populations is disregarded here.

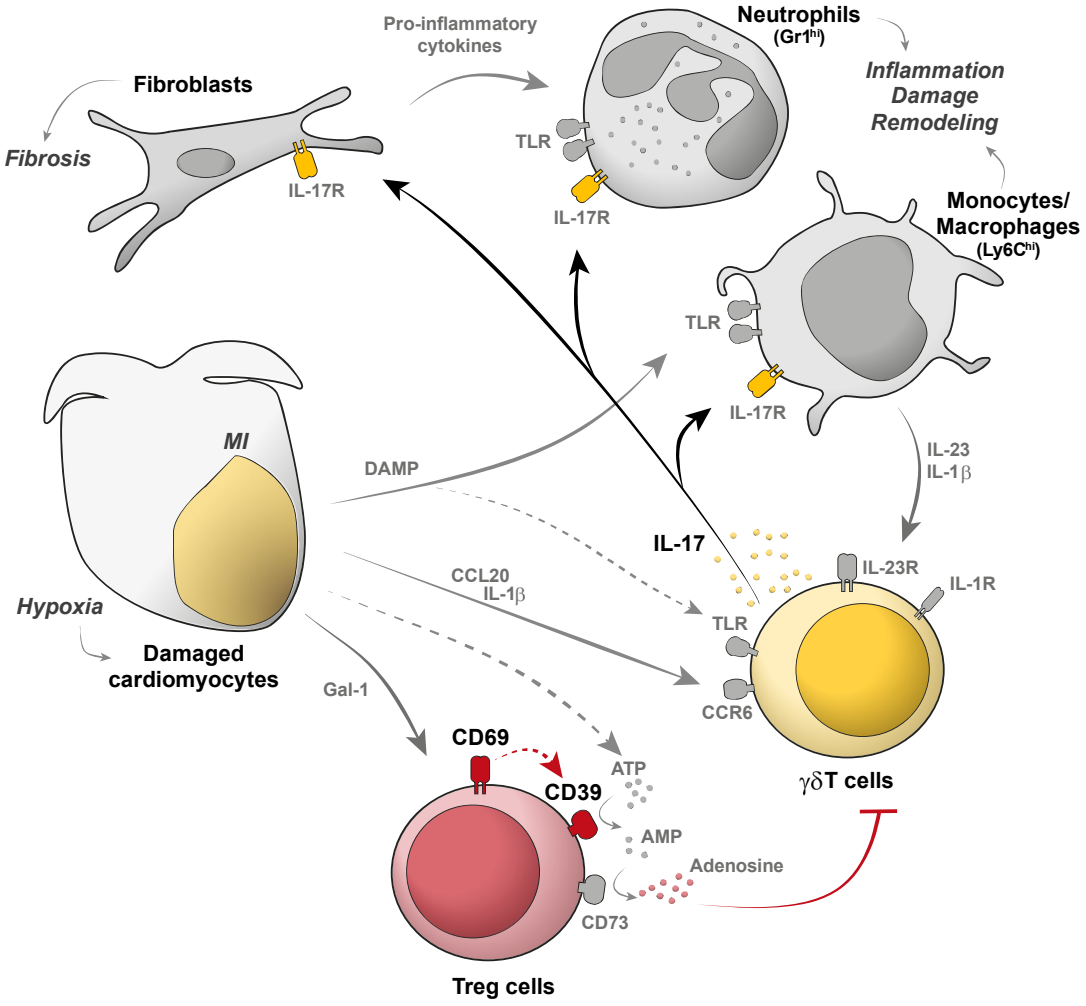

Figure D.2. **Proposed model with CD69$^+$ Treg cells as regulators of the post MI inflammation and damage**. After MI, the ischemic myocardium releases signals that rapidly recruit immune cells. For instance, damaged cardiomyocytes release CCL20, which is recognized by CCR6 on the membrane of γδT cells, favoring their accumulation in the myocardium. The injured heart also releases DAMPs that activate innate cells to produce IL-23 and IL-1β. These cytokines promote the production of IL-17 by γδT cells. The release of abundant IL-17 by γδT cells acts on fibroblast to promote fibrosis, on neutrophils to accelerate recruitment and on monocytes/macrophages to switch toward pro-inflammatory phenotypes. Activated fibroblasts also secrete cytokines that accelerate the activation of monocytes and neutrophils, boosting inflammation, myocardial damage and remodeling. At the same time, the release of DAMPs and IL-1β by cardiomyocytes sustains locally the activation γδT cells. Hypoxic conditions also induce the production of Gal-1, a ligand of CD69, which is essential for the recruitment of Treg cells. To counteract the inflammatory feedback loop, CD69$^+$ Treg cells inhibit γδT cells in an antigen-independent manner. The presence of CD69 on Treg cells increases CD39, which converts extracellular ATP, released by the damaged myocardium, to AMP. Consecutively, CD73 transforms AMP to adenosine, which inhibits γδT cells. Lines in black and red denote inflammatory and regulatory signaling pathways, respectively, explored in our study.

In agreement with our data, different studies have reported a protective role of CD39 after MI. Increased expression of CD39 was reported in infarcted heart extracts in response to hypoxia (Kohler et al. 2007; Eltzschig et al. 2009). According to existing literature, CD39 overexpression ameliorates the progression of mice after MI (Cai, Huttinger, et al. 2011; Wheeler et al. 2012; Smith et al. 2017) and *Cd39*$^{-/-}$ mice develop exacerbated MI-induced cardiac damage (Kohler et al. 2007). A single-chain antibody CD39 fusion protein directed to platelets has been proposed as an effective therapy for I/R (Ziegler et al. 2018). Furthermore, adoptive transfer of *Cd39*$^{-/-}$ iTreg cells fails to prevent inflammation and achieve cardiac protection after MI (Xia et al. 2015). Thus, Treg cells deficient for CD69 present similar dysfunctional properties to what is described for CD39-deficient Treg cells early after MI. All these evidences advocate for a possible co-regulation of both molecules early after MI on Treg cells to prevent exacerbated inflammatory-mediated cardiac deterioration.

In summary, all these evidences propose a novel molecular mechanism of Treg protection against inflammatory-mediated cardiac damage (**figure D.2**), encouraging a further exploration in a clinical setting.

4. CD69 expression on Treg cells predicts the risk of CHF development after MI

Acute MI is the leading cause of mortality worldwide, but CHF secondary to MI is also a major concern (Pfeffer, Pfeffer, and Lamas 1993). Although primary percutaneous coronary intervention is the reference treatment for MI patients (Ibanez et al. 2018), reducing significantly the area of damaged myocardium, an important proportion of patients may develop severe CHF within months or years (Kelly et al. 2011). Although reduced left ventricular ejection fraction as well as old age have been associated with decreased post-MI survival (Halkin et al. 2004; Halkin et al. 2005; van der Vleuten et al. 2008), there is a lack of contemporary multicenter studies evaluating causes and predictors behind CHF development following MI.

We observed a specific deployment of CD69^{+} Treg cells in the peripheral blood of patients with acute MI as in LAD-ligation mice, leading to think that the aforementioned immunomodulatory effect of CD69 might also be true for the human pathology. In agreement, other studies have suggested an elevation of CD69 expression in PBLs during MI, although certainly missing the cellular mechanisms and pathological implications (Pasqui et al. 2003; Steppich et al. 2007; de Dios et al. 2021). Our data showed that based on the expression of CD69 on Treg cells at admission, two groups of patients can be distinguished: those with low-to-normal levels of CD69, comparable to healthy individuals, and those with high levels of CD69 expression. Interestingly, this differential expression of CD69 appeared to be related to differences in the immune repertoire, as well as in the progression toward CHF scenarios. The

reason underlying the variability in the extent of CD69 upregulation after MI remains unknown. Genetic variants, concomitant inflammatory conditions or other factors might explain differences in the CD69 response.

In a follow-up of two independent cohorts of MI patients from Barcelona and Madrid (Spain), we found that low levels of CD69 expression during the first hours after admission for acute MI is associated with a higher risk of re-hospitalization for CHF. We also determined that *CD69* mRNA expression in PBLs is linked to the Treg cell subset. Thus, either the levels of *CD69* mRNA, measured by qPCR, or the surface CD69 on Treg cells, measured by FACS, predict CHF development. Even after adjusting by conventional biomarkers of cardiac injury and confounder factors, CD69 expression on Treg cells remains a predictor of heart failure readmission after MI. After multivariate correction, only $CD69^+$ Treg cells and age, and neither cardiac injury biomarkers nor left ventricular ejection fraction (even though the last one was significant when analyzed independently), measured at the time of acute MI, significantly distinguished patients that developed CHF. Therefore, congruently with preclinical data, CD69 expression during MI is related to a better prognosis of MI patients.

Although the proportion of patients that developed CHF in our study is consistent to what it is described for this period of time of follow up (Kelly et al. 2011), the number of included CHF patients may still appear limited. However, our results have been statistically validated in two independent patient cohorts and after multivariate adjustment. Indeed, exploration of these parameters in larger cohorts would be needed to further confirm our observations. Also, performing these analyses over longer intervals of follow up would be of interest to investigate the involvement of CD69 in the chronic damage after MI in a longer term. Although further studies are needed to prospectively validate the diagnostic and therapeutic value of circulating $CD69^+$ Treg cells, this target opens new specific cellular avenues for precision medicine to improve management of MI patients.

5. Perspectives of the $CD69^+$ Treg cells/miR-155-5p axis in MI

A high number of evidences highlights miR-155-5p as an abundant miRNA with multicellular regulatory properties in different inflammatory processes and disease conditions (Mahesh and Biswas 2019; Bruen, Fitzsimons, and Belton 2019; Chen et al. 2020). In particular, miR-155-5p and CD69 are coregulated in a positive-feedback loop in Treg cells to promote cell differentiation and homeostasis (Sanchez-Diaz et al. 2017). Here we have described that the expression of these two molecules coincides in peripheral Treg cells after MI.

Different studies in mouse models have acknowledged a role for miR-155 in the post-MI inflammation, although the specific contribution of Treg cells has been disregarded. This miRNA can be expressed by multiple cell types, so different experimental approaches may lead to apparently opposing outcomes. In

general, full-body depletion of miR-155 improves progression after LAD-ligation (He et al. 2016; Wang et al. 2017) and I/R (Eisenhardt et al. 2015). However, under particular situations, such as in mice also lacking ApoE, which present a state of dyslipidemia, this protection is not achieved (Schumacher et al. 2021). Moreover, this miRNA is actively secreted into EVs after MI, with different effects according to the target cell type. For instance, macrophage-derived extracellular miR-155 in fibroblast promotes fibrosis (Wang et al. 2017), whereas in endothelial cells inhibits angiogenesis (Liu et al. 2020).

Previous literature on clinical data have reported changes in the levels of circulating hsa-miR-155-5p in MI, although leading to confrontational conclusions and without exploring the miRNA source. Depending on the comparators, the heterogeneity of the cohorts and the time frame of analysis, some studies described either an upregulation of hsa-miR-155-5p in peripheral blood after MI (Li et al. 2017; Kazimierczyk et al. 2019), a downregulation (Yao et al. 2011) or not significant changes (Li et al. 2019). Therefore, a controlled homogeneous clinical study is a need. It has been reported that this miRNA increases rapidly in plasma overtime after the coronary plaque rupture, emphasizing that the time point of measurement is important (Kazimierczyk et al. 2019). Our data indicate that hsa-miR-155-5p levels in plasma of acute MI patients within the first 24h from the ischemic event are higher compared with those in healthy individuals.

It is important to determine the source of this circulating miRNA for the understanding of its role and development as a clinical target. In our cohort of patients, we have extensively analyzed the peripheral immune signature of MI patients and the elevation of hsa-miR-155-5p in circulation only correlated directly with circulating $CD69^+$ Treg cells, suggesting that this cell type might drive the expression of this miRNA. After sorting Treg cells from PBLs of MI patients, we have confirmed that this population specifically synthesizes hsa-miR-155-5p in alignment with CD69 expression. Cell sorting of different immune cell types and miRNA secretion assays would be of interest in order to corroborate that $CD69^+$ Treg cells are the main source of circulating hsa-miR-155-5p after MI. At the same time, we have previously demonstrated that hsa-miR-155-5p is able to trigger the upregulation of CD69 in Treg cells (Sanchez-Diaz et al. 2017), so the increased circulating levels of this miRNA after infarction might also contribute to the activation $CD69^+$ Treg cells. In any case, our data support a parallelism between the $CD69^+$ Treg cell and hsa-miR-155-5p responses in peripheral blood. In this direction, patients with higher levels of peripheral $CD69^+$ Treg cells, related to a lower risk of CHF development, also showed higher levels of hsa-miR-155-5p. Although analysis in larger and independent validation cohorts of MI patients with follow-up is required, our data advocate for the exploration of this miRNA as a potential prognostic marker.

CONCLUSIONS

CONCLUSIONS

The findings presented herein support the following conclusions:

1. Peripheral Th17 cells are abundant during the acute phase of myocardial injury in mice and patients with myocarditis, and not in those with myocardial infarction.
2. Th17 cells secrete mmu-miR-721 into circulating plasma extracellular vesicles in murine models of experimental myocarditis.
3. Mmu-miR-721 promotes Th17 cell responses and myocarditis development by inhibiting *Pparg*.
4. The human hsa-miR-Chr8:96 contains an 18 nucleotides-long consensus sequence with the murine mmu-miR-721, and exhibits processing and functionality compatible with a novel miRNA.
5. Hsa-miR-Chr8:96 is upregulated in plasma from patients with myocarditis and is synthesized by human Th17 cells from these patients, behaving as an efficient non-invasive biomarker to distinguish patients with myocarditis from healthy individuals and patients with myocardial infarction.
6. $CD69^+$ Treg cells increase in peripheral blood of myocardial infarction patients and mice and are recruited to infarcted myocardium after coronary artery ligation in mice.
7. CD69 expression on Treg cells prevents excessive cardiac inflammation and damage, as well as subsequent heart failure, thus improving survival of mice after myocardial infarction.
8. $CD69^+$ Treg cells control cardiac inflammation following MI by inhibiting $IL\text{-}17^+$ γδT cells in a CD39-dependent manner.
9. CD69 expression on peripheral Treg cells during acute MI correlates with circulating hsa-miR-155-5p levels and is associated with a lower risk of developing chronic heart failure within 2.5 years.

CONCLUSIONES

CONCLUSIONES

Los resultados presentados en este trabajo permiten concluir que:

1. Las células Th17 son abundantes durante la fase aguda de daño cardiaco en pacientes y ratones con miocarditis, pero no en aquellos con infarto de miocardio.
2. Las células Th17 secretan el mmu-miR-721 dentro de vesículas extracelulares al plasma en modelos de ratón de miocarditis experimental.
3. El mmu-miR-721 promueve las respuestas Th17, y por consiguiente el desarrollo de la miocarditis mediante la inhibición de su target *Pparg*.
4. La secuencia humana hsa-miR-Chr8:96 es consenso con la del mmu-miR-721 murino y presenta un procesamiento y funcionalidad compatible con la de un miRNA novel.
5. El hsa-miR-Chr8:96 está aumentado en plasma de pacientes con miocarditis y es sintetizado por células Th17 humanas de estos pacientes, comportándose como un biomarcador no invasivo y eficiente para el diagnóstico de pacientes con miocarditis frente a sujetos sanos o pacientes con infarto de miocardio.
6. Las células $CD69^+$ Treg se expanden en sangre periférica de pacientes y ratones con infarto de miocardio, acumulándose en el corazón de ratones con infarto inducido por la ligadura permanente de la arteria coronaria.
7. La expresión de CD69 en células Treg reduce la inflamación y el daño miocárdico, así como el consecuente fallo cardiaco, mejorando la supervivencia de ratones tras infarto de miocardio.
8. Las células $CD69^+$ Treg controlan la inflamación cardiaca tras infarto mediante la inhibición de células γδT que secretan IL-17, en un mecanismo mediado por CD39.
9. La expresión de CD69 en células Treg periféricas se correlaciona con los niveles del hsa-miR-155-5p en plasma en pacientes con infarto de miocardio y se asocia con un menor riesgo de re-hospitalización por fallo cardiaco crónico en 2.5 años.

REFERENCES

REFERENCES

Abarbanell, A. M., J. L. Herrmann, B. R. Weil, Y. Wang, J. Tan, S. P. Moberly, J. W. Fiege, and D. R. Meldrum. 2010. 'Animal models of myocardial and vascular injury', *J Surg Res*, 162: 239-49.

Abbate, A., R. Bussani, G. Liuzzo, G. G. Biondi-Zoccai, E. Barresi, P. Mellone, G. Sinagra, A. Dobrina, F. De Giorgio, R. Sharma, F. Bassan, A. Severino, F. Baldi, L. M. Biasucci, F. Pandolfi, F. Silvestri, G. W. Vetrovec, A. Baldi, and F. Crea. 2008. 'Sudden coronary death, fatal acute myocardial infarction and widespread coronary and myocardial inflammation', *Heart*, 94: 737-42.

Afanasyeva, M., Y. Wang, Z. Kaya, S. Park, M. J. Zilliox, B. H. Schofield, S. L. Hill, and N. R. Rose. 2001. 'Experimental autoimmune myocarditis in A/J mice is an interleukin-4-dependent disease with a Th2 phenotype', *Am J Pathol*, 159: 193-203.

Aggarwal, S., N. Ghilardi, M. H. Xie, F. J. de Sauvage, and A. L. Gurney. 2003. 'Interleukin-23 promotes a distinct CD4 T cell activation state characterized by the production of interleukin-17', *J Biol Chem*, 278: 1910-4.

Ahmad, Farida B., and Robert N. Anderson. 2021. 'The Leading Causes of Death in the US for 2020', *JAMA*, 325: 1829-30.

Al-Salam, S., and S. Hashmi. 2014. 'Galectin-1 in early acute myocardial infarction', *PLoS One*, 9: e86994.

Amber-Vitos, O., N. Chaturvedi, E. Nachliel, M. Gutman, and Y. Tsfadia. 2016. 'The effect of regulating molecules on the structure of the PPAR-RXR complex', *Biochim Biophys Acta*, 1861: 1852-63.

Andreu, Z., E. Rivas, A. Sanguino-Pascual, A. Lamana, M. Marazuela, I. González-Alvaro, F. Sánchez-Madrid, H. de la Fuente, and M. Yáñez-Mó. 2016. 'Comparative analysis of EV isolation procedures for miRNAs detection in serum samples', *J Extracell Vesicles*, 5: 31655.

Attur, M. G., R. N. Patel, S. B. Abramson, and A. R. Amin. 1997. 'Interleukin-17 up-regulation of nitric oxide production in human osteoarthritis cartilage', *Arthritis Rheum*, 40: 1050-3.

Aujla, S. J., Y. R. Chan, M. Zheng, M. Fei, D. J. Askew, D. A. Pociask, T. A. Reinhart, F. McAllister, J. Edeal, K. Gaus, S. Husain, J. L. Kreindler, P. J. Dubin, J. M. Pilewski, M. M. Myerburg, C. A. Mason, Y. Iwakura, and J. K. Kolls. 2008. 'IL-22 mediates mucosal host defense against Gram-negative bacterial pneumonia', *Nat Med*, 14: 275-81.

Bahit, M. C., A. Kochar, and C. B. Granger. 2018. 'Post-Myocardial Infarction Heart Failure', *JACC Heart Fail*, 6: 179-86.

Baldeviano, G. C., J. G. Barin, M. V. Talor, S. Srinivasan, D. Bedja, D. Zheng, K. Gabrielson, Y. Iwakura, N. R. Rose, and D. Cihakova. 2010. 'Interleukin-17A is dispensable for myocarditis but essential for the progression to dilated cardiomyopathy', *Circ Res*, 106: 1646-55.

Bankovich, A. J., L. R. Shiow, and J. G. Cyster. 2010. 'CD69 suppresses sphingosine 1-phosophate receptor-1 (S1P1) function through interaction with membrane helix 4', *J Biol Chem*, 285: 22328-37.

Bansal, S. S., M. A. Ismahil, M. Goel, G. Zhou, G. Rokosh, T. Hamid, and S. D. Prabhu. 2019. 'Dysfunctional and Proinflammatory Regulatory T-Lymphocytes Are Essential for Adverse Cardiac Remodeling in Ischemic Cardiomyopathy', *Circulation*, 139: 206-21.

Barczyk, A., W. Pierzchala, and E. Sozañska. 2003. 'Interleukin-17 in sputum correlates with airway hyperresponsiveness to methacholine', *Respir Med*, 97: 726-33.

Barin, J. G., G. C. Baldeviano, M. V. Talor, L. Wu, S. Ong, D. Fairweather, D. Bedja, N. R. Stickel, J. A. Fontes, A. B. Cardamone, D. Zheng, K. L. Gabrielson, N. R. Rose, and D. Cihákova. 2013. 'Fatal eosinophilic myocarditis develops in the absence of IFN-γ and IL-17A', *J Immunol*, 191: 4038-47.

Barin, J. G., G. C. Baldeviano, M. V. Talor, L. Wu, S. Ong, F. Quader, P. Chen, D. Zheng, P. Caturegli, N. R. Rose, and D. Cihákova. 2012. 'Macrophages participate in IL-17-mediated inflammation', *Eur J Immunol*, 42: 726-36.

Barnden, M. J., J. Allison, W. R. Heath, and F. R. Carbone. 1998. 'Defective TCR expression in transgenic mice constructed using cDNA-based alpha- and beta-chain genes under the control of heterologous regulatory elements', *Immunol Cell Biol*, 76: 34-40.

Barros-Martins, J., N. Schmolka, D. Fontinha, M. Pires de Miranda, J. P. Simas, I. Brok, C. Ferreira, M. Veldhoen, B. Silva-Santos, and K. Serre. 2016. 'Effector γδ T Cell Differentiation Relies on Master but Not Auxiliary Th Cell Transcription Factors', *J Immunol*, 196: 3642-52.

Barthlott, T., H. Kohler, and K. Eichmann. 1997. 'Asynchronous coreceptor downregulation after positive thymic selection: prolonged maintenance of the double positive state in CD8 lineage differentiation due to sustained biosynthesis of the CD4 coreceptor', *J Exp Med*, 185: 357-62.

Bertoli, G., C. Cava, and I. Castiglioni. 2015. 'MicroRNAs: New Biomarkers for Diagnosis, Prognosis, Therapy Prediction and Therapeutic Tools for Breast Cancer', *Theranostics*, 5: 1122-43.

Bettelli, E., Y. Carrier, W. Gao, T. Korn, T. B. Strom, M. Oukka, H. L. Weiner, and V. K. Kuchroo. 2006. 'Reciprocal developmental pathways for the generation of pathogenic effector TH17 and regulatory T cells', *Nature*, 441: 235-8.

Bigby, M., J. S. Markowitz, P. A. Bleicher, M. J. Grusby, S. Simha, M. Siebrecht, M. Wagner, C. Nagler-Anderson, and L. H. Glimcher. 1993. 'Most gamma delta T cells develop normally in the absence of MHC class II molecules', *J Immunol*, 151: 4465-75.

Blanton, R. M., F. J. Carrillo-Salinas, and P. Alcaide. 2019. 'T-cell recruitment to the heart: friendly guests or unwelcome visitors?', *Am J Physiol Heart Circ Physiol*, 317: H124-h40.

Blaschitz, Christoph, and Manuela Raffatellu. 2010. 'Th17 cytokines and the gut mucosal barrier', *J Clin Immunol*, 30: 196-203.

Bluestone, J. A., and A. K. Abbas. 2003. 'Natural versus adaptive regulatory T cells', *Nat Rev Immunol*, 3: 253-7.

Bluestone, J. A., C. R. Mackay, J. J. O'Shea, and B. Stockinger. 2009. 'The functional plasticity of T cell subsets', *Nat Rev Immunol*, 9: 811-6.

Boehncke, W. H. 2018. 'Systemic Inflammation and Cardiovascular Comorbidity in Psoriasis Patients: Causes and Consequences', *Front Immunol*, 9: 579.

Bonner, F., N. Borg, S. Burghoff, and J. Schrader. 2012. 'Resident cardiac immune cells and expression of the ectonucleotidase enzymes CD39 and CD73 after ischemic injury', *PLoS One*, 7: e34730.

Born, Willi, Craig Miles, Janicé White, Rebecca O'Brien, John H. Freed, Philippa Marrack, John Kappler, and Ralph T. Kubo. 1987. 'Peptide sequences of T-cell receptor δ and γ chains are identical to predicted X and γ proteins', *Nature*, 330: 572-74.

Borsellino, G., M. Kleinewietfeld, D. Di Mitri, A. Sternjak, A. Diamantini, R. Giometto, S. Hopner, D. Centonze, G. Bernardi, M. L. Dell'Acqua, P. M. Rossini, L. Battistini, O. Rotzschke, and K. Falk. 2007. 'Expression of ectonucleotidase CD39 by Foxp3+ Treg cells: hydrolysis of extracellular ATP and immune suppression', *Blood*, 110: 1225-32.

Brenner, Michael B., Joanne McLean, Deno P. Dialynas, Jack L. Strominger, John A. Smith, Frances L. Owen, J. G. Seidman, Stephen Ip, Fred Rosen, and Michael S. Krangel. 1986. 'Identification of a putative second T-cell receptor', *Nature*, 322: 145-49.

Bruen, R., S. Fitzsimons, and O. Belton. 2019. 'miR-155 in the Resolution of Atherosclerosis', *Front Pharmacol*, 10: 463.

Burchill, M. A., J. Yang, K. B. Vang, J. J. Moon, H. H. Chu, C. W. Lio, A. L. Vegoe, C. S. Hsieh, M. K. Jenkins, and M. A. Farrar. 2008. 'Linked T cell receptor and cytokine signaling govern the development of the regulatory T cell repertoire', *Immunity*, 28: 112-21.

Bush, K. A., K. M. Farmer, J. S. Walker, and B. W. Kirkham. 2002. 'Reduction of joint inflammation and bone erosion in rat adjuvant arthritis by treatment with interleukin-17 receptor IgG1 Fc fusion protein', *Arthritis Rheum*, 46: 802-5.

Caforio, A. L., R. Marcolongo, C. Basso, and S. Iliceto. 2015. 'Clinical presentation and diagnosis of myocarditis', *Heart*, 101: 1332-44.

Caforio, A. L. P., C. Cheng, M. Perazzolo Marra, G. Tarantini, C. Basso, R. Marcolongo, and S. Iliceto. 2019. 'How to improve therapy in myocarditis: role of cardiovascular magnetic resonance and of endomyocardial biopsy', *Eur Heart J Suppl*, 21: B19-b22.

Caforio, A. L., S. Pankuweit, E. Arbustini, C. Basso, J. Gimeno-Blanes, S. B. Felix, M. Fu, T. Heliö, S. Heymans, R. Jahns, K. Klingel, A. Linhart, B. Maisch, W. McKenna, J. Mogensen, Y. M. Pinto, A. Ristic, H. P. Schultheiss, H. Seggewiss, L. Tavazzi, G. Thiene, A. Yilmaz, P. Charron, and

P. M. Elliott. 2013. 'Current state of knowledge on aetiology, diagnosis, management, and therapy of myocarditis: a position statement of the European Society of Cardiology Working Group on Myocardial and Pericardial Diseases', *Eur Heart J*, 34: 2636-48, 48a-48d.

Cai, M., Z. M. Huttinger, H. He, W. Zhang, F. Li, L. A. Goodman, D. G. Wheeler, L. J. Druhan, J. L. Zweier, K. M. Dwyer, G. He, A. J. d'Apice, S. C. Robson, P. J. Cowan, and R. J. Gumina. 2011. 'Transgenic over expression of ectonucleotide triphosphate diphosphohydrolase-1 protects against murine myocardial ischemic injury', *J Mol Cell Cardiol*, 51: 927-35.

Cai, Y., X. Shen, C. Ding, C. Qi, K. Li, X. Li, V. R. Jala, H. G. Zhang, T. Wang, J. Zheng, and J. Yan. 2011. 'Pivotal role of dermal IL-17-producing γδ T cells in skin inflammation', *Immunity*, 35: 596-610.

Caiazzo, G., G. Fabbrocini, R. Di Caprio, A. Raimondo, E. Scala, N. Balato, and A. Balato. 2018. 'Psoriasis, Cardiovascular Events, and Biologics: Lights and Shadows', *Front Immunol*, 9: 1668.

Calame, K. 2007. 'MicroRNA-155 function in B Cells', *Immunity*, 27: 825-7.

Cebrián, M., E. Yagüe, M. Rincón, M. López-Botet, M. O. de Landázuri, and F. Sánchez-Madrid. 1988. 'Triggering of T cell proliferation through AIM, an activation inducer molecule expressed on activated human lymphocytes', *J Exp Med*, 168: 1621-37.

Chaikijurajai, T., and W. H. W. Tang. 2020. 'Reappraisal of Inflammatory Biomarkers in Heart Failure', *Curr Heart Fail Rep*, 17: 9-19.

Chen, J., M. Y. Liao, X. L. Gao, Q. Zhong, T. T. Tang, X. Yu, Y. H. Liao, and X. Cheng. 2013. 'IL-17A induces pro-inflammatory cytokines production in macrophages via MAPKinases, NF-κB and AP-1', *Cell Physiol Biochem*, 32: 1265-74.

Chen, L., D. Gao, Z. Shao, Q. Zheng, and Q. Yu. 2020. 'miR-155 indicates the fate of CD4(+) T cells', *Immunol Lett*, 224: 40-49.

Chen, W., W. Jin, N. Hardegen, K. J. Lei, L. Li, N. Marinos, G. McGrady, and S. M. Wahl. 2003. 'Conversion of peripheral CD4+CD25- naive T cells to CD4+CD25+ regulatory T cells by TGF-beta induction of transcription factor Foxp3', *J Exp Med*, 198: 1875-86.

Chen, X. M., T. Zhang, D. Qiu, J. Y. Feng, Z. Y. Jin, Q. Luo, X. Y. Wang, and X. L. Wu. 2018. 'Gene expression pattern of TCR repertoire and alteration expression of IL-17A gene of gammadelta T cells in patients with acute myocardial infarction', *J Transl Med*, 16: 189.

Childs, R. A., C. Galustian, A. M. Lawson, G. Dougan, K. Benwell, G. Frankel, and T. Feizi. 1999. 'Recombinant soluble human CD69 dimer produced in Escherichia coli: reevaluation of saccharide binding', *Biochem Biophys Res Commun*, 266: 19-23.

Cibrian, D., M. L. Saiz, H. de la Fuente, R. Sánchez-Díaz, O. Moreno-Gonzalo, I. Jorge, A. Ferrarini, J. Vázquez, C. Punzón, M. Fresno, M. Vicente-Manzanares, E. Daudén, P. M. Fernández-Salguero, P. Martín, and F. Sánchez-Madrid. 2016. 'CD69 controls the uptake of L-tryptophan through LAT1-CD98 and AhR-dependent secretion of IL-22 in psoriasis', *Nat Immunol*, 17: 985-96.

Cihakova, D., J. G. Barin, M. Afanasyeva, M. Kimura, D. Fairweather, M. Berg, M. V. Talor, G. C. Baldeviano, S. Frisancho, K. Gabrielson, D. Bedja, and N. R. Rose. 2008. 'Interleukin-13 protects against experimental autoimmune myocarditis by regulating macrophage differentiation', *Am J Pathol*, 172: 1195-208.

Cihakova, D., and N. R. Rose. 2008. 'Pathogenesis of myocarditis and dilated cardiomyopathy', *Adv Immunol*, 99: 95-114.

Clark, R. B., D. Bishop-Bailey, T. Estrada-Hernandez, T. Hla, L. Puddington, and S. J. Padula. 2000. 'The nuclear receptor PPAR gamma and immunoregulation: PPAR gamma mediates inhibition of helper T cell responses', *J Immunol*, 164: 1364-71.

Cobb, Bradley S., Arnulf Hertweck, James Smith, Eric O'Connor, Daniel Graf, Terence Cook, Stephen T. Smale, Shimon Sakaguchi, Frederick J. Livesey, Amanda G. Fisher, and Matthias Merkenschlager. 2006. 'A role for Dicer in immune regulation', *Journal of Experimental Medicine*, 203: 2519-27.

Collison, L. W., C. J. Workman, T. T. Kuo, K. Boyd, Y. Wang, K. M. Vignali, R. Cross, D. Sehy, R. S. Blumberg, and D. A. Vignali. 2007. 'The inhibitory cytokine IL-35 contributes to regulatory T-cell function', *Nature*, 450: 566-9.

Cooper, L. T., K. L. Baughman, A. M. Feldman, A. Frustaci, M. Jessup, U. Kuhl, G. N. Levine, J. Narula, R. C. Starling, J. Towbin, and R. Virmani. 2007. 'The role of endomyocardial biopsy in the management of cardiovascular disease: a scientific statement from the American Heart Association, the American College of Cardiology, and the European Society of Cardiology. Endorsed by the Heart Failure Society of America and the Heart Failure Association of the European Society of Cardiology', *J Am Coll Cardiol*, 50: 1914-31.

Cooper, L. T., Jr. 2009. 'Myocarditis', *N Engl J Med*, 360: 1526-38.

Cortes, J. R., R. Sanchez-Diaz, E. R. Bovolenta, O. Barreiro, S. Lasarte, A. Matesanz-Marin, M. L. Toribio, F. Sanchez-Madrid, and P. Martin. 2014. 'Maintenance of immune tolerance by Foxp3+ regulatory T cells requires CD69 expression', *J Autoimmun*, 55: 51-62.

Coutinho, A., I. Caramalho, E. Seixas, and J. Demengeot. 2005. 'Thymic commitment of regulatory T cells is a pathway of TCR-dependent selection that isolates repertoires undergoing positive or negative selection', *Curr Top Microbiol Immunol*, 293: 43-71.

Coventry, B. J., S. C. Weeks, S. E. Heckford, P. J. Sykes, J. Bradley, and J. M. Skinner. 1996. 'Lack of IL-2 cytokine expression despite Il-2 messenger RNA transcription in tumor-infiltrating lymphocytes in primary human breast carcinoma: selective expression of early activation markers', *J Immunol*, 156: 3486-92.

Cruz-Adalia, A., L. J. Jimenez-Borreguero, M. Ramirez-Huesca, I. Chico-Calero, O. Barreiro, E. Lopez-Conesa, M. Fresno, F. Sanchez-Madrid, and P. Martin. 2010. 'CD69 limits the severity of cardiomyopathy after autoimmune myocarditis', *Circulation*, 122: 1396-404.

Cua, D. J., J. Sherlock, Y. Chen, C. A. Murphy, B. Joyce, B. Seymour, L. Lucian, W. To, S. Kwan, T. Churakova, S. Zurawski, M. Wiekowski, S. A. Lira, D. Gorman, R. A. Kastelein, and J. D. Sedgwick. 2003. 'Interleukin-23 rather than interleukin-12 is the critical cytokine for autoimmune inflammation of the brain', *Nature*, 421: 744-8.

Daniels, M. D., K. V. Hyland, K. Wang, and D. M. Engman. 2008. 'Recombinant cardiac myosin fragment induces experimental autoimmune myocarditis via activation of Th1 and Th17 immunity', *Autoimmunity*, 41: 490-9.

de Dios, E., C. Rios-Navarro, N. Pérez-Solé, J. Gavara, V. Marcos-Garcés, M. J. Forteza, R. Oltra, J. M. Vila, F. J. Chorro, and V. Bodi. 2021. 'Overexpression of genes involved in lymphocyte activation and regulation are associated with reduced CRM-derived cardiac remodelling after STEMI', *Int Immunopharmacol*, 95: 107490.

de la Fuente, H., A. Cruz-Adalia, G. Martinez Del Hoyo, D. Cibrian-Vera, P. Bonay, D. Perez-Hernandez, J. Vazquez, P. Navarro, R. Gutierrez-Gallego, M. Ramirez-Huesca, P. Martin, and F. Sanchez-Madrid. 2014. 'The leukocyte activation receptor CD69 controls T cell differentiation through its interaction with galectin-1', *Mol Cell Biol*, 34: 2479-87.

Deaglio, S., K. M. Dwyer, W. Gao, D. Friedman, A. Usheva, A. Erat, J. F. Chen, K. Enjyoji, J. Linden, M. Oukka, V. K. Kuchroo, T. B. Strom, and S. C. Robson. 2007. 'Adenosine generation catalyzed by CD39 and CD73 expressed on regulatory T cells mediates immune suppression', *J Exp Med*, 204: 1257-65.

Deseke, M., and I. Prinz. 2020. 'Ligand recognition by the γδ TCR and discrimination between homeostasis and stress conditions', *Cell Mol Immunol*, 17: 914-24.

Ding, H., Y. Wang, L. Hu, S. Xue, Y. Wang, L. Zhang, Y. Zhang, H. Qi, H. Yu, L. H. H. Aung, Y. An, and P. Li. 2020. 'Combined detection of miR-21-5p, miR-30a-3p, miR-30a-5p, miR-155-5p, miR-216a and miR-217 for screening of early heart failure diseases', *Biosci Rep*, 40.

Dionne, A., F. Sperotto, S. Chamberlain, A. L. Baker, A. J. Powell, A. Prakash, D. A. Castellanos, S. F. Saleeb, S. D. de Ferranti, J. W. Newburger, and K. G. Friedman. 2021. 'Association of Myocarditis With BNT162b2 Messenger RNA COVID-19 Vaccine in a Case Series of Children', *JAMA Cardiol*.

Dolmatova, E., G. Spagnol, D. Boassa, J. R. Baum, K. Keith, C. Ambrosi, M. I. Kontaridis, P. L. Sorgen, G. E. Sosinsky, and H. S. Duffy. 2012. 'Cardiomyocyte ATP release through pannexin 1 aids in early fibroblast activation', *Am J Physiol Heart Circ Physiol*, 303: H1208-18.

Doolan, A., N. Langlois, and C. Semsarian. 2004. 'Causes of sudden cardiac death in young Australians', *Med J Aust*, 180: 110-2.

Due, H., P. Svendsen, J. S. Bødker, A. Schmitz, M. Bøgsted, H. E. Johnsen, T. C. El-Galaly, A. S. Roug, and K. Dybkær. 2016. 'miR-155 as a Biomarker in B-Cell Malignancies', *Biomed Res Int*, 2016: 9513037.

Duong Van Huyen, J. P., M. Tible, A. Gay, R. Guillemain, O. Aubert, S. Varnous, F. Iserin, P. Rouvier, A. François, D. Vernerey, X. Loyer, P. Leprince, J. P. Empana, P. Bruneval, A. Loupy, and X. Jouven. 2014. 'MicroRNAs as non-invasive biomarkers of heart transplant rejection', *Eur Heart J*, 35: 3194-202.

Dutton, R. W., L. M. Bradley, and S. L. Swain. 1998. 'T cell memory', *Annu Rev Immunol*, 16: 201-23.

Eis, Peggy S., Wayne Tam, Liping Sun, Amy Chadburn, Zongdong Li, Mario F. Gomez, Elsebet Lund, and James E. Dahlberg. 2005. 'Accumulation of miR-155 and BIC RNA in human B cell lymphomas', *Proc Natl Acad Sci U S A*, 102: 3627.

Eisenhardt, S. U., J. B. Weiss, C. Smolka, J. Maxeiner, F. Pankratz, X. Bemtgen, M. Kustermann, J. R. Thiele, Y. Schmidt, G. Bjoern Stark, M. Moser, C. Bode, and S. Grundmann. 2015. 'MicroRNA-155 aggravates ischemia-reperfusion injury by modulation of inflammatory cell recruitment and the respiratory oxidative burst', *Basic Res Cardiol*, 110: 32.

Ekström, K., J. Lehtonen, R. Kandolin, A. Räisänen-Sokolowski, K. Salmenkivi, and M. Kupari. 2016. 'Long-term outcome and its predictors in giant cell myocarditis', *Eur J Heart Fail*, 18: 1452-58.

Eltzschig, H. K., D. Kohler, T. Eckle, T. Kong, S. C. Robson, and S. P. Colgan. 2009. 'Central role of Sp1-regulated CD39 in hypoxia/ischemia protection', *Blood*, 113: 224-32.

Eriksson, U., M. O. Kurrer, R. Bingisser, H. P. Eugster, P. Saremaslani, F. Follath, S. Marsch, and U. Widmer. 2001. 'Lethal autoimmune myocarditis in interferon-gamma receptor-deficient mice: enhanced disease severity by impaired inducible nitric oxide synthase induction', *Circulation*, 103: 18-21.

Eriksson, U., M. O. Kurrer, W. Sebald, F. Brombacher, and M. Kopf. 2001. 'Dual role of the IL-12/IFN-gamma axis in the development of autoimmune myocarditis: induction by IL-12 and protection by IFN-gamma', *J Immunol*, 167: 5464-9.

Fabbiano, S., M. Menacho-Marquez, J. Robles-Valero, M. Pericacho, A. Matesanz-Marin, C. Garcia-Macias, M. A. Sevilla, M. J. Montero, B. Alarcon, J. M. Lopez-Novoa, P. Martin, and X. R. Bustelo. 2015. 'Immunosuppression-Independent Role of Regulatory T Cells against Hypertension-Driven Renal Dysfunctions', *Mol Cell Biol*, 35: 3528-46.

Fabre, A., and M. N. Sheppard. 2006. 'Sudden adult death syndrome and other non-ischaemic causes of sudden cardiac death', *Heart*, 92: 316-20.

Fairweather, D., S. Frisancho-Kiss, and N. R. Rose. 2005. 'Viruses as adjuvants for autoimmunity: evidence from Coxsackievirus-induced myocarditis', *Rev Med Virol*, 15: 17-27.

Fairweather, D., S. Frisancho-Kiss, S. A. Yusung, M. A. Barrett, S. E. Davis, S. J. Gatewood, D. B. Njoku, and N. R. Rose. 2004. 'Interferon-gamma protects against chronic viral myocarditis by reducing mast cell degranulation, fibrosis, and the profibrotic cytokines transforming growth factor-beta 1, interleukin-1 beta, and interleukin-4 in the heart', *Am J Pathol*, 165: 1883-94.

Fairweather, D., Z. Kaya, G. R. Shellam, C. M. Lawson, and N. R. Rose. 2001. 'From infection to autoimmunity', *J Autoimmun*, 16: 175-86.

Ferreira, V. M., J. Schulz-Menger, G. Holmvang, C. M. Kramer, I. Carbone, U. Sechtem, I. Kindermann, M. Gutberlet, L. T. Cooper, P. Liu, and M. G. Friedrich. 2018. 'Cardiovascular Magnetic Resonance in Nonischemic Myocardial Inflammation: Expert Recommendations', *J Am Coll Cardiol*, 72: 3158-76.

Flajnik, M. F., and L. Du Pasquier. 2004. 'Evolution of innate and adaptive immunity: can we draw a line?', *Trends Immunol*, 25: 640-4.

Fleisher, T. A. 1997. 'Immune function', *Pediatr Rev*, 18: 351-6.

Fontenot, J. D., M. A. Gavin, and A. Y. Rudensky. 2003. 'Foxp3 programs the development and function of CD4+CD25+ regulatory T cells', *Nat Immunol*, 4: 330-6.

Fontenot, J. D., J. P. Rasmussen, M. A. Gavin, and A. Y. Rudensky. 2005. 'A function for interleukin 2 in Foxp3-expressing regulatory T cells', *Nat Immunol*, 6: 1142-51.

Fossiez, F., O. Djossou, P. Chomarat, L. Flores-Romo, S. Ait-Yahia, C. Maat, J. J. Pin, P. Garrone, E. Garcia, S. Saeland, D. Blanchard, C. Gaillard, B. Das Mahapatra, E. Rouvier, P. Golstein, J.

Banchereau, and S. Lebecque. 1996. 'T cell interleukin-17 induces stromal cells to produce proinflammatory and hematopoietic cytokines', *J Exp Med*, 183: 2593-603.
Frangogiannis, N. G. 2014. 'The inflammatory response in myocardial injury, repair, and remodelling', *Nat Rev Cardiol*, 11: 255-65.
Friedman, R. C., K. K. Farh, C. B. Burge, and D. P. Bartel. 2009. 'Most mammalian mRNAs are conserved targets of microRNAs', *Genome Res*, 19: 92-105.
Friedrich, M. G., U. Sechtem, J. Schulz-Menger, G. Holmvang, P. Alakija, L. T. Cooper, J. A. White, H. Abdel-Aty, M. Gutberlet, S. Prasad, A. Aletras, J. P. Laissy, I. Paterson, N. G. Filipchuk, A. Kumar, M. Pauschinger, and P. Liu. 2009. 'Cardiovascular magnetic resonance in myocarditis: A JACC White Paper', *J Am Coll Cardiol*, 53: 1475-87.
Fujino, S., A. Andoh, S. Bamba, A. Ogawa, K. Hata, Y. Araki, T. Bamba, and Y. Fujiyama. 2003. 'Increased expression of interleukin 17 in inflammatory bowel disease', *Gut*, 52: 65-70.
Gannon, M. P., E. Schaub, C. L. Grines, and S. G. Saba. 2019. 'State of the art: Evaluation and prognostication of myocarditis using cardiac MRI', *J Magn Reson Imaging*, 49: e122-e31.
García-Monzón, C., R. Moreno-Otero, J. M. Pajares, A. García-Sánchez, M. López-Botet, M. O. de Landázuri, and F. Sánchez-Madrid. 1990. 'Expression of a novel activation antigen on intrahepatic CD8+ T lymphocytes in viral chronic active hepatitis', *Gastroenterology*, 98: 1029-35.
Garg, A., B. Seeliger, A. A. Derda, K. Xiao, A. Gietz, K. Scherf, K. Sonnenschein, I. Pink, M. M. Hoeper, T. Welte, J. Bauersachs, S. David, C. Bär, and T. Thum. 2021. 'Circulating cardiovascular microRNAs in critically ill COVID-19 patients', *Eur J Heart Fail*, 23: 468-75.
George, J., S. Schwartzenberg, D. Medvedovsky, M. Jonas, G. Charach, A. Afek, and A. Shamiss. 2012. 'Regulatory T cells and IL-10 levels are reduced in patients with vulnerable coronary plaques', *Atherosclerosis*, 222: 519-23.
Gil-Cruz, C., C. Perez-Shibayama, A. De Martin, F. Ronchi, K. van der Borght, R. Niederer, L. Onder, M. Lütge, M. Novkovic, V. Nindl, G. Ramos, M. Arnoldini, E. M. C. Slack, V. Boivin-Jahns, R. Jahns, M. Wyss, C. Mooser, B. N. Lambrecht, M. T. Maeder, H. Rickli, L. Flatz, U. Eriksson, M. B. Geuking, K. D. McCoy, and B. Ludewig. 2019. 'Microbiota-derived peptide mimics drive lethal inflammatory cardiomyopathy', *Science*, 366: 881-86.
Glass, C. K., and S. Ogawa. 2006. 'Combinatorial roles of nuclear receptors in inflammation and immunity', *Nat Rev Immunol*, 6: 44-55.
Golpour, A., D. Patriki, P. J. Hanson, B. McManus, and B. Heidecker. 2021. 'Epidemiological Impact of Myocarditis', *J Clin Med*, 10.
Gondek, D. C., L. F. Lu, S. A. Quezada, S. Sakaguchi, and R. J. Noelle. 2005. 'Cutting edge: contact-mediated suppression by CD4+CD25+ regulatory cells involves a granzyme B-dependent, perforin-independent mechanism', *J Immunol*, 174: 1783-6.
Gonzalez-Amaro, R., J. R. Cortes, F. Sanchez-Madrid, and P. Martin. 2013. 'Is CD69 an effective brake to control inflammatory diseases?', *Trends Mol Med*, 19: 625-32.
Grabie, N., A. H. Lichtman, and R. Padera. 2019. 'T cell checkpoint regulators in the heart', *Cardiovasc Res*, 115: 869-77.
Grogan, J. L., M. Mohrs, B. Harmon, D. A. Lacy, J. W. Sedat, and R. M. Locksley. 2001. 'Early transcription and silencing of cytokine genes underlie polarization of T helper cell subsets', *Immunity*, 14: 205-15.
Grossman, W. J., J. W. Verbsky, W. Barchet, M. Colonna, J. P. Atkinson, and T. J. Ley. 2004. 'Human T regulatory cells can use the perforin pathway to cause autologous target cell death', *Immunity*, 21: 589-601.
Haas, J. D., F. H. González, S. Schmitz, V. Chennupati, L. Föhse, E. Kremmer, R. Förster, and I. Prinz. 2009. 'CCR6 and NK1.1 distinguish between IL-17A and IFN-gamma-producing gammadelta effector T cells', *Eur J Immunol*, 39: 3488-97.
Haasch, D., Y. W. Chen, R. M. Reilly, X. G. Chiou, S. Koterski, M. L. Smith, P. Kroeger, K. McWeeny, D. N. Halbert, K. W. Mollison, S. W. Djuric, and J. M. Trevillyan. 2002. 'T cell activation induces a noncoding RNA transcript sensitive to inhibition by immunosuppressant drugs and encoded by the proto-oncogene, BIC', *Cell Immunol*, 217: 78-86.

Hajjo, R., D. A. Sabbah, S. K. Bardaweel, and A. Tropsha. 2021. 'Shedding the Light on Post-Vaccine Myocarditis and Pericarditis in COVID-19 and Non-COVID-19 Vaccine Recipients', *Vaccines (Basel)*, 9.

Haks, M. C., J. M. Lefebvre, J. P. Lauritsen, M. Carleton, M. Rhodes, T. Miyazaki, D. J. Kappes, and D. L. Wiest. 2005. 'Attenuation of gammadeltaTCR signaling efficiently diverts thymocytes to the alphabeta lineage', *Immunity*, 22: 595-606.

Halkin, A., E. Aymong, D. A. Cox, R. Mehran, A. J. Lansky, M. Fahy, G. Weisz, E. Garcia, J. E. Tcheng, C. L. Grines, and G. W. Stone. 2004. 'Relation between late patency of the infarct-related artery, left ventricular function, and clinical outcomes after primary percutaneous intervention for acute myocardial infarction (CADILLAC trial)', *Am J Cardiol*, 93: 349-53.

Halkin, A., M. Singh, E. Nikolsky, C. L. Grines, J. E. Tcheng, E. Garcia, D. A. Cox, M. Turco, T. D. Stuckey, Y. Na, A. J. Lansky, B. J. Gersh, W. W. O'Neill, R. Mehran, and G. W. Stone. 2005. 'Prediction of mortality after primary percutaneous coronary intervention for acute myocardial infarction: the CADILLAC risk score', *J Am Coll Cardiol*, 45: 1397-405.

Hamada, S., M. Umemura, T. Shiono, K. Tanaka, A. Yahagi, M. D. Begum, K. Oshiro, Y. Okamoto, H. Watanabe, K. Kawakami, C. Roark, W. K. Born, R. O'Brien, K. Ikuta, H. Ishikawa, S. Nakae, Y. Iwakura, T. Ohta, and G. Matsuzaki. 2008. 'IL-17A produced by gammadelta T cells plays a critical role in innate immunity against listeria monocytogenes infection in the liver', *J Immunol*, 181: 3456-63.

Han, Y., Q. Guo, M. Zhang, Z. Chen, and X. Cao. 2009. 'CD69+ CD4+ CD25- T cells, a new subset of regulatory T cells, suppress T cell proliferation through membrane-bound TGF-beta 1', *J Immunol*, 182: 111-20.

Harrington, L. E., R. D. Hatton, P. R. Mangan, H. Turner, T. L. Murphy, K. M. Murphy, and C. T. Weaver. 2005. 'Interleukin 17-producing CD4+ effector T cells develop via a lineage distinct from the T helper type 1 and 2 lineages', *Nat Immunol*, 6: 1123-32.

Hayes, S. M., L. Li, and P. E. Love. 2005. 'TCR signal strength influences alphabeta/gammadelta lineage fate', *Immunity*, 22: 583-93.

He, D., L. Wu, H. K. Kim, H. Li, C. A. Elmets, and H. Xu. 2006. 'CD8+ IL-17-producing T cells are important in effector functions for the elicitation of contact hypersensitivity responses', *J Immunol*, 177: 6852-8.

He, W., H. Huang, Q. Xie, Z. Wang, Y. Fan, B. Kong, D. Huang, and Y. Xiao. 2016. 'MiR-155 Knockout in Fibroblasts Improves Cardiac Remodeling by Targeting Tumor Protein p53-Inducible Nuclear Protein 1', *J Cardiovasc Pharmacol Ther*, 21: 423-35.

Heymans, S., U. Eriksson, J. Lehtonen, and L. T. Cooper, Jr. 2016. 'The Quest for New Approaches in Myocarditis and Inflammatory Cardiomyopathy', *J Am Coll Cardiol*, 68: 2348-64.

Higgins, S. C., A. G. Jarnicki, E. C. Lavelle, and K. H. Mills. 2006. 'TLR4 mediates vaccine-induced protective cellular immunity to Bordetella pertussis: role of IL-17-producing T cells', *J Immunol*, 177: 7980-9.

Hofmann, U., N. Beyersdorf, J. Weirather, A. Podolskaya, J. Bauersachs, G. Ertl, T. Kerkau, and S. Frantz. 2012. 'Activation of CD4+ T lymphocytes improves wound healing and survival after experimental myocardial infarction in mice', *Circulation*, 125: 1652-63.

Hofmann, U., and S. Frantz. 2016. 'Role of T-cells in myocardial infarction', *Eur Heart J*, 37: 873-9.

Hommel, M. 2004. 'On the dynamics of T-cell activation in lymph nodes', *Immunol Cell Biol*, 82: 62-6.

Hong, Fan, Shijia Pan, Yuan Guo, Pengfei Xu, and Yonggong Zhai. 2019. 'PPARs as Nuclear Receptors for Nutrient and Energy Metabolism', *Molecules*, 24.

Hori, S., T. Nomura, and S. Sakaguchi. 2003. 'Control of regulatory T cell development by the transcription factor Foxp3', *Science*, 299: 1057-61.

Hsieh, C. S., Y. Liang, A. J. Tyznik, S. G. Self, D. Liggitt, and A. Y. Rudensky. 2004. 'Recognition of the peripheral self by naturally arising CD25+ CD4+ T cell receptors', *Immunity*, 21: 267-77.

Hsieh, C. S., Y. Zheng, Y. Liang, J. D. Fontenot, and A. Y. Rudensky. 2006. 'An intersection between the self-reactive regulatory and nonregulatory T cell receptor repertoires', *Nat Immunol*, 7: 401-10.

Hsu, S. C., L. T. Wang, C. L. Yao, H. Y. Lai, K. Y. Chan, B. S. Liu, P. Chong, O. K. Lee, and H. W. Chen. 2013. 'Mesenchymal stem cells promote neutrophil activation by inducing IL-17 production in CD4+ CD45RO+ T cells', *Immunobiology*, 218: 90-5.

Huber, S. A. 2000. 'T cells expressing the gamma delta T cell receptor induce apoptosis in cardiac myocytes', *Cardiovasc Res*, 45: 579-87.

Humphreys, D. T., C. J. Hynes, H. R. Patel, G. H. Wei, L. Cannon, D. Fatkin, C. M. Suter, J. L. Clancy, and T. Preiss. 2012. 'Complexity of murine cardiomyocyte miRNA biogenesis, sequence variant expression and function', *PLoS One*, 7: e30933.

Hunter, M. P., N. Ismail, X. Zhang, B. D. Aguda, E. J. Lee, L. Yu, T. Xiao, J. Schafer, M. L. Lee, T. D. Schmittgen, S. P. Nana-Sinkam, D. Jarjoura, and C. B. Marsh. 2008. 'Detection of microRNA expression in human peripheral blood microvesicles', *PLoS One*, 3: e3694.

Hutvágner, G., J. McLachlan, A. E. Pasquinelli, E. Bálint, T. Tuschl, and P. D. Zamore. 2001. 'A cellular function for the RNA-interference enzyme Dicer in the maturation of the let-7 small temporal RNA', *Science*, 293: 834-8.

Ibanez, B., S. James, S. Agewall, M. J. Antunes, C. Bucciarelli-Ducci, H. Bueno, A. L. P. Caforio, F. Crea, J. A. Goudevenos, S. Halvorsen, G. Hindricks, A. Kastrati, M. J. Lenzen, E. Prescott, M. Roffi, M. Valgimigli, C. Varenhorst, P. Vranckx, and P. Widimský. 2018. '2017 ESC Guidelines for the management of acute myocardial infarction in patients presenting with ST-segment elevation: The Task Force for the management of acute myocardial infarction in patients presenting with ST-segment elevation of the European Society of Cardiology (ESC)', *Eur Heart J*, 39: 119-77.

Ivanov, II, B. S. McKenzie, L. Zhou, C. E. Tadokoro, A. Lepelley, J. J. Lafaille, D. J. Cua, and D. R. Littman. 2006. 'The orphan nuclear receptor RORgammat directs the differentiation program of proinflammatory IL-17+ T helper cells', *Cell*, 126: 1121-33.

Iwakawa, H. O., and Y. Tomari. 2015. 'The Functions of MicroRNAs: mRNA Decay and Translational Repression', *Trends Cell Biol*, 25: 651-65.

Jensen, K. D., X. Su, S. Shin, L. Li, S. Youssef, S. Yamasaki, L. Steinman, T. Saito, R. M. Locksley, M. M. Davis, N. Baumgarth, and Y. H. Chien. 2008. 'Thymic selection determines gammadelta T cell effector fate: antigen-naive cells make interleukin-17 and antigen-experienced cells make interferon gamma', *Immunity*, 29: 90-100.

Jensen, L. D., and D. J. Marchant. 2016. 'Emerging pharmacologic targets and treatments for myocarditis', *Pharmacol Ther*, 161: 40-51.

Jianjun, Yang, R. Zhang, G. Lu, Y. Shen, L. Peng, C. Zhu, M. Cui, W. Wang, P. Arnaboldi, M. Tang, M. Gupta, C. F. Qi, P. Jayaraman, H. Zhu, B. Jiang, S. H. Chen, J. C. He, A. T. Ting, M. M. Zhou, V. K. Kuchroo, H. C. Morse, 3rd, K. Ozato, A. G. Sikora, and H. Xiong. 2013. 'T cell–derived inducible nitric oxide synthase switches off Th17 cell differentiation', *J Exp Med*, 210: 1447-62.

Josefowicz, S. Z., L. F. Lu, and A. Y. Rudensky. 2012. 'Regulatory T cells: mechanisms of differentiation and function', *Annu Rev Immunol*, 30: 531-64.

Jovanovic, D. V., J. A. Di Battista, J. Martel-Pelletier, F. C. Jolicoeur, Y. He, M. Zhang, F. Mineau, and J. P. Pelletier. 1998. 'IL-17 stimulates the production and expression of proinflammatory cytokines, IL-beta and TNF-alpha, by human macrophages', *J Immunol*, 160: 3513-21.

Jovičić, Ana, and Aaron D. Gitler. 2017. 'Distinct repertoires of microRNAs present in mouse astrocytes compared to astrocyte-secreted exosomes', *PLoS One*, 12: e0171418-e18.

Kanda, N., S. Koike, and S. Watanabe. 2005. 'IL-17 suppresses TNF-alpha-induced CCL27 production through induction of COX-2 in human keratinocytes', *J Allergy Clin Immunol*, 116: 1144-50.

Kanegane, H., and G. Tosato. 1996. 'Activation of naive and memory T cells by interleukin-15', *Blood*, 88: 230-5.

Kawakami, R., A. Sakamoto, K. Kawai, A. Gianatti, D. Pellegrini, A. Nasr, B. Kutys, L. Guo, A. Cornelissen, M. Mori, Y. Sato, I. Pescetelli, M. Brivio, M. Romero, G. Guagliumi, R. Virmani, and A. V. Finn. 2021. 'Pathological Evidence for SARS-CoV-2 as a Cause of Myocarditis: JACC Review Topic of the Week', *J Am Coll Cardiol*, 77: 314-25.

Kazimierczyk, E., A. Eljaszewicz, P. Zembko, E. Tarasiuk, M. Rusak, A. Kulczynska-Przybik, M. Lukaszewicz-Zajac, K. Kaminski, B. Mroczko, M. Szmitkowski, M. Dabrowska, B. Sobkowicz, M. Moniuszko, and A. Tycinska. 2019. 'The relationships among monocyte

subsets, miRNAs and inflammatory cytokines in patients with acute myocardial infarction', *Pharmacol Rep*, 71: 73-81.
Ke, B., X. Ke, X. Wan, Y. Yang, Y. Huang, J. Qin, C. Hu, and L. Shi. 2017. 'Astragalus polysaccharides attenuates TNF-α-induced insulin resistance via suppression of miR-721 and activation of PPAR-γ and PI3K/AKT in 3T3-L1 adipocytes', *Am J Transl Res*, 9: 2195-206.
Kebir, H., K. Kreymborg, I. Ifergan, A. Dodelet-Devillers, R. Cayrol, M. Bernard, F. Giuliani, N. Arbour, B. Becher, and A. Prat. 2007. 'Human TH17 lymphocytes promote blood-brain barrier disruption and central nervous system inflammation', *Nat Med*, 13: 1173-5.
Kelly, D. J., T. Gershlick, B. Witzenbichler, G. Guagliumi, M. Fahy, G. Dangas, R. Mehran, and G. W. Stone. 2011. 'Incidence and predictors of heart failure following percutaneous coronary intervention in ST-segment elevation myocardial infarction: the HORIZONS-AMI trial', *Am Heart J*, 162: 663-70.
Ketting, R. F., S. E. Fischer, E. Bernstein, T. Sijen, G. J. Hannon, and R. H. Plasterk. 2001. 'Dicer functions in RNA interference and in synthesis of small RNA involved in developmental timing in C. elegans', *Genes Dev*, 15: 2654-9.
Kim, J. H., and I. A. Choi. 2021. 'Cardiovascular morbidity and mortality in patients with spondyloarthritis: A meta-analysis', *Int J Rheum Dis*, 24: 477-86.
Kim, V. N. 2005. 'MicroRNA biogenesis: coordinated cropping and dicing', *Nat Rev Mol Cell Biol*, 6: 376-85.
Kindermann, I., M. Kindermann, R. Kandolf, K. Klingel, B. Bültmann, T. Müller, A. Lindinger, and M. Böhm. 2008. 'Predictors of outcome in patients with suspected myocarditis', *Circulation*, 118: 639-48.
Kirkham, B. W., M. N. Lassere, J. P. Edmonds, K. M. Juhasz, P. A. Bird, C. S. Lee, R. Shnier, and I. J. Portek. 2006. 'Synovial membrane cytokine expression is predictive of joint damage progression in rheumatoid arthritis: a two-year prospective study (the DAMAGE study cohort)', *Arthritis Rheum*, 54: 1122-31.
Klingenberg, R., C. E. Brokopp, A. Grives, A. Courtier, M. Jaguszewski, N. Pasqual, E. Vlaskou Badra, A. Lewandowski, O. Gaemperli, S. P. Hoerstrup, W. Maier, U. Landmesser, T. F. Luscher, and C. M. Matter. 2015. 'Clonal restriction and predominance of regulatory T cells in coronary thrombi of patients with acute coronary syndromes', *Eur Heart J*, 36: 1041-8.
Klotz, L., S. Burgdorf, I. Dani, K. Saijo, J. Flossdorf, S. Hucke, J. Alferink, N. Nowak, M. Beyer, G. Mayer, B. Langhans, T. Klockgether, A. Waisman, G. Eberl, J. Schultze, M. Famulok, W. Kolanus, C. Glass, C. Kurts, and P. A. Knolle. 2009. 'The nuclear receptor PPAR gamma selectively inhibits Th17 differentiation in a T cell-intrinsic fashion and suppresses CNS autoimmunity', *J Exp Med*, 206: 2079-89.
Klotz, L., I. Dani, F. Edenhofer, L. Nolden, B. Evert, B. Paul, W. Kolanus, T. Klockgether, P. Knolle, and L. Diehl. 2007. 'Peroxisome proliferator-activated receptor gamma control of dendritic cell function contributes to development of CD4+ T cell anergy', *J Immunol*, 178: 2122-31.
Kobayashi, H., and Y. Tomari. 2016. 'RISC assembly: Coordination between small RNAs and Argonaute proteins', *Biochim Biophys Acta*, 1859: 71-81.
Kohler, D., T. Eckle, M. Faigle, A. Grenz, M. Mittelbronn, S. Laucher, M. L. Hart, S. C. Robson, C. E. Muller, and H. K. Eltzschig. 2007. 'CD39/ectonucleoside triphosphate diphosphohydrolase 1 provides myocardial protection during cardiac ischemia/reperfusion injury', *Circulation*, 116: 1784-94.
Kohlhaas, S., O. A. Garden, C. Scudamore, M. Turner, K. Okkenhaug, and E. Vigorito. 2009. 'Cutting edge: the Foxp3 target miR-155 contributes to the development of regulatory T cells', *J Immunol*, 182: 2578-82.
Korn, T., E. Bettelli, W. Gao, A. Awasthi, A. Jäger, T. B. Strom, M. Oukka, and V. K. Kuchroo. 2007. 'IL-21 initiates an alternative pathway to induce proinflammatory T(H)17 cells', *Nature*, 448: 484-87.
Kotanidis, C. P., M. A. Bazmpani, A. B. Haidich, C. Karvounis, C. Antoniades, and T. D. Karamitsos. 2018. 'Diagnostic Accuracy of Cardiovascular Magnetic Resonance in Acute Myocarditis: A Systematic Review and Meta-Analysis', *JACC Cardiovasc Imaging*, 11: 1583-90.
Kühl, U., M. Pauschinger, P. L. Schwimmbeck, B. Seeberg, C. Lober, M. Noutsias, W. Poller, and H. P. Schultheiss. 2003. 'Interferon-beta treatment eliminates cardiotropic viruses and improves

left ventricular function in patients with myocardial persistence of viral genomes and left ventricular dysfunction', *Circulation*, 107: 2793-8.

Kullberg, M. C., D. Jankovic, C. G. Feng, S. Hue, P. L. Gorelick, B. S. McKenzie, D. J. Cua, F. Powrie, A. W. Cheever, K. J. Maloy, and A. Sher. 2006. 'IL-23 plays a key role in Helicobacter hepaticus-induced T cell-dependent colitis', *J Exp Med*, 203: 2485-94.

Kunzmann, V., B. Kimmel, T. Herrmann, H. Einsele, and M. Wilhelm. 2009. 'Inhibition of phosphoantigen-mediated gammadelta T-cell proliferation by CD4+ CD25+ FoxP3+ regulatory T cells', *Immunology*, 126: 256-67.

Kwak, P. B., and Y. Tomari. 2012. 'The N domain of Argonaute drives duplex unwinding during RISC assembly', *Nat Struct Mol Biol*, 19: 145-51.

Laan, M., Z. H. Cui, H. Hoshino, J. Lötvall, M. Sjöstrand, D. C. Gruenert, B. E. Skoogh, and A. Lindén. 1999. 'Neutrophil recruitment by human IL-17 via C-X-C chemokine release in the airways', *J Immunol*, 162: 2347-52.

Laffón, A., R. García-Vicuña, A. Humbría, A. A. Postigo, A. L. Corbí, M. O. de Landázuri, and F. Sánchez-Madrid. 1991. 'Upregulated expression and function of VLA-4 fibronectin receptors on human activated T cells in rheumatoid arthritis', *J Clin Invest*, 88: 546-52.

Laggner, U., P. Di Meglio, G. K. Perera, C. Hundhausen, K. E. Lacy, N. Ali, C. H. Smith, A. C. Hayday, B. J. Nickoloff, and F. O. Nestle. 2011. 'Identification of a novel proinflammatory human skin-homing Vγ9Vδ2 T cell subset with a potential role in psoriasis', *J Immunol*, 187: 2783-93.

Lagos-Quintana, Mariana, Reinhard Rauhut, Abdullah Yalcin, Jutta Meyer, Winfried Lendeckel, and Thomas Tuschl. 2002. 'Identification of Tissue-Specific MicroRNAs from Mouse', *Current Biology*, 12: 735-39.

Laird, R. M., K. Laky, and S. M. Hayes. 2010. 'Unexpected role for the B cell-specific Src family kinase B lymphoid kinase in the development of IL-17-producing γδ T cells', *J Immunol*, 185: 6518-27.

Landgraf, Pablo, Mirabela Rusu, Robert Sheridan, Alain Sewer, Nicola Iovino, Alexei Aravin, Sébastien Pfeffer, Amanda Rice, Alice O. Kamphorst, Markus Landthaler, Carolina Lin, Nicholas D. Socci, Leandro Hermida, Valerio Fulci, Sabina Chiaretti, Robin Foà, Julia Schliwka, Uta Fuchs, Astrid Novosel, Roman-Ulrich Müller, Bernhard Schermer, Ute Bissels, Jason Inman, Quang Phan, Minchen Chien, David B. Weir, Ruchi Choksi, Gabriella De Vita, Daniela Frezzetti, Hans-Ingo Trompeter, Veit Hornung, Grace Teng, Gunther Hartmann, Miklos Palkovits, Roberto Di Lauro, Peter Wernet, Giuseppe Macino, Charles E. Rogler, James W. Nagle, Jingyue Ju, F. Nina Papavasiliou, Thomas Benzing, Peter Lichter, Wayne Tam, Michael J. Brownstein, Andreas Bosio, Arndt Borkhardt, James J. Russo, Chris Sander, Mihaela Zavolan, and Thomas Tuschl. 2007. 'A Mammalian microRNA Expression Atlas Based on Small RNA Library Sequencing', *Cell*, 129: 1401-14.

Lang, R. M., L. P. Badano, V. Mor-Avi, J. Afilalo, A. Armstrong, L. Ernande, F. A. Flachskampf, E. Foster, S. A. Goldstein, T. Kuznetsova, P. Lancellotti, D. Muraru, M. H. Picard, E. R. Rietzschel, L. Rudski, K. T. Spencer, W. Tsang, and J. U. Voigt. 2015. 'Recommendations for cardiac chamber quantification by echocardiography in adults: an update from the American Society of Echocardiography and the European Association of Cardiovascular Imaging', *Eur Heart J Cardiovasc Imaging*, 16: 233-70.

Langrish, C. L., Y. Chen, W. M. Blumenschein, J. Mattson, B. Basham, J. D. Sedgwick, T. McClanahan, R. A. Kastelein, and D. J. Cua. 2005. 'IL-23 drives a pathogenic T cell population that induces autoimmune inflammation', *J Exp Med*, 201: 233-40.

Lauritsen, J. P., G. W. Wong, S. Y. Lee, J. M. Lefebvre, M. Ciofani, M. Rhodes, D. J. Kappes, J. C. Zúñiga-Pflücker, and D. L. Wiest. 2009. 'Marked induction of the helix-loop-helix protein Id3 promotes the gammadelta T cell fate and renders their functional maturation Notch independent', *Immunity*, 31: 565-75.

Lee, R. C., R. L. Feinbaum, and V. Ambros. 1993. 'The C. elegans heterochronic gene lin-4 encodes small RNAs with antisense complementarity to lin-14', *Cell*, 75: 843-54.

Lee, Y., C. Ahn, J. Han, H. Choi, J. Kim, J. Yim, J. Lee, P. Provost, O. Rådmark, S. Kim, and V. N. Kim. 2003. 'The nuclear RNase III Drosha initiates microRNA processing', *Nature*, 425: 415-9.

Li, J., R. Panganiban, A. T. Kho, M. J. McGeachie, L. Farnam, R. P. Chase, S. T. Weiss, Q. Lu, and K. G. Tantisira. 2020. 'Circulating MicroRNAs and Treatment Response in Childhood Asthma', *Am J Respir Crit Care Med*, 202: 65-72.

Li, L., S. Li, M. Wu, C. Chi, D. Hu, Y. Cui, J. Song, C. Lee, and H. Chen. 2019. 'Early diagnostic value of circulating microRNAs in patients with suspected acute myocardial infarction', *J Cell Physiol*, 234: 13649-58.

Li, S., C. Lee, J. Song, C. Lu, J. Liu, Y. Cui, H. Liang, C. Cao, F. Zhang, and H. Chen. 2017. 'Circulating microRNAs as potential biomarkers for coronary plaque rupture', *Oncotarget*, 8: 48145-56.

Lichtman, A. H. 2013. 'The heart of the matter: protection of the myocardium from T cells', *J Autoimmun*, 45: 90-6.

Lin, C. R., T. Y. Wei, H. Y. Tsai, Y. T. Wu, P. Y. Wu, and S. T. Chen. 2015. 'Glycosylation-dependent interaction between CD69 and S100A8/S100A9 complex is required for regulatory T-cell differentiation', *Faseb j*, 29: 5006-17.

Liu, S., J. Chen, J. Shi, W. Zhou, L. Wang, W. Fang, Y. Zhong, X. Chen, Y. Chen, A. Sabri, and S. Liu. 2020. 'M1-like macrophage-derived exosomes suppress angiogenesis and exacerbate cardiac dysfunction in a myocardial infarction microenvironment', *Basic Res Cardiol*, 115: 22.

Liu, Y. H., Y. S. Tsai, S. C. Lin, N. S. Liao, M. S. Jan, C. T. Liang, S. W. Hsu, W. C. Chen, J. M. Sung, N. Maeda, and P. J. Tsai. 2016. 'Quantitative PPARγ expression affects the balance between tolerance and immunity', *Scientific reports*, 6: 26646.

Liu, Y., P. Zhang, J. Li, A. B. Kulkarni, S. Perruche, and W. Chen. 2008. 'A critical function for TGF-beta signaling in the development of natural CD4+CD25+Foxp3+ regulatory T cells', *Nat Immunol*, 9: 632-40.

López-Cabrera, M., A. G. Santis, E. Fernández-Ruiz, R. Blacher, F. Esch, P. Sánchez-Mateos, and F. Sánchez-Madrid. 1993. 'Molecular cloning, expression, and chromosomal localization of the human earliest lymphocyte activation antigen AIM/CD69, a new member of the C-type animal lectin superfamily of signal-transmitting receptors', *J Exp Med*, 178: 537-47.

Lu, L. F., T. H. Thai, D. P. Calado, A. Chaudhry, M. Kubo, K. Tanaka, G. B. Loeb, H. Lee, A. Yoshimura, K. Rajewsky, and A. Y. Rudensky. 2009. 'Foxp3-dependent microRNA155 confers competitive fitness to regulatory T cells by targeting SOCS1 protein', *Immunity*, 30: 80-91.

Lurz, P., C. Luecke, I. Eitel, F. Fohrenbach, C. Frank, M. Grothoff, S. de Waha, K. P. Rommel, J. A. Lurz, K. Klingel, R. Kandolf, G. Schuler, H. Thiele, and M. Gutberlet. 2016. 'Comprehensive Cardiac Magnetic Resonance Imaging in Patients With Suspected Myocarditis: The MyoRacer-Trial', *J Am Coll Cardiol*, 67: 1800-11.

Lv, H., E. Havari, S. Pinto, R. V. Gottumukkala, L. Cornivelli, K. Raddassi, T. Matsui, A. Rosenzweig, R. T. Bronson, R. Smith, A. L. Fletcher, S. J. Turley, K. Wucherpfennig, B. Kyewski, and M. A. Lipes. 2011. 'Impaired thymic tolerance to α-myosin directs autoimmunity to the heart in mice and humans', *J Clin Invest*, 121: 1561-73.

Ma, X., C. Ma, and X. Zheng. 2013. 'MicroRNA-155 in the pathogenesis of atherosclerosis: a conflicting role?', *Heart Lung Circ*, 22: 811-8.

Mack, D. G., A. M. Lanham, B. E. Palmer, L. A. Maier, and A. P. Fontenot. 2009. 'CD27 expression on CD4+ T cells differentiates effector from regulatory T cell subsets in the lung', *J Immunol*, 182: 7317-24.

Mahesh, G., and R. Biswas. 2019. 'MicroRNA-155: A Master Regulator of Inflammation', *J Interferon Cytokine Res*, 39: 321-30.

Maisel, A., D. Cesario, S. Baird, J. Rehman, P. Haghighi, and S. Carter. 1998. 'Experimental autoimmune myocarditis produced by adoptive transfer of splenocytes after myocardial infarction', *Circ Res*, 82: 458-63.

Malhotra, N., K. Narayan, O. H. Cho, K. E. Sylvia, C. Yin, H. Melichar, M. Rashighi, V. Lefebvre, J. E. Harris, L. J. Berg, and J. Kang. 2013. 'A network of high-mobility group box transcription factors programs innate interleukin-17 production', *Immunity*, 38: 681-93.

Malik, S., M. Y. Want, and A. Awasthi. 2016. 'The Emerging Roles of Gamma-Delta T Cells in Tissue Inflammation in Experimental Autoimmune Encephalomyelitis', *Front Immunol*, 7: 14.

Maloy, K. J., and M. C. Kullberg. 2008. 'IL-23 and Th17 cytokines in intestinal homeostasis', *Mucosal Immunol*, 1: 339-49.

Mangan, P. R., L. E. Harrington, D. B. O'Quinn, W. S. Helms, D. C. Bullard, C. O. Elson, R. D. Hatton, S. M. Wahl, T. R. Schoeb, and C. T. Weaver. 2006. 'Transforming growth factor-beta induces development of the T(H)17 lineage', *Nature*, 441: 231-4.

Mao, X., R. Zhu, F. Zhang, Y. Zhong, K. Yu, Y. Wei, H. Sun, W. Xu, Q. Luo, Y. Wang, Y. Ding, and Q. Zeng. 2019. 'IL-37 Plays a Beneficial Role in Patients with Acute Coronary Syndrome', *Mediators Inflamm*, 2019: 9515346.

Marketou, M., J. Kontaraki, A. Patrianakos, G. Kochiadakis, I. Anastasiou, K. Fragkiadakis, A. Plevritaki, S. T. Papadaki, G. Chlouverakis, and F. Parthenakis. 2021. 'Peripheral Blood MicroRNAs as Potential Biomarkers of Myocardial Damage in Acute Viral Myocarditis', *Genes (Basel)*, 12.

Markle, J. G., S. Mortin-Toth, A. S. Wong, L. Geng, A. Hayday, and J. S. Danska. 2013. 'γδ T cells are essential effectors of type 1 diabetes in the nonobese diabetic mouse model', *J Immunol*, 190: 5392-401.

Marson, Alexander, Karsten Kretschmer, Garrett M. Frampton, Elizabeth S. Jacobsen, Julia K. Polansky, Kenzie D. MacIsaac, Stuart S. Levine, Ernest Fraenkel, Harald von Boehmer, and Richard A. Young. 2007. 'Foxp3 occupancy and regulation of key target genes during T-cell stimulation', *Nature*, 445: 931-35.

Martin, B., K. Hirota, D. J. Cua, B. Stockinger, and M. Veldhoen. 2009. 'Interleukin-17-producing gammadelta T cells selectively expand in response to pathogen products and environmental signals', *Immunity*, 31: 321-30.

Martín, P., R. Blanco-Domínguez, and R. Sánchez-Díaz. 2021. 'Novel human immunomodulatory T cell receptors and their double-edged potential in autoimmunity, cardiovascular disease and cancer', *Cell Mol Immunol*, 18: 919-35.

Martín, P., M. Gómez, A. Lamana, A. Cruz-Adalia, M. Ramírez-Huesca, M. A. Ursa, M. Yáñez-Mo, and F. Sánchez-Madrid. 2010. 'CD69 association with Jak3/Stat5 proteins regulates Th17 cell differentiation', *Mol Cell Biol*, 30: 4877-89.

Martín, P., M. Gómez, A. Lamana, A. Matesanz Marín, J. R. Cortés, M. Ramírez-Huesca, O. Barreiro, P. López-Romero, C. Gutiérrez-Vázquez, H. de la Fuente, A. Cruz-Adalia, and F. Sánchez-Madrid. 2010. 'The leukocyte activation antigen CD69 limits allergic asthma and skin contact hypersensitivity', *J Allergy Clin Immunol*, 126: 355-65, 65.e1-3.

Maserati, Marc, Melanie Walentuk, Xiangpeng Dai, Olivia Holston, Danielle Adams, and Jesse Mager. 2011. 'Wdr74 is required for blastocyst formation in the mouse', *PLoS One*, 6: e22516-e16.

Massilamany, C., A. Gangaplara, D. Steffen, and J. Reddy. 2011. 'Identification of novel mimicry epitopes for cardiac myosin heavy chain-α that induce autoimmune myocarditis in A/J mice', *Cell Immunol*, 271: 438-49.

Matsumoto, S., Y. Sakata, D. Nakatani, S. Suna, H. Mizuno, M. Shimizu, M. Usami, T. Sasaki, H. Sato, Y. Kawahara, T. Hamasaki, S. Nanto, M. Hori, and I. Komuro. 2012. 'A subset of circulating microRNAs are predictive for cardiac death after discharge for acute myocardial infarction', *Biochem Biophys Res Commun*, 427: 280-4.

McGeachy, M. J., and D. J. Cua. 2007. 'The link between IL-23 and Th17 cell-mediated immune pathologies', *Semin Immunol*, 19: 372-6.

Mei, R., E. Raschi, E. Forcesi, I. Diemberger, F. De Ponti, and E. Poluzzi. 2018. 'Myocarditis and pericarditis after immunization: Gaining insights through the Vaccine Adverse Event Reporting System', *Int J Cardiol*, 273: 183-86.

Meijer, H. A., E. M. Smith, and M. Bushell. 2014. 'Regulation of miRNA strand selection: follow the leader?', *Biochem Soc Trans*, 42: 1135-40.

Mevorach, D., E. Anis, N. Cedar, M. Bromberg, E. J. Haas, E. Nadir, S. Olsha-Castell, D. Arad, T. Hasin, N. Levi, R. Asleh, O. Amir, K. Meir, D. Cohen, R. Dichtiar, D. Novick, Y. Hershkovitz, R. Dagan, I. Leitersdorf, R. Ben-Ami, I. Miskin, W. Saliba, K. Muhsen, Y. Levi, M. S. Green, L. Keinan-Boker, and S. Alroy-Preis. 2021. 'Myocarditis after BNT162b2 mRNA Vaccine against Covid-19 in Israel', *N Engl J Med*.

Michlewski, G., and J. F. Cáceres. 2019. 'Post-transcriptional control of miRNA biogenesis', *Rna*, 25: 1-16.

Misra, N., J. Bayry, S. Lacroix-Desmazes, M. D. Kazatchkine, and S. V. Kaveri. 2004. 'Cutting edge: human CD4+CD25+ T cells restrain the maturation and antigen-presenting function of dendritic cells', *J Immunol*, 172: 4676-80.

Mocan-Hognogi, Diana Larisa, Sebastian Trancă, Anca Daniela Farcaş, Radu Florin Mocan-Hognogi, Andrada Viorica Pârvu, and Anca Simona Bojan. 2021. 'Immune Checkpoint Inhibitors and the Heart', *Frontiers in cardiovascular medicine*, 8: 726426-26.

Mokuno, Y., T. Matsuguchi, M. Takano, H. Nishimura, J. Washizu, T. Ogawa, O. Takeuchi, S. Akira, Y. Nimura, and Y. Yoshikai. 2000. 'Expression of toll-like receptor 2 on gamma delta T cells bearing invariant V gamma 6/V delta 1 induced by Escherichia coli infection in mice', *J Immunol*, 165: 931-40.

Molet, S., Q. Hamid, F. Davoine, E. Nutku, R. Taha, N. Pagé, R. Olivenstein, J. Elias, and J. Chakir. 2001. 'IL-17 is increased in asthmatic airways and induces human bronchial fibroblasts to produce cytokines', *J Allergy Clin Immunol*, 108: 430-8.

Moltó, A., and E. Nikiphorou. 2018. 'Comorbidities in Spondyloarthritis', *Front Med (Lausanne)*, 5: 62.

Momose, F., N. Seo, Y. Akahori, S. Sawada, N. Harada, T. Ogura, K. Akiyoshi, and H. Shiku. 2016. 'Guanine-Rich Sequences Are a Dominant Feature of Exosomal microRNAs across the Mammalian Species and Cell Types', *PLoS One*, 11: e0154134.

Moody, L., H. He, Y. X. Pan, and H. Chen. 2017. 'Methods and novel technology for microRNA quantification in colorectal cancer screening', *Clin Epigenetics*, 9: 119.

Mora-Ruiz, M. D., F. Blanco-Favela, A. K. Chavez Rueda, M. V. Legorreta-Haquet, and L. Chavez-Sanchez. 2019. 'Role of interleukin-17 in acute myocardial infarction', *Mol Immunol*, 107: 71-78.

Muñoz-Ruiz, M., N. Sumaria, D. J. Pennington, and B. Silva-Santos. 2017. 'Thymic Determinants of γδ T Cell Differentiation', *Trends Immunol*, 38: 336-44.

Muxel, Sandra Marcia, Maria Fernanda Laranjeira-Silva, Ricardo Andrade Zampieri, and Lucile Maria Floeter-Winter. 2017. 'Leishmania (Leishmania) amazonensis induces macrophage miR-294 and miR-721 expression and modulates infection by targeting NOS2 and L-arginine metabolism', *Scientific reports*, 7: 44141-41.

Myers, J. M., L. T. Cooper, D. C. Kem, S. Stavrakis, S. D. Kosanke, E. M. Shevach, D. Fairweather, J. A. Stoner, C. J. Cox, and M. W. Cunningham. 2016. 'Cardiac myosin-Th17 responses promote heart failure in human myocarditis', *JCI Insight*, 1.

Myers, J. M., D. Fairweather, S. A. Huber, and M. W. Cunningham. 2013. 'Autoimmune myocarditis, valvulitis, and cardiomyopathy', *Curr Protoc Immunol*, Chapter 15: Unit 15.14.1-51.

Nahrendorf, M., F. K. Swirski, E. Aikawa, L. Stangenberg, T. Wurdinger, J. L. Figueiredo, P. Libby, R. Weissleder, and M. J. Pittet. 2007. 'The healing myocardium sequentially mobilizes two monocyte subsets with divergent and complementary functions', *J Exp Med*, 204: 3037-47.

Nakae, S., Y. Komiyama, A. Nambu, K. Sudo, M. Iwase, I. Homma, K. Sekikawa, M. Asano, and Y. Iwakura. 2002. 'Antigen-specific T cell sensitization is impaired in IL-17-deficient mice, causing suppression of allergic cellular and humoral responses', *Immunity*, 17: 375-87.

Nakae, S., H. Suto, G. J. Berry, and S. J. Galli. 2007. 'Mast cell-derived TNF can promote Th17 cell-dependent neutrophil recruitment in ovalbumin-challenged OTII mice', *Blood*, 109: 3640-8.

Nakahama, T., H. Hanieh, N. T. Nguyen, I. Chinen, B. Ripley, D. Millrine, S. Lee, K. K. Nyati, P. K. Dubey, K. Chowdhury, Y. Kawahara, and T. Kishimoto. 2013. 'Aryl hydrocarbon receptor-mediated induction of the microRNA-132/212 cluster promotes interleukin-17-producing T-helper cell differentiation', *Proc Natl Acad Sci U S A*, 110: 11964-9.

Nakasone, C., N. Yamamoto, M. Nakamatsu, T. Kinjo, K. Miyagi, K. Uezu, K. Nakamura, F. Higa, H. Ishikawa, L. O'Brien R, K. Ikuta, M. Kaku, J. Fujita, and K. Kawakami. 2007. 'Accumulation of gamma/delta T cells in the lungs and their roles in neutrophil-mediated host defense against pneumococcal infection', *Microbes Infect*, 9: 251-8.

Narayan, K., K. E. Sylvia, N. Malhotra, C. C. Yin, G. Martens, T. Vallerskog, H. Kornfeld, N. Xiong, N. R. Cohen, M. B. Brenner, L. J. Berg, and J. Kang. 2012. 'Intrathymic programming of effector fates in three molecularly distinct γδ T cell subtypes', *Nat Immunol*, 13: 511-8.

Navickas, R., D. Gal, A. Laucevičius, A. Taparauskaitė, M. Zdanytė, and P. Holvoet. 2016. 'Identifying circulating microRNAs as biomarkers of cardiovascular disease: a systematic review', *Cardiovasc Res*, 111: 322-37.

Nie, X., M. He, J. Wang, P. Chen, F. Wang, J. Lai, C. Li, T. Yu, H. Zuo, G. Cui, K. Miao, J. Jiang, D. W. Wang, and C. Chen. 2020. 'Circulating miR-4763-3p Is a Novel Potential Biomarker Candidate for Human Adult Fulminant Myocarditis', *Mol Ther Methods Clin Dev*, 17: 1079-87.

Niedbala, Wanda, Jose C. Alves-Filho, Sandra Y. Fukada, Silvio Manfredo Vieira, Akio Mitani, Fabiane Sonego, Ananda Mirchandani, Daniele C. Nascimento, Fernando Q. Cunha, and Foo Y. Liew. 2011. 'Regulation of type 17 helper T-cell function by nitric oxide during inflammation', *Proc Natl Acad Sci U S A*, 108: 9220-25.

Nielsen, O. H., I. Kirman, N. Rüdiger, J. Hendel, and B. Vainer. 2003. 'Upregulation of interleukin-12 and -17 in active inflammatory bowel disease', *Scand J Gastroenterol*, 38: 180-5.

Niino, M., K. Iwabuchi, S. Kikuchi, M. Ato, T. Morohashi, A. Ogata, K. Tashiro, and K. Onoé. 2001. 'Amelioration of experimental autoimmune encephalomyelitis in C57BL/6 mice by an agonist of peroxisome proliferator-activated receptor-gamma', *J Neuroimmunol*, 116: 40-8.

O'Brien, R. L., and W. K. Born. 2010. 'gammadelta T cell subsets: a link between TCR and function?', *Semin Immunol*, 22: 193-8.

O'Connell, R. M., D. Kahn, W. S. Gibson, J. L. Round, R. L. Scholz, A. A. Chaudhuri, M. E. Kahn, D. S. Rao, and D. Baltimore. 2010. 'MicroRNA-155 promotes autoimmune inflammation by enhancing inflammatory T cell development', *Immunity*, 33: 607-19.

O'Connell, R. M., K. D. Taganov, M. P. Boldin, G. Cheng, and D. Baltimore. 2007. 'MicroRNA-155 is induced during the macrophage inflammatory response', *Proc Natl Acad Sci U S A*, 104: 1604-9.

Obermajer, N., J. L. Wong, R. P. Edwards, K. Chen, M. Scott, S. Khader, J. K. Kolls, K. Odunsi, T. R. Billiar, and P. Kalinski. 2013. 'Induction and stability of human Th17 cells require endogenous NOS2 and cGMP-dependent NO signaling', *J Exp Med*, 210: 1433-445.

Obradovic, D., K. P. Rommel, S. Blazek, K. Klingel, M. Gutberlet, C. Lücke, P. Büttner, H. Thiele, V. Adams, P. Lurz, F. Emrich, and C. Besler. 2021. 'The potential role of plasma miR-155 and miR-206 as circulatory biomarkers in inflammatory cardiomyopathy', *ESC Heart Fail*, 8: 1850-60.

Ohta, A., and M. Sitkovsky. 2014. 'Extracellular adenosine-mediated modulation of regulatory T cells', *Front Immunol*, 5: 304.

Ooi, D. S., P. A. Isotalo, and J. P. Veinot. 2000. 'Correlation of antemortem serum creatine kinase, creatine kinase-MB, troponin I, and troponin T with cardiac pathology', *Clin Chem*, 46: 338-44.

Ouyang, W., O. Beckett, Q. Ma, and M. O. Li. 2010. 'Transforming growth factor-beta signaling curbs thymic negative selection promoting regulatory T cell development', *Immunity*, 32: 642-53.

Paliard, X., R. de Waal Malefijt, H. Yssel, D. Blanchard, I. Chrétien, J. Abrams, J. de Vries, and H. Spits. 1988. 'Simultaneous production of IL-2, IL-4, and IFN-gamma by activated human CD4+ and CD8+ T cell clones', *J Immunol*, 141: 849-55.

Pandiyan, P., L. Zheng, S. Ishihara, J. Reed, and M. J. Lenardo. 2007. 'CD4+CD25+Foxp3+ regulatory T cells induce cytokine deprivation-mediated apoptosis of effector CD4+ T cells', *Nat Immunol*, 8: 1353-62.

Papiernik, M., M. L. de Moraes, C. Pontoux, F. Vasseur, and C. Pénit. 1998. 'Regulatory CD4 T cells: expression of IL-2R alpha chain, resistance to clonal deletion and IL-2 dependency', *Int Immunol*, 10: 371-8.

Papotto, P. H., J. C. Ribot, and B. Silva-Santos. 2017. 'IL-17(+) gammadelta T cells as kick-starters of inflammation', *Nat Immunol*, 18: 604-11.

Park, S. G., R. Mathur, M. Long, N. Hosh, L. Hao, M. S. Hayden, and S. Ghosh. 2010. 'T regulatory cells maintain intestinal homeostasis by suppressing gammadelta T cells', *Immunity*, 33: 791-803.

Pasqui, A. L., M. Di Renzo, G. Bova, F. Bruni, L. Puccetti, G. Pompella, and A. Auteri. 2003. 'T cell activation and enhanced apoptosis in non-ST elevation myocardial infarction', *Clin Exp Med*, 3: 37-44.

Paul, Sourav, and Girdhari Lal. 2016. 'Regulatory and effector functions of gamma–delta (γδ) T cells and their therapeutic potential in adoptive cellular therapy for cancer', *International Journal of Cancer*, 139: 976-85.

Pfaff, Nils, Jan Fiedler, Angelika Holzmann, Axel Schambach, Thomas Moritz, Tobias Cantz, and Thomas Thum. 2011. 'miRNA screening reveals a new miRNA family stimulating iPS cell generation via regulation of Meox2', *EMBO reports*, 12: 1153-59.
Pfeffer, M. A., J. M. Pfeffer, and G. A. Lamas. 1993. 'Development and prevention of congestive heart failure following myocardial infarction', *Circulation*, 87: Iv120-5.
Pillai, R. S. 2005. 'MicroRNA function: multiple mechanisms for a tiny RNA?', *Rna*, 11: 1753-61.
Pollack, A., A. R. Kontorovich, V. Fuster, and G. W. Dec. 2015. 'Viral myocarditis--diagnosis, treatment options, and current controversies', *Nat Rev Cardiol*, 12: 670-80.
Poller, W., S. Dimmeler, S. Heymans, T. Zeller, J. Haas, M. Karakas, D. M. Leistner, P. Jakob, S. Nakagawa, S. Blankenberg, S. Engelhardt, T. Thum, C. Weber, B. Meder, R. Hajjar, and U. Landmesser. 2018. 'Non-coding RNAs in cardiovascular diseases: diagnostic and therapeutic perspectives', *Eur Heart J*, 39: 2704-16.
Porcuna, Jesús, Jorge Mínguez-Martínez, and Mercedes Ricote. 2021. 'The PPARα and PPARγ Epigenetic Landscape in Cancer and Immune and Metabolic Disorders', *Int J Mol Sci*, 22.
Pot, Caroline, Lionel Apetoh, and Vijay K. Kuchroo. 2011. 'Type 1 regulatory T cells (Tr1) in autoimmunity', *Semin Immunol*, 23: 202-08.
Qureshi, O. S., Y. Zheng, K. Nakamura, K. Attridge, C. Manzotti, E. M. Schmidt, J. Baker, L. E. Jeffery, S. Kaur, Z. Briggs, T. Z. Hou, C. E. Futter, G. Anderson, L. S. Walker, and D. M. Sansom. 2011. 'Trans-endocytosis of CD80 and CD86: a molecular basis for the cell-extrinsic function of CTLA-4', *Science*, 332: 600-3.
Radulovic, K., C. Manta, V. Rossini, K. Holzmann, H. A. Kestler, U. M. Wegenka, T. Nakayama, and J. H. Niess. 2012. 'CD69 regulates type I IFN-induced tolerogenic signals to mucosal CD4 T cells that attenuate their colitogenic potential', *J Immunol*, 188: 2001-13.
Rahman, M. S., and K. Woollard. 2017. 'Atherosclerosis', *Adv Exp Med Biol*, 1003: 121-44.
Ramachandran, S., and V. Palanisamy. 2012. 'Horizontal transfer of RNAs: exosomes as mediators of intercellular communication', *Wiley Interdiscip Rev RNA*, 3: 286-93.
Rangachari, M., N. Mauermann, R. R. Marty, S. Dirnhofer, M. O. Kurrer, V. Komnenovic, J. M. Penninger, and U. Eriksson. 2006. 'T-bet negatively regulates autoimmune myocarditis by suppressing local production of interleukin 17', *J Exp Med*, 203: 2009-19.
Rao, D. S., R. M. O'Connell, A. A. Chaudhuri, Y. Garcia-Flores, T. L. Geiger, and D. Baltimore. 2010. 'MicroRNA-34a perturbs B lymphocyte development by repressing the forkhead box transcription factor Foxp1', *Immunity*, 33: 48-59.
Read, S., V. Malmström, and F. Powrie. 2000. 'Cytotoxic T lymphocyte-associated antigen 4 plays an essential role in the function of CD25(+)CD4(+) regulatory cells that control intestinal inflammation', *J Exp Med*, 192: 295-302.
Ribot, J. C., M. Chaves-Ferreira, F. d'Orey, M. Wencker, N. Gonçalves-Sousa, J. Decalf, J. P. Simas, A. C. Hayday, and B. Silva-Santos. 2010. 'Cutting edge: adaptive versus innate receptor signals selectively control the pool sizes of murine IFN-γ- or IL-17-producing γδ T cells upon infection', *J Immunol*, 185: 6421-25.
Ribot, J. C., A. deBarros, D. J. Pang, J. F. Neves, V. Peperzak, S. J. Roberts, M. Girardi, J. Borst, A. C. Hayday, D. J. Pennington, and B. Silva-Santos. 2009. 'CD27 is a thymic determinant of the balance between interferon-gamma- and interleukin 17-producing gammadelta T cell subsets', *Nat Immunol*, 10: 427-36.
Ribot, J. C., S. T. Ribeiro, D. V. Correia, A. E. Sousa, and B. Silva-Santos. 2014. 'Human γδ thymocytes are functionally immature and differentiate into cytotoxic type 1 effector T cells upon IL-2/IL-15 signaling', *J Immunol*, 192: 2237-43.
Ricote, M., A. F. Valledor, and C. K. Glass. 2004. 'Decoding transcriptional programs regulated by PPARs and LXRs in the macrophage: effects on lipid homeostasis, inflammation, and atherosclerosis', *Arterioscler Thromb Vasc Biol*, 24: 230-9.
Rieckmann, M., M. Delgobo, C. Gaal, L. Buchner, P. Steinau, D. Reshef, C. Gil-Cruz, E. N. T. Horst, M. Kircher, T. Reiter, K. G. Heinze, H. W. Niessen, P. A. Krijnen, A. M. van der Laan, J. J. Piek, C. Koch, H. J. Wester, C. Lapa, W. R. Bauer, B. Ludewig, N. Friedman, S. Frantz, U. Hofmann, and G. C. Ramos. 2019. 'Myocardial infarction triggers cardioprotective antigen-specific T helper cell responses', *J Clin Invest*, 130: 4922-36.

Roark, C. L., J. D. French, M. A. Taylor, A. M. Bendele, W. K. Born, and R. L. O'Brien. 2007. 'Exacerbation of collagen-induced arthritis by oligoclonal, IL-17-producing gamma delta T cells', *J Immunol*, 179: 5576-83.

Rodriguez, A., S. Griffiths-Jones, J. L. Ashurst, and A. Bradley. 2004. 'Identification of mammalian microRNA host genes and transcription units', *Genome Res*, 14: 1902-10.

Rodriguez, A., E. Vigorito, S. Clare, M. V. Warren, P. Couttet, D. R. Soond, S. van Dongen, R. J. Grocock, P. P. Das, E. A. Miska, D. Vetrie, K. Okkenhaug, A. J. Enright, G. Dougan, M. Turner, and A. Bradley. 2007. 'Requirement of bic/microRNA-155 for normal immune function', *Science*, 316: 608-11.

Roth, Gregory A., George A. Mensah, Catherine O. Johnson, Giovanni Addolorato, Enrico Ammirati, Larry M. Baddour, Noël C. Barengo, Andrea Z. Beaton, Emelia J. Benjamin, Catherine P. Benziger, Aimé Bonny, Michael Brauer, Marianne Brodmann, Thomas J. Cahill, Jonathan Carapetis, Alberico L. Catapano, Sumeet S. Chugh, Leslie T. Cooper, Josef Coresh, Michael Criqui, Nicole DeCleene, Kim A. Eagle, Sophia Emmons-Bell, Valery L. Feigin, Joaquim Fernández-Solà, Gerry Fowkes, Emmanuela Gakidou, Scott M. Grundy, Feng J. He, George Howard, Frank Hu, Lesley Inker, Ganesan Karthikeyan, Nicholas Kassebaum, Walter Koroshetz, Carl Lavie, Donald Lloyd-Jones, Hong S. Lu, Antonio Mirijello, Awoke Misganaw Temesgen, Ali Mokdad, Andrew E. Moran, Paul Muntner, Jagat Narula, Bruce Neal, Mpiko Ntsekhe, Glaucia Moraes de Oliveira, Catherine Otto, Mayowa Owolabi, Michael Pratt, Sanjay Rajagopalan, Marissa Reitsma, Antonio Luiz P. Ribeiro, Nancy Rigotti, Anthony Rodgers, Craig Sable, Saate Shakil, Karen Sliwa-Hahnle, Benjamin Stark, Johan Sundström, Patrick Timpel, Imad M. Tleyjeh, Marco Valgimigli, Theo Vos, Paul K. Whelton, Magdi Yacoub, Liesl Zuhlke, Christopher Murray, Valentin Fuster, Gregory A. Roth, George A. Mensah, Catherine O. Johnson, Giovanni Addolorato, Enrico Ammirati, Larry M. Baddour, Noel C. Barengo, Andrea Beaton, Emelia J. Benjamin, Catherine P. Benziger, Aime Bonny, Michael Brauer, Marianne Brodmann, Thomas J. Cahill, Jonathan R. Carapetis, Alberico L. Catapano, Sumeet Chugh, Leslie T. Cooper, Josef Coresh, Michael H. Criqui, Nicole K. DeCleene, Kim A. Eagle, Sophia Emmons-Bell, Valery L. Feigin, Joaquim Fernández-Sola, F. Gerry R. Fowkes, Emmanuela Gakidou, Scott M. Grundy, Feng J. He, George Howard, Frank Hu, Lesley Inker, Ganesan Karthikeyan, Nicholas J. Kassebaum, Walter J. Koroshetz, Carl Lavie, Donald Lloyd-Jones, Hong S. Lu, Antonio Mirijello, Awoke T. Misganaw, Ali H. Mokdad, Andrew E. Moran, Paul Muntner, Jagat Narula, Bruce Neal, Mpiko Ntsekhe, Gláucia M.M. Oliveira, Catherine M. Otto, Mayowa O. Owolabi, Michael Pratt, Sanjay Rajagopalan, Marissa B. Reitsma, Antonio Luiz P. Ribeiro, Nancy A. Rigotti, Anthony Rodgers, Craig A. Sable, Saate S. Shakil, Karen Sliwa, Benjamin A. Stark, Johan Sundström, Patrick Timpel, Imad I. Tleyjeh, Marco Valgimigli, Theo Vos, Paul K. Whelton, Magdi Yacoub, Liesl J. Zuhlke, Mohsen Abbasi-Kangevari, Alireza Abdi, Aidin Abedi, Victor Aboyans, Woldu A. Abrha, Eman Abu-Gharbieh, Abdelrahman I. Abushouk, Dilaram Acharya, Tim Adair, Oladimeji M. Adebayo, Zanfina Ademi, Shailesh M. Advani, Khashayar Afshari, Ashkan Afshin, Gina Agarwal, Pradyumna Agasthi, Sohail Ahmad, Sepideh Ahmadi, Muktar B. Ahmed, Budi Aji, Yonas Akalu, Wuraola Akande-Sholabi, Addis Aklilu, Chisom J. Akunna, Fares Alahdab, Ayman Al-Eyadhy, Khalid F. Alhabib, Sheikh M. Alif, Vahid Alipour, Syed M. Aljunid, François Alla, Amir Almasi-Hashiani, Sami Almustanyir, Rajaa M. Al-Raddadi, Adeladza K. Amegah, Saeed Amini, Arya Aminorroaya, Hubert Amu, Dickson A. Amugsi, Robert Ancuceanu, Deanna Anderlini, Tudorel Andrei, Catalina Liliana Andrei, Alireza Ansari-Moghaddam, Zelalem A. Anteneh, Ippazio Cosimo Antonazzo, Benny Antony, Razique Anwer, Lambert T. Appiah, Jalal Arabloo, Johan Ärnlöv, Kurnia D. Artanti, Zerihun Ataro, Marcel Ausloos, Leticia Avila-Burgos, Asma T. Awan, Mamaru A. Awoke, Henok T. Ayele, Muluken A. Ayza, Samad Azari, Darshan B. B, Nafiseh Baheiraei, Atif A. Baig, Ahad Bakhtiari, Maciej Banach, Palash C. Banik, Emerson A. Baptista, Miguel A. Barboza, Lingkan Barua, Sanjay Basu, Neeraj Bedi, Yannick Béjot, Derrick A. Bennett, Isabela M. Bensenor, Adam E. Berman, Yihienew M. Bezabih, Akshaya S. Bhagavathula, Sonu Bhaskar, Krittika Bhattacharyya, Ali Bijani, Boris Bikbov, Mulugeta M. Birhanu, Archith Boloor, Luisa C. Brant, Hermann Brenner, Nikolay I. Briko, Zahid A. Butt, Florentino Luciano Caetano dos Santos, Leah E. Cahill, Lucero Cahuana-Hurtado, Luis A. Cámera, Ismael R. Campos-Nonato, Carlos Cantu-Brito, Josip Car, Juan J.

Carrero, Felix Carvalho, Carlos A. Castañeda-Orjuela, Ferrán Catalá-López, Ester Cerin, Jaykaran Charan, Vijay Kumar Chattu, Simiao Chen, Ken L. Chin, Jee-Young J. Choi, Dinh-Toi Chu, Sheng-Chia Chung, Massimo Cirillo, Sean Coffey, Sara Conti, Vera M. Costa, David K. Cundiff, Omid Dadras, Baye Dagnew, Xiaochen Dai, Albertino A.M. Damasceno, Lalit Dandona, Rakhi Dandona, Kairat Davletov, Vanessa De la Cruz-Góngora, Fernando P. De la Hoz, Jan-Walter De Neve, Edgar Denova-Gutiérrez, Meseret Derbew Molla, Behailu T. Derseh, Rupak Desai, Günther Deuschl, Samath D. Dharmaratne, Meghnath Dhimal, Raja Ram Dhungana, Mostafa Dianatinasab, Daniel Diaz, Shirin Djalalinia, Klara Dokova, Abdel Douiri, Bruce B. Duncan, Andre R. Duraes, Arielle W. Eagan, Sanam Ebtehaj, Aziz Eftekhari, Sahar Eftekharzadeh, Michael Ekholuenetale, Nevine El Nahas, Islam Y. Elgendy, Muhammed Elhadi, Shaimaa I. El-Jaafary, Sadaf Esteghamati, Atkilt E. Etisso, Oghenowede Eyawo, Ibtihal Fadhil, Emerito Jose A. Faraon, Pawan S. Faris, Medhat Farwati, Farshad Farzadfar, Eduarda Fernandes, Carlota Fernandez Prendes, Pietro Ferrara, Irina Filip, Florian Fischer, David Flood, Takeshi Fukumoto, Mohamed M. Gad, Shilpa Gaidhane, Morsaleh Ganji, Jalaj Garg, Abadi K. Gebre, Birhan G. Gebregiorgis, Kidane Z. Gebregzabiher, Gebreamlak G. Gebremeskel, Lemma Getacher, Abera Getachew Obsa, Alireza Ghajar, Ahmad Ghashghaee, Nermin Ghith, Simona Giampaoli, Syed Amir Gilani, Paramjit S. Gill, Richard F. Gillum, Ekaterina V. Glushkova, Elena V. Gnedovskaya, Mahaveer Golechha, Kebebe B. Gonfa, Amir Hossein Goudarzian, Alessandra C. Goulart, Jenny S. Guadamuz, Avirup Guha, Yuming Guo, Rajeev Gupta, Vladimir Hachinski, Nima Hafezi-Nejad, Teklehaimanot G. Haile, Randah R. Hamadeh, Samer Hamidi, Graeme J. Hankey, Arief Hargono, Risky K. Hartono, Maryam Hashemian, Abdiwahab Hashi, Shoaib Hassan, Hamid Y. Hassen, Rasmus J. Havmoeller, Simon I. Hay, Khezar Hayat, Golnaz Heidari, Claudiu Herteliu, Ramesh Holla, Mostafa Hosseini, Mehdi Hosseinzadeh, Mihaela Hostiuc, Sorin Hostiuc, Mowafa Househ, Junjie Huang, Ayesha Humayun, Ivo Iavicoli, Charles U. Ibeneme, Segun E. Ibitoye, Olayinka S. Ilesanmi, Irena M. Ilic, Milena D. Ilic, Usman Iqbal, Seyed Sina N. Irvani, Sheikh Mohammed Shariful Islam, Rakibul M. Islam, Hiroyasu Iso, Masao Iwagami, Vardhmaan Jain, Tahereh Javaheri, Sathish Kumar Jayapal, Shubha Jayaram, Ranil Jayawardena, Panniyammakal Jeemon, Ravi P. Jha, Jost B. Jonas, Jitendra Jonnagaddala, Farahnaz Joukar, Jacek J. Jozwiak, Mikk Jürisson, Ali Kabir, Tanvir Kahlon, Rizwan Kalani, Rohollah Kalhor, Ashwin Kamath, Ibrahim Kamel, Himal Kandel, Amit Kandel, André Karch, Ayele Semachew Kasa, Patrick D.M.C. Katoto, Gbenga A. Kayode, Yousef S. Khader, Mohammad Khammarnia, Muhammad S. Khan, Md Nuruzzaman Khan, Maseer Khan, Ejaz A. Khan, Khaled Khatab, Gulam M.A. Kibria, Yun Jin Kim, Gyu Ri Kim, Ruth W. Kimokoti, Sezer Kisa, Adnan Kisa, Mika Kivimäki, Dhaval Kolte, Ali Koolivand, Vladimir A. Korshunov, Sindhura Lakshmi Koulmane Laxminarayana, Ai Koyanagi, Kewal Krishan, Vijay Krishnamoorthy, Barthelemy Kuate Defo, Burcu Kucuk Bicer, Vaman Kulkarni, G. Anil Kumar, Nithin Kumar, Om P. Kurmi, Dian Kusuma, Gene F. Kwan, Carlo La Vecchia, Ben Lacey, Tea Lallukka, Qing Lan, Savita Lasrado, Zohra S. Lassi, Paolo Lauriola, Wayne R. Lawrence, Avula Laxmaiah, Kate E. LeGrand, Ming-Chieh Li, Bingyu Li, Shanshan Li, Stephen S. Lim, Lee-Ling Lim, Hualiang Lin, Ziqiang Lin, Ro-Ting Lin, Xuefeng Liu, Alan D. Lopez, Stefan Lorkowski, Paulo A. Lotufo, Alessandra Lugo, Nirmal K. M, Fabiana Madotto, Morteza Mahmoudi, Azeem Majeed, Reza Malekzadeh, Ahmad A. Malik, Abdullah A. Mamun, Navid Manafi, Mohammad Ali Mansournia, Lorenzo G. Mantovani, Santi Martini, Manu R. Mathur, Giampiero Mazzaglia, Suresh Mehata, Man Mohan Mehndiratta, Toni Meier, Ritesh G. Menezes, Atte Meretoja, Tomislav Mestrovic, Bartosz Miazgowski, Tomasz Miazgowski, Irmina Maria Michalek, Ted R. Miller, Erkin M. Mirrakhimov, Hamed Mirzaei, Babak Moazen, Masoud Moghadaszadeh, Yousef Mohammad, Dara K. Mohammad, Shafiu Mohammed, Mohammed A. Mohammed, Yaser Mokhayeri, Mariam Molokhia, Ahmed A. Montasir, Ghobad Moradi, Rahmatollah Moradzadeh, Paula Moraga, Lidia Morawska, Ilais Moreno Velásquez, Jakub Morze, Sumaira Mubarik, Walter Muruet, Kamarul Imran Musa, Ahamarshan J. Nagarajan, Mahdi Nalini, Vinay Nangia, Atta Abbas Naqvi, Sreenivas Narasimha Swamy, Bruno R. Nascimento, Vinod C. Nayak, Javad Nazari, Milad Nazarzadeh, Ruxandra I. Negoi, Sandhya Neupane Kandel, Huong L.T. Nguyen, Molly R. Nixon, Bo Norrving, Jean Jacques Noubiap, Brice E. Nouthe, Christoph Nowak, Oluwakemi O. Odukoya, Felix A. Ogbo, Andrew T. Olagunju, Hans Orru,

Alberto Ortiz, Samuel M. Ostroff, Jagadish Rao Padubidri, Raffaele Palladino, Adrian Pana, Songhomitra Panda-Jonas, Utsav Parekh, Eun-Cheol Park, Mojtaba Parvizi, Fatemeh Pashazadeh Kan, Urvish K. Patel, Mona Pathak, Rajan Paudel, Veincent Christian F. Pepito, Arokiasamy Perianayagam, Norberto Perico, Hai Q. Pham, Thomas Pilgrim, Michael A. Piradov, Farhad Pishgar, Vivek Podder, Roman V. Polibin, Akram Pourshams, Dimas R.A. Pribadi, Navid Rabiee, Mohammad Rabiee, Amir Radfar, Alireza Rafiei, Fakher Rahim, Vafa Rahimi-Movaghar, Mohammad Hifz Ur Rahman, Muhammad Aziz Rahman, Amir Masoud Rahmani, Ivo Rakovac, Pradhum Ram, Sudha Ramalingam, Juwel Rana, Priyanga Ranasinghe, Sowmya J. Rao, Priya Rathi, Lal Rawal, Wasiq F. Rawasia, Reza Rawassizadeh, Giuseppe Remuzzi, Andre M.N. Renzaho, Aziz Rezapour, Seyed Mohammad Riahi, Ross L. Roberts-Thomson, Leonardo Roever, Peter Rohloff, Michele Romoli, Gholamreza Roshandel, Godfrey M. Rwegerera, Seyedmohammad Saadatagah, Maha M. Saber-Ayad, Siamak Sabour, Simona Sacco, Masoumeh Sadeghi, Sahar Saeedi Moghaddam, Saeed Safari, Amirhossein Sahebkar, Sana Salehi, Hamideh Salimzadeh, Mehrnoosh Samaei, Abdallah M. Samy, Itamar S. Santos, Milena M. Santric-Milicevic, Nizal Sarrafzadegan, Arash Sarveazad, Thirunavukkarasu Sathish, Monika Sawhney, Mete Saylan, Maria I. Schmidt, Aletta E. Schutte, Subramanian Senthilkumaran, Sadaf G. Sepanlou, Feng Sha, Saeed Shahabi, Izza Shahid, Masood A. Shaikh, Mahdi Shamali, Morteza Shamsizadeh, Md Shajedur Rahman Shawon, Aziz Sheikh, Mika Shigematsu, Min-Jeong Shin, Jae Il Shin, Rahman Shiri, Ivy Shiue, Kerem Shuval, Soraya Siabani, Tariq J. Siddiqi, Diego A.S. Silva, Jasvinder A. Singh, Ambrish Singh Mtech, Valentin Y. Skryabin, Anna A. Skryabina, Amin Soheili, Emma E. Spurlock, Leo Stockfelt, Stefan Stortecky, Saverio Stranges, Rizwan Suliankatchi Abdulkader, Hooman Tadbiri, Eyayou G. Tadesse, Degena B. Tadesse, Masih Tajdini, Md Tariqujjaman, Berhane F. Teklehaimanot, Mohamad-Hani Temsah, Ayenew K. Tesema, Bhaskar Thakur, Kavumpurathu R. Thankappan, Rekha Thapar, Amanda G. Thrift, Binod Timalsina, Marcello Tonelli, Mathilde Touvier, Marcos R. Tovani-Palone, Avnish Tripathi, Jaya P. Tripathy, Thomas C. Truelsen, Guesh M. Tsegay, Gebiyaw W. Tsegaye, Nikolaos Tsilimparis, Biruk S. Tusa, Stefanos Tyrovolas, Krishna Kishore Umapathi, Brigid Unim, Bhaskaran Unnikrishnan, Muhammad S. Usman, Muthiah Vaduganathan, Pascual R. Valdez, Tommi J. Vasankari, Diana Z. Velazquez, Narayanaswamy Venketasubramanian, Giang T. Vu, Isidora S. Vujcic, Yasir Waheed, Yanzhong Wang, Fang Wang, Jingkai Wei, Robert G. Weintraub, Abrha H. Weldemariam, Ronny Westerman, Andrea S. Winkler, Charles S. Wiysonge, Charles D.A. Wolfe, Befikadu Legesse Wubishet, Gelin Xu, Ali Yadollahpour, Kazumasa Yamagishi, Lijing L. Yan, Srikanth Yandrapalli, Yuichiro Yano, Hiroshi Yatsuya, Tomas Y. Yeheyis, Yigizie Yeshaw, Christopher S. Yilgwan, Naohiro Yonemoto, Chuanhua Yu, Hasan Yusefzadeh, Geevar Zachariah, Sojib Bin Zaman, Muhammed S. Zaman, Maryam Zamanian, Ramin Zand, Alireza Zandifar, Afshin Zarghi, Mikhail S. Zastrozhin, Anasthasia Zastrozhina, Zhi-Jiang Zhang, Yunquan Zhang, Wangjian Zhang, Chenwen Zhong, Zhiyong Zou, Yves Miel H. Zuniga, Christopher J.L. Murray, and Valentin Fuster. 2020. 'Global Burden of Cardiovascular Diseases and Risk Factors, 1990–2019', *J Am Coll Cardiol*, 76: 2982-3021.

Roy, P., M. Orecchioni, and K. Ley. 2021. 'How the immune system shapes atherosclerosis: roles of innate and adaptive immunity', *Nat Rev Immunol*.

Saito, H., D. M. Kranz, Y. Takagaki, A. C. Hayday, H. N. Eisen, and S. Tonegawa. 1984. 'Complete primary structure of a heterodimeric T-cell receptor deduced from cDNA sequences', *Nature*, 309: 757-62.

Sakaguchi, S., N. Sakaguchi, M. Asano, M. Itoh, and M. Toda. 1995. 'Immunologic self-tolerance maintained by activated T cells expressing IL-2 receptor alpha-chains (CD25). Breakdown of a single mechanism of self-tolerance causes various autoimmune diseases', *J Immunol*, 155: 1151-64.

Samat, A. A. K., J. van der Geest, S. J. Vastert, J. van Loosdregt, and F. van Wijk. 2021. 'Tissue-Resident Memory T Cells in Chronic Inflammation-Local Cells with Systemic Effects?', *Cells*, 10.

Sanchez-Diaz, R., R. Blanco-Dominguez, S. Lasarte, K. Tsilingiri, E. Martin-Gayo, B. Linillos-Pradillo, H. de la Fuente, F. Sanchez-Madrid, R. Nakagawa, M. L. Toribio, and P. Martin. 2017.

'Thymus-Derived Regulatory T Cell Development Is Regulated by C-Type Lectin-Mediated BIC/MicroRNA 155 Expression', *Mol Cell Biol*, 37.

Sánchez-Mateos, P., and F. Sánchez-Madrid. 1991. 'Structure-function relationship and immunochemical mapping of external and intracellular antigenic sites on the lymphocyte activation inducer molecule, AIM/CD69', *Eur J Immunol*, 21: 2317-25.

Sancho, D., M. Gómez, F. Viedma, E. Esplugues, M. Gordón-Alonso, M. A. García-López, H. de la Fuente, A. C. Martínez, P. Lauzurica, and F. Sánchez-Madrid. 2003. 'CD69 downregulates autoimmune reactivity through active transforming growth factor-beta production in collagen-induced arthritis', *J Clin Invest*, 112: 872-82.

Santangelo, L., G. Giurato, C. Cicchini, C. Montaldo, C. Mancone, R. Tarallo, C. Battistelli, T. Alonzi, A. Weisz, and M. Tripodi. 2016. 'The RNA-Binding Protein SYNCRIP Is a Component of the Hepatocyte Exosomal Machinery Controlling MicroRNA Sorting', *Cell Rep*, 17: 799-808.

Sardella, G., L. De Luca, V. Francavilla, D. Accapezzato, M. Mancone, M. I. Sirinian, F. Fedele, and M. Paroli. 2007. 'Frequency of naturally-occurring regulatory T cells is reduced in patients with ST-segment elevation myocardial infarction', *Thromb Res*, 120: 631-4.

Sato, N. 2019. 'Call for action to establish standard diagnostic and therapeutic approaches for myocarditis', *Int J Cardiol*, 284: 61-62.

Saxena, A., M. Dobaczewski, V. Rai, Z. Haque, W. Chen, N. Li, and N. G. Frangogiannis. 2014. 'Regulatory T cells are recruited in the infarcted mouse myocardium and may modulate fibroblast phenotype and function', *Am J Physiol Heart Circ Physiol*, 307: H1233-42.

Schumacher, D., A. Curaj, S. Simsekyilmaz, A. Schober, E. A. Liehn, and S. F. Mause. 2021. 'miR155 Deficiency Reduces Myofibroblast Density but Fails to Improve Cardiac Function after Myocardial Infarction in Dyslipidemic Mouse Model', *Int J Mol Sci*, 22.

Schwarzenberger, P., W. Huang, P. Ye, P. Oliver, M. Manuel, Z. Zhang, G. Bagby, S. Nelson, and J. K. Kolls. 2000. 'Requirement of endogenous stem cell factor and granulocyte-colony-stimulating factor for IL-17-mediated granulopoiesis', *J Immunol*, 164: 4783-9.

Schwarzenberger, P., V. La Russa, A. Miller, P. Ye, W. Huang, A. Zieske, S. Nelson, G. J. Bagby, D. Stoltz, R. L. Mynatt, M. Spriggs, and J. K. Kolls. 1998. 'IL-17 stimulates granulopoiesis in mice: use of an alternate, novel gene therapy-derived method for in vivo evaluation of cytokines', *J Immunol*, 161: 6383-9.

Seropian, I. M., J. P. Cerliani, S. Toldo, B. W. Van Tassell, J. M. Ilarregui, G. E. Gonzalez, M. Matoso, F. N. Salloum, R. Melchior, R. J. Gelpi, J. C. Stupirski, A. Benatar, K. A. Gomez, C. Morales, A. Abbate, and G. A. Rabinovich. 2013. 'Galectin-1 controls cardiac inflammation and ventricular remodeling during acute myocardial infarction', *Am J Pathol*, 182: 29-40.

Shao, C., F. Yang, Z. Qin, X. Jing, Y. Shu, and H. Shen. 2019. 'The value of miR-155 as a biomarker for the diagnosis and prognosis of lung cancer: a systematic review with meta-analysis', *BMC Cancer*, 19: 1103.

Sharir, R., J. Semo, S. Shimoni, T. Ben-Mordechai, N. Landa-Rouben, S. Maysel-Auslender, A. Shaish, M. Entin-Meer, G. Keren, and J. George. 2014. 'Experimental myocardial infarction induces altered regulatory T cell hemostasis, and adoptive transfer attenuates subsequent remodeling', *PLoS One*, 9: e113653.

Sheridan, Brian S., Pablo A. Romagnoli, Quynh-Mai Pham, Han-Hsuan Fu, Francis Alonzo, 3rd, Wolf-Dieter Schubert, Nancy E. Freitag, and Leo Lefrançois. 2013. 'γδ T cells exhibit multifunctional and protective memory in intestinal tissues', *Immunity*, 39: 184-95.

Shevach, E. M. 2009. 'Mechanisms of foxp3+ T regulatory cell-mediated suppression', *Immunity*, 30: 636-45.

Shibata, K., H. Yamada, T. Sato, T. Dejima, M. Nakamura, T. Ikawa, H. Hara, S. Yamasaki, R. Kageyama, Y. Iwakura, H. Kawamoto, H. Toh, and Y. Yoshikai. 2011. 'Notch-Hes1 pathway is required for the development of IL-17-producing γδ T cells', *Blood*, 118: 586-93.

Shimizu, J., S. Yamazaki, T. Takahashi, Y. Ishida, and S. Sakaguchi. 2002. 'Stimulation of CD25(+)CD4(+) regulatory T cells through GITR breaks immunological self-tolerance', *Nat Immunol*, 3: 135-42.

Shiow, L. R., D. B. Rosen, N. Brdicková, Y. Xu, J. An, L. L. Lanier, J. G. Cyster, and M. Matloubian. 2006. 'CD69 acts downstream of interferon-alpha/beta to inhibit S1P1 and lymphocyte egress from lymphoid organs', *Nature*, 440: 540-4.

Silverstein, A. M. 2003. 'Cellular versus humoral immunology: a century-long dispute', *Nat Immunol*, 4: 425-8.
Simon, T., S. Taleb, N. Danchin, L. Laurans, B. Rousseau, S. Cattan, J. M. Montely, O. Dubourg, A. Tedgui, S. Kotti, and Z. Mallat. 2013. 'Circulating levels of interleukin-17 and cardiovascular outcomes in patients with acute myocardial infarction', *Eur Heart J*, 34: 570-7.
Singh, R. P., S. Hasan, S. Sharma, S. Nagra, D. T. Yamaguchi, D. T. Wong, B. H. Hahn, and A. Hossain. 2014. 'Th17 cells in inflammation and autoimmunity', *Autoimmun Rev*, 13: 1174-81.
Smith, S. B., Z. Xu, T. Novitskaya, B. Zhang, E. Chepurko, X. A. Pu, D. G. Wheeler, M. Ziolo, and R. J. Gumina. 2017. 'Impact of cardiac-specific expression of CD39 on myocardial infarct size in mice', *Life Sci*, 179: 54-59.
Smith, S. C., and P. M. Allen. 1991. 'Myosin-induced acute myocarditis is a T cell-mediated disease', *J Immunol*, 147: 2141-7.
Sonderegger, I., G. Iezzi, R. Maier, N. Schmitz, M. Kurrer, and M. Kopf. 2008. 'GM-CSF mediates autoimmunity by enhancing IL-6-dependent Th17 cell development and survival', *J Exp Med*, 205: 2281-94.
Sonderegger, I., T. A. Röhn, M. O. Kurrer, G. Iezzi, Y. Zou, R. A. Kastelein, M. F. Bachmann, and M. Kopf. 2006. 'Neutralization of IL-17 by active vaccination inhibits IL-23-dependent autoimmune myocarditis', *Eur J Immunol*, 36: 2849-56.
Sontheimer, E. J. 2005. 'Assembly and function of RNA silencing complexes', *Nat Rev Mol Cell Biol*, 6: 127-38.
Spinner, C. A., and V. Lazarevic. 2020. 'Transcriptional regulation of adaptive and innate lymphoid lineage specification', *Immunol Rev*.
Squadrito, M. L., M. Etzrodt, M. De Palma, and M. J. Pittet. 2013. 'MicroRNA-mediated control of macrophages and its implications for cancer', *Trends Immunol*, 34: 350-9.
Sreejit, G., A. Abdel-Latif, B. Athmanathan, R. Annabathula, A. Dhyani, S. K. Noothi, G. A. Quaife-Ryan, A. Al-Sharea, G. Pernes, D. Dragoljevic, H. Lal, K. Schroder, B. Y. Hanaoka, C. Raman, M. B. Grant, J. E. Hudson, S. S. Smyth, E. R. Porrello, A. J. Murphy, and P. R. Nagareddy. 2020. 'Neutrophil-Derived S100A8/A9 Amplify Granulopoiesis After Myocardial Infarction', *Circulation*, 141: 1080-94.
Steppich, B. A., P. Moog, C. Matissek, N. Wisniowski, J. Kühle, N. Joghetaei, F. J. Neumann, A. Schomig, and I. Ott. 2007. 'Cytokine profiles and T cell function in acute coronary syndromes', *Atherosclerosis*, 190: 443-51.
Straus, D. S., and C. K. Glass. 2007. 'Anti-inflammatory actions of PPAR ligands: new insights on cellular and molecular mechanisms', *Trends Immunol*, 28: 551-8.
Strungs, E. G., E. L. Ongstad, M. P. O'Quinn, J. A. Palatinus, L. J. Jourdan, and R. G. Gourdie. 2013. 'Cryoinjury models of the adult and neonatal mouse heart for studies of scarring and regeneration', *Methods Mol Biol*, 1037: 343-53.
Sucato, V., G. Testa, S. Puglisi, S. Evola, A. R. Galassi, and G. Novo. 2021. 'Myocardial infarction with non-obstructive coronary arteries (MINOCA): Intracoronary imaging-based diagnosis and management', *J Cardiol*, 77: 444-51.
Sutton, C., C. Brereton, B. Keogh, K. H. Mills, and E. C. Lavelle. 2006. 'A crucial role for interleukin (IL)-1 in the induction of IL-17-producing T cells that mediate autoimmune encephalomyelitis', *J Exp Med*, 203: 1685-91.
Sutton, C. E., S. J. Lalor, C. M. Sweeney, C. F. Brereton, E. C. Lavelle, and K. H. Mills. 2009. 'Interleukin-1 and IL-23 induce innate IL-17 production from gammadelta T cells, amplifying Th17 responses and autoimmunity', *Immunity*, 31: 331-41.
Swat, W., M. Dessing, H. von Boehmer, and P. Kisielow. 1993. 'CD69 expression during selection and maturation of CD4+8+ thymocytes', *Eur J Immunol*, 23: 739-46.
Swirski, F. K., and M. Nahrendorf. 2013. 'Leukocyte behavior in atherosclerosis, myocardial infarction, and heart failure', *Science*, 339: 161-6.
———. 2018. 'Cardioimmunology: the immune system in cardiac homeostasis and disease', *Nat Rev Immunol*, 18: 733-44.
Swirski, F. K., M. Nahrendorf, M. Etzrodt, M. Wildgruber, V. Cortez-Retamozo, P. Panizzi, J. L. Figueiredo, R. H. Kohler, A. Chudnovskiy, P. Waterman, E. Aikawa, T. R. Mempel, P. Libby,

R. Weissleder, and M. J. Pittet. 2009. 'Identification of splenic reservoir monocytes and their deployment to inflammatory sites', *Science*, 325: 612-6.
Szabo, S. J., S. T. Kim, G. L. Costa, X. Zhang, C. G. Fathman, and L. H. Glimcher. 2000. 'A novel transcription factor, T-bet, directs Th1 lineage commitment', *Cell*, 100: 655-69.
Szatmari, I., D. Töröcsik, M. Agostini, T. Nagy, M. Gurnell, E. Barta, K. Chatterjee, and L. Nagy. 2007. 'PPARgamma regulates the function of human dendritic cells primarily by altering lipid metabolism', *Blood*, 110: 3271-80.
Taams, L. S., J. M. van Amelsfort, M. M. Tiemessen, K. M. Jacobs, E. C. de Jong, A. N. Akbar, J. W. Bijlsma, and F. P. Lafeber. 2005. 'Modulation of monocyte/macrophage function by human CD4+CD25+ regulatory T cells', *Hum Immunol*, 66: 222-30.
Tada, T., T. Takemori, K. Okumura, M. Nonaka, and T. Tokuhisa. 1978. 'Two distinct types of helper T cells involved in the secondary antibody response: independent and synergistic effects of Ia- and Ia+ helper T cells', *J Exp Med*, 147: 446-58.
Tamis-Holland, J. E., H. Jneid, H. R. Reynolds, S. Agewall, E. S. Brilakis, T. M. Brown, A. Lerman, M. Cushman, D. J. Kumbhani, C. Arslanian-Engoren, A. F. Bolger, and J. F. Beltrame. 2019. 'Contemporary Diagnosis and Management of Patients With Myocardial Infarction in the Absence of Obstructive Coronary Artery Disease: A Scientific Statement From the American Heart Association', *Circulation*, 139: e891-e908.
Tarassishin, Leonid, Olivier Loudig, Avital Bauman, Bridget Shafit-Zagardo, Hyeon-Sook Suh, and Sunhee C. Lee. 2011. 'Interferon regulatory factor 3 inhibits astrocyte inflammatory gene expression through suppression of the proinflammatory miR-155 and miR-155*', *Glia*, 59: 1911-22.
Testi, R., D. D'Ambrosio, R. De Maria, and A. Santoni. 1994. 'The CD69 receptor: a multipurpose cell-surface trigger for hematopoietic cells', *Immunol Today*, 15: 479-83.
Teunissen, M. B., C. W. Koomen, R. de Waal Malefyt, E. A. Wierenga, and J. D. Bos. 1998. 'Interleukin-17 and interferon-gamma synergize in the enhancement of proinflammatory cytokine production by human keratinocytes', *J Invest Dermatol*, 111: 645-9.
Thai, T. H., D. P. Calado, S. Casola, K. M. Ansel, C. Xiao, Y. Xue, A. Murphy, D. Frendewey, D. Valenzuela, J. L. Kutok, M. Schmidt-Supprian, N. Rajewsky, G. Yancopoulos, A. Rao, and K. Rajewsky. 2007. 'Regulation of the germinal center response by microRNA-155', *Science*, 316: 604-8.
Thygesen, Kristian, Joseph S. Alpert, Allan S. Jaffe, Bernard R. Chaitman, Jeroen J. Bax, David A. Morrow, and Harvey D. White. 2018. 'Fourth Universal Definition of Myocardial Infarction (2018)', *Circulation*, 138: e618-e51.
Tone, Y., K. Furuuchi, Y. Kojima, M. L. Tykocinski, M. I. Greene, and M. Tone. 2008. 'Smad3 and NFAT cooperate to induce Foxp3 expression through its enhancer', *Nat Immunol*, 9: 194-202.
Tsai, Y. S., L. Xu, O. Smithies, and N. Maeda. 2009. 'Genetic variations in peroxisome proliferator-activated receptor gamma expression affect blood pressure', *Proc Natl Acad Sci U S A*, 106: 19084-9.
Tsilingiri, K., H. de la Fuente, M. Relano, R. Sanchez-Diaz, C. Rodriguez, J. Crespo, F. Sanchez-Cabo, A. Dopazo, J. L. Alonso-Lebrero, A. Vara, J. Vazquez, J. M. Casasnovas, F. Alfonso, B. Ibanez, V. Fuster, J. Martinez-Gonzalez, P. Martin, and F. Sanchez-Madrid. 2019. 'Oxidized Low-Density Lipoprotein Receptor in Lymphocytes Prevents Atherosclerosis and Predicts Subclinical Disease', *Circulation*, 139: 243-55.
Tsujioka, H., T. Imanishi, H. Ikejima, A. Kuroi, S. Takarada, T. Tanimoto, H. Kitabata, K. Okochi, Y. Arita, K. Ishibashi, K. Komukai, H. Kataiwa, N. Nakamura, K. Hirata, A. Tanaka, and T. Akasaka. 2009. 'Impact of heterogeneity of human peripheral blood monocyte subsets on myocardial salvage in patients with primary acute myocardial infarction', *J Am Coll Cardiol*, 54: 130-8.
Unutmaz, D., P. Pileri, and S. Abrignani. 1994. 'Antigen-independent activation of naive and memory resting T cells by a cytokine combination', *J Exp Med*, 180: 1159-64.
Vaca, L. 2014. 'Point-of-care diagnostic tools to detect circulating microRNAS as biomarkers of disease', *Sensors (Basel)*, 14: 9117-31.

Valadi, H., K. Ekström, A. Bossios, M. Sjöstrand, J. J. Lee, and J. O. Lötvall. 2007. 'Exosome-mediated transfer of mRNAs and microRNAs is a novel mechanism of genetic exchange between cells', *Nat Cell Biol*, 9: 654-9.

van der Vleuten, P. A., S. Rasoul, W. Huurnink, I. C. van der Horst, R. H. Slart, S. Reiffers, R. A. Dierckx, R. A. Tio, J. P. Ottervanger, M. J. De Boer, and F. Zijlstra. 2008. 'The importance of left ventricular function for long-term outcome after primary percutaneous coronary intervention', *BMC Cardiovasc Disord*, 8: 4.

Veldhoen, M., and B. Stockinger. 2006. 'TGFbeta1, a "Jack of all trades": the link with pro-inflammatory IL-17-producing T cells', *Trends Immunol*, 27: 358-61.

Villarroya-Beltri, C., C. Gutiérrez-Vázquez, F. Sánchez-Cabo, D. Pérez-Hernández, J. Vázquez, N. Martin-Cofreces, D. J. Martinez-Herrera, A. Pascual-Montano, M. Mittelbrunn, and F. Sánchez-Madrid. 2013. 'Sumoylated hnRNPA2B1 controls the sorting of miRNAs into exosomes through binding to specific motifs', *Nat Commun*, 4: 2980.

Wang, C., C. Zhang, L. Liu, X. A, B. Chen, Y. Li, and J. Du. 2017. 'Macrophage-Derived mir-155-Containing Exosomes Suppress Fibroblast Proliferation and Promote Fibroblast Inflammation during Cardiac Injury', *Mol Ther*, 25: 192-204.

Wang, F., G. Long, C. Zhao, H. Li, S. Chaugai, Y. Wang, C. Chen, and D. W. Wang. 2014. 'Atherosclerosis-related circulating miRNAs as novel and sensitive predictors for acute myocardial infarction', *PLoS One*, 9: e105734.

Wang, Y., K. Dembowsky, E. Chevalier, P. Stuve, M. Korf-Klingebiel, M. Lochner, L. C. Napp, H. Frank, E. Brinkmann, A. Kanwischer, J. Bauersachs, M. Gyongyosi, T. Sparwasser, and K. C. Wollert. 2019. 'C-X-C Motif Chemokine Receptor 4 Blockade Promotes Tissue Repair After Myocardial Infarction by Enhancing Regulatory T Cell Mobilization and Immune-Regulatory Function', *Circulation*, 139: 1798-812.

Wang, Y. M., J. L. McRae, S. C. Robson, P. J. Cowan, G. Y. Zhang, M. Hu, T. Polhill, Y. Wang, G. Zheng, Y. Wang, V. W. Lee, R. J. Unwin, D. C. Harris, K. M. Dwyer, and S. I. Alexander. 2012. 'Regulatory T cells participate in CD39-mediated protection from renal injury', *Eur J Immunol*, 42: 2441-51.

Weirather, J., U. D. Hofmann, N. Beyersdorf, G. C. Ramos, B. Vogel, A. Frey, G. Ertl, T. Kerkau, and S. Frantz. 2014. 'Foxp3+ CD4+ T cells improve healing after myocardial infarction by modulating monocyte/macrophage differentiation', *Circ Res*, 115: 55-67.

Wheeler, D. G., M. E. Joseph, S. D. Mahamud, W. L. Aurand, P. J. Mohler, V. J. Pompili, K. M. Dwyer, M. B. Nottle, S. J. Harrison, A. J. d'Apice, S. C. Robson, P. J. Cowan, and R. J. Gumina. 2012. 'Transgenic swine: expression of human CD39 protects against myocardial injury', *J Mol Cell Cardiol*, 52: 958-61.

Wheeler, G., S. Ntounia-Fousara, B. Granda, T. Rathjen, and T. Dalmay. 2006. 'Identification of new central nervous system specific mouse microRNAs', *FEBS Lett*, 580: 2195-200.

Wightman, B., I. Ha, and G. Ruvkun. 1993. 'Posttranscriptional regulation of the heterochronic gene lin-14 by lin-4 mediates temporal pattern formation in C. elegans', *Cell*, 75: 855-62.

Wilson, N. J., K. Boniface, J. R. Chan, B. S. McKenzie, W. M. Blumenschein, J. D. Mattson, B. Basham, K. Smith, T. Chen, F. Morel, J. C. Lecron, R. A. Kastelein, D. J. Cua, T. K. McClanahan, E. P. Bowman, and R. de Waal Malefyt. 2007. 'Development, cytokine profile and function of human interleukin 17-producing helper T cells', *Nat Immunol*, 8: 950-7.

Wolf, D., and K. Ley. 2019. 'Immunity and Inflammation in Atherosclerosis', *Circ Res*, 124: 315-27.

Wu, L., S. Ong, M. V. Talor, J. G. Barin, G. C. Baldeviano, D. A. Kass, D. Bedja, H. Zhang, A. Sheikh, J. B. Margolick, Y. Iwakura, N. R. Rose, and D. Cihákóvá. 2014. 'Cardiac fibroblasts mediate IL-17A-driven inflammatory dilated cardiomyopathy', *J Exp Med*, 211: 1449-64.

Wu, Lei, Nicola L. Diny, SuFey Ong, Jobert G. Barin, Xuezhou Hou, Noel R. Rose, Monica V. Talor, and Daniela Čihákóvá. 2016. 'Pathogenic IL-23 signaling is required to initiate GM-CSF-driven autoimmune myocarditis in mice', *Eur J Immunol*, 46: 582-92.

Xi, H., R. Schwartz, I. Engel, C. Murre, and G. J. Kersh. 2006. 'Interplay between RORgammat, Egr3, and E proteins controls proliferation in response to pre-TCR signals', *Immunity*, 24: 813-26.

Xia, N., J. Jiao, T. T. Tang, B. J. Lv, Y. Z. Lu, K. J. Wang, Z. F. Zhu, X. B. Mao, S. F. Nie, Q. Wang, X. Tu, H. Xiao, Y. H. Liao, G. P. Shi, and X. Cheng. 2015. 'Activated regulatory T-cells

attenuate myocardial ischaemia/reperfusion injury through a CD39-dependent mechanism', *Clin Sci (Lond)*, 128: 679-93.
Xie, M., and J. A. Steitz. 2014. 'Versatile microRNA biogenesis in animals and their viruses', *RNA Biol*, 11: 673-81.
Yamamura, Y., R. Gupta, Y. Morita, X. He, R. Pai, J. Endres, A. Freiberg, K. Chung, and D. A. Fox. 2001. 'Effector function of resting T cells: activation of synovial fibroblasts', *J Immunol*, 166: 2270-5.
Yan, X., A. Anzai, Y. Katsumata, T. Matsuhashi, K. Ito, J. Endo, T. Yamamoto, A. Takeshima, K. Shinmura, W. Shen, K. Fukuda, and M. Sano. 2013. 'Temporal dynamics of cardiac immune cell accumulation following acute myocardial infarction', *J Mol Cell Cardiol*, 62: 24-35.
Yan, X., T. Shichita, Y. Katsumata, T. Matsuhashi, H. Ito, K. Ito, A. Anzai, J. Endo, Y. Tamura, K. Kimura, J. Fujita, K. Shinmura, W. Shen, A. Yoshimura, K. Fukuda, and M. Sano. 2012. 'Deleterious effect of the IL-23/IL-17A axis and gammadeltaT cells on left ventricular remodeling after myocardial infarction', *J Am Heart Assoc*, 1: e004408.
Yang, J. S., and E. C. Lai. 2011. 'Alternative miRNA biogenesis pathways and the interpretation of core miRNA pathway mutants', *Mol Cell*, 43: 892-903.
Yang, X. O., A. D. Panopoulos, R. Nurieva, S. H. Chang, D. Wang, S. S. Watowich, and C. Dong. 2007. 'STAT3 regulates cytokine-mediated generation of inflammatory helper T cells', *J Biol Chem*, 282: 9358-63.
Yang, X. O., B. P. Pappu, R. Nurieva, A. Akimzhanov, H. S. Kang, Y. Chung, L. Ma, B. Shah, A. D. Panopoulos, K. S. Schluns, S. S. Watowich, Q. Tian, A. M. Jetten, and C. Dong. 2008. 'T helper 17 lineage differentiation is programmed by orphan nuclear receptors ROR alpha and ROR gamma', *Immunity*, 28: 29-39.
Yang, Y., W. Bai, L. Zhang, G. Yin, X. Wang, J. Wang, H. Zhao, Y. Han, and Y. Q. Yao. 2008. 'Determination of microRNAs in mouse preimplantation embryos by microarray', *Dev Dyn*, 237: 2315-27.
Yao, R., Y. Ma, Y. Du, M. Liao, H. Li, W. Liang, J. Yuan, Z. Ma, X. Yu, H. Xiao, and Y. Liao. 2011. 'The altered expression of inflammation-related microRNAs with microRNA-155 expression correlates with Th17 differentiation in patients with acute coronary syndrome', *Cell Mol Immunol*, 8: 486-95.
Yi, R., Y. Qin, I. G. Macara, and B. R. Cullen. 2003. 'Exportin-5 mediates the nuclear export of pre-microRNAs and short hairpin RNAs', *Genes Dev*, 17: 3011-6.
Yuan, J., A. L. Cao, M. Yu, Q. W. Lin, X. Yu, J. H. Zhang, M. Wang, H. P. Guo, and Y. H. Liao. 2010. 'Th17 cells facilitate the humoral immune response in patients with acute viral myocarditis', *J Clin Immunol*, 30: 226-34.
Yuan, Z., Y. Liu, Y. Liu, J. Zhang, C. Kishimoto, Y. Wang, A. Ma, and Z. Liu. 2003. 'Peroxisome proliferation-activated receptor-gamma ligands ameliorate experimental autoimmune myocarditis', *Cardiovasc Res*, 59: 685-94.
Zajac, A. J., J. N. Blattman, K. Murali-Krishna, D. J. Sourdive, M. Suresh, J. D. Altman, and R. Ahmed. 1998. 'Viral immune evasion due to persistence of activated T cells without effector function', *J Exp Med*, 188: 2205-13.
Zeng, X., Y. L. Wei, J. Huang, E. W. Newell, H. Yu, B. A. Kidd, M. S. Kuhns, R. W. Waters, M. M. Davis, C. T. Weaver, and Y. H. Chien. 2012. 'γδ T cells recognize a microbial encoded B cell antigen to initiate a rapid antigen-specific interleukin-17 response', *Immunity*, 37: 524-34.
Zhang, Y., J. Bauersachs, and H. F. Langer. 2017. 'Immune mechanisms in heart failure', *Eur J Heart Fail*, 19: 1379-89.
Zhao, Z., Y. Wu, M. Cheng, Y. Ji, X. Yang, P. Liu, S. Jia, and Z. Yuan. 2011. 'Activation of Th17/Th1 and Th1, but not Th17, is associated with the acute cardiac event in patients with acute coronary syndrome', *Atherosclerosis*, 217: 518-24.
Zheng, S. G., J. H. Wang, W. Stohl, K. S. Kim, J. D. Gray, and D. A. Horwitz. 2006. 'TGF-beta requires CTLA-4 early after T cell activation to induce FoxP3 and generate adaptive CD4+CD25+ regulatory cells', *J Immunol*, 176: 3321-9.
Zheng, W., and R. A. Flavell. 1997. 'The transcription factor GATA-3 is necessary and sufficient for Th2 cytokine gene expression in CD4 T cells', *Cell*, 89: 587-96.

Zheng, Y., D. M. Danilenko, P. Valdez, I. Kasman, J. Eastham-Anderson, J. Wu, and W. Ouyang. 2007. 'Interleukin-22, a T(H)17 cytokine, mediates IL-23-induced dermal inflammation and acanthosis', *Nature*, 445: 648-51.

Zheng, Y. J., T. S. Liang, J. Wang, J. Y. Zhao, S. N. Zhai, D. K. Yang, and L. D. Wang. 2020. 'MicroRNA-155 acts as a diagnostic and prognostic biomarker for oesophageal squamous cell carcinoma', *Artif Cells Nanomed Biotechnol*, 48: 977-82.

Zheng, Y., S. Josefowicz, A. Chaudhry, X. P. Peng, K. Forbush, and A. Y. Rudensky. 2010. 'Role of conserved non-coding DNA elements in the Foxp3 gene in regulatory T-cell fate', *Nature*, 463: 808-12.

Zheng, Ye, Steven Z. Josefowicz, Arnold Kas, Tin-Tin Chu, Marc A. Gavin, and Alexander Y. Rudensky. 2007. 'Genome-wide analysis of Foxp3 target genes in developing and mature regulatory T cells', *Nature*, 445: 936-40.

Zhou, Haibo, Xinfang Huang, Huijuan Cui, Xiaobing Luo, Yuanjia Tang, Shunle Chen, Li Wu, and Nan Shen. 2010. 'miR-155 and its star-form partner miR-155* cooperatively regulate type I interferon production by human plasmacytoid dendritic cells', *Blood*, 116: 5885-94.

Zhou, L., Ivanov, II, R. Spolski, R. Min, K. Shenderov, T. Egawa, D. E. Levy, W. J. Leonard, and D. R. Littman. 2007. 'IL-6 programs T(H)-17 cell differentiation by promoting sequential engagement of the IL-21 and IL-23 pathways', *Nat Immunol*, 8: 967-74.

Zhu, G. F., L. X. Yang, R. W. Guo, H. Liu, Y. K. Shi, J. S. Ye, and Z. H. Yang. 2014. 'microRNA-155 is inversely associated with severity of coronary stenotic lesions calculated by the Gensini score', *Coron Artery Dis*, 25: 304-10.

Ziegler, M., J. D. Hohmann, A. K. Searle, M. K. Abraham, H. H. Nandurkar, X. Wang, and K. Peter. 2018. 'A single-chain antibody-CD39 fusion protein targeting activated platelets protects from cardiac ischaemia/reperfusion injury', *Eur Heart J*, 39: 111-16.

Ziegler, S. F., S. D. Levin, L. Johnson, N. G. Copeland, D. J. Gilbert, N. A. Jenkins, E. Baker, G. R. Sutherland, A. L. Feldhaus, and F. Ramsdell. 1994. 'The mouse CD69 gene. Structure, expression, and mapping to the NK gene complex', *J Immunol*, 152: 1228-36.

ANNEXES

ANNEXES

1. Relevant analyses of miRNA microarrays performed in this study

   a. Table A.1. List of miRNAs differentially expressed by sorted or cultured antigen-specific Th17 cells (Th17ag-sp) *versus* activated $CD4^+$ T cells and polyclonal Th17 cells (Th17poly) after differentiation in culture.

   b. Table A.2. List of miRNAs differentially expressed by sorted antigen-specific Th17 cells (Th17ag-sp) from *Cd69*$^{-/-}$ mice *versus* sorted Th17ag-sp cells from wild type (WT) mice.

   c. Table A.3. List of miRNAs differentially expressed by sorted $CD4^+$ T cells from mice with autoimmune myocarditis and myocardial infarction.

   d. Table A.4. Receiver operating characteristic curves of plasma miRNAs and blood T cells.

2. List of publications in which the PhD candidate has contributed during the research period (only attached those already peer-reviewed and accepted for publication)

   a. Sánchez-Díaz R, **Blanco-Dominguez R**, Lasarte S, Tsilingiri K, Martín-Gayo E, Linillos-Pradillo B, de la Fuente H, Sánchez-Madrid F, Nakagawa R, Toribio ML, Martín P. Thymus-derived Treg cell development is regulated by C-type-lectin–mediated BIC/miRNA155 expression. *Molecular and Cellular Biology* 2017 Apr 14;37(9):e00341-16. doi: 10.1128/MCB.00341-16.

   b. Martin P, **Blanco-Dominguez R**, Sanchez-Diaz R. Novel human immunomodulatory T cell receptors and their double-edged potential in autoimmunity, cardiovascular disease, and cancer. *Cellular & Molecular Immunology*, 2021 Apr;18(4):919-935. doi: 10.1038/s41423-020-00586-4.

   c. **Blanco-Dominguez R**, Sánchez-Díaz R, de la Fuente H, Jiménez-Borreguero LJ, Matesanz-Marín A, Relaño M, Jiménez-Alejandre R, Linillos-Pradillo B, Tsilingiri K, Martín-Mariscal ML, Alonso-Herranz L, Moreno G, Martín-Asenjo R, García-Guimaraes MM, Bruno KA, Dauden E, González-Álvaro I, Villar Guimerans LM, Martínez-León A, Salvador-Garicano AM, Michelhaugh SA, Ibrahim NE, Januzzi JL, Kottwitz J, Iliceto S, Plebani M, Basso C, Baritussio A, Seguso M, Marcolongo R, Ricote M, Fairweather D, Bueno H, Fernández-Friera L, Alfonso F, Caforio ALP, Pascual-Figal DA, Heidecker B, Lüscher TF, Das S, Fuster V, Ibáñez B, Sánchez-Madrid F, Martín P. A novel circulating microRNA for the detection of acute myocarditis. *The New England Journal of Medicine***.** 2021 May 27;384(21):2014-2027. doi: 10.1056/NEJMoa2003608.

   d. Vallejo J, Saigusa R, Gulati R, Ghosheh Y, Durant CP, Roy P, Ehinger E, Suryawanshi V, Pattarabanjird T, Pafgett LE, Olingy CE, Hanna DB, Landay AL, Tracy RP, Lazar JM, Mack WJ, Weber KM, Adimora AA, Hodis HN, Tien PC, Ofotokun I, Heath SL, **Blanco-Dominguez R**, Dinh HQ, Shemesh A, McNamara CA, Lanier LL, Hedrick CC, Kaplan RC, Ley K. Combined protein and transcript single cell

RNA sequencing in human peripheral blood mononuclear cells. *Preprint* doi: https://doi.org/10.1101/2020.09.10.292086.

e. **Blanco-Domínguez R,** De la Fuente H, Rodríguez C, Rodríguez-Arabaolaza I, Sánchez-Díaz R, Jiménez-Alexandre R, Martín-Aguado L, García-Guimaraes MM, Vera A, Rivero F, Cuesta J, Jiménez-Borreguero LJ, Cecconi A, Duran A, Taurón M, Alonso J, Alfonso F, Sánchez-Madrid F, Martínez-González and Martín P. CD69 expression on regulatory T cells protects from immune damage after Myocardial Infarction. *Manuscript submitted*

f. Cecconi A, Navarrete G, García-Guimaraes M, Vera A, **Blanco-Dominguez R**, Sanz-García A, Lozano-Prieto M, Martín P, Sánchez-Madrid F, De la Fuente H, Jiménez-Borreguero LJ, Alfonso F. Influence of Air Pollutants on Circulating Inflammatory Cells and microRNA Expression in Acute Myocardial Infarction. *Manuscript submitted*.

g. **Blanco-Domínguez R,** Martín-Aguado L, Cases I, Nuñez V, De la Fuente H, Romero-Carramiñana I, Alonso-Herranz L, Alfonso F, Sánchez-Madrid F, Rojas AM, Martín P, Ricote M. Changes in circulating macrophage-derived microRNAs after myocardial infarction. *Manuscript in preparation*.

Table A.1. List of miRNAs differentially expressed by sorted or cultured antigen-specific Th17 cells (Th17ag-sp) *versus* activated CD4$^+$ T cells and polyclonal Th17 cells (Th17poly) after differentiation in culture. Mouse microRNA microarray (Agilent mouse miRNA array, 8x15K) was performed to analyze expression of miRNAs. Sorted-Th17ag-sp n=4; cultured Th17ag-sp n=1; Th17poly n=1 and CD4$^+$ T cells n=1. The 27 microRNAs detected in both cultured Th17ag-sp and sorted Th17ag-sp samples are highlighted in bold.

	Th17ag-sp *vs* CD4	Th17ag-sp *vs* Th17poly
miRNA name	**Log Fold Change**	**Log Fold Change**
mmu-miR-19a	6.955512	1.711149
mmu-miR-301a	5.833094	0.306646
mmu-miR-210	**5.422674**	**5.422674**
mmu-miR-181b	4.816477	-1.79107
mmu-miR-223	**4.329713**	**4.329713**
mmu-miR-206	4.208049	4.208049
mmu-miR-212	4.162022	-0.65632
mmu-miR-16*	3.983226	3.983226
mmu-let-7e	3.961208	3.961208
mmu-miR-181a	3.941559	-2.4166
mmu-miR-350	**3.844374**	**3.844374**
mmu-miR-15a*	3.789114	3.789114
mmu-miR-128	**3.729743**	**3.729743**
mmu-miR-96	3.690472	3.690472
mmu-miR-670	3.503866	3.503866
mmu-miR-721	**3.501172**	**3.501172**
mmu-miR-181d	3.4864	-0.83425
mmu-miR-331-3p	**3.482866**	**3.482866**
mmu-miR-214*	3.474831	3.474831
mmu-miR-18a	3.455006	1.646696
mmu-miR-483-5p	**3.404238**	**3.404238**
mmu-miR-539	**3.375458**	**3.375458**
mmu-miR-181c	3.263462	3.263462
mmu-miR-28	**3.223385**	**3.223385**
mmu-miR-106a	**3.194242**	**3.194242**
mmu-miR-466a-5p	3.12738	3.12738
mmu-miR-324-5p	3.104556	3.104556
mmu-miR-17	**2.995375**	**2.995375**
mmu-miR-466b-5p	2.934609	2.934609
mmu-miR-363	**2.920245**	**2.920245**
mmu-miR-877*	**2.903015**	**2.903015**
mmu-miR-185	2.794519	2.794519
mmu-miR-183	2.580362	2.580362
mmu-miR-705	**2.538815**	**2.538815**
mmu-miR-322	2.513221	2.513221
mmu-miR-338-5p	2.496938	2.496938
mmu-miR-483*	**2.489482**	**2.489482**
mmu-miR-342-5p	**2.473516**	**2.473516**
mmu-miR-467e	**2.424829**	**2.424829**
mmu-miR-671-5p	**2.423298**	**2.423298**
mmu-miR-101b	2.391533	2.391533
mmu-miR-702	**2.381283**	**2.381283**
mmu-miR-449a	2.323647	2.323647
mmu-miR-149	**2.323199**	**2.323199**
mmu-miR-680	2.316846	-2.46102

mmu-miR-151-5p	**2.310454**	**2.310454**
mmu-miR-219	2.204745	2.204745
mmu-miR-148a	2.193035	2.193035
mmu-miR-18b	2.175362	2.175362
mmu-let-7b*	**2.160693**	**2.160693**
mmu-miR-106b	2.144256	1.287673
mmu-miR-125a-5p	2.11614	2.11614
mmu-miR-362-3p	2.111872	2.111872
mmu-miR-207	2.073385	2.073385
mmu-miR-382	2.04969	2.04969
mmu-miR-125a-3p	1.991296	-2.42808
mmu-miR-30e	1.960979	1.197295
mmu-miR-191*	**1.951643**	**1.951643**
mmu-miR-532-5p	1.912263	1.912263
mmu-miR-712	1.826083	1.826083
mmu-miR-24-1*	1.821628	1.821628
mmu-miR-465b-5p	1.768309	1.768309
mmu-miR-301b	1.745878	1.745878
mmu-miR-27a	1.736565	0.860198
mmu-miR-19b	1.716949	1.20001
mmu-miR-696	1.689179	1.689179
mmu-miR-374	1.686894	1.686894
mmu-miR-182	1.644674	1.644674
mmu-miR-30a	1.622375	1.622375
mmu-miR-20a	1.611714	0.864535
mmu-miR-30b*	1.572994	1.572994
mmu-miR-574-5p	1.548114	2.969683
mmu-miR-148b	1.520209	1.520209
mmu-miR-700	1.464536	1.464536
mmu-miR-33	1.427502	1.427502
mmu-miR-188-5p	1.41284	-0.43185
mmu-miR-324-3p	1.406973	1.406973
mmu-let-7f*	**1.401869**	**1.401869**
mmu-miR-21*	1.39425	1.39425
mmu-miR-290-3p	**1.380107**	**1.380107**
mmu-miR-30e*	1.372421	1.372421
mmu-miR-484	1.362419	1.362419
mmu-miR-99b*	1.316186	1.316186
mmu-miR-192	1.290998	1.290998
mmu-miR-872	1.257301	1.257301
mmu-miR-18a*	**1.252466**	**1.252466**
mmu-miR-29b	1.238676	1.748291
mmu-miR-298	**1.238358**	**1.238358**
mmu-miR-674*	1.21804	1.21804
mmu-miR-328	1.087073	1.087073
mmu-miR-21	1.043861	1.444974
mmu-miR-140	0.948637	1.072688
mmu-miR-29a	0.899576	1.039132
mmu-miR-669n	0.85258	3.640549
mmu-miR-34a	0.82432	0.321198
mmu-miR-93	0.803905	-0.8705
mmu-let-7i	0.801364	0.545795
mmu-miR-466c-5p	0.743993	8.301777
mmu-miR-672	0.687503	6.940064
mmu-miR-689	0.604063	-0.79165
mmu-miR-17*	0.540405	-0.85359
mmu-miR-468	0.474999	7.95964
mmu-miR-296-5p	0.455498	4.073336

mmu-miR-466f-5p	0.334993	4.025996
mmu-miR-466h	0.321187	6.400558
mmu-miR-669b	0.214234	7.294101
mmu-miR-132	0.209548	-1.05013
mmu-miR-27b	0.165781	-0.70159
mmu-miR-669a	0.091264	2.860682
mmu-miR-1224	-0.00795	-0.60129
mghv-miR-M1-6	-0.07284	4.621456
mmu-miR-467c	-0.10437	5.139989
mmu-miR-361	-0.26453	-0.71582
mmu-miR-297c	-0.44586	4.33201
mmu-miR-140*	-0.48335	-1.22355
mmu-miR-16	-0.56397	-1.33836
mmu-miR-30b	-0.58494	-0.63867
mmu-miR-345-5p	-0.69433	-1.80101
mmu-miR-23a	-0.76298	-1.46141
mmu-miR-423-5p	-0.76689	-1.58363
mghv-miR-M1-2	-0.76962	-1.59821
mmu-miR-720	-0.8621	-0.8621
mmu-miR-378	-0.86915	3.451508
mmu-miR-294	-0.88453	4.212159
mmu-miR-23b	-1.02052	-1.26499
mmu-miR-652	-1.1929	-0.74743
mmu-miR-801_v10.1	-1.19418	-2.29453
mmu-miR-26a	-1.23808	-0.72114
mmu-miR-500	-1.32335	5.671071
mmu-miR-709	-1.56003	-3.20714
mmu-miR-690	-1.58232	-3.36911
mmu-miR-202-3p	-1.68889	-2.87193
mmu-miR-29b*	-1.89906	2.327672
mmu-miR-467b	-2.08672	2.332656
mmu-miR-494	-2.18369	-1.84832
mmu-miR-146a	-2.22218	-1.52898
mmu-miR-7a	-2.80574	-0.64554
mmu-miR-150	-2.88063	-2.36179
mmu-miR-714	-3.00526	-2.21798
mmu-miR-685	-3.48811	-2.43369
mmu-miR-139-5p	-3.76633	2.716089

Table A.2. List of miRNAs differentially expressed by sorted antigen-specific Th17 cells (Th17ag-sp) from *Cd69*$^{-/-}$ mice *versus* sorted Th17ag-sp cells from wild type (WT) mice. Mouse microRNA microarray (Agilent mouse miRNA array, 8x15K) was performed to analyze expression of miRNAs. N=1 for both CD69KO and WT. The 4 microRNAs specific for antigen-specific Th17 cells (table A1) are highlighted in bold.

	Th17ag-sp-*Cd69*$^{-/-}$ *vs* Th17ag-sp-WT
miRNA name	**Log2 Fold Change**
mmu-miR-721	**7.567371352**
mmu-miR-483-5p	**7.027359548**
mmu-miR-466c-5p	5.912043585
mmu-miR-468	5.83899353
mmu-miR-500	5.613617399
mmu-miR-669b	5.322333796
mmu-miR-296-5p	5.052658598
mmu-miR-672	4.729078283
mmu-miR-134	4.598318572
mmu-miR-466h	4.519452583
mmu-miR-671-5p	**4.238984529**
mmu-miR-706	3.916053997
mmu-miR-705	**3.177433252**
mmu-miR-467c	2.676399506
mmu-miR-301a	2.495856485
mmu-miR-715	2.066501183
mmu-miR-714	2.026329576
mmu-miR-34a	2.00790293
mmu-miR-689	2.003679334
mmu-miR-669c	1.829499293
mmu-miR-680	1.798895556
mmu-miR-669a	1.730754845
mmu-miR-17*	1.482301194
mmu-miR-574-5p	1.472600479
mmu-miR-345-5p	1.319989716
mmu-miR-423-5p	1.303836322
mmu-miR-188-5p	1.246854782
mmu-miR-720	1.197282913
mmu-miR-202-3p	1.069019767
mmu-miR-146a	1.037978717
mmu-miR-1224	1.005818327
mmu-miR-709	0.991997652
mmu-miR-18a	0.969662645
mmu-miR-30e	0.952162819
mmu-miR-15a	0.925698775
mmu-miR-155	0.860405868
mmu-miR-26b	0.852272484
mmu-miR-125a-3p	0.84959725
mmu-miR-181a	0.832513346
mmu-miR-150	0.758791896
mmu-miR-425	0.756246116
mmu-miR-181b	0.74850271
mmu-miR-685	0.718522081
mmu-miR-93	0.674017832
mmu-miR-20a	0.673038498
mmu-let-7c	0.661908087

mmu-let-7b	0.661152883
mmu-miR-142-5p	0.64600658
mmu-miR-20b	0.640338376
mmu-let-7a	0.601025543
mmu-miR-23b	0.598586071
mmu-miR-142-3p	0.594537753
mmu-miR-21	0.58191009
mmu-let-7f	0.56854535
mmu-miR-19a	0.554045854
mmu-miR-29a	0.457515812
mmu-miR-29c	0.448521784
mmu-miR-103	0.427951842
mmu-miR-132	0.41916563
mmu-miR-15b	0.418740253
mmu-miR-107	0.414192157
mmu-miR-140*	0.409203543
mmu-miR-130b	0.355623332
mmu-miR-26a	0.353528134
mmu-miR-27b	0.336568813
mmu-let-7i	0.327925648
mmu-miR-494	0.300413113
mmu-let-7g	0.254759708
mmu-miR-361	0.248227563
mmu-miR-29b	0.246320763
mmu-miR-24	0.236756244
mmu-miR-22	0.20908636
mmu-miR-30d	0.201643395
mmu-miR-16	0.190650888
mmu-miR-690	0.184398245
mmu-miR-92a	0.182811649
mmu-miR-106b	0.179649772
mmu-miR-30c	0.162502285
mmu-miR-19b	0.128051304
mmu-miR-25	0.111909753
mmu-miR-652	0.104285259
mmu-miR-711	0.092974867
mmu-miR-466f-5p	0.092974867
mmu-let-7d	0.080634062
mmu-miR-23a	0.078772539
mmu-miR-27a	0.070750643
mmu-miR-342-3p	0.067336105
mmu-miR-30b	0.053777812
mmu-miR-801_v10.1	0

Table A.3. List of miRNAs differentially expressed by sorted CD4$^+$ T cells from mice with autoimmune myocarditis and myocardial infarction. CD4$^+$ T cells isolated from axillary or inguinal lymph nodes 6 days after the induction of experimental autoimmune myocarditis (CD4^{EAM}), or from mediastinal lymph nodes 3 days after induction of myocardial infarction by ligation of the left anterior descending coronary artery (CD4^{MI}). Mouse microRNA microarray (Agilent mouse miRNA array, 8x15K) was performed to analyze expression of miRNAs. Sorted CD4^{EAM} n=4; sorted CD4^{MI} n=3. In bold, 4 miRNAs specific for antigen-specific Th17 cells (table A1) and also upregulated in *Cd69*$^{-/-}$ Th17 cells (table A2) are upregulated in CD4^{EAM} compared with CD4^{MI}. M: log2 of the mean difference, A: normalized average expression, t: test statistic (= log2 mean difference / standard error). Benjamini-Hochberg adjusted p-value.

	CD4^{EAM} vs CD4^{MI}				
miRNA name	M	A	t	P-value	Adjusted p-value
mmu-miR-681	0.196	5.708	15.265	0	0.00526
mmu-miR-3075-5p	0.192	5.659	13.021	0.00001	0.00526
mmu-miR-149-5p	-0.675	6.409	-12.941	0.00001	0.00526
mmu-miR-6394	0.162	5.604	12.744	0.00001	0.00526
mmu-miR-7014-5p	0.2	5.632	12.28	0.00001	0.00526
mmu-let-7g-5p	0.811	12.681	11.341	0.00002	0.00664
mmu-miR-200a-3p	0.441	6.041	11.162	0.00002	0.00664
mmu-miR-3473b	2.108	10.191	10.5	0.00004	0.0083
mmu-miR-7216-5p	0.379	5.881	10.225	0.00004	0.0083
mmu-miR-342-5p	0.386	5.879	9.614	0.00006	0.0083
mmu-miR-18b-3p	-0.265	5.943	-9.553	0.00006	0.0083
mmu-miR-142a-3p	1.288	14.819	9.534	0.00006	0.0083
mmu-miR-7009-5p	0.149	5.643	9.51	0.00006	0.0083
mmu-miR-7222-3p	0.296	5.793	9.477	0.00006	0.0083
mmu-miR-8100	0.184	5.604	9.445	0.00007	0.0083
mmu-miR-6516-5p	0.758	6.335	9.316	0.00007	0.00843
mmu-miR-3552	-0.165	5.791	-8.968	0.00009	0.00903
mmu-miR-7031-5p	0.139	5.589	8.905	0.00009	0.00903
mmu-miR-7048-5p	0.31	5.798	8.859	0.0001	0.00903
mmu-miR-6998-5p	0.091	5.524	8.792	0.0001	0.00903
mmu-miR-6981-5p	0.251	5.655	8.786	0.0001	0.00903
mmu-miR-3473a	1.295	7.037	8.493	0.00012	0.01012
mmu-miR-3473e	0.418	5.836	8.47	0.00012	0.01012
mmu-miR-203-3p	0.584	5.978	8.416	0.00013	0.01012
mmu-miR-7008-5p	0.161	5.639	8.205	0.00015	0.01125
mmu-miR-7665-5p	0.121	5.552	8.102	0.00016	0.01162
mmu-miR-326-3p	0.171	5.704	7.996	0.00017	0.0117
mmu-miR-151-5p	1.036	6.818	7.988	0.00017	0.0117
mmu-miR-7050-3p	-0.142	5.788	-7.92	0.00018	0.01187
mmu-miR-3962	0.575	6.053	7.872	0.00019	0.01187
mmu-miR-345-5p	-0.42	7.009	-7.777	0.0002	0.01205
mmu-miR-6934-5p	0.133	5.548	7.763	0.00021	0.01205
mmu-miR-29c-3p	2.228	9.706	7.623	0.00023	0.01296
mmu-miR-690	2.034	9.073	7.529	0.00024	0.01346
mmu-miR-378d	1.228	8.386	7.439	0.00026	0.01346

mmu-miR-7057-3p	-0.262	5.909	-7.409	0.00027	0.01346
mmu-let-7f-5p	0.616	12.647	7.397	0.00027	0.01346
mmu-miR-547-5p	-0.234	5.837	-7.351	0.00028	0.01346
mmu-miR-155-5p	1.382	9.135	7.331	0.00028	0.01346
mmu-miR-1966-5p	0.125	5.57	7.307	0.00029	0.01346
mmu-miR-6970-5p	0.294	5.773	7.287	0.00029	0.01346
mmu-miR-378a-5p	0.707	6.387	7.145	0.00033	0.01467
mmu-miR-98-3p	-0.072	5.645	-7.083	0.00034	0.01485
mmu-miR-330-3p	0.108	5.533	7.071	0.00035	0.01485
mmu-miR-7674-5p	0.113	5.551	7.023	0.00036	0.01486
mmu-miR-383-5p	0.186	5.644	7.014	0.00036	0.01486
mmu-miR-292b-3p	-0.256	5.961	-6.921	0.00039	0.01567
mmu-miR-7046-5p	0.078	5.521	6.821	0.00042	0.01635
mmu-miR-592-5p	0.343	5.79	6.817	0.00043	0.01635
mmu-miR-874-3p	0.289	5.724	6.715	0.00046	0.01733
mmu-miR-3572-5p	0.144	5.546	6.677	0.00048	0.01733
mmu-miR-6973a-5p	0.084	5.499	6.674	0.00048	0.01733
mmu-miR-1839-5p	0.65	6.106	6.592	0.00051	0.0182
mmu-miR-1907	0.095	5.56	6.521	0.00054	0.01863
mmu-miR-7063-5p	0.106	5.588	6.503	0.00055	0.01863
mmu-miR-290b-3p	-0.25	5.95	-6.499	0.00055	0.01863
mmu-miR-3100-3p	-0.404	6.133	-6.405	0.0006	0.01888
mmu-miR-101b-3p	0.346	5.822	6.385	0.00061	0.01888
mmu-miR-700-3p	-0.329	6.077	-6.361	0.00062	0.01888
mmu-miR-375-5p	-0.122	5.713	-6.35	0.00063	0.01888
mmu-miR-7034-5p	0.23	5.708	6.346	0.00063	0.01888
mmu-miR-5046	-0.151	5.834	-6.33	0.00064	0.01888
mmu-miR-3535	0.717	6.169	6.326	0.00064	0.01888
mmu-miR-7b-5p	0.278	5.832	6.31	0.00065	0.01888
mmu-miR-7005-3p	-0.158	5.861	-6.267	0.00068	0.01888
mmu-miR-6973b-5p	0.529	6.961	6.257	0.00068	0.01888
mmu-miR-7083-3p	-0.14	5.789	-6.235	0.0007	0.01888
mmu-miR-6385	0.297	5.863	6.21	0.00071	0.01888
mmu-miR-6922-3p	-0.086	5.597	-6.181	0.00073	0.01888
mmu-miR-8112	-0.172	5.79	-6.178	0.00073	0.01888
mmu-miR-3544-3p	-0.515	6.237	-6.17	0.00074	0.01888
mmu-miR-129-1-3p	-0.225	5.899	-6.143	0.00075	0.01888
mmu-miR-378c	0.518	6.003	6.139	0.00076	0.01888
mmu-miR-698-5p	0.101	5.518	6.117	0.00077	0.01888
mmu-miR-6968-3p	-0.391	6.137	-6.115	0.00077	0.01888
mmu-miR-713	-0.089	5.484	-6.112	0.00078	0.01888
mmu-miR-338-3p	-0.126	5.657	-6.109	0.00078	0.01888
mmu-miR-6388	0.07	5.554	6.09	0.00079	0.01888
mmu-miR-7221-3p	0.184	5.642	6.087	0.00079	0.01888
mmu-miR-6953-3p	-0.165	5.827	-6.068	0.00081	0.01895
mmu-miR-497a-5p	0.155	5.686	6.005	0.00085	0.01905
mmu-miR-7006-3p	-0.266	5.86	-6.002	0.00086	0.01905
mmu-miR-6516-3p	1.069	6.847	5.986	0.00087	0.01905
mmu-miR-7023-3p	-0.109	5.713	-5.958	0.00089	0.01905
mmu-miR-7224-5p	-0.06	5.688	-5.948	0.0009	0.01905
mmu-miR-7658-3p	-0.228	5.811	-5.937	0.00091	0.01905
mmu-miR-6415	0.521	5.996	5.933	0.00091	0.01905

mmu-miR-7056-5p	0.327	5.817	5.915	0.00093	0.01905
mmu-miR-6962-3p	-0.13	5.65	-5.91	0.00093	0.01905
mmu-miR-652-3p	0.633	8.103	5.909	0.00093	0.01905
mmu-miR-3085-3p	-0.625	6.465	-5.889	0.00095	0.01905
mmu-miR-7666-5p	-0.566	6.403	-5.88	0.00096	0.01905
mmu-miR-28a-3p	0.14	5.548	5.872	0.00096	0.01905
mmu-miR-29b-3p	1.701	11.051	5.869	0.00097	0.01905
mmu-miR-191-3p	-0.256	6.068	-5.862	0.00097	0.01905
mmu-miR-92b-3p	-0.476	6.126	-5.86	0.00097	0.01905
mmu-miR-7007-5p	0.285	5.723	5.842	0.00099	0.01918
mmu-miR-3102-5p.2-5p	0.264	5.843	5.83	0.001	0.0192
mmu-miR-3470a	0.776	6.938	5.787	0.00104	0.01939
mmu-miR-7646-3p	-0.058	5.496	-5.773	0.00105	0.01939
mmu-miR-1843a-5p	0.239	5.858	5.755	0.00107	0.01939
mmu-miR-6938-5p	0.16	5.668	5.748	0.00108	0.01939
mmu-miR-18a-3p	-0.173	5.724	-5.723	0.0011	0.01939
mmu-miR-6402	-0.341	6.382	-5.723	0.0011	0.01939
mmu-miR-378b	0.981	7.695	5.721	0.00111	0.01939
mmu-miR-668-3p	-0.411	6.086	-5.69	0.00114	0.01939
mmu-miR-6904-3p	-0.237	5.889	-5.69	0.00114	0.01939
mmu-miR-3473c	-0.258	5.985	-5.689	0.00114	0.01939
mmu-miR-1930-3p	0.117	5.614	5.684	0.00115	0.01939
mmu-miR-3475-5p	-0.517	6.289	-5.682	0.00115	0.01939
mmu-miR-1952	-0.123	5.724	-5.654	0.00118	0.01939
mmu-miR-6967-3p	-0.223	5.82	-5.65	0.00118	0.01939
mmu-miR-5107-5p	0.576	6.523	5.647	0.00119	0.01939
mmu-let-7f-1-3p	-0.541	6.227	-5.644	0.00119	0.01939
mmu-miR-702-3p	-0.761	6.579	-5.635	0.0012	0.01939
mmu-miR-129-2-3p	-0.162	5.783	-5.634	0.0012	0.01939
mmu-miR-7002-3p	-0.067	5.613	-5.628	0.00121	0.01939
mmu-miR-101c	1.702	7.384	5.62	0.00122	0.01939
mmu-miR-3110-3p	0.195	5.733	5.591	0.00125	0.01951
mmu-miR-6982-3p	-0.221	5.879	-5.587	0.00125	0.01951
mmu-miR-7242-5p	0.132	5.561	5.583	0.00126	0.01951
mmu-miR-7070-5p	0.485	6.097	5.577	0.00127	0.01951
mmu-miR-3971	0.373	5.9	5.543	0.00131	0.02000
mmu-miR-5128	0.44	6.483	5.532	0.00132	0.02006
mmu-miR-7057-5p	0.098	5.552	5.52	0.00134	0.02012
mmu-miR-7062-3p	-0.232	5.924	-5.486	0.00138	0.02055
mmu-miR-3620-3p	-0.848	6.72	-5.481	0.00139	0.02055
mmu-miR-29a-5p	0.114	5.654	5.457	0.00142	0.02087
mmu-miR-3092-3p	-0.695	6.468	-5.426	0.00146	0.02118
mmu-miR-223-3p	-1.136	7.453	-5.426	0.00146	0.02118
mmu-miR-344g-3p	0.065	5.487	5.38	0.00153	0.02118
mmu-miR-7668-3p	0.08	5.534	5.371	0.00154	0.02118
mmu-miR-6909-3p	-0.068	5.637	-5.37	0.00155	0.02118
mmu-miR-29b-1-5p	0.201	5.676	5.359	0.00156	0.02118
mmu-miR-3067-3p	0.124	5.649	5.359	0.00156	0.02118
mmu-miR-7115-3p	-0.427	6.176	-5.352	0.00157	0.02118
mmu-miR-5113	0.482	6.057	5.344	0.00158	0.02118
mmu-miR-6906-5p	0.296	5.881	5.337	0.0016	0.02118
mmu-miR-1843a-3p	0.176	5.754	5.335	0.0016	0.02118

mmu-miR-7036a-3p	-0.255	5.833	-5.32	0.00162	0.02118
mmu-miR-140-3p	1.063	8.58	5.315	0.00163	0.02118
mmu-miR-7239-3p	0.127	5.6	5.312	0.00164	0.02118
mmu-miR-6384	-0.095	5.586	-5.308	0.00164	0.02118
mmu-miR-146a-5p	1.856	8.503	5.304	0.00165	0.02118
mmu-miR-466n-3p	0.351	5.841	5.302	0.00165	0.02118
mmu-miR-5620-3p	-0.519	6.213	-5.296	0.00166	0.02118
mmu-miR-3068-3p	0.647	6.174	5.272	0.0017	0.02118
mmu-miR-6354	0.068	5.552	5.267	0.00171	0.02118
mmu-miR-8103	-0.429	6.125	-5.258	0.00172	0.02118
mmu-miR-7076-3p	-0.22	5.855	-5.255	0.00173	0.02118
mmu-miR-6934-3p	-0.45	6.237	-5.253	0.00173	0.02118
mmu-miR-6972-5p	0.068	5.595	5.25	0.00174	0.02118
mmu-miR-6931-3p	-0.286	5.964	-5.247	0.00174	0.02118
mmu-miR-5127	-0.241	5.807	-5.246	0.00174	0.02118
mmu-miR-200b-3p	0.253	5.91	5.239	0.00176	0.02118
mmu-miR-710	0.191	5.575	5.236	0.00176	0.02118
mmu-miR-6978-5p	0.395	5.844	5.232	0.00177	0.02118
mmu-miR-7088-5p	0.301	5.828	5.225	0.00178	0.02118
mmu-miR-7020-5p	0.152	5.743	5.215	0.0018	0.02118
mmu-miR-6977-3p	-0.158	5.78	-5.214	0.0018	0.02118
mmu-miR-6924-3p	-0.187	5.888	-5.2	0.00183	0.02133
mmu-miR-5118	0.112	5.596	5.173	0.00188	0.02158
mmu-miR-142a-5p	0.624	12.893	5.171	0.00188	0.02158
mmu-miR-1967	0.157	5.601	5.163	0.00189	0.02158
mmu-miR-6370	0.135	5.645	5.158	0.0019	0.02158
mmu-miR-1291	0.195	5.653	5.156	0.00191	0.02158
mmu-miR-7069-3p	-0.229	5.998	-5.152	0.00192	0.02158
mmu-miR-7665-3p	-0.171	5.837	-5.135	0.00195	0.02176
mmu-miR-214-3p	0.108	5.626	5.13	0.00196	0.02176
mmu-miR-7022-3p	-0.814	6.662	-5.122	0.00197	0.02176
mmu-miR-7025-5p	-0.287	5.958	-5.115	0.00199	0.02176
mmu-miR-6418-5p	0.316	5.786	5.101	0.00202	0.02176
mmu-miR-3084-5p	0.08	5.551	5.098	0.00202	0.02176
mmu-miR-101a-3p	1.694	7.95	5.088	0.00204	0.02176
mmu-miR-7224-3p	-0.7	6.463	-5.083	0.00205	0.02176
mmu-miR-99a-5p	0.223	5.692	5.081	0.00206	0.02176
mmu-miR-3970	0.128	5.661	5.078	0.00206	0.02176
mmu-miR-133a-3p	-0.097	5.714	-5.07	0.00208	0.02176
mmu-miR-6912-5p	0.155	5.63	5.07	0.00208	0.02176
mmu-miR-3059-3p	0.138	5.586	5.055	0.00211	0.02176
mmu-miR-3547-3p	-0.225	5.913	-5.055	0.00211	0.02176
mmu-miR-7024-3p	-0.141	5.741	-5.053	0.00212	0.02176
mmu-miR-7241-5p	-0.677	6.471	-5.049	0.00213	0.02176
mmu-miR-7687-3p	-0.403	6.129	-5.048	0.00213	0.02176
mmu-miR-3473d	-0.115	5.602	-5.039	0.00215	0.02183
mmu-miR-6921-5p	0.121	5.541	5.022	0.00218	0.0221
mmu-miR-671-3p	-0.193	5.816	-5.01	0.00221	0.02219
mmu-miR-6980-3p	-0.332	6.102	-5.004	0.00222	0.02219
mmu-miR-7653-3p	-0.343	6.07	-5.002	0.00223	0.02219
mmu-miR-7211-3p	0.163	5.58	4.983	0.00227	0.02251
mmu-miR-7027-5p	0.064	5.525	4.965	0.00232	0.02271

mmu-miR-291b-5p	-0.553	6.24	-4.955	0.00234	0.02271
mmu-miR-28c	0.329	5.879	4.954	0.00234	0.02271
mmu-miR-6945-3p	-0.216	5.837	-4.954	0.00234	0.02271
mmu-miR-219a-5p	1.267	7.644	4.944	0.00237	0.02277
mmu-miR-671-5p	**0.186**	**5.727**	**4.932**	**0.0024**	**0.02277**
mmu-miR-6943-3p	-0.617	6.411	-4.929	0.0024	0.02277
mmu-miR-7034-3p	-0.264	5.955	-4.928	0.00241	0.02277
mmu-miR-194-2-3p	0.079	5.617	4.926	0.00241	0.02277
mmu-miR-5130	0.124	5.666	4.901	0.00247	0.02277
mmu-miR-7075-5p	0.138	5.627	4.895	0.00249	0.02277
mmu-miR-3110-5p	-0.053	5.598	-4.895	0.00249	0.02277
mmu-miR-7019-5p	0.079	5.539	4.894	0.00249	0.02277
mmu-miR-467b-5p	0.95	8.08	4.893	0.0025	0.02277
mmu-miR-7083-5p	0.082	5.563	4.891	0.0025	0.02277
mmu-miR-7236-5p	-0.077	5.485	-4.888	0.00251	0.02277
mmu-miR-7033-5p	0.551	6.067	4.888	0.00251	0.02277
mmu-miR-7073-3p	-0.126	5.759	-4.884	0.00252	0.02277
mmu-miR-8095	-0.522	6.443	-4.866	0.00257	0.02309
mmu-miR-6897-3p	-0.319	6.075	-4.851	0.00261	0.02335
mmu-let-7k	0.11	5.643	4.842	0.00263	0.02345
mmu-miR-290a-3p	-0.37	6.096	-4.823	0.00268	0.02369
mmu-miR-7054-3p	-0.112	5.734	-4.823	0.00268	0.02369
mmu-miR-6963-3p	-0.295	5.897	-4.81	0.00272	0.02392
mmu-miR-6238	0.198	5.69	4.801	0.00275	0.02402
mmu-miR-5132-3p	-0.338	6.054	-4.79	0.00278	0.02418
mmu-miR-6407	0.07	5.54	4.78	0.00281	0.02434
mmu-miR-5104	0.087	5.547	4.765	0.00285	0.02462
mmu-miR-6987-3p	-0.079	5.572	-4.743	0.00292	0.02493
mmu-miR-30b-5p	0.9	9.751	4.74	0.00293	0.02493
mmu-miR-483-3p	**-0.284**	**5.942**	**-4.74**	**0.00293**	**0.02493**
mmu-miR-139-5p	0.736	6.461	4.72	0.00299	0.02514
mmu-miR-6923-3p	-0.426	6.138	-4.72	0.00299	0.02514
mmu-miR-669f-3p	-0.455	8.015	-4.715	0.00301	0.02514
mmu-miR-351-5p	-0.064	5.544	-4.712	0.00302	0.02514
mmu-miR-7686-3p	0.091	5.58	4.711	0.00302	0.02514
mmu-miR-7053-3p	-0.206	5.841	-4.699	0.00306	0.02534
mmu-miR-7018-5p	0.298	5.867	4.693	0.00308	0.02541
mmu-let-7b-3p	-0.662	6.349	-4.687	0.0031	0.02545
mmu-miR-6383	0.088	5.568	4.683	0.00311	0.02545
mmu-miR-6769b-3p	-0.296	6.043	-4.673	0.00314	0.0256
mmu-miR-7067-3p	-0.258	5.988	-4.661	0.00318	0.02579
mmu-miR-3102-3p.2-3p	-0.33	6.016	-4.658	0.00319	0.02579
mmu-miR-3095-3p	0.708	6.444	4.651	0.00322	0.0258
mmu-miR-140-5p	0.929	8.203	4.65	0.00322	0.0258
mmu-miR-6936-3p	0.061	5.581	4.626	0.00331	0.02624
mmu-miR-6976-3p	-0.479	6.278	-4.626	0.00331	0.02624
mmu-miR-7117-3p	-0.298	6.057	-4.616	0.00334	0.02639
mmu-miR-9769-5p	-0.383	6.083	-4.613	0.00335	0.02639
mmu-miR-500-3p	0.473	7.316	4.585	0.00345	0.02701
mmu-miR-1306-3p	0.208	5.743	4.584	0.00346	0.02701
mmu-miR-411-3p	-0.089	5.568	-4.565	0.00353	0.02744
mmu-miR-678	0.132	5.619	4.544	0.00361	0.0279

mmu-miR-692	-0.064	5.562	-4.542	0.00362	0.0279
mmu-miR-29a-3p	1.897	12.717	4.539	0.00363	0.0279
mmu-miR-6961-5p	0.18	5.609	4.523	0.0037	0.02814
mmu-miR-7667-5p	-0.105	5.711	-4.523	0.0037	0.02814
mmu-miR-483-5p	0.15	5.628	4.515	0.00373	0.02825
mmu-miR-1947-3p	-0.848	6.417	-4.512	0.00374	0.02825
mmu-miR-133b-3p	-0.136	5.708	-4.508	0.00376	0.02825
mmu-miR-6914-3p	-0.165	5.751	-4.505	0.00377	0.02825
mmu-miR-7085-3p	-0.507	6.247	-4.495	0.00381	0.02844
mmu-miR-767	0.112	5.596	4.489	0.00384	0.02844
mmu-miR-7085-5p	0.107	5.573	4.488	0.00384	0.02844
mmu-miR-3099-3p	0.393	6.213	4.477	0.00389	0.02867
mmu-miR-6957-5p	0.253	5.748	4.468	0.00393	0.02885
mmu-miR-3104-3p	-0.137	5.816	-4.455	0.00398	0.02914
mmu-miR-7030-5p	0.123	5.61	4.449	0.00401	0.0292
mmu-miR-5627-3p	-0.058	5.697	-4.443	0.00403	0.02929
mmu-miR-200a-5p	0.074	5.527	4.436	0.00407	0.02942
mmu-miR-7045-5p	0.459	6.246	4.427	0.00411	0.0296
mmu-miR-195a-5p	0.562	6.548	4.41	0.00418	0.03004
mmu-miR-6936-5p	-0.27	5.887	-4.402	0.00422	0.03018
mmu-miR-188-5p	0.143	5.594	4.395	0.00425	0.0302
mmu-miR-6944-5p	0.206	5.672	4.395	0.00425	0.0302
mmu-miR-185-3p	-0.054	5.51	-4.378	0.00434	0.03059
mmu-miR-8093	0.104	5.546	4.374	0.00436	0.03059
mmu-miR-5624-3p	-0.074	5.485	-4.371	0.00437	0.03059
mmu-miR-3073b-3p	-0.066	5.535	-4.37	0.00437	0.03059
mmu-miR-217-3p	-0.083	5.543	-4.361	0.00442	0.03075
mmu-miR-6958-5p	0.118	5.586	4.341	0.00451	0.03075
mmu-miR-6927-3p	-0.052	5.562	-4.337	0.00454	0.03075
mmu-miR-6989-5p	0.116	5.558	4.335	0.00455	0.03075
mmu-miR-344h-3p	-0.047	5.5	-4.335	0.00455	0.03075
mmu-miR-142b	0.182	5.702	4.334	0.00455	0.03075
mmu-miR-7052-3p	-0.349	6.091	-4.334	0.00455	0.03075
mmu-miR-99b-5p	0.091	5.638	4.333	0.00456	0.03075
mmu-miR-7055-3p	-0.418	6.178	-4.333	0.00456	0.03075
mmu-miR-409-3p	-0.074	5.703	-4.332	0.00456	0.03075
mmu-miR-802-3p	-0.074	5.535	-4.315	0.00465	0.03109
mmu-miR-467e-5p	1.049	7.998	4.315	0.00465	0.03109
mmu-miR-6980-5p	0.282	6.579	4.312	0.00467	0.03109
mmu-miR-7081-5p	0.067	5.469	4.307	0.00469	0.03109
mmu-miR-378a-3p	1.095	7.417	4.307	0.00469	0.03109
mmu-miR-298-5p	-0.357	6.065	-4.296	0.00475	0.0311
mmu-miR-3089-3p	0.079	5.581	4.295	0.00475	0.0311
mmu-miR-6904-5p	0.39	6.64	4.292	0.00477	0.0311
mmu-miR-24-3p	0.585	9.076	4.292	0.00477	0.0311
mmu-miR-7653-5p	0.512	6.154	4.291	0.00478	0.0311
mmu-miR-365-3p	-0.154	6.039	-4.273	0.00488	0.03155
mmu-miR-5103	0.167	5.69	4.272	0.00488	0.03155
mmu-miR-7a-1-3p	0.64	6.677	4.267	0.00491	0.03159
mmu-miR-7211-5p	-0.616	6.297	-4.265	0.00492	0.03159
mmu-miR-1a-3p	-0.069	5.512	-4.25	0.005	0.0319
mmu-miR-465b-5p	0.095	5.585	4.247	0.00502	0.0319

mmu-miR-365-1-5p	0.086	5.541	4.246	0.00502	0.0319
mmu-miR-295-5p	0.159	5.623	4.242	0.00505	0.0319
mmu-miR-7235-5p	0.056	5.527	4.238	0.00507	0.0319
mmu-miR-6917-3p	-0.151	5.736	-4.238	0.00507	0.0319
mmu-miR-466f-5p	0.094	5.584	4.234	0.00509	0.03192
mmu-miR-21a-3p	0.21	5.668	4.226	0.00514	0.03212
mmu-miR-8108	0.059	5.532	4.223	0.00516	0.03214
mmu-miR-344i	0.285	5.83	4.208	0.00525	0.03248
mmu-miR-6419	-0.052	5.501	-4.206	0.00526	0.03248
mmu-let-7a-1-3p	-0.098	5.682	-4.204	0.00527	0.03248
mmu-miR-7080-3p	-0.514	6.304	-4.187	0.00537	0.03302
mmu-miR-511-5p	-0.136	5.623	-4.178	0.00543	0.03324
mmu-miR-6416-3p	0.046	5.501	4.176	0.00544	0.03324
mmu-miR-6954-5p	0.067	5.528	4.165	0.00551	0.03352
mmu-miR-6908-5p	-0.357	6.521	-4.156	0.00556	0.03376
mmu-miR-7004-5p	0.095	5.549	4.146	0.00563	0.034
mmu-miR-23a-5p	0.142	5.582	4.141	0.00566	0.034
mmu-miR-877-3p	-0.96	6.559	-4.14	0.00567	0.034
mmu-miR-1934-3p	0.143	5.617	4.139	0.00568	0.034
mmu-miR-130a-5p	-0.052	5.568	-4.131	0.00573	0.03406
mmu-miR-8094	0.095	5.595	4.127	0.00575	0.03406
mmu-miR-7651-5p	0.087	5.567	4.127	0.00575	0.03406
mmu-miR-7670-5p	0.142	5.577	4.126	0.00576	0.03406
mmu-miR-1190	-0.052	5.598	-4.12	0.0058	0.0342
mmu-miR-24-2-5p	0.157	5.667	4.116	0.00583	0.0342
mmu-miR-6905-3p	-0.083	5.526	-4.115	0.00584	0.0342
mmu-miR-186-5p	0.383	6.258	4.107	0.00589	0.03433
mmu-miR-1247-5p	-0.063	5.558	-4.106	0.00589	0.03433
mmu-miR-760-3p	0.087	5.542	4.1	0.00594	0.03446
mmu-miR-195a-3p	0.082	5.702	4.08	0.00607	0.03506
mmu-miR-7a-5p	1.051	7.755	4.077	0.00609	0.03506
mmu-miR-6985-3p	-0.091	5.603	-4.077	0.00609	0.03506
mmu-miR-7008-3p	-0.075	5.574	-4.067	0.00617	0.03537
mmu-miR-7654-3p	-0.112	5.64	-4.056	0.00624	0.03568
mmu-miR-6910-3p	-0.126	5.725	-4.053	0.00627	0.03571
mmu-miR-7017-3p	-0.337	5.88	-4.048	0.0063	0.03575
mmu-miR-6405	0.101	5.553	4.047	0.00631	0.03575
mmu-miR-6931-5p	0.48	6.046	4.042	0.00634	0.03584
mmu-let-7b-5p	0.95	10.641	4.04	0.00636	0.03584
mmu-miR-29c-5p	0.127	5.704	4.028	0.00645	0.03621
mmu-miR-467c-5p	0.666	6.942	4.019	0.00652	0.03648
mmu-miR-9769-3p	-0.26	5.924	-4.014	0.00656	0.0366
mmu-miR-34c-5p	-0.093	5.523	-4.006	0.00662	0.03677
mmu-miR-329-3p	-0.065	5.634	-4.005	0.00663	0.03677
mmu-let-7c-5p	0.76	10.623	3.996	0.0067	0.03695
mmu-miR-6984-5p	0.33	6.137	3.996	0.0067	0.03695
mmu-miR-7072-3p	-0.216	5.841	-3.988	0.00676	0.03717
mmu-miR-7656-5p	-0.058	5.511	-3.983	0.0068	0.03727
mmu-miR-33-5p	0.604	6.277	3.981	0.00682	0.03727
mmu-miR-6922-5p	0.108	5.574	3.972	0.00689	0.03746
mmu-miR-5122	0.182	5.69	3.971	0.00689	0.03746
mmu-miR-7045-3p	-0.15	5.884	-3.963	0.00696	0.03771

mmu-miR-6540-3p	-0.07	5.544	-3.951	0.00706	0.03817
mmu-miR-92b-5p	0.125	5.611	3.941	0.00714	0.03839
mmu-miR-328-3p	-0.226	5.864	-3.941	0.00714	0.03839
mmu-miR-7046-3p	-0.253	6.021	-3.934	0.0072	0.03859
mmu-miR-147-5p	-0.049	5.549	-3.926	0.00727	0.03883
mmu-miR-691	0.248	5.682	3.921	0.00731	0.03894
mmu-miR-98-5p	1.124	7.226	3.916	0.00736	0.03907
mmu-miR-1962	0.07	5.528	3.914	0.00737	0.03907
mmu-miR-7011-3p	-0.244	5.771	-3.905	0.00745	0.03933
mmu-miR-6959-5p	0.098	5.569	3.903	0.00747	0.03933
mmu-miR-6947-5p	0.06	5.481	3.901	0.00748	0.03933
mmu-miR-6916-3p	-0.138	5.631	-3.897	0.00752	0.03939
mmu-miR-6987-5p	0.389	6.188	3.892	0.00756	0.03951
mmu-miR-6916-5p	0.057	5.519	3.88	0.00767	0.03997
mmu-miR-338-5p	0.206	5.698	3.875	0.00772	0.04013
mmu-miR-7047-3p	-0.968	6.49	-3.862	0.00784	0.04059
mmu-miR-6241	-0.056	5.641	-3.857	0.00789	0.04059
mmu-miR-1191a	0.076	5.623	3.855	0.00791	0.04059
mmu-miR-465d-3p	-0.06	5.491	-3.854	0.00791	0.04059
mmu-miR-6546-5p	0.121	5.622	3.853	0.00793	0.04059
mmu-miR-26a-5p	0.305	11.4	3.849	0.00796	0.04059
mmu-miR-7657-3p	-0.048	5.476	-3.847	0.00798	0.04059
mmu-miR-3058-5p	0.187	5.754	3.847	0.00798	0.04059
mmu-miR-7038-5p	0.122	5.671	3.834	0.0081	0.04098
mmu-let-7i-5p	0.321	11.532	3.834	0.0081	0.04098
mmu-miR-191-5p	0.088	5.619	3.83	0.00814	0.04107
mmu-miR-7649-5p	0.163	5.672	3.824	0.0082	0.04121
mmu-miR-6395	-0.152	5.669	-3.821	0.00823	0.04121
mmu-miR-6952-3p	-0.225	5.784	-3.82	0.00824	0.04121
mmu-miR-6984-3p	-0.296	5.876	-3.809	0.00835	0.04164
mmu-miR-28a-5p	0.523	6.193	3.795	0.00849	0.04227
mmu-miR-7066-3p	-0.154	5.754	-3.792	0.00852	0.0423
mmu-miR-6905-5p	0.339	6.494	3.786	0.00858	0.04243
mmu-miR-7016-3p	-0.249	5.909	-3.785	0.00859	0.04243
mmu-miR-6351	0.114	5.589	3.78	0.00864	0.04256
mmu-miR-376b-5p	-0.065	5.563	-3.776	0.00869	0.04267
mmu-miR-1966-3p	-0.06	5.58	-3.763	0.00882	0.04312
mmu-miR-34a-3p	-0.099	5.539	-3.761	0.00885	0.04312
mmu-miR-320-3p	0.272	5.778	3.761	0.00885	0.04312
mmu-miR-3569-3p	-0.077	5.587	-3.746	0.009	0.04377
mmu-miR-6942-3p	-0.128	5.601	-3.743	0.00904	0.04384
mmu-miR-196a-1-3p	-0.055	5.544	-3.738	0.00909	0.04396
mmu-miR-6901-5p	0.06	5.528	3.731	0.00917	0.04421
mmu-miR-7226-3p	0.112	5.644	3.727	0.00922	0.04435
mmu-miR-3964	0.234	5.731	3.721	0.00928	0.04441
mmu-miR-6896-3p	-0.073	5.615	-3.72	0.0093	0.04441
mmu-miR-6973a-3p	-0.242	5.897	-3.719	0.0093	0.04441
mmu-miR-744-5p	0.366	5.993	3.712	0.00939	0.0447
mmu-miR-150-5p	1.77	11.772	3.709	0.00942	0.04473
mmu-miR-6372	-0.08	5.527	-3.698	0.00954	0.04519
mmu-miR-5622-5p	-0.077	5.539	-3.696	0.00957	0.04524
mmu-miR-3070-3p	0.206	5.735	3.684	0.00971	0.04577

mmu-miR-7032-5p	0.064	5.507	3.674	0.00983	0.04623
mmu-miR-6360	0.447	6.028	3.67	0.00987	0.0463
mmu-miR-7088-3p	-0.085	5.595	-3.665	0.00993	0.04638
mmu-miR-7051-5p	0.073	5.499	3.665	0.00994	0.04638
mmu-miR-714	0.198	5.838	3.663	0.00996	0.04638
mmu-miR-3077-5p	0.063	5.526	3.654	0.01007	0.04662
mmu-miR-3085-5p	0.047	5.505	3.654	0.01007	0.04662
mmu-miR-3572-3p	-0.133	5.756	-3.652	0.01009	0.04662
mmu-miR-7656-3p	-0.048	5.492	-3.649	0.01013	0.04662
mmu-miR-6918-3p	-0.06	5.554	-3.649	0.01014	0.04662
mmu-miR-6908-3p	0.059	5.545	3.644	0.01019	0.04675
mmu-miR-7048-3p	-0.114	5.761	-3.634	0.01032	0.04722
mmu-miR-1839-3p	0.885	8.342	3.609	0.01064	0.04849
mmu-miR-7017-5p	0.062	5.517	3.608	0.01065	0.04849
mmu-miR-6946-5p	0.215	5.637	3.598	0.01078	0.04892
mmu-miR-7234-3p	0.315	6.288	3.597	0.01079	0.04892
mmu-miR-26b-5p	0.885	11.121	3.595	0.01082	0.04892
mmu-miR-7647-3p	0.075	5.54	3.591	0.01087	0.04905
mmu-miR-8119	0.41	6.434	3.583	0.01099	0.04945
mmu-miR-136-3p	-0.054	5.558	-3.577	0.01106	0.04965
mmu-miR-7055-5p	0.367	6.341	3.573	0.01112	0.04982
mmu-miR-425-5p	0.9	7.36	3.567	0.0112	0.04991
mmu-miR-16-2-3p	0.155	5.894	3.567	0.0112	0.04991
mmu-miR-5134-5p	0.116	5.545	3.565	0.01122	0.04991
mmu-miR-5116	-0.046	5.659	-3.558	0.01133	0.05027
mmu-miR-188-3p	0.374	6.087	3.552	0.01141	0.0504
mmu-miR-107-3p	0.796	8.395	3.552	0.01142	0.0504
mmu-miR-3077-3p	-0.052	5.511	-3.54	0.01159	0.05105
mmu-miR-6986-3p	-0.355	5.897	-3.535	0.01165	0.05122
mmu-miR-7225-3p	-0.053	5.52	-3.529	0.01173	0.05145
mmu-miR-2183	-0.298	5.858	-3.514	0.01196	0.05211
mmu-miR-6937-3p	-0.064	5.731	-3.514	0.01196	0.05211
mmu-miR-6990-5p	0.296	5.858	3.512	0.01199	0.05211
mmu-miR-504-3p	0.266	6.96	3.512	0.012	0.05211
mmu-miR-9768-3p	-0.059	5.477	-3.509	0.01203	0.05214
mmu-miR-5129-3p	-0.048	5.636	-3.507	0.01206	0.05215
mmu-miR-6359	0.065	5.507	3.505	0.01209	0.05215
mmu-miR-335-3p	-0.125	5.634	-3.503	0.01212	0.05215
mmu-miR-202-5p	-0.055	5.607	-3.502	0.01214	0.05215
mmu-miR-7005-5p	0.309	5.853	3.497	0.01222	0.05232
mmu-miR-206-5p	-0.059	5.613	-3.494	0.01226	0.05232
mmu-let-7a-5p	0.503	12.18	3.493	0.01228	0.05232
mmu-miR-7012-5p	0.209	5.683	3.492	0.01229	0.05232
mmu-miR-3112-3p	-0.12	5.673	-3.483	0.01243	0.0528
mmu-miR-8102	0.313	5.894	3.477	0.01252	0.05304
mmu-miR-1927	0.302	6.593	3.474	0.01256	0.05311
mmu-miR-7070-3p	-0.117	5.617	-3.47	0.01264	0.05329
mmu-miR-1188-3p	-0.478	6.074	-3.465	0.01271	0.05347
mmu-miR-487b-3p	0.301	5.863	3.462	0.01276	0.05347
mmu-miR-499-3p	0.089	5.625	3.461	0.01277	0.05347
mmu-miR-1957a	0.09	5.59	3.46	0.01279	0.05347
mmu-miR-1982-5p	0.255	5.82	3.457	0.01285	0.05358

mmu-miR-337-5p	-0.042	5.493	-3.45	0.01295	0.05381
mmu-miR-134-3p	-0.115	5.682	-3.45	0.01296	0.05381
mmu-miR-6954-3p	-0.092	5.694	-3.445	0.01304	0.05381
mmu-miR-5625-5p	-0.036	5.476	-3.445	0.01304	0.05381
mmu-miR-1943-3p	-0.843	6.23	-3.444	0.01305	0.05381
mmu-miR-1934-5p	-0.069	5.531	-3.429	0.0133	0.05473
mmu-miR-32-3p	-0.978	6.581	-3.403	0.01373	0.05624
mmu-miR-3060-5p	0.048	5.637	3.403	0.01373	0.05624
mmu-miR-33-3p	-0.047	5.571	-3.4	0.0138	0.05624
mmu-miR-6988-5p	0.094	5.558	3.396	0.01386	0.05624
mmu-miR-3064-5p	0.057	5.516	3.396	0.01386	0.05624
mmu-miR-1946a	-0.075	5.525	-3.393	0.01391	0.05624
mmu-miR-7658-5p	0.078	5.531	3.393	0.01391	0.05624
mmu-miR-423-5p	0.721	6.894	3.392	0.01393	0.05624
mmu-miR-328-5p	0.332	6.018	3.391	0.01396	0.05624
mmu-miR-6975-5p	0.417	6.275	3.389	0.01398	0.05624
mmu-miR-7219-3p	0.225	6.027	3.388	0.01399	0.05624
mmu-miR-365-2-5p	0.097	5.54	3.376	0.01422	0.05704
mmu-miR-1843b-3p	-0.113	5.801	-3.372	0.01428	0.05715
mmu-miR-1971	0.135	5.61	3.37	0.01433	0.05722
mmu-miR-7659-5p	-0.062	5.525	-3.359	0.01452	0.05782
mmu-miR-541-5p	-0.049	5.522	-3.358	0.01454	0.05782
mmu-let-7c-1-3p	-0.049	5.598	-3.356	0.01458	0.05786
mmu-miR-216b-5p	-0.048	5.462	-3.353	0.01464	0.05796
mmu-miR-487b-5p	-0.064	5.561	-3.347	0.01474	0.05822
mmu-miR-6918-5p	0.237	6.993	3.346	0.01477	0.05822
mmu-miR-1896	0.207	5.748	3.338	0.01492	0.05862
mmu-miR-668-5p	-0.05	5.476	-3.335	0.01497	0.05862
mmu-miR-6955-5p	0.074	5.494	3.335	0.01498	0.05862
mmu-miR-664-3p	-0.102	6.049	-3.334	0.01499	0.05862
mmu-let-7d-5p	0.573	10.605	3.331	0.01505	0.05872
mmu-miR-129b-5p	0.315	6.664	3.321	0.01525	0.05937
mmu-miR-181a-5p	-2.456	8.978	-3.316	0.01534	0.05948
mmu-miR-299b-5p	-0.171	5.729	-3.315	0.01537	0.05948
mmu-miR-6925-3p	-0.108	5.665	-3.314	0.01537	0.05948
mmu-miR-7094b-2-5p	0.277	5.81	3.312	0.01541	0.05954
mmu-miR-152-3p	0.051	5.546	3.31	0.01545	0.05955
mmu-let-7d-3p	-0.207	5.853	-3.308	0.01549	0.05957
mmu-let-7j	0.151	5.725	3.301	0.01564	0.06003
mmu-miR-3473f	0.323	6.269	3.291	0.01584	0.06068
mmu-miR-1193-3p	-0.039	5.572	-3.287	0.01591	0.06083
mmu-miR-1251-3p	-0.041	5.491	-3.282	0.01601	0.06107
mmu-miR-345-3p	0.047	5.473	3.269	0.01629	0.06202
mmu-miR-6960-3p	-0.194	5.65	-3.267	0.01633	0.06203
mmu-miR-7678-3p	-0.045	5.596	-3.265	0.01636	0.06203
mmu-miR-6352	-0.176	5.845	-3.258	0.01651	0.06249
mmu-miR-711	0.052	5.525	3.249	0.01671	0.06305
mmu-miR-700-5p	0.094	5.687	3.248	0.01673	0.06305
mmu-miR-1188-5p	0.145	5.62	3.239	0.01692	0.0636
mmu-miR-3063-3p	-2.137	6.676	-3.238	0.01694	0.0636
mmu-miR-30d-5p	0.455	8.359	3.236	0.01699	0.06367
mmu-miR-207	-0.906	6.261	-3.233	0.01704	0.06373

mmu-miR-669a-3-3p	-0.79	6.212	-3.226	0.0172	0.06419
mmu-miR-293-3p	-0.056	5.502	-3.224	0.01725	0.06423
mmu-miR-3620-5p	0.188	5.8	3.223	0.01728	0.06423
mmu-miR-32-5p	0.44	6.112	3.219	0.01737	0.06444
mmu-miR-1897-5p	0.287	6.09	3.213	0.01749	0.06476
mmu-miR-7086-5p	0.336	6.092	3.209	0.01759	0.06491
mmu-miR-669m-3p	-0.249	5.885	-3.208	0.0176	0.06491
mmu-miR-425-3p	-0.067	5.746	-3.205	0.01768	0.06507
mmu-miR-551b-5p	0.179	5.675	3.201	0.01776	0.06513
mmu-miR-6999-5p	0.06	5.579	3.201	0.01776	0.06513
mmu-miR-434-3p	-0.087	5.64	-3.196	0.01789	0.06546
mmu-miR-7000-3p	-0.047	5.528	-3.188	0.01808	0.06597
mmu-miR-190a-5p	-0.065	5.567	-3.187	0.0181	0.06597
mmu-miR-361-5p	0.799	7.759	3.185	0.01815	0.06603
mmu-miR-141-3p	0.309	5.933	3.182	0.01821	0.06612
mmu-miR-7084-5p	0.091	5.557	3.177	0.01833	0.06643
mmu-miR-362-3p	0.709	6.863	3.175	0.01838	0.06648
mmu-miR-30c-5p	0.544	9.424	3.171	0.01847	0.06668
mmu-miR-1224-3p	-0.157	5.621	-3.167	0.01857	0.06691
mmu-miR-6926-3p	-0.071	5.544	-3.165	0.01862	0.06695
mmu-miR-7080-5p	0.318	6.749	3.162	0.01868	0.06704
mmu-miR-669h-5p	0.136	5.665	3.16	0.01874	0.06714
mmu-miR-421-5p	-0.053	5.548	-3.147	0.01905	0.06814
mmu-miR-7684-3p	0.081	5.58	3.145	0.01911	0.06821
mmu-miR-5623-3p	-0.08	5.57	-3.14	0.01923	0.06851
mmu-miR-6920-3p	-0.063	5.614	-3.136	0.01933	0.06874
mmu-miR-298-3p	-0.057	5.556	-3.133	0.01941	0.06884
mmu-miR-222-3p	0.121	5.641	3.13	0.01947	0.06884
mmu-miR-450b-5p	-0.062	5.541	-3.13	0.01947	0.06884
mmu-miR-1197-3p	-0.047	5.557	-3.128	0.01953	0.06891
mmu-miR-3080-3p	-0.044	5.455	-3.125	0.01959	0.06891
mmu-miR-193b-5p	0.061	5.505	3.125	0.0196	0.06891
mmu-miR-7226-5p	0.15	5.642	3.123	0.01966	0.06896
mmu-miR-7219-5p	0.389	6.202	3.122	0.01969	0.06896
mmu-miR-539-3p	-0.051	5.575	-3.117	0.0198	0.06923
mmu-miR-466h-3p	-1.252	7.43	-3.113	0.01991	0.06932
mmu-miR-721	**0.074**	**5.56**	**3.112**	**0.01993**	**0.06932**
mmu-miR-7081-3p	-0.17	5.612	-3.111	0.01997	0.06932
mmu-miR-5132-5p	0.089	5.55	3.109	0.02001	0.06932
mmu-miR-211-5p	-0.175	6.05	-3.109	0.02001	0.06932
mmu-miR-127-3p	-0.069	5.558	-3.096	0.02035	0.07035
mmu-miR-6926-5p	0.206	5.702	3.095	0.02039	0.07036
mmu-miR-3092-5p	-0.059	5.589	-3.088	0.02058	0.07088
mmu-miR-7676-3p	-0.408	5.767	-3.083	0.02069	0.07115
mmu-miR-615-3p	-0.136	5.606	-3.079	0.0208	0.07127
mmu-miR-3081-5p	0.163	5.621	3.079	0.0208	0.07127
mmu-miR-7014-3p	-0.067	5.581	-3.077	0.02087	0.07127
mmu-miR-148b-3p	0.434	6.334	3.074	0.02094	0.07127
mmu-miR-705	**0.302**	**5.853**	**3.074**	**0.02095**	**0.07127**
mmu-miR-3067-5p	0.1	5.615	3.074	0.02095	0.07127
mmu-miR-873a-5p	-0.04	5.542	-3.07	0.02106	0.07149
mmu-miR-7241-3p	0.247	5.867	3.044	0.02178	0.07373

mmu-miR-297b-5p	0.071	5.58	3.044	0.02179	0.07373
mmu-miR-802-5p	-0.06	5.555	-3.042	0.02183	0.07373
mmu-miR-370-3p	0.162	5.674	3.039	0.02192	0.07389
mmu-miR-7063-3p	-0.162	5.801	-3.035	0.02205	0.07416
mmu-miR-7233-5p	0.296	6.175	3.034	0.02208	0.07416
mmu-miR-6911-5p	0.063	5.542	3.026	0.02232	0.07476
mmu-miR-146b-3p	-0.051	5.483	-3.025	0.02234	0.07476
mmu-miR-6413	0.059	5.528	3.023	0.02239	0.0748
mmu-miR-7671-5p	-0.041	5.548	-3.021	0.02245	0.07488
mmu-miR-6964-3p	-0.053	5.56	-3.016	0.0226	0.07498
mmu-miR-3963	0.381	15.2	3.016	0.02261	0.07498
mmu-miR-290a-5p	0.132	5.683	3.016	0.02261	0.07498
mmu-miR-3076-5p	-0.079	5.671	-3.015	0.02264	0.07498
mmu-miR-6939-5p	0.051	5.542	3.01	0.02278	0.0753
mmu-miR-376c-3p	-1.988	6.442	-3.007	0.02286	0.0754
mmu-miR-6919-3p	-0.045	5.534	-3.006	0.02289	0.0754
mmu-miR-196b-5p	-0.032	5.521	-3.001	0.02304	0.07556
mmu-miR-494-3p	0.701	8.911	3.001	0.02304	0.07556
mmu-miR-6971-5p	0.39	6.301	3.001	0.02306	0.07556
mmu-miR-5121	0.628	7.778	2.997	0.02318	0.07577
mmu-miR-449c-3p	-0.061	5.562	-2.996	0.0232	0.07577
mmu-miR-135a-1-3p	0.065	5.601	2.988	0.02344	0.07641
mmu-miR-7678-5p	0.075	5.5	2.987	0.02349	0.07641
mmu-miR-7043-5p	0.207	5.939	2.986	0.02352	0.07641
mmu-miR-582-3p	-0.048	5.507	-2.982	0.02364	0.07667
mmu-miR-466f-3p	-1.476	7.017	-2.977	0.0238	0.07694
mmu-miR-6902-3p	0.364	6.068	2.977	0.02381	0.07694
mmu-miR-291a-3p	0.048	5.572	2.975	0.02387	0.07697
mmu-miR-216c-3p	-0.051	5.499	-2.972	0.02394	0.07697
mmu-miR-7649-3p	-0.046	5.512	-2.971	0.02399	0.07697
mmu-miR-5618-5p	-0.038	5.481	-2.971	0.024	0.07697
mmu-miR-568	-0.124	5.546	-2.97	0.02402	0.07697
mmu-miR-6410	0.082	5.575	2.969	0.02406	0.07697
mmu-miR-744-3p	-0.048	5.672	-2.966	0.02413	0.07706
mmu-miR-7657-5p	0.31	6.058	2.963	0.02423	0.07725
mmu-miR-7116-3p	-0.074	5.568	-2.959	0.02436	0.07755
mmu-miR-196b-3p	-0.078	5.553	-2.957	0.02442	0.07755
mmu-miR-6898-5p	0.393	6.09	2.956	0.02445	0.07755
mmu-miR-6348	-0.925	6.331	-2.954	0.02453	0.07766
mmu-miR-101a-5p	0.088	5.588	2.946	0.02481	0.07842
mmu-miR-1251-5p	-0.045	5.491	-2.938	0.02504	0.07903
mmu-miR-6991-3p	-0.06	5.57	-2.929	0.02534	0.07984
mmu-miR-6974-5p	0.063	5.478	2.927	0.02543	0.07997
mmu-miR-7040-5p	0.064	5.581	2.925	0.02548	0.08002
mmu-miR-204-5p	-0.165	5.673	-2.922	0.0256	0.08027
mmu-miR-302c-3p	-1.08	6.049	-2.917	0.02576	0.08063
mmu-miR-185-5p	0.68	6.594	2.915	0.02584	0.08073
mmu-miR-1231-3p	-0.063	5.515	-2.912	0.02593	0.08088
mmu-miR-7044-5p	0.113	5.612	2.909	0.02604	0.08108
mmu-miR-669d-3p	-0.717	5.996	-2.906	0.02614	0.08126
mmu-miR-6236	0.085	5.56	2.902	0.02627	0.08138
mmu-miR-574-3p	-1.608	6.665	-2.902	0.02629	0.08138

mmu-miR-3068-5p	0.056	5.657	2.901	0.0263	0.08138
mmu-miR-6988-3p	-0.049	5.552	-2.899	0.02638	0.08149
mmu-miR-1b-5p	-0.067	5.62	-2.896	0.0265	0.08171
mmu-miR-1893	-0.042	5.478	-2.894	0.02654	0.08172
mmu-miR-1894-3p	0.333	6.391	2.893	0.0266	0.08176
mmu-miR-6915-3p	-0.059	5.549	-2.884	0.02691	0.08257
mmu-miR-7064-3p	-0.4	5.816	-2.881	0.02702	0.08266
mmu-miR-7578	-0.066	5.535	-2.881	0.02703	0.08266
mmu-miR-485-3p	-0.456	5.78	-2.879	0.02708	0.08269
mmu-miR-764-5p	-0.52	5.838	-2.877	0.02717	0.08278
mmu-miR-376c-5p	-0.041	5.538	-2.876	0.0272	0.08278
mmu-miR-182-3p	-0.042	5.538	-2.874	0.02729	0.08292
mmu-miR-878-5p	-0.064	5.447	-2.87	0.02742	0.08316
mmu-miR-6906-3p	-0.112	5.579	-2.868	0.02751	0.08316
mmu-miR-546	0.059	5.446	2.867	0.02754	0.08316
mmu-miR-466g	-1.63	6.85	-2.866	0.02757	0.08316
mmu-miR-7218-5p	0.25	6.68	2.866	0.02759	0.08316
mmu-miR-30c-1-3p	0.389	6.288	2.86	0.02778	0.08361
mmu-miR-6995-5p	0.417	6.11	2.859	0.02783	0.08363
mmu-miR-467b-3p	-1.319	6.267	-2.854	0.02801	0.08404
mmu-miR-7056-3p	-0.127	5.729	-2.853	0.02807	0.08407
mmu-miR-7093-5p	0.037	5.541	2.85	0.02816	0.08422
mmu-miR-466i-3p	-1.097	7.287	-2.844	0.0284	0.08474
mmu-miR-6975-3p	-0.401	5.784	-2.843	0.02843	0.08474
mmu-miR-878-3p	0.178	5.762	2.84	0.02855	0.08496
mmu-miR-6993-3p	-0.067	5.524	-2.836	0.02871	0.0853
mmu-miR-3108-5p	-0.043	5.465	-2.834	0.02878	0.08538
mmu-miR-7235-3p	-1.148	6.165	-2.83	0.02893	0.08558
mmu-miR-6927-5p	0.045	5.563	2.829	0.02895	0.08558
mmu-miR-3070-2-3p	0.326	6.689	2.828	0.02899	0.08558
mmu-miR-467g	-1.211	6.253	-2.827	0.02903	0.08558
mmu-miR-6401	0.259	6.662	2.826	0.02909	0.08562
mmu-miR-7652-3p	-0.034	5.576	-2.824	0.02916	0.08569
mmu-miR-8105	0.129	5.688	2.822	0.02923	0.08569
mmu-miR-468-3p	-0.657	6.421	-2.821	0.02929	0.08569
mmu-miR-1938	-0.037	5.495	-2.821	0.02929	0.08569
mmu-miR-6412	0.481	6.964	2.818	0.02938	0.08582
mmu-miR-6933-3p	-0.072	5.519	-2.814	0.02957	0.08613
mmu-miR-29b-2-5p	-0.032	5.5	-2.813	0.02958	0.08613
mmu-miR-669e-3p	-1.547	6.406	-2.812	0.02962	0.08613
mmu-miR-8109	0.052	5.476	2.809	0.02975	0.08636
mmu-miR-3091-3p	-0.042	5.506	-2.803	0.02998	0.08689
mmu-miR-7a-2-3p	-0.069	5.596	-2.798	0.03021	0.08743
mmu-miR-471-3p	-0.067	5.547	-2.793	0.03041	0.08785
mmu-miR-599	-0.035	5.525	-2.791	0.0305	0.08798
mmu-miR-6973b-3p	-0.083	5.63	-2.788	0.0306	0.08803
mmu-miR-382-3p	-0.066	5.626	-2.788	0.03061	0.08803
mmu-miR-136-5p	-0.046	5.578	-2.787	0.03066	0.08804
mmu-miR-669l-5p	0.335	6.844	2.785	0.03074	0.08813
mmu-let-7e-5p	0.27	6.026	2.779	0.03096	0.08863
mmu-miR-6538	0.158	5.732	2.777	0.03106	0.08879
mmu-miR-6998-3p	-0.857	5.905	-2.776	0.03112	0.08882

mmu-miR-181c-3p	-0.066	5.516	-2.771	0.03131	0.08901
mmu-miR-7666-3p	0.142	5.643	2.771	0.03131	0.08901
mmu-miR-6404	0.033	5.49	2.771	0.03133	0.08901
mmu-miR-7031-3p	-0.176	5.693	-2.765	0.03155	0.08947
mmu-miR-495-3p	-0.046	5.562	-2.765	0.03158	0.08947
mmu-miR-466m-3p	-1.065	6.233	-2.763	0.03164	0.0895
mmu-miR-6969-5p	0.406	6.044	2.759	0.03182	0.08986
mmu-miR-16-1-3p	0.122	5.634	2.755	0.03201	0.09028
mmu-miR-6957-3p	-0.46	5.824	-2.742	0.03256	0.09169
mmu-miR-8107	0.185	5.744	2.738	0.03273	0.09201
mmu-miR-5617-3p	-0.054	5.555	-2.732	0.03299	0.0925
mmu-miR-3102-5p	0.458	6.185	2.732	0.033	0.0925
mmu-miR-34b-3p	-0.188	5.667	-2.729	0.03315	0.09279
mmu-miR-7671-3p	0.239	5.774	2.727	0.03321	0.09283
mmu-miR-344b-5p	-0.052	5.522	-2.721	0.03352	0.09345
mmu-miR-3093-3p	0.051	5.458	2.72	0.03354	0.09345
mmu-miR-138-1-3p	0.077	5.589	2.716	0.03374	0.09387
mmu-miR-7681-5p	-0.564	5.85	-2.714	0.03382	0.09397
mmu-miR-7028-5p	0.31	6.339	2.71	0.034	0.09423
mmu-miR-3105-3p	-0.05	5.549	-2.71	0.03402	0.09423
mmu-miR-1895	0.426	6.71	2.705	0.03423	0.09468
mmu-miR-698-3p	-0.146	5.604	-2.703	0.03432	0.09477
mmu-miR-7118-3p	-0.184	5.655	-2.702	0.03436	0.09477
mmu-miR-217-5p	-0.03	5.449	-2.697	0.0346	0.0953
mmu-miR-190b-5p	0.236	6.482	2.694	0.03473	0.09552
mmu-miR-6952-5p	0.067	5.508	2.69	0.03495	0.09577
mmu-miR-7039-3p	-0.09	5.74	-2.689	0.03499	0.09577
mmu-miR-467d-3p	-0.971	7.232	-2.688	0.03502	0.09577
mmu-miR-125a-3p	0.124	5.662	2.688	0.03503	0.09577
mmu-miR-8114	-0.206	5.65	-2.685	0.03517	0.09602
mmu-miR-6997-3p	-0.095	5.679	-2.684	0.03523	0.09604
mmu-miR-7027-3p	-0.146	5.624	-2.681	0.03537	0.09614
mmu-miR-7212-3p	-1.26	6.083	-2.68	0.03539	0.09614
mmu-miR-1930-5p	-0.049	5.484	-2.68	0.03542	0.09614
mmu-miR-327	0.073	5.49	2.678	0.03551	0.09614
mmu-miR-1894-5p	-0.527	5.893	-2.678	0.03552	0.09614
mmu-miR-1906	0.612	6.608	2.667	0.03603	0.09727
mmu-miR-5126	-0.441	7.485	-2.667	0.03604	0.09727
mmu-miR-7661-3p	-0.642	5.923	-2.665	0.03612	0.09735
mmu-miR-30a-5p	0.315	6.461	2.66	0.03638	0.0979
mmu-miR-509-3p	-0.034	5.521	-2.647	0.03702	0.09936
mmu-miR-7084-3p	-0.216	5.727	-2.647	0.03703	0.09936
mmu-miR-7012-3p	-0.191	5.668	-2.644	0.03719	0.09954
mmu-miR-3474	0.044	5.478	2.644	0.0372	0.09954
mmu-miR-467c-3p	-1.127	6.48	-2.643	0.03726	0.09955

Table A.4. Receiver operating characteristic curves of plasma miRNAs and blood T cells. A. ROC curves analyzed using the normalized qPCR values ($2^{-\Delta\Delta Ct}$) for each plasma miRNA to compare myocarditis *versus* healthy donors or myocardial infarction patients. B. C. ROC curves calculated for different peripheral blood T cell populations measured by FACs. AUC: area under the curve; CI: confidence interval; Sensitivity: true positive rate; Specificity: false positive rate. Cut-off value estimated as the value that resulted in both sensitivity and specificity over 90% or the value with the highest likelihood ratio.

A. Circulating miRNAs	AUC	95% CI	Cut-off value ($2^{-\Delta\Delta Ct}$)	Sensitivity (%)	Specificity (%)
Myocarditis vs Healthy Controls					
Hsa-miR-Chr8:96	0.9882	0.9702 - 1.006	> 2.937	97.30	93.75
Hsa-miR-483-5p	0.9421	0.8838 - 1.000	> 3.514	78.79	95.45
Hsa-miR-21-5p	0.7159	0.5587 - 0.8731	> 2.190	40.91	95.00
Hsa-miR-212-3p	0.7156	0.5472 - 0.8841	> 2.083	45.00	93.75
Hsa-miR-132-3p	0.8006	0.6606 - 0.9406	> 3.097	47.62	93.75
Myocarditis vs Myocardial Infarction (STEMI + NSTEMI) patients					
Hsa-miR-Chr8:96	0.9268	0.8787 - 0.9749	> 20.03	70.27	98.61
Hsa-miR-483-5p	0.5094	0.3863 - 0.6325	< 0.999	9.091	96.55
Hsa-miR-21-5p	0.5293	0.3618 - 0.6969	> 3.340	28.57	80.77
Hsa-miR-212-3p	0.5673	0.3992 - 0.7354	> 4.966	25.00	88.46
Hsa-miR-132-3p	0.6412	0.4862 - 0.7961	> 40.82	14.29	96.43
Myocarditis vs ST-elevation Myocardial Infarction (STEMI) patients					
Hsa-miR-Chr8:96	0.9309	0.8778 - 0.9841	> 16.64	75.68	97.02
Hsa-miR-483-5p	0.5015	0.3567 - 0.6462	> 5.700	72.73	41.94
Hsa-miR-21-5p	0.5970	0.4028 - 0.7911	> 3.340	36.36	80.00
Hsa-miR-212-3p	0.6462	0.4409 - 0.8514	> 4.966	25.00	92.31
Hsa-miR-132-3p	0.7245	0.5441 - 0.9049	> 8.108	23.81	92.86
Myocarditis vs non-ST-elevation Myocardial Infarction (NSTEMI) patients					
Hsa-miR-Chr8:96	0.9227	0.8655 - 0.9798	> 20.03	70.27	97.22
Hsa-miR-483-5p	0.5219	0.3735 - 0.6703	< 8.025	54.55	62.96
Hsa-miR-21-5p	0.5289	0.3224 - 0.7355	< 0.820	27.27	90.91
Hsa-miR-212-3p	0.5115	0.3111 - 0.7120	< 0.791	20.00	92.31
Hsa-miR-132-3p	0.5578	0.3638 - 0.7519	> 6.240	28.57	92.86

B. Blood T cells	AUC	95% CI	Cut-off value (%)	Sensitivity (%)	Specificity (%)
Myocarditis vs Healthy Donors					
Th17	0.8825	0.7981 - 0.9669	> 1.785	57.14	98.39
Treg	0.7429	0.6099 - 0.8759	> 9.500	27.27	98.70
Th17/ Treg	0.7143	0.5952 - 0.8334	> 0.654	32.14	98.25
IFNγ	0.5977	0.4223 - 0.7732	< 0.655	15.00	90.91
Myocarditis vs Myocardial Infarction (STEMI + NSTEMI) patients					
Th17	0.8664	0.7819 - 0.9508	> 2.545	39.23	92.88
Treg	0.5700	0.4287 - 0.7114	> 13.40	13.64	96.72
Th17/ Treg	0.7659	0.6602 - 0.8717	> 0.741	28.57	98.21
IFNγ	0.5338	0.3852 - 0.6824	> 16.10	12.16	95.45

AMERICAN SOCIETY FOR MICROBIOLOGY | Molecular and Cellular Biology®

RESEARCH ARTICLE

Thymus-Derived Regulatory T Cell Development Is Regulated by C-Type Lectin-Mediated BIC/MicroRNA 155 Expression

Raquel Sánchez-Díaz,[a,e] Rafael Blanco-Dominguez,[a] Sandra Lasarte,[a,e] Katerina Tsilingiri,[a] Enrique Martín-Gayo,[b] Beatriz Linillos-Pradillo,[a] Hortensia de la Fuente,[c,e] Francisco Sánchez-Madrid,[c,e] Rinako Nakagawa,[d] María L. Toribio,[b] Pilar Martín[a,e]

Signaling and Inflammation Program, Centro Nacional de Investigaciones Cardiovasculares (CNIC), Madrid, Spain[a]; Centro de Biología Molecular Severo Ochoa, Consejo Superior de Investigaciones Científicas, Universidad Autónoma de Madrid, Madrid, Spain[b]; Department of Immunology, Hospital de la Princesa, Madrid, Spain[c]; Immunity and Cancer Laboratory, The Francis Crick Institute, London, United Kingdom[d]; CIBER de Enfermedades Cardiovasculares, Instituto de Salud Carlos III, Madrid, Spain[e]

ABSTRACT Thymus-derived regulatory T (tTreg) cells are key to preventing autoimmune diseases, but the mechanisms involved in their development remain unsolved. Here, we show that the C-type lectin receptor CD69 controls tTreg cell development and peripheral Treg cell homeostasis through the regulation of BIC/microRNA 155 (miR-155) and its target, suppressor of cytokine signaling 1 (SOCS-1). Using Foxp3-mRFP/*cd69*$^{+/-}$ or Foxp3-mRFP/*cd69*$^{-/-}$ reporter mice and short hairpin RNA (shRNA)-mediated silencing and miR-155 transfection approaches, we found that CD69 deficiency impaired the signal transducer and activator of transcription 5 (STAT5) pathway in Foxp3^{+} cells. This results in BIC/miR-155 inhibition, increased SOCS-1 expression, and severely impaired tTreg cell development in embryos, adults, and Rag2$^{-/-}$ γc$^{-/-}$ hematopoietic chimeras reconstituted with *cd69*$^{-/-}$ stem cells. Accordingly, *mirn155*$^{-/-}$ mice have an impaired development of CD69^{+} tTreg cells and overexpression of the miR-155-induced CD69 pathway, suggesting that both molecules might be concomitantly activated in a positive-feedback loop. Moreover, *in vitro*-inducible CD25^{+} Treg (iTreg) cell development is inhibited in *Il2r*$\gamma^{-/-}$/*cd69*$^{-/-}$ mice. Our data highlight the contribution of CD69 as a nonredundant key regulator of BIC/miR-155-dependent Treg cell development and homeostasis.

KEYWORDS regulatory T cell development, C-type lectin, miR-155, autoimmunity, microRNA

Received 14 June 2016 **Returned for modification** 28 July 2016 **Accepted** 27 January 2017

Accepted manuscript posted online 6 February 2017

Citation Sánchez-Díaz R, Blanco-Dominguez R, Lasarte S, Tsilingiri K, Martín-Gayo E, Linillos-Pradillo B, de la Fuente H, Sánchez-Madrid F, Nakagawa R, Toribio ML, Martín P. 2017. Thymus-derived regulatory T cell development is regulated by C-type lectin-mediated BIC/microRNA 155 expression. Mol Cell Biol 37:e00341-16. https://doi.org/10.1128/MCB.00341-16.

Address correspondence to Pilar Martín, pmartinf@cnic.es.

Regulatory T (Treg) cells are a specialized subset of lymphocytes with a dominant role in the prevention of autoimmune diseases (1). Treg cell subtypes have been classified according to their origin in the thymus, peripheral lymphoid organs, or *in vitro* and have been extensively characterized; however, the mechanisms that regulate their generation in the thymus remain poorly understood. Understanding how thymus-derived Treg (tTreg) cells (2) become a distinct lineage is crucial for the development of strategies to control immune responses by targeting these cells (3). A central event in tTreg cell differentiation is the induction of the transcription factor Foxp3 by early signals delivered from the T cell (TC) receptor (TCR), which results in transcriptional activation and enhanced function of the interleukin-2 (IL-2) signaling pathway (4). Among other mechanisms, Foxp3 expression is promoted by the microRNA (miRNA) 155 (miR-155) through the inhibition of SOCS-1 (suppressor of cytokine signaling 1), enhancing the activation and binding of STAT5 (signal transducer and activator of

transcription 5) to the Foxp3 promoter and the Foxp3-CNS (conserved noncoding sequence) (5, 6). In a positive-feedback loop, Foxp3 increases the expression of miR-155 by binding to an intronic element of BIC, the gene encoding the miR-155 precursor transcript. Nevertheless, the mechanisms by which miRNAs impact tTreg cell differentiation and function are not fully elucidated, and the data are somewhat contradictory. For example, Dicer, a member of the RNase III complex that processes pre-miRNAs into mature miRNAs, plays a key role in tTreg cell differentiation (7) and function (8); however, the lack of Dicer is linked to enhanced miR-155 expression in MRL/lpr mice (9), suggesting that there are Dicer-independent mechanisms for miRNA regulation in Treg cells. The Treg cells of lupus-prone mice have an altered phenotype, low levels of Dicer, and a weak suppressive capacity linked to the expression of the C-type lectin receptor CD69 (9). Moreover, increased CD69 expression has been detected in activated *Dicer*$^{-/-}$ TCs, which show defective egress from lymphoid organs (10). In addition, CD4^{+} CD8^{+} thymocytes include a CD69^{high} TCR^{high} Treg cell progenitor subpopulation, indicating that CD69 expression is relevant to tTreg cell differentiation (11). We hypothesized that CD69, which contributes to the maintenance of immunological tolerance through the regulation of Treg cell function, makes a substantial contribution to Treg cell development in the thymus. The C-type lectin CD69 is expressed constitutively by a subpopulation of peripheral Treg (pTreg) cells and tTreg cells (12). Here, we report that CD69 is required for the development of Treg cells in the thymus through the promotion of STAT5 phosphorylation and the transcription of BIC/miR-155. FoxP3-mRFP/*cd69*$^{-/-}$ reporter mice have a significantly below-normal number of tTreg cells, and Treg cell differentiation was also impaired in fetal thymus organ cultures (FTOCs) of *cd69*$^{-/-}$ embryonic thymuses or wild-type embryonic thymuses treated with anti-CD69. Consistently, FoxP3^{+} tTreg cells are poorly generated from *cd69*$^{-/-}$ precursors in mixed bone marrow chimeras. An impairment of STAT5 phosphorylation in FoxP3-mRFP/*cd69*$^{-/-}$ tTreg cells leads to the enhanced transcription of SOCS-1 and the inhibition of miR-155-dependent tTreg cell development. CD69 thus maintains miR-155-dependent tTreg cell development through a positive-feedback regulatory mechanism, giving rise to a functional pTreg cell subset. Our results strongly support a role for CD69 as a critical receptor in the control of Treg cell development and homeostasis.

RESULTS

CD69 expression is required for development of the tTreg cell subset. To determine whether CD69 is necessary for tTreg cell development in the thymus, we analyzed CD69 membrane expression in tTreg cells from *cd69*$^{+/+}$, *cd69*$^{+/-}$, and *cd69*$^{-/-}$ littermates bearing a Foxp3-mRFP reporter gene (monomeric red fluorescent protein inserted into the *foxp3* locus). In agreement with previously reported data for nonreporter mice (12), about 30% of tTreg cells expressing Foxp3-mRFP in wild-type thymuses also express CD69 (Fig. 1A and B). This percentage is lower in Foxp3-mRFP/*cd69*$^{+/-}$ heterozygous mice, and this subset is absent in Foxp3-mRFP/*cd69*$^{-/-}$ mice (Fig. 1A and B). The proportions of CD4^{+} single-positive (SP) (CD4SP) thymocytes and the other thymocyte subsets are unaffected in *cd69* heterozygous and *cd69*-deficient reporter littermates (Fig. 1C), but compared with Foxp3-mRFP/*cd69*$^{+/+}$ mice, both genotypes showed a 30% lower cellularity of total and CD4SP thymocytes (Fig. 1D). These results are consistent with previously reported data showing that the overexpression of CD69 in the thymus increases the levels of SP thymocytes controlling egress to the periphery (13, 14). However, Foxp3-mRFP/*cd69*$^{-/-}$ and *cd69*$^{+/-}$ mice showed a marked reduction in the proportion of tTreg cells compared with that in *cd69*$^{+/+}$ adult reporter mice (Fig. 1E and F), while total tTreg cell numbers were not altered in the *cd69*$^{+/-}$ and *cd69*$^{-/-}$ groups (Fig. 1F), indicating that CD69 could be playing an important role in the regulation of tTreg cell development masked by thymocyte egress defects in Foxp3-mRFP/*cd69*$^{-/-}$ mice. In addition, we found that *cd69*$^{-/-}$ adult reporter mice also showed a reduction in the proportion of pTreg cells compared with that in *cd69*$^{+/+}$ littermates (see Fig. S1A and B in the supplemental material). These

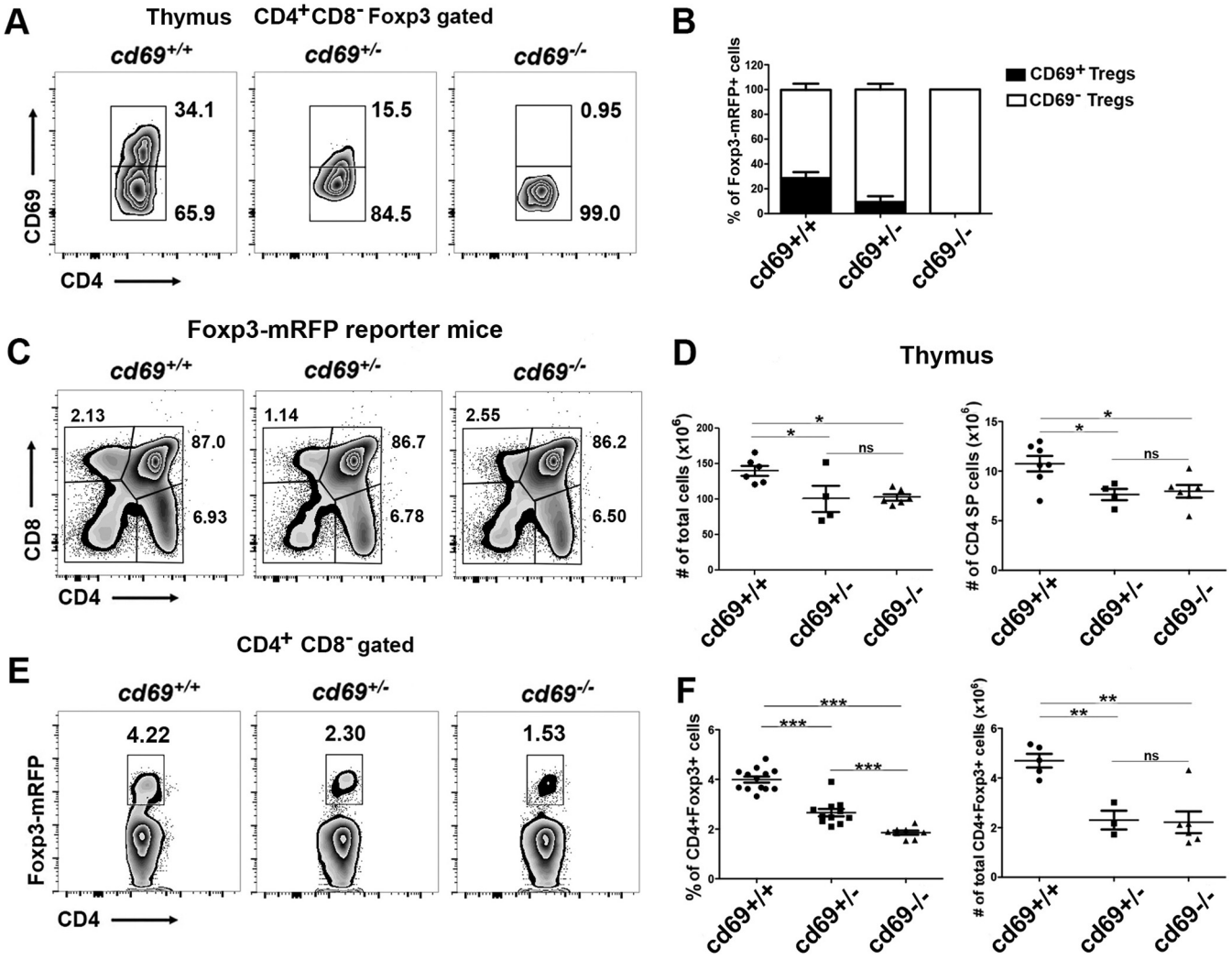

FIG 1 CD69 expression is required for thymus-derived Treg cell homeostasis in adult mice. (A) Density plots showing CD69 expression in $CD4^+$ $CD8^-$ $Foxp3^+$-gated thymocytes from 8- to 12-week-old Foxp3-mRFP/*cd69*$^{+/+}$ (wild-type), Foxp3-mRFP/*cd69*$^{+/-}$ (heterozygous), and Foxp3-mRFP/*cd69*$^{-/-}$ (deficient) reporter littermates. Numbers indicate the proportions (percentages) of gated cells. (B) Bar chart showing the percentages (±standard deviations) of $CD69^+$ and $CD69^-$ tTreg cells within the thymus of the indicated reporter mice. (C) Flow cytometry analysis of thymocyte subsets in 8- to 10-week-old reporter littermates. The percentages of thymus-derived T cell subsets are shown. (D) Cellularity of the thymus (left) and total numbers of CD4SP cells (right) in reporter littermates. (E) Analysis of endogenous Foxp3 expression in tTreg cells in the thymuses of reporter littermates. (F) Percentages (left) and total cell numbers (right) of gated $CD4^+$ $CD8^-$ $Foxp3^+$ tTreg cells in adult reporter littermates. Data are from at least 7 litters with 3 to 12 littermates each. Totals of 16 Foxp3-mRFP/*cd69*$^{+/+}$ (wild-type), 11 Foxp3-mRFP/*cd69*$^{+/-}$ (heterozygous), and 12 Foxp3-mRFP/*cd69*$^{-/-}$ (deficient) mice were analyzed. Error bars show standard deviations. Data were evaluated by ANOVA followed by Bonferroni's multiple-comparison test. *, $P < 0.05$; **, $P < 0.01$; ***, $P < 0.001$; ns, not significant.

data are not consistent with data reported previously for nonreporter mice (12). To clarify the differences observed with Foxp3 reporter mice, we performed Foxp3 staining in thymuses and spleens from Foxp3-mRFP mice. The data indicate that exogenous staining with anti-Foxp3 antibodies (Abs) differs from the endogenous print of Foxp3-mRFP depending on the tissue (Fig. S2), suggesting that the use of anti-Foxp3 antibodies is not always as accurate as the use of reporter genes. In summary, CD69 could be playing a role in both tTreg cell development and pTreg cell homeostasis.

Deletion of CD69 inhibits tTreg cell differentiation in fetal thymus organ cultures. To determine if *cd69* deficiency leads to decreased tTreg cell development, independently of the thymic maturation state or the sphingosine 1-phosphate receptor 1 ($S1P_1$)-induced thymocyte egress capacity, we performed an FTOC assay on thymuses from 15- to 17-day-old mouse embryos (embryonic day 15 [E15] to E17) and analyzed total CD4SP thymocytes and tTreg cell differentiation over 5 days of culture. Compared

with *cd69*$^{+/+}$ FTOCs, *cd69*$^{-/-}$ E15 to E17 FTOCs displayed marked reductions in the proportions and absolute cell numbers of Foxp3^{+} tTreg cells, with insignificant changes in total cell numbers (Fig. 2A and B), indicating that CD69 is required during tTreg cell differentiation at early stages of development. To confirm these results, we treated E15 FTOCs with an anti-CD69 monoclonal antibody (MAb) (2.2), which downregulates CD69 expression and hence blocks downstream signaling (15), and monitored Treg cell development over 14 days of culture. Consistent with the *cd69*$^{-/-}$ FTOC data, throughout the culture period, anti-CD69-treated FTOCs showed notably lower proportions and cell numbers of Foxp3^{+} tTreg cells than did FTOCs treated with the isotype control antibody (2.8) (Fig. 2C and D), whereas total FTOC cell numbers were unaltered by either treatment (Fig. 2D). These findings are consistent with previously reported evidence indicating that immature activated CD69^{+} thymocytes are the precursors of intrathymic Treg cells in humans and mice (11, 16).

Defective tTreg and pTreg cell generation from *cd69*$^{-/-}$ progenitors is a cell-autonomous defect. To further explore the role of CD69 in tTreg cell differentiation, we transferred bone marrow (BM) hematopoietic stem cells from Foxp3-mRFP/*cd69*$^{+/+}$ or Foxp3-mRFP/*cd69*$^{-/-}$ littermates into lethally γ-irradiated C57BL/6 recipients (Fig. 3A). Twelve weeks after reconstitution, percentages and numbers of CD4^{+} Foxp3^{+} Treg cells derived from *cd69*$^{-/-}$ BM precursors were markedly lower in the thymus (Fig. 3A) and blood (see Fig. S3 in the supplemental material) than in those derived from *cd69*$^{+/+}$ precursors, indicating an impaired Treg cell regeneration capacity of *cd69*$^{-/-}$ BM hematopoietic stem cells. Moreover, we analyzed the potential of these precursors to differentiate into tTreg cells in sublethally irradiated Rag2$^{-/-}$ γc$^{-/-}$ recipients, which lack lymphoid cells (Fig. 3B). Because Rag2$^{-/-}$ γc$^{-/-}$ recipient mice lack NK cells, we depleted donor BM precursors of T cells before transplantation to avoid graft-versus-host disease (17). As described above, *cd69*$^{-/-}$ BM precursors had the lowest tTreg cell regeneration potential, even though in both systems, there were no differences in CD4SP cell numbers between thymuses of chimeric mice from *cd69*$^{+/+}$ and those from *cd69*$^{-/-}$ BM precursors (Fig. 3A and B). These results suggest that the differences observed in the percentages of CD4^{+} Foxp3^{+} tTreg cells in the thymus are due to an impaired differentiation of this cell subset and not to defective thymocyte egress (Fig. 3A and B).

Finally, to definitely rule out that the differences observed are due to differential egress between *cd69*$^{+/+}$ and *cd69*$^{-/-}$ thymocytes (Fig. 1D), we generated mixed BM chimeric mice by reconstituting sublethally irradiated Rag2$^{-/-}$ γc$^{-/-}$ mice with a 1:1 mixture of wild-type (B6SJL) CD45.1 and *cd69*$^{-/-}$ CD45.2 BM hematopoietic stem cells from either Foxp3 reporter (Fig. 3C) or nonreporter (see Fig. S4A in the supplemental material) mice. Thymuses, spleens, lymph nodes, and blood were harvested starting from 8 to 10 weeks after transfer. CD4^{+} Foxp3^{+} Treg cells generated from *cd69*$^{+/+}$ and *cd69*$^{-/-}$ precursors were analyzed separately (Fig. 3D; Fig. S4B and S5). We detected a marked difference in the frequencies of CD4^{+} Foxp3^{+} tTreg cells and pTreg cells originating from the two precursors in both models, with a lower proportion of Treg cells being derived from *cd69*$^{-/-}$ CD45.2 CD4^{+} SP precursors than from *cd69*$^{+/+}$ CD45.1 precursors (Fig. 3D and E; Fig. S4C and S5A to C); this occurred even though CD4^{+} SP cells originated from both precursors in equal proportions in the thymuses (Fig. 3E), spleens (Fig. S5A), and lymph nodes (Fig. S5B). These data indicate that *cd69*$^{+/+}$ BM hematopoietic stem cells are necessary for the generation of CD4^{+} Foxp3^{+} tTreg cells and, subsequently, pTreg cell homeostasis. Our data are consistent with the finding that Treg cell precursors in the human thymus form part of the CD69^{+} thymocyte cell subset (11).

CD69 deficiency impairs STAT5 signaling and BIC/miR-155-dependent tTreg cell differentiation. To investigate the mechanism of CD69-modulated tTreg cell development, we examined the STAT5 pathway that stimulates the *foxp3* promoter, inducing tTreg cell development (4). Sorted Foxp3-mRFP^{+}-CD69^{+} and -CD69^{-} Treg cells from wild-type reporter mice (see Fig. S6 in the supplemental material) were analyzed by intracellular staining and Western blotting. The analyses showed dimin-

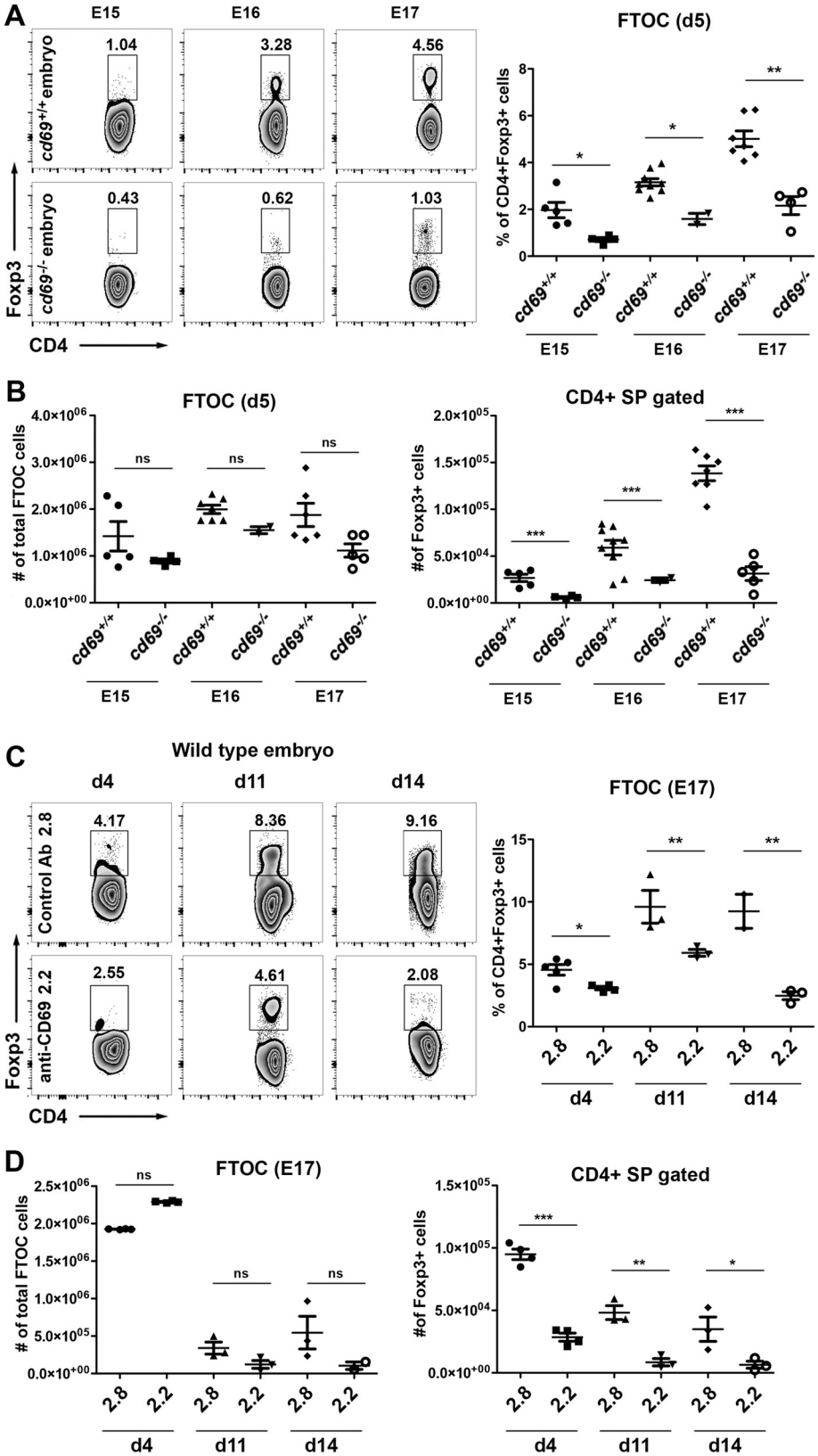

FIG 2 tTreg cell differentiation in fetal thymus organ culture requires CD69 expression. (A) Representative density plots of 5-day FTOCs from *cd69*$^{+/+}$ and *cd69*$^{-/-}$ embryos in the C57BL/6 background. Embryonic thymuses were removed from 15- to 17-day-old embryos, and the percentages of tTreg development in the lobes were determined by FACS analysis. (B) Cellularity of fetal thymus lobes (left) and total cell numbers of CD4^{+} Foxp3^{+} cells (right) from *cd69*$^{+/+}$ and *cd69*$^{-/-}$ embryos. (C) FTOCs from wild-type 17-day-old embryos

(Continued on next page)

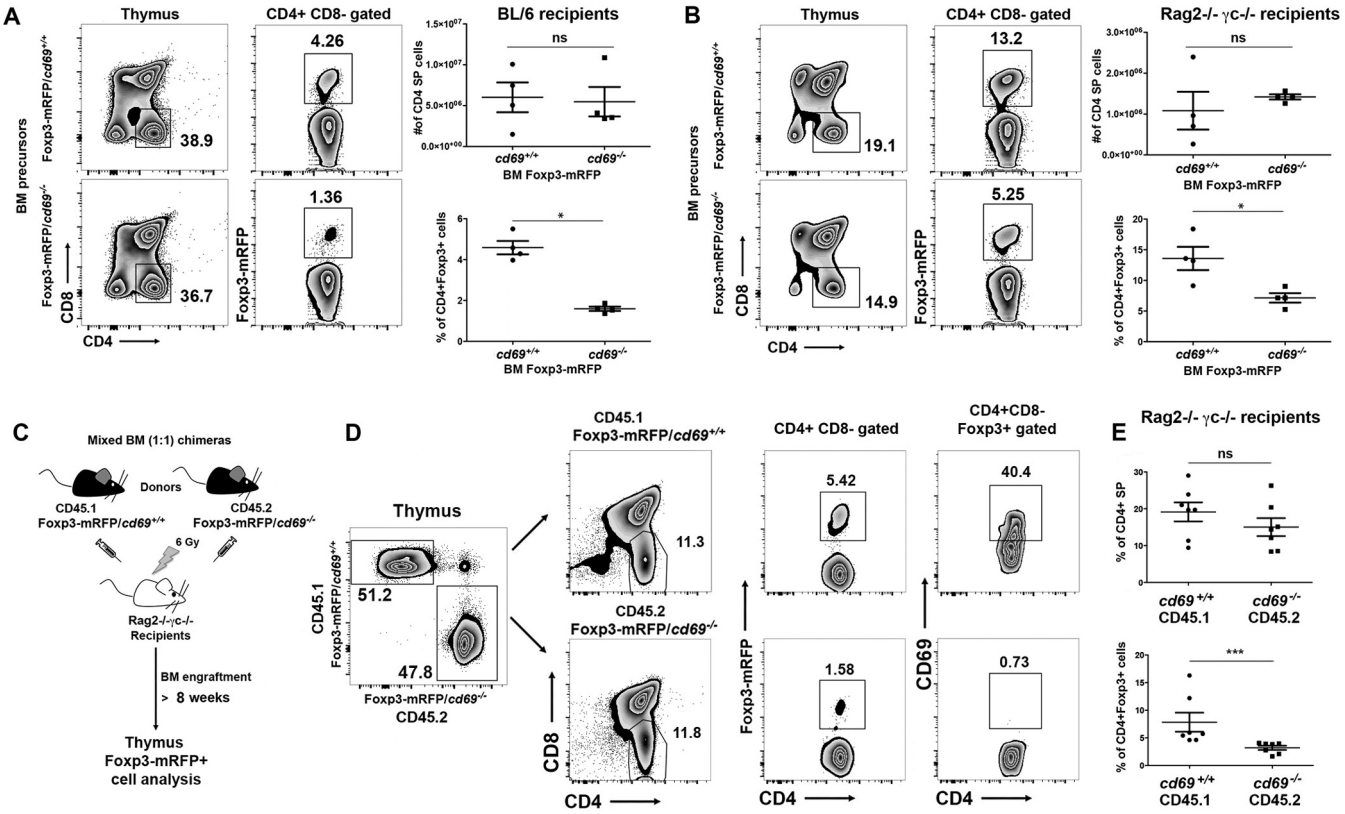

FIG 3 CD69$^+$ hematopoietic stem cells are more prone to developing tTreg cells after reconstitution. (A and B) Eight- to twelve-week-old C57BL/6 (A) or Rag2$^{-/-}$ γc$^{-/-}$ (B) recipient mice received two or one split dose of 6.5 Gy gamma radiation, respectively, and were i.v. injected with bone marrow cells from Foxp3-mRFP/*cd69*$^{+/+}$ or Foxp3-mRFP/*cd69*$^{-/-}$ littermates. (C) In mixed chimeras, irradiated Rag2$^{-/-}$ γc$^{-/-}$ recipients were transplanted with a mixture of CD45.1-Foxp3-mRFP/*cd69*$^{+/+}$ or CD45.2-Foxp3-mRFP/*cd69*$^{-/-}$ bone marrow precursors at a ratio of 1:1. (D) After at least 10 weeks, the contributions of the different donor bone marrow precursors to tTreg cell development and CD69 expression in tTreg cells were determined by FACS analysis. (E) Percentages of gated CD4$^+$ SP cells and CD4$^+$ CD8$^-$ Foxp3$^+$ tTreg cells within CD45.1 or CD45.2 donors in the thymus. All data are representative of results from at least 3 independent experiments with at least 3 recipient mice per group or 6 recipient mice for mixed chimeras. Error bars show standard deviations. *, $P < 0.05$; **, $P < 0.01$; ***, $P < 0.001$ (Student's *t* test).

ished STAT5 phosphorylation in sorted CD69$^-$ tTreg cells in steady state (Fig. 4A and B), indicating that CD69 expression maintains STAT5 bystander activation of tTreg cells within the thymus. The analysis of sorted pTreg cells in the spleen confirmed diminished STAT5 phosphorylation in secondary lymphoid organs (Fig. S7A). Although we detected no differences in Foxp3 activation or expression between CD69-expressing and nonexpressing tTreg cells (Fig. 1E and 4C) or pTreg cells (12), the transcriptional activation of *bic* was abrogated in CD69$^-$ tTreg cells, and consequently, miR-155 expression was inhibited in these cells (Fig. 4D) and pTreg cells (Fig. S7B). It has been reported that miR-155 inhibits the expression of SOCS-1, supporting Foxp3$^+$ tTreg cell development (6). Importantly, expression levels of both the *socs-1* gene and protein were upregulated in CD69$^-$ tTreg cells (Fig. 4E and F) and pTreg cells (Fig. S7B), which had very low levels of miR-155. Moreover, we analyzed the STAT5 pathway in sorted tTreg cells from *cd69*$^{+/+}$, *cd69*$^{+/-}$, and *cd69*$^{-/-}$ Foxp3-mRFP reporter mice. STAT5 phosphorylation is partially inhibited in *cd69*$^{+/-}$ compared to *cd69*$^{-/-}$ tTreg cells,

FIG 2 Legend (Continued)
(E17) were maintained for up to 14 days in culture in the presence of anti-CD69 monoclonal antibody (2.2) or the isotype control antibody (2.8). Density plots shows the percentages of tTreg cells on days 4, 11, and 14 after culture. (D) Cellularity of fetal thymus lobes (left) and total numbers of CD4$^+$ Foxp3$^+$ cells (right) under each condition. Totals of 31 and 36 embryos from five *cd69*$^{+/+}$ and four *cd69*$^{-/-}$ females, respectively, were analyzed. The 2 lobes from each fetal thymus were analyzed separately. Error bars show standard deviations. Values were calculated relative to data for *cd69*$^{+/+}$ control lobes from four independent FTOC assays. *, $P < 0.05$; **, $P < 0.01$; ***, $P < 0.001$ (Student's *t* test).

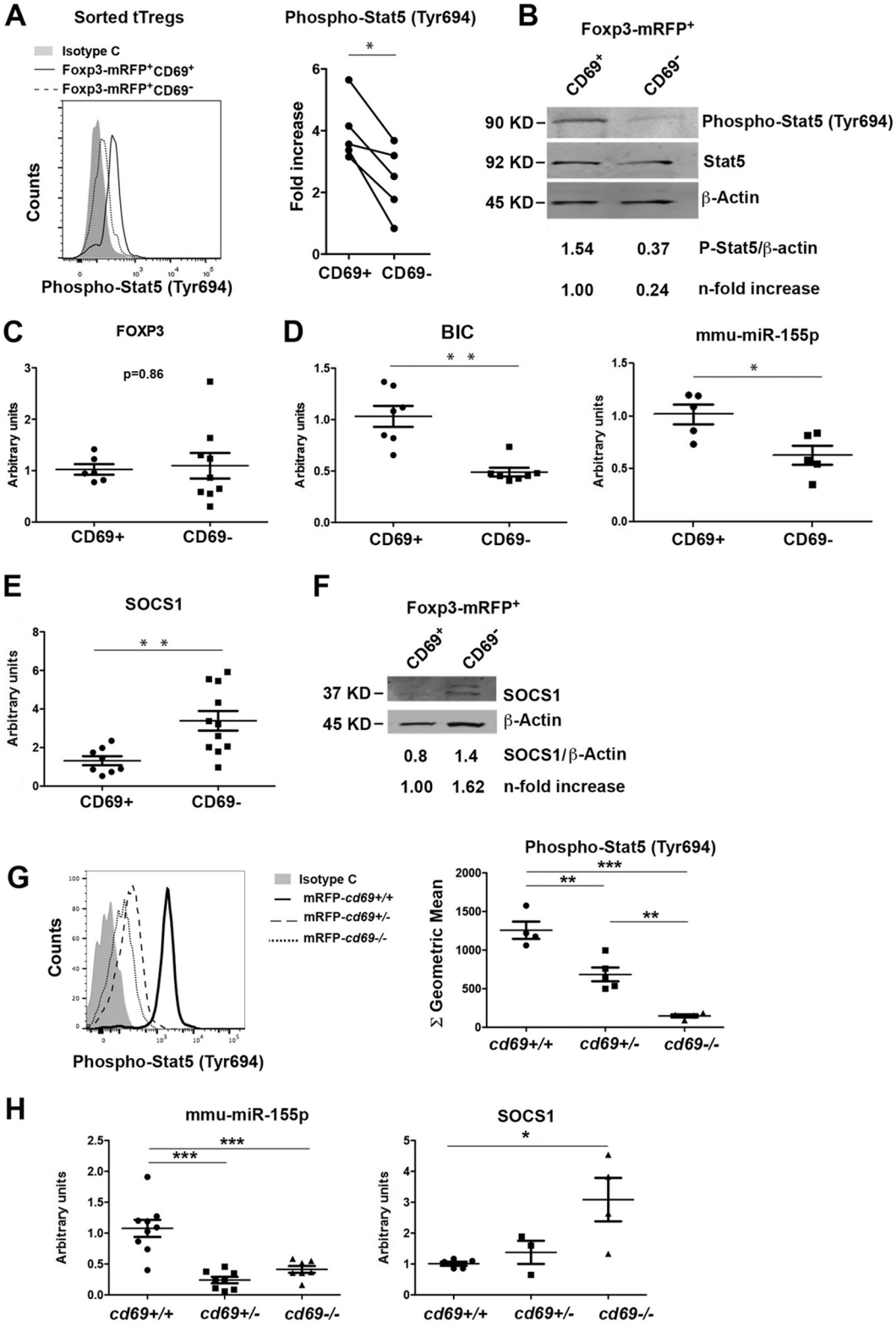

FIG 4 Expression of miR-155 and target proteins in CD69-deficient and -proficient Treg cells. (A, left) Representative histogram showing the levels of STAT5 phosphorylation determined by FACS analysis in sorted CD69$^+$ or CD69$^-$ tTreg cells. (Right) Levels of STAT5 phosphorylation shown as fold differences compared with isotype control-treated cells. Lines link measurements of CD69$^+$ and CD69$^-$ tTreg cells from the same mouse. (B) Representative Western blot showing the levels of STAT5 phosphorylation in tTreg cells sorted as described above for panel A. Phosphorylation levels are normalized to STAT5 and β-actin total protein levels. (C to E) qPCR analysis of the relative expression levels of Foxp3 (C), the BIC promoter, mmu-miR-155 (D), and *socs-1* (E) in CD69$^+$ and CD69$^-$ tTreg cells. Expression was normalized to the levels in CD69$^+$ tTreg cells. (F) Representative Western blot of SOCS-1 protein expression in sorted CD69$^+$ and CD69$^-$ Foxp3-mRFP$^+$ tTreg cells. SOCS-1 levels

(Continued on next page)

which almost abrogated the pathway (Fig. 4G). Thus, *cd69*$^{+/-}$ and *cd69*$^{-/-}$ tTreg cells have very low levels of miR-155 compared to those of *cd69*$^{+/+}$ cells. Accordingly, the *socs-1* gene is modestly and strongly upregulated in *cd69*$^{+/-}$ and *cd69*$^{-/-}$ tTreg cells, respectively (Fig. 4H). Our data suggest that the loss of at least one *cd69* allele modifies at least in part the expression of the receptor on the membrane (Fig. 1A and B) but is sufficient to fully prevent the activation of the STAT5 pathway, miR-155 transcription, SOCS-1 inhibition, and the proper differentiation of tTreg cells.

The overexpression of SOCS-1 regulates STAT5 signaling, reducing the proportions of tTreg cells in *cd69*$^{-/-}$ mice to levels similar to those in *mirn155*$^{-/-}$ mice (6). We analyzed the CD69^{+}/CD69^{-} ratio within tTreg and pTreg cells from *mirn155*$^{-/-}$ mice (Fig. 5A and C). Consistent with data from previous work, *mirn155*$^{-/-}$ mice display impaired numbers of tTreg cells and pTreg cells as well as an important reduction in the development of CD69^{+} Treg cells in both thymuses (Fig. 5A) and spleens (Fig. 5C). Interestingly, *cd69* gene expression was almost abrogated in the thymuses of *mirn155*$^{-/-}$ mice (Fig. 5B), suggesting that *cd69* and *mirn155* could have common regulation pathways.

In agreement, we found that *cd69*$^{+/-}$ and *cd69*$^{-/-}$ thymic precursors are less able to differentiate toward tTreg cells than are CD69-proficient precursors in the same mice (Fig. 1F and 3E). These data thus strongly suggest that the maintenance of miR-155 expression in tTreg cells is dependent on CD69-induced STAT5 phosphorylation, reflecting a unique property of CD69 in the development of tTreg cells.

Signaling of both IL-2 receptor γ (IL-2Rγ) and CD69 is required for the development of *in vitro*-inducible CD25^{+} Treg cells. To further explore the nonredundant role of CD69 in the development of iTreg cells, we analyzed the levels of Foxp3 in the absence of Jak3-STAT5 signaling. We cultured naive CD4 T cells under Treg-skewed conditions with transforming growth factor β (TGF-β) plus IL-2 in the presence of antigen-presenting cells. The use of Jak3 chemical inhibitors decreased STAT5 phosphorylation in *cd69*$^{+/+}$ iTreg cells to *cd69*$^{-/-}$ iTreg cell levels (Fig. 6A); however, the percentages of Foxp3-mRFP^{+} cells are comparable for both genotypes, even high in *cd69*$^{-/-}$ Treg cell cultures and independently of Jak-STAT5 inhibition (Fig. 6B), indicating that the Jak3-STAT5 signaling pathway is not required for Foxp3 expression of inducible Treg cells, corroborating the above-described data for tTreg cells (Fig. 4C).

It has been described that Foxp3 expression is dependent on IL-2Rγc; thus, *Il2r*$\gamma^{-/-}$ mice had no detectable Foxp3^{+} cells in thymus or spleen (18). However, the expression of CD25^{+} Treg cells is detectable in thymus and spleen of these mice (18). We aimed to address the role of CD69 in the development of CD25^{+} iTreg cells in the absence of IL-2Rγ/Foxp3 signaling pathways. For this purpose, we generated *Il2r*$\gamma^{-/-}$/*cd69*$^{-/-}$ double-knockout mice. We analyzed the levels of CD25^{+} iTreg cells after induction with TGF-β plus IL-2 in the presence of Jak3 inhibitors in cells from *Il2r*$\gamma^{-/-}$ mice compared to *Il2r*$\gamma^{-/-}$/*cd69*$^{-/-}$ mice. Jak3 inhibition decreased STAT5 phosphorylation in *Il2r*$\gamma^{-/-}$ iTreg cells to the levels in *Il2r*$\gamma^{-/-}$/*cd69*$^{-/-}$ Treg cells (Fig. 6C). Interestingly, the differentiation of CD25^{+} iTreg cells is completely abolished in both *Il2r*$\gamma^{-/-}$/*cd69*$^{-/-}$ iTreg cells and *Il2r*$\gamma^{-/-}$ iTreg cells plus Jak3 inhibitors (Fig. 6D). These data indicate that in the absence of the IL-2Rγ/Foxp3 pathway, CD69-induced Jak3-STAT5 activation is pivotal for the development of CD25^{+} iTreg cells.

It has been proposed that miR-155 could regulate different cell type functions depending on the biological context, and miR-155-mediated SOCS-1 repression regu-

FIG 4 Legend (Continued)

are normalized to mean β-actin levels from of at least 4 independent sortings. (G, left) Representative histogram showing the levels of STAT5 phosphorylation in sorted tTreg cells from *cd69*$^{+/+}$, *cd69*$^{+/-}$, and *cd69*$^{-/-}$ Foxp3 reporter mice. (Right) Quantification of STAT5 phosphorylation levels shown as geometric mean fluorescence intensities. (H) mmu-miR-155 and *socs-1* transcriptional levels analyzed by qPCR in tTreg cells from *cd69*$^{+/+}$, *cd69*$^{+/-}$, and *cd69*$^{-/-}$ Foxp3 reporter mice. All data are derived from at least 5 independent sortings/experiments (3 animals per sorting). For panels A to E, data were analyzed by a *t* test, except for Western blot analyses, for which representative gels are shown. Error bars show standard deviations. **, $P < 0.01$; ***, $P < 0.001$ (Student's *t* test). For panels G and H, data were analyzed by ANOVA followed by Bonferroni's multiple-comparison test. *, $P < 0.05$; **, $P < 0.01$; ***, $P < 0.001$.

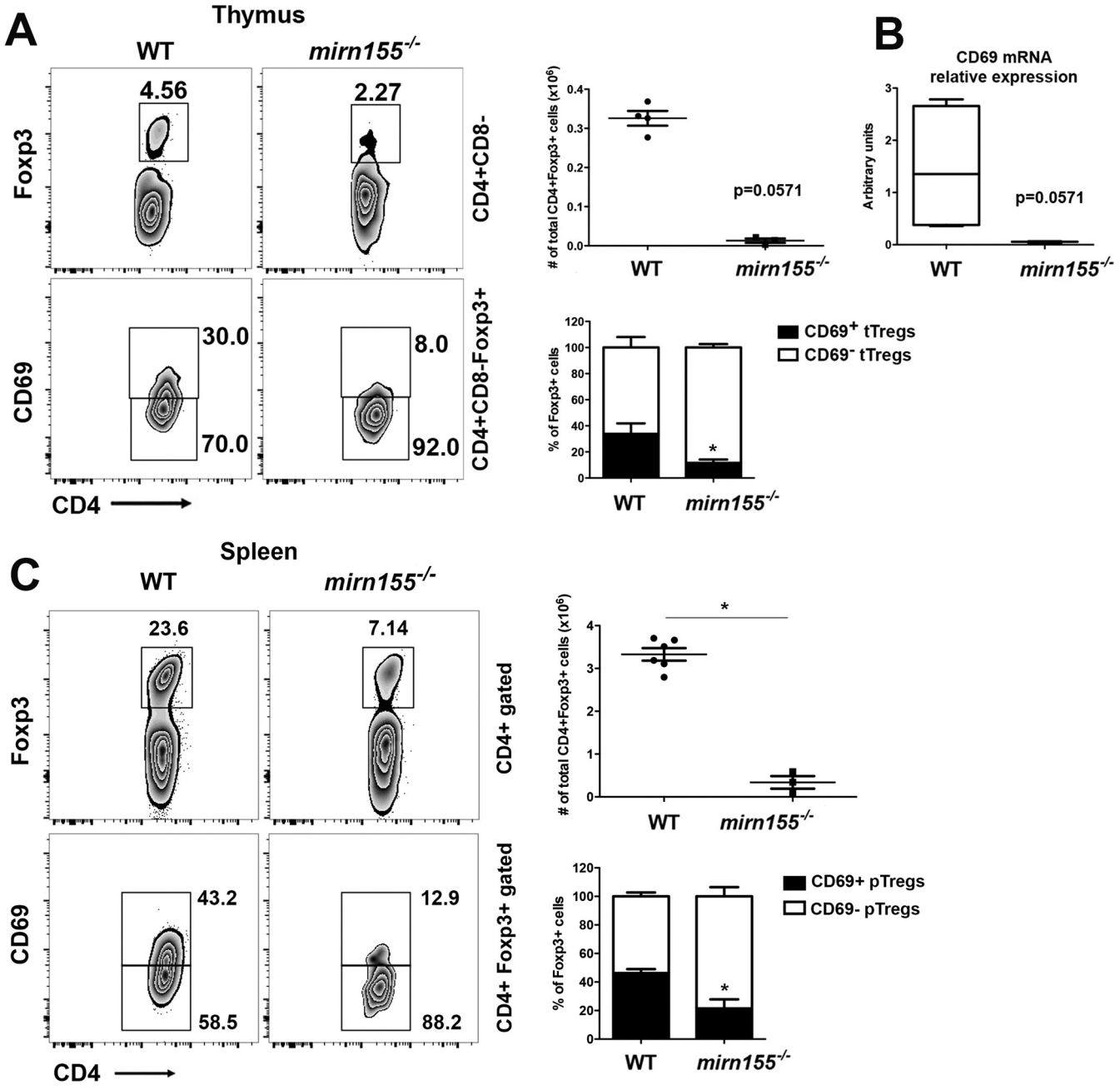

FIG 5 CD69$^+$ Treg cell development is impaired in the thymus and spleen of *mirn155*$^{-/-}$ mice. (A and C) Density plots showing CD4$^+$ CD8$^-$ Foxp3$^+$ tTreg cells and CD69 expression in gated CD4$^+$ CD8$^-$ Foxp3$^+$ thymocytes (A) or splenocytes (C) from wild-type (WT) or *mirn155*$^{-/-}$ mice. Numbers indicate the proportions (percentages) of gated cells. Bar charts show total cell numbers of gated CD4$^+$ CD8$^-$ Foxp3$^+$ tTreg cells (top) and percentages (±standard deviations) of CD69$^+$ and CD69$^-$ tTreg cells (bottom) within thymuses from wild-type or *mirn155*$^{-/-}$ mice. (B) Relative expression levels of *cd69* in thymocytes from wild-type or *mirn155*$^{-/-}$ mice analyzed by qPCR. All data are derived from 5 wild-type mice and 3 *mirn155*$^{-/-}$ mice. Data were analyzed by a *t* test. Error bars show standard deviations. *, $P < 0.05$ (Student's *t* test).

lates the competitive fitness of Treg cells (19). We analyzed the expression of *mir-155*, *socs-1*, *T-bet*, and *Eomes* in order to investigate if other miR-155 target genes are affected in iTreg cell differentiation in the absence of Jak3-STAT5 signaling pathway activation through CD69. We observed a diminished expression of miR-155 in *cd69*$^{-/-}$ compared to *cd69*$^{+/+}$ iTreg cells (see Fig. S8A in the supplemental material), as in *ex vivo* CD69$^-$ thymus-derived Treg cells (Fig. 4D and G). However, Jak3 inhibition does not contribute to miR-155 inhibition (Fig. S8A), suggesting that other signaling pathways could contribute to miR-155 regulation in iTreg cells. Moreover, *socs-1* expression

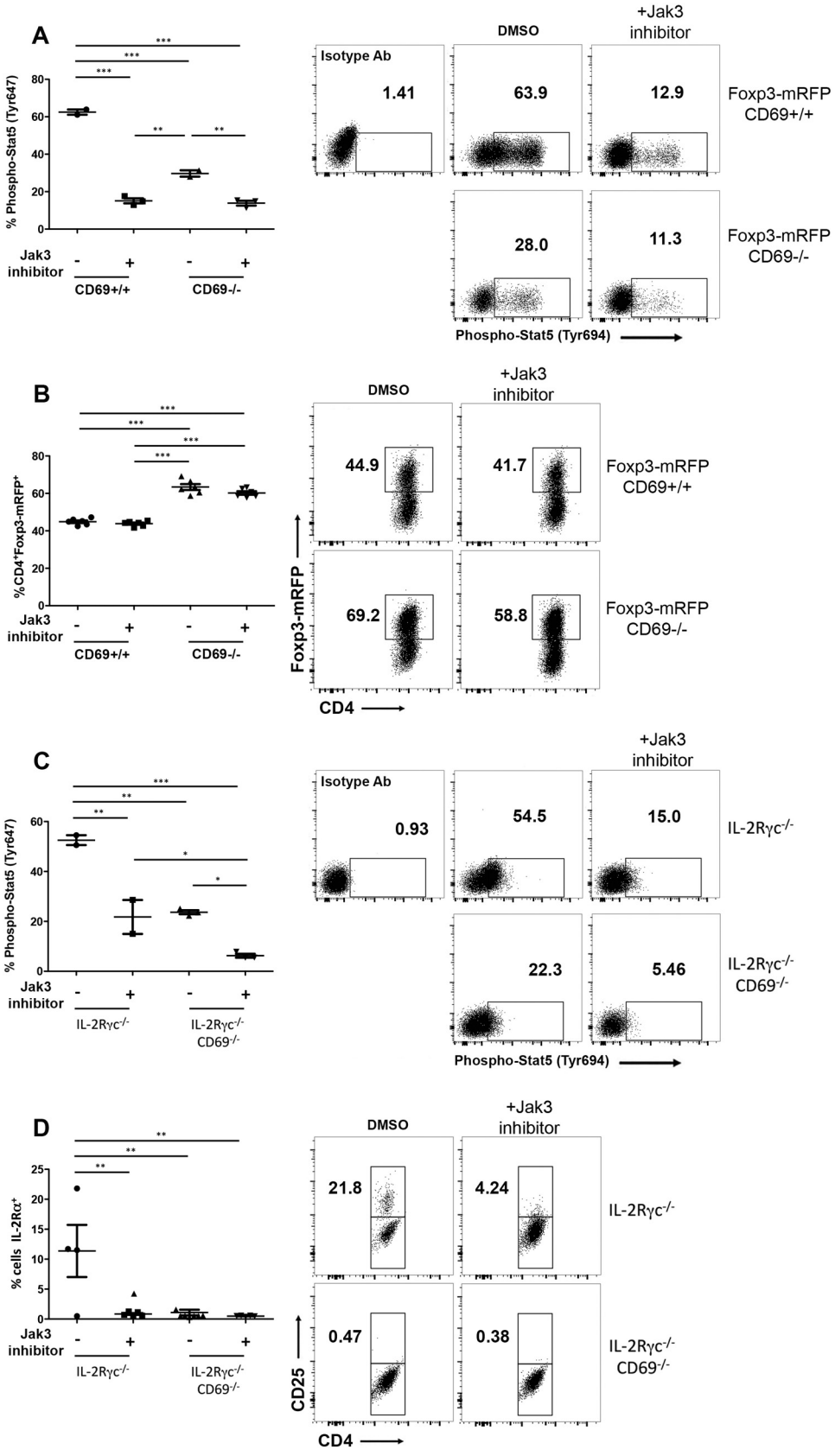

FIG 6 CD69 expression rescues iTreg cell differentiation in the absence of the IL-2Rγc/Foxp3 signaling pathway. (A) Naive CD4$^+$ T cells from Foxp3-mRFP/*cd69*$^{+/+}$ or Foxp3-mRFP/*cd69*$^{-/-}$ littermates were cultured for 72 h under Treg-skewed conditions and treated with a chemical Jak3 inhibitor or an equal concentration of dimethyl sulfoxide

(Continued on next page)

is strongly induced in *cd69*$^{-/-}$ iTreg cells compared to *cd69*$^{+/+}$ iTreg cells (Fig. S8B), but the expression of other miR-155 target genes such as *T-bet* and *Eomes* is not (Fig. S8C). Interestingly, Jak3 inhibits the expression of *socs-1*, *T-bet*, and *Eomes* in the absence of CD69 (Fig. S8B and C), supporting the hypothesis that other CD69-dependent mechanisms could be involved in the regulation of these target genes. Altogether, these data suggest that CD69 controls *socs-1* expression and Treg cell differentiation through miR-155 regulation, although other molecules could be involved in this process.

Expression levels of miR-155 and CD69 are coregulated in a positive-feedback loop. CD69 and BIC/miR-155 promoter sequences have two putative STAT5 binding elements upstream of the TATA box and AP-1 element (20) (see Fig. S9 in the supplemental material). Moreover, the transcription factor AP-1, highly induced after TCR stimulation, regulates the activation of both promoters (20, 21), suggesting that both promoters might be concomitantly activated, in a positive-feedback loop, by the same TCR/CD3-triggered pathway (Fig. S9). To test this hypothesis, we next investigated whether CD69 downstream signaling regulates miR-155 expression in tTreg cells. Sorted Foxp3^{+} tTreg cells from Foxp3-mRFP/*cd69*$^{+/+}$ mice, expressing CD69 at steady state, were incubated with anti-CD69 antibody (2.2), which downregulates CD69 membrane expression and dampens its signaling (22) (Fig. 7A). As described above, we observed strong CD69 dampening on the membrane compared with that in cells incubated with control mouse IgG1 MAb (2.8) (Fig. 7A). Quantitative PCR (qPCR) analysis revealed decreased miR-155 expression in 2.2-treated CD69^{+} tTreg cells (Fig. 7B), to levels comparable to those in CD69^{-} or *cd69*$^{-/-}$ tTreg cells (Fig. 7B and 4D and H). Moreover, CD69 blockade with 2.2 Abs impairs STAT5 phosphorylation (Fig. 7C) and prevents SOCS-1 inhibition (Fig. 7D), meaning that CD69 expression is necessary for the miR-155-dependent inhibition of SOCS-1 and the bona fide formation of tTreg cells.

To verify whether these findings could be extended to human cells, activated CD4^{+} CD25^{+} peripheral blood lymphocytes (PBLs) were infected with lentiviruses (LVs) carrying different short hairpin RNA (shRNA) sequences targeting CD69 (shCD69-1 to -3). Endogenous levels of membrane CD69 and hsa-miR-155 were analyzed by fluorescence-activated cell sorter (FACS) analysis and qPCR, respectively (Fig. 8A and B). LV infection of PBLs with three shCD69 sequences fully inhibited CD69 expression compared to mock LV infection (Fig. 8A), inducing the loss of hsa-miR-155 transcription (Fig. 8B). Our data indicate that human CD69 and hsa-miR-155 are regulated together as in mouse cells. In parallel, we induced the expression of CD69 *in vitro* (Fig. 8C) to corroborate that the STAT5 pathway and hsa-miR-155 are activated together with the receptor, whereas SOCS-1 is inhibited (Fig. 8D).

To test this mechanism functionally, we performed loss- and gain-of-function assays by transfecting human Treg cells with anti-hsa-miR-155 or hsa-pre-miR-155. First, we transfected control and anti-CD3 (OKT3)-stimulated CD4^{+} CD25^{+} human PBLs with anti-hsa-miR-155-5p or scrambled anti-miRNA (Fig. 8E). CD69 expression in activated PBLs dropped dramatically after the inhibition of hsa-miR-155 (Fig. 8F). Moreover, STAT5 activation was reduced, and in agreement, *socs-1* gene expression was enhanced, indicating that miR-155 blockade regulates the CD69 signaling pathway. In contrast, the overexpression of hsa-miR-155 in CD69^{-} Treg cells (Fig. 8G) revealed significant increases in the expression of CD69, STAT5 activation, and *socs-1* inhibition (Fig. 8H). Thus, the reciprocal modulation of the C-type lectin and miR-155 in a positive-feedback loop could be pivotal to maintaining tTreg cell fitness and pTreg cell homeostasis.

FIG 6 Legend (Continued)

(DMSO) for the last 9 h. The percentages of phospho-STAT5^{+} cells and the levels of STAT5 phosphorylation determined by FACS analysis and compared to an isotype Ab are shown. (B) Quantification of reporter Foxp3-mRFP^{+} cells treated as described above for panel A. (C) Naive CD4^{+} T cells from *Il2rγ*$^{-/-}$/*cd69*$^{-/-}$ and *Il2rγ*$^{-/-}$ mice were cultured as described above for panel A, and the percentages of phospho-STAT5^{+} cells and the levels of STAT5 phosphorylation were determined by FACS analysis. (D) Quantification of CD25^{+} Treg cells by FACS analysis. Data are from two independent experiments ($n = 3$ for each genotype). Error bars show standard deviations. Data were evaluated by ANOVA followed by Bonferroni's multiple-comparison test. *, $P < 0.05$; **, $P < 0.01$; ***, $P < 0.001$.

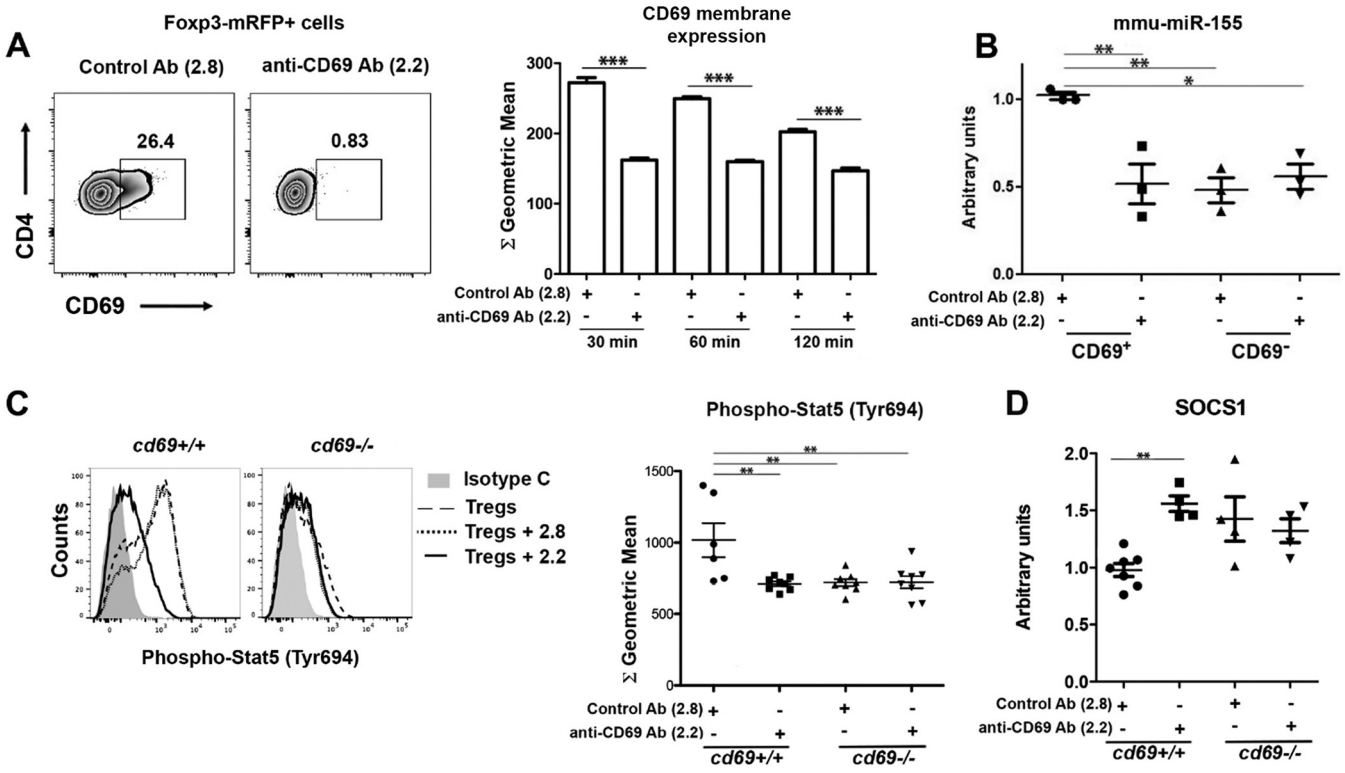

FIG 7 CD69 downstream signaling regulates miR-155, STAT5, and *socs-1* expression in Treg cells. (A, left) Representative plots of CD69 expression in sorted mouse Foxp3-mRFP/*cd69*$^{+/+}$ tTreg cells treated with anti-CD69 Ab 2.2 or the 2.8 isotype control antibody. (Right) CD69 expression after Ab treatment determined by FACS analysis. Bars correspond to the means ± standard deviations of data from one representative experiment of four. (B) qPCR analysis of mmu-miR-155 expression in sorted CD69^{+} or CD69^{-} Foxp3-mRFP^{+} tTreg cells after Ab treatment. Results are normalized by sno135 snRNA expression, and expression is relative to that in 2.8-treated CD69^{+} cells. (C, left) Representative histogram showing the levels of STAT5 phosphorylation in iTreg cells from *cd69*$^{+/+}$ or *cd69*$^{-/-}$ reporter mice treated with anti-CD69 Ab 2.2 or the 2.8 isotype control Ab. (Right) Quantification of STAT5 phosphorylation levels shown as geometric mean fluorescence intensities. (D) *socs-1* transcriptional levels analyzed by qPCR. Data shown in panels A and B are derived from 3 independent sortings/experiments (3 animals per sorting), and data shown in panels C and D are iTreg cells differentiated from at least 4 mice per group. Data were analyzed by 1-way ANOVA and Bonferroni's posttest (B). CD69 expression after Ab treatment was analyzed by a *t* test (A). *, $P < 0.05$; **, $P < 0.01$; ***, $P < 0.001$ (Student's *t* test).

DISCUSSION

In this study, we have shown that the C-type lectin CD69 plays a key role in the development and homeostasis of Treg cells. Using a combined genetic model of Foxp3 reporter and *cd69* knockout mice and genetic inhibition approaches, we unequivocally demonstrate that the activation of the CD69 pathway promotes STAT5 phosphorylation, BIC/miR-155 expression, and SOCS-1 inhibition. The role of CD69 as a negative regulator of the immune system has remained a controversial issue during the last years (23). However, very recent studies by independent groups show that CD69 plays a crucial role in the suppressor function of mouse and human Treg cells as well as in the generation of *in vitro*-induced Treg cells (12, 16, 24–26). Nevertheless, the specific role of the C-type lectin in the development of Treg cells in the thymus remains elusive.

A major issue that has limited this study has been the key role of CD69 in the egress of lymphocytes from lymphoid organs and in particular from the thymus to the periphery (13, 14, 27–29). Although thymic positive and negative T cell selection processes are unaffected by CD69 deficiency (30), CD69 controls the egress of mature T cells into the periphery via corticomedullary blood vessels, through the negative regulation of $S1P_1$ receptors (27, 28), making it not an easy task to study its role in the development of Treg cells in the thymus. With the help of Foxp3 reporter mice, we have performed studies of tTreg cell differentiation in FTOC and in mixed chimeric mice to avoid the effects derived from the different migratory potentials of CD69^{+} and CD69^{-} cells. We demonstrate that the expression of the C-type lectin CD69 is pivotal for the development of tTreg cells, as they are virtually absent in FTOCs from *cd69*$^{-/-}$

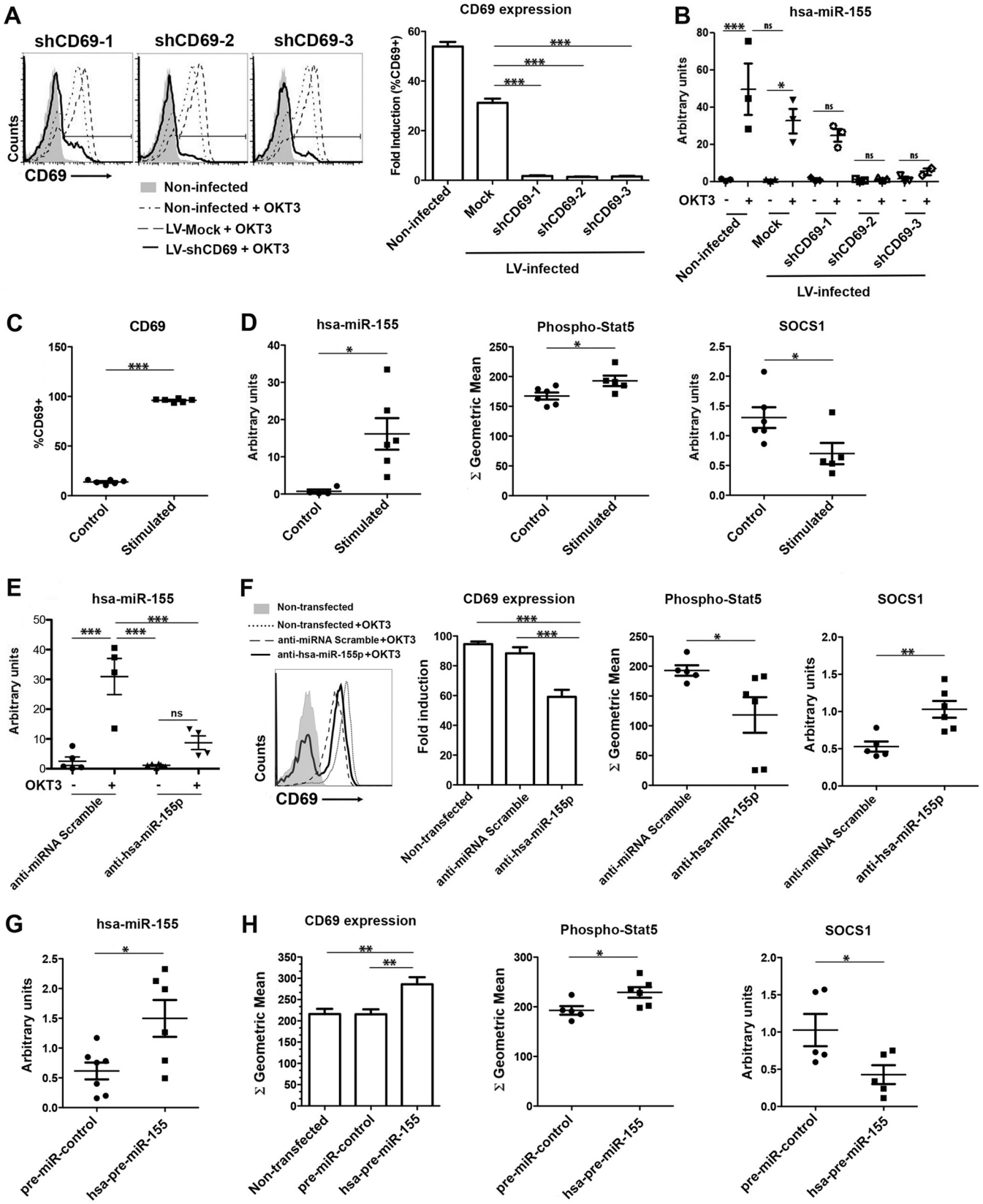

FIG 8 Coregulation of CD69 and miR-155 expression in human Treg cells. (A, left) Representative histograms of CD69 expression after LV infection with 3 different shCD69 sequences (shCD691 to -3) or an shRNA control sequence, stimulated with human anti-CD3 Abs (OKT3 clone) or not stimulated. (Right) Fold CD69 induction relative to values for nonstimulated cells. (B) qPCR analysis of hsa-miR-155 expression in human $CD4^+$ T cells after LV infection. (C and D) Human PBLs were stimulated with PMA-ionomycin for 4 h or not stimulated, and the percentages of $CD69^+$ cells (C) and phospho-STAT5 (D) were determined by FACS

(Continued on next page)

or anti-CD69-treated embryonic thymuses or in mixed bone marrow chimeras from *cd69*$^{-/-}$ precursors. In both systems, total numbers of cells within the thymus do not change, whereas tTreg cell proportions originating from CD69^{-} precursors are consistently diminished, demonstrating unequivocally that this effect is not due to a different migratory behavior.

We have found that proportions of Foxp3^{+} pTreg cells are also diminished after analysis of spleen and lymph nodes from adult Foxp3-mRFP/*cd69*$^{-/-}$ reporter mice compared to *cd69*$^{+/+}$ and *cd69*$^{+/-}$ littermates. In addition, CD69-deficient pTreg cells have a defective suppressive function (12). Thus, defects observed in CD69-deficient precursors affect both tTreg cell development and pTreg cell homeostasis, strongly indicating that CD69-proficient precursors give rise to the CD69^{+} functionally active pTreg cell subset. In this regard, two different genetic approaches in mice and a recent study in humans indicate that CD69 expression in pTreg cells is required to maintain immunological tolerance. CD69 deficiency in mice compromises T cell-induced colitis and the establishment of oral tolerance after antigen challenge *in vivo* (24), and CD69^{+} pTreg cells are essential for the prevention of asthmatic reactions to harmless antigens (12). Furthermore, a subset of CD69^{+} Treg cells in the blood of healthy human donors seems to have a relevant immune-regulatory role (25).

The C-type lectin CD69 interacts with Jak3/STAT5 proteins independently of the IL-2 pathway, thus inhibiting Th17 responses (31) and controlling the suppressor potential of pTreg cells (12). STAT5 phosphorylation stimulates the *foxp3* promoter, inducing tTreg cell development (4), and Foxp3 binds to an intron within the promoter region of the miR-155 host gene *bic* in Treg cells (32). Both *mirn155*$^{-/-}$ and *bic*$^{-/-}$ mice have below-normal numbers of Foxp3^{+} Treg cells in thymuses and secondary lymphoid organs, indicating an essential role for miR-155 in the development of Foxp3^{+} Treg cells (5, 6). We have explored if this pathway could be the responsible for the defects observed in Treg cell development in *cd69*-deficient mice, finding a strong inhibition of STAT5 phosphorylation in freshly isolated Foxp3-mRFP^{+}-CD69^{-} compared to Foxp3-mRFP^{+}-CD69^{+} tTreg cells. Moreover, the transcriptional level of *bic*/miR-155 is reduced in Foxp3-mRFP^{+}-CD69^{-} Treg cells, and consequently, its target SOCS-1 is upregulated at both the mRNA and protein levels. In a mouse model of SOCS-1 overexpression, negative regulation of STAT5 signaling reduces the proportion of Foxp3^{+} thymocytes to levels similar to those seen in *mirn155*$^{-/-}$ mice (6). miR-155 inhibits SOCS-1 expression, enhancing Foxp3^{+} tTreg cell development (6). Our data demonstrate that CD69 expression enhanced BIC/miR-155 transcription, inhibited SOCS-1, and therefore maintained Treg cell differentiation and the fitness of Treg cells. However, IL-2R signaling also activates the Jak/STAT5 pathway in Treg cells; specifically, Foxp3 expression is dependent on IL-2Rγc signaling, as *Il2r*$\gamma^{-/-}$ mice have no detectable Foxp3^{+} cells, although a small proportion of CD25^{+} Treg cells is still detectable in these mice (18). Our study shows that the differentiation of CD25^{+} iTreg cells is inhibited in *Il2r*$\gamma^{-/-}$ cultures plus Jak3 inhibitors or *Il2r*$\gamma^{-/-}$/*cd69*$^{-/-}$ mice, indicating that Jak3-STAT5 signaling pathway activation through CD69 is essential for the development of Treg cells.

CD69 does not appear as an miR-155 target in the PicTar, Targetscan, or miRanda miRNA target prediction database, and there are no miR-155 target sequences in the CD69 3′ untranslated region (UTR) (33). However, several studies have shown a correlation between Dicer, a member of the RNase III complex that processes pre-miRNAs into mature miRNAs, miR-155 regulation, and CD69 expression. Treg cells from MRL/lpr

FIG 8 Legend (Continued)

analysis. (D) hsa-miR-155 and human *socs-1* gene expression levels were analyzed by qPCR. (E) Human PBLs were transfected with anti-hsa-miR-155-5p or an anti-miRNA scramble control, and hsa-miR-155 expression was analyzed by qPCR. (F) Representative histograms and quantification of CD69 expression, STAT5 phosphorylation, and human *socs-1* transcription levels in CD4^{+} PBLs treated as described above for panel E. (G) Human PBLs were transfected with hsa-pre-miR-155-5p or the pre-miRNA control, and hsa-miR-155 expression was analyzed by qPCR. (H) CD69 expression, STAT5 phosphorylation, and human *socs-1* transcription in CD4^{+} PBLs treated as described above for panel G. Results from miRNA qPCRs are normalized to sno135 snRNA expression levels. All data are means ± standard deviations of results from at least 3 independent donors for a total of 10 donors. Data were analyzed by 1-way ANOVA and Bonferroni's posttest or by a *t* test. *, $P < 0.05$; **, $P < 0.01$; ***, $P < 0.001$.

mice are Dicer insufficient and yet overexpress miR-155 and show increased CD69 expression (9), suggesting that there are Dicer-alternative mechanisms for miRNA regulation. In another study, *Dicer*$^{-/-}$ TCs showed increased CD69 expression after TCR stimulation and, consequently, defective egress from lymphoid organs (10). As described above for CD69, Dicer plays a key role in tTreg cell differentiation (7) and Treg cell function (8). In this regard, CD69 is expressed in lymphocytes early after TCR/CD3 stimulation (34), and its cytoplasmic tail interacts with Jak3/STAT5 molecules (35), triggering this pathway in pTreg cells (12) and tTreg cells and therefore inhibiting SOCS-1 transcription and protein expression. Similarly, TCR-induced IL-2 signaling triggers STAT5 signaling and enhances Foxp3-dependent miR-155 expression, limiting SOCS-1 expression and promoting Treg cell homeostasis (6). Recent data show that microRNAs could regulate different cell type functions modulating different target genes, depending on the biological context (19). We analyzed the expression of miR-155 and SOCS-1 in the absence of Jak3-STAT5 signaling pathway activation through CD69 in the differentiation of iTreg cells. miR-155 expression is inhibited and SOCS-1 is upregulated in *cd69*$^{-/-}$ compared to *cd69*$^{+/+}$ iTreg cells; however, Jak3 inhibition does not contribute to miR-155 dampening, suggesting that other microRNAs and/or target genes could be involved. Interestingly, the STAT5 binding elements of the BIC/miR-155 and CD69 promoter sequences are similar, with each element containing two putative STAT binding elements upstream of the TATA box and AP-1 element (20). Moreover, the transcription factor AP-1, which is highly induced after TCR stimulation, regulates the activation of both promoters (20, 21). This suggests that both promoters might be concomitantly activated, in a positive-feedback loop, by the same TCR/CD3-triggered pathway.

Our present study shows that Foxp3-RFP/*cd69*$^{-/-}$ reporter mice have a dramatically reduced tTreg cell population in adult thymuses. Moreover, tTreg cells are unable to develop properly in FTOCs from *cd69*$^{-/-}$ or anti-CD69-treated embryonic thymuses or in mixed bone marrow chimeras from *cd69*$^{-/-}$ precursors. The *in vitro* data confirm that the phosphorylation of STAT5 is abrogated in CD69-deficient tTreg cells and results in the inhibition of the BIC/miR-155 pathway, increased SOCS-1 expression, and impaired tTreg cell development. Our previous studies show that the suppressor function of Treg cells is compromised in *cd69*-deficient mice (12), indicating that CD69 is a key molecule in the development of Foxp3$^+$ CD69$^+$ Treg cells in the thymus that will give rise to the functionally active subset of Treg cells in the periphery. Therefore, we postulated that the C-type lectin CD69 is a pivotal molecule for the maintenance of immune homeostasis in health and disease.

MATERIALS AND METHODS

Mice. *cd69*$^{-/-}$ mice were generated in the 129/Sv background as described previously (31) and backcrossed onto the C57BL/6 strain for at least 12 generations. C57BL/6.Ly5.1 mice (CD45.1$^+$) were purchased from The Jackson Laboratory (B6.SJL-Ptprc^a Pepc^b/BoyJ, stock number 002014). Rag2$^{-/-}$ $\gamma c^{-/-}$ (Rag2/Il2rg) mice were provided by the laboratory of M. L. Toribio (Centro de Biología Molecular, CSIC, Spain) and were intercrossed with C57BL/6 mice to generate *Il2r*$\gamma^{-/-}$ mice, which were subsequently intercrossed with *cd69*$^{-/-}$ mice to generate *Il2r*$\gamma^{-/-}$/*cd69*$^{-/-}$ mice. FoxP3-mRFP reporter mice (FIR mice; C57BL/6 background) were generated and provided by the Flavell laboratory (Yale University School of Medicine, New Haven, CT) (36) and were intercrossed with *cd69*$^{-/-}$ mice to generate Foxp3-mRFP/*cd69*$^{+/+}$ wild-type, Foxp3-mRFP/*cd69*$^{+/-}$ heterozygous, and Foxp3-mRFP/*cd69*$^{-/-}$ *CD69*-deficient littermates. Animals were housed and used under specific-pathogen-free (SPF) conditions at the Centro Nacional de Investigaciones Cardiovasculares (CNIC) animal facility. *mirn155*$^{-/-}$ mice were provided by R. Nakagawa (The Francis Crick Institute, London, United Kingdom). All animal procedures were approved by the ethics committee of the Comunidad Autónoma de Madrid and conducted in accordance with the institutional guidelines that comply with European Institutes of Health directives (37).

Intracellular staining and FACS analysis. Single-cell suspensions were obtained from adult or fetal thymuses and incubated in FACS buffer (phosphate-buffered saline [PBS], 0.5% bovine serum albumin [BSA], 1 μM EDTA, 0.1% NaN_3) with fluorochrome-conjugated mouse-specific antibodies against CD4, CD8, CD69, CD45.1, and CD45.2. All antibodies were purchased from BD Biosciences. For Foxp3 intracellular staining, we used the Foxp3 staining kit (eBioscience). CD69$^+$- and CD69$^-$-Foxp3-mRFP$^+$ tTreg cells were sorted from Foxp3-mRFP/*cd69*$^{+/+}$ thymuses by using a FACSAria III instrument (BD Biosciences). For intracellular STAT5 staining, sorted tTreg cells were fixed with 0.2% paraformaldehyde and permeabilized with 90% methanol, and cells were incubated with anti-phospho-STAT5 (Tyr694) (Cell

Signaling), an Alexa Fluor 647-IgG1 isotype control, and Alexa Fluor 647–anti-phospho-STAT5 (pY694) (Becton Dickinson). Human PBLs were obtained after Ficoll separation from buffy coats and maintained in RPMI medium supplemented with 10% fetal calf serum (FCS), 20 mM HEPES, L-glutamine, antibiotics, nonessential amino acids, sodium pyruvate, and β-mercaptoethanol. Treated PBLs were incubated with fluorochrome-conjugated human-specific antibodies against CD4, CD25, and CD69 (BD Biosciences) and Foxp3 (Miltenyi Biotec). Cells were analyzed in an LSRFortessa flow cytometer (BD Biosciences) equipped with four lasers (405, 488, 561, and 640 nm), and the data were processed with FlowJo v10.0.4 (TreeStar).

Fetal thymus organ culture. Uteri were removed from female mice at the indicated gestational time points, and the embryos were placed into a petri dish with fresh cold PBS for the extraction of thymuses. To place the fetal thymus lobes in culture, we placed 0.8-μm nitrocellulose membrane filters (Millipore) on top of 12- to 7-mm Gelfoam sponges embedded in prewarmed Iscove´s modified Dulbecco´s medium (IMDM) (supplemented with 10% FCS, L-glutamine, antibiotics, and β-mercaptoethanol). FTOCs were maintained for 4 to 14 days, with medium being replaced every 3 days. An anti-CD69 monoclonal antibody (2.2) or the isotype control antibody (2.8) was added (50 μg/ml) to the culture medium as indicated and replaced every 3 days. At the end of the culture period, single-cell suspensions were prepared from the lobes, and cells were counted and analyzed by FACS analysis.

Western blotting. Lysates of sorted CD69$^+$- and CD69$^-$-Foxp3-mRFP$^+$ tTreg cells were prepared in PD buffer (40 mM Tris HCl [pH 8.0], 0.5 M NaCl, 6 mM EDTA, 6 mM EGTA, 0.1% NP-40) containing a protease inhibitor cocktail (Complete Mini; Roche). Proteins (20 μg) were size separated on 12% SDS-polyacrylamide gels and transferred onto Trans-Blot nitrocellulose membranes (Bio-Rad). Primary antibodies for immunoblotting were as follows: anti-β-actin, anti-SOCS-1, and anti-STAT5 (Santa Cruz) and anti-phospho-STAT5 (Cell Signaling). Quantitative assessment of protein expression was performed with the Odyssey scanner and analyzed with Image Studio Lite v4.0 Western blot analysis software (Li-Cor).

***In vitro* differentiation of Treg cells.** Inducible Treg cells were differentiated from Foxp3-mRFP/*cd69*$^{+/+}$, Foxp3-mRFP/*cd69*$^{-/-}$, *Il2rγ*$^{-/-}$/*cd69*$^{-/-}$, and *Il2rγ*$^{-/-}$ mice. Naive CD4 T cells from these mice were isolated and cocultured for 72 h with irradiated antigen-presenting cells in the presence of plate-bound anti-CD3 (2 μg/ml) and soluble anti-CD28 (2 μg/ml) plus recombinant TGF-β1 (10 ng/ml) and IL-2 (2 ng/ml). The last 9 h, the cells were incubated with or without Jak3 inhibitor I (catalog number CAS 202475-60-3; Calbiochem) (10 μg/ml). For experiments with inhibitor antibodies, after differentiation, Treg cells were cultured for 4 h with anti-2.2 Ab or the 2.8 isotype control Ab.

RNA extraction and gene expression analysis. RNA and microRNA were extracted from 2×10^4 to 6×10^4 sorted mouse tTreg cells or 10^6 human PBLs with the miRNeasy minikit (Qiagen), followed by DNase treatment with the Turbo DNase-free kit (Ambion). For analysis of SOCS-1, Foxp3, and BIC transcripts, reverse transcription was performed by using the High Capacity cDNA reverse transcription kit (Applied Biosystems). SOCS-1 and Foxp3 gene expression levels were analyzed by real-time PCR using SYBR green PCR mix (Applied Biosystems). Mouse and human *Gapdh* genes were used as the endogenous controls. The following primers were used to amplify murine genes: forward (F) primer 5′-CTGCG GTTCTATTGGGGAC-3′ and reverse (R) primer 5′-AAAAGGCAGTCGAAGGTCTCG-3′ for *socs-1*, F primer 5′-CACCCAGGAAAGACAGCAACC-3′ and R primer 5′-GCAAGAGCTCTTGTCCATTGA-3′ for *Foxp3*, F primer 5′-CCCTTGGGCTGTGTTAATAGTG-3′ and R primer 5′-AACTTCTCGTACAAGCCTGGG-3′for *cd69*, and F primer 5′-TGAAGCAGGCATCTGAGGG-3′ and R primer 5′-CGAAGGTGGAAGAGTGGGAG-3′ for *Gapdh*. The following primers were used to amplify human genes: F primer 5′-TTTTCGCCCTTAGCGTGAAGA-3′ and R primer 5′-GAGGCAGTCGAAGCTCTCG-3′ for *socs-1* and F primer 5′-AATGGACTGGTCGTGGAG-3′ and R primer 5′-CCCTCCAGGGGATCGTTTG-3′ for *gapdh*. BIC gene expression was analyzed by real-time PCR using TaqMan universal PCR master mix and specific TaqMan probe and primers for *bic* (catalog numbers Mm01716204-m1 and Hs01374570-m1; Applied Biosystems). The expression of microRNA was analyzed by using a TaqMan microRNA reverse transcription kit, individual TaqMan microRNA assays for mmu-miR-155-5p (catalog number 002571) and hsa-miR-155-5p (catalog number 002287), and TaqMan universal PCR master mix (Applied Biosystems). sno135 snRNA (catalog number 001230) was used as the endogenous control. Real-time quantitative PCR analysis was performed with an ABI Prism 7900HT 384 thermal cycler (Applied Biosystems). The relative gene expression level was determined by using the $2^{-\Delta\Delta C_T}$ method.

Chimeric mice. Eight- to twelve-week-old Rag2$^{-/-}$ γc$^{-/-}$ recipient mice were irradiated with one split dose of 6.5 Gy gamma radiation, whereas C57BL/6 recipients were irradiated with two split 6.5-Gy doses. The mice were intravenously (i.v.) injected with bone marrow cells from Foxp3-mRFP/*cd69*$^{+/+}$ or Foxp3-mRFP/*cd69*$^{-/-}$ littermates. In mixed chimeras, irradiated Rag2$^{-/-}$ γc$^{-/-}$ recipients were transplanted with a mixture of CD45.1 *cd69*$^{+/+}$ or CD45.2 *cd69*$^{-/-}$ bone marrow precursors from nonreporter or reporter Foxp3-mRFP$^+$ cells, at a ratio of 1:1. After at least 10 weeks, the contribution of the different donor bone marrow precursors to the tTreg cell subset was determined by FACS analysis.

Transient transfection. PBLs (10^6) were transiently transfected for 4 h with 50 pM anti-miR-155 (catalog number AM12601; Ambion) by using Lipotransfectin (Niborlab) according to the manufacturer's instructions. As a negative control, a random anti-miRNA sequence control (negative control 1, catalog number AM1701; Ambion) was included in the assay mixture. Transfected cells were stimulated with plate-bound anti-CD3 antibody (OKT3; 3 μg/ml) for 24 h. When indicated, PBLs (0.5×10^6) were transfected for 7 h with 50 pM pre-miR-hsa-miR-155 or a pre-miRNA negative control (Ambion) by using Lipofectamine RNA iMAX (Invitrogen). Transfected cells were stimulated with phorbol myristate acetate (PMA) during 4 h with 50 ng/ml PMA and 750 ng/ml ionomycin (P+I). After stimulation, the levels of CD69 and phospho-STAT5 were monitored by flow cytometry, and transcriptional levels of hsa-miR-155 and *socs-1* were monitored by qPCR.

Plasmids. The pLKO lentiviral plasmids containing shCD69 sequences were obtained from Sigma-Aldrich (catalog numbers TRCN0000057693, TRCN0000057694, and TRCN0000057695), and the pLKO lentiviral control plasmid is a pLKO empty vector from Sigma-Aldrich (catalog number SHC001). The shCD69 sequences used were as follows (5′ to 3′): CCGGGCATGGAATGTGAGAAGAATTCTCGAGAATTCT TCTCACATTCCATGCTTTTTG for shCD69-1, CCGGAGGCCAATACACATTCTCAATCTCGAGATTGAGAATGTGT ATTGGCCTTTTTTG for shCD69-2, and CCGGGTGGTCAAATGGCAAAGAATTCTCGAGAATTCTTTGCCATTTGA CCACTTTTTG for shCD69-3.

LV production, titration, and infection. HEK-293 cells were cultured in Dulbecco's modified Eagle's medium (DMEM) containing 10% fetal bovine serum (FBS) (Sigma-Aldrich) and L-glutamine plus antibiotics. HEK-293 cells were transiently transfected by the calcium phosphate method with 3 HIV-derived plasmids and the vesicular stomatitis virus (VSV)-pseudotyped LV system (provided by F. Sánchez-Madrid, Hospital de la Princesa, Spain) to obtain LVs expressing the shCD69 sequences. The supernatant containing LV particles was collected 48 h after the removal of the calcium phosphate precipitate and ultracentrifuged for 2 h (Optima L-100 XP ultracentrifuge; Beckman). LVs were collected by adding cold PBS and were titrated by qPCR. PBLs isolated from healthy donors were infected with LV particles (multiplicity of infection [MOI] of 10) for 5 h. Subsequently, virus-containing medium was replaced with fresh complete RPMI medium supplemented with 10% FBS. After 12 h, infected cells were selected with puromycin for 48 h. Selected cells were stimulated with plate-bound anti-CD3 antibody (OKT3; 3 μg/ml) for 24 h. After stimulation, the levels of CD69 were monitored by flow cytometry, and levels of miR-155 were monitored by TaqMan qPCR.

Statistical analysis. Experiments were performed according to a randomized complete block design (treatments and different time points have been taken into account) or a fully randomized design. To determine significant differences, *P* values were calculated by Student's *t* test as appropriate, and differences were considered significant at *P* values of <0.05. Means from more than two experimental groups were compared by 1-way analysis of variance (ANOVA). To account for multiple comparisons, the Tukey test was used to compared selected pairs of means, and the Bonferroni posttest was used to compare all pairs of means. All statistical analyses were carried out with Prism v5 (GraphPad Software). Each experiment was repeated at least three times, unless otherwise indicated in the figure legends.

SUPPLEMENTAL MATERIAL

Supplemental material for this article may be found at https://doi.org/10.1128/MCB.00341-16.

SUPPLEMENTAL FILE 1, PDF file, 6.1 MB.

ACKNOWLEDGMENTS

We thank S. Bartlett for editorial assistance and Richard A. Flavell (Yale University, New Haven, CT) for kindly providing the *foxp3*-mRFP reporter mice.

This study was funded by a grant from the Spanish Ministry of Economy and Competitiveness (SAF2013-44857-R to M.L.T.), grant INDISNET 01592006 from the Comunidad de Madrid to P.M. and F.S.-M., and grants from the Instituto de Salud Carlos III (PI-FIS-2016-9488 to P.M.), the CIBER de Enfermedades Cardiovasculares to F.S.-M. and P.M., and the Fundació La Marató TV3 (20152330 31) to P.M. and F.S.-M. R.S.-D. was funded by a predoctoral fellowship from the Comunidad de Madrid, S.L. was funded by a contract from the RETICS Enfermedades Cardiovasculares (Instituto de Salud Carlos III), and K.T. is cofunded by the European Union Marie Curie Program (COFUND CNIC IPP). This research has been cofinanced by FEDER. The CNIC is supported by the Ministry of Economy, Industry, and Competitiveness (MINECO) and the Pro CNIC Foundation and is a Severo Ochoa Center of Excellence (MINECO award SEV-2015-0505).

R.S.-D. and R.B.-D. performed research and analyzed the data; S.L., K.T., H.D.L.F., B.L.-P., and E.M.-G. performed research; R.N. contributed with *mirn155*$^{-/-}$ mice; F.S.-M. and M.L.T. designed research and analyzed the data; and P.M. designed research, collected and analyzed the data, and wrote the paper.

We declare that we have no competing interests.

REFERENCES

1. Campbell DJ, Koch MA. 2011. Phenotypical and functional specialization of FOXP3+ regulatory T cells. Nat Rev Immunol 11:119–130. https://doi.org/10.1038/nri2916.
2. Abbas AK, Benoist C, Bluestone JA, Campbell DJ, Ghosh S, Hori S, Jiang S, Kuchroo VK, Mathis D, Roncarolo MG, Rudensky A, Sakaguchi S, Shevach EM, Vignali DA, Ziegler SF. 2013. Regulatory T cells: recommendations to simplify the nomenclature. Nat Immunol 14:307–308. https://doi.org/10.1038/ni.2554.
3. Josefowicz SZ, Lu LF, Rudensky AY. 2012. Regulatory T cells: mechanisms of differentiation and function. Annu Rev Immunol 30:531–564. https://doi.org/10.1146/annurev.immunol.25.022106.141623.
4. Burchill MA, Yang J, Vang KB, Moon JJ, Chu HH, Lio CW, Vegoe AL, Hsieh CS, Jenkins MK, Farrar MA. 2008. Linked T cell receptor and cytokine signaling govern the development of the regulatory T cell repertoire. Immunity 28:112–121. https://doi.org/10.1016/j.immuni.2007.11.022.

5. Kohlhaas S, Garden OA, Scudamore C, Turner M, Okkenhaug K, Vigorito E. 2009. Cutting edge: the Foxp3 target miR-155 contributes to the development of regulatory T cells. J Immunol 182:2578–2582. https://doi.org/10.4049/jimmunol.0803162.
6. Lu LF, Thai TH, Calado DP, Chaudhry A, Kubo M, Tanaka K, Loeb GB, Lee H, Yoshimura A, Rajewsky K, Rudensky AY. 2009. Foxp3-dependent microRNA155 confers competitive fitness to regulatory T cells by targeting SOCS1 protein. Immunity 30:80–91. https://doi.org/10.1016/j.immuni.2008.11.010.
7. Cobb BS, Hertweck A, Smith J, O'Connor E, Graf D, Cook T, Smale ST, Sakaguchi S, Livesey FJ, Fisher AG, Merkenschlager M. 2006. A role for Dicer in immune regulation. J Exp Med 203:2519–2527. https://doi.org/10.1084/jem.20061692.
8. Liston A, Lu LF, O'Carroll D, Tarakhovsky A, Rudensky AY. 2008. Dicer-dependent microRNA pathway safeguards regulatory T cell function. J Exp Med 205:1993–2004. https://doi.org/10.1084/jem.20081062.
9. Divekar AA, Dubey S, Gangalum PR, Singh RR. 2011. Dicer insufficiency and microRNA-155 overexpression in lupus regulatory T cells: an apparent paradox in the setting of an inflammatory milieu. J Immunol 186:924–930. https://doi.org/10.4049/jimmunol.1002218.
10. Zhang N, Bevan MJ. 2010. Dicer controls CD8$^+$ T-cell activation, migration, and survival. Proc Natl Acad Sci U S A 107:21629–21634. https://doi.org/10.1073/pnas.1016299107.
11. Martin-Gayo E, Sierra-Filardi E, Corbi AL, Toribio ML. 2010. Plasmacytoid dendritic cells resident in human thymus drive natural Treg cell development. Blood 115:5366–5375. https://doi.org/10.1182/blood-2009-10-248260.
12. Cortes JR, Sanchez-Diaz R, Bovolenta ER, Barreiro O, Lasarte S, Matesanz-Marin A, Toribio ML, Sanchez-Madrid F, Martin P. 2014. Maintenance of immune tolerance by Foxp3+ regulatory T cells requires CD69 expression. J Autoimmun 55:51–62. https://doi.org/10.1016/j.jaut.2014.05.007.
13. Feng C, Woodside KJ, Vance BA, El-Khoury D, Canelles M, Lee J, Gress R, Fowlkes BJ, Shores EW, Love PE. 2002. A potential role for CD69 in thymocyte emigration. Int Immunol 14:535–544. https://doi.org/10.1093/intimm/dxf020.
14. Nakayama T, Kasprowicz DJ, Yamashita M, Schubert LA, Gillard G, Kimura M, Didierlaurent A, Koseki H, Ziegler SF. 2002. The generation of mature, single-positive thymocytes in vivo is dysregulated by CD69 blockade or overexpression. J Immunol 168:87–94. https://doi.org/10.4049/jimmunol.168.1.87.
15. Lamana A, Sancho D, Cruz-Adalia A, del Hoyo GM, Herrera AM, Feria M, Diaz-Gonzalez F, Gomez M, Sanchez-Madrid F. 2006. The role of CD69 in acute neutrophil-mediated inflammation. Eur J Immunol 36:2632–2638. https://doi.org/10.1002/eji.200636355.
16. Wirnsberger G, Mair F, Klein L. 2009. Regulatory T cell differentiation of thymocytes does not require a dedicated antigen-presenting cell but is under T cell-intrinsic developmental control. Proc Natl Acad Sci U S A 106:10278–10283. https://doi.org/10.1073/pnas.0901877106.
17. Noval Rivas M, Hazzan M, Weatherly K, Gaudray F, Salmon I, Braun MY. 2010. NK cell regulation of CD4 T cell-mediated graft-versus-host disease. J Immunol 184:6790–6798. https://doi.org/10.4049/jimmunol.0902598.
18. Fontenot JD, Rasmussen JP, Gavin MA, Rudensky AY. 2005. A function for interleukin 2 in Foxp3-expressing regulatory T cells. Nat Immunol 6:1142–1151. https://doi.org/10.1038/ni1263.
19. Lu LF, Gasteiger G, Yu IS, Chaudhry A, Hsin JP, Lu Y, Bos PD, Lin LL, Zawislak CL, Cho S, Sun JC, Leslie CS, Lin SW, Rudensky AY. 2015. A single miRNA-mRNA interaction affects the immune response in a context- and cell-type-specific manner. Immunity 43:52–64. https://doi.org/10.1016/j.immuni.2015.04.022.
20. Yin Q, Wang X, McBride J, Fewell C, Flemington E. 2008. B-cell receptor activation induces BIC/miR-155 expression through a conserved AP-1 element. J Biol Chem 283:2654–2662. https://doi.org/10.1074/jbc.M708218200.
21. Castellanos MC, Munoz C, Montoya MC, Lara-Pezzi E, Lopez-Cabrera M, de Landazuri MO. 1997. Expression of the leukocyte early activation antigen CD69 is regulated by the transcription factor AP-1. J Immunol 159:5463–5473.
22. Esplugues E, Sancho D, Vega-Ramos J, Martinez C, Syrbe U, Hamann A, Engel P, Sanchez-Madrid F, Lauzurica P. 2003. Enhanced antitumor immunity in mice deficient in CD69. J Exp Med 197:1093–1106. https://doi.org/10.1084/jem.20021337.
23. Gonzalez-Amaro R, Cortes JR, Sanchez-Madrid F, Martin P. 2013. Is CD69 an effective brake to control inflammatory diseases? Trends Mol Med 19:625–632. https://doi.org/10.1016/j.molmed.2013.07.006.
24. Radulovic K, Manta C, Rossini V, Holzmann K, Kestler HA, Wegenka UM, Nakayama T, Niess JH. 2012. CD69 regulates type I IFN-induced tolerogenic signals to mucosal CD4 T cells that attenuate their colitogenic potential. J Immunol 188:2001–2013. https://doi.org/10.4049/jimmunol.1100765.
25. Vitales-Noyola M, Doniz-Padilla L, Alvarez-Quiroga C, Monsivais-Urenda A, Portillo-Salazar H, Gonzalez-Amaro R. 2015. Quantitative and functional analysis of CD69(+) NKG2D(+) T regulatory cells in healthy subjects. Hum Immunol 76:511–518. https://doi.org/10.1016/j.humimm.2015.06.003.
26. Lin CR, Wei TW, Tsai HY, Wu YT, Wu PY, Chen ST. 2015. Glycosylation-dependent interaction between CD69 and S100A8/S100A9 complex is required for regulatory T-cell differentiation. FASEB J 29:5006–5017. https://doi.org/10.1096/fj.15-273987.
27. Matloubian M, Lo CG, Cinamon G, Lesneski MJ, Xu Y, Brinkmann V, Allende ML, Proia RL, Cyster JG. 2004. Lymphocyte egress from thymus and peripheral lymphoid organs is dependent on S1P receptor 1. Nature 427:355–360. https://doi.org/10.1038/nature02284.
28. Shiow LR, Rosen DB, Brdickova N, Xu Y, An J, Lanier LL, Cyster JG, Matloubian M. 2006. CD69 acts downstream of interferon-alpha/beta to inhibit S1P1 and lymphocyte egress from lymphoid organs. Nature 440:540–544. https://doi.org/10.1038/nature04606.
29. Weinreich MA, Hogquist KA. 2008. Thymic emigration: when and how T cells leave home. J Immunol 181:2265–2270. https://doi.org/10.4049/jimmunol.181.4.2265.
30. Lauzurica P, Sancho D, Torres M, Albella B, Marazuela M, Merino T, Bueren JA, Martinez AC, Sanchez-Madrid F. 2000. Phenotypic and functional characteristics of hematopoietic cell lineages in CD69-deficient mice. Blood 95:2312–2320.
31. Martin P, Gomez M, Lamana A, Cruz-Adalia A, Ramirez-Huesca M, Ursa MA, Yanez-Mo M, Sanchez-Madrid F. 2010. CD69 association with Jak3/Stat5 proteins regulates Th17 cell differentiation. Mol Cell Biol 30:4877–4889. https://doi.org/10.1128/MCB.00456-10.
32. Zheng Y, Josefowicz SZ, Kas A, Chu TT, Gavin MA, Rudensky AY. 2007. Genome-wide analysis of Foxp3 target genes in developing and mature regulatory T cells. Nature 445:936–940. https://doi.org/10.1038/nature05563.
33. Ziegler SF, Levin SD, Johnson L, Copeland NG, Gilbert DJ, Jenkins NA, Baker E, Sutherland GR, Feldhaus AL, Ramsdell F. 1994. The mouse CD69 gene. Structure, expression, and mapping to the NK gene complex. J Immunol 152:1228–1236.
34. Testi R, Phillips JH, Lanier LL. 1989. T cell activation via Leu-23 (CD69). J Immunol 143:1123–1128.
35. Martin P, Sanchez-Madrid F. 2011. CD69: an unexpected regulator of TH17 cell-driven inflammatory responses. Sci Signal 4:pe14. https://doi.org/10.1126/scisignal.2001825.
36. Wan YY, Flavell RA. 2005. Identifying Foxp3-expressing suppressor T cells with a bicistronic reporter. Proc Natl Acad Sci U S A 102:5126–5131. https://doi.org/10.1073/pnas.0501701102.
37. European Institutes of Health. 2010. Directive 2010/63/EU of the European Parliament and the Council on the Protection of Animals Used for Scientific Purposes. Official J Eur Union 53:33–79.

REVIEW ARTICLE OPEN

Novel human immunomodulatory T cell receptors and their double-edged potential in autoimmunity, cardiovascular disease and cancer

Pilar Martín[1,2], Rafael Blanco-Domínguez[1] and Raquel Sánchez-Díaz[1,2]

In the last decade, approaches based on T cells and their immunomodulatory receptors have emerged as a solid improvement in treatments for various types of cancer. However, the roles of these molecules in the therapeutic context of autoimmune and cardiovascular diseases are still relatively unexplored. Here, we review the best known and most commonly used immunomodulatory T cell receptors in clinical practice (PD-1 and CTLA-4), along with the rest of the receptors with known functions in animal models, which have great potential as modulators in human pathologies in the medium term. Among these other receptors is the receptor CD69, which has recently been described to be expressed in mouse and human T cells in autoimmune and cardiovascular diseases and cancer. However, inhibition of these receptors individually or in combination by drugs or monoclonal antibodies generates a loss of immunological tolerance and can trigger multiple autoimmune disorders in different organs and immune-related adverse effects. In the coming decades, knowledge on the functions of different immunomodulatory receptors will be pivotal for the development of new and better therapies with less harmful side effects. In this review, we discuss the roles of these receptors in the control of immunity from a perspective focused on therapeutic potential in not only cancer but also autoimmune diseases, such as systemic lupus erythematosus, autoimmune diabetes and rheumatoid arthritis, and cardiovascular diseases, such as atherosclerosis, acute myocardial infarction, and myocarditis.

Keywords: Immunomodulatory receptors; Autoimmune diseases; T cells; Immunotherapy

Cellular & Molecular Immunology _####################_; https://doi.org/10.1038/s41423-020-00586-4

INTRODUCTION

Targeting immunomodulatory T cell receptors has emerged as a successful approach to manipulate the immune system, generating spectacular outcomes in certain diseases, such as cancer. Advances in the knowledge on the mechanisms by which tumors affect the balance between effector and regulatory T cells have revealed new therapeutic strategies for the treatment of autoimmune diseases[1] and are also very promising for cardiovascular diseases.[2] In this review article, we focus on receptors with the main function of triggering immunosuppressive signaling pathways in T cells, mainly programmed cell death protein (PD1), cytotoxic T-lymphocyte-associated protein-4 (CTLA-4), B- and T-lymphocyte attenuator (BTLA), *Lymphocyte-activation gene 3* (LAG-3), T cell immunoglobulin and mucin domain-containing protein 3 (TIM-3), T cell immunoglobulin and immunoreceptor tyrosine-based inhibitory motif [ITIM] domain (TIGIT), 2B4 (CD244), and V-domain Ig suppressor of T cell activation (VISTA), all of which belong to the immunoglobulin (Ig) superfamily;[3] CD5, a scavenger-receptor cysteine-rich (SRCR) superfamily receptor; and CD69, a C-type lectin with a role as an immunomodulatory T cell receptor that has been demonstrated in recent years.[4] We summarize the main characteristics of each of the above immunomodulatory T cell receptors, their expression in different T cell subsets, the mechanism of suppression, or negative regulation of T cell activation and associated positive and negative repercussions in the contexts of human autoimmunity, cardiovascular disease, and cancer (Table 1). Moreover, we also discuss the role of the new generation of targeted immunotherapies (immune checkpoint inhibitors, ICIs) in cancer and how checkpoint inhibition is also being adapted to treat autoimmune diseases.[1]

OVERVIEW OF THE IMMUNOMODULATORY RECEPTORS EXPRESSED BY T CELLS

PD1, CTLA-4, and BTLA belong to the CD28 Ig superfamily and share similar protein structures.[5] PD-1 (CD279) is expressed by all T cells during activation, B cells, natural killer, and myeloid cells.[6] PD-L1 and PD-L2 are known ligands of PD-1 expressed by T, B, and antigen-presenting cells. The binding of PD-1 to PD-L1 induces resistance to activation by positive signals from the T cell receptor (TCR) and CD28 in conventional T cells.[6] CTLA-4 (CD165) is expressed on activated $CD4^+$ T cells and competitively binds B7.1 and B7.2, acting as a coinhibitory signal to down-regulate early T cell activation and proliferation.[7] Constitutive CTLA-4 expression on regulatory T (Treg) cells enhances their regulatory function through suppression of antigen-presenting cells.[8] BTLA (CD272) is expressed in single-positive thymocytes,

[1]Vascular Pathophysiology Area, Centro Nacional de Investigaciones Cardiovasculares (CNIC), Madrid, Spain and [2]CIBERCV, Madrid, Spain
Correspondence: Pilar Martín (pmartinf@cnic.es)

Received: 21 August 2020 Accepted: 28 October 2020
Published online: 24 November 2020

Table 1. Pathologies and treatments associated with different T cell immunoreceptors in the fields of autoimmunity, cardiovascular disease, and cancer

Immunoreceptor	T cell type	Disease	Treatment	Ref.
PD-1				
Autoimmunity	T cell	Type 1 diabetes		81
	gd T cell	Psoriasis	Nivolumab	210
	Treg	Inflammatory bowel disease	Anti-PD-L1 monoclonal antibodies: MIH2	230
	Treg	RA	TNF blockade	94
	Treg	MS		231
CVD	T cell	Atherosclerosis		123
	CD8 T cell	Atherosclerosis	Anti-PD-1 monoclonal antibody (clone 29E.2A3, BioLegend)	121
	T cell	DC and myocarditis	Anti-PD1 and anti-PD1L antibodies	152
	Treg	ACS		122
Cancer	$CD8^+$ T cells/Treg cells	Melanoma, lung cancer, kidney cancer, BC, head and neck cancer, urothelial carcinoma, hepatocellular carcinoma, gastric cancer, metastatic Merkel cell carcinoma and Hodgkin lymphoma	Anti-PD-1 mAbs: atezolizumab, pembrolizumab and nivolumab	191,210
	CD8 T cell	AML		232
CTLA-4				
Autoimmunity	CD8 T cell	RA	Fusion protein: CTLA4 Ig	97
CVD	T cell	DC and myocarditis	Anti-CTLA4 antibody	152
		Chronic heart failure		233
Cancer	CD8 T cell	Melanoma	Ipilimumab	178
	T cell	Melanoma, NSCLC, breast cancer, prostate cancer, pancreatic cancer, hepatocellular carcinoma, and mesothelioma	Anti-CTLA-4 mAbs: ipilimumab and tremelimumab	187
LAG-3				
Autoimmunity		MS		234
CVD	CD4 T cells	Cardiac dysfunction in chronic HIV	Anti-LAG-3 immunotherapy	235
	CD4 T cells	CAD		128
Cancer	CD8 T cells	Multiple human cancers, breast cancer, ovarian cancer	Anti-LAG-3 immunotherapy	12,206
	CD8 T cells	Melanoma	Anti-LAG3 mAb: relatlimab	206
	CD8 T cells	Metastatic breast cancer	LAG3-Ig fusion protein: EOC202	206
Tim-3				
Autoimmunity	CD4 T cell, CD8 T cell, NKT cell	RA		12,103
	CD8 T cell	Asthma and allergy		12
	Th1 cell	MS		12
	Treg	Autoimmune hepatitis		236
CVD	CD8	Atherosclerosis	Anti-Tim-3 mAb: F38-2E2	121
Cancer	T cells	Hepatocellular carcinoma		237
	CD8 T cell	Prostate cancer		238
	$CD8^+$ T cells/Treg cells	Hepatocellular, ovarian, colon and cervical carcinomas		237
TIGIT				
Autoimmunity	Treg cell	Type 1 diabetes		12
		MS		12
		RA		12
Cancer	CD8 T cell	NSCLC, colon cancer, melanoma, and myelogenous leukemia		12,88
	Treg cell	Melanoma		88

Table 1. continued

Immunoreceptor	T cell type	Disease	Treatment	Ref.
2B4				
Autoimmunity	CD8 T cell	RA		18
	CD8 T cell	SLE		18
Cancer	CD8 T cell	Multiple myeloma		239
	CD8 T cell	Melanoma, hepatocarcinoma, and AML		239
	CD8 T cell	AML		239
VISTA				
Cancer	CD8 T cells, Tregs	Endometrial and ovarian cancers, solid tumors	Anti-VISTA mAb: JNJ 61610588 (clinical trial)	207
	T cell, Treg	Solid tumors and lymphomas, NSCLC	CA-170 (clinical trial)	207
	T cells	Prostate cancer		131
CD69				
Autoimmunity	T cells	RA		4,111
	CD4 T cells	Type 1 diabetes		90
	T cells	Osteoarthritis		4
	Treg cells	SLE		4,44,68,69
	Th17 cells	Wegener's granulomatosis		4
	Th17 cells	MS		4
	T cells	Optic neuromyelitis		4
	T cells/Treg cells	Autoimmune thyroiditis		4,74
CVD	T cells	MI		149
	Th17/Treg cells	Atherosclerosis		4,32,149
	CD4 T cells	Coronary heart disease		240
Cancer	CD4 T cells	Lung adenocarcinoma		241
	Treg cells	Hepatocellular carcinoma		4
	CD4 T cells	NSCLC		242
BTLA				
Autoimmunity	CD4 and CD8 T cells	RA		243
	$CD4^+$ T cell	Ulcerative colitis		243
	$CD4^+$ T cells	SLE		243
	$CD8^+$ T cells	MS		243
	$CD4^-CD8^-$ T cells	Vasculitis		243
	$CD4^+$ T cells	Vasculitis (Behçet's disease)		243
CVD	Treg	Atherosclerosis		243
Cancer	T cells	Epithelial ovarian carcinoma		243
	$CD8^+$ T cell	Melanoma		243
	T cells	Diffuse large B cell lymphoma		243
	$CD4^+$ T	Hepatocellular carcinoma		243
CD5				
Autoimmunity	T cell	CTCL	Anti-CD5 mAb: T101; and radioimmunoconjugate 90Y-T101	244
	T cells	MS		244
Cancer	T cell	Lung carcinoma		244
	T cell	Melanoma		244

CVD cardiovascular diseases, *mAb* monoclonal antibody, *CD* cluster of differentiation, *NKT* natural killer T, *gd T cell* gamma delta T cell, *Treg* regulatory T cell, *TNF* tumor necrosis factor, *Ig* immunoglobulin, *Th* T helper, *PD1* programmed cell death, *PD1L* programmed cell death ligand, *CTLA4* cytotoxic T-lymphocyte-associated protein-4, *LAG3 Lymphocyte-activation gene 3, TIM3* T cell immunoglobulin and mucin domain-containing protein 3, *TIGIT* T cell immunoreceptor with Ig and ITIM domains, *VISTA* V-domain Ig suppressor of T cell activation, *BTLA* B and T lymphocyte associated, *AML* acute myeloid leukemia, *NSCLC* non-small cell lung cancer, *MS* multiple sclerosis, *SLE* systemic lupus erythematosus, *CAD* coronary artery disease, *RA* rheumatoid arthritis, *DC* dilated cardiomyopathy, *MI* myocardial infarction, *ACS* acute coronary syndrome

mature T cells, B cells, macrophages, and dendritic cells. BTLA maintains T cell immune tolerance[9], and the binding of BTLA to its ligand, herpes virus entry mediator, prevents excessive activation of T cells.[10]

LAG-3 is a transmembrane protein homolog to the CD4 coreceptor that binds to major histocompatibility complex (MHC) class II with high affinity.[11] LAG-3 (CD223) is expressed in activated $CD4^+$ T cells, Treg cells, Tr1 cells, activated $CD8^+$ T cells, natural killer cells, dendritic cells, B cells, and exhausted effector T cells.[12] The interaction of LAG-3 with MHC II leads to decreased proliferation and cytokine secretion by antigen-specific $CD4^+$ T cell clones.[11] T cell immunoglobulin and mucin domain 3 is a transmembrane protein belonging to the Ig superfamily that is expressed in CD4 helper 1 (Th1) cells, CD8 T cytotoxic 1 (Tc1) cells, Treg cells, dendritic cells, natural killer cells, monocytes, macrophages, and mast cells. Galectin-9, the first reported Tim-3 ligand, was shown to induce apoptosis in Th1 cells,[13] and carcinoembryonic antigen cell adhesion molecule 1 forms a heterodimer with Tim-3 to mediate T cell inhibition and exhaustion.[14] TIGIT is a coinhibitory transmembrane protein expressed by regulatory and memory $CD4^+$ T cells, $CD8^+$ T cells, and natural killer cells. The poliovirus receptor (CD155) shared with CD226, poliovirus receptor-related 2 (CD112, also known as Nectin-2), and Nectin4 are the ligands for TIGIT and deliver stimulatory signals.[15,16] TIGIT also blocks T cell activation, proliferation, and maturation by targeting downstream TCR signaling pathways.[17] The signaling lymphocyte activation molecule 2B4/CD244 is a CD2-related receptor expressed in antigen-experienced $CD8^+$ αβ T cells, natural killer cells, dendritic cells, and myeloid-derived suppressor cells (MDSCs).[18] The engagement of 2B4 by its receptor, CD48, contributes to $CD8^+$ T cell exhaustion and cell function inhibition.[19] VISTA is expressed in T cells, natural killer cells, and myeloid cells.[20] VISTA is a member of the B7 family, and although the receptor shares homology with members of the CD28 family, the gene is located on a different chromosome. VISTA can act as both a ligand and a receptor in regulating $CD4^+$ and $CD8^+$ T cell proliferation and cytokine production.[21]

The T cell receptor-inhibiting molecule CD5, also known as Leu-1 in humans, is a transmembrane glycoprotein that belongs to the highly conserved SRCR.[22] CD5 is constitutively expressed on lymphocyte precursors, mature T cells, and B1a cells and is associated with both TCR/CD3 and B cell receptor.[23] The known ligands for CD5 are CD5L, CD72, and CD5 itself, but little is known about their physiological functions. CD5 clusters with the TCRζ/CD3-pMHC complex and inhibits signaling through immunological synapses in thymocytes and peripheral T cells.[24,25]

Last but not least, the early leukocyte activation antigen CD69 is a type II C-lectin membrane receptor[26] that belongs to a family of immunomodulatory receptors involved in the immune response, the NK complex.[4] CD69 is expressed early after cell activation in all hematopoietic cells except erythrocytes[27] and has emerged as a new immunoregulatory receptor expressed by T cells in the last decade.[28] Additionally, a number of ligands for CD69 with the ability to modulate T cell responses through different pathways and triggers have been identified recently. Galectin-1 (Gal-1) binds to CD69, inhibiting naive and helper T cell activation and differentiation,[29,30] and interaction with the S100A8/S100A9 complex is required for the differentiation of regulatory T cells.[31] Oxidized low-density lipoprotein (OxLDL) has been shown to bind specifically to $CD69^+$ human T lymphocytes, enhancing Treg cell differentiation and inhibiting Th17 cells.[32] Interestingly, the CD69 cluster with the aromatic amino acid-transporter complex LAT-1-CD98 in γδ T cells regulates L-tryptophan transport and cytokine secretion in these cells.[33] The immunomodulatory T cell receptors, their ligands, and the cellular functions triggered by signaling through each receptor are summarized in Fig. 1.

OPPORTUNITIES RELATED TO IMMUNOMODULATORY T CELL RECEPTORS IN HUMAN AUTOIMMUNE DISEASES

Autoimmune diseases are the consequence of deterioration or loss of self-tolerance resulting from defects in the thymic elimination of potentially self-reactive T cells (central tolerance) or in the control mechanisms of potentially self-reactive T cells in the periphery (peripheral tolerance). The nature of autoimmune diseases is multifactorial since the mechanisms that trigger these conditions can be genetic, epigenetic, molecular, and/or cellular in origin. However, the generation of pathogenic inflammatory responses in peripheral tissues upon activation of autoantigen-specific T cells is a common denominator in all autoimmune diseases.[34] T cells with a potentially autoreactive TCR escape thymic selection, and powerful mechanisms are required to control these autoreactive T cells and maintain peripheral tolerance.[34] Therefore, approaches targeting immunomodulatory T cell receptors have emerged in recent years as therapeutic opportunities to restore tolerance in autoimmune diseases (Table 1).

Systemic lupus erythematosus (SLE)

The immunomodulatory receptors PD-1, CTLA-4, and BTLA play nonredundant roles in the modulation of central tolerance during the thymocyte selection process and in maintaining peripheral tolerance. We analyzed the performance of these receptors in the development of SLE since patients with this autoimmune disease display abnormal levels of these receptors in T cells with a characteristic hyperactive phenotype. PD-1 has a pivotal role in the negative regulation of positive TCR-α/β thymocyte selection by affecting the threshold of pre-TCR/CD3 complex downstream signaling.[35,36] In addition, *PD-1* gene ablation in mice with the additional *lpr/lpr* mutation also results in the development of lupus-like glomerulonephritis and destructive arthritis with age,[37] which indicates the involvement of this immunomodulatory receptor in the maintenance of peripheral self-tolerance. Different animal models demonstrate that PD-1 expression can be tuned finely with anti-PD-1 monoclonal antibodies (mAbs) to preserve the number of $Foxp3^+$ T cells or reduce the number of $CD4^+PD\text{-}1^+$ T cells and alleviate lupus-like nephritis.[38,39] However, a completely opposite effect was observed with anti-PD-1 mAb therapy in experimental autoimmune encephalomyelitis and NOD diabetes animal models.[40,41] The discovery that the PD-1 pathway modulates T follicular helper cell-mediated humoral immunity by negatively regulating T follicular regulatory (Tfr) cells[42] indicates that PD-1 blockade may preferentially influence the Tfr cell function controlling the development of lupus, reconciling previous contradictory results. In patients with SLE, it has been reported that PD-1 expression levels in $CD4^+$ T cells are very low[43] and the frequency of $PD\text{-}1^+$ cells is greatly decreased. It was found that patients with the PD-1.3 A/G allele have significantly lower expression of PD-1 in $CD4^+$ T cells than other patients. Although PD-1 expression is higher in $CD25^+$ Tregs than in effector T cells, PD-1 expression is significantly lower in SLE patients than in healthy subjects, which leads to functional and numerical reductions in Tregs in SLE patients. This was confirmed in another study in which PD-1 was found to be highly induced in $CD4^+CD25^+$ and $CD4^+CD69^+$ T cells from healthy controls but not in those from patients with SLE.[44] A recent study found elevated levels of coinhibitory IgG autoantibodies against PD-1 in the serum of new-onset SLE patients that were associated with SLE Disease Activity Index (SLEDAI) scores, revealing a new pathway of PD-1 modulation.[45] In contrast, a pilot study with a small number of patients showed that PD-1 expression levels in peripheral blood mononuclear cells (PBMCs) were significantly increased in SLE patients and associated with SLEDAI scores, suggesting that PD-1 inhibitors are useful tools in the treatment of SLE.[46] In summary, these data indicate that both the regulation and aberrant expression of PD-1 play key roles in the regulation of

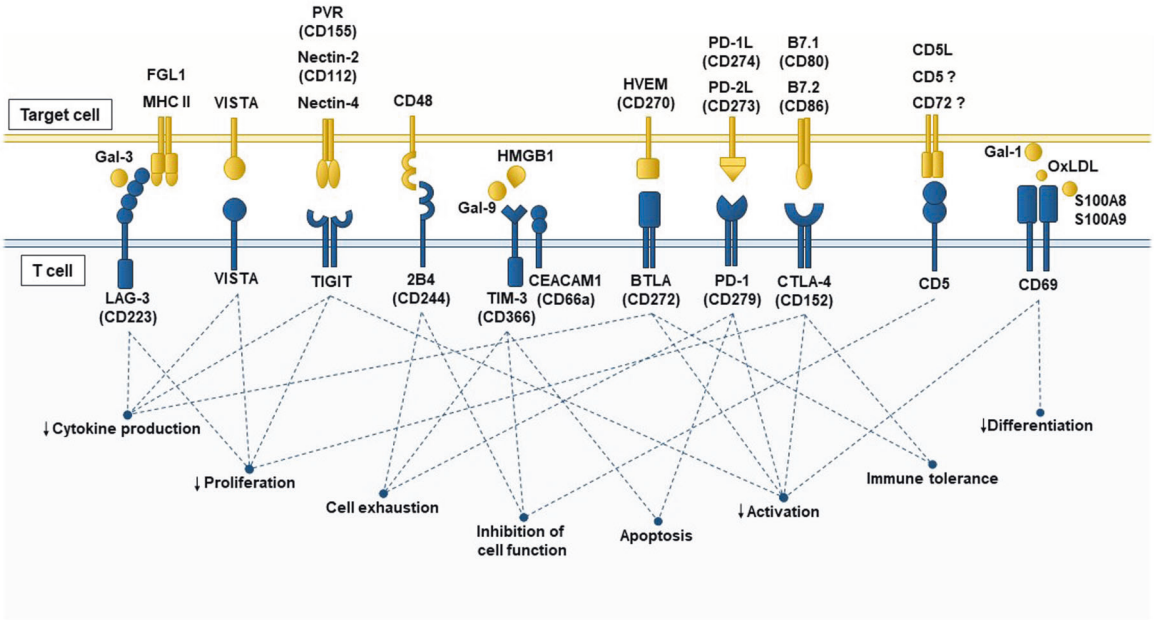

Fig. 1 Membrane receptors with immunomodulatory activity in T cells and their ligands. T cell responses are controlled by multiple inhibitory signals to prevent excessive inflammation that can occasionally cause more damage than repair. T cells express a battery of different receptors with immunomodulatory capacity in the membrane, such as LAG-3, VISTA, TIGIT, 2B4, TIM-3, CEACAM-1, BTLA, PD-1, CTLA-4, CD5, and CD69, which can interact with either soluble ligands or membrane proteins expressed by antigen-presenting cells (APCs), inflammatory cells, tumor cells, or damaged cells. Ligand–receptor interactions induce inhibitory signals in the T cell and sometimes also in the target cell to control inflammation, and the effects include decreasing proliferation, differentiation, activation, cytokine production and cell function and promoting apoptosis, T cell exhaustion and tolerance. LAG-3 *Lymphocyte-activation Gene 3*, MHC II major histocompatibility complex class II, *Gal-3* Galectin-3, *VISTA* V-domain immunoglobulin suppressor of T cell activation, TIGIT T cell immunoreceptor with immunoglobulin and ITIM domains, PVR poliovirus receptor, Tim-3 T cell immunoglobulin and mucin domain 3, CEACAM-1 carcinoembryonic antigen cell adhesion molecule 1, Gal-9 Galectin-9, HMGB1 high-mobility group box 1, BTLA B- and T-lymphocyte attenuator, HVEM herpes virus entry mediator, PD-1 programmed cell death protein, PD-L1/PD-L2 PD-1 ligand 1/PD-1 ligand 2, CTLA-4 cytotoxic T-lymphocyte-associated protein-4, Gal-1 Galectin 1, CD5L CD5 antigen-like, OxLDL oxidized low-density lipoprotein

this autoimmune disease. However, the clinical efficacy of manipulating this pathway requires more basic research and clinical studies. In this regard, an ongoing clinical trial (ClinicalTrials.gov Identifier: NCT03816345) is now testing the efficacy of an anti-PD1 mAb (nivolumab) in SLE and several other autoimmune diseases (Chron's disease, inflammatory bowel disease, multiple sclerosis, rheumatoid arthritis (RA), ulcerative colitis, etc.).

CTLA-4-deficient mice develop lethal lymphoproliferative syndrome and autoimmunity,[47,48] as well as a rapid and severe lupus-like autoimmune syndrome.[49] These mice exhibit global T cell dysregulation promoting systemic humoral autoimmunity that triggers lupus-like autoimmunity.[49] The relevance of the *CTLA* gene in the susceptibility to SLE is supported by evidence from different human populations with different polymorphisms.[50–52] Interestingly, SLE patients display increased expression of CTLA in isolated responder T cells (Foxp3$^-$) compared to healthy controls and patients with other autoimmune rheumatic diseases (RA or psoriatic arthritis).[53] However, these T cells exhibit defective inhibition of T cell activation by CTLA-4 after CD3/CD28 costimulation. CTLA-4 receptors are displaced from membrane microdomains in SLE patients and are unable to regulate the intracellular signaling molecules triggered by T cell activation.[53] Therefore, the receptor CTLA-4 in responding T cells could be a possible target to restore the function of T cells in patients with SLE, and there is in vitro evidence that soluble CTLA-4 from lupus patient PBMCs regulates effector responses.[54] The administration of abatacept, a fusion protein comprising CTLA-4 linked to the Fc portion of IgG1, has been tested clinically in several autoimmune diseases. Abatacept has also been tested in different clinical trials as a therapy for SLE[55] and lupus nephritis[56] patients in randomized studies and, although it showed evidence of biological activity, it did not meet the endpoint criteria of achieving a complete response during treatment.[56]

BTLA expression in effector T cells is associated with SLEDAI scores.[57,58] Lupus patients have a defect in the upregulation of BTLA expression upon activation of CD4$^+$ T cells in comparison with healthy controls.[58] BTLA is recruited to the immunological synapse and acts as an inhibitory receptor that negatively regulates the immune response; this function is defective in SLE patients but can be corrected by restoring intracellular trafficking and lipid metabolism in lupus CD4$^+$ T cells.[58] This gives BTLA characteristics similar to those of CTLA-4 and PD-1, and human anti-BTLA antibodies have been developed;[59,60] however, the potential of BTLA as a possible target in autoimmune diseases has not yet been tested.

CD69-deficient mice are healthy and do not present an autoimmune phenotype,[61] although the expression of this receptor in Treg cells is necessary for the development of natural Treg cells in the thymus[62] and their suppressive activity in inflammatory conditions,[63] indicating that the immunomodulatory receptor CD69 plays a pivotal role in the maintenance of central and peripheral tolerance.[4,26] CD69 expression in Tregs negatively regulates the production of proinflammatory cytokines and is necessary for the suppressive function of these cells in mouse models of autoimmune colitis.[64,65] CD4$^+$CD69$^+$ cell numbers are increased in lupus-prone (NZBxNZW)F_1 mice and pristine-induced SLE mice, and these cells regulate cytokine production by effector T cells.[66,67] SLE patients also present an increased CD69/CD3 ratio in PMBCs compared to healthy controls, which correlates with SLEDAI scores,[68,69] and increased levels of CD4$^+$CD69$^+$TGF-β$^+$IL-10$^+$Foxp3$^-$ Treg cells.[70–72] The CD69$^+$ Treg cell population appears to be increased in a number of

autoimmune and inflammatory disorders.[73–75] However, although increased in number, CD69$^+$TGF-β$^+$ Foxp3$^-$ Treg cells from SLE patients are not able to inhibit the release of cytokines by autologous lymphocytes, indicating that they do not contribute to the regulation of autoimmunity in these patients.[70] Moreover, SLE patients who do not respond to immunosuppressive therapy have significantly higher levels of P-glycoprotein (P-gp)$^+$CD69$^+$CD4$^+$ cells in the blood and renal tissue than responsive patients. P-gp expression in lymphocytes plays a role in the active efflux of intracellular drugs, and the high proportion of P-gp$^+$CD69$^+$CD4$^+$ cells in nonresponsive SLE patients is suggestive of corticosteroid resistance and renal damage.[76] Therefore, CD69 plays a role in regulating the secretion of cytokines and could be a potential target to control SLE in patients refractory to immunosuppressive therapy. Clinical trials need to be conducted to underscore the real value of this molecule as a therapeutic target.

Autoimmune diabetes

The PD-1-PD-L1 interaction has central roles in regulating the initiation and progression of autoimmune diabetes in nonobese diabetic (NOD) mice. PD-1 blockade rapidly precipitates diabetes in prediabetic NOD mice,[41] while overexpression of PD-L1 in pancreatic beta cells prevents diabetes in these animals.[77,78] PD-1 expression is downregulated specifically in CD8$^+$ T cells from type 2 diabetes (T2D) patients,[79] suggesting that immunomodulatory receptors have a role in the development of T2D. Moreover, PD-L1 is expressed in beta cells from type 1 diabetes (T1D) mellitus patients, possibly to attenuate the autoimmune response mediated by type I and II interferons through IRF1.[80,81] Along with animal evidence, these data provide the rationale for developing new therapies to target this costimulatory pathway in this disease without eliminating the protective role of the PD-1–PD-L1 pathway.

In contrast, CTLA blockade only negatively regulates autoimmune diabetes in neonatal NOD mice,[40] and CTLA-4 Ig or anti-B7-2 mAb treatment was shown to reduce the incidence of diabetes in young mice, whereas treatment with any of these reagents had no effect on disease progression in older mice.[82]

Targeting the BTLA pathway in NOD mice with an mAb that selectively depletes pathogenic helper CD4$^+$ T cells increases the proportion of Treg cells and protects against spontaneous disease onset in NOD mice.[83] Adoptive transfer of OVA-specific CD8$^+$ T cells isolated from BTLA-deficient mice into RIP-mOVA-recipient mice (expressing membrane-bound OVA in pancreatic beta cells) induces diabetes.[9] Moreover, BTLA limits γδ T cell numbers and sustains normal γδ T cell subset frequencies by restricting interleukin-7 (IL-7) responsiveness and CD27$^-$RORγt$^+$ population expansion.[84] γδ T cells have been implicated in the development of diabetes; however, the putative role of BTLA targeting in clinical autoimmune diabetes treatment has not been addressed. LAG-3-deficient NOD mice exhibit accelerated autoimmune diabetes development mediated by expansion of pathogenic T cell clones in the islets, which are normally restrained by LAG-3.[85] However, the onset of diabetes is accelerated even more in animals doubly deficient in LAG-3 and PD-1, which also develop other autoimmune diseases, such as myocarditis.[86] More recently, LAG-3 has been shown to act by limiting the function and proliferation of Tregs due to enhanced IL-2–Stat5 signaling pathway and Eos expression.[87] TIGIT is a repressor of the CD226-activating pathway that functions by binding the common ligand CD155. This costimulatory axis has also been postulated to be a therapeutic target for the treatment of T1D, as targeting TIGIT would control the suppressive function of Tregs.[88]

Finally, the expression of CD69 has been associated with the development of T2D complicated by coronary artery disease in patients.[89] Although whether there is a causal relationship is unknown, CD69 could exert its function through the regulation of the hypoxia-inducible factor short isoform I.1.[90]

Rheumatoid arthritis

T cells play a central role in the pathogenesis of RA; however, the first attempts to target T cells for therapeutic purposes produced a high risk of infection. Thus, the immunomodulatory receptors on T cells have been explored as better targets for the treatment of this often progressive and destructive chronic joint disease. CTLA-4 deficiency affects both central tolerance and peripheral tolerance as well as Treg-mediated suppression. Mice deficient in CTLA-4 develop severe collagen-induced arthritis,[91] and patients with CTLA-4 mutations show expansion of Treg cells, which leads to subsequent inflammation and autoimmunity probably through the production of organ-specific autoantibodies.[92,93] The therapeutic agent *abatacept* (CTLA-4-Ig) has shown efficacy in a broad spectrum of RA patients from early-stage disease to refractory disease resistant to tumor necrosis factor-α (TNF-α) blockers.[94] *Abatacept* treatment results in significant improvement in the signs and symptoms of RA[95] and in patients with juvenile idiopathic arthritis who did not respond to traditional TNF blockers.[96] Treatment with *belatacept*, an alternative human CTLA-4 Ig, in a phase I/II clinical trial evaluating multiple doses revealed the preliminary efficacy of this drug in the treatment of RA.[97]

BTLA polymorphism is associated with susceptibility to RA,[98] and the expression of BTLA is decreased in T cells from patients with RA.[99] LAG-3$^+$ Treg cells have been associated with the development of RA, and their frequency is lower in patients with RA than in healthy individuals.[100] Moreover, LAG-3$^+$Foxp3$^-$ Tregs are highly effective in relieving joint severity and local and systemic inflammation.[101] TIM-3 is associated with RA disease activity[102] and involved in the immune dysregulation mediated by TNF-α, IL-17, and interferon-γ (IFN-γ) in this disease;[103] thus, TIM-3 may play an important role in the pathogenesis of RA. TIGIT overexpression in vivo improves the severity of RA by decreasing the production of IFN-γ and IL-17, increasing IL-10 cytokine levels and removing anti-collagen II antibodies.[104] CD4$^+$CD28$^-$ T cells from RA patients overexpress 2B4 together with CD226 and CRACC, suggesting that these receptors could modulate this disease.[105] The roles of VISTA and CD5 in RA have been studied, and the relevant expression of these molecules in the pathology of RA relies on macrophages[106] and B cells,[107] respectively. Signaling by these receptors begins in the innate phase of inflammation, and their roles in T cells during RA need to be explored further. The above data suggest that these immunomodulatory receptors could have therapeutic roles in the development of RA, although at the moment, there are no data on their clinical effectiveness.

CD69-deficient mice show no overt signs of autoimmunity,[97] although they are more susceptible to asthma,[63] contact dermatitis,[108] myocarditis,[109] colitis,[64] and RA[110] than wild-type mice due to exacerbated Th1 and Th17 responses. The role of CD69 was first described in the synovial fluid T cells of RA patients;[111] these T cells fail to express CD25 or produce IL-2, and consequently, they are not able to proliferate properly. Moreover, CD69 expression by synovial T cells in RA patients correlates with disease activity.[112] CD69-deficient mice show a higher incidence and severity of collagen-induced arthritis (CIA), with exacerbated T and B cell responses, than wild-type mice.[110] These mice also show reductions in the levels of tumor growth factor-β1 (TGF-β1) and TGF-β2, which are protective cytokines in CIA, in inflammatory foci and parallel increases in the levels of proinflammatory cytokines, such as RANTES and IL-1β, leading to increased joint inflammation and cartilage and bone erosion. The immunomodulatory receptor CD69 expressed by T cells regulates the immune response through control of TGF-β production[26] and regulates the differentiation and activation of Treg and Th17 cells through control of the Stat5/miR-155/SOCS1 (ref. [62]) and Jak3–Stat5 pathways,[28] respectively. CD69 is also a hallmark of tissue-resident memory T cells, together with CD103 and CD49a, with

direct implications on this pathology and autoimmune diseases in general.[113] However, the potential of this receptor as a possible therapeutic tool in RA has not been explored in the clinic.[4] The potential roles of T cell immunoreceptors and their involvement in autoimmune pathologies are outlined in Fig. 2.

The efficacy of these immunomodulatory receptors in modulating autoimmune diseases is experimentally associated with certain changes in immune markers, which can be exploited as biomarkers. Some of the receptors mentioned above may indicate the immune process that is taking place due to different treatments. In the next few years, more research will be needed to decipher whether these receptors should be exploited not only to predict the efficiency of treatments and identify autoimmune patients that could possibly benefit from the treatments but also to predict possible adverse effects of treatments.

IMMUNOMODULATORY T CELL RECEPTORS IN CARDIOVASCULAR DISEASE

Increasing numbers of clinical trials have been conducted in patients with acute myocardial infarction (MI) and heart failure, such as cardiomyopathy and myocarditis, using a variety of cell types, including bone marrow stem cells, mesenchymal stem cells, and cardiac resident stem cells. However, none of these preclinical trials or studies have yielded clear results in terms of regeneration of cardiac tissue. In this scenario, immunomodulation has gained interest for its use not only as an adjuvant in cellular therapies but also as cardioprotective therapy in different cardiovascular diseases. T cell responses are important in the onset, progression, and resolution of acute myocardial events and chronic heart failure.[114] Here, we review the roles of immunomodulatory T cell receptors in different cardiovascular diseases, including atherosclerosis as the trigger of MI.

Immunomodulation in atherosclerosis treatment

T lymphocytes are present during all stages of development in human atherosclerotic lesions,[115] although their role in the disease has been controversial for decades. Increasing evidence demonstrates the modulatory role of the immune system in experimental and clinical arteriosclerosis. The most recent and definitive evidence comes from the CANTOS (Canakinumab Antiinflammatory Thrombosis Outcome Study) clinical trial in which anti-inflammatory treatment was found to be associated with reduced cardiovascular risk.[116] These works provide strong evidence that immunomodulatory therapies have therapeutic potential in the development and management of clinical atherosclerosis and other chronic inflammatory conditions. Even statins have been seen to regulate certain immune molecules, such as modulating MHC II through arterial cells and restraining T cell responses[117] through IFN-gamma.[118] T cell-mediated immunity plays a significant role in atherosclerosis development.[119] The role of $CD4^+$ T cells is quite complex; Th1 cells have a proatherogenic role, while Treg cells protect against disease development. However, the roles of Th2, Th17, and follicular helper T cells are still controversial. $CD8^+$ T cells have pleiotropic effects on the development of atherosclerosis; they can induce an inflammatory response via inflammatory cytokines, and cytotoxic activity towards endothelial cells increases the progression of atheroma plaques, whereas the same cytotoxic activity towards macrophages and regulatory $CD8^+$ T cell subsets can inhibit inflammatory responses and atherosclerosis progression.[120] Interestingly, $CD8^+$ T cell function is regulated by the PD-1 and Tim-3 signaling pathways in atherosclerosis.[121] In humans, the $CD8^+PD\text{-}1^+Tim3^+$ T cell subset, which is enriched in central memory T cells, is abundant in patients with atherosclerosis presenting with increased antiatherogenic cytokine production and decreased proatherogenic cytokine production. In patients with acute coronary syndrome, the expression of PD-1 and PD-L1 on circulating T cells is very low.[122,123] Blockade of $CD8^+PD\text{-}1^+Tim3^+$ T cells increases TNFα and IFNγ production. Ab-mediated inhibition of TIM-3 was shown to aggravate atherosclerosis by limiting efferocytosis and T cell responses in mice.[124] In parallel, pretreatment of apolipoprotein-deficient (apoE−/−) mice with CTLA-4-IgG can reverse disease acceleration, blocking the signaling pathway in T cells and T cell activation,[125] whereas CTLA-4-blocking antibodies strongly increase atherosclerotic lesion numbers,[126] and the overexpression of transgenic CTLA-4 in apoE−/− mice enhances Treg-mediated suppression and prevents atherosclerosis development.[127] Together, these studies demonstrate that CTLA-4 limits plaque development by inducing anti-inflammatory T cell responses, positioning CTLA-4 as a promising target in atherosclerosis.

The lipoprotein scavenger receptor BI (SCARB1) rs10846744 noncoding variant has been associated with atherosclerosis, independent of traditional cardiovascular risk factors, and with LAG3. A novel study proposed plasma LAG3 as an independent predictor of HDL-C levels and coronary heart disease risk.[128]

BTLA was recently described to be mostly expressed on B cells in patients with cardiovascular disease and in follicular B2 cells in Ldlr−/− mice fed a high-fat diet. However, the use of an agonistic anti-BTLA antibody was shown to inhibit atherosclerosis development in an animal model with significant increases in regulatory B and T cell numbers,[129] indicating an immunomodulatory effect mediated through T cells in atherosclerosis.[129] These findings suggest BTLA as a new promising target for the treatment of atherosclerosis.

Treatment with agonistic anti-TIGIT antibodies inhibits $CD4^+$ T cell responses, although this treatment does not affect atherosclerotic lesions in LDLr−/− mice fed a high-fat diet.[130] These data suggest that myeloid cells can increase their activity by crosstalk with T cells, negatively influencing disease. Similarly, VISTA is a receptor and a ligand with immunosuppressive effects on IFNγ and TNFα in both T cells and macrophages,[131] which adopt an anti-inflammatory M2 phenotype that can also play a role in atherosclerosis development.[132]

Although CD5 is expressed in T cells from atherosclerotic lesions of apoE−/− and ldlr−/− mice,[133] the role of CD5 expression in T cells during disease development is unknown. However, the role of CD69 in atherosclerosis was described recently.[32] An interaction between CD69 and OxLDL was identified to be responsible for the anti-inflammatory phenotype of T cells needed to restrain plaque development. The binding of OxLDL to CD69 in mouse and human T cells induces the expression of NR4A1 and NR4A2, members of the NR4A subfamily of human nuclear receptors involved in regulatory T cell differentiation.[134] CD69 depletion in the lymphoid compartment of ldlr−/− mice results in reduced expression of NR4A1 and NR4A3 in T cells in mice fed a high-fat diet. The inhibition of these signaling pathways favors the development of Th17 cells, promoting a proinflammatory environment and accelerating the development of atheroma plaques.[32,135] In addition, the expression of the CD69 and NR4A1 genes in peripheral blood cells was studied in a cohort of subjects with exhaustive characterization of subclinical atherosclerosis belonging to the *Progression of Early Subclinical Atherosclerosis* (PESA) study,[136] including in healthy and asymptomatic individuals. The data showed that CD69 and NR4A1 mRNA levels decreased with the progression of the atheroma plaque, validating the data from the in vivo model. Analysis of the CD69 receptor in the PBLs of this cohort showed that the loss of CD69 expression was very significantly associated with the development of atheroma plaques, even when this association was corrected for other cardiovascular risk parameters, such as the levels of OxLDL. Further studies on the new regulatory OxLDL/CD69 pair in

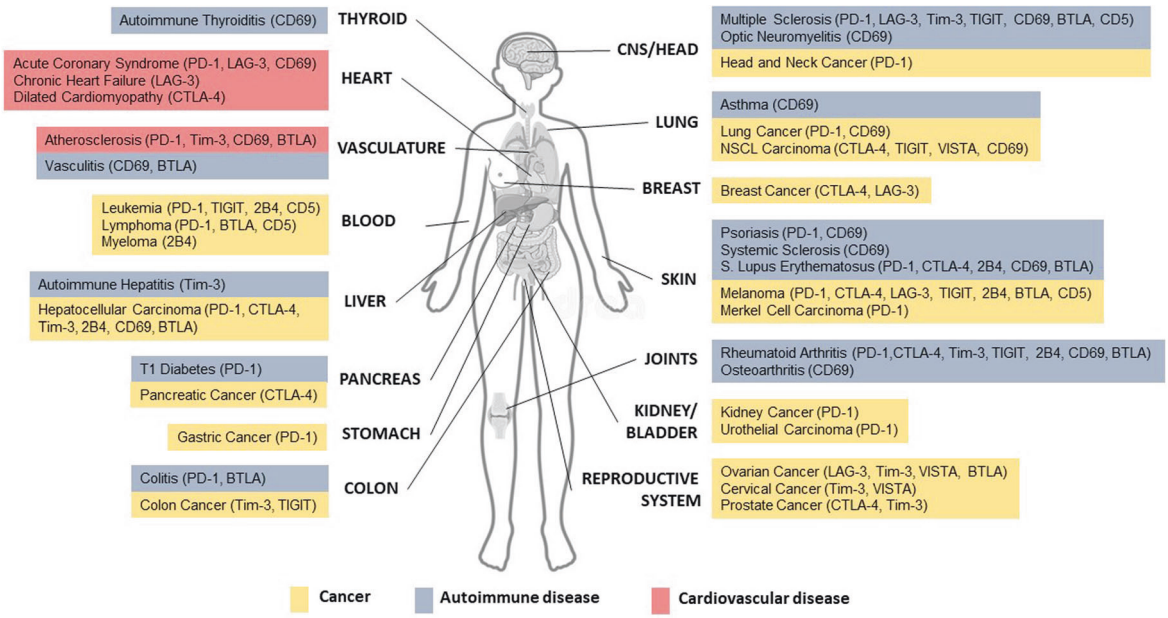

Fig. 2 Contributions of inhibitory receptors on T cells to human autoimmune diseases (blue), cardiovascular diseases (red), and cancer (yellow) in different organs. Signaling through immunomodulatory membrane receptors is pivotal to promoting immune tolerance and avoiding excess deleterious T cell activation and reactivity. Activation or inhibition of immunomodulatory receptors on T cells may be beneficial or detrimental, depending on the disease context. In different cancer types, immunotherapy based on the blockade of these inhibitory receptors leads to increased and relatively long-lasting T cell responses against tumor cells, resulting in efficient tumor clearance. However, autoimmunity due to self-reactivity, which is related to excessive T cell activation, is the main side effect of cancer immunotherapy. Additionally, dysfunction of inhibitory receptors on T cells is linked to different autoimmune disorders, such as thyroiditis, vasculitis, hepatitis, type 1 diabetes, colitis, multiple and systemic sclerosis, optic neuromyelitis, asthma, psoriasis, systemic lupus erythematosus, rheumatoid arthritis, and osteoarthritis. Favoring signaling through these receptors has emerged as a strategy to restore tolerance in autoimmune patients. The T cell response is also an important mediator of atherosclerosis and acute and chronic myocardial disease development and progression. Thus, different immunomodulatory receptors on T cells are therapeutic candidates in cardiovascular diseases. This schematic summarizes the immunomodulatory T cell receptors (in parentheses) that have been implicated in different human diseases

human lymphoid cells during atherosclerotic disease progression will provide novel insights into targeting these pathways for the prognostic evaluation/treatment of cardiovascular diseases.

Acute myocardial infarction

MI results from occlusion of the coronary arteries, mainly due to a thrombus caused by rupture of a lipid atherosclerotic plaque, which causes ischemia in a region of the heart. Ischemia causes subsequent cardiomyocyte death and triggers inflammatory and repair mechanisms. In recent years, multiple studies have highlighted the roles of T cells not only in the development of atherosclerosis but also in the progression after MI, contributing to cardiac function and remodeling.[137] Since immunomodulatory T cell receptors are also checkpoints in the inflammation underlying atherosclerosis, ICI therapy may create an increased risk for atherosclerotic cardiovascular events, such as MI, in cancer patients.[138] Acute cardiovascular manifestations derived from atherosclerosis appear progressively after several years of subclinical disease. Although ICI therapy has been implemented in the clinic for the past decade, it may be too early to have a clear picture of the effect of ICIs on the incidence of acute MI. However, in recent cumulative studies, MI has been reported to be a complication in patients treated with ICIs, with an incidence ranging from 1 to 3%.[139,140] Some studies indicate that MI occurs less than a year after ICI treatment, suggesting that immunomodulatory therapy can accelerate the progression and instability of pre-existing atherosclerotic lesions rather than cause de novo plaque formation.[141] An analysis of coronary plaques suggested that the T cell proportion was higher in ICI-treated patients than in untreated patients,[142] consistent with an exacerbated T cell response after ICI therapy in the coronary arteries, a possible trigger of acute events.[142]

Beyond their roles in atherosclerotic plaque instability and rupture, some immunomodulatory receptors have been proposed to be involved in regulatory mechanisms limiting the degree of inflammation after myocardial ischemic events. Variants of the PD-1-[143] and CTLA-4-encoding genes[144] are associated with an altered risk of MI,[145] and proteomic profiling analysis identified CD5 antigen-like and others as marker proteins associated with new-onset atherosclerotic cardiovascular disease risk.[145] PD-1 expression is upregulated in peripheral leukocytes when they increase in number during the first hours after MI and then decrease after reperfusion. In contrast, lower levels of PD-1 expression in T cells are associated with larger infarction lesions.[146]

Furthermore, analyses of the peripheral blood phenotype of MI patients revealed that circulating $CD4^+$ T cells overexpress CD69 (ref. [147]) and that regulatory T cells overexpress CTLA-4 early after MI.[148] T cells show evident CD69 expression not only in the peripheral blood but also in the culprit coronary artery plaque.[149] This evidence suggests that anti-inflammatory molecules are rapidly stimulated after infarction to prevent excessive inflammation and damage, although little is known about the particular mechanisms underlying these processes.

Myocarditis and dilated cardiomyopathy

Inflammation of the myocardium, or myocarditis, can be caused by infectious or noninfectious triggers. Self-reactive $CD4^+$ T cells are a common feature of different types of myocarditis. These cells recognize cardiac antigens and increase the inflammatory response. If inflammation persists, cardiomyocyte death results

in the loss of myocardial tissue and fibrosis, leading to the development of dilated chronic cardiomyopathy.[150] Thymic epithelial cells present self-antigens to immature T lymphocytes to deplete the lymphocytes with self-reactive potential. Interestingly, some cardiac antigens, such as alpha myosin heavy chain (αMyHC), are poorly represented in the thymic epithelial cells (TEC) repertoire of autoantigens. As a result, heart-specific autoreactive T cells escape thymic negative selection.[151] These naive T cells can recognize cardiac autoantigens presented by dendritic cells in the lymph nodes that drain the heart, but their activation may be dampened by peripheral tolerance mechanisms. Peripheral tolerance includes suppression by Treg cells and immunomodulatory receptors or immune checkpoints. Dysfunction or inhibition of immune checkpoints can cause activation and expansion of these self-reactive T cell clones. In addition, a storm of costimulatory signals occurring in the context of heart infection or tissue damage can contribute to overcoming peripheral tolerance and triggering autoimmune responses to the heart.[152] The potential roles of T cell immunoreceptors and their involvement in cardiovascular diseases are outlined in Fig. 2.

CARDIOVASCULAR IMMUNE-RELATED ADVERSE EVENTS (IRAES) OF IMMUNOMODULATORY RECEPTOR THERAPY

Myocarditis is one of the irAEs of ICI therapy for cancer. Patients with ICI-related myocarditis have T cell infiltration of the myocardium usually accompanied by a severe clinical presentation, such as a decreased ejection fraction, cardiogenic shock, severe arrhythmia, and advanced atrioventricular block.[153–155] The lack of myocarditis-specific biomarkers makes diagnosis difficult, so only severe cases are usually reported, which could explain the observed low incidence and high mortality. Approximately 0.1–1.1% of patients treated with ICI therapy develop myocarditis, although myocarditis is fulminant in up to 50% of these patients. According to different studies, the time to onset of symptoms of ICI-induced myocarditis varies between 1 and 2.5 months after the start of treatment with an ICI.[154,156,157]

ICI-induced myocarditis has been described in patients administered an anti-PD-1 antibody, an anti-CTLA-4 antibody or a combination of both,[154] although additional studies with larger sample sizes should be performed to attribute specific myocardial adverse effects to each ICI.

Preclinical data indicate critical roles for the PD-1/PD-L1 and CTLA-4 pathways in regulating autoimmune responses to the heart. Depletion of functional PD-1 in BALB/c mice but not in BALB/c Rag2−/− mice leads to the spontaneous development of fatal autoimmune dilated cardiomyopathy,[158] suggesting a critical role for PD-1 in the regulation of cardiac autoimmunity mediated by lymphoid cells. Subsequent studies have described the increased susceptibility of PD-1-deficient mice to experimental autoimmune myocarditis, which is established by immunization with an αMyHC peptide.[159] Mice lacking CTLA-4 die within the first month from severe lymphoproliferative disease with involvement of the heart and development of fulminant myocarditis.[160] In addition, the administration of anti-PD-1 plus anti-CTLA-4 combination therapy to nonhuman primates results in the development of multiple organ toxicities, including myocarditis, with cardiac infiltration of mononuclear cells consisting primarily of T cells and with a composition similar to that observed in patients with ICI-induced myocarditis.[161] PD-L1 was first described as highly expressed in the mouse heart.[162] In addition, different studies have identified PD-L1 expression in the myocardium of patients with ICI-induced myocarditis.[153] Other studies have shown that the cardiac endothelium positively regulates PD-L1 in response to IFNγ as a mechanism of tissue-based tolerance and T cell depletion[163] in a negative feedback loop in the heart to maintain resistance to local effector T cell-mediated responses.

The exact mechanism of ICI-induced myocarditis development remains unclear. A suggested explanation is that T cells may recognize homologous antigens in the heart and tumors by a molecular mimicry mechanism.[153] Specific muscle antigens, such as troponin and desmin, were found in tumor biopsies, supporting the idea that the same T cell clones can detect antigens present in both the myocardium and tumors. Consistently, myocarditis secondary to treatment with ICIs is more common when there is also autoimmune involvement of the skeletal muscle or myositis.[164] As an alternative explanation, T cell clones that recognize different antigens can undergo aberrant activation. As discussed above, some T cell clones that recognize cardiac epitopes escape negative selection in the thymus, so when peripheral tolerance mechanisms are blocked by immunotherapy, the expansion of a heart-specific T cell response can be triggered.[151]

Although CD69 involvement in human disease remains unexplored, preclinical studies indicate that a lack of other immunomodulatory T cell receptors increases susceptibility to myocarditis and dilated cardiomyopathy. CD69 deficiency leads to exacerbated Th17-mediated autoimmune myocarditis and subsequent cardiomyopathy after immunization with the αMyHC peptide.[109] Although LAG-3 deficiency alone does not induce cardiac autoimmunity, depletion of LAG-3 in PD-1-deficient mice increases the susceptibility to spontaneous T cell-mediated fulminant myocarditis.[86] Finally, administration of an anti-Tim-3 antibody exacerbates male myocardial inflammation in a mouse model of viral myocarditis.[165,166] Taken together, this evidence suggests that multiple inhibitory signals in T cells prevent cardiac autoimmunity.

ICIS IN CANCER

In recent years, there has been a large increase in the development and implementation of cancer immunotherapies. FDA approval of the use of blocking antibodies specific for CTLA-4 (ipilimumab) or PD-1 (nivolumab) in humans and biologics such as CTLA-4-Ig (abatacept) has been key to producing significant improvements in the treatment of various types of cancer, especially melanoma. Unlike radiotherapy and chemotherapy, which are intended to directly interfere with the growth and survival of tumor cells, immunotherapies target tumors indirectly, favoring an increase in antitumor immune responses that arise spontaneously in many patients. ICI therapy could therefore be used to modulate the immune response to improve the treatment of many types of cancer (Fig. 2).

Cancer mechanisms to bypass the immune system

To understand the modes of action of ICIs, it is important to recognize the dynamic interaction between cancer and the immune system that occurs during the course of the disease. Cancer cells are genetically unstable, which contributes to their uncontrolled proliferation and expression of antigens that the immune system can recognize. These antigens include normal proteins overexpressed by cancer cells and new proteins that are generated by mutation and genetic rearrangement.[167] Cytotoxic $CD8^+$ T cells are particularly effective in mediating antitumor immune responses by recognizing tumor-specific antigens presented by MHC I. $CD8^+$ T cells become licensed effector cells after appropriate stimulation by antigen-presenting cells, which collect antigens at the tumor site. In addition to displaying antigenic peptides presented on MHC molecules, antigen-presenting cells must provide costimulatory signals via surface receptors, such as CD28, and cytokines, such as IL-12, for effective stimulation of T cells.[168]

Tumor cells adopt a variety of mechanisms to prevent immune recognition and immune-mediated destruction. Established

tumors arise through the selection of clones that can evade the immune system, a process known as immunoediting.[169] Tumor cells can evade immune recognition directly by inhibiting molecules that make them vulnerable, such as tumor antigens or MHC class I.[170] Alternatively, tumors can evade immune responses by taking advantage of mechanisms the body has developed to prevent immunopathologies. The mediators involved in these mechanisms include inhibitory cytokines, such as IL-10 and TGF-β; inhibitory cell types, such as Tregs, regulatory B cells, and MDSCs; metabolic modulators, such as indoleamine 2,3-dioxygenase; and immunomodulatory receptors, such as PD-1 and CTLA-4.[171,172]

Immune exhaustion also contributes to immune dysfunction in cancer. Originally described in the context of chronic viral infection, where the host cannot eliminate the pathogen, it is now evident that exhausted T cells can also promote cancer development.[173,174] Under these conditions, the persistent high antigenic load leads T cells to regulate immunomodulatory receptors, whose signaling subsequently leads to a progressive loss of proliferative potential and effector functions and, in some cases, exhausted T cell elimination.[175] Therefore, exhaustion is a physiological mechanism designed to limit immunopathology during persistent infection and a major obstacle to antitumor immune responses.[176]

Anti-CTLA4 treatment

CTLA-4 blockade has been shown to promote T cell activation and intratumoral Treg cell depletion.[177] Ipilimumab (IgG1) and tremelimumab (IgG2) are the two human anti-CTLA-4 antibodies that have undergone clinical evaluation. In a 2010 phase III clinical trial, in previously treated patients, treatment with ipilimumab at a dose of 3 mg/kg with or without administration of a gp100 peptide vaccine was evaluated and compared to peptide vaccine administration alone, finding an improvement in overall survival (OS) in both groups of patients who received ipilimumab, which led to the approval of ipilimumab for patients with metastatic melanoma.[178] A similar test was performed with a combination of dacarbazine with or without ipilimumab at a dose of 10 mg/kg, which improved survival but increased liver toxicity.[179] In addition, a pharmacokinetic analysis showed that ipilimumab had linear pharmacokinetics in the dose range of 3–10 mg/kg.[180] The efficacy of ipilimumab was validated in a randomized, double-blind, phase III trial after complete resection of high-risk stage III melanoma.[181] Studies in other types of cancer have shown the efficacy of ipilimumab in some renal cell carcinoma patients, including patients who did not respond to other immunotherapies.[182] In patients with B cell lymphoma, CTLA-4 blockade with ipilimumab had antitumor activity and was well tolerated at doses of 1 and 3 mg/kg;[183] however, a phase III trial did not show a significant difference in terms of survival between the ipilimumab group and the placebo group in patients with castration-resistant metastatic prostate cancer.[184] Tremelimumab, an alternative antibody that blocks CTLA-4, continues to be investigated in clinical trials and has also demonstrated long-lasting responses and acceptable tolerability in patients with melanoma,[185] refractory metastatic colorectal cancer,[186] hepatocellular carcinoma,[187] or malignant mesothelioma.[188]

Anti-PD1 treatment

PD-1 regulates the activation of T cells in peripheral tissues and is expressed in activated T cells, Treg cells, activated B cells, and NK cells. The endogenous PD1 ligands, PD-L1 and PD-L2, are expressed in activated immune cells and nonhematopoietic cells, including tumor cells; tumor cell expression is the mechanism by which these cells circumvent the immune system[189]. Inhibition of these interactions with therapeutic antibodies improves the T cell response and stimulates antitumor activity.[162]

The first anti-PD-1 inhibitor evaluated was nivolumab (BMS-936558), a human mAb (IgG4) that blocks the immunomodulatory receptor PD1.[190]

A phase I trial in which different doses were tested found that nivolumab is safe and produces positive responses in 16–31% of pretreated patients across all types of solid tumors tested, with a duration of at least 1 year.[191] For ipilimumab, both adverse effects and efficacy depend on the dose, but for nivolumab, these correlation are not observed, which can be explained by the high correlation between the receptor and antibody even at low doses.[192]

Pembrolizumab (MK-3475) is an alternative humanized high-affinity IgG4 antibody recognizing PD1. It has been evaluated in several phase I clinical trials, and three different doses have been tested in patients with metastatic melanoma who were never previously treated and in a cohort patients including patients previously treated with *ipilimumab* and those who were not previously treated with *ipilimumab*. Most of the adverse effects observed were seen with the highest dose, and no significant differences among the three treatment subgroups were, but patients with a smaller tumor burden had a greater capacity to respond to pembrolizumab.[193]

Pidilizumab (formerly CT-011) is a humanized anti-PD-1 IgG1 antibody. It was one of the first anti-PD-1 agents used in cancer patients. Several clinical trials at different stages, which treated patients with hematological malignancies or metastatic melanoma, have shown that treatment is generally well tolerated, with no treatment-related deaths, but in some patients, previous treatment with ipilimumab did not produce an advantage in treatment response. Pidilizumab appears to be associated with lower response rates in melanoma than nivolumab or pembrolizumab, but the 1-year OS rate is similar to that reported in studies of nivolumab.[193,194]

Anti-PD-L1 treatment

MPDL-3280A is an anti-human IgG1 antibody engineered to block PD-L1, with the Fc domain of IgG1 mutated to completely nullify the effects of antibody-dependent cellular cytotoxicity and complement-dependent toxicity. Furthermore, PD-L1 is particularly expressed in tumors infiltrated by immune cells, which implies that this treatment mainly benefits patients with more inflamed tumors.[193] This antibody exerts its mechanism of action by blocking PD-1/PD-L1 signaling, and unlike antibodies that block PD-1, those that block PD-L1 avoid the side effects that result from blocking the interaction of PD1 with PD-L2 and that of PD-L1 with CD80. *MPDL3280A* has been evaluated in multiple tumor types, with safety and preliminary efficacy identified in melanoma, renal cell carcinoma, non-small cell lung carcinoma, colorectal cancer, gastric cancer, and squamous cell carcinoma of the head/neck. Other PD-L1-inhibiting antibodies are *BMS-936559*, which has been shown to be safe and clinically active in various types of tumors in phase I clinical trials, and *MEDI-4736*, which is currently in clinical development.[191]

Combination therapies

Blocking immune checkpoint molecules with multiple inhibitory antibodies can improve treatment efficacy. For example, for ipilimumab, the percentage of patients with a reduction in tumor size or the ORR (objective response ratio) achieved with monotherapy was 6%, and the OS time was 10 months.[178] In phase I work, nivolumab had an ORR of 31%, and the OS time was 17 months. However, in a phase I trial combining ipilimumab with nivolumab, the ORR was 53% at the maximum tolerated dose, and all subjects who responded to treatment showed a ≥80% decrease in their tumor burden after 12 weeks of treatment.[195] Patients treated with this combination therapy showed a more frequent rate (53%) of adverse effects. This combination, and other

combinations of mAbs, should be confirmed in other phase III clinical trials, which are currently underway.[191] Combination therapy with other noninhibitory immune checkpoint agents is also being evaluated. The feasibility of other combination therapy strategies is being explored in different trials, each with compelling preclinical justification. The most direct combination therapy approach would be a combination of immunotherapy and chemotherapy, as there is a multitude of preliminary data from patients who have been included in clinical trials evaluating immunoregulators after an insufficient response to conventional chemotherapy; in particular, there are treatments that combine ipilimumab with cycles of chemotherapy with carboplatin, etoposide or paclitaxel in patients with lung cancer[196–198] and advanced melanoma.[199]

The combination of ICIs with alternative treatments that favor systemic stimulation of the immune system, such as vaccines, cytokine therapy, and adoptive cell therapy,[200–202] would be an interesting approach. The combination of immunomodulatory agents with agents producing a local effect that causes tumor regression, such as radiotherapy, is based on the *abscopal* effect, which describes the phenomenon of tumor regression outside the irradiated field caused by the release of cytokines and antigens induced by irradiation that enhances the systemic immune response against the tumor. The combination of radiotherapy with ipilimumab has been evaluated in phase I/II trials in prostate cancer, which showed an improvement in treatment response with tolerable adverse effects.[203] Similar to the combination with radiotherapy, other combinations are being investigated with different alternatives strategies for local control, such as cryoablation and electrochemotherapy. The *abscopal* effect is also observed after treatment with cytotoxic therapies, such as B-Raf protein or VEGF inhibitors, capable of stimulating the immune system by favoring the production of antigens.[202,204] Some of these studies, such as one combining ipilimumab with GM-CSF, showed an improved survival rate with few side effects for the patients treated with the combination therapy compared to those treated only with ipilimumab. The combination of ipilimumab with bevacizumab, a VEGF-blocking antibody, improves the immune responses against tumors with tolerable toxicity. However, some combined therapies, such as treatment with vemurafenib and ipilimumab, produce high liver toxicity.[205] In summary, the use of combined therapies seems to be a step forward in the search for a cure for cancer, but more studies are needed to adjust the doses very precisely and reduce adverse effects.

The dual blockade of LAG-3/PD-1 was recently identified to be clinically relevant and is being tested in clinical trials. A recombinant fusion protein with four extracellular domains of LAG-3 has been tested safely in combination with pembrolizumab or nivolumab in patients with melanoma with progressive disease after immunotherapy.[206] Similarly, the combination of anti-VISTA molecules with anti-PD-1 therapy is under investigation. Combination of CA-170, an oral inhibitor of VISTA, with PD-1 has shown positive results in different clinical trials.[207]

ICI-based therapies have been able to increase the average life expectancy of cancer patients, yet mortality remains high among patients with advanced-stage disease, highlighting the need for further innovation in the field. These therapies appear to be most effective in patients with pre-existing antitumor immunity, suggesting that, in patients without such immunity, these drugs cannot mediate de novo antitumor immune responses. It would therefore be interesting to implement de novo generation of antitumor immunity with these treatments. To achieve this objective, it is essential to improve the understanding of the mechanisms of action of these treatments to identify ways to improve their use not only through specific guidance in certain types of patients who are more likely to respond but also through a correct combination with other therapies that will increase the responses of patients in whom these treatments are less efficient. Furthermore, as the understanding of the mechanisms of action of these therapies improves, it will also be easier to prevent possible adverse effects caused by these therapies.

ICIS AND IRAES

Although there is no doubt that treatments targeting these immunomodulatory T cell receptors have created a new era in cancer treatment and increased patient survival, different adverse events related to the immune system have been observed. These adverse events are called irAEs and are directly related to the mechanisms of action of PD-1 and CTLA-4.[139] Under physiological conditions, these molecules prevent autoimmunity and limit activation of the immune system, but inhibition of these two receptors as a cancer therapy causes a wide range of side effects that resemble autoimmune reactions. Analysis of sera and biopsies from patients with irAEs has revealed that these reactions are mediated by activated $CD4^+$ and $CD8^+$ T cells infiltrating tissues, as well as by increases in the levels of proinflammatory cytokines.[208] IrAEs can impact multiple organs and systems, including the skin, gastrointestinal tract, liver, endocrine system, eyes, kidneys, nervous system, pancreas, and heart. Almost all patients treated with ICIs experience mild side effects, such as diarrhea, fatigue, itching, rash, nausea, and decreased appetite. Apart from myocarditis mentioned earlier in this review, serious adverse reactions include severe diarrhea, colitis, increased alanine aminotransferase levels, inflammatory pneumonitis, and interstitial nephritis.[209] Patients who experience exacerbation of pre-existing autoimmune conditions, such as psoriasis,[210] or who develop new autoimmune conditions, such as T1D mellitus,[211] have also been reported. Particularly serious side effects may require cessation of treatment, although these patients may still respond thereafter.

Anti-CTLA-4 antibody-induced IrAEs are common but generally low grade, although severe and life-threatening cases have also been reported. The skin and gastrointestinal tract are more frequently affected, while hepatic, endocrine, and neurological events are less common.[212] Rash is generally the first irAE to manifest after the first or second dose of ipilimumab.[213] Colitis and diarrhea are the most common gastrointestinal IrAEs after the first few months of ipilimumab treatment, which can be very serious, particularly in rare cases where perforation of the gastrointestinal tract occurs. A phase III trial in patients with advanced melanoma demonstrated that ipilimumab adverse events were mild, with sporadic life-threatening cases.[214] Anti-CTLA-4 antibodies can induce a severe and extensive form of inflammatory bowel disease, suggesting the need to avoid nonsteroidal anti-inflammatory drugs in patients treated with anti-CTLA-4 therapy.[215] Hepatic irAEs are rare and may manifest as an acute hepatitis or biliary pattern, which can be reversed with corticosteroids.[216] In addition, autoimmune hypophysitis has been reported in up to 17% of patients with melanoma or renal cell carcinoma treated with anti-CTLA-4 therapy, which may be related to pituitary gland enlargement and hormonal deficiencies.[217] The risk of irAEs in the case of ipilimumab treatment depends on the dose, and the mean time to onset of adverse effects is 10 weeks.[218]

In anti-PD-1/PD-L1 treatment, 30–40% of patients experience skin toxicities.[219] The most common skin toxicities are lichenoid reactions, vitiligo, pruritus, and eczema. Vitiligo is observed only in patients with metastatic melanoma. Antibodies targeting the PD-1/PD-L1 axis have shown a favorable toxicity profile in preliminary trials with rates of relatively severe adverse events of 13% in patients receiving *MK-3475*, 9% in patients receiving *BMS-936559*, and 14% in patients receiving *nivolumab*. A unique and life-threatening toxicity for these agents is pneumonitis, which was the cause of death in three patients (1%) in a phase I clinical trial of nivolumab despite corticosteroid treatment.[219] Cardiac irAEs

due to PD-1 axis blockade have attracted attention due to the high mortality rates but have an incidence of less than 1%. Endocrinopathies derived from PD1 axis blockade include hypophysitis, thyroiditis, hypothyroidism, hyperthyroidism, and T1DM. In addition to the previously described pathologies, there are some rare ICI-mediated toxicities that have neurological, ocular, or hematological manifestations.

The incidence of adverse effects is higher in patients treated with combination therapies, who are more susceptible to acute kidney injury than those treated with ipilimumab, nivolumab, or pembrolizumab monotherapy. Up to 7% of people treated with anti-PD-1 monotherapy and up to 33% of patients treated with combination anti-PD-1 and anti-CTLA-4 therapy develop hepatitis.[220] Combined treatment with these ICIs causes a decrease and blockade in Treg cell function, which also produces other pathologies that are included within the irAEs, such as increases in the incidence of proatherogenic lesions or pneumonitis. Another event considered an irAE is the generation of autoantibodies, as occurs in thyroiditis, since treatment with PD1 inhibitors can promote the mobilization of pre-existing autoantibodies against the thyroid.[220] The study of the pathophysiology of these adverse effects and toxicities should produce a more precise understanding of the functions of ICIs in the tumor and tissue contexts and thus favor the improvement of therapies, with avoidance of possible adverse effects.

Autoimmune diabetes mellitus is related to blockade of CTLA-4, PD-1, its ligand (PD-L1), and combination ICI therapy.

Recently, it has been demonstrated that a constitutive reduction in CTLA-4 signaling does not accelerate SLE in a susceptible NZM2328 animal model.[221] Although a patient with de novo SLE nephritis after ipilimumab treatment was reported,[222] SLE patients treated with ICIs do not seem to exhibit disease worsening.[223] De novo cases of SLE have yet to be reported in patients treated with other ICIs.

In general, the knowledge of possible biomarkers in the field of immunotherapy is very limited in aspects related to predicting the efficiency and suitability of different treatments. The field of biomarkers for predicting possible adverse effects induced by immunotherapy is even less investigated. Therefore, the development of the field of biomarkers to cover the negative aspects of immunotherapy and potentially predictand the suitability of treatments will be very important.

CONCLUDING REMARKS AND FUTURE DIRECTIONS

T cells are key in the development and control of inflammatory diseases of autoimmune origin or cancer; very recently, it has been shown that they also play key roles in pathologies such as acute MI, atherosclerosis, and myocarditis, highlighting the relevance of T cells in cardiovascular disease.[224] Different molecular tools blocking immunomodulatory receptors on T cells have emerged as some of the most promising cancer therapies in the last decade. However, the potential of targeting immunomodulatory T cell receptors in other diseases, such as autoimmunity or cardiovascular disease, which is the leading cause of death worldwide,[225] has been little explored. In addition to the most well-known receptors in clinical practice, PD-1 and CTLA-4, there is a battery of immunomodulatory receptors whose immunoregulatory properties have been described more recently, but their therapeutic potential in clinical practice remains unexplored. In contrast, other T cell receptors, such as CD69, have roles in the development of autoimmunity and in cardiovascular disease in mice and humans, and blockade of this receptor has antitumor properties;[226] however, its role in human cancer has never been addressed.[227] In this review article, we have summarized the mechanisms of action of these immunomodulatory receptors expressed by T cells, paying special attention to the less explored receptors, including their potential development in the clinic for treatment of cancer, cardiovascular disease, or autoimmune diseases, such as diabetes, lupus, or RA.

The use of inhibitory drugs and mAbs against these immunomodulatory receptors can be equally effective in cancer and autoimmune diseases. An example is *abatacept* (CTLA-4-Ig), which is used mainly in melanoma, but recent clinical trials show that it has potential in the treatment of autoimmune diseases, such as RA, in patients refractory to treatment with TNF-α blockers, indicating the potential of immunomodulatory receptor-based therapies in several pathologies that have not yet been explored. In this regard, the integration of technologies to deliver and control drug or mAb release has become one of the more important challenges in the field of immunotherapy. The strategies to deliver these drugs to the target organ are almost as important as the mechanism of action. For this reason, research in nanotechnology, one of the known strategies to improve the nanodelivery of chemotherapeutic agents, is becoming of interest in the field of immunotherapy.[228] In addition, the development of cellular therapies (e.g., CAR T cells) as targeted vehicles for use with regulatory molecules and/or combination with immunotherapy is a trend that we will see developed in the coming years and that, hopefully, will further improve the therapeutic potential not only in cancer but also in autoimmune and cardiovascular diseases.[229] In parallel, we need to advance the knowledge on the molecular and cellular mechanisms triggered by these receptors in each tissue, especially to prevent the triggering of adverse immune effects associated with these therapies in the most vulnerable tissues.

The field of biomedicine faces a challenge in the coming years, in which the study of the immunomodulatory receptors of T cells in the context of numerous pathologies can represent a great step forward in the treatment of fatal or chronic diseases that are highly prevalent in the world and lack cures. The enormous success of targeting the immune checkpoints PD-1 and CTLA4 in cancer should be enough to encourage the scientific community to study the other immunomodulatory T cell receptors in depth in the coming years and bring therapies related to these receptors closer to clinical practice in autoimmune and cardiovascular diseases.

ACKNOWLEDGEMENTS

This study was supported by competitive grants from the Ministerio de Ciencia, Innovación y Universidades, through the Carlos III Institute of Health-Fondo de Investigación Sanitaria (PI19/00545) to P.M.; CIBER Cardiovascular (Fondo de Investigación Sanitaria del Instituto de Salud Carlos III and cofunding by Fondo Europeo de Desarrollo Regional FEDER) to P.M.; and CAM (S2017/BMD-3671-INFLAMUNE-CM) from the Comunidad de Madrid to P.M. The CNIC is supported by the Instituto de Salud Carlos III (ISCIII), the Ministerio de Ciencia e Innovación and the Pro CNIC Foundation and is a Severo Ochoa Center of Excellence (SEV-2015-0505). R. B.-D. is supported by the Formación de Profesorado Universitario (FPU16/02780) program of the Spanish Ministry of Education, Culture and Sports.

ADDITIONAL INFORMATION

Competing interests: The authors declare no competing interests.

REFERENCES

1. Boardman, D. A. & Levings, M. K. Cancer immunotherapies repurposed for use in autoimmunity. *Nat. Biomed. Eng.* **3**, 259–263 (2019).
2. Lutgens, E. et al. Immunotherapy for cardiovascular disease. *Eur. Heart J.* **40**, 3937–3946 (2019).
3. Murphy, K. A. et al. Immunomodulatory receptors are differentially expressed in B and T cell subsets relevant to autoimmune disease. *Clin. Immunol.* **209**, 108276 (2019).

4. Gonzalez-Amaro, R., Cortes, J. R., Sanchez-Madrid, F. & Martin, P. Is CD69 an effective brake to control inflammatory diseases? *Trends Mol. Med.* **19**, 625–632 (2013).
5. Watanabe, N. et al. BTLA is a lymphocyte inhibitory receptor with similarities to CTLA-4 and PD-1. *Nat. Immunol.* **4**, 670–679 (2003).
6. Sharpe, A. H. & Pauken, K. E. The diverse functions of the PD1 inhibitory pathway. *Nat. Rev. Immunol.* **18**, 153–167 (2018).
7. Krummel, M. F. & Allison, J. P. CD28 and CTLA-4 have opposing effects on the response of T cells to stimulation. *J. Exp. Med.* **182**, 459–465 (1995).
8. Wing, K. et al. CTLA-4 control over Foxp3+ regulatory T cell function. *Science* **322**, 271–275 (2008).
9. Liu, X. et al. Cutting edge: a critical role of B and T lymphocyte attenuator in peripheral T cell tolerance induction. *J. Immunol.* **182**, 4516–4520 (2009).
10. Sedy, J. R. et al. B and T lymphocyte attenuator regulates T cell activation through interaction with herpesvirus entry mediator. *Nat. Immunol.* **6**, 90–98 (2005).
11. Huard, B., Prigent, P., Tournier, M., Bruniquel, D. & Triebel, F. CD4/major histocompatibility complex class II interaction analyzed with CD4- and lymphocyte activation gene-3 (LAG-3)-Ig fusion proteins. *Eur. J. Immunol.* **25**, 2718–2721 (1995).
12. Anderson, A. C., Joller, N. & Kuchroo, V. K. Lag-3, Tim-3, and TIGIT: co-inhibitory receptors with specialized functions in immune regulation. *Immunity* **44**, 989–1004 (2016).
13. Zhu, C. et al. The Tim-3 ligand galectin-9 negatively regulates T helper type 1 immunity. *Nat. Immunol.* **6**, 1245–1252 (2005).
14. Huang, Y. H. et al. CEACAM1 regulates TIM-3-mediated tolerance and exhaustion. *Nature* **517**, 386–390 (2015).
15. Harjunpaa, H. & Guillerey, C. TIGIT as an emerging immune checkpoint. *Clin. Exp. Immunol.* **200**, 108–119 (2020).
16. Reches, A. et al. Nectin4 is a novel TIGIT ligand which combines checkpoint inhibition and tumor specificity. *J. Immunother. Cancer* **8**, https://doi.org/10.1136/jitc-2019-000266 (2020).
17. Yu, X. et al. The surface protein TIGIT suppresses T cell activation by promoting the generation of mature immunoregulatory dendritic cells. *Nat. Immunol.* **10**, 48–57 (2009).
18. Cannons, J. L., Tangye, S. G. & Schwartzberg, P. L. SLAM family receptors and SAP adaptors in immunity. *Annu. Rev. Immunol.* **29**, 665–705 (2011).
19. Blackburn, S. D. et al. Coregulation of CD8+ T cell exhaustion by multiple inhibitory receptors during chronic viral infection. *Nat. Immunol.* **10**, 29–37 (2009).
20. Nowak, E. C. et al. Immunoregulatory functions of VISTA. *Immunol. Rev.* **276**, 66–79 (2017).
21. Wang, L. et al. VISTA, a novel mouse Ig superfamily ligand that negatively regulates T cell responses. *J. Exp. Med.* **208**, 577–592 (2011).
22. Jones, N. H. et al. Isolation of complementary DNA clones encoding the human lymphocyte glycoprotein T1/Leu-1. *Nature* **323**, 346–349 (1986).
23. Huang, H. J., Jones, N. H., Strominger, J. L. & Herzenberg, L. A. Molecular cloning of Ly-1, a membrane glycoprotein of mouse T lymphocytes and a subset of B cells: molecular homology to its human counterpart Leu-1/T1 (CD5). *Proc. Natl Acad. Sci. USA* **84**, 204–208 (1987).
24. Brossard, C., Semichon, M., Trautmann, A. & Bismuth, G. CD5 inhibits signaling at the immunological synapse without impairing its formation. *J. Immunol.* **170**, 4623–4629 (2003).
25. Tabbekh, M., Mokrani-Hammani, M., Bismuth, G. & Mami-Chouaib, F. T-cell modulatory properties of CD5 and its role in antitumor immune responses. *Oncoimmunology* **2**, e22841 (2013).
26. Sancho, D., Gomez, M. & Sanchez-Madrid, F. CD69 is an immunoregulatory molecule induced following activation. *Trends Immunol.* **26**, 136–140 (2005).
27. Lopez-Cabrera, M. et al. Molecular cloning, expression, and chromosomal localization of the human earliest lymphocyte activation antigen AIM/CD69, a new member of the C-type animal lectin superfamily of signal-transmitting receptors. *J. Exp. Med.* **178**, 537–547 (1993).
28. Martin, P. & Sanchez-Madrid, F. CD69: an unexpected regulator of TH17 cell-driven inflammatory responses. *Sci. Signal.* **4**, pe14 (2011).
29. Martin, P. et al. CD69 association with Jak3/Stat5 proteins regulates Th17 cell differentiation. *Mol. Cell Biol.* **30**, 4877–4889 (2010).
30. de la Fuente, H. et al. The leukocyte activation receptor CD69 controls T cell differentiation through its interaction with galectin-1. *Mol. Cell Biol.* **34**, 2479–2487 (2014).
31. Lin, C. R. et al. Glycosylation-dependent interaction between CD69 and S100A8/S100A9 complex is required for regulatory T-cell differentiation. *FASEB J.* **29**, 5006–5017 (2015).
32. Tsilingiri, K. et al. Oxidized low-density lipoprotein receptor in lymphocytes prevents atherosclerosis and predicts subclinical disease. *Circulation* **139**, 243–255 (2019).
33. Cibrian, D. et al. CD69 controls the uptake of L-tryptophan through LAT1-CD98 and AhR-dependent secretion of IL-22 in psoriasis. *Nat. Immunol.* **17**, 985–996 (2016).
34. Rosenblum, M. D., Remedios, K. A. & Abbas, A. K. Mechanisms of human autoimmunity. *J. Clin. Invest.* **125**, 2228–2233 (2015).
35. Nishimura, H., Honjo, T. & Minato, N. Facilitation of beta selection and modification of positive selection in the thymus of PD-1-deficient mice. *J. Exp. Med.* **191**, 891–898 (2000).
36. Sharpe, A. H., Wherry, E. J., Ahmed, R. & Freeman, G. J. The function of programmed cell death 1 and its ligands in regulating autoimmunity and infection. *Nat. Immunol.* **8**, 239–245 (2007).
37. Nishimura, H., Nose, M., Hiai, H., Minato, N. & Honjo, T. Development of lupus-like autoimmune diseases by disruption of the PD-1 gene encoding an ITIM motif-carrying immunoreceptor. *Immunity* **11**, 141–151 (1999).
38. Kasagi, S. et al. Anti-programmed cell death 1 antibody reduces CD4+PD-1+ T cells and relieves the lupus-like nephritis of NZB/W F1 mice. *J. Immunol.* **184**, 2337–2347 (2010).
39. Wong, M., La Cava, A., Singh, R. P. & Hahn, B. H. Blockade of programmed death-1 in young (New Zealand black x New Zealand white)F1 mice promotes the activity of suppressive CD8+ T cells that protect from lupus-like disease. *J. Immunol.* **185**, 6563–6571 (2010).
40. Salama, A. D. et al. Critical role of the programmed death-1 (PD-1) pathway in regulation of experimental autoimmune encephalomyelitis. *J. Exp. Med.* **198**, 71–78 (2003).
41. Ansari, M. J. et al. The programmed death-1 (PD-1) pathway regulates autoimmune diabetes in nonobese diabetic (NOD) mice. *J. Exp. Med.* **198**, 63–69 (2003).
42. Sage, P. T., Francisco, L. M., Carman, C. V. & Sharpe, A. H. The receptor PD-1 controls follicular regulatory T cells in the lymph nodes and blood. *Nat. Immunol.* **14**, 152–161 (2013).
43. Kristjansdottir, H. et al. Lower expression levels of the programmed death 1 receptor on CD4+CD25+ T cells and correlation with the PD-1.3A genotype in patients with systemic lupus erythematosus. *Arthritis Rheum.* **62**, 1702–1711 (2010).
44. Bertsias, G. K. et al. Genetic, immunologic, and immunohistochemical analysis of the programmed death 1/programmed death ligand 1 pathway in human systemic lupus erythematosus. *Arthritis Rheum.* **60**, 207–218 (2009).
45. Shi, H. et al. Elevated serum autoantibodies against co-inhibitory PD-1 facilitate T cell proliferation and correlate with disease activity in new-onset systemic lupus erythematosus patients. *Arthritis Res. Ther.* **19**, 52 (2017).
46. Jiao, Q. et al. Upregulated PD-1 expression is associated with the development of systemic lupus erythematosus, but not the PD-1.1 allele of the PDCD1 gene. *Int J. Genomics* **2014**, 950903 (2014).
47. Waterhouse, P. et al. Lymphoproliferative disorders with early lethality in mice deficient in Ctla-4. *Science* **270**, 985–988 (1995).
48. Tivol, E. A. et al. Loss of CTLA-4 leads to massive lymphoproliferation and fatal multiorgan tissue destruction, revealing a critical negative regulatory role of CTLA-4. *Immunity* **3**, 541–547 (1995).
49. Stohl, W. et al. Global T cell dysregulation in non-autoimmune-prone mice promotes rapid development of BAFF-independent, systemic lupus erythematosus-like autoimmunity. *J. Immunol.* **181**, 833–841 (2008).
50. Barreto, M. et al. Evidence for CTLA4 as a susceptibility gene for systemic lupus erythematosus. *Eur. J. Hum. Genet.* **12**, 620–626 (2004).
51. Ahmed, S. et al. Association of CTLA-4 but not CD28 gene polymorphisms with systemic lupus erythematosus in the Japanese population. *Rheumatology* **40**, 662–667 (2001).
52. Hudson, L. L., Rocca, K., Song, Y. W. & Pandey, J. P. CTLA-4 gene polymorphisms in systemic lupus erythematosus: a highly significant association with a determinant in the promoter region. *Hum. Genet.* **111**, 452–455 (2002).
53. Jury, E. C. et al. Abnormal CTLA-4 function in T cells from patients with systemic lupus erythematosus. *Eur. J. Immunol.* **40**, 569–578 (2010).
54. Dahal, L. N. et al. Immunoregulatory soluble CTLA-4 modifies effector T-cell responses in systemic lupus erythematosus. *Arthritis Res. Ther.* **18**, 180 (2016).
55. Merrill, J. T. et al. The efficacy and safety of abatacept in patients with non-life-threatening manifestations of systemic lupus erythematosus: results of a twelve-month, multicenter, exploratory, phase IIb, randomized, double-blind, placebo-controlled trial. *Arthritis Rheum.* **62**, 3077–3087 (2010).
56. Furie, R. et al. Efficacy and safety of abatacept in lupus nephritis: a twelve-month, randomized, double-blind study. *Arthritis Rheumatol.* **66**, 379–389 (2014).
57. Oster, C. et al. BTLA expression on Th1, Th2 and Th17 effector T-cells of patients with systemic lupus erythematosus is associated with active disease. *Int. J. Mol. Sci.* **20**, https://doi.org/10.3390/ijms20184505 (2019).
58. Sawaf, M. et al. Defective BTLA functionality is rescued by restoring lipid metabolism in lupus CD4+ T cells. *JCI Insight* **3**, https://doi.org/10.1172/jci.insight.99711 (2018).

59. Vendel, A. C. et al. B and T lymphocyte attenuator regulates B cell receptor signaling by targeting Syk and BLNK. *J. Immunol.* **182**, 1509–1517 (2009).
60. Otsuki, N., Kamimura, Y., Hashiguchi, M. & Azuma, M. Expression and function of the B and T lymphocyte attenuator (BTLA/CD272) on human T cells. *Biochem. Biophys. Res. Commun.* **344**, 1121–1127 (2006).
61. Lauzurica, P. et al. Phenotypic and functional characteristics of hematopoietic cell lineages in CD69-deficient mice. *Blood* **95**, 2312–2320 (2000).
62. Sanchez-Diaz, R. et al. Thymus-derived regulatory T cell development is regulated by C-type lectin-mediated BIC/MicroRNA 155 expression. *Mol. Cell. Biol.* **37**, https://doi.org/10.1128/MCB.00341-16 (2017).
63. Cortes, J. R. et al. Maintenance of immune tolerance by Foxp3+ regulatory T cells requires CD69 expression. *J. Autoimmun.* **55**, 51–62 (2014).
64. Radulovic, K. et al. CD69 regulates type I IFN-induced tolerogenic signals to mucosal CD4 T cells that attenuate their colitogenic potential. *J. Immunol.* **188**, 2001–2013 (2012).
65. Yu, L. et al. CD69 enhances immunosuppressive function of regulatory T-cells and attenuates colitis by prompting IL-10 production. *Cell Death Dis.* **9**, 905 (2018).
66. Ishikawa, S. et al. A subset of CD4+ T cells expressing early activation antigen CD69 in murine lupus: possible abnormal regulatory role for cytokine imbalance. *J. Immunol.* **161**, 1267–1273 (1998).
67. Peixoto, T. V. et al. CD4(+)CD69(+) T cells and CD4(+)CD25(+)FoxP3(+) Treg cells imbalance in peripheral blood, spleen and peritoneal lavage from pristane-induced systemic lupus erythematosus (SLE) mice. *Adv. Rheumatol.* **59**, 30 (2019).
68. Su, C. C., Shau, W. Y., Wang, C. R., Chuang, C. Y. & Chen, C. Y. CD69 to CD3 ratio of peripheral blood mononuclear cells as a marker to monitor systemic lupus erythematosus disease activity. *Lupus* **6**, 449–454 (1997).
69. Portales-Perez, D., Gonzalez-Amaro, R., Abud-Mendoza, C. & Sanchez-Armass, S. Abnormalities in CD69 expression, cytosolic pH and Ca2+ during activation of lymphocytes from patients with systemic lupus erythematosus. *Lupus* **6**, 48–56 (1997).
70. Vitales-Noyola, M. et al. Patients with systemic lupus erythematosus show increased levels and defective function of CD69(+) T regulatory cells. *Mediators Inflamm.* **2017**, 2513829 (2017).
71. Han, Y., Guo, Q., Zhang, M., Chen, Z. & Cao, X. CD69+ CD4+ CD25- T cells, a new subset of regulatory T cells, suppress T cell proliferation through membrane-bound TGF-beta 1. *J. Immunol.* **182**, 111–120 (2009).
72. Crispin, J. C., Martinez, A., de Pablo, P., Velasquillo, C. & Alcocer-Varela, J. Participation of the CD69 antigen in the T-cell activation process of patients with systemic lupus erythematosus. *Scand. J. Immunol.* **48**, 196–200 (1998).
73. Vitales-Noyola, M. et al. Quantitative and functional analysis of CD69(+) NKG2D (+) T regulatory cells in healthy subjects. *Hum. Immunol.* **76**, 511–518 (2015).
74. Rodriguez-Munoz, A. et al. Levels of regulatory T cells CD69(+)NKG2D(+)IL-10 (+) are increased in patients with autoimmune thyroid disorders. *Endocrine* **51**, 478–489 (2016).
75. Vitales-Noyola, M. et al. Quantitative and functional analysis of CD69(+) T regulatory lymphocytes in patients with periodontal disease. *J. Oral. Pathol. Med.* **46**, 549–557 (2017).
76. Tsujimura, S., Adachi, T., Saito, K. & Tanaka, Y. Role of P-glycoprotein on CD69(+) CD4(+) cells in the pathogenesis of proliferative lupus nephritis and non-responsiveness to immunosuppressive therapy. *RMD Open* **3**, e000423 (2017).
77. El Khatib, M. M. et al. beta-Cell-targeted blockage of PD1 and CTLA4 pathways prevents development of autoimmune diabetes and acute allogeneic islets rejection. *Gene Ther.* **22**, 430–438 (2015).
78. Li, R. et al. PD-L1-driven tolerance protects neurogenin3-induced islet neogenesis to reverse established type 1 diabetes in NOD mice. *Diabetes* **64**, 529–540 (2015).
79. Sun, P. et al. Unlike PD-L1, PD-1 is downregulated on partial immune cells in type 2 diabetes. *J. Diabetes Res.* **2019**, 5035261 (2019).
80. Colli, M. L. et al. PDL1 is expressed in the islets of people with type 1 diabetes and is up-regulated by interferons-alpha and-gamma via IRF1 induction. *EBioMedicine* **36**, 367–375 (2018).
81. Osum, K. C. et al. Interferon-gamma drives programmed death-ligand 1 expression on islet beta cells to limit T cell function during autoimmune diabetes. *Sci. Rep.* **8**, 8295 (2018).
82. Lenschow, D. J. et al. Differential effects of anti-B7-1 and anti-B7-2 monoclonal antibody treatment on the development of diabetes in the nonobese diabetic mouse. *J. Exp. Med.* **181**, 1145–1155 (1995).
83. Truong, W. et al. BTLA targeting modulates lymphocyte phenotype, function, and numbers and attenuates disease in nonobese diabetic mice. *J. Leukoc. Biol.* **86**, 41–51 (2009).
84. Bekiaris, V., Sedy, J. R., Macauley, M. G., Rhode-Kurnow, A. & Ware, C. F. The inhibitory receptor BTLA controls gammadelta T cell homeostasis and inflammatory responses. *Immunity* **39**, 1082–1094 (2013).
85. Bettini, M. et al. Cutting edge: accelerated autoimmune diabetes in the absence of LAG-3. *J. Immunol.* **187**, 3493–3498 (2011).
86. Okazaki, T. et al. PD-1 and LAG-3 inhibitory co-receptors act synergistically to prevent autoimmunity in mice. *J. Exp. Med.* **208**, 395–407 (2011).
87. Zhang, Q. et al. LAG3 limits regulatory T cell proliferation and function in autoimmune diabetes. *Sci. Immunol.* **2**, https://doi.org/10.1126/sciimmunol.aah4569 (2017).
88. Fuhrman, C. A. et al. Divergent phenotypes of human regulatory T cells expressing the receptors TIGIT and CD226. *J. Immunol.* **195**, 145–155 (2015).
89. Diarte-Anazco, E. M. G. et al. Novel insights into the role of HDL-associated sphingosine-1-phosphate in cardiometabolic diseases. *Int. J. Mol. Sci.* **20**, https://doi.org/10.3390/ijms20246273 (2019).
90. Srinivasan, S. et al. Sphingosine-1-phosphate reduces CD4+ T-cell activation in type 1 diabetes through regulation of hypoxia-inducible factor short isoform I.1 and CD69. *Diabetes* **57**, 484–493 (2008).
91. Klocke, K., Sakaguchi, S., Holmdahl, R. & Wing, K. Induction of autoimmune disease by deletion of CTLA-4 in mice in adulthood. *Proc. Natl Acad. Sci. USA* **113**, E2383–E2392 (2016).
92. Verma, N., Burns, S. O., Walker, L. S. K. & Sansom, D. M. Immune deficiency and autoimmunity in patients with CTLA-4 (CD152) mutations. *Clin. Exp. Immunol.* **190**, 1–7 (2017).
93. Kuehn, H. S. et al. Immune dysregulation in human subjects with heterozygous germline mutations in CTLA4. *Science* **345**, 1623–1627 (2014).
94. Lin, J. et al. TNFalpha blockade in human diseases: an overview of efficacy and safety. *Clin. Immunol.* **126**, 13–30 (2008).
95. Genant, H. K. et al. Abatacept inhibits progression of structural damage in rheumatoid arthritis: results from the long-term extension of the AIM trial. *Ann. Rheum. Dis.* **67**, 1084–1089 (2008).
96. Ruperto, N. et al. Abatacept in children with juvenile idiopathic arthritis: a randomised, double-blind, placebo-controlled withdrawal trial. *Lancet* **372**, 383–391 (2008).
97. Larsen, C. P. et al. Rational development of LEA29Y (belatacept), a high-affinity variant of CTLA4-Ig with potent immunosuppressive properties. *Am. J. Transpl.* **5**, 443–453 (2005).
98. Oki, M. et al. A functional polymorphism in B and T lymphocyte attenuator is associated with susceptibility to rheumatoid arthritis. *Clin. Dev. Immunol.* **2011**, 305656 (2011).
99. Yang, B. et al. The expression of BTLA was increased and the expression of HVEM and LIGHT were decreased in the T cells of patients with rheumatoid arthritis [corrected]. *PLoS ONE* **11**, e0155345 (2016).
100. Nakachi, S. et al. Interleukin-10-producing LAG3(+) regulatory T cells are associated with disease activity and abatacept treatment in rheumatoid arthritis. *Arthritis Res. Ther.* **19**, 97 (2017).
101. Chen, S. Y., Hsu, W. T., Chen, Y. L., Chien, C. H. & Chiang, B. L. Lymphocyte-activation gene 3(+) (LAG3(+)) forkhead box protein 3(-) (FOXP3(-)) regulatory T cells induced by B cells alleviates joint inflammation in collagen-induced arthritis. *J. Autoimmun.* **68**, 75–85 (2016).
102. Lee, J. et al. Expression of human TIM-3 and its correlation with disease activity in rheumatoid arthritis. *Scand. J. Rheumatol.* **40**, 334–340 (2011).
103. Koohini, Z. et al. Analysis of PD-1 and Tim-3 expression on CD4(+) T cells of patients with rheumatoid arthritis; negative association with DAS28. *Clin. Rheumatol.* **37**, 2063–2071 (2018).
104. Zhao, W. et al. TIGIT overexpression diminishes the function of CD4 T cells and ameliorates the severity of rheumatoid arthritis in mouse models. *Exp. Cell Res.* **340**, 132–138 (2016).
105. Fasth, A. E., Bjorkstrom, N. K., Anthoni, M., Malmberg, K. J. & Malmstrom, V. Activating NK-cell receptors co-stimulate CD4(+)CD28(−) T cells in patients with rheumatoid arthritis. *Eur. J. Immunol.* **40**, 378–387 (2010).
106. Ceeraz, S. et al. VISTA deficiency attenuates antibody-induced arthritis and alters macrophage gene expression in response to simulated immune complexes. *Arthritis Res. Ther.* **19**, 270 (2017).
107. Verwilghen, J., Corrigall, V., Pope, R. M., Rodrigues, R. & Panayi, G. S. Expression and function of CD5 and CD28 in patients with rheumatoid arthritis. *Immunology* **80**, 96–102 (1993).
108. Martin, P. et al. The leukocyte activation antigen CD69 limits allergic asthma and skin contact hypersensitivity. *J. Allergy Clin. Immunol.* **126**, 355–365, 365 e351–e353 (2010).
109. Cruz-Adalia, A. et al. CD69 limits the severity of cardiomyopathy after autoimmune myocarditis. *Circulation* **122**, 1396–1404 (2010).
110. Sancho, D. et al. CD69 downregulates autoimmune reactivity through active transforming growth factor-beta production in collagen-induced arthritis. *J. Clin. Invest*. **112**, 872–882 (2003).
111. Hernandez-Garcia, C., Fernandez-Gutierrez, B., Morado, I. C., Banares, A. A. & Jover, J. A. The CD69 activation pathway in rheumatoid arthritis synovial fluid T cells. *Arthritis Rheum.* **39**, 1277–1286 (1996).

112. Iannone, F., Corrigal, V. M. & Panayi, G. S. CD69 on synovial T cells in rheumatoid arthritis correlates with disease activity. *Br. J. Rheumatol.* **35**, 397 (1996).
113. Steinbach, K., Vincenti, I., Merkler, D. & Resident-Memory, T. Cells in tissue-restricted immune responses: for better or worse? *Front. Immunol.* **9**, 2827 (2018).
114. Blanton, R. M., Carrillo-Salinas, F. J. & Alcaide, P. T-cell recruitment to the heart: friendly guests or unwelcome visitors? *Am. J. Physiol. Heart Circ. Physiol.* **317**, H124–H140 (2019).
115. Munro, J. M., van der Walt, J. D., Munro, C. S., Chalmers, J. A. & Cox, E. L. An immunohistochemical analysis of human aortic fatty streaks. *Hum. Pathol.* **18**, 375–380 (1987).
116. Ridker, P. M. et al. Antiinflammatory therapy with Canakinumab for atherosclerotic disease. *N. Engl. J. Med* **377**, 1119–1131 (2017).
117. Palinski, W. Immunomodulation: a new role for statins? *Nat. Med.* **6**, 1311–1312 (2000).
118. Mach, F. Statins as immunomodulatory agents. *Circulation* **109**, II15–II17 (2004).
119. Tse, K., Tse, H., Sidney, J., Sette, A. & Ley, K. T cells in atherosclerosis. *Int Immunol.* **25**, 615–622 (2013).
120. van Duijn, J., Kuiper, J. & Slutter, B. The many faces of CD8+ T cells in atherosclerosis. *Curr. Opin. Lipido.* **29**, 411–416 (2018).
121. Qiu, M. K. et al. PD-1 and Tim-3 pathways regulate CD8+ T cells function in atherosclerosis. *PLoS ONE* **10**, e0128523 (2015).
122. Li, S. H., Chen, W. J., Yan, M., Shu, Y. W. & Liao, Y. H. Expression of coinhibitory PD-L1 on CD4(+)CD25(+)FOXP3(+) regulatory T cells is elevated in patients with acute coronary syndrome. *Coron. Artery Dis.* **26**, 598–603 (2015).
123. Lee, J. et al. Contributions of PD-1/PD-L1 pathway to interactions of myeloid DCs with T cells in atherosclerosis. *J. Mol. Cell Cardiol.* **46**, 169–176 (2009).
124. Foks, A. C. et al. T-cell immunoglobulin and mucin domain 3 acts as a negative regulator of atherosclerosis. *Arterioscler. Thromb. Vasc. Biol.* **33**, 2558–2565 (2013).
125. Ma, K. et al. CTLA4-IgG ameliorates homocysteine-accelerated atherosclerosis by inhibiting T-cell overactivation in apoE(−/−) mice. *Cardiovasc. Res.* **97**, 349–359 (2013).
126. Ewing, M. M. et al. T-cell co-stimulation by CD28-CD80/86 and its negative regulator CTLA-4 strongly influence accelerated atherosclerosis development. *Int. J. Cardiol.* **168**, 1965–1974 (2013).
127. Matsumoto, T. et al. Overexpression of cytotoxic T-lymphocyte-associated antigen-4 prevents atherosclerosis in mice. *Arterioscler. Thromb. Vasc. Biol.* **36**, 1141–1151 (2016).
128. Golden, D. et al. Lymphocyte activation gene 3 and coronary artery disease. *JCI Insight* **1**, e88628 (2016).
129. Douna, H. et al. B- and T-lymphocyte attenuator stimulation protects against atherosclerosis by regulating follicular B cells. *Cardiovasc. Res.* **116**, 295–305 (2020).
130. Foks, A. C. et al. Agonistic anti-TIGIT treatment inhibits T cell responses in LDLr deficient mice without affecting atherosclerotic lesion development. *PLoS ONE* **8**, e83134 (2013).
131. Gao, J. et al. VISTA is an inhibitory immune checkpoint that is increased after ipilimumab therapy in patients with prostate cancer. *Nat. Med*. **23**, 551–555 (2017).
132. Decano, J. L. & Aikawa, M. Dynamic macrophages: understanding mechanisms of activation as guide to therapy for atherosclerotic vascular disease. *Front. Cardiovasc. Med.* **5**, 97 (2018).
133. Roselaar, S. E., Kakkanathu, P. X. & Daugherty, A. Lymphocyte populations in atherosclerotic lesions of apoE −/− and LDL receptor −/− mice. Decreasing density with disease progression. *Arterioscler. Thromb. Vasc. Biol.* **16**, 1013–1018 (1996).
134. Sekiya, T. et al. Nr4a receptors are essential for thymic regulatory T cell development and immune homeostasis. *Nat. Immunol.* **14**, 230–237 (2013).
135. Lim, H. et al. Proatherogenic conditions promote autoimmune T helper 17 cell responses in vivo. *Immunity* **40**, 153–165 (2014).
136. Fernandez-Friera, L. et al. Prevalence, vascular distribution, and multiterritorial extent of subclinical atherosclerosis in a middle-aged cohort: The PESA (Progression of Early Subclinical Atherosclerosis) Study. *Circulation* **131**, 2104–2113 (2015).
137. Swirski, F. K. & Nahrendorf, M. Cardioimmunology: the immune system in cardiac homeostasis and disease. *Nat. Rev. Immunol.* **18**, 733–744 (2018).
138. Lutgens, E. & Seijkens, T. T. P. Cancer patients receiving immune checkpoint inhibitor therapy are at an increased risk for atherosclerotic cardiovascular disease. *J. Immunother. Cancer* **8**, https://doi.org/10.1136/jitc-2019-000300 (2020).
139. Ramos-Casals, M. et al. Immune-related adverse events of checkpoint inhibitors. *Nat. Rev. Dis. Prim.* **6**, 38 (2020).
140. Zaha, V. G., Meijers, W. C. & Moslehi, J. Cardio-immuno-oncology. *Circulation* **141**, 87–89 (2020).
141. Bar, J. et al. Acute vascular events as a possibly related adverse event of immunotherapy: a single-institute retrospective study. *Eur. J. Cancer* **120**, 122–131 (2019).
142. Newman, J. L. & Stone, J. R. Immune checkpoint inhibition alters the inflammatory cell composition of human coronary artery atherosclerosis. *Cardiovasc. Pathol.* **43**, 107148 (2019).
143. Bennet, A. M., Alarcon-Riquelme, M., Wiman, B., de Faire, U. & Prokunina-Olsson, L. Decreased risk for myocardial infarction and lower tumor necrosis factor-alpha levels in carriers of variants of the PDCD1 gene. *Hum. Immunol.* **67**, 700–705 (2006).
144. Yip, H. K. et al. Cytotoxic T lymphocyte antigen 4 gene polymorphism associated with ST-segment elevation acute myocardial infarction. *Circ. J.* **71**, 1213–1218 (2007).
145. Yin, X. et al. Protein biomarkers of new-onset cardiovascular disease: prospective study from the systems approach to biomarker research in cardiovascular disease initiative. *Arterioscler. Thromb. Vasc. Biol.* **34**, 939–945 (2014).
146. Forteza, M. J. et al. Programmed death-1 (PD-1): a novel mechanism for understanding the acute immune deregulation in ST-segment elevation myocardial infarction. *Int J. Cardiol.* **177**, 8–10 (2014).
147. Pasqui, A. L. et al. T cell activation and enhanced apoptosis in non-ST elevation myocardial infarction. *Clin. Exp. Med.* **3**, 37–44 (2003).
148. Carvalheiro, T. et al. Phenotypic and functional alterations on inflammatory peripheral blood cells after acute myocardial infarction. *J. Cardiovasc. Transl. Res.* **5**, 309–320 (2012).
149. Hosono, M. et al. Increased expression of T cell activation markers (CD25, CD26, CD40L and CD69) in atherectomy specimens of patients with unstable angina and acute myocardial infarction. *Atherosclerosis* **168**, 73–80 (2003).
150. Bruestle, K., Hackner, K., Kreye, G. & Heidecker, B. Autoimmunity in acute myocarditis: how immunopathogenesis steers new directions for diagnosis and treatment. *Curr. Cardiol. Rep.* **22**, 28 (2020).
151. Lv, H. et al. Impaired thymic tolerance to alpha-myosin directs autoimmunity to the heart in mice and humans. *J. Clin. Invest.* **121**, 1561–1573 (2011).
152. Grabie, N., Lichtman, A. H. & Padera, R. T cell checkpoint regulators in the heart. *Cardiovasc. Res.* **115**, 869–877 (2019).
153. Johnson, D. B. et al. Fulminant myocarditis with Combination Immune Checkpoint Blockade. *N. Engl. J. Med* **375**, 1749–1755 (2016).
154. Mahmood, S. S. et al. Myocarditis in patients treated with immune checkpoint inhibitors. *J. Am. Coll. Cardiol.* **71**, 1755–1764 (2018).
155. Shrestha, K. P. & Carrera, A. E. Hair trace elements and mental retardation among children. *Arch. Environ. Health* **43**, 396–398 (1988).
156. Moslehi, J. J., Salem, J. E., Sosman, J. A., Lebrun-Vignes, B. & Johnson, D. B. Increased reporting of fatal immune checkpoint inhibitor-associated myocarditis. *Lancet* **391**, 933 (2018).
157. Escudier, M. et al. Clinical features, management, and outcomes of immune checkpoint inhibitor-related cardiotoxicity. *Circulation* **136**, 2085–2087 (2017).
158. Nishimura, H. et al. Autoimmune dilated cardiomyopathy in PD-1 receptor-deficient mice. *Science* **291**, 319–322 (2001).
159. Tarrio, M. L., Grabie, N., Bu, D. X., Sharpe, A. H. & Lichtman, A. H. PD-1 protects against inflammation and myocyte damage in T cell-mediated myocarditis. *J. Immunol.* **188**, 4876–4884 (2012).
160. Tivol, E. A. et al. CTLA4Ig prevents lymphoproliferation and fatal multiorgan tissue destruction in CTLA-4-deficient mice. *J. Immunol.* **158**, 5091–5094 (1997).
161. Ji, C. et al. Myocarditis in cynomolgus monkeys following treatment with immune checkpoint inhibitors. *Clin. Cancer Res.* **25**, 4735–4748 (2019).
162. Freeman, G. J. et al. Engagement of the PD-1 immunoinhibitory receptor by a novel B7 family member leads to negative regulation of lymphocyte activation. *J. Exp. Med*. **192**, 1027–1034 (2000).
163. Rodig, N. et al. Endothelial expression of PD-L1 and PD-L2 down-regulates CD8+ T cell activation and cytolysis. *Eur. J. Immunol.* **33**, 3117–3126 (2003).
164. Koelzer, V. H. et al. Systemic inflammation in a melanoma patient treated with immune checkpoint inhibitors-an autopsy study. *J. Immunother. Cancer* **4**, 13 (2016).
165. Frisancho-Kiss, S. et al. Cutting edge: T cell Ig mucin-3 reduces inflammatory heart disease by increasing CTLA-4 during innate immunity. *J. Immunol.* **176**, 6411–6415 (2006).
166. Frisancho-Kiss, S. et al. Cutting edge: cross-regulation by TLR4 and T cell Ig mucin-3 determines sex differences in inflammatory heart disease. *J. Immunol.* **178**, 6710–6714 (2007).
167. Lawrence, M. S. et al. Mutational heterogeneity in cancer and the search for new cancer-associated genes. *Nature* **499**, 214–218 (2013).
168. Pennock, N. D. et al. T cell responses: naive to memory and everything in between. *Adv. Physiol. Educ.* **37**, 273–283 (2013).
169. Teng, M. W., Galon, J., Fridman, W. H. & Smyth, M. J. From mice to humans: developments in cancer immunoediting. *J. Clin. Invest.* **125**, 3338–3346 (2015).
170. Otsuka, A. et al. Hedgehog pathway inhibitors promote adaptive immune responses in basal cell carcinoma. *Clin. Cancer Res.* **21**, 1289–1297 (2015).

171. Vinay, D. S. et al. Immune evasion in cancer: mechanistic basis and therapeutic strategies. *Semin. Cancer Biol.* **35**(Suppl), S185–S198 (2015).
172. Sarvaria, A., Madrigal, J. A. & Saudemont, A. B cell regulation in cancer and anti-tumor immunity. *Cell Mol. Immunol.* **14**, 662–674 (2017).
173. Day, C. L. et al. PD-1 expression on HIV-specific T cells is associated with T-cell exhaustion and disease progression. *Nature* **443**, 350–354 (2006).
174. Baitsch, L. et al. Exhaustion of tumor-specific CD8(+) T cells in metastases from melanoma patients. *J. Clin. Invest*. **121**, 2350–2360 (2011).
175. Wherry, E. J. T cell exhaustion. *Nat. Immunol.* **12**, 492–499 (2011).
176. Speiser, D. E. et al. T cell differentiation in chronic infection and cancer: functional adaptation or exhaustion? *Nat. Rev. Immunol.* **14**, 768–774 (2014).
177. Peggs, K. S., Quezada, S. A., Chambers, C. A., Korman, A. J. & Allison, J. P. Blockade of CTLA-4 on both effector and regulatory T cell compartments contributes to the antitumor activity of anti-CTLA-4 antibodies. *J. Exp. Med.* **206**, 1717–1725 (2009).
178. Hodi, F. S. et al. Improved survival with ipilimumab in patients with metastatic melanoma. *N. Engl. J. Med*. **363**, 711–723 (2010).
179. Robert, C. et al. Ipilimumab plus dacarbazine for previously untreated metastatic melanoma. *N. Engl. J. Med.* **364**, 2517–2526 (2011).
180. Wolchok, J. D. et al. Ipilimumab monotherapy in patients with pretreated advanced melanoma: a randomised, double-blind, multicentre, phase 2, dose-ranging study. *Lancet Oncol.* **11**, 155–164 (2010).
181. Eggermont, A. M. et al. Adjuvant ipilimumab versus placebo after complete resection of high-risk stage III melanoma (EORTC 18071): a randomised, double-blind, phase 3 trial. *Lancet Oncol.* **16**, 522–530 (2015).
182. Yang, J. C. et al. Ipilimumab (anti-CTLA4 antibody) causes regression of metastatic renal cell cancer associated with enteritis and hypophysitis. *J. Immunother.* **30**, 825–830 (2007).
183. Ansell, S. M. et al. Phase I study of ipilimumab, an anti-CTLA-4 monoclonal antibody, in patients with relapsed and refractory B-cell non-Hodgkin lymphoma. *Clin. Cancer Res.* **15**, 6446–6453 (2009).
184. Kwon, E. D. et al. Ipilimumab versus placebo after radiotherapy in patients with metastatic castration-resistant prostate cancer that had progressed after docetaxel chemotherapy (CA184-043): a multicentre, randomised, double-blind, phase 3 trial. *Lancet Oncol.* **15**, 700–712 (2014).
185. Ribas, A. et al. Phase III randomized clinical trial comparing tremelimumab with standard-of-care chemotherapy in patients with advanced melanoma. *J. Clin. Oncol.* **31**, 616–622 (2013).
186. Chung, K. Y. et al. Phase II study of the anti-cytotoxic T-lymphocyte-associated antigen 4 monoclonal antibody, tremelimumab, in patients with refractory metastatic colorectal cancer. *J. Clin. Oncol.* **28**, 3485–3490 (2010).
187. Sangro, B. et al. A clinical trial of CTLA-4 blockade with tremelimumab in patients with hepatocellular carcinoma and chronic hepatitis C. *J. Hepatol.* **59**, 81–88 (2013).
188. Calabro, L. et al. Tremelimumab for patients with chemotherapy-resistant advanced malignant mesothelioma: an open-label, single-arm, phase 2 trial. *Lancet Oncol.* **14**, 1104–1111 (2013).
189. Dong, H. et al. Tumor-associated B7-H1 promotes T-cell apoptosis: a potential mechanism of immune evasion. *Nat. Med.* **8**, 793–800 (2002).
190. Topalian, S. L. et al. Safety, activity, and immune correlates of anti-PD-1 antibody in cancer. *N. Engl. J. Med.* **366**, 2443–2454 (2012).
191. Page, D. B., Postow, M. A., Callahan, M. K., Allison, J. P. & Wolchok, J. D. Immune modulation in cancer with antibodies. *Annu. Rev. Med.* **65**, 185–202 (2014).
192. Lipson, E. J. et al. Durable cancer regression off-treatment and effective reinduction therapy with an anti-PD-1 antibody. *Clin. Cancer Res.* **19**, 462–468 (2013).
193. Mahoney, K. M., Freeman, G. J. & McDermott, D. F. The next immune-checkpoint inhibitors: PD-1/PD-L1 blockade in melanoma. *Clin. Ther.* **37**, 764–782 (2015).
194. Berger, R. et al. Phase I safety and pharmacokinetic study of CT-011, a humanized antibody interacting with PD-1, in patients with advanced hematologic malignancies. *Clin. Cancer Res*. **14**, 3044–3051 (2008).
195. Wolchok, J. D. et al. Nivolumab plus ipilimumab in advanced melanoma. *N. Engl. J. Med.* **369**, 122–133 (2013).
196. Lynch, T. J. et al. Ipilimumab in combination with paclitaxel and carboplatin as first-line treatment in stage IIIB/IV non-small-cell lung cancer: results from a randomized, double-blind, multicenter phase II study. *J. Clin. Oncol.* **30**, 2046–2054 (2012).
197. Horinouchi, H. et al. Phase I study of ipilimumab in phased combination with paclitaxel and carboplatin in Japanese patients with non-small-cell lung cancer. *Invest. N. Drugs* **33**, 881–889 (2015).
198. Arriola, E. et al. Outcome and biomarker analysis from a multicenter phase 2 study of ipilimumab in combination with carboplatin and etoposide as first-line therapy for extensive-stage SCLC. *J. Thorac. Oncol.* **11**, 1511–1521 (2016).
199. Hersh, E. M. et al. A phase II multicenter study of ipilimumab with or without dacarbazine in chemotherapy-naive patients with advanced melanoma. *Invest N. Drugs* **29**, 489–498 (2011).
200. Chi, M. & Dudek, A. Z. Vaccine therapy for metastatic melanoma: systematic review and meta-analysis of clinical trials. *Melanoma Res.* **21**, 165–174 (2011).
201. Bernatchez, C., Radvanyi, L. G. & Hwu, P. Advances in the treatment of metastatic melanoma: adoptive T-cell therapy. *Semin. Oncol.* **39**, 215–226 (2012).
202. Boni, A. et al. Selective BRAFV600E inhibition enhances T-cell recognition of melanoma without affecting lymphocyte function. *Cancer Res.* **70**, 5213–5219 (2010).
203. Slovin, S. F. et al. Ipilimumab alone or in combination with radiotherapy in metastatic castration-resistant prostate cancer: results from an open-label, multicenter phase I/II study. *Ann. Oncol.* **24**, 1813–1821 (2013).
204. Wilmott, J. S. et al. Selective BRAF inhibitors induce marked T-cell infiltration into human metastatic melanoma. *Clin. Cancer Res.* **18**, 1386–1394 (2012).
205. Ribas, A., Hodi, F. S., Callahan, M., Konto, C. & Wolchok, J. Hepatotoxicity with combination of vemurafenib and ipilimumab. *N. Engl. J. Med.* **368**, 1365–1366 (2013).
206. Puhr, H. C. & Ilhan-Mutlu, A. New emerging targets in cancer immunotherapy: the role of LAG3. *ESMO Open* **4**, e000482 (2019).
207. Tagliamento, M., Bironzo, P. & Novello, S. New emerging targets in cancer immunotherapy: the role of VISTA. ESMO Open **4**, https://doi.org/10.1136/esmoopen-2020-000683 (2020).
208. Johnston, R. L., Lutzky, J., Chodhry, A. & Barkin, J. S. Cytotoxic T-lymphocyte-associated antigen 4 antibody-induced colitis and its management with infliximab. *Dig. Dis. Sci.* **54**, 2538–2540 (2009).
209. Abdel-Rahman, O. & Fouad, M. A network meta-analysis of the risk of immune-related renal toxicity in cancer patients treated with immune checkpoint inhibitors. *Immunotherapy* **8**, 665–674 (2016).
210. Nonomura, Y. et al. ADAMTSL5 is upregulated in melanoma tissues in patients with idiopathic psoriasis vulgaris induced by nivolumab. *J. Eur. Acad. Dermatol. Venereol.* **31**, e100–e101 (2017).
211. Chae, Y. K. et al. A case of pembrolizumab-induced type-1 diabetes mellitus and discussion of immune checkpoint inhibitor-induced type 1 diabetes. *Cancer Immunol. Immunother.* **66**, 25–32 (2017).
212. Tarhini, A. Immune-mediated adverse events associated with ipilimumab ctla-4 blockade therapy: the underlying mechanisms and clinical management. *Science (Cairo)* **2013**, 857519 (2013).
213. Fecher, L. A., Agarwala, S. S., Hodi, F. S. & Weber, J. S. Ipilimumab and its toxicities: a multidisciplinary approach. *Oncologist* **18**, 733–743 (2013).
214. Weber, J. S. et al. Patterns of onset and resolution of immune-related adverse events of special interest with ipilimumab: detailed safety analysis from a phase 3 trial in patients with advanced melanoma. *Cancer* **119**, 1675–1682 (2013).
215. Marthey, L. et al. Cancer Immunotherapy with anti-CTLA-4 monoclonal antibodies induces an inflammatory bowel disease. *J. Crohns Colitis* **10**, 395–401 (2016).
216. Kim, K. W. et al. Ipilimumab associated hepatitis: imaging and clinicopathologic findings. *Invest N. Drugs* **31**, 1071–1077 (2013).
217. Dillard, T., Yedinak, C. G., Alumkal, J. & Fleseriu, M. Anti-CTLA-4 antibody therapy associated autoimmune hypophysitis: serious immune related adverse events across a spectrum of cancer subtypes. *Pituitary* **13**, 29–38 (2010).
218. Bertrand, A., Kostine, M., Barnetche, T., Truchetet, M. E. & Schaeverbeke, T. Immune related adverse events associated with anti-CTLA-4 antibodies: systematic review and meta-analysis. *BMC Med.* **13**, 211 (2015).
219. Naidoo, J. et al. Toxicities of the anti-PD-1 and anti-PD-L1 immune checkpoint antibodies. *Ann. Oncol.* **26**, 2375–2391 (2015).
220. Qin, W. et al. The diverse gunction of PD-1/PD-L pathway beyond vancer. *Front. Immunol.* **10**, 2298 (2019).
221. Stohl, W., Yu, N., Chalmers, S. A., Putterman, C. & Jacob, C. O. Constitutive reduction in the checkpoint inhibitor, CTLA-4, does not accelerate SLE in NZM 2328 mice. *Lupus Sci. Med.* **6**, e000313 (2019).
222. Fadel, F., El Karoui, K. & Knebelmann, B. Anti-CTLA4 antibody-induced lupus nephritis. *N. Engl. J. Med.* **361**, 211–212 (2009).
223. Richter, M. D. et al. Brief Report: Cancer immunotherapy in patients with preexisting rheumatic disease: The Mayo Clinic experience. *Arthritis Rheumatol.* **70**, 356–360 (2018).
224. Simons, K. H. et al. T cell co-stimulation and co-inhibition in cardiovascular disease: a double-edged sword. *Nat. Rev. Cardiol.* **16**, 325–343 (2019).
225. Mensah, G. A., Roth, G. A. & Fuster, V. The global burden of cardiovascular diseases and risk factors: 2020 and beyond. *J. Am. Coll. Cardiol.* **74**, 2529–2532 (2019).
226. Esplugues, E. et al. Enhanced antitumor immunity in mice deficient in CD69. *J. Exp. Med* **197**, 1093–1106 (2003).

227. Cibrian, D. & Sanchez-Madrid, F. CD69: from activation marker to metabolic gatekeeper. *Eur. J. Immunol.* **47**, 946–953 (2017).
228. Song, W., Das, M. & Chen, X. Nanotherapeutics for immuno-oncology: a crossroad for new paradigms. *Trends Cancer* **6**, 288–298 (2020).
229. Grosser, R., Cherkassky, L., Chintala, N. & Adusumilli, P. S. Combination immunotherapy with CAR T cells and checkpoint blockade for the treatment of solid tumors. *Cancer Cell* **36**, 471–482 (2019).
230. Gianchecchi, E. & Fierabracci, A. Inhibitory receptors and pathways of lymphocytes: the role of PD-1 in Treg development and their involvement in autoimmunity onset and cancer progression. *Front. Immunol.* **9**, 2374 (2018).
231. Michel, L. et al. Patients with relapsing-remitting multiple sclerosis have normal Treg function when cells expressing IL-7 receptor alpha-chain are excluded from the analysis. *J. Clin. Invest.* **118**, 3411–3419 (2008).
232. Zelle-Rieser, C. et al. T cells in multiple myeloma display features of exhaustion and senescence at the tumor site. *J. Hematol. Oncol.* **9**, 116 (2016).
233. Heinzerling, L. et al. Cardiotoxicity associated with CTLA4 and PD1 blocking immunotherapy. *J. Immunother. Cancer* **4**, 50 (2016).
234. Zhang, Z. et al. Two genes encoding immune-regulatory molecules (LAG3 and IL7R) confer susceptibility to multiple sclerosis. *Genes Immun.* **6**, 145–152 (2005).
235. Pallikkuth, S. et al. Cardiac morbidity in HIV infection is associated with checkpoint inhibitor LAG-3 on CD4 T cells. *PLoS One* **13**, e0206256 (2018).
236. Liberal, R. et al. The impaired immune regulation of autoimmune hepatitis is linked to a defective galectin-9/tim-3 pathway. *Hepatology* **56**, 677–686 (2012).
237. Das, M., Zhu, C. & Kuchroo, V. K. Tim-3 and its role in regulating anti-tumor immunity. *Immunol. Rev.* **276**, 97–111 (2017).
238. Japp, A. S. et al. Dysfunction of PSA-specific CD8+ T cells in prostate cancer patients correlates with CD38 and Tim-3 expression. *Cancer Immunol. Immunother.* **64**, 1487–1494 (2015).
239. Agresta, L., Hoebe, K. H. N. & Janssen, E. M. The emerging role of CD244 signaling in immune cells of the tumor microenvironment. *Front. Immunol.* **9**, 2809 (2018).
240. Peng, J. & Xiang, Y. Value analysis of CD69 combined with EGR1 in the diagnosis of coronary heart disease. *Exp. Ther. Med.* **17**, 2047–2052 (2019).
241. Wald, O. et al. CD4+CXCR4highCD69+ T cells accumulate in lung adenocarcinoma. *J. Immunol.* **177**, 6983–6990 (2006).
242. Oja, A. E. et al. Functional heterogeneity of CD4(+) tumor-infiltrating lymphocytes with a resident memory phenotype in NSCLC. *Front. Immunol.* **9**, 2654 (2018).
243. Yu, X., Zheng, Y., Mao, R., Su, Z. & Zhang, J. BTLA/HVEM signaling: milestones in research and role in chronic hepatitis B virus infection. *Front. Immunol.* **10**, 617 (2019).
244. Burgueno-Bucio, E., Mier-Aguilar, C. A. & Soldevila, G. The multiple faces of CD5. *J. Leukoc. Biol.* **105**, 891–904 (2019).

ORIGINAL ARTICLE

A Novel Circulating MicroRNA for the Detection of Acute Myocarditis

R. Blanco-Domínguez, R. Sánchez-Díaz, H. de la Fuente, L.J. Jiménez-Borreguero, A. Matesanz-Marín, M. Relaño, R. Jiménez-Alejandre, B. Linillos-Pradillo, K. Tsilingiri, M.L. Martín-Mariscal, L. Alonso-Herranz, G. Moreno, R. Martín-Asenjo, M.M. García-Guimaraes, K.A. Bruno, E. Dauden, I. González-Álvaro, L.M. Villar-Guimerans, A. Martínez-León, A.M. Salvador-Garicano, S.A. Michelhaugh, N.E. Ibrahim, J.L. Januzzi, J. Kottwitz, S. Iliceto, M. Plebani, C. Basso, A. Baritussio, M. Seguso, R. Marcolongo, M. Ricote, D.L. Fairweather, H. Bueno, L. Fernández-Friera, F. Alfonso, A.L.P. Caforio, D.A. Pascual-Figal, B. Heidecker, T.F. Lüscher, S. Das, V. Fuster, B. Ibáñez, F. Sánchez-Madrid, and P. Martín

ABSTRACT

BACKGROUND

The diagnosis of acute myocarditis typically requires either endomyocardial biopsy (which is invasive) or cardiovascular magnetic resonance imaging (which is not universally available). Additional approaches to diagnosis are desirable. We sought to identify a novel microRNA for the diagnosis of acute myocarditis.

METHODS

To identify a microRNA specific for myocarditis, we performed microRNA microarray analyses and quantitative polymerase-chain-reaction (qPCR) assays in sorted CD4+ T cells and type 17 helper T (Th17) cells after inducing experimental autoimmune myocarditis or myocardial infarction in mice. We also performed qPCR in samples from coxsackievirus-induced myocarditis in mice. We then identified the human homologue for this microRNA and compared its expression in plasma obtained from patients with acute myocarditis with the expression in various controls.

RESULTS

We confirmed that Th17 cells, which are characterized by the production of interleukin-17, are a characteristic feature of myocardial injury in the acute phase of myocarditis. The microRNA mmu-miR-721 was synthesized by Th17 cells and was present in the plasma of mice with acute autoimmune or viral myocarditis but not in those with acute myocardial infarction. The human homologue, designated hsa-miR-Chr8:96, was identified in four independent cohorts of patients with myocarditis. The area under the receiver-operating-characteristic curve for this novel microRNA for distinguishing patients with acute myocarditis from those with myocardial infarction was 0.927 (95% confidence interval, 0.879 to 0.975). The microRNA retained its diagnostic value in models after adjustment for age, sex, ejection fraction, and serum troponin level.

CONCLUSIONS

After identifying a novel microRNA in mice and humans with myocarditis, we found that the human homologue (hsa-miR-Chr8:96) could be used to distinguish patients with myocarditis from those with myocardial infarction. (Funded by the Spanish Ministry of Science and Innovation and others.)

The authors' full names, academic degrees, and affiliations are listed in the Appendix. Address reprint requests to Dr. Martín at the Vascular Pathophysiology Area, Centro Nacional de Investigaciones Cardiovasculares, Melchor Fernández Almagro 3, E-28029 Madrid, Spain, or at pmartinf@cnic.es.

Mr. Blanco-Domínguez and Dr. Sánchez-Díaz contributed equally to this article.

N Engl J Med 2021;384:2014-27.
DOI: 10.1056/NEJMoa2003608

Myocarditis is a disease with multiple causes[1,2] (e.g., infectious pathogens, toxins, drugs, and autoimmune disorders[3,4]) that may resolve spontaneously, cause sudden cardiac death, or evolve into dilated cardiomyopathy.[5] The actual prevalence of the disease remains uncertain because of the difficulty of reaching a confirmatory diagnosis in many cases. Myocarditis is a frequent final diagnosis in patients who receive an initial diagnosis of acute myocardial infarction with nonobstructive coronary arteries (MINOCA),[6] a clinical entity that occurs in approximately 10 to 20% of patients who meet the criteria for myocardial infarction.[7,8] The diagnosis of myocarditis is usually established after ruling out coronary artery disease by means of coronary angiography or computed tomography and confirming the presence of Lake Louise criteria on cardiac magnetic resonance imaging (MRI).[9] However, cardiac MRI is not available in all centers.[10,11] The reference standard for diagnosis relies on endomyocardial biopsy, which is usually reserved for severe cases.[1] Therefore, reliable and accessible diagnostic tools for the early diagnosis of acute myocarditis are an unmet clinical need.

The phenotypes of circulating T cells are altered in both myocarditis[12] and myocardial infarction.[13] Cardiac myosin-specific type 17 helper T (Th17) lymphocytes[14] play a central role in the development of myocarditis and dilated cardiomyopathy[15] and in the production of anti–myocardial antibodies in viral myocarditis.[16] MicroRNAs (miRNAs) have emerged as innovative biomarkers for cardiovascular disease.[17] We sought to identify a novel miRNA that could be used to distinguish acute myocarditis from myocardial infarction.

Methods

Overview of Study Strategy

By analyzing circulating T cells obtained from mice and humans with myocarditis and myocardial infarction, we confirmed that Th17 cells are a characteristic feature of myocardial injury in the acute phase of myocarditis. Screening of miRNAs that are synthesized by Th17 cells with the use of microarrays and quantitative polymerase-chain-reaction (qPCR) assays showed that mmu-miR-721 was specific for Th17 cells and plasma in mice with autoimmune or viral myocarditis. Since the human homologue of mmu-miR-721 had not been described previously, we cloned and sequenced the putative human homologue in plasma obtained from patients with myocarditis. Coimmunoprecipitation and luciferase assays showed that the human homologue, which we designated hsa-miR-Chr8:96, is a new functional human miRNA. We validated hsa-miR-Chr8:96 as a suitable myocarditis detector in four independent cohorts using qPCR. The animal models and human study participants are described below; details regarding the study methods are provided in the Supplementary Appendix, available with the full text of this article at NEJM.org.

This multicenter study was approved by the ethics committee of the Carlos III Institute of Health and the research ethics committee at each of the participating hospitals; a list of centers is provided in the Supplementary Appendix. All the participants provided written informed consent for the use of their samples and data.

Murine Models of Autoimmune Myocarditis and Myocardial Infarction

Wild-type BALB/c mice and CD69 knockout mice were bred at the National Center for Cardiovascular Research (CNIC) animal facility for use in our experimental autoimmune myocarditis model. Mice between the ages of 8 and 12 weeks were immunized subcutaneously on days 0 and 7 with 100 μg per 0.2 ml of cardiac α-myosin heavy-chain peptide (residues 614–629; Ac-RSLKLMATLFSTYASADR-OH), emulsified in a 1:1 ratio in complete Freund's adjuvant. Severe experimental autoimmune myocarditis was induced in the CD69 knockout mice[18]; less severe (moderate) experimental autoimmune myocarditis was induced in the wild-type mice. Sex- and age-matched littermates were immunized with complete Freund's adjuvant and saline as controls. In separate experiments, wild-type BALB/c mice between the ages of 8 and 12 weeks underwent permanent ligation of the left anterior descending coronary artery to induce myocardial infarction, with sham-operated mice used as controls, as described in the Supplementary Appendix.

Experimental autoimmune myocarditis was also induced in mice expressing antigen-specific T-cell receptors. We purchased C57BL/6-Tg (TcraTcrb) 425Cbn/J mice (called OT-II) expressing a T-cell receptor specific for peptide 323–339 of ovalbumin in the context of murine major histocompatibility complex class II alleles H-2

I-Ab from the Jackson Laboratory (stock number 004194). Additional OT-II mice were backcrossed with CD69 knockout mice, which are both from the same inbred strain (C57BL/6 background).

The mice were housed under specific pathogen-free conditions at the CNIC animal facility. All procedures involving the mice were approved by the Comunidad Autónoma de Madrid and conducted in accordance with Directive 2010/63/EU of the European Parliament and of the Council of September 22, 2010, on the protection of animals used for scientific purposes.

MURINE MODEL OF VIRAL MYOCARDITIS

Wild-type BALB/c or C57BL/6 mice were obtained from the Jackson Laboratory. Eight-week-old mice were inoculated intraperitoneally with 10^3 plaque-forming units of coxsackievirus B3 that had been isolated from a patient (Nancy strain) and passaged through Vero cells and then through the heart (i.e., heart-passaged) in saline, as described in the Supplementary Appendix. Control mice received intraperitoneal saline injections. Serum and hearts were collected 10 days after infection, as described previously.[19] Mice were maintained under pathogen-free conditions in the animal facility at Mayo Clinic Jacksonville, and approval was obtained from the Animal Care and Use Committee of Mayo Clinic for all procedures.

STUDY PATIENTS

The main study cohort included 132 patients with initial clinical suspicion of acute myocarditis and myocardial injury, ventricular dysfunction, or both (Tables S1 and S2 in the Supplementary Appendix). Of these patients, 42 had a final diagnosis of myocarditis on the basis of cardiac MRI that met the typical Lake Louise diagnostic criteria; 90 patients were diagnosed with myocardial infarction and were included in the analysis as comparators. A total of 80 healthy participants with no abnormal findings on electrocardiography or echocardiography were included as additional controls.

We validated the use of hsa-miR-Chr8:96 for the diagnosis of human myocarditis using four additional patient cohorts. Validation cohort 1 was provided by the Partners Biobank (Boston) and included 34 patients with an established diagnosis of acute myocarditis and 11 patients with myocardial infarction as comparators (Table S3). Validation cohort 2, which has been described previously,[20] was provided by the Center for Molecular Cardiology of the University Hospital Zurich (Switzerland). This cohort included 35 patients with an established diagnosis of acute myocarditis and 20 patients with MINOCA (Table S4). Validation cohort 3 included samples

Figure 1 (facing page). Circulating Th17 Cells in Acute Myocarditis.

Panel A shows the kinetics of biomarkers of myocardial injury — troponin I, lactate dehydrogenase (LDH), and creatine kinase MB (CK-MB) — in the serum of BALB/c mice after induction of experimental autoimmune myocarditis (following immunization with cardiac α-myosin heavy-chain peptide) as compared with control mice (following immunization with phosphate-buffered saline). Also shown are the changes in the same biomarkers after the induction of myocardial infarction (following ligation of the left anterior descending coronary artery) as compared with control mice (following a sham operation). Dashed lines represent basal levels of each biomarker. P values, which are shown for the comparisons with controls, were calculated by two-way analysis of variance with Sidak's multiple comparisons test. Data are representative of more than three independent experiments in 3 to 10 pools of two mice each. **Panel B** shows the time course of changes in the left ventricular ejection fraction after the induction of myocarditis or myocardial infarction, as quantified by transthoracic echocardiography (TTE), with 4 to 7 mice per group. **Panel C** shows the time course of changes in the percentage of type 17 helper T (Th17) cells in CD4+ T cells in the blood of BALB/c mice after myocarditis or myocardial infarction (and respective controls), according to the results of fluorescence-activated cell sorting (FACS) in 6 mice per group. P values were calculated by means of two-way repeated-measures analysis of variance (Sidak's post hoc test). Data in Panels B and C are representative of more than three independent experiments. **Panel D** shows the left ventricular ejection fraction, as measured by TTE, in samples obtained from 43 patients with myocarditis, 43 patients with ST-segment elevation myocardial infarction (STEMI), 35 patients with non-STEMI (NSTEMI), and 23 healthy controls. Data were analyzed by means of the Kruskal–Wallis test with Dunn's multiple comparisons test. **Panel E** shows the quantification of Th17 cells on FACS as a percentage of all CD4+ T cells in peripheral-blood samples obtained from patients with acute myocarditis, STEMI, or NSTEMI and from healthy controls. P values were calculated by the same method used in Panel D and were performed in the analysis of samples from 33 patients with myocarditis, 45 with STEMI, and 41 with NSTEMI, along with 62 healthy controls. In all five panels, the data are represented as means, with I bars representing standard errors.

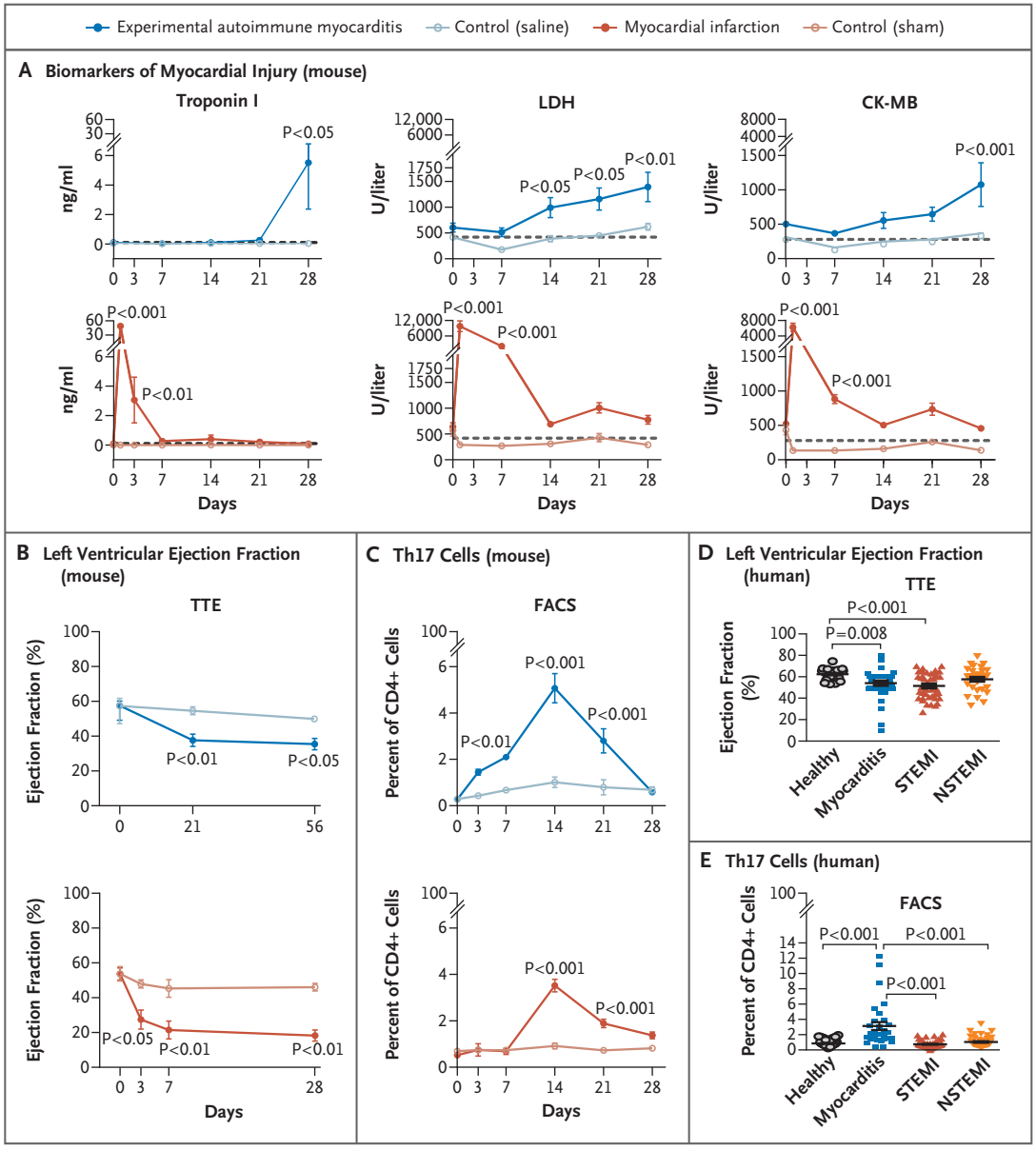

from 40 patients selected from a prospective cohort recruited at the University of Padua (Italy) with a biopsy-proven diagnosis of myocarditis. In addition, samples from 49 patients with acute myocardial infarction from the Biobank Regional Platform (Murcia, Spain) were analyzed in parallel as comparators (Table S5). Finally, as a control cohort, we included samples obtained from patients with Th17-related immunologic diseases without cardiac involvement (Table S6). A detailed description of the cohorts is provided in the Supplementary Appendix.

STATISTICAL ANALYSIS

We first evaluated the normality of the distributions using the D'Agostino–Pearson test. If distributions were normal, we used the unpaired Student's t-test for two-group comparisons and one-way analysis of variance analysis with Tukey's post hoc test when more than two groups were compared. If distributions were nonnormal, we used the Mann–Whitney U-test for the analysis of two groups and the Kruskal–Wallis test with Dunn's post hoc test for multiple-group comparisons. In the kinetic experiments, one-way

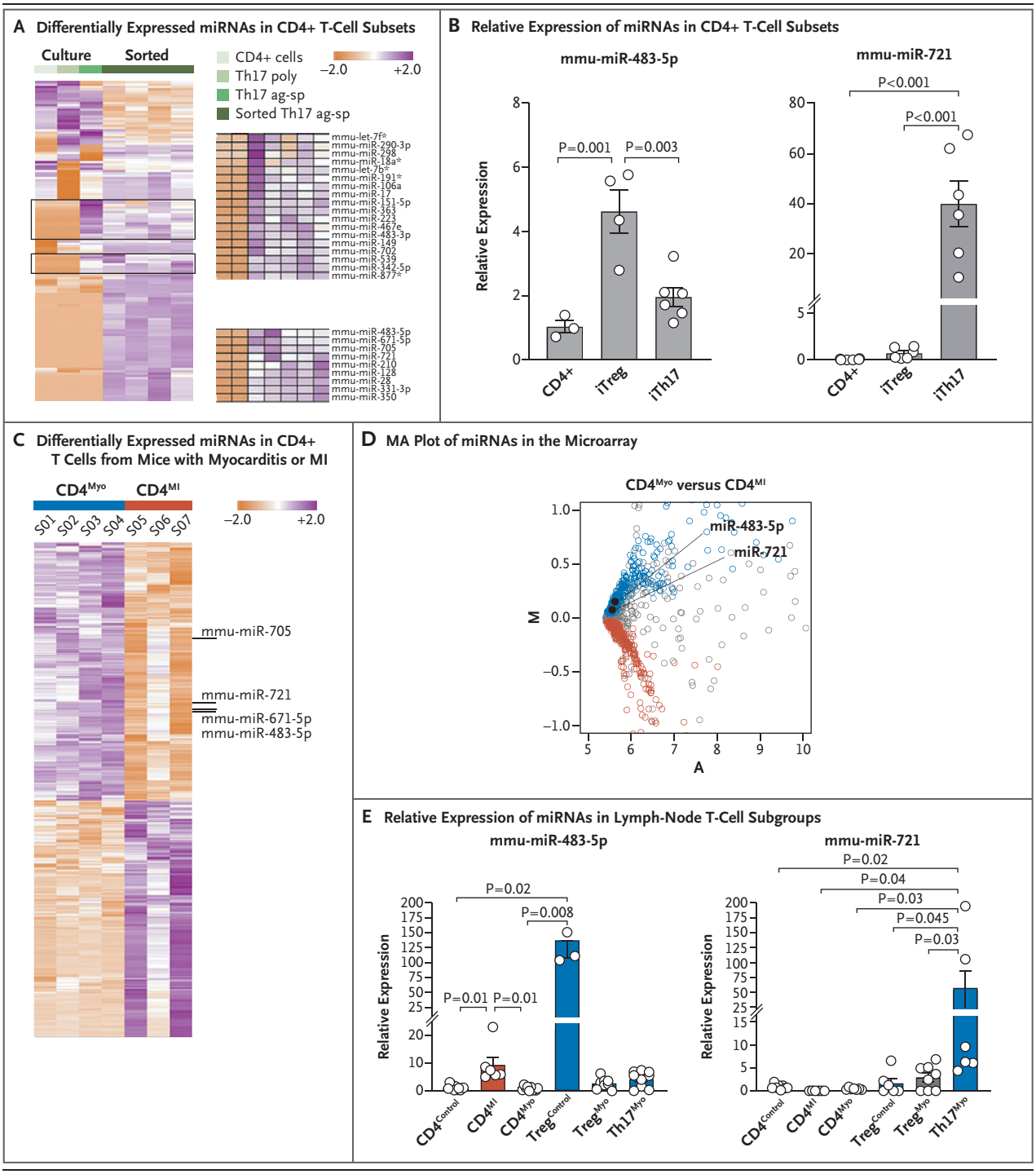

repeated-measures analysis of variance with Dunnett's multiple comparison post hoc test or two-way repeated-measures analysis of variance with Sidak's multiple comparison post hoc test were performed. To assess the association of hsa-miR-Chr8:96 with myocarditis, we performed logistic-regression analyses after adjustment for sex, age, troponin level (normalized value), and ejection fraction with or without the addition of hsa-miR-Chr8:96 as an independent variable. We

Figure 2 (facing page). Synthesis of miRNAs by Circulating Th17 Cells in Myocarditis.

Panel A shows a heat map representing unsupervised hierarchical clustering for the murine microRNAs (miRNAs) expressed in common among the cell types displayed, as analyzed by means of miRNA microarray. Lymph node CD4+ T cells were activated for 48 hours with monoclonal antibodies against T-cell activation molecules CD3 and CD28 or underwent polyclonal differentiation into Th17 (Th17 poly) cells or ovalbumin antigen-specific Th17 (Th17ag-sp) cells in vitro, before sorting or in parallel with sorted interleukin-17+ cells (sorted Th17ag-sp in 4 samples). All data have been normalized by the median of each miRNA. The color scale indicates the relative expression level of each miRNA, with white indicating 0 expression, purple indicating an expression of more than 0, and orange indicating an expression of less than 0. The two gates include 27 miRNAs that were differentially expressed by Th17ag-sp cells (magnified on the right). **Panel B** shows the relative expression of mmu-miR-483-5p and mmu-miR-721 in freshly isolated CD4+ T cells and in vitro differentiated Th17ag-sp (iTh17) and regulatory T (Treg) ag-sp (iTreg) cultures analyzed by quantitative polymerase-chain-reaction (qPCR) assay (3 to 6 experiments for each cell type). Data are represented as means (±SE), and P values were calculated by one-way analysis of variance with Tukey's post hoc test. **Panel C** shows a heat map for the differentially expressed miRNAs with significant expression variance between sorted CD4+ T cells obtained from axillary lymph nodes 6 days after the induction of experimental autoimmune myocarditis ($CD4^{Myo}$, in 4 mice) and from mediastinal lymph nodes obtained 3 days after myocardial infarction (MI) following coronary-artery ligation ($CD4^{MI}$, 3 pools of 2 mice each) in BALB/c mice, after normalization by the median of each miRNA. Individual miRNAs of interest are identified to the right of the heat map. **Panel D** shows an "MA" plot indicating the average expression (A) versus the $\log_2$ of the mean difference (M) of miRNAs detected in the microarray. In the plot, miRNAs that are significantly overrepresented ($P<0.1$ after adjustment) in $CD4^{Myo}$ cells (blue) and $CD4^{MI}$ cells (red) are indicated. In both these cell populations, miRNAs that are indistinctly represented ($P>0.1$ after adjustment) are indicated in gray. **Panel E** shows the relative expression of mmu-miR-483-5p and mmu-miR-721 by qPCR in T-cell subgroups isolated from mediastinal or axillary lymph nodes normalized to CD4+ control cells; $CD4^{Control}$ corresponds to CD4+ T cells isolated from axillary lymph nodes from saline-injected control mice, $CD4^{MI}$ to CD4+ T cells isolated from mediastinal lymph nodes after myocardial infarction, $CD4^{Myo}$ to CD4+ T cells isolated from axillary lymph nodes after the induction of experimental autoimmune myocarditis, $Treg^{Control}$ to CD4+Foxp3+ cells isolated from axillary lymph nodes from saline-injected control mice, $Treg^{Myo}$ to CD4+Foxp3+ cells isolated from axillary lymph nodes after the induction of experimental autoimmune myocarditis, and $Th17^{Myo}$ to CD4+ interleukin-17 cells sorted from axillary lymph nodes after the induction of experimental autoimmune myocarditis. Histograms indicate the mean relative expression of each miRNA in cells pooled from three independent experiments; I bars indicate standard errors. P values were calculated by one-way analysis of variance with Tukey's post hoc test (in 5 to 7 pools of 2 mice each for mmu-miR-721) and by the Kruskal–Wallis test with Dunn's post hoc test (in 3 to 7 pools of 2 mice each for mmu-miR-483-5p).

performed analysis of the receiver-operating-characteristic (ROC) curves to evaluate diagnostic performance and DeLong's test for comparisons. We estimated the best cutoff value for hsa-miR-Chr8:96 (expressed as a relative gene-expression value calculated by the delta–delta Ct [cycle threshold] method for the qPCR analysis) for achieving both a sensitivity and specificity of more than 90% or the value presenting the highest likelihood ratio. Data analyses were performed with GraphPad Prism software, version 7.0, and R software, version 3.6.2.

RESULTS

TH17-SPECIFIC RESPONSES IN ACUTE MYOCARDITIS AND MYOCARDIAL INFARCTION

We assessed myocardial injury and T-cell responses after inducing experimental autoimmune myocarditis or myocardial infarction in mice (Fig. S1). Substantial elevations in levels of cardiac troponin I, creatine kinase MB, and lactate dehydrogenase above the basal level suggested that myocardial injury peaked approximately 21 days after the induction of myocarditis and 3 days after the induction of myocardial infarction (Fig. 1A and Fig. S1A and S1B). The left ventricular ejection fraction dropped promptly after myocardial infarction (>50% reduction at day 3) and also declined in myocarditis (significant decrease at day 21) (Fig. 1B and Fig. S2A). An analysis of circulating T cells showed a significant increase in the number of Th17 cells 14 days after either myocarditis or myocardial infarction (Fig. 1C and Fig. S2B through S2F). The number of Th17 cells was not significantly increased at days 3 or 7 after myocardial infarction (the time of peak biomarker elevation). Therefore, Th17 cells appear to be characteristic of the acute phase of myocardial injury in myocarditis (on day 21) but not the acute phase of myocardial injury in myocardial infarction (on day 3) (Fig. 1C).

We also assessed T-cell responses in 42 patients with acute myocarditis, in 45 patients with ST-segment elevation myocardial infarction (STEMI), in 45 patients with non–ST-segment elevation myocardial infarction (NSTEMI), and in 80 healthy controls. Demographic and clinical data are summarized in Tables S1 and S2. Patients with myocarditis and those with STEMI had significantly greater reductions in the ejection fraction than did healthy controls (Fig. 1D). T-cell subgroups that were analyzed in blood showed a significant increase in Th17 cells in patients with acute myocarditis (Fig. 1E and Fig. S3A). The prominent role of Th17 cells in patients

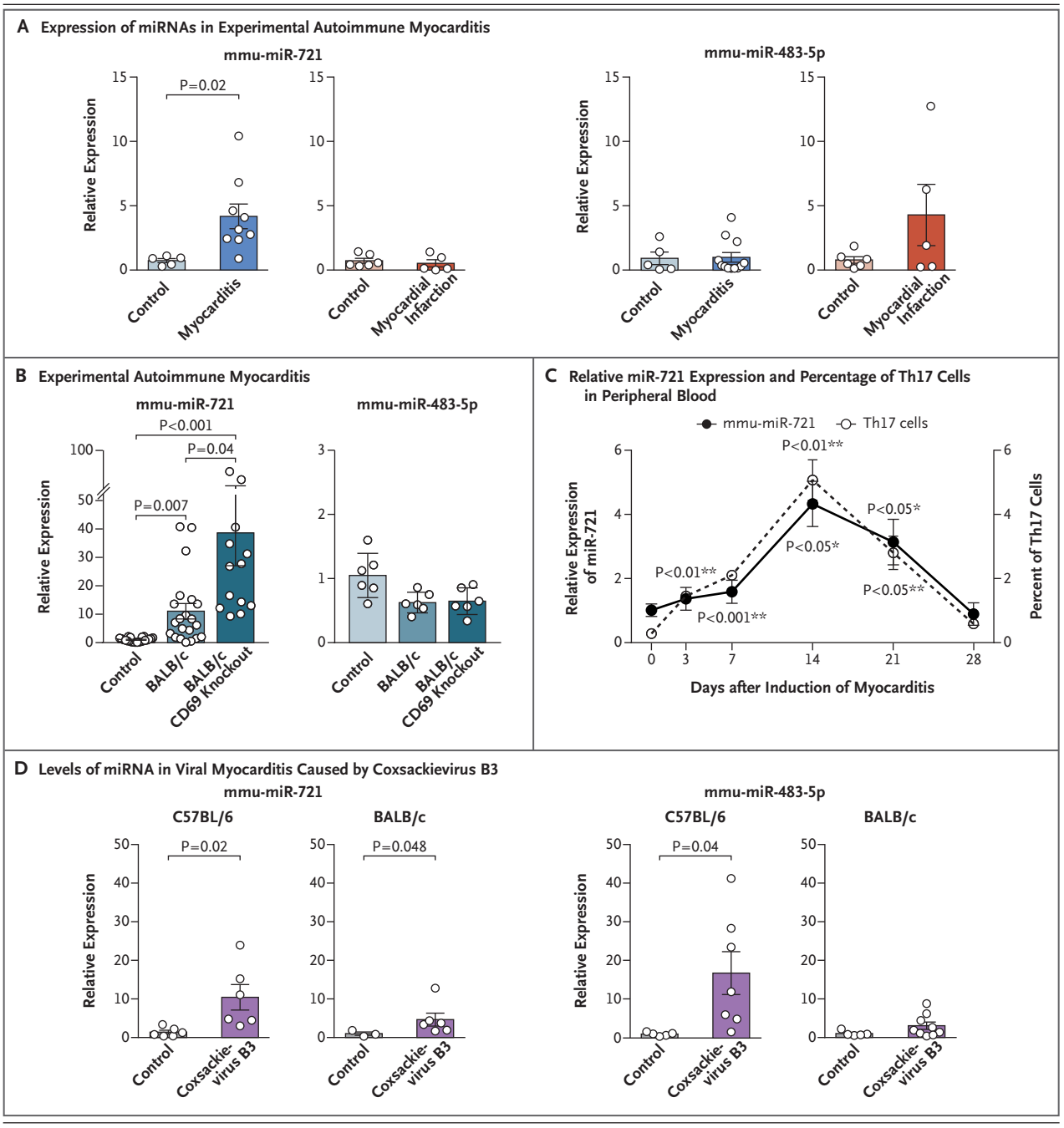

with myocarditis is highlighted by increased ratios of Th17 cells to both Th1 cells and regulatory T cells (Fig. S3B) and by increased absolute numbers of Th17 cells (Fig. S3C).

SYNTHESIS OF MMU-MIR-721 BY TH17 CELLS IN AUTOIMMUNE MYOCARDITIS

We performed miRNA screening of T-cell subgroups obtained from the peripheral blood of mice that had experimental autoimmune myocarditis. The T-cell subgroups that were analyzed included CD4+ T cells, polyclonal Th17 cells, and cultures enriched with ovalbumin antigen-specific Th17 (Th17ag-sp) cells or Th17ag-sp sorted cells (Fig. S4A). Microarray analysis identified 27 miRNAs that were up-regulated in both Th17ag-sp cultures and Th17ag-sp sorted cells (Fig. 2A, Fig. S4B, and Table S7). MiRNA profil-

Figure 3 (facing page). Circulating miRNAs in Mice with Autoimmune or Viral Myocarditis.

Panel A shows the expression of mmu-miR-721 and mmu-miR-483-5p in an analysis performed by qPCR in plasma obtained from BALB/c mice 21 days after the induction of experimental autoimmune myocarditis (following immunization with cardiac α-myosin heavy-chain peptide) or control mice (following immunization with phosphate-buffered saline), or 3 days after the induction of myocardial infarction (following ligation of the left anterior descending coronary artery) or control mice (following sham operation). Data are represented as means (±SE) from one representative among three independent experiments involving 5 to 9 mice per group. The P value was calculated by the unpaired t-test. **Panel B** shows the relative expression of mmu-miR-721 and mmu-miR-483-5p in serum obtained from mice with moderate myocarditis (BALB/c background) or severe myocarditis (BALB/c CD69 knockout background), and control mice immunized with saline (with 6 to 21 mice per group), analyzed by qPCR. Histogram values are means (±SE), with calculations performed by one-way analysis of variance with Tukey's post hoc test. **Panel C** shows the relative expression of mmu-miR-721 (analyzed by qPCR) and the percentage of Th17 cells in peripheral blood (analyzed by flow cytometry) in samples obtained from mice at different time points after the induction of experimental autoimmune myocarditis in 6 mice. I bars represent standard errors. P values were determined by one-way repeated-measures analysis of variance. Dunnett's multiple-comparison test was performed between values at day 3 to day 28 as compared with day 0 after induction of myocarditis for mmu-miR-721 relative expression (*) and for the percentage of Th17 cells (**) individually. **Panel D** shows levels of circulating miRNA that were assessed by qPCR during viral myocarditis at 10 days after infection with coxsackievirus B3. The expression in BALB/c and C57BL/6 mouse strains was analyzed in parallel with uninfected control groups (5 to 7 mice per group). Data that are reported as means (±SE) were analyzed by means of the unpaired t-test (in C57BL/6 mice) and the Mann–Whitney U test (in BALB/c mice).

ing of Th17ag-sp sorted cells obtained from CD69 knockout mice (in which severe myocarditis develops[18]) as compared with wild-type mice (in which moderate myocarditis develops) showed mmu-miR-721 and mmu-miR-483-5p as the most strongly up-regulated miRNAs (Table S8). Analysis by qPCR showed that mmu-miR-721 expression was specific for Th17ag-sp cells (Fig. 2B and Fig. S4C). Pathway analysis software (Ingenuity) identified roles for the selected miRNAs in T-cell homeostasis and differentiation (Fig. S4D) and identified validated target genes related to Th17 cells, such as *Pparγ*, *Nos2*, *Stat3*, *Tgfβ*, and *Cd69* (Fig. S4E).

MiRNA profiling in sorted CD4+ T cells from draining lymph nodes 6 days after the induction of myocarditis or 3 days after coronary artery ligation in mice (Fig. S4F) revealed that mmu-miR-721 and mmu-miR-483-5p were overexpressed in myocarditis-associated CD4+ T cells as compared with myocardial infarction-associated CD4+ T cells (Fig. 2C and 2D and Table S9). Analysis of sorted T cells by qPCR (Fig. S4G) confirmed that mmu-miR-721 was synthesized by Th17ag-sp cells in myocarditis (Fig. 2E).

DETECTION OF MMU-MIR-721 IN PLASMA FROM MICE WITH AUTOIMMUNE AND VIRAL MYOCARDITIS

We detected expression of mmu-miR-721 in plasma from mice with experimental autoimmune myocarditis and expression of mmu-miR-483-5p in plasma from mice with acute myocardial infarction (Fig. 3A). The relative expression of mmu-miR-721 increased in CD69 knockout mice (Fig. 3B). During the development of experimental autoimmune myocarditis, the time course of the rise and fall of circulating Th17 cells was similar to that of circulating mmu-miR-721 (Fig. 3C). In a murine model of viral myocarditis caused by coxsackievirus B3 infection (Fig. S5), circulating mmu-miR-721 expression at 10 days was significantly higher in C57BL/6 mice, in which severe heart inflammation developed, than in BALB/c mice, in which less severe inflammation developed (Fig. 3D).

IDENTIFICATION, CLONING, AND VALIDATION OF THE MMU-MIR-721 HUMAN HOMOLOGUE

The human homologue of mmu-miR-721 had not been identified,[21] so we screened the genome of human and other mammalian species for homologous sequences (Fig. S6A). The yield of amplification product with the murine probe for mmu-miR-721 (Fig. 4A and Fig. S6B) and cloning efficiency (Fig. 4B) were higher with plasma from patients with myocarditis than with plasma from patients with myocardial infarction or healthy controls. Screened colonies yielded an 18-nucleotide sequence identical to mmu-miR-721 (Fig. 4B), which was highly conserved across mammalian species (Fig. S6A) and located on chromosome 8 in the human genome (genomic sequence, NC_018919.2) (Fig. S6C). We postulated that the 3 nucleotides (TCT) at the 5′ end complete the putative mature human miR-721 homologue (*TCT*TGCAATTAAAAGGGGGAA), which we called hsa-miR-Chr8:96.

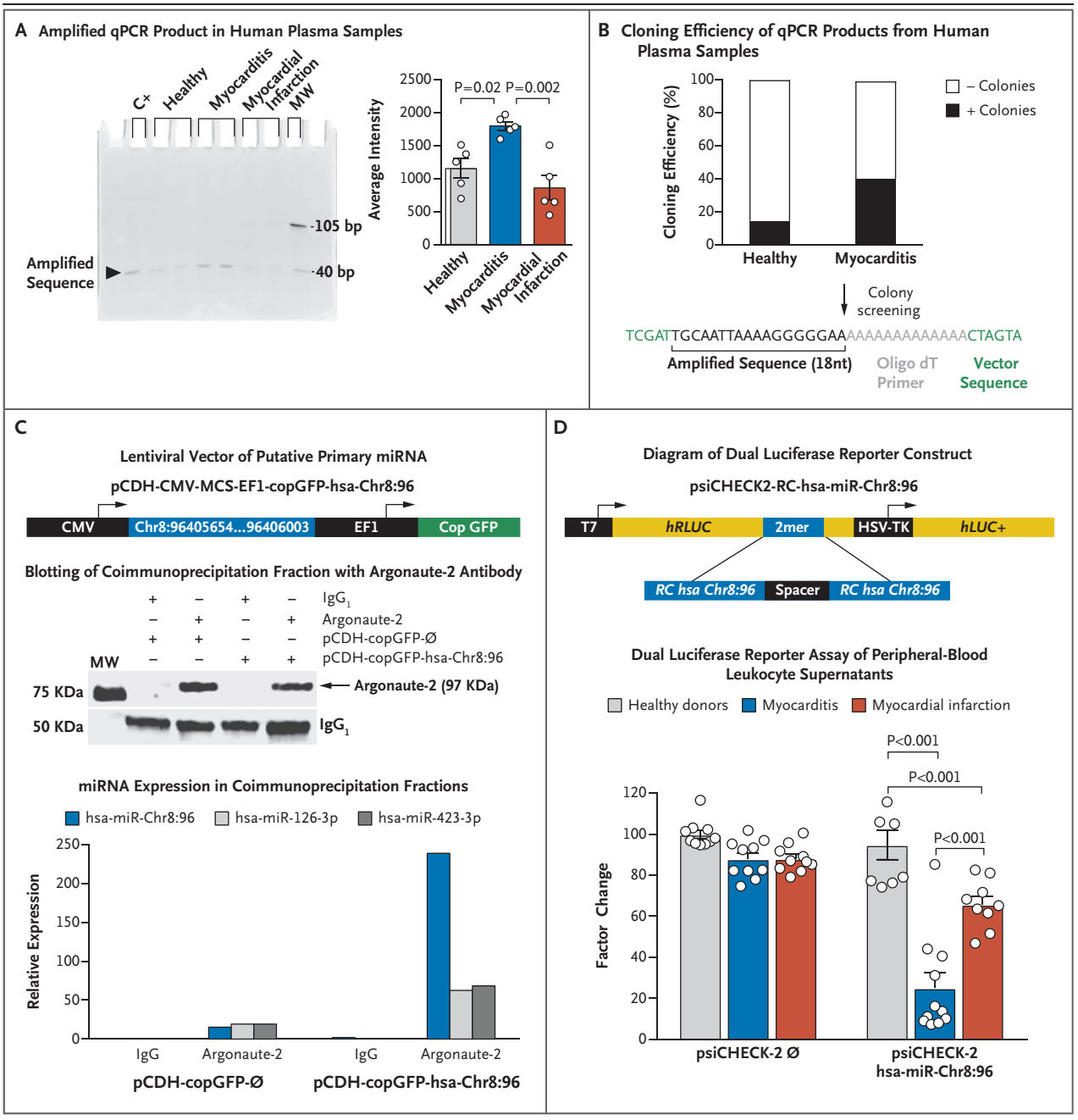

MiRNAs are defined by their length and their association with the Argonaute protein family.[22] We cloned the pre-miRNA (Fig. 4C) and performed coimmunoprecipitation of RNA with Argonaute-2 or IgG subclass 1, followed by qPCR analysis, which showed that the cloned fragment was processed as a mature miRNA. For functional validation,[23] we cloned the reverse-complementary sequence of hsa-miR-Chr8:96 (Fig. 4D) in a luciferase dual reporter vector. Supernatants from peripheral-blood leukocytes obtained from patients with myocarditis inhibited the luciferase activity, which supports the conclusion that hsa-miR-Chr8:96 is a mature and functionally active miRNA.

PRESENCE OF HSA-MIR-CHR8:96 IN ACUTE MYOCARDITIS

We performed qPCR to assay plasma samples from the main cohort for miRNA profiling (Table S1). We analyzed hsa-miR-483-5p and hsa-miR-21, which are abundant after myocardial

Figure 4 (facing page). Cloning and Validation of hsa-miR-Chr8:96.

Panel A shows the results of analyses with the use of polyacrylamide gel electrophoresis (at left) indicating the qPCR product (black arrowhead) in human plasma samples obtained from patients with acute myocarditis or acute myocardial infarction or from healthy controls with the mmu-miR-721 probe. Transfected mmu-miR-721 in human cells was used as a positive control (C+). MW denotes molecular-weight markers. Quantification of the average intensity of the qPCR product (stained with methylene blue and quantified with Image Studio Lite, version 4.0) is shown at right. Data are pooled from two independent gels. Histograms represent the mean values (±SE) and were analyzed by one-way analysis of variance with Tukey's post hoc test (with 5 patients per group). **Panel B** shows quantification of pGEM-T cloning efficiency of the qPCR products from human plasma samples. The product obtained from sequencing the colonies included 18 nucleotides (nt) (black) and a polyadenine tail (gray) from the reverse primer poly dT (a short sequence of deoxythymidine nucleotide) used for qPCR, inserted into the vector sequence (green). **Panel C** shows a diagram of pCDH-CMV-MCS-EF1-copGFP–based lentiviral vector used to express the sequence of Chr8:96405654–96406003, containing 350 nucleotides including the putative primary miRNA pri-hsa-miR-Chr8:96 (at top). Also shown is representative blotting with Argonaute-2 antibody of the RNA–Argonaute-2–IgG_1 coimmunoprecipitation fraction (middle graph) and the expression of the indicated miRNAs in the coimmunoprecipitation fractions evaluated by qPCR (lower graph). To quantify the expression of hsa-miR-Chr8:96, a custom-made probe was used to amplify the putative mature hsa-miR-Chr8:96 (TCT TGC AAT TAA AAG GGG GAA). RNU1A1, a small nuclear RNA that is processed independently of Argonaute-2, was used as an endogenous control for miRNA relative expression (1 of 4 independent experiments). **Panel D** shows a diagram of psiCHECK2-RC-hsa-miR-Chr8:96 luciferase dual reporter vector (at top). The 2-mer insert consists of a tandem repeat of the reverse complementary (RC) sequence to the mature hsa-miR-Chr8:96. Also shown are peripheral-blood leukocytes obtained from patients with acute myocarditis, from those with acute myocardial infarction, and from healthy controls that were cultured overnight, followed by collection of supernatants (bottom graph). Renilla and firefly dual luciferase reporter assays were performed after transiently transfecting HEK293T cells with an empty plasmid (psiCHECK2 Ø) or psiCHECK2-RC-hsa-miR-Chr8:96–expressing plasmid, by adding the supernatant of the different human samples. Firefly luciferase and renilla signals were analyzed (5 supernatants from 5 different study participants from each group). Data are means (±SE) and analyzed by two-way analysis of variance with Sidak's post hoc test. CMV denotes cytomegalovirus promoter, CopGFP superbright green fluorescent protein, EF1 elongation factor 1 promoter, hLUC+ synthetic firefly luciferase gene, hRLUC synthetic renilla luciferase reporter gene, HSV-TK herpes simplex virus-1 thymidine kinase promoter, MCS multicloning site, Ø empty plasmid, pCDH complementary DNA cloning and expression lentivector, and T7 T7 promoter.

injury,[24] and hsa-miR-132-3p and hsa-miR-212-3p, which promote Th17-cell differentiation,[25] together with hsa-miR-Chr8:96. The expression of the novel miRNA in plasma was greater in patients with myocarditis than in either patients with myocardial infarction or healthy controls (Fig. 5A). The novel miRNA was specifically synthesized by Th17 cells obtained from patients with myocarditis (Fig. S6D and S6E). ROC curves were generated to determine the diagnostic characteristics of hsa-miR-Chr8:96 expression measured in plasma. Among the patients with myocarditis, the area under the ROC curve was 0.927 (95% confidence interval [CI], 0.879 to 0.975) as compared with patients with myocardial infarction and 0.988 (95% CI, 0.970 to 1.006) as compared with healthy controls (Fig. 5B and Table S10). We analyzed additional validation cohorts with different comparators, which confirmed that the novel miRNA was specifically expressed in plasma from patients with myocarditis, as compared with those with myocardial infarction (Fig. 5C and Table S3) or MINOCA (Fig. 5D and Table S4). These data were also validated in a cohort of patients with biopsy-proven myocarditis (Fig. 5E and Table S5), along with patients who had other Th17-related diseases (rheumatoid arthritis, spondyloarthritis, psoriasis, and multiple sclerosis) (Table S6 and Fig. S6F). The ability of the novel miRNA to distinguish acute myocarditis from myocardial infarction remained significant after adjustment for age, sex, ejection fraction, and serum troponin level (Fig. 5F and 5G and Fig. S6G).

DISCUSSION

In this study, we identified a novel miRNA, mmu-miR-721, as a marker of myocarditis in murine models (including experimental autoimmune myocarditis and viral myocarditis) and its human homologue, which we designated hsa-miR-Chr8:96. The diagnostic ability of the detection of hsa-miR-Chr8:96 in plasma to discriminate myocarditis from other conditions was confirmed in several patient cohorts with different comparators, including myocardial infarction, MINOCA, and autoimmune diseases, as compared with healthy volunteers.

Previous studies of miRNA expression in the heart during autoimmune or viral myocarditis[26,27] and of circulating miRNAs in patients with heart failure[28-30] suggest that the discovery strategies

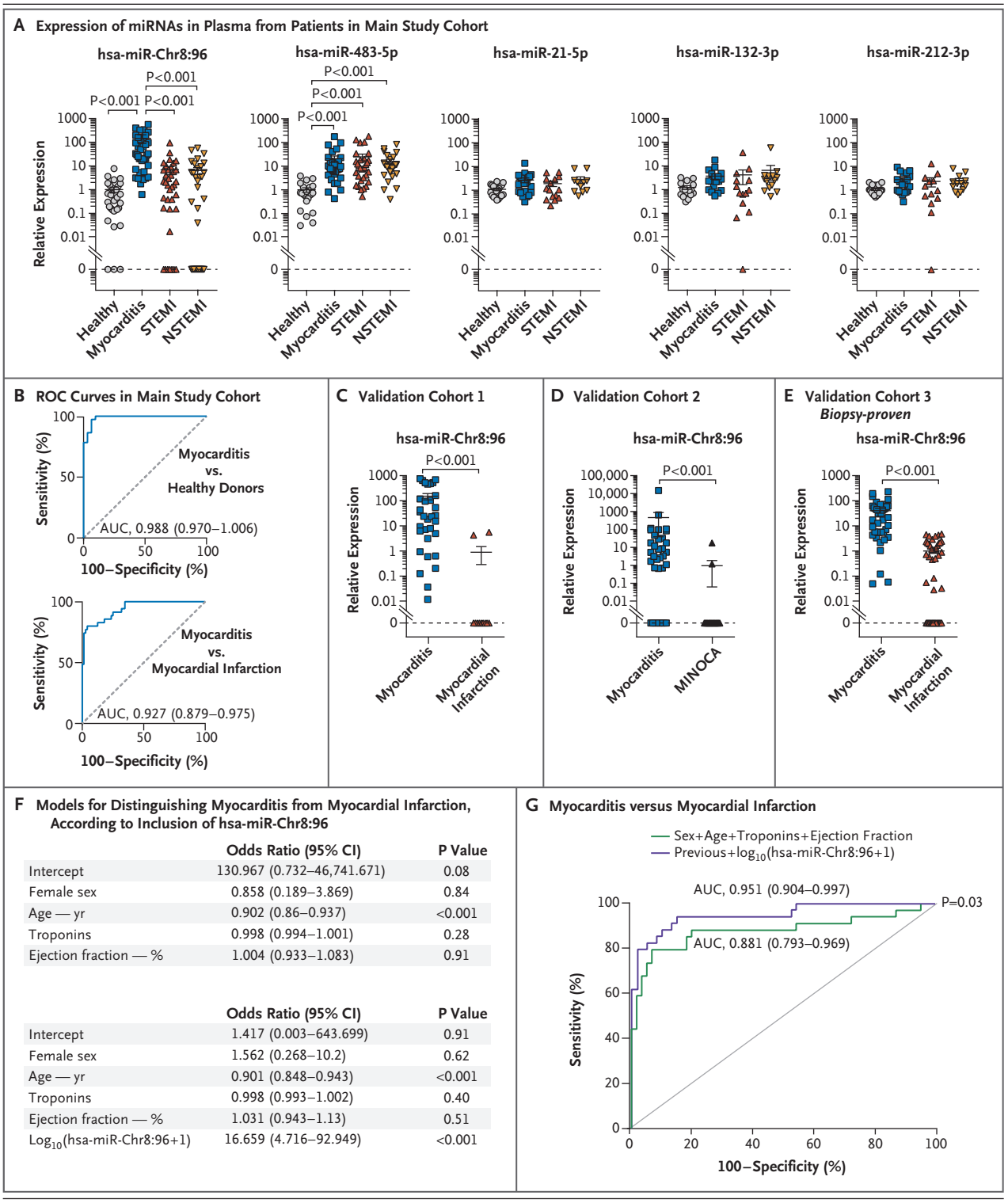

F Models for Distinguishing Myocarditis from Myocardial Infarction, According to Inclusion of hsa-miR-Chr8:96

	Odds Ratio (95% CI)	P Value
Intercept	130.967 (0.732–46,741.671)	0.08
Female sex	0.858 (0.189–3.869)	0.84
Age — yr	0.902 (0.86–0.937)	<0.001
Troponins	0.998 (0.994–1.001)	0.28
Ejection fraction — %	1.004 (0.933–1.083)	0.91

	Odds Ratio (95% CI)	P Value
Intercept	1.417 (0.003–643.699)	0.91
Female sex	1.562 (0.268–10.2)	0.62
Age — yr	0.901 (0.848–0.943)	<0.001
Troponins	0.998 (0.993–1.002)	0.40
Ejection fraction — %	1.031 (0.943–1.13)	0.51
Log_{10}(hsa-miR-Chr8:96+1)	16.659 (4.716–92.949)	<0.001

that were used in those studies would not identify candidate miRNAs that are differentially expressed among different causes of cardiac injury. In comparison, we have investigated the expression of novel miRNAs by Th17 cells, which play an important role in both myocarditis[15] and myo-

Figure 5 (facing page). Analysis of Circulating hsa-miR-Chr8:96 for the Detection of Acute Myocarditis.

Panel A shows quantification of miRNAs by qPCR in circulating plasma obtained from 39 patients with acute myocarditis, 39 patients with STEMI, and 38 patients with NSTEMI, along with plasma from 31 healthy controls in the main study cohort in Spain. Data are represented as $\log_{10}$ of miRNA relative expression in plasma. I bars represent standard errors. Data were analyzed by Kruskal–Wallis with Dunn's post hoc test. **Panel B** shows receiver-operating-characteristic (ROC) curves of hsa-miR-Chr8:96 determinations in plasma, based on the relative gene-expression values calculated by the delta–delta Ct (cycle threshold) method for the qPCR analysis, which were generated to distinguish patients with acute myocarditis from those with acute myocardial infarction and from healthy controls. Also indicated are the area under the ROC curve (AUC), 95% confidence interval (CI), and P value for each comparison. **Panel C** shows validation cohort 1 of patients with myocarditis or acute myocardial infarction from the Partners Biobank (Boston) (AUC, 0.952; 95% CI, 0.883 to 1.000). **Panel D** shows validation cohort 2 of patients with myocarditis, as compared with those with acute myocardial infarction with nonobstructive coronary arteries (MINOCA), from University Hospital Zurich (AUC, 0.831; 95% CI, 0.722 to 0.941). **Panel E** shows validation cohort 3 of patients with biopsy-proven acute myocarditis from the University of Padua and patients with acute myocardial infarction from the Biobank Regional Platform (Murcia, Spain) (AUC, 0.938; 95% CI, 0.889 to 0.988). In Panels C, D, and E, circulating miRNA levels are represented as means (±SE) and were analyzed by the Mann–Whitney U test. **Panel F** shows multivariable logistic-regression models with or without inclusion of hsa-miR-Chr8:96 after adjustment for potential confounders (age, sex, serum troponin levels, and left ventricular ejection fraction) to distinguish patients with myocarditis from those with myocardial infarction. **Panel G** shows ROC curves for the multivariable logistic-regression models with or without hsa-miR-Chr8:96 and the variables of sex, age, serum troponin levels, and left ventricular ejection fraction. DeLong's test was used for the comparison of the AUC.

cardial infarction,[31] and detected an miRNA that could be used to differentiate between these conditions.

In clinical practice, the diagnosis of myocarditis remains a challenge because of the lack of easily accessible diagnostic methods that are both sensitive and specific.[32] Endomyocardial biopsy remains the reference standard, but it is not routinely performed owing to its associated risks as an invasive procedure.[33] Although cardiac MRI is noninvasive,[34,35,10] it also has limitations, including the lack of availability in many hospitals and in the ambulatory setting; in addition, the sensitivity of cardiac MRI to detect edema and vascular permeability decreases over time.[35] Therefore, there is a need for new diagnostic methods.

Additional work will be necessary to determine whether hsa-miR-Chr8:96 is suitable for use as a diagnostic test for myocarditis. This miRNA has not yet been evaluated in other cardiac disorders, such as dilated cardiomyopathy, from which myocarditis must be distinguished in the clinical setting. In addition, in our study, we note great variability in the expression of hsa-miR-Chr8:96, which remains unexplained; it is not clear whether this variation reflects the severity of the disease or is attributable to some other factor.

We identified a novel miRNA in mice and humans with myocarditis and found that the human homologue, hsa-miR-Chr8:96, can be used to distinguish patients with myocarditis from those with myocardial infarction and from healthy controls.

Supported by a grant (PI19/00545, to Dr. Martín) from the Ministry of Science and Innovation through the Carlos III Institute of Health–Fondo de Investigación Sanitaria; by a grant from the Biomedical Research Networking Center on Cardiovascular Diseases (to Drs. Martín, Sánchez-Madrid, and Ibáñez); by grants (S2017/BMD-3671-INFLAMUNE-CM, to Drs. Martín and Sánchez-Madrid; and S2017/BMD-3867-RENIM-CM, to Dr. Ibáñez) from Comunidad de Madrid; by a grant (20152330 31, to Drs. Martín, Sánchez-Madrid, and Alfonso) from Fundació La Marató de TV3; by grants (ERC-2011-AdG 294340-GENTRIS, to Dr. Sánchez-Madrid; and ERC-2018-CoG 819775-MATRIX, to Dr. Ibáñez) from the European Research Council; by grants (SAF2017-82886R, to Dr. Sánchez-Madrid; RETOS2019-107332RB-I00, to Dr. Ibáñez; and SAF2017-90604-REDT-NurCaMeIn and RTI2018-095928-BI00, to Dr. Ricote) from the Ministry of Science and Innovation; by Fondo Europeo de Desarrollo Regional (FEDER); and by a 2016 Leonardo Grant for Researchers and Cultural Creators from the BBVA Foundation to Dr. Martín. The National Center for Cardiovascular Research (CNIC) is supported by the Carlos III Institute of Health, the Ministry of Science and Innovation, the Pro CNIC Foundation, and by a Severo Ochoa Center of Excellence grant (SEV-2015-0505). Mr. Blanco-Domínguez is supported by a grant (FPU16/02780) from the Formación de Profesorado Universitario program of the Spanish Ministry of Education, Culture, and Sports. Ms. Linillos-Pradillo is supported by a fellowship (PEJD-2016/BMD-2789) from Fondo de Garantía de Empleo Juvenil de Comunidad de Madrid. Dr. Relaño is supported by a grant (BES-2015-072625) from Contratos Predoctorales Severo Ochoa para la Formación de Doctores of the Ministry of Economy and Competitiveness. Dr. Alonso-Herranz is supported by a fellowship from La Caixa–CNIC. Dr. Caforio is supported by Budget Integrato per la Ricerca dei Dipartimenti BIRD-2019 from Università di Padova. Dr. Das is supported by grants (UG3 TR002878 and R35 HL150807) from the National Institutes of Health and the American Heart Association through its Strategically Focused Research Networks.

Disclosure forms provided by the authors are available with the full text of this article at NEJM.org.

We thank the patients and other volunteers for their participation in this study; Manuel Gómez for his critical reading of the manuscript; Ana Vanesa Alonso and Lorena Flores for their excellent technical work with the echocardiography acquisition and analysis in the murine models; Ramón F. Maruri for his work analyzing data for the patients from Hospital de la Princesa; Laura Fernández and Belen Díaz from HM Hospitales for patient recruitment; Juan José Lazcano Duque and Elisabet Daniel Palomares for their work with mouse colony management; and the staff members at the Bioinformatics, Genomics, Advanced Imaging, Cellomics, and Comparative Medicine units at the CNIC for their support in this work.

APPENDIX

The authors' full names and academic degrees are as follows: Rafael Blanco-Domínguez, M.Sc., Raquel Sánchez-Díaz, Ph.D., Hortensia de la Fuente, M.D., Ph.D., Luis J. Jiménez-Borreguero, M.D., Adela Matesanz-Marín, Ph.D., Marta Relaño, Ph.D., Rosa Jiménez-Alejandre, M.Sc., Beatriz Linillos-Pradillo, M.Sc., Katerina Tsilingiri, Ph.D., María L. Martín-Mariscal, M.D., Laura Alonso-Herranz, Ph.D., Guillermo Moreno, M.Sc., Roberto Martín-Asenjo, M.D., Marcos M. García-Guimaraes, M.D., Katelyn A. Bruno, Ph.D., Esteban Dauden, M.D., Ph.D., Isidoro González-Álvaro, M.D., Ph.D., Luisa M. Villar-Guimerans, M.D., Ph.D., Amaia Martínez-León, M.D., Ane M. Salvador-Garicano, Ph.D., Sam A. Michelhaugh, B.A., Nasrien E. Ibrahim, M.D., James L. Januzzi, M.D., Jan Kottwitz, M.D., Sabino Iliceto, M.D., Mario Plebani, M.D., Cristina Basso, M.D., Ph.D., Anna Baritussio, M.D., Ph.D., Mara Seguso, M.Sc., Renzo Marcolongo, M.D., Mercedes Ricote, Ph.D., DeLisa Fairweather, Ph.D., Héctor Bueno, M.D., Ph.D., Leticia Fernández-Friera, M.D., Ph.D., Fernando Alfonso, M.D., Ph.D., Alida L.P. Caforio, M.D., Ph.D., Domingo A. Pascual-Figal, M.D., Ph.D., Bettina Heidecker, M.D., Ph.D., Thomas F. Lüscher, M.D., Ph.D., Saumya Das, M.D., Ph.D., Valentín Fuster, M.D., Ph.D., Borja Ibáñez, M.D., Ph.D., Francisco Sánchez-Madrid, Ph.D., and Pilar Martín, Ph.D.

The authors' affiliations are as follows: the Vascular Pathophysiology Area (R.B.-D., R.S.-D., A.M.-M., M. Relaño, R.J.-A., B.L.-P., K.T., D.A.P.-F., V.F., F.S.-M., P.M.) and the Myocardial Pathophysiology Area (L.A.-H., M. Ricote, H.B., L.F.-F., B.I.), Centro Nacional de Investigaciones Cardiovasculares (CNIC), the Department of Immunology (H.F., F.S.-M.), the Department of Cardiology (L.J.J.-B., M.M.G.-G., F.A.), the Department of Dermatology (E.D.), and the Department of Rheumatology (I.G.-A.), Instituto de Investigación Sanitaria, Hospital Universitario de la Princesa, Fundación Jiménez Díaz (M.L.M.-M., B.I.), the Cardiology Department, Hospital Universitario 12 de Octubre, and Instituto de Investigación Sanitaria Hospital 12 de Octubre (G.M., R.M.-A., H.B.), the Department of Immunology, Hospital Ramón y Cajal (L.M.V.-G.), HM Hospitales–Centro Integral de Enfermedades Cardiovasculares (L.F.-F.), and CIBER de Enfermedades Cardiovasculares (R.S.-D., H.F., L.J.J.-B., F.A., D.A.P.-F., B.I., F.S.-M., P.M.), Madrid, Hospital Universitario Central de Asturias, Oviedo (A.M.-L.), and the Cardiology Department, Hospital Universitario Virgen de la Arrixaca, Murcia (D.A.P.-F.) — all in Spain; the Department of Cardiovascular Medicine, Mayo Clinic, Jacksonville, FL (K.A.B., D.F.); the Cardiovascular Division and Corrigan Minehan Heart Center, Massachusetts General Hospital, and Harvard Medical School, Boston (A.M.S.-G., S.A.M., N.E.I., J.L.J., S.D.); Kanntonsspital St. Gallen Klinik für Anesthesiologie und Intensivmedizin, St. Gallen, Switzerland (J.K.); Cardiology (S.I., A.B., A.L.P.C.) and the Cardiovascular Pathology Unit (C.B.), the Department of Cardiac, Thoracic, Vascular Sciences and Public Health, the Department of Laboratory Medicine (M.P., M.S.), and the Department of Medicine, Hematology and Clinical Immunology (R.M.), University of Padua, Padua, Italy; Charite Universitätsmedizin Berlin, Campus Benjamin Franklin, Berlin (B.H.); Imperial College and Royal Brompton and Harefield Hospital, London (T.F.L.); and the Cardiovascular Institute, Icahn School of Medicine at Mount Sinai, New York (V.F.).

REFERENCES

1. Heymans S, Eriksson U, Lehtonen J, Cooper LT Jr. The quest for new approaches in myocarditis and inflammatory cardiomyopathy. J Am Coll Cardiol 2016;68:2348-64.
2. Cooper LT Jr. Myocarditis. N Engl J Med 2009;360:1526-38.
3. Frustaci A, Russo MA, Chimenti C. Randomized study on the efficacy of immunosuppressive therapy in patients with virus-negative inflammatory cardiomyopathy: the TIMIC study. Eur Heart J 2009;30:1995-2002.
4. Caforio AL, Marcolongo R, Basso C, Iliceto S. Clinical presentation and diagnosis of myocarditis. Heart 2015;101:1332-44.
5. Felker GM, Thompson RE, Hare JM, et al. Underlying causes and long-term survival in patients with initially unexplained cardiomyopathy. N Engl J Med 2000;342:1077-84.
6. Thygesen K, Alpert JS, Jaffe AS, et al. Fourth universal definition of myocardial infarction (2018). J Am Coll Cardiol 2018;72:2231-64.
7. Ibanez B, James S, Agewall S, et al. 2017 ESC guidelines for the management of acute myocardial infarction in patients presenting with ST-segment elevation: the task force for the management of acute myocardial infarction in patients presenting with ST-segment elevation of the European Society of Cardiology (ESC). Eur Heart J 2018;39:119-77.
8. Tamis-Holland JE, Jneid H, Reynolds HR, et al. Contemporary diagnosis and management of patients with myocardial infarction in the absence of obstructive coronary artery disease: a scientific statement from the American Heart Association. Circulation 2019;139(18):e891-e908.
9. Gannon MP, Schaub E, Grines CL, Saba SG. State of the art: evaluation and prognostication of myocarditis using cardiac MRI. J Magn Reson Imaging 2019;49(7):e122-e131.
10. Ferreira VM, Schulz-Menger J, Holmvang G, et al. Cardiovascular magnetic resonance in nonischemic myocardial inflammation: expert recommendations. J Am Coll Cardiol 2018;72:3158-76.
11. Caforio ALP, Cheng C, Perazzolo Marra M, et al. How to improve therapy in myocarditis: role of cardiovascular magnetic resonance and of endomyocardial biopsy. Eur Heart J Suppl 2019;21:Suppl B:B19-B22.
12. Cihakova D, Rose NR. Pathogenesis of myocarditis and dilated cardiomyopathy. Adv Immunol 2008;99:95-114.
13. Kovalcsik E, Antunes RF, Baruah P, Kaski JC, Dumitriu IE. Proteasome-mediated reduction in proapoptotic molecule Bim renders $CD4^+CD28^{null}$ T cells resistant to apoptosis in acute coronary syndrome. Circulation 2015;131:709-20.
14. Rangachari M, Mauermann N, Marty RR, et al. T-bet negatively regulates autoimmune myocarditis by suppressing local production of interleukin 17. J Exp Med 2006;203:2009-19.
15. Myers JM, Cooper LT, Kem DC, et al. Cardiac myosin-Th17 responses promote heart failure in human myocarditis. JCI Insight 2016;1(9):e85851.
16. Yuan J, Cao AL, Yu M, et al. Th17 cells facilitate the humoral immune response in patients with acute viral myocarditis. J Clin Immunol 2010;30:226-34.
17. Boon RA, Dimmeler S. MicroRNAs in

myocardial infarction. Nat Rev Cardiol 2015;12:135-42.
18. Cruz-Adalia A, Jiménez-Borreguero LJ, Ramírez-Huesca M, et al. CD69 limits the severity of cardiomyopathy after autoimmune myocarditis. Circulation 2010; 122:1396-404.
19. Myers JM, Fairweather D, Huber SA, Cunningham MW. Autoimmune myocarditis, valvulitis, and cardiomyopathy. Curr Protoc Immunol 2013;15:Unit 15.14.1-51.
20. Patriki D, Gresser E, Manka R, Emmert MY, Lüscher TF, Heidecker B. Approximation of the incidence of myocarditis by systematic screening with cardiac magnetic resonance imaging. JACC Heart Fail 2018;6:573-9.
21. Wheeler G, Ntounia-Fousara S, Granda B, Rathjen T, Dalmay T. Identification of new central nervous system specific mouse microRNAs. FEBS Lett 2006;580: 2195-200.
22. Ha M, Kim VN. Regulation of microRNA biogenesis. Nat Rev Mol Cell Biol 2014;15:509-24.
23. Rao DS, O'Connell RM, Chaudhuri AA, Garcia-Flores Y, Geiger TL, Baltimore D. MicroRNA-34a perturbs B lymphocyte development by repressing the forkhead box transcription factor Foxp1. Immunity 2010;33:48-59.
24. Halushka PV, Goodwin AJ, Halushka MK. Opportunities for microRNAs in the crowded field of cardiovascular biomarkers. Annu Rev Pathol 2019;14:211-38.
25. Nakahama T, Hanieh H, Nguyen NT, et al. Aryl hydrocarbon receptor-mediated induction of the microRNA-132/212 cluster promotes interleukin-17-producing T-helper cell differentiation. Proc Natl Acad Sci U S A 2013;110:11964-9.
26. Corsten MF, Papageorgiou A, Verhesen W, et al. MicroRNA profiling identifies microRNA-155 as an adverse mediator of cardiac injury and dysfunction during acute viral myocarditis. Circ Res 2012;111:415-25.
27. Xu HF, Ding YJ, Zhang ZX, et al. MicroRNA-21 regulation of the progression of viral myocarditis to dilated cardiomyopathy. Mol Med Rep 2014;10:161-8.
28. Aleshcheva G, Pietsch H, Escher F, Schultheiss HP. MicroRNA profiling as a novel diagnostic tool for identification of patients with inflammatory and/or virally induced cardiomyopathies. ESC Heart Fail 2021;8:408-22.
29. Zhang J, Xing Q, Zhou X, et al. Circulating miRNA-21 is a promising biomarker for heart failure. Mol Med Rep 2017;16: 7766-74.
30. Zhang B, Li B, Qin F, Bai F, Sun C, Liu Q. Expression of serum microRNA-155 and its clinical importance in patients with heart failure after myocardial infarction. J Int Med Res 2019;47:6294-302.
31. Simon T, Taleb S, Danchin N, et al. Circulating levels of interleukin-17 and cardiovascular outcomes in patients with acute myocardial infarction. Eur Heart J 2013;34:570-7.
32. Caforio AL, Pankuweit S, Arbustini E, et al. Current state of knowledge on aetiology, diagnosis, management, and therapy of myocarditis: a position statement of the European Society of Cardiology Working Group on Myocardial and Pericardial Diseases. Eur Heart J 2013;34: 2636-48.
33. Sato N. Call for action to establish standard diagnostic and therapeutic approaches for myocarditis. Int J Cardiol 2019;284:61-2.
34. Kotanidis CP, Bazmpani MA, Haidich AB, Karvounis C, Antoniades C, Karamitsos TD. Diagnostic accuracy of cardiovascular magnetic resonance in acute myocarditis: a systematic review and meta-analysis. JACC Cardiovasc Imaging 2018; 11:1583-90.
35. Lurz P, Luecke C, Eitel I, et al. Comprehensive cardiac magnetic resonance imaging in patients with suspected myocarditis: the MyoRacer-trial. J Am Coll Cardiol 2016;67:1800-11.